347

IMPERIAL COLLEGE OF SCIENCE AND TECHNOLOGY

University of London

THE EFFECT OF RUBBER CONTENT ON THE STRENGTH OF IMPACT POLYSTYRENE

by

KAMYAR NIKPUR, B.Sc.(Eng.), M.Sc.

Thesis submitted for the degree of

Doctor of Philosophy

of the

University of London

Department of Mechanical Engineering
Imperial College of Science and Technology
London SW7 2BX

October 1977

ABSTRACT

Most glassy polymers are susceptible to fail in a brittle manner. In order to improve the fracture behaviour, these polymers are commonly grafted with a rubbery material and it is generally thought that the toughness of the rubber-modified derivatives increases substantially. The work presented in this thesis aims at analysing the mechanical properties of various types of commercial and specially prepared high impact polystyrenes (HIPS). Having studied the specially prepared grades of these polymers which contained different nominal rubber fractional volumes, the analysis is mainly centred upon the effect of rubber content on the fracture and tensile properties. Although the work was carried out on HIPS polymers alone, the findings of this study may be applied for various types of rubber particulate-filled polymer composites.

Contributions are made in three areas. Firstly, the tensile behaviour of the rubber-modified polymers are studied and it is shown that the moduli and yield stress of these materials decrease significantly with increasing rubber. The prediction of the low strain properties were made possible by introducing a two-stage calculation model in which the composite particles (consisting of relatively rigid polystyrene beads floated in a rubbery media) and the HIPS aggregate (consisting of the relatively soft composite particles suspended in the polystyrene matrix) were analysed using Hill's and modified Kerner's theories of composite materials. The theoretical discussion following has provided a better understanding of the effect of anisotropic dispersion of rubber particles on the overall behaviour of the material. The subsequent theoretical model proposed for the effect of craze formation upon the elongation to break can be used as a basis on which to assess the apparent toughness

of modified polymers. Finally, the effect of temperature and strain rate on the tensile properties of HIPS was demonstrated by employing the non-resonance forced vibration method and also the standard tensile tests.

Secondly, attempts were made to measure the fracture toughness of HIPS under brittle conditions, using the standard linear fracture mechanics theories. On researching the fracture behaviour of some commercial types of HIPS, it was shown that, under plane strain conditions with the aid of utilising wider specimens and also crack constraining media (such as coating the crack specimens by a fragile glue), a brittle fracture can be induced. Hence, on the basis of these findings, the effect of rubber content, strain rate and temperature on the fracture toughness of certain specially prepared HIPS was analysed and it was shown that the toughness increases with decreasing temperature, increasing strain rate and increasing rubber content up to 2% fractional volume, and thereafter remains fairly constant.

Finally, the impact properties of certain commercial and specially prepared HIPS were analysed. The basic theories derived for homogeneous brittle or ductile materials were shown to be inadequate for describing the impact strengths of these materials. Consequently, a composite theory is proposed for rubber-modified polymers which clearly describes the effect of rubber content on their impact strengths. By this theory, it is shown that the resistance to impact can be considered to be made up of two components, one being the initiation resistance, depending on the properties of the matrix alone, and the other the propagation resistance, being independent of the matrix material but proportional to the level of rubber grafting.

ACKNOWLEDGEMENTS

The author would like to thank the members of the Mechanical Engineering Department at Imperial College for the assistance and advice given to him during the course of his study. In particular, he is indebted to Professor J.G. Williams, who suggested this project and who has supervised it with enthusiasm and encouragement to its completion.

It is a pleasant duty to acknowledge the kindness of Dr D.P. Isherwood, who provided stimulation and substantial aid during the earlier part of the study and the preparation of the manuscript.

Special thanks are also due to Messrs L.H. Coutts, M.W. Birch, P.D. Ewing, J.A. Briffa and R. White for their invaluable assistance on the technical aspects of the experimental work, and to Mr J.M. Hodgkinson and Dr S.H. Joseph for their helpful discussions and valuable comments.

The experiments described in Chapter 8 were performed in the Polymer Characterisation Laboratory of the Chemistry Department and the author wishes to express his gratitude to Dr J.A. Barrie and Mr R.N. Sheppard for their technical assistance. The electron microscopic photography in Chapter 5 was carried out in the Chemical Engineering and the Mining & Mineral Technology Departments, and the help and advice of the technicians of these departments are very much appreciated.

The author is also grateful to the US Steel Corporation for their financial support during the first two years of this work.

Thanks are also due to Miss E.A. Quin for her skilful and careful typing of this thesis.

CONTENTS

		Page
Abstract		2
Acknowledgements		4
Contents		5
Nomenclature		11
Abbreviations		21
CHAPTER 1 :	INTRODUCTION	22
1.1	Production of High Impact Polystyrene	22
1.2	Plan of Thesis	25
	PART I	
CHAPTER 2 :	ELASTIC PROPERTIES OF PARTICULATE-FILLED COMPOSITES	28
2.1	Introduction	28
2.2	A Brief Historial Review of Theories on Particulate-Filled Polymers	32
2.3	Dewey's Dilute Suspension Theory	37
2.4	Kerner's Theory of Finite Suspension	43
2.5	Self-Consistent Composite Theories	47
CHAPTER 3 :	FRACTURE TOUGHNESS	50
3.1	Introduction	50
3.2	Energy Balance Criterion	52
3.3	Stress Intensity Analysis	56
3.4	Modification of Linear Fracture Mechanics	63
3.5	Non-Linearity in Fracture Mechanism	66

		Page
3.6	Bimodal Fracture Criterion	73
3.7	The Generalised Theory of Fracture Mechanics	76
CHAPTER 4 :	IMPACT RESISTANCE	79
4.1	Historical Review	79
4.2	Problems and Limitations of Impact Testing	87
4.3	Initiation, Propagation and Plastic Energy Losses	95
4.4	Impact Strength of Brittle Materials	98
4.5	Modification of Linear Theory of Impact	106
	PART II	
CHAPTER 5 :	EFFECT OF RUBBER ON VISCOELASTIC PROPERTIES OF HIPS	111
5.1	Introduction	111
5.2	Morphology of HIPS	114
5.3	Previous Studies of Mechanical Properties of HIPS	122
5.4	Experimental Programme	128
5.4.1	Test conditions and apparatus	128
5.4.2	Materials	128
5.4.3	Results	128
5.5	Theoretical Prediction of Modulus of Elasticity of Composite Polymers	137
5.5.1	Composite model	137
5.5.2	Bulk modulus	139
5.5.3	Shear modulus bounds	139
5.5.4	Approximate expressions for shear modulus of particulate-filled composites	143

		Page
5.5.5	Proposed method to evaluate the modulus of elasticity of toughened polymers	144
5.6	Some Physical Parameters Affecting the Overall Mechanical Behaviour of Modified Polymers	148
5.7	Distribution of Rubber Particles	151
5.8	The Craze Effect	157
5.8.1	Craze formation model	157
5.8.2	Single penny-shaped crack in an infinite body	160
5.8.3	An infinite number of penny-shaped cracks in an elastic body	162
5.9	Closure	167
CHAPTER 6 :	FRACTURE OF HIPS AT ROOM TEMPERATURE	168
6.1	Introduction	168
6.2	Basic Linear Fracture Criterion	172
6.3	Previous Studies of Fracture of HIPS	175
6.4	Experimental Programme	178
6.4.1	Materials	178
6.4.2	Specimen and notching technique	179
6.4.3	Test conditions and apparatus	181
6.5	Inducement of Brittle Fracture by Means of Covering the Crack	182
6.5.1	Glueing method	182
6.5.2	Experimental results	184
6.6	Effect of Notch Geometry	194
6.6.1	Surface notched specimens	195

		Page
6.6.2	Single-edge notched specimens	195
6.7	Influence of Specimens Dimensions on the Mode of Fracture	203
6.7.1	Thickness effect	203
6.7.2	Width effect	205
6.7.3	100 mm wide surface notched specimens	206
6.7.4	100 mm wide single-edge notched specimens	207
6.8	Ductility and Brittleness	217
6.9	Discussion on the Validity of Linear Fracture Criterion in HIPS	227
6.10	Strain Rate Effect	242
6.11	Fracture Toughness as a Function of Rubber Content	245
6.11.1	Testing procedure and results	246
6.12	Conclusion	266
CHAPTER 7 :	IMPACT STRENGTH OF RUBBER-MODIFIED POLYMERS	269
7.1	Introduction	269
7.2	Previous Work on Impact Testing of Toughened Polymers	271
7.3	Fundamentals of Linear and Yielding Fracture Mechanics Approaches to Impact	273
7.4	Impact Test Instrumentation	277
7.5	Calibration of the Impact Machine	279
7.6	Experimental Programme	282
7.6.1	Test conditions	282
7.6.2	Materials	282
7.6.3	Notching technique	287

		Page
7.7	Analysis of the Experimental Data	291
	7.7.1 Fracture of CPS	292
	7.7.2 Low level impact PS	296
	7.7.3 Medium and high level HIPS	296
	7.7.4 Application of composite impact theory	304
7.8	Effect of Rubber Content on Impact Strength of HIPS	309
7.9	An Analysis of Commercial Grades of HIPS	312
7.10	The Effect of Rubber-Matrix Interface on Impact Strength	335
7.11	Closure	340
CHAPTER 8 :	DYNAMIC MECHANICAL PROPERTIES	341
8.1	Introduction	341
8.2	Theoretical Approach	344
8.3	Experiments	347
	8.3.1 Apparatus	347
	8.3.2 Operating procedure	350
	8.3.3 Specimen preparation and experimental procedure	351
8.4	Results	353
8.5	Discussion and Conclusions	367
CHAPTER 9 :	THE EFFECT OF TEMPERATURE ON THE STRENGTH OF HIPS	369
9.1	Introduction	369
9.2	Experimental Programme	371
	9.2.1 Cooling and heating apparatus	371
	9.2.2 Test procedure	373

		Page
9.3	Results and Discussion	377
	9.3.1 Effect of temperature on the ultimate stress of HIPS	377
	9.3.2 Effect of temperature on the fracture toughness of CPS	384
	9.3.3 Effect of temperature on the fracture toughness of HIPS	390
9.4	The Rôle of Rubber in HIPS with Reference to Temperature Variations	404
CHAPTER 10 :	CONCLUSION	409
10.1	Contributions	410
10.2	Recommendations for Future Research	415
APPENDIX A :	THE ISOLATED SPHERICAL INCLUSION	416
APPENDIX B :	THE CHARPY SPECIMEN	419
APPENDIX C :	PROGRAM FOR CALCULATING FRACTURE TOUGHNESS	424
APPENDIX D :	COMPUTER PROGRAM FOR IMPACT ANALYSIS	432
References		444

NOMENCLATURE

Symbol		Description
$\bar{a}$	:	normalised a
a	:	crack length (SEN); crack depth (SN)
a_o	:	initial crack length
a'	:	characteristic dimension of a rectangular parallelpiped particle
a_{eff}	:	effective crack length
a_c	:	characteristic crack length
A	:	area of the crack interface
A_o	:	exponential constant in the modulus-rubber content relationship
$\tilde{A}_j$ $(j = 1,3)$	:	general elastic constants of the composite polymer
A^m_j $(j = 1,3)$	:	general elastic constants of the matrix
A^p_j $(j = 1,3)$	:	general elastic constants of the inclusion phase
b	:	half crack width in centrally notched or surface notched specimens
b'	:	characteristic thickness of a rectangular parallelpiped particle
B	:	specimen thickness
B_o	:	exponential constant in the yield stress-rubber content relationship
c	:	radius of a penny-shaped crack
c_s	:	cross-head speed
C	:	compliance of a cracked specimen
C_o	:	initial compliance of a cantilever specimen
C'_o	:	initial compliance of a three-point bend specimen
d	:	particle alignment factor

Symbol		Description
d_o	:	characteristic particle alignment factor
D	:	specimen width along the crack
e	:	characteristic length of the Dugdale hypothetical crack
e'	:	restitution factor
e_1	:	output voltage of the stress transducer
e_2	:	output voltage of the strain transducer
E	:	modulus of elasticity (matrix)
E'	:	modulus of elasticity (composite particle)
$\tilde{E}$	:	modulus of elasticity (composite polymer)
E_o	:	nominal modulus of elasticity
E_1	:	in-phase modulus
E_2	:	out-of-phase modulus
E_r	:	modulus of elasticity of rubber
E_{red}	:	reduced modulus of elasticity
E_s	:	modulus of elasticity of PS
E^*	:	complex modulus of elasticity
f_1	:	calibration factor for the stress transducer in the Rheovibron
f_2	:	calibration factor for the strain transducer in the Rheovibron
$F_{jk}(\theta)$	:	geometry function introduced in Westergaard's expression
F_o	:	amplitude of the applied force
g_1	:	input voltage to the stress transducer in the Rheovibron
g_2	:	input voltage to the strain transducer in the Rheovibron
G	:	strain energy release rate
G_1	:	potentiometer ratio of the strain gauge (Rheovibron)

Symbol		Description
G_2	:	potentiometer ratio of the stress gauge (Rheovibron)
G_b	:	brittle impact strength
G_c	:	critical strain energy release rate
G_d	:	ductile impact strength
G_i	:	initiation impact resistance
G_p	:	propagation impact resistance
h_c	:	critical value of shear lip width
h'	:	characteristic dimension of a rectangular composite element
H_i $(i = 1,6)$	:	Goodier's constants
i	:	index varying from 1 to N
I	:	total recorded energy loss in an impact test
I_b	:	impact energy (brittle fracture)
I_c	:	impact energy (composite fracture)
I_{cs}	:	impact energy per unit cross-sectional area
I_d	:	impact energy (ductile fracture)
I_i	:	initiation impact energy
I_p	:	propagation impact energy
I_r	:	reduced impact energy
j	:	index varying from 1 to 3
J	:	value of Rice's contour integral
J_o	:	zero order J-type Bessel function
J_1	:	first order J-type Bessel function
J_c	:	critical J
k	:	bulk modulus (matrix)
k'	:	bulk modulus (inclusion)
$\tilde{k}$	:	bulk modulus (composite)

Symbol		Description
k_o	:	shear bulk moduli ratio (= $4/3\ \mu_s/k_s$)
k_o'	:	shear bulk moduli ratio (= $4/3\ \mu_s/k_r$)
k_r	:	bulk modulus (rubber)
k_s	:	bulk modulus (polystyrene)
K	:	intensity factor
K_{0c}	:	minimum value of K_c
K_{1c}	:	plane strain fracture toughness
K_{2c}	:	plane stress fracture toughness
K_c	:	critical value of K
K_{cm}	:	mean K_c
ΔK_c	:	estimated spread from K_{cm}
l	:	arc length along Γ contour
l'	:	characteristic thickness of a rectangular composite element
L	:	specimen length
m	:	mass of an impact specimen
M	:	pendulum mass (impact test)
M_c	:	number of cracks (crazes) generated in a sample of HIPS subjected to a uniform tensile stress
$\vec{n}_j$ $(j = 1,3)$	:	unit vectors along the X_j axes
n_o	:	shear modulus ratio (= μ/μ')
N	:	number of particles
N_o	:	proportional coefficient in the dynamic mechanical test
o	:	particle radius
p	:	third power of the ratio of the crack radius to the particle radius
P	:	load

Symbol		Description
P_o	:	value of dynamic force dial in Rheovibron apparatus
P_c	:	percentage of cracked area
P_f	:	load at fracture
q_1, q_2	:	constants in Petrenko's expression
q_3, q_4	:	constants in Fillunger's expression
Q	:	potential energy
Q_o	:	input energy density
Q_a	:	local energy density
r	:	radial coordinate from the crack tip
r_c	:	craze zone length
r_i $(i = 1,N)$	:	radial coordinates from the centre of the ith particle
r_p	:	plastic zone radius
r_s	:	slow crack growth length
R_m	:	cutter radius
s	:	ligament area (of an impact specimen)
s_o	:	gross cross-sectional area
S	:	surface (of integration)
S_e	:	standard error
S_K	:	elastic stress concentration factor
S_p	:	supporting span in impact
$\overline{S}_p$	:	normalised S_p
t	:	time
T	:	temperature
$\vec{T}$	:	stress vector
T_j $(j = 1,3)$	:	principle stresses along cartesian axes
T_g	:	gross transition temperature

Symbol		Description
u_r, u_ψ, u_θ	:	displacement components in spherical coordinates
u_z, u_r, u_θ	:	displacement components in cylindrical coordinates (a cracked body subjected to a tensile stress)
u^*	:	displacement component of an uncracked body (along the z axis)
U	:	strain energy
U_o	:	strain energy density
$\tilde{U}_o$	:	strain energy density (composite)
U_f	:	strain energy at fracture
U_k	:	linear kinetic energy of the flying pieces in impact
U'_k	:	rotational kinetic energy of the flying pieces in impact
U_s	:	elastic energy dissipated in slow crack growth
ΔU	:	strain energy variance due to the presence of a crack
v	:	effective volume (on an impact specimen)
v_z, v_r, v_θ	:	displacement components in cylindrical coordinates (a cracked body subjected to an internal pressure, σ)
V	:	volume (of integration)
V_l	:	impact pendulum velocity
V_r	:	variance
V'_r	:	skewness
V''_r	:	Kurtosis
w	:	specific fracture work
W	:	fracture work
W_d	:	dissipation energy density in a dynamic mechanical test
x_j $(j = 1,3)$	:	cartesian coordinates

Symbol		Description
x_{ij} $(i = 1,N,\ j = 1,3)$	:	cartesian coordinates from the centre of the ith particle
$\tilde{X}_o$	:	elongation per unit length (composite polymer)
$\vec{X}$	:	displacement vector (composite polymer)
$\vec{X}$	:	displacement vector
$\tilde{X}_j$ $(j = 1,3)$	:	displacement components in cartesian coordinates (composite)
X_j $(j = 1,3)$	:	displacement components in cartesian coordinates (matrix)
X_f	:	load point deflection at fracture
X_n	:	fraction of specimens having a value equal to or greater than K_c
ΔX_{ij} $(i = 1,N,\ j = 1,3)$	:	displacement variances due to the ith particle (along the x_j axes)
Y	:	geometry function in fracture toughness expression
z	:	normal ordinate (in cylindrical coordinates)
$z = z_i$	:	equatorial plane of the ith penny-shaped crack

Greek Symbols

α	:	constant in Kerner's equation
α_o	:	constant in Hashin's equation
α_s	:	crack angle in surface notched specimens
β	:	constant in Kerner's equation
β_o	:	displacement error in dynamic mechanical test
β_p	:	fractional surface of particles in a composite polymer
γ	:	specific fracture energy
γ_p	:	specific plastic energy

Symbol		Description
γ_s	:	specific surface energy
Γ	:	arbitrary contour surrounding the crack tip
δ	:	crack opening displacement
δ_o	:	minor axis of a penny-shaped crack
δ_c	:	critical δ
δ_{jk} $(j,k = 1,3)$	:	Kroneker constant
Δ	:	damping coefficient
Δ_{mid}	:	displacement variance (mid-layer of the composite element)
Δ_{top}	:	displacement variance (top layers of the composite element)
ε	:	strain
ε_{jk}	:	strain tensor
$\bar{\varepsilon}$	:	elongation
$\bar{\varepsilon}_o$	:	amplitude of elongation
$\dot{\varepsilon}$	:	strain rate
$\dot{\varepsilon}_o$	:	nominal strain rate
$\Delta\dot{\varepsilon}_o$	:	strain rate variance
ε_o	:	amplitude of strain
ε_y	:	yield strain
ζ	:	normalised z $(= z/c)$
ζ_i	:	ζ of the ith particle
η	:	constant in Parvin-Bluhm expression
η_i $(i = 1,6)$	:	polynomial coefficients of K factor for Charpy specimens
θ	:	angular ordinate (from the crack plane)
Θ	:	a coefficient in the intensity factor expression for SN specimens
λ	:	Lamé's constant (matrix)

Symbol		Description
λ'	:	Lamé's constant (inclusion)
$\tilde{\lambda}$	:	Lamé's constant (composite
Λ	:	load point displacement
μ	:	shear modulus (matrix)
μ'	:	shear modulus (inclusion)
$\tilde{\mu}$	:	shear modulus (composite)
μ_o	:	shear moduli ratio (= μ_r/μ_s)
μ_o'	:	shear moduli ratio (= μ'/μ_s)
μ_o''	:	shear moduli ratio (= $\tilde{\mu}/\mu_s$)
μ_r	:	shear modulus (rubber)
μ_s	:	shear modulus (polystyrene)
ν	:	Poisson ratio (matrix)
ν'	:	Poisson ratio (inclusion)
$\tilde{\nu}$	:	Poisson ratio (composite polymer)
ν_r	:	Poisson ratio (rubber)
ν_s	:	Poisson ratio (polystyrene)
ξ	:	constant in Dewey's equation
ξ_o	:	Young's moduli ratio (= E_r/E_s)
Π_1, Π_2	:	coefficients of K_c expression (experimental)
ρ	:	normalised r (= r/c)
ρ_c	:	notch tip radius
ρ_i	:	ρ of the ith particle
σ	:	tensile (gross) stress
σ_o	:	amplitude of the applied stress
σ_z, σ_r, σ_θ	:	normal stress components in cylindrical coordinates
σ_c	:	critical stress at fracture

Symbol		Description
σ_e	:	effective stress in the vicinity of the crack tip
σ_m	:	maximum stress at the crack tip
σ_y	:	yield stress
$\sigma_{y,eff}$	:	effective yield stress
$\tilde{\sigma}_y$	:	yield stress of a composite polymer
σ_{jk} $(j,k = 1,3)$	:	stress tensor (in the cartesian system)
Σ	:	summation notation
τ	:	integral variable in the Sneddon integral
τ_{rz}, $\tau_{r\theta}$, $\tau_{z\theta}$	:	shear stress components (cylindrical coordinates)
ϕ	:	nominal rubber content
ϕ_m	:	maximum packing fraction of particles
ϕ_p	:	fractional volume of rubber particles in HIPS
ϕ_s	:	fractional volume of occluded PS
Φ	:	calibration factor for impact test
χ	:	constant in the ductile impact formula
ψ	:	correction function in modified Kerner's expression
ψ_o	:	frequency (angular)
ω_1, ω_2, ω_p	:	constants in the Lethersich expression
Ω	:	phase angle

ABBREVIATIONS

PS	:	polystyrene
CPS	:	crystal polystyrene
IPS	:	impact polystyrene
HIPS	:	high impact polystyrene
PBD	:	polybutadiene rubber
ABS	:	acrylonitrile butadiene styrene
PVC	:	polyvinyl chloride
U A0, U B0, and U C0	:	Various types of CPS supplied by the Chemical section of the US Steel Corporation
U A1.11, U A2.22, U A3.33, U A5.55, U B1.11, U B2.22, U B3.33, U B5.55, U C1.11, U C2.22, and U C3.33	:	Various types of HIPS supplied by the US Steel Corporation. The first two letters specify the type and the subsequent digits specify the nominal rubber fractional volumes.
PTFE	:	polytetrafluorethylene
PMMA	:	polymethylmethacrylate (Perspex)
COD	:	crack opening displacement
BCP	:	a commercial type of HIPS (grade CP40 of BP Chemicals Limited)
BCF	:	a commercial type of HIPS (grade 83CFT of BP Chemicals Limited)
PET	:	polyethyleneterephthalate
SEN	:	single-edge notched (specimen)
SN	:	surface notched (specimen)
PC	:	polycarbonate
T1	:	stress transducer
T2	:	strain transducer
VR1 and VR2	:	potentiometers in the Rheovibron apparatus

CHAPTER 1

INTRODUCTION

1.1 PRODUCTION OF HIGH IMPACT POLYSTYRENE

It has been generally conjectured by the plastics manufacturers that the addition of a rubbery phase to inherently brittle materials would significantly improve their impact resistance, fracture toughness and elongation to break. This assumption, combined with the relatively cheap production of crystal polystyrene and similar base brittle materials, has led to the development of many types of rubber modified polymers which have been produced in large quantities. Historically, high impact polystyrenes were the first impact composite polymers produced, based on a thermoplastic matrix with a particulate rubber phase. This was followed by the production of a vast number of polymer/rubber combinations, ranging from ABS (acrylonitrile butadiene styrene) and PVC/nitrile rubber blends to modified epoxide resins. The best of these materials have an excellent balance of mechanical and physical properties achieved by controlling the blending procedure, qualities and quantities of the constituent phases in the composite.

In principle, rubber can be added to polystyrene in three ways:

1. Mechanical mixing which results in the dispersion of discrete irregular rubber particles in a continuous phase of polystyrene.

2. Solution grafting which results in suspension of discrete quasi-spherical grafted particles (which usually consist of 80% to 85% occluded polystyrene in the rubber matrix) in a continuous phase of polystyrene.

3. Latex mixing (or emulsion polymerisation) which involves blending small amounts of rubber latex with emulsion-polymerised polystyrene.

The choice of processing technique for making a toughened polymer is governed by a variety of technical and economic factors. However, the toughest modified polystyrene for the least amount of rubber used is generally achieved by the solution grafting process which is the principal commercial technique (Boyer et al (1970)).

In summary, the behaviour of toughened polymers is determined by the manufacturing methods, the choice of principal ingredients (the type and molecular weights of polystyrene and rubber used) and the quantity of other possible processing additives (e.g. initiators, chain transfer agents, and mineral oil). In view of the morphology of the composite, the quantity, size, shape, internal structure of the particles and the state of its interface with the surrounding matrix, it can be seen that many factors contribute to the overall mechanical properties of the polymer. It is, therefore, of prime importance to any company manufacturing rubber modified polystyrene to have a clear understanding of the effects of all these possible variables in their products. The obvious approach to this is to manufacture materials varying only one component at a time and then to examine the performance of the composite. However, this is not usually feasible since a specific modification of the grafting process normally involves more than one change in the resultant polymer. Recent problems with rubber supplies have added urgency to the need for more insight into the effect of rubber content, assuming the other processing factors are kept constant.

An attempt has therefore been made in this thesis to study the effects

of the controlling parameters, especially the rubber content, on the behaviour of some commercial and specially prepared grades of HIPS. It is believed that an experimental analysis of these polymers would provide the basis of a better theoretical understanding of the problem and thus permit the prediction of mechanical and fracture properties of rubber modified polymers. In this work, four parameters are considered to be of prime importance:

1. The modulus of elasticity as the best estimate of stiffness;

2. Average rupture stress of unnotched materials describing the general yield strength;

3. The fracture toughness as measured in a slow test which reflects the breaking strength and elongation directly;

4. The impact strength as measured by employing a fast test using fracture mechanics theories and a pendulum-type testing machine.

1.2 PLAN OF THE THESIS

The work to be presented in this thesis has been arranged into two parts: Part I contains historical reviews and essential theoretical principles employed in the second part. Part II comprises all the theoretical and experimental work performed in this project. The appendices and the paper following the two main parts contain information which is not directly essential to an understanding of the main text but provide a more detailed analysis of some relevant problems. The computer programs attached can be used in further research on impact and fracture toughness measurements; cross-references are used to link the appendices to the main text.

Chapters 2, 3 and 4, which follow this introductory chapter, provide a literature survey on viscoelastic properties, fracture and impact strength of polymers.

Chapter 5 deals with the low strain and the large strain deformations and stresses in particulate-filled composite polymers. The experimental investigation on some specially prepared impact polystyrene is a study of the effect of rubber content on the stiffness and rupture stress of these materials. The theoretical work developed is not necessarily an attempt to predict accurate moduli and rupture stresses due to the presence of rubber phase inclusions, but rather to provide a basis for an understanding of the influence of a rubber phase structure, its arrangement and its configuration, on the overall behaviour of the material. Last, but of more importance, the possibilities of reduction in stiffness of the material as a result of craze generation around particles was studied.

Chapter 6 deals with the fracture of impact polystyrene in air at $20^{o}C$ and at medium cross-head speeds. Previous work by Ferguson (1973) and Parvin (1975) has shown that commercial grades of these materials

behave in a ductile manner even at the highest Instron cross-head speed (about 50 cm/min). In practice, on the other hand, it is occasionally observed that similar materials break in a brittle manner at apparently lower stresses under the same ambient conditions. Therefore, several tests on some commercial and specially prepared impact polystyrene were performed with a view to defining the lowest fracture toughness at normal ambient environments. Finally, the effect of rubber content on the fracture toughness of modified polystyrene is studied at the most severe circumstances of brittle failure.

Chapter 7 is effectively a continuation of Chapter 6 since the fracture behaviour of the same materials under impact loading is investigated. As it turned out, the available theories on impact resistance of brittle or ductile materials failed to describe the impact behaviour of composite materials. Prior to analysis of the effect of rubber content on the impact strength of modified polystyrene, an attempt was made to provide a comprehensive theoretical basis to give an account of semi-ductile behaviour of composite polymers under impact loads.

In Chapters 8 and 9, the effect of temperature on the moduli, rupture stress and fracture toughness were studied for various grades of special impact polystyrenes which had different rubber contents. Chapter 8 deals with the dynamic modulus and loss factor measurement at $-140^{o}C$ to $+140^{o}C$. Chapter 9 describes the effect of rubber content on the fracture strength of impact polystyrene in the temperature range of $-120^{o}C$ to $+60^{o}C$.

A general conclusion and discussion of the contribution made by this thesis and a plan for further research on this subject are provided in the final chapter, Chapter 10.

PART I

LITERATURE SURVEY

CHAPTER 2

ELASTIC PROPERTIES OF PARTICULATE-FILLED COMPOSITES

2.1 INTRODUCTION

High impact polystyrene (HIPS) is a solution grafted polymer which may be approximated as a two-phase suspension composite. A suspension, or particulate-filled, composite is a special kind of heterogeneous multi-phase material in which one phase is regarded as the matrix and all other phases are embedded in the form of inclusions. The study of morphology of HIPS shows that the inclusion phase does not merely consist of rubber particles but is itself a two-phase suspension composite in which polystyrene (PS) sub-inclusions are dispersed in a continuous rubber matrix (see Figure 2.1). With regard to this point, Bucknall (1977) has shown that a composite inclusion has a similar, but not identical, effect on properties of rubber modified polymers to that produced by a pure rubber inclusion of the same volume.

In general, elastic particulate fillers are often added to different basic brittle polymers in order to improve their fracture resistance. In particular, a small addition of polybutadiene rubber (PBD) in crystal PS, which is an extremely brittle material, increases its impact strength and fracture toughness by several times . This is understood to be engendered by multiple-craze creation emanating from rubber phase particles. However, a large reduction in the materials stiffness is an inevitable penalty to be weighed against the improvement of the fracture properties.

Prediction of mechanical properties of a composite from the structure and the elastic characteristics of its constituents is a prerequisite for the design of a polymer having specific required properties. The purpose

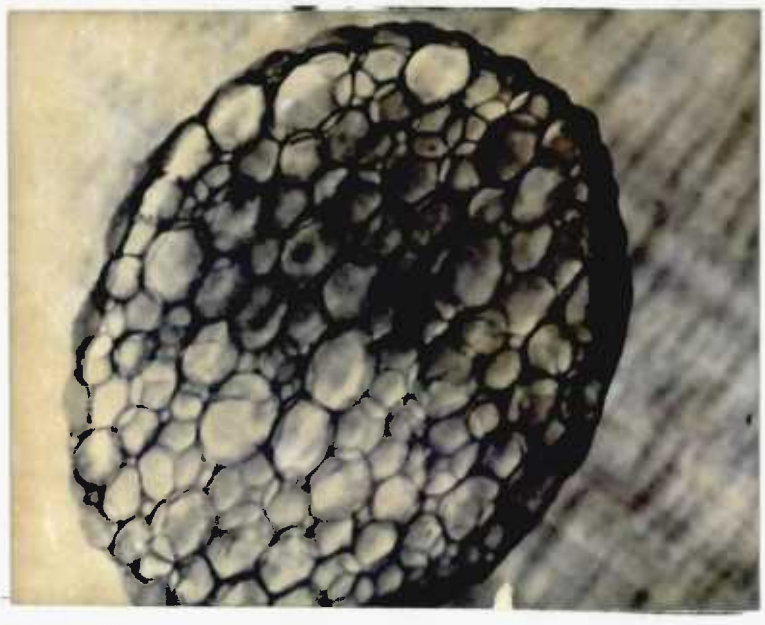


Figure 2.1: Inclusion phase in HIPS, the inclusion comprising of 80-85% occluded PS grafted in PBD rubber matrix

of the present survey is to review theoretical methods in the field of prediction of elastic properties of composite materials. Literature surveys on fracture toughness and impact measurements are given in subsequent chapters.

Although, in principle, it should be possible to evaluate the low strain properties (e.g. modulus of elasticity) of a composite polymer, there are numerous difficulties in formulating an exact relationship describing the overall behaviour of the material in terms of mechanical properties and geometry of its constituents. In general, the evaluation of mechanical constants of a randomly particulate-filled composite should be of a statistical nature. To simplify the work, however, it is more convenient to incorporate the statistical nature of the problem by employing continuum mechanics and variational principles rather than a systematic statistical study of the problem. As a first approximation, this approach basically deals with a hypothetical composite model which contains an infinite number of small particles, distributed uniformly and symmetrically in a homogeneous and isotropic matrix. In a statistical analysis, any kind of symmetry is defined by spatial independence of all volume average properties of the material. The average theories of bulk behaviour are, therefore, concerned with homogeneously heterogeneous media that is to say the mechanical behaviour of the material at any macroscopically large region is independent of the location of that region in space.

In fact, the main benefit of the mean theories of heterogeneous materials is due to the possibility of by-passing the more complicated problem of stress-strain determination within the composite elements, and therefore obtaining an average solution for overall properties of the bulk composite.

An accurate analytical solution for large strain properties (such as yield stress and fracture) of a composite material is much harder to achieve. The Broutman & Panizza (1971) and the Agarwal & Broutman (1974) finite element solutions only highlight the effect of the presence of rubber phase particles in an elastic matrix as stress concentrating elements and thereby are the main source of craze creation. The craze growth around the rubber particles is, therefore, responsible for large reductions in the final rupture stress, but also enhances the fracture toughness of rubber modified polymers. The effect of craze generation on modulus and yield stress of HIPS is discussed in Chapter 5.

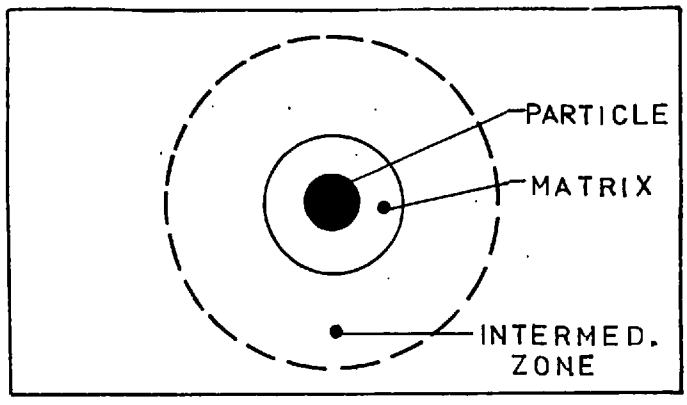
2.2 A BRIEF HISTORICAL REVIEW OF THEORIES ON PARTICULATE-FILLED POLYMERS

The first step in studying the elastic behaviour of a heterogeneous material is to choose a suitable mathematical model to represent the composite. The simplest approximation to rubber modified polymers is a dilute suspension composite model in which the fractional volume of the inclusion phase is usually assumed to be less than 2%. The special case of the suspension of elastic spherical inclusions in an elastic matrix of differing moduli was first analysed by Bruggeman (1937), who found a correct expression for bulk modulus and an erroneous expression for shear modulus. Dewey (1947) re-evaluated the elastic properties of a dilute suspension composite using Goodier's (1933) solution in which the deformations and stresses in an elastic body containing a single spherical inclusion are described. His results were later derived independently by Eshelby (1957) and Hashin (1959). Moreover, Eshelby extended the theory to composites containing ellipsoidal inclusions. In all the works mentioned above, the matrix and the fillers were assumed to be linearly elastic materials. However, in general, the mechanical properties of polymers, as well as the rubbery inclusions, are functions of time and strain, that is the strain history. Bucknall (1977) has shown that PS and HIPS can both be treated as approximately linear visco-elastic materials at small strains . Oldroyd (1956) and Hashin (1970) developed some general methods to describe the behaviour of composites whose constituents were linearly visco-elastic.

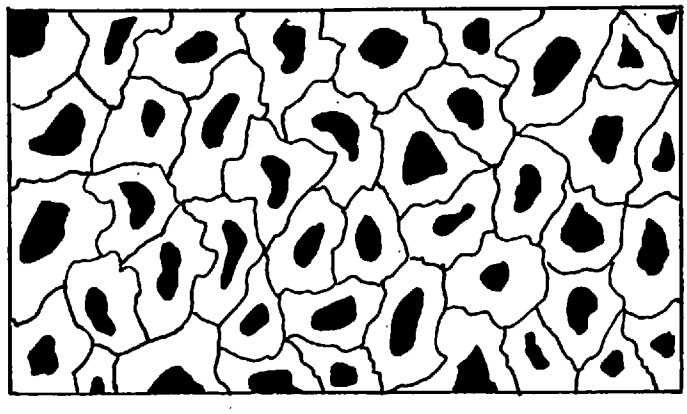
When the fractional volume of the suspended phase is finite, the interaction of neighbouring particles and the consequent distortion of stress fields have an important role in determining the overall bulk properties of the material. Hence, the dilute suspension assumptions are no longer valid and a more suitable modelling of composites is required.

The first study on the modulus of finite suspension composites known to the author is the work of Kerner (1956b) who derived an approximate solution for shear and bulk moduli of composites having spherical inclusions. Hashin & Shtrikman (1961,1962,1963) and Hashin (1962) used variational principles of minimum potential energy and minimum complementary energy and thereby derived expressions for the lower and upper limits of the effective elastic moduli of composites composed of homogeneous and isotropic elastic phases. These bounds do not reflect any particular geometry and spacing order of the composite constituents and are, in general, a function of fractional phase volumes and the modulus ratio of matrix and inclusions. The hypothetical models used by Kerner and Hashin & Shtrikman are shown in Figure 2.2. In these models, the material was divided into spheroidal (or spherical) composite elements, each containing a concentric inclusion. If the particles are assumed to be spherical, it can be shown that the lower or the upper Hashin-Shtrikman bounds coincide with Kerner's solution when the matrix has higher or lower shear and bulk moduli than the inclusion, respectively (Hashin (1961)). Moreover, the dilute suspension expression obtained by Dewey tends to that of Hashin's and Kerner's expression as the volume fraction of inclusions vanishes.

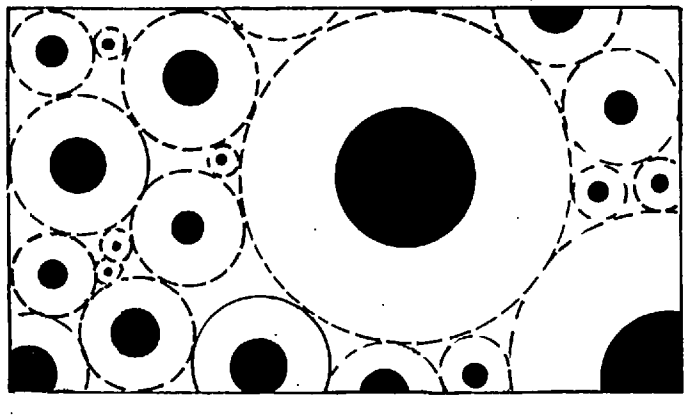
Sato & Furukawa (1962), Budiansky (1965), Nielsen (1966), Lavengood, Nicolais & Narkis (1973), and Leidner & Woodhams (1974) studied the mechanical properties of rigid bead-filled composites. Although their studies are not of direct interest for this present work, they still serve as a useful guide in describing the internal deformation and the state of the particle-matrix interface in composite materials. In particular, Yoshiyasu Sato analysed the molecular reinforcement mechanism of filled composites, and thus expressed the composite moduli in terms of volume



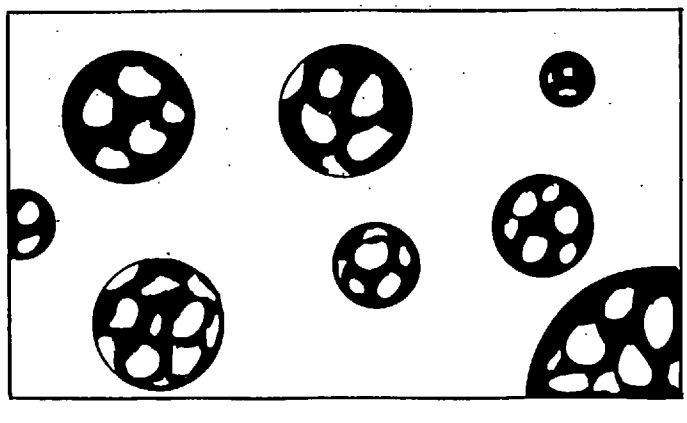
1. Kerner's Model: Concentric phases surrounded by unknown intermediate zone



2. Hashin's Model: Irregular composite elements containing rubber cores



3. Hill's Model: Concentric composite elements of differing sizes



4. Bucknall's Model: Grafted spherical particles suspended in an elastic media

Figure 2.2: Composite models

effect, surface effect and cavitation effect engendered by imperfect adhesion between filler and polymer.

In 1965, Hill developed a self-consistent theory for two-phase composites by considering the strain within ellipsoidal inclusions which were suspended in a composite media having unknown properties. Figure 2.3 shows Hashin's bounds and Hill's self-consistent prediction for the elastic modulus of a rubber modified polystyrene containing 0% to 99% rubber-phase inclusions. The main restriction to Hill's theory is that it does not distinguish between matrix and dispersed inclusions, and thus ignores the phase inversion as the fractional volume phase exceeds 50% of the composite volume. Turley (1963), Budiansky (1965), Halpin (1969), Davies (1971), Dickie (1973), Nielsen (1973), and many others, extended the theory of heterogeneous materials and gave suitable expressions for the moduli of a composite containing interpenetrating continuous phases.

The Takayanagi et al (1963) treatment of viscoelastic composites is also based on Kerner's equation. They analysed a combined model of series and parallel composite elements and thereby deduced a complex modulus for composites containing spherical viscoelastic inclusions. This solution was, in effect, a curve-fitting procedure.

Bucknall (1969) proposed a two-stage method to calculate the shear modulus of HIPS containing 5% nominal rubber content. In the first step, the modulus of the composite inclusions (comprising 80% PS and 20% PBD) was evaluated using the Hashin bound equations. The overall modulus of HIPS was then calculated for a composite containing 75% PS and 25% grafted inclusions. Hence, he showed that toughened polymers containing pure rubber particles are substantially stiffer than those containing grafted particles (see Figure 2.2 - Bucknall's model).

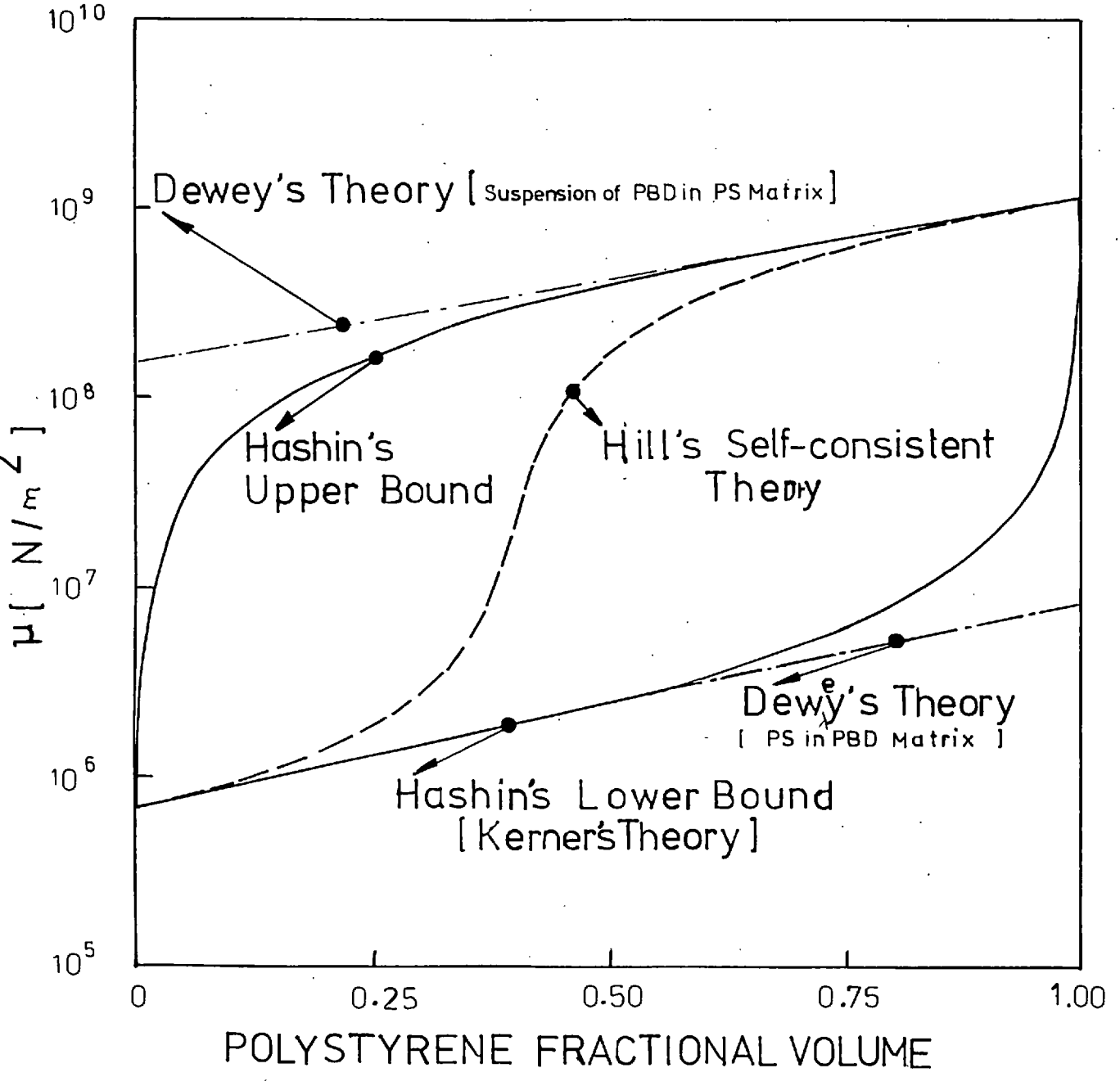


Figure 2.3: Comparison of various composite theories

2.3 DEWEY'S DILUTE SUSPENSION THEORY

The effect of spherical inclusions in infinitely large elastic media, subjected to a uniform tensile load, has been studied analytically by Goodier (1933). In his work, three-dimensional elasticity equations were used to evaluate the stress and strain changes in a homogeneous matrix containing one spherical elastic inclusion. Figure 2.4 illustrates Goodier's model in a spherical system of coordinates. The details of Goodier's solution are given in Appendix A.

Dewey extended Goodier's solution to determine the moduli of a composite containing infinite small spherical beads. The following assumptions were made by Dewey to construct his hypothetical composite model:

(a) The particles are spherical and infinitely small compared to the general dimensions of the composite region over which integration should be performed.

(b) The distribution of particles in the matrix is assumed to be uniform, and the composite in the aggregate is considered as homogeneous heterogeneous media.

(c) Particles (inclusions) and the surrounding medium(matrix) are assumed to behave as perfect elastic materials, thus neglecting the time-dependence of their mechanical properties.

(d) The effect of other viscous additives (impurities) are neglected, e.g. mineral oil, which is usually added for processing facility in rubber modified polymers.

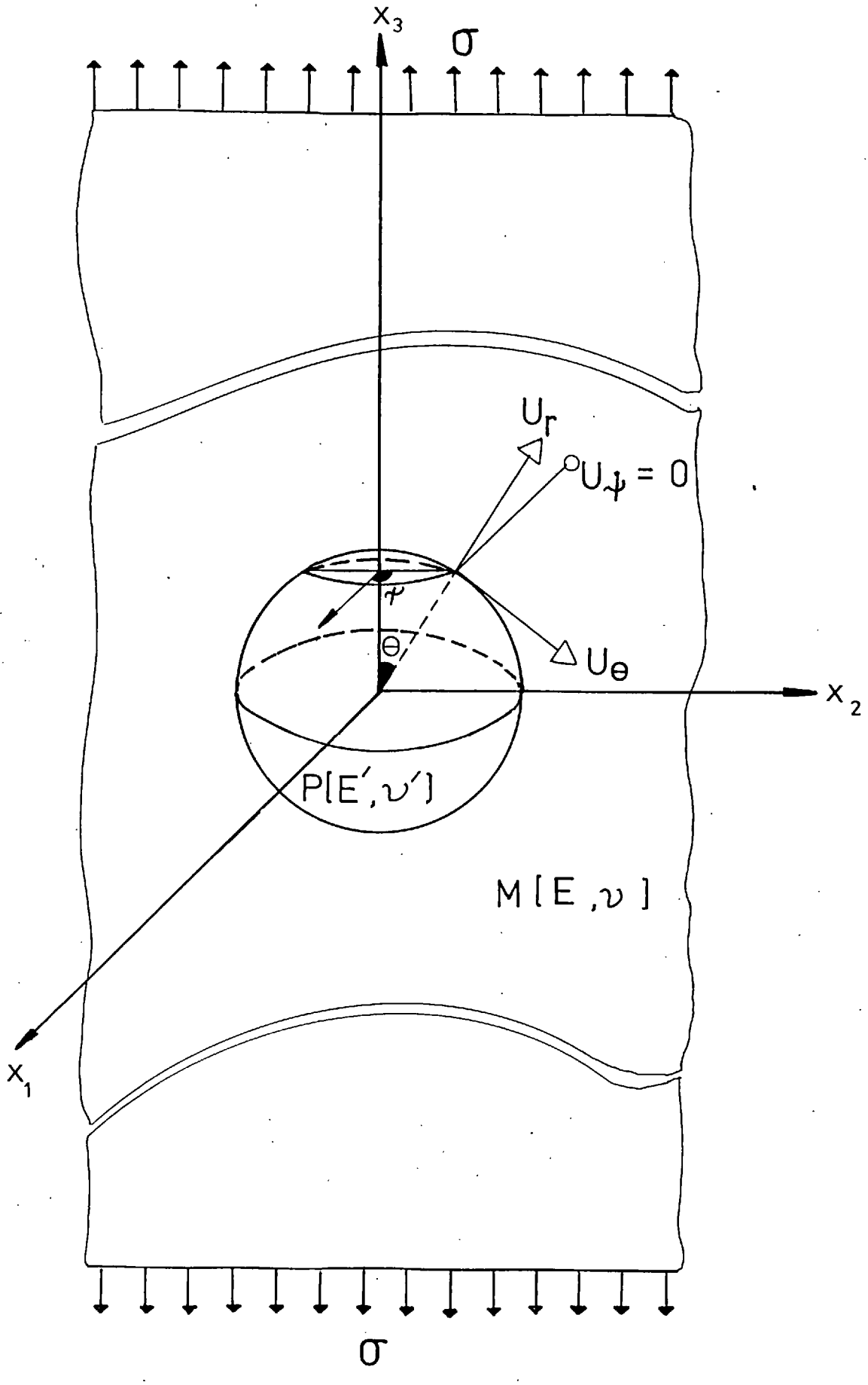


Figure 2.4: A spherical inclusion in an infinite body

(e) It is assumed that there is good adhesion between the matrix and the particles, therefore molecular dislocation cannot appear before complete fracture. Having assumed complete molecular bonds between the composite components, the stress and strain field can be studied in a mathematically infinitesimal element of the material. Hence, stress and strain in the matrix-particle interface may transfer from the matrix to the particles in two ways: one being by shear stresses, due to perfect adhesion and frictional forces; and the other by normal stresses, due to adhesion only.

(f) The inter-effects of particles on each other are neglected and, therefore, the properties of the composite, as a whole, would merely be the summation of the properties of each particle in a plain medium,plus the one of the matrix itself. It is also assumed that the latter does not alter due to particles present in the matrix. This assumption is approximately correct if the dilute suspended inclusions in the matrix are surrounded by regions free of particles of dimensions three to four times greater than the radii of the particles.

(g) Thermal stresses, which may be generated in composite processing, due to differences between the coefficients of thermal contraction of the composite components, are ignored.

By assumptions (b) and (c), the displacement vector of an arbitrary point in the composite subjected to a stress vector $\vec{T}$ can be expressed linearly as:

$$\vec{\tilde{X}} = \tilde{A}_1 x_1 \vec{n}_1 + \tilde{A}_2 x_2 \vec{n}_2 + \tilde{A}_3 x_3 \vec{n}_3 \tag{2.1}$$

where x_j and $\vec{n}_j$ are the cartesian coordinates and the unit vectors along the cartesian axes. Coefficients $\tilde{A}_j$ denote the elastic *variances* of the composite. In the special case of simple tension, we have:

$$\tilde{A}_1 = \tilde{A}_2 = -\frac{\tilde{\nu}}{\tilde{E}}\sigma \quad , \quad \tilde{A}_3 = \frac{\sigma}{\tilde{E}} \tag{2.2}$$

where σ is the applied tensile stress, and $\tilde{E}$ and $\tilde{\nu}$ are the modulus of elasticity and Poisson's ratio of the composite, respectively, and are to be determined. The coefficients $\tilde{A}_j$ can be calculated by the method applied by Einstein (1906) to calculate the viscosity of composites. The displacement vector of the composite can be described as the sum of displacements due to the presence of each particle and the one of the matrix (assumption (f)). Thus:

$$\tilde{X}_j = \tilde{A}_j x_j = A_j^m x_j + \sum_{i=1}^{N} \Delta X_{ij}^p \qquad (j = 1, 3) \tag{2.3}$$

where N is the number of particles, and A_j^m are the elastic constants of the matrix. ΔX_{ij}^p denotes the displacement *differences* due to the presence of a single spherical inclusion, and are defined by equations (A.3) and (A.4) (see Appendix A).

Statistically, the summation $\sum_{i=1}^{N} \Delta X_{ij}^p$ can be replaced by N times the mean value of ΔX_{ij}^p. Thus, by applying Green's integration transformation, we have:

$$\sum_{i=1}^{N} \Delta X_{ij}^p = \frac{N}{V} \int_S \Delta X_{ij}^p \frac{x_{ij}}{r_i} \, dS \tag{2.4}$$

where the integration must be carried out over the outer surface of the composite model (V and S denote the volume and surface of integration, and x_{ij} and r_i are cartesian and radial coordinates from the centre of each particle, respectively). The elasticity constants of the composite, $\tilde{A}_j$, can therefore be calculated by substituting for ΔX^p_{ij} from equations (A.3) and (A.4).

Assuming that the total energy stored in the composite is the sum of the energies due to the presence of N spherical particles and the one of the matrix, and equating the results with the apparent composite strain energy per unit volume, defined by:

$$\tilde{U}_o = \tfrac{1}{2} \tilde{\lambda} (\tilde{A}_1 + \tilde{A}_2 + \tilde{A}_3)^2 + \tilde{\mu} (\tilde{A}_1^2 + \tilde{A}_2^2 + \tilde{A}_3^2) \qquad (2.5)$$

expressions for the elastic moduli of the composite can be deduced ($\tilde{\lambda}$ and $\tilde{\mu}$ are Lamé's constant and the shear modulus of the composite, respectively). Denoting Lamé's constant and the shear modulus of the matrix by λ and μ, and those of the particles by λ' and μ', we have:

$$\tilde{\mu} = \mu \{1 + 15 (\mu' - \mu)(\lambda + 2\mu) (2\mu' (3\lambda + 8\mu) + \mu (9\lambda + 14\mu))^{-1} \phi\} \qquad (2.6)$$

$$\tilde{k}^{-1} = \frac{k^{-1} + (3 + 4\mu k^{-1})(k'^{-1} - k^{-1}) \phi}{(3 + 4\mu k'^{-1})} \qquad (2.7)$$

where $\tilde{k}$, k and k' are the bulk moduli of the composite, matrix and particles, respectively. ϕ denotes the nominal fractional volume of rubber particles.

In the special case of rubber particles suspended in a polystyrene matrix, we have:

$$\mu' \simeq 0 \qquad (2.8)$$

and:

$$(\tilde{\mu}/\mu) = 1 - \xi \phi \tag{2.9}$$

where:

$$\xi = 15 \frac{\lambda + 2\mu}{9\lambda + 14\mu} \tag{2.10}$$

Equations (2.9) and (2.10) predict a linear change in elastic moduli of a rubber modified polymer containing different rubber contents (see Figure 2.3).

2.4 KERNER'S THEORY OF FINITE SUSPENSION

A substantial fraction of the mysteries associated with the elastic behaviour of particulate-filled composites, in particular rubber modified polymers, might be eradicated if an accurate modelling of these composites could be constructed. In this regard, Kerner's hypothetical model is a close approximation to the case of finite suspension composites having a relatively large fractional volume of spherical inclusions. Schematically, the composite is subdivided into spherical elements, each containing a spherical inclusion core (characterised by μ' and k') and surrounded by a shell of matrix (characterised by μ and k)*. The intermediate zone adjacent to the spherical elements have properties which vary, in some unknown way, between those of a suspending medium and those of an average composite characterised by $\tilde{\mu}$ and $\tilde{k}$. By using the averaging procedure due to Bruggeman (1937), and analysing the effect of uniform elongation and uniform compression on the model described, expressions for the moduli of the composite are deduced. To evaluate the average stresses and strains in inclusions, in the matrix shell, and at a point far from the spherical element representing the average composite, the Goodier's solutions were invoked by Kerner. The intermediate zone does not need to be analysed, as by averaging the elongation and normal stresses across a plane orthogonal to the applied stress, its effect is eliminated. Kerner's calculations for the bulk modulus, $\tilde{k}$, and the shear modulus, $\tilde{\mu}$, of a two-phase composite results in:

$$\tilde{k} = \left[\frac{k\,(1-\phi)}{3k+4\mu} + \frac{k'\,\phi}{3k'+4\mu}\right] \Big/ \left[\frac{1-\phi}{3k+4\mu} + \frac{\phi}{3k'+4\mu}\right] \qquad (2.11)$$

---

* μ, μ' and $\tilde{\mu}$ are the shear moduli of the matrix, inclusions and average composite, respectively.

and:

$$\tilde{\mu} = \mu \frac{1 + \alpha \beta \phi}{1 - \beta \phi} \tag{2.12}$$

where: $\alpha = \frac{7 - 5\nu}{8 - 10\nu}$, $\beta = \frac{\mu'/\mu - 1}{\mu'/\mu + \alpha}$

where ν and ν' denote the Poisson ratios of the matrix and particles, respectively. The Kerner expressions are not self-consistent since, at the limiting case of the suspending matrix vanishing (i.e. the composite is a mere aggregate of packed particles), the elastic moduli still depends on the properties of the vanished media*. Lewis & Nielsen (1970) modified Kerner's equations by introducing an additional function, ψ, and taking into account that the maximum packing fraction of particles suspended in a matrix, ϕ_m, cannot exceed a definite fraction of the composite volume (Scott (1960), McGeary (1961)). Hence, the shear modulus of a two-phase composite was described by:

$$\tilde{\mu} = \mu \frac{1 + \alpha \beta \phi}{1 - \beta \psi \phi} \tag{2.13}$$

The ψ-function must satisfy the following boundary conditions:

1. $\psi \phi = 0$ at $\phi = 0$
2. $d(\psi\phi)/d\phi = 1$ at $\phi = 0$
3. $\psi \phi = 1$ at $\phi = \phi_m$

Lewis & Nielsen proposed two simple functions which satisfied these conditions and were in reasonably good agreement with experimental data;

---

* Except for two-phase composites.

these are:

$$\psi = 1 + \frac{1 - \phi_m}{\phi_m^2}\,\phi \tag{2.14}$$

$$\psi = \left[1 - e^{\frac{-\phi}{1 - \phi/\phi_m}}\right]/\phi \tag{2.15}$$

Figure 2.5 shows the modified Kerner theory assuming $\phi_m = 0.64$, together with some experimental data on a glass-filled epoxy resin composite performed by Lewis & Nielsen.

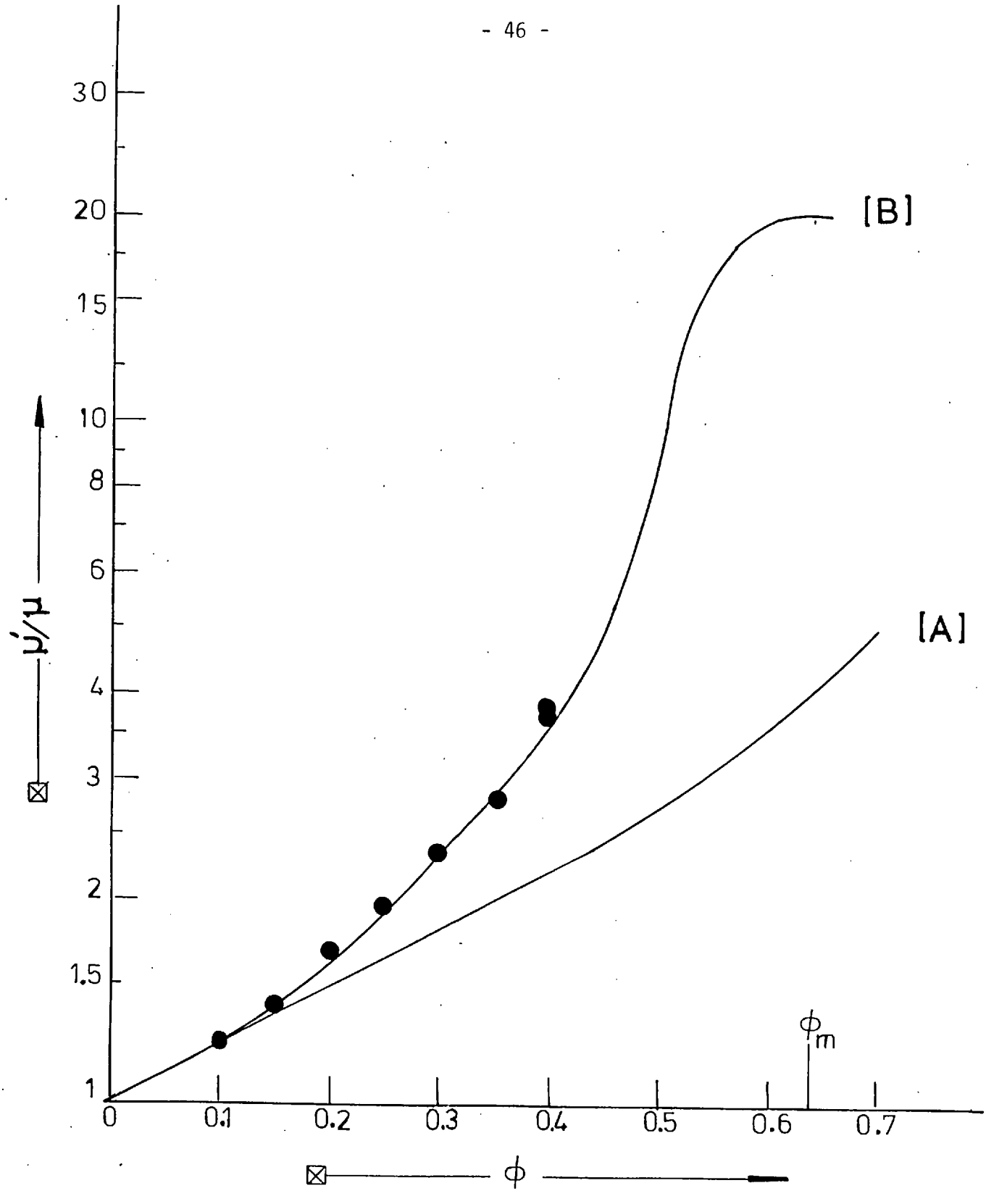


Figure 2.5: Dependence of relative modulus on volume fraction of filler
A = Original Kerner's equation
B = Modified Kerner's equation
Circles correspond to experimental results (solid curves are calculated for $\upsilon = \upsilon' = 0.35$, $\mu'/\mu = 25$, $\phi_m = 0.64$)
(after Lewis & Neilsen)

2.5 SELF-CONSISTENT COMPOSITE THEORIES

In general, the arrangement and geometry of inclusions in particulate-filled composites are of complete random form. When the composite is viewed macroscopically, the random characteristics of its constituents contributes an homogeneous and isotropic behaviour to the material as a whole. An oscillation in statistical characteristics describing the quantity (i.e. average volume fraction), order (arrangement of particles in the matrix), and geometry (size and shape) of composite constituents should generally engender a change in average behaviour of the composite. In practice, apart from fractional volumes, the detailed characteristics of the composite elements are very difficult to measure experimentally. Thence, when single fractional volumes are given alone, the prediction of composite behaviour, such as modulus of elasticity, in general should be merely restricted to defining the lower and upper bounds. The bounding values are essentially deduced by determining the admissable stress and strain fields within a specified composite of varying composition.

Hashin & Shtrikman (1961,1962) derived expressions for bounds of shear and bulk moduli of particulate-filled composites having spherical constituent geometry. In brief, their treatment is based on some new variational theorems for linear elastic theory and analyse the change in strain energy in a loaded homogeneous body due to insertion of inhomogeneities. In the Hashin-Shtrikman equations, the bulk modulus bounds coincide and are identical to the solution given by Kerner (equation (2.11)). The lower and upper bounds for shear modulus are given by:

$$\tilde{\mu}_{upper} = \mu' + (1 - \phi)/\left(\frac{1}{\mu - \mu'} + \frac{6\,(k' + 2\mu')\,\phi}{5\mu'\,(3k' + 4\mu')}\right) \qquad (2.16)$$

$$\tilde{\mu}_{lower} = \mu + \phi/\left(\frac{1}{\mu' - \mu} + \frac{6\,(k + 2\mu)(1 - \phi)}{5\mu\,(3k + 4\mu)}\right) \qquad (2.17)$$

The closeness of these bounds depends on the ratio of bulk and shear moduli of composite components. In the case of rubber modified polymers, the shear modulus of the matrix polymer is about 1000 times greater than that of the rubbery inclusions. Therefore, the Hashin-Shtrikman bounds are widely separated and hence are of limited practical value.

On the other hand, when the particle configuration is known, numerous approximate equations have been proposed for the moduli of homogeneous heterogeneous composites (e.g. Turley (1963); Budiansky (1965,1970); Hill (1965); Halpin (1969); Davies (1971); Dickie (1973); Laws (1973, 1974); and Nielsen (1973,1974)). Among these, the self-consistent expression developed by Hill (1965) is apparently the most suitable expression for components containing variously-sized elastic spherical particles (Bucknall (1977)). The theoretical technique is essentially an extension of Hershey's (1954) theory for aggregates of crystals. In applying this theory, the properties of a typical crystal are attributed to the particle inclusions, and the macroscopic properties of the polycrystal to the matrix polymer. The shear modulus of such composites was then calculated by Hill, and can be expressed implicitly by the following equation:

$$\left[\frac{(1-\phi)\,k}{k+(4/3)\,\tilde{\mu}}+\frac{\phi\,k'}{k'+(4/3)\,\tilde{\mu}}\right]+5\left[\frac{(1-\phi)\,\mu'}{\tilde{\mu}-\mu'}+\frac{\phi\,\mu}{\tilde{\mu}-\mu}\right]+2=0 \qquad (2.18)$$

From the above equation, the shear modulus, $\tilde{\mu}$, can be evaluated using iteration or graphical techniques. Figure 2.3 shows Hill's modulus of elasticity versus the volume fraction of inclusions for HIPS. As previously stated, the main disadvantage of Hill's solution is that the method neglects the phase inversion as the fractional volume of inclusions exceeds 50% of the composite volume. This is a particularly serious

problem when analysing the elastic behaviour of HIPS, as the composite particles comprise about 80% occluded PS particles in a 20% rubber matrix.

CHAPTER 3

FRACTURE TOUGHNESS

3.1 INTRODUCTION

An understanding of fracture phenomena of polymers is vital to the accurate and safe design of any mechanical structure. Design on the basis of material yield stress, even with a high safety factor, is not adequate, since a disasterous premature fracture can occur from unexpected brittle failure. In practice, a brittle fracture normally takes place at loads far below the yield strength and this is due to the presence of intrinsic flaws or stress concentrations in the component designed.

Most glassy polymers (e.g. PS and its rubber-modified derivatives) are, by nature, apt to fail in a brittle manner so that, under certain loading and environmental conditions, the initiation of a small crack in these materials leads to a sudden shattering fracture. That is to say, the resistance to crack propagation of these materials is often insignificant. Since most polymeric materials are liable to certain processing defects, which act as sources for cracks, it can be seen that the design of plastic components requires an exhaustive and careful consideration.

The fracture of polymers subjected to tensile stresses is predominantly governed by the severity of the stress concentrating elements contained in the material, rather than being merely determined by their final yield strengths. From this it is clear that any valid fracture theory should focus upon the phenomena of crack initiation and crack propagation in the material. Accordingly, fracture mechanics, which is based on the analysis of cracks and their growth, has been developed and applied to a wide variety of materials, including polymers. The main

benefit is to provide a clearer appraisal of the role of stress concentrators, either as intrinsic flaws or as design features, in controlling the fracture behaviour of stressed components and to offer a design technique by which the final strength of a material is categorised by a single fracture parameter. Having evaluated this fracture parameter experimentally, the design of brittle or semi-brittle articles and parts containing various stress singularities can be accomplished by using these fracture techniques and the normal theories of elasticity.

Fracture mechanics concepts have been expounded in various publications, e.g. Andrews (1968); Liebowitz (1968); Hayes (1970); Turner (1972); Sih (1973); Knott (1973); Williams (1973); and others. An outline of the basic principles of the subject, employed in the present work, is briefly reviewed below.

3.2 THE ENERGY BALANCE CRITERION

The fracture of materials can be categorised as either brittle or ductile. When the material fails in a brittle manner, the maximum applied stress is often well below the yield stress. An intrinsic or artificial flaw in such materials grows almost instantly and the parts fail suddenly, often with violent shattering. Ductile materials, however, normally break at stresses above the yield point and work hardening occurs before complete failure. In polymers, the phenomenon of work hardening is usually combined with the appearance of crazes. A fracture criterion which could accurately predict failure of brittle materials would be a useful engineering tool, both for the structural design of bodies having stress singularities and the classification of materials.

The fracture energy balance criterion based on the first law of thermodynamics disregards the problem of plastic work hardening and craze formation in materials. This theory has been basically founded by Griffith (1921,1924) who was a pioneer in explaining the significant discrepancy between the observed fracture toughness of glass and that predicted from consideration of its intermolecular attraction. For a certain glass, Griffith found a theoretical strength in tension of the order of 1.1×10^4 MN/m^2, while tensile tests with glass rods gave a strength of only 1.9×10^2 MN/m^2. Griffith attributed this difference to the presence of numerous internal flaws in the glass and similar materials which are incapable of visible plastic deformation. Recent developments in the manufacturing technology of strong fibres has shown that the theoretical strength can nearly be achieved if microscopic flaws and local defects can be eliminated (Kelly (1973)). On the other hand, infra red observations in most common materials clearly show that an uneven stress distribution on molecular bonds exists and that fracture of highly

stressed bonds usually forms the nucleus for subsequent crack expansion.

The linear fracture criterion was primarily derived for a centrally cracked specimen of infinite width, undergoing a uniaxial tensile load. It postulates that the energy absorbed in the formation of fresh surfaces of a crack is provided by the release of potential energy stored in the material. The instability conditions can therefore be determined if the energy balance at the inception of crack growth is described. By integrating the product of stress and strain in each element of a centrally notched specimen, Griffith obtained the following expression for the reduction in strain energy due to the introduction of the crack*:

$$\Delta U = \frac{\pi\, b^2\, B\, \sigma^2}{E_{red}} \tag{3.1}$$

where b = half crack width

B = specimen thickness

σ = gross applied stress

E_{red} = reduced modulus of elasticity ($E_{red} = (1 - \nu^2)\, E$ for plane stress, and $E_{red} = E$ for plane strain conditions; ν denotes Poisson's ratio)

If the crack is extended and new surfaces are produced over the length $4\ \delta b$, the amount of potential energy dissipated is given by:

$$\delta W = -\gamma\, (4\ \delta b)\, B \tag{3.2}$$

---

* The stress and strain analysis of this model was previously made by Inglis (1913).

where γ is the work absorbed per unit area in forming new surfaces. Griffith initially defined the coefficient γ as the surface energy per unit area, γ_s. The energy δW therefore describes the work spent against the molecular interaction in producing the fracture surfaces. Despite the importance of the fracture concept introduced by Griffith, it took almost a quarter of a century before the theory was reconsidered by Zener & Holloman (1944) to describe the brittle fracture of some metallic materials. Irwin (1948) argued that, for almost all materials, the energy dissipated due to molecular disbonding is usually smaller than that used in plastic work and hence γ should be interpreted as the plastic energy absorbed per unit area of fracture surface, γ_p. Orowan (1945,1949) also noted that γ_p is approximately three orders of magnitude greater than γ_s, thereby dominating the fracture mechanism. Following Irwin and other researchers, the coefficient 2γ is usually termed as the critical strain energy release rate, G_c, which comprises all forms of energy, such as debonding, plastic and crazing work dissipated in the crack formation process (Irwin & Kies (1952,1954)).

From equations (3.1) and (3.2), the current potential energy preserved in the specimen is given by:

$$Q = U - \Delta U + W = \frac{\sigma^2 B D}{2 E} - \frac{\pi B \sigma^2 b^2}{E_{red}} + 2 G B b \qquad (3.3)$$

where U denotes the elastic energy of an uncracked specimen, and D is the width of the specimen along the crack.

As the crack grows, the current potential energy decreases, having its maximum value at instability conditions (i.e. at crack initiation), that is:

$$dQ = \frac{d}{db}\left(-\frac{\pi\, b^2\, B\, \sigma^2}{E_{red}} + \frac{\sigma^2\, B\, D}{2\, E} + 2\, G\, B\, b\right) \delta b$$

$$= -\frac{2\, \pi\, b\, B\, \sigma^2}{E_{red}} + 2\, G\, B = 0$$

The critical strain energy release rate, G_c, is therefore defined as:

$$G_c = \frac{\pi\, b\, \sigma_c^{\,2}}{E_{red}} \tag{3.4}$$

where the suffix c denotes the instability conditions.

Although the modified Irwin-Griffith theory of fracture accounts for a small local plastic zone in the vicinity of the crack tip, its application remains restricted to mainly brittle materials where the plastic deformation is negligible and does not distort the elastic field which is macroscopically remote from the crack tip.

3.3 STRESS INTENSITY ANALYSIS

The linear theory of elasticity provides a unique relationship between the stress, strain and energy. Therefore, a fracture criterion described in terms of an energy balance concept should be expressible in some way or another by a critical stress or strain criterion. In 1956, Irwin introduced a new approach according to which fracture occurs when a critical stress distribution (expressed in terms of a stress intensity factor) is reached. In 1957, Irwin showed that the stress intensity approach is equivalent to the energy balance approach and hence linear fracture mechanics was, for the first time, correlated to the classical elasticity analysis. In a critical appraisal of fracture mechanics, Weiss & Yukawa (1965) indicated that, while the stress criterion of fracture may not resolve the plastic work problem in the energy balance criterion, it can reassert the feasibility of fracture mechanics theory by avoiding the use of an intricate concept of strain energy release rate, which encompasses various types of energy mechanism.

In 1939, Westergaard analysed an infinite plate with a central crack undergoing a traction perpendicular to the crack plane. He showed that the stresses near the crack tip can approximately be given by:

$$\sigma_{jk} = \frac{K}{(2\pi r)^{\frac{1}{2}}} F_{jk}(\theta) + \textit{terms of order } r^0 \qquad (3.5)$$

where σ_{jk} = the stress tensor, r = radial distance from the crack tip, θ = the angle from the crack plane, and K, the intensity factor, is given by:

$$K = \sigma (\pi b)^{\frac{1}{2}} \qquad (3.6)$$

and the geometry function, $F_{jk}(\theta)$, is defined by:

$$F_{jk} = \cos\frac{\theta}{2}\begin{bmatrix} 1 + \sin\frac{\theta}{2}\sin\frac{3\theta}{2} \\ 1 - \sin\frac{\theta}{2}\sin\frac{3\theta}{2} \\ \sin\frac{\theta}{2}\cos\frac{3\theta}{2} \end{bmatrix} \tag{3.7}$$

In studying the critical conditions at the crack tip, it is convenient to direct attention to the plane of the crack where the normal stresses are at a maximum; hence, for $\theta = 0$:

$$\sigma_{jk} = \frac{K}{(2\pi r)^{\frac{1}{2}}}\delta_{jk} \tag{3.8}$$

where δ_{jk} is the Kronecker delta.

From equation (3.8), it is immediately seen that all stresses tend to infinity at the crack tip. The continuum stress analysis of Westergaard, therefore, does not hold at the vicinity of the crack tip and, in practice, the elastic stress field will be distorted by the creation of plastic zones and subsequent crack bluntening. However, by comparing the stress field near a mathematically sharp crack with those calculated for rounded cracks, Bucknall (1977) showed that the general form of stress distribution does not alter, except in a very small space close to the crack tip.

In papers by Wigglesworth (1957), M.L. Williams (1957), Erdogan (1962), Irwin (1962), Paris et al (1962), Sih (1962,1973), Bowie (1964), and many others, it was proved that the solution obtained for an infinite plate with a central notch is universal for any combination of specimen geometries and loading configurations, except for the way in which K is specified. The factor K, which is a function of geometry and loading, was designated the stress intensity factor and can be generally expressed as:

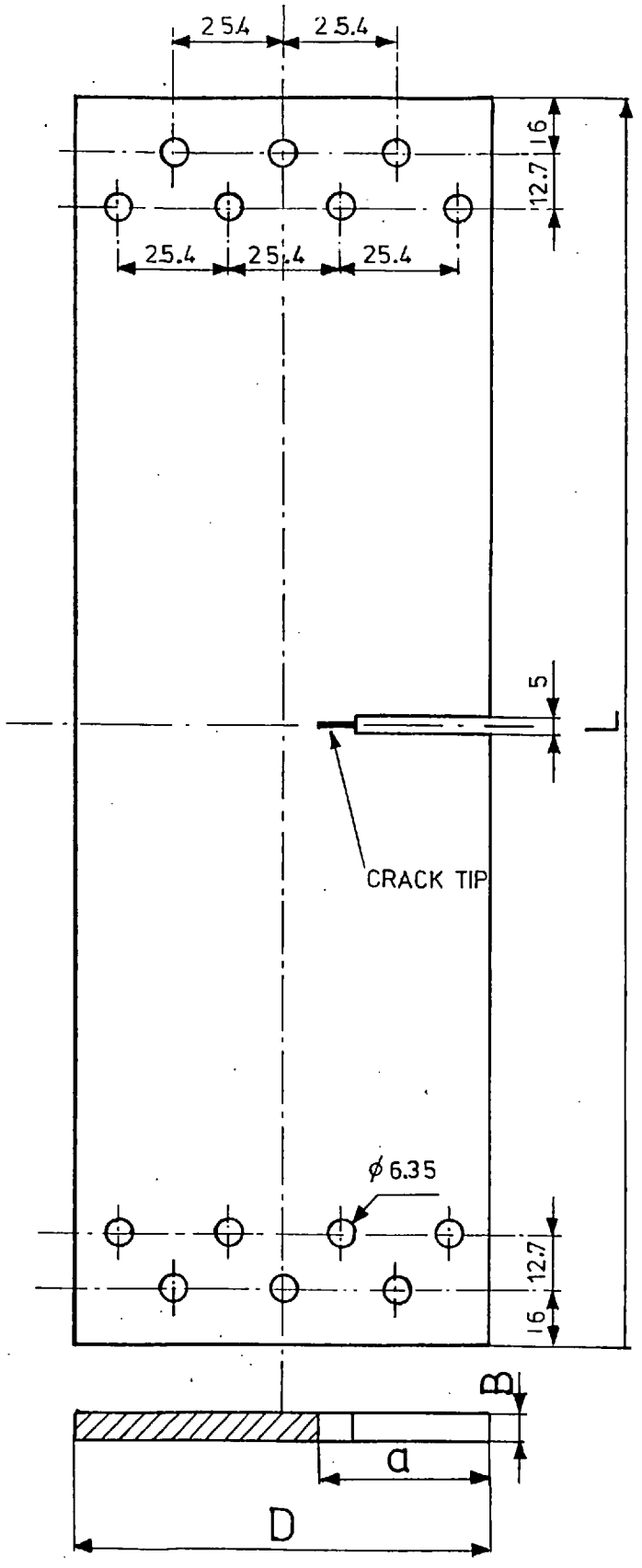


Figure 3.1: Single-edge notch specimen

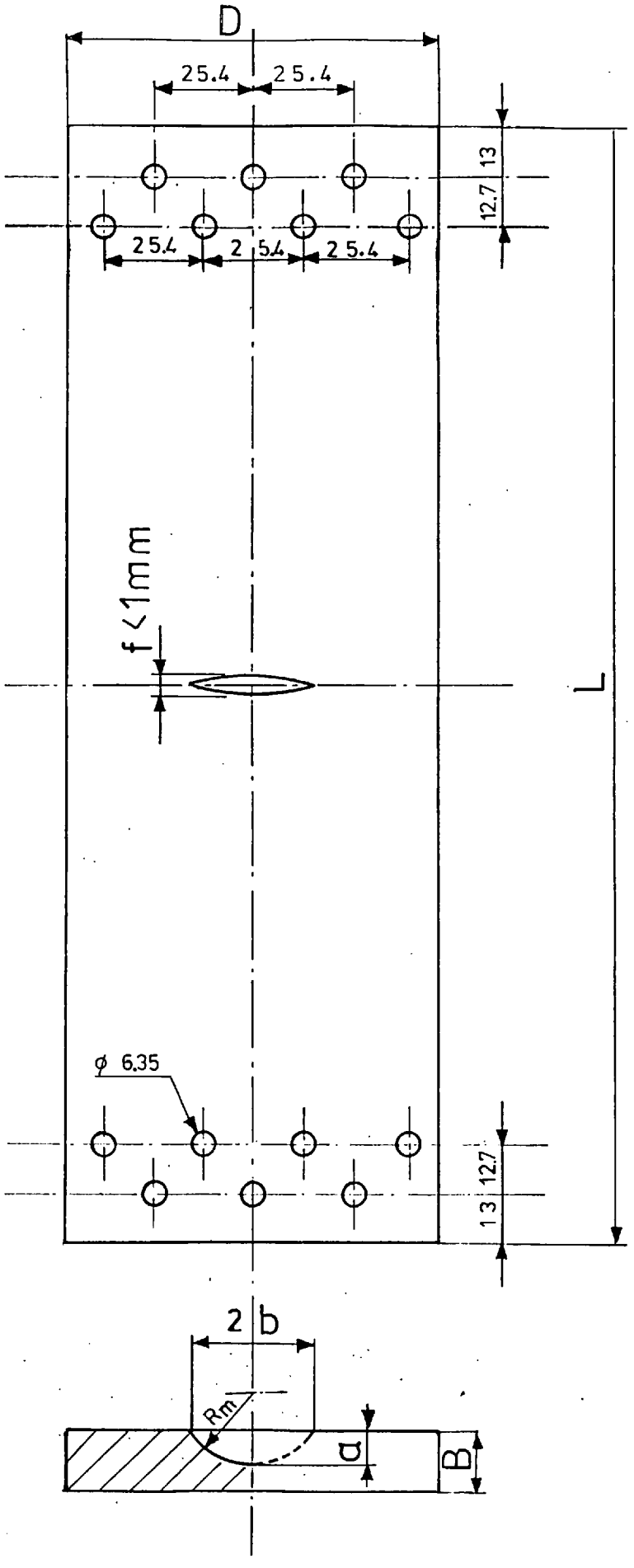


Figure 3.2: Surface notch specimen

$$K = Y \sigma \sqrt{a_c} \tag{3.9}$$

where a_c is a characteristic crack dimension (e.g. $a_c = b$ for surface notched specimens, and $a_c = a$ for single-edge notched specimens, where b and a denote the half crack width and crack length, respectively - see Figures 3.1 and 3.2), and Y is a geometrical factor and its values may be found in standard textbooks and publications (e.g. Knott (1973); Brown & Srawley (1966)). For example, in the case of a single-edge notched specimen in tension:

$$Y = 1.99 - 0.41 \left(\frac{a}{D}\right) + 18.7 \left(\frac{a}{D}\right)^2 - 38.48 \left(\frac{a}{D}\right)^3 + 53.85 \left(\frac{a}{D}\right)^4 \tag{3.10}$$

The geometry factors, Y, for tensile surface notched specimens and for single-edge notched specimens in bending, are given in section 6.4 of Chapter 6 and Appendix B, respectively.

The critical value of the stress intensity factor at the instant of crack growth can serve as a fracture criterion, simply by postulating that the instability occurs when:

$$K \geq K_c \tag{3.11}$$

The quantity K_c is known as the fracture toughness and, like G_c, is a material property influenced only by the changes in temperature, environmental conditions and strain rate. Since, in an elastic deformation mode, the potential energy is defined by the stress field, the critical intensity factor, K_c, and the strain energy release, G_c, should yield equivalent fracture criteria. Consequently, Irwin showed that

these quantities are related by:

$$K_c^2 = G_c E (1 - \nu^2) \qquad \text{for plane strain} \tag{3.12}$$

$$K_c^2 = G_c E \qquad \text{for plane stress} \tag{3.13}$$

where E and ν are the modulus of elasticity and Poisson's ratio, respectively.

Ferguson (1973), and many others, argued that, when testing plastics for the purpose of evaluating their fracture toughness, it is advisable to measure K_c directly rather than G_c, because calculation of the appropriate modulus in the vicinity of the crack tip is extremely difficult as the strain rate in that region is an unknown variable. However, in impact testing, while the experimental measurement of applied stresses and strains demand expensive and complicated instrumentation, the energy to fracture, and consequently G_c, can be obtained by using simpler devices.

Irwin (1960a) has further shown that a simple relation exists between K and elastic stress concentration analysis. The stress concentration factor is an important engineering parameter denoting the ratio of the applied gross stress to the maximum stress at the most critical point in a loaded body. The Irwin relationship is given by:

$$K = \lim_{\rho_c \to 0} \left((\tfrac{1}{2} \sigma \pi \rho_c)^{\frac{1}{2}} S_K \right) \tag{3.14}$$

where $S_K = \sigma_m / \sigma$ denotes the stress concentration factor (σ_m = the maximum stress at the notch tip, and ρ_c = notch tip radius). Under unstable conditions, equation (3.14) indicates that, if K_c is insensitive to the crack tip radius, σ_m must be inversely proportional to the square root of

ρ_c. Weiss & Yukawa (1965) showed experimentally that this is a valid assumption, provided that the crack tip radii are small compared to the crack length and specimen dimensions.

3.4 MODIFICATION OF LINEAR FRACTURE MECHANICS

As discussed previously, linear fracture mechanics is essentially an elastic deformation criterion. Hence, the distortion of the elastic field resulting from limited plastic flow, and the subsequent increase in the apparent fracture toughness of the material is considered as a theoretical error which is either negligible or must be adequately corrected.

Irwin (1960b,c) suggested that, to allow for limited plastic flow at the crack tip, the crack length should be adjusted to include this plastic zone. He estimated the plastic zone correction by setting $\sigma = \sigma_y$ (where σ_y is the yield stress of the material) in equation (3.8), which results in:

$$r_p = \frac{1}{2\pi} \frac{K_c^2}{\sigma_y^2} \tag{3.15}$$

Irwin proposed that, if the ratio of fracture strength to yield stress (σ/σ_y) does not exceed 0.7, the error due to the plastic work can be eliminated by substituting the effective crack length ($a_{eff} = a_o + r_p$, where a_o denotes the initial crack length) for the initial crack length in equation (3.8). Weiss & Yukawa (1965) argued that the error will not only depend on the above ratio, but also on the load-carrying capacity (i.e. the stress and strain in the plastic zone) which itself is a function of the work hardening characteristic of the material. Liu (1965) introduced further restrictions for the applicability of modified linear fracture mechanics. He concluded that the amount of plastic zone which can be tolerated is limited by the dimensions of the specimen and the crack length, that is:

$$r_p \ll B \text{ and } D \tag{3.16}$$

$$r_p < 0.1\, a_c \tag{3.17}$$

In order to calculate the plastic zone radius from equation (3.15), the effective yield stress in the vicinity of the crack tip, $\sigma_{y,eff}$, rather than the general yield stress, must be considered. Theoretical $\sigma_{y,eff}$ for plane strain conditions is three times larger than the nominal σ_y^*, since the transverse tensions in the region near the crack tip raise the effective strength of the material. In practice, however, plane strain only prevails in the middle core of the specimen thickness, and the average $\sigma_{y,eff}$ is, therefore, lower than $3\,\sigma_y$. Allowing for this consideration, Irwin (1960b) proposed to modify equation (3.15) for plane strain conditions to:

$$r_p = \frac{1}{6\pi}\frac{K_c^2}{\sigma_y^2} \tag{3.18}$$

If the plastic zone and craze zone sizes are assumed to be interchangeable quantities (Hoffman & Richmond (1976)), one can evaluate the plastic correction radius by employing various models proposed for crazing mechanisms. A model of craze shape suggested by Hayes & Williams (1972) (on a basis similar to that originally put forward by Dugdale (1960) and Bilby et al (1963) for plastic zones in steels) envisions a thin band of craze ahead of a crack tip. From this model, the craze zone size, r_c, was found to be:

$$r_c = \frac{\pi}{8}\frac{K_c^2}{\sigma_y^2} \qquad (\text{for } \sigma \ll \sigma_y) \tag{3.19}$$

which is identical in form to the Irwin plastic zone size but quantitatively is almost 2.5 times greater in value. It is believed, however, that one must distinguish between the plastic bands which are formed in planes of

---

* assuming $\upsilon = .33$

maximum shear stress (in a tensile test, having an angle of about 45^{o} with the crack plane), and the craze bands which are formed in the plane of a crack. Thence, the plastic correction should be based on Irwin's suggestion which is further verified by Duffy et al (1969) using the Von Mises yielding criterion.

3.5 NON-LINEARITY IN FRACTURE MECHANISMS

In situations were large scale yielding takes place at the crack tip prior to crack extension, the concept of critical stress or energy release associated with an elastic analysis becomes unrealistic. Two fracture criteria were therefore proposed to describe the failure of more ductile materials: the critical crack opening concept based on a strain criterion, and Rice's contour integral based on a path-independent energy. Cottrell (1961), Wells (1965), Hayes (1970), Ferguson et al (1973), Hoffman & Richmond (1976), and others, pointed out that the crack tip faces open up before crack extension begins, which reflects the strain environment existing in the region near the crack tip. They further argued that the critical value of the crack opening displacement (COD) can provide a useful fracture criterion for ductile materials, where G_c and K_c concepts are not applicable.

Analysis using the COD criterion is essentially based on the Dugdale model which attempts to negate the stress infinities at the crack tip by introduction of "cohesive stresses" associated with yielding behaviour. Figure 3.3 shows Dugdale's stress analysis for an infinitely wide specimen with a central crack. In order to eliminate singularities at the crack tip, the cohesive stresses must be applied over a length $(e - b)$ such that the stress intensity factor at the crack tip vanishes. By superimposing the solutions for two identical components with a crack length of $2e$, in which one undergoes a tensile load at its boundaries and the other is subjected to a uniform stress of $-\sigma_e$ on the crack faces in the interval $(e - b)$, it can be concluded that:

$$\frac{\sigma}{\sigma_e} = \frac{2}{\pi} \cos^{-1} \frac{b}{e} \tag{3.20}$$

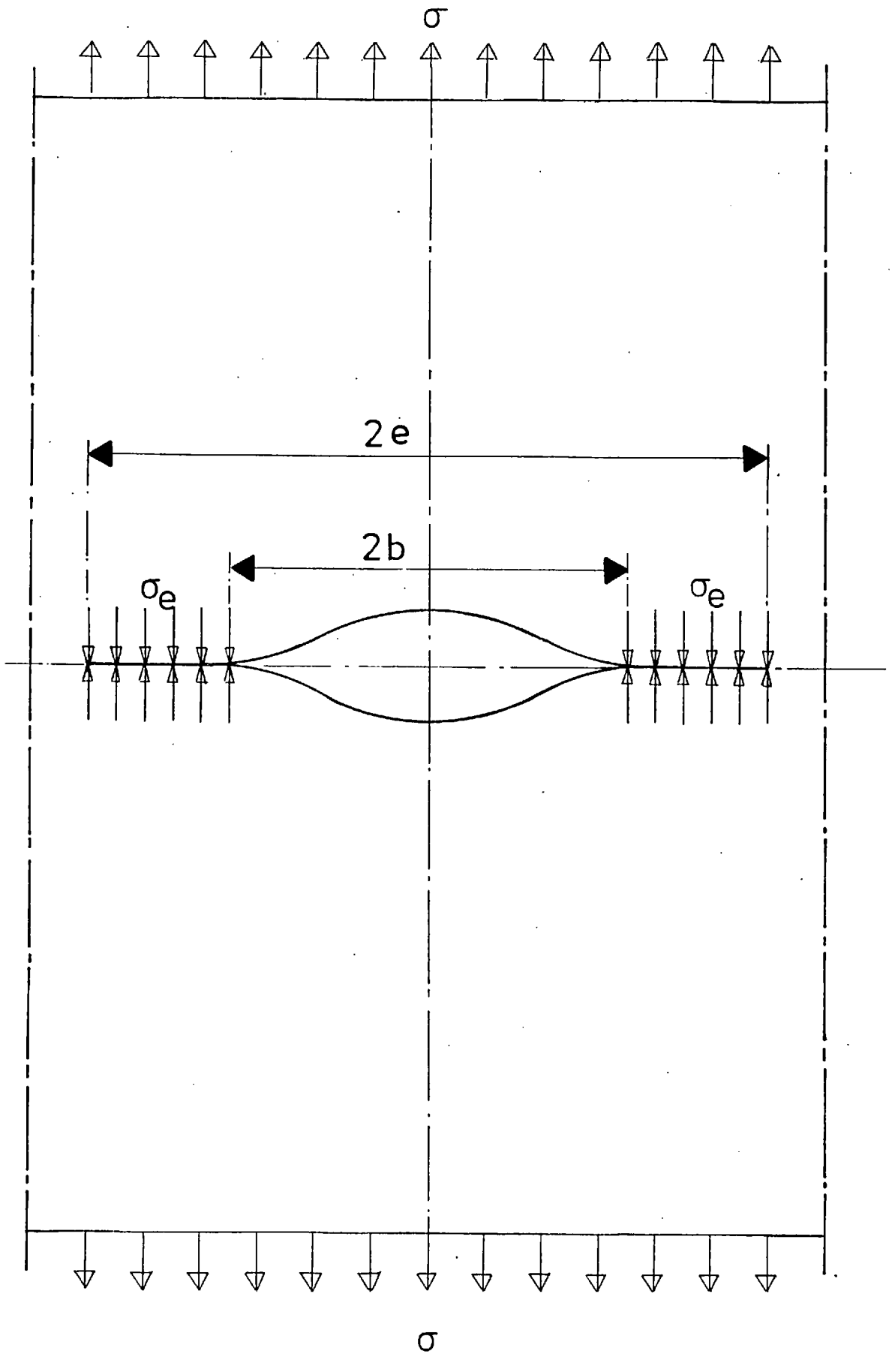


Figure 3.3: The Dugdale model

where σ_e denotes the effective stress in the plastic zone.

Goodier & Field (1962) and Burdekin & Stone (1966) showed that the COD (δ) associated with Dugdale's model, expressed in terms of yield strain, ε_y, or yield stress, σ_y, are given by:

$$\frac{\delta}{\varepsilon_y} = \frac{8b}{\pi} \ln \frac{e}{b} \tag{3.21}$$

$$\frac{\delta}{\sigma_y} = \frac{8}{\pi E_{red}} \ln \left(\sec \frac{\pi}{2} \frac{\sigma}{\sigma_y}\right) \tag{3.22}$$

where σ is the applied stress.

For moderately large initial crack lengths and small craze zones (i.e. in the case of $\sigma << \sigma_y$), these equations are reduced to:

$$\delta_c = \frac{K_c^2}{E_{red}\, \sigma_y} = \frac{G_c}{\sigma_y} \tag{3.23}$$

where E_{red} is the reduced modulus. Equation (3.23) correlates the strain and stress criteria for a dominantly brittle fracture (that is, when the applied stress is much lower than the yield stress).

Evaluation of COD for various practical specimen shapes is given by many workers (among them, Isherwood & Williams (1970), Hayes & Williams (1972), Fenner (1973), Chell (1975), Howard & Otter (1975)). According to Hoffman & Richmond (1976), none of these theories adequately characterise craze growth and crack opening displacement. However, they argued that, if the philosophy of COD can be verified (i.e. to show that it is not a function of geometry and loading) and if it could be conveniently measured experimentally, no theory would be necessary to evaluate COD from a stress analysis. Direct measurement of COD can be made by using a flat-tipped, parallel-sided tool (Codmeter) which runs into the crack

within approximately 0.5 mm to 0.75 mm (Hoffman & Richmond (1976)) from the tip.

Experimental work for metallic materials (Burdekin & Stone (1966); Cottrell (1961); Wells (1965)) and for plastics (Ferguson (1973); Williams (1972); Theocaris (1974)) has shown that the COD criterion is a useful tool to study the fracture behaviour of materials where considerable plastic work takes place. The work by Ferguson (1973) on HIPS, in particular, showed that, within some experimental error, the final failure of a material occurs at a constant COD, and he further noted that the values obtained were independent of geometry. He also stated that the experimental measurements of COD and those predicted theoretically were in good agreement. Unfortunately, the work of Hoffman & Richmond (1976) using similar materials has shown that the calculated values were about two or three times the measured values. He speculated that the reason for the discrepancy between theory and experiment could be attributed to the non-linearity in displacement, whereas all theories assume a linear elastic deformation.

The critical value of the J-integral, as formulated by Rice (1967, 1968,1973) can be viewed as a more sophisticated elastic-plastic criterion. As shown previously, linear fracture mechanics is essentially an elastic analysis of a cracked body manifesting a unique stress-strain field with a singularity at the crack tip. The fracture toughness of a material then can be determined by its resistance to this stress singularity, characterised by the stress intensity factor, K. The J-integral concept similarly assumes the existance of a stress singularity at the crack tip but its application is not confined to linear elastic bodies. Rice (1968) and Begley & Landes (1972) have shown that the J-integral is truly a path independent parameter for non-linear elastic materials and those which

obey the Hencky law of plasticity. Hayes (1970) further proved that, in the case of a monotonic loading, the J-integral would also be approximately path independent if a Prandtl-Reuss presentation is adopted. Hence, the J-integral can be calculated at a contour sufficiently far from the uncertain crack tip region, although its value depends on the stress-strain field and the material strength in that region. The evaluation of crack resistance of an elastic-plastic body, without focusing attention directly at the crack tip, is a rigorous advantage over the COD and similar criteria which are based on the analysis of strain or stress at the ambiguous crack tip region. Moreover, the COD concept principally denies the existence of the stress singularities at the crack tip by assuming a uniform cohesive stress acting along the plastic bands at crack ends. Rice & Rosengren (1968), however, have shown that a singularity does exist and its strength depends upon the flow properties of the material.

The energy line integral, J, is basically defined for a two-dimensional cracked body and is given by the following equation:

$$J = \oint_{\Gamma} U_o \, dx_2 - \vec{T} \frac{\partial \vec{X}}{\partial x_1} \, dl \tag{3.24}$$

where Γ is any closed contour around the crack tip, $\vec{T}$ is the stress vector exerted on the material normal to the contour ($\vec{T}_j = \sigma_{jk} \vec{n}_j$, where $\vec{n}_j$ denotes the unit vectors along the cartesian axes), $\vec{X}$ is the displacement vector, l is the arc length along Γ, x_1 and x_2 are rectangular coordinates along and normal to the crack, respectively, and U_o is the strain energy density function defined by:

$$U_o = \int_o^{\varepsilon_{mn}} \sigma_{jk} \, d\varepsilon_{jk} \tag{3.25}$$

where ε_{jk} is the strain tensor. Equation (3.24) describes the strain

field near the crack tip and is restricted only by the assumption that the strain energy be a single valued function of displacements (the effect of unloading is therefore disregarded) and ignores the secondary types of energy transfer (such as heat and kinetic energy losses).

Begley & Landes (1972) proved that the critical value of Rice's integral at fracture, J_c, can be used as a valid failure criterion by showing experimentally that it is independent of geometry and loading system. They also showed that the J-integral can be alternatively defined as:

$$J = \int_0^{\Lambda_o} \left(-\frac{\partial P}{\partial a_c}\right)_{at\ constant\ \Lambda} d\Lambda = \int_0^{P_o} \left(\frac{\partial \Lambda}{\partial a_c}\right)_{at\ constant\ P} dP \qquad (3.26)$$

These equations relate J to the rate of change of the area under the load-displacement curve at constant load or displacement (P and Λ are load and displacement at the point of loading, respectively, and a_c denotes the characteristic crack length) with respect to crack length. The J-integral can therefore be interpreted as the potential energy difference between two identically loaded bodies having different crack lengths of a_c and $(a_c + \delta a_c)$. From these equations, the J-integral can be directly evaluated by measuring the area under the load-displacement graphs for a family of specimens differing only in their crack sizes. Rice, Paris & Merkle (1973) further showed that the J-integral can be calculated from a single load-displacement record for certain commonly used test configurations.

When the plastic deformation is negligible, J_c and K_c are related by:

$$J_c = \frac{K_c^2}{E_{red}} = G_c \qquad (3.27)$$

or, on the other hand, if the material is rigid-perfectly-plastic, the

J_c and the crack opening displacement, δ_c, are related by:

$$J_c = \delta_c \sigma_y = G_c \tag{3.28}$$

3.6 THE BIMODAL FRACTURE CRITERION

Linear fracture mechanics is based on the two-dimensional approximation of an inherently three-dimensional problem (Srawley & Brown (1965)). The plane stress and plane strain solutions are therefore appropriate for the two extremes of infinitely thin and infinitely thick plates. In the former extreme, there is an insignificant through-thickness constraint and, consequently, the plastic deformation is not restricted, whereas in the latter case, the elastic in-plane constraint is a maximum and plastic shear formation is not allowed. Consequently, under plane strain conditions, materials are apt to break in a brittle manner since the plastic formation is less probable. The transition from ductile to brittle fracture can therefore be attributed to a change in fracture mode from plane stress to plane strain conditions, which manifests itself by the presence or absence of plastic deformation. In most cases, the experimental results have shown that the fracture toughness decreases on changing from plane stress to plane strain conditions. However, the relative variation differs from material to material (Weiss & Yukawa (1965)). The determination of the fracture toughness value in the latter condition is of greater importance because it is pertinent to a weaker configuration and therefore is a useful parameter for design purposes.

Although the philosophy of plane stress and plane strain is very much discussed (e.g. McClintock & Irwin (1965); Weiss & Yukawa (1965); Weiss & Sessler (1962); Bluhm (1961)), there is not yet an accurate method that predicts the fracture mode. In general, an increase in crack sharpness and specimen size (including thickness and width) causes a brittle fracture pertaining to the plane strain conditions. For sharply notched specimens ($B/\rho_c \geq 10$, where B and ρ_c are the specimen thickness and crack

tip radius*, respectively), the plane strain condition prevails if (ASTM (1973)):

$$B \geq 2.5 \left(\frac{K_c}{\sigma_y}\right)^2 \tag{3.29}$$

In practice, the above condition does not hold in most experiments (for example, in a medium grade of HIPS, the sheet thickness required by equation (3.29) is about 10 cm). Bluhm (1961,1962), Anderson (1969), and Parvin & Williams (1975) proposed various quantitative fracture models, all essentially assuming a composite fracture behaviour. Thus, they argued that a material can be viewed as a three-layer sandwich model where its outer layers are always under plane stress conditions, while the middle core may be constrained (if the material is sufficiently thick) and undergoes a plane strain condition. Bluhm suggested that the width of each surface layer, h_c, which is distinguishable by shear lips in metallic materials, is independent of geometry. Thus, if the material is thicker than $2h_c$, the mid-thick layer of width $(B - 2h_c)$ undergoes plane strain deformation. He further postulated that the apparent fracture toughness of the material is a function of the energies absorbed in the fracturing of plane stress and plane strain layers of the sandwich model and is defined by†:

$$K_c^2 = (1-\nu^2)\, K_{1c}^2 + \frac{1}{\pi^2\, \sigma_y^2\, B} \left(\eta\, K_{2c}^2 - (1-\nu^2)\, K_{1c}^2\right) \qquad (\text{for } B > 2h_c) \tag{3.30}$$

where K_{1c} and K_{2c} are the fracture toughnesses of the plane strain and

---

* This is suggested by Weiss & Sessler (1962) for steel and alloys, which can be somewhat different where the fracture of plastics is concerned.

† Equation (3.30) is Parvin's modification of Bluhm's (1962) model, in which it was assumed $h_c = r_p$ (r_p being defined by equation (3.15)).

plane stress layers, respectively, and η is a material constant.

Parvin (1973) postulated that the extent to which the plane stress effect penetrates the thickness is determined by the plastic zone size, r_p. He then assumed that the apparent fracture toughness, K_c, can be calculated by an arithmetic averaging of K_{1c} and K_{2c} over the relevant thicknesses $(B - 2r_p)$ and $2r_p$, respectively, that is:

$$K_c = \frac{(B - 2r_p)}{B} K_{1c} + \frac{2r_p}{B} K_{2c} \tag{3.31}$$

where r_p is defined by equation (3.15).

Parvin's (1973) experimental results for polycarbonate (PC) and HIPS showed that the above model provides a more satisfactory description of thickness effects than that of Bluhm.

3.7 THE GENERALISED THEORY OF FRACTURE MECHANICS

The principles of linear fracture mechanics originally put forward by Griffith (1921) and formulated and generalised by Irwin (1948,1956), Orowan (1948), and Weiss & Yukawa (1965), and many others, are essentially based upon linear elasticity theories. To accommodate for a limited plastic deformation prior to fracture, Irwin (1960a,b) and Duffy et al (1969) proposed a correction method for materials which do not break in a perfectly brittle manner. The limitations of this modified linear fracture mechanics, discussed by many researchers (e.g. Liu (1965)), has been briefly reviewed in section 3.4.

The concept of the critical crack opening displacement based on a strain criterion has been shown to be a useful tool with which the comparison of a wide spectrum of brittle to ductile materials can be made in a satisfactory manner (Ferguson (1973); Theocaris (1974)). The underlying philosophy of the COD criterion is, however, purely based on empirical observations and therefore its theoretical foundation is not fully justified. On the other hand, the concept of the path independent energy integral as a fracture criterion, formulated by Rice (1967,1968), and others, can be viewed as a more sophisticated fracture criterion. This theory is essentially deduced for non-linear elastic materials (and, in the case of monotonic loading, for those materials which obey the Prandtl-Reuss law of plasticity) and hence it does not take into account the energy dissipated during the crack propagation.

While the aforementioned fracture mechanics criteria already incorporate a considerable number of valuable theoretical results, the whole subject is still in an evolutionary stage. Most of the work discussed principally invokes a unique fracture parameter for describing the composite process of failure. Even within this restricted framework, there remains much

work to be done, in particular in the area of more complicated viscoelastic and elastic-plastic behaviour. For example, a generalised theory which obviates the constraints imposed by the requirements of linear elasticity, reversibility and infinitesimal strains has not yet been seriously investigated. The introductory analysis on a universal fracture mechanics criterion by Andrews (1974) provides a systematic approach to this problem and outlines the difficulties encountered in such generalisation. Andrew's generalised fracture criterion can be formulated as follows:

$$2\gamma = -\frac{dQ_a}{dA} = a_c\, Q_o\, f(\sigma, \varepsilon, T, \dot{\varepsilon}, a_c/B, a_c/D) \qquad (3.32)$$

where D and B = specimen dimensions along and perpendicular to crack surface, respectively

A = $a_c\, B$ = area of crack interface

Q_o = input energy density (i.e. the specific work during a monotonic deformation)

Q_a = local energy density

σ = applied stress on the material boundaries

ε = applied strain on the material boundaries

T = temperature

$\dot{\varepsilon}$ = strain rate

The fracture parameter γ is the actual energy available for forming new crack surfaces after the deduction of all energy losses throughout the material. At instability conditions, it must therefore equal the surface energy, γ_s. Equation (3.32) describes the fracture behaviour as a function of stress, strain, strain rate and temperature. The inclusion of ε and $\dot{\varepsilon}$ is redundant for linear materials but for non-linear viscoelastic

polymers, the stress-strain field is not independent of the local stress and strain rate. The temperature variable, T, is included for the thermodynamic consideration of heat losses during crack propagation.

The practical application of this new approach remains to be examined in an exhaustive experimental analysis of fracture.

CHAPTER 4

IMPACT RESISTANCE

Impact strength is a material property describing the material's resistance against shock loads. Determination of the resistance of the materials to impact ha been the subject of exhaustive research for many years. Thus, numerous techniques have been devised to describe the material's ability to absorb impact energy without fracture. An historical survey of impact testing is therefore useful in highlighting the main difficulties encountered in studying the impact resistances of various types of materials.

4.1 HISTORICAL SURVEY OF IMPACT TESTING

An extensive résumé of impact testing up to 1928 is given by Fettweiss (1929) who quoted more than 700 references. In 1948, Lethersich briefly discussed the works of his predecessors and, in so doing, referred to more than 200 papers among the 2000 papers available in his time. Articles on the impact behaviour of plastic materials by Turley (1967), Vincent (1971), Marshall, Williams & Turner (1973), Plati (1975), Bucknall (1977), and Williams & Birch (1977) study the recent developments on this subject and advance the theoretical understanding of impact measurement.

The science of impact testing originally started when metallurgists of Réaurmur's time (circa 1720) attempted to distinguish between flawless and defective steels by nick-bend tests. According to Lethersich, the earliest quoted reference to the subject was in 1734 by Swedenborg who judged iron bars by throwing them against sharp edges. Tredgold (1824), Thurston (1874,1875,1876), Dunn (1897,1898), Russell (1898), Charpy (1901), Izod (1903), Lavery & Southwell (1934), Church & Daynes (1937), Callendar

(1942), Stock (1944), and many others, developed various types of impact machines and thereby studied the impact resistance of diverse types of materials at different testing conditions.

Lever & Rhys (1957) listed numerous impact devices which is by no means exhaustive and, as cited by Bucknall (1977), "... This plethora of tests serves only to emphasise the difficulty of correlating standard test results with service performances". In general, impact measurement techniques fall into the two categories of limited and excess impact energy methods. Falling weight machines were first introduced by Frémont, Olsen & Hatt-Turner for testing various materials such as steel and wood (Lethersich (1948)) and were later modified by other researchers (Dunn (1897), Church & Daynes (1937), and Callendar (1942)). In these machines, a weight is allowed to fall vertically from variable heights upon specimens which are mounted on Izod or Charpy supports.

The Charpy and Izod supports are illustrated in Figures 4.1 and 4.2, respectively. In the Charpy method, the specimen is rested horizontally on anvils at its ends and struck by the falling weight at its centre. In the Izod support, the cantilever specimen is clamped at the lower ends and the weight strikes the specimen at a fixed distance from the edge of the vice.

In falling weight machines, a certain percentage of specimens are fractured (usually 50%) in a single blow test. The absorbed energy is estimated either by measuring the velocity of the weight before and after fracture using a rotating drum and recording pen attached to the weight, or by evaluating the compression of a spring on which the weight falls after fracturing the specimen.

The drop dart testing apparatus is a type of falling weight machine in which plastics sheets or pipes are tested. This machine was first

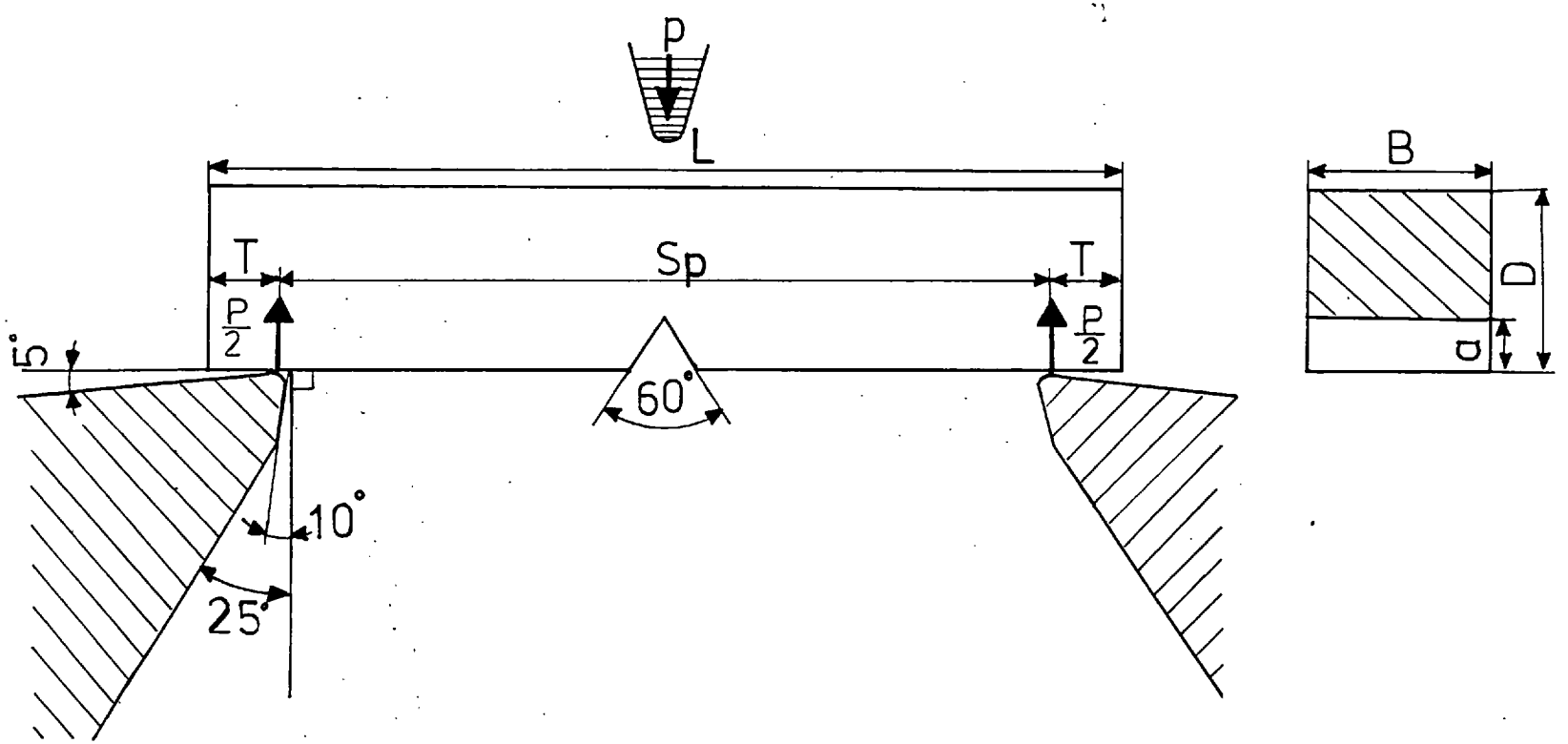


Figure 4.1: Charpy specimen and support

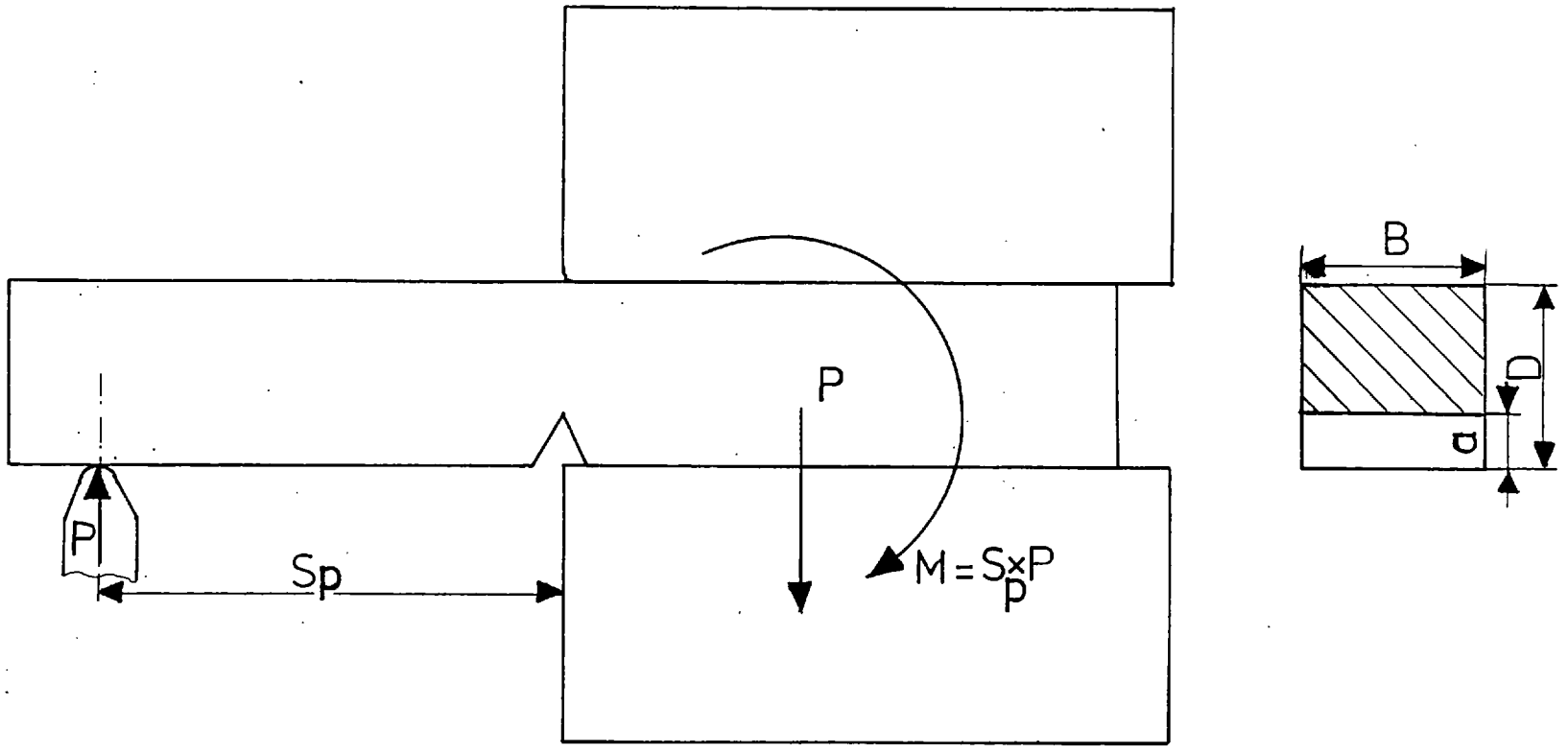


Figure 4.2: Izod specimen and support

constructed and used in America, and Lubin & Winans (1944), Stock (1944), and Morris (1968) proposed several testing procedures to study the experimental data obtained.

The drop dart machine essentially consists of a release mechanism and a heavy rigid base on which a hollow steel cylinder support is fixed so that its axis coincides with the line of fall of the striker. The striking dart has a burnished hemi-spherical head and may be guided through a slider in order to reduce the friction when using small weights (Figure 4.3). Two test procedures can be programmed by these machines:

(a) Bruceton Staircase Method: The aim of this method is to evaluate the necessary impact energy which will be just sufficient to break 50% of the specimens. This can be achieved by performing at least twenty repeated trials (British Standards Institution (1965)) using a "staircase" procedure so that the product of the height of fall and weight of the striker is equal to the required impact energy.

(b) Probit Method: The aim of this method is to obtain the fraction of fractures for a given number of specimens subjected to a fixed level of impact energy. Morris (1968) statistically analysed the experimental data obtained at each level of impact energy and thus showed that the probability distribution of failures was Gaussian for HIPS, ABS and many other polymers. Although the Probit technique requires a larger number of specimens, it provides more informative data than the Staircase method. This is so because, in practice, it supplies the designer of such materials with a wide

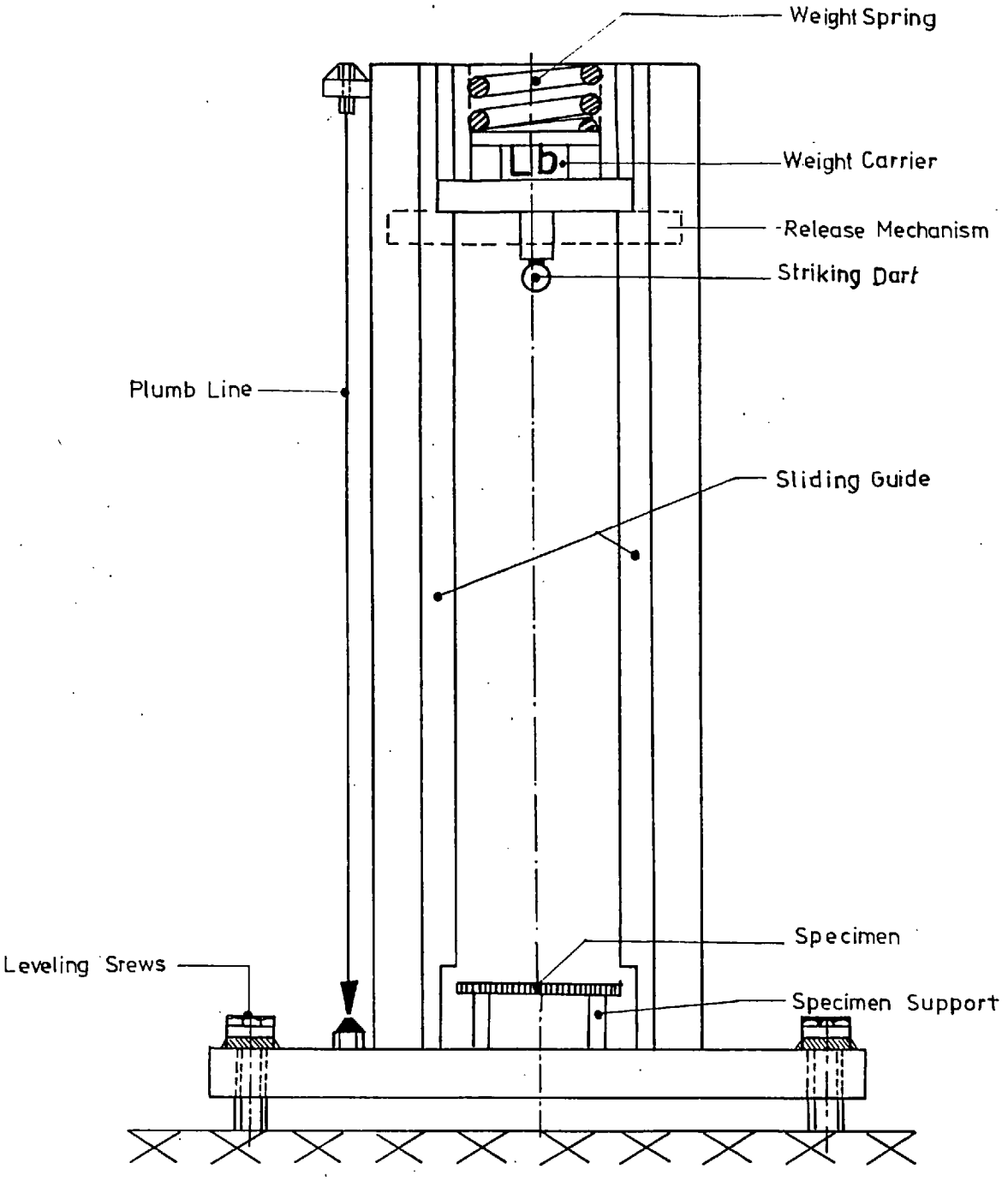


Figure 4.3: Falling weight apparatus

spectrum of impact energies necessary to cause failure in a given small fraction of specimens.

The impact machines, as described above, are mainly limited energy testing machines. The pendulum impact machines are contrarily designed to conduct excess energy impact testings on Charpy, Izod and tensile specimens. This machine was primarily developed by Russell in 1898 who employed a similar testing procedure as described previously.

In 1901, Charpy constructed his pendulum impact machine on which the cantilever and three-point bend types of specimen could be used. In 1903, Izod tested a sample of a burst gun barrel. He clamped one end in a vice and struck the other end with a hammer, thereby displaying the weak resistance of the faulty steel under impact loads. (He later designed his pendulum machine on a similar basis, and since the work of Charpy was not known in Britain, it was considered a new discovery and thence named after him.)

At the present time, the pendulum-type impact machine is extensively used for testing the resistances of metallic and non-metallic materials. The machine consists mainly of a pendulum which can swing freely in a vertical plane, with different supports for Charpy, Izod and tensile specimens fixed on a rigid base which can be levelled by adjusting screws, and a recording device. The energy absorbed in fractured specimens can be calculated by subtracting the kinetic energy of the pendulum from its effective potential energy at the releasing position. In Chapter 7, a detailed description of a recent design of pendulum-type impact machine used in the present work will be given.

In addition to the above standardised machines, many other types of impact devices were used by certain researchers. Among them are the

Guillery flywheel machine, torsion impact machines, and the Stock horizontal drop ball test, which are essentially based on similar principles to the aforementioned machines but have different loading systems, specimen geometries and impact velocities.

Falling weight machines essentially provide a statistical knowledge of failure of a particular range of materials under an impact shock, and therefore provide a useful method to distinguish between faulty and sound materials which are newly processed. These machines are simpler to construct than pendulum machines, but a much larger number of tests must be conducted in order to obtain consistent values. It must be mentioned that these values will still be dependent on the specimen geometry, loading system, instrumentation and experimental procedure, and hence can be compared only if a standard specimen and testing technique is used. It is the author's belief that the use of these machines should be restricted to the determination of fracture occurrence probabilities in samples of fabricated plastic sheets, pipes and parts, rather than a tool for the comparative evaluation of impact resistances. Otherwise, the tests on specimens of differing geometry and loading systems often rank materials in a different order of merit.

The experimental data obtained using a pendulum-type impact machine can be analysed theoretically if fracture mechanics principles are employed. It is only on this basis that the intrinsic resistances of materials subjected to impact pulses can be deduced. Before proceeding with the fracture mechanics approach, the practical shortcomings of standard impact analyses will be reviewed.

4.2 PROBLEMS AND LIMITATIONS OF STANDARD IMPACT TESTING

In the standard testing of notched Charpy or Izod specimens, impact strengths can be expressed in general forms, e.g. energy per unit length of notch, energy per unit ligament area (i.e. net cross-sectional area), and energy per unit volume of plastically deformed zone. In British Standard (1965), the impact strength is defined as the energy absorbed per 12.7 mm width of specimen, i.e.

$$\textit{Impact strength} = \frac{I \times 12.7}{D} \tag{4.1}$$

where I and D are the impact energy and the specimen width along the crack, respectively.

The total recorded energy in a pendulum impact machine is a composite quantity, consisting of various forms of energy dissipated during a test. For this reason, from early stages, many investigators attempted to study the different possible modes of energy loss in an impact test (among them are Ludwik (1923), Callendar (1942), Telfair & Nason (1943), and Lethersich (1948)). In the ASTM Book of Standards (1972b), the energy losses sufferred by the pendulum during the impact test are assumed to be the sum of the energies absorbed in the following processes:

1. Crack initiation (the inception of crack growth);
2. Propagation of the crack across the specimen width;
3. Kinetic energy due to the ejection of the broken pieces of specimen;
4. Plastic indentation or deformation at the line of impact;
5. Bending of the specimen;
6. Pendulum vibration;

7. Horizontal movement or vibration of the machine frame or base;
8. Friction in pendulum bearing and windage resistance;
9. Friction between the specimen and pendulum striking nose;
10. Plastic deformation at the crack tip.

The last mode of energy loss was not mentioned in this reference, but many other workers (e.g. Plati (1975); Bucknall (1977)) considered the plastic work as an important factor.

Factors 6, 7 and 8 are associated with the design and calibration accuracy of the impact machines and must be regarded as testing errors, and are discussed in Chapter 7 when the Charpy testing apparatus is described. The energy absorbed in elastic bending of a specimen is a reversible energy and must not be considered separately, since it will eventually resolve into the other forms of energy during crack propagation or when the broken halves are ejected. The indentation losses (factor 4) and the friction between specimen and pendulum are usually assumed to be negligible for most plastics.

The energy absorbed in the projection of fractured specimens is termed in various references as the "broken half error", the "kinetic energy of flying pieces", or the "toss factor". Noticeably, among the various factors which are assumed to contribute to the existing discrepancy in an impact test, most attention is given to the evaluation of the kinetic energy of flying pieces. Although the error is insignificant when tough materials are tested (Charpy (1901)), for most plastics whose impact resistances are low, the error is appreciable. Callendar (1942), Zinzow (a discussion on the paper by Burns & Werring (1938)), Hazen (1943), Lethersich (1948), Stephenson (1957), Marshall, Williams & Turner (1973), Williams & Birch (1977), and many others, attempted to evaluate the

kinetic energy of broken pieces and showed that the error can be as high as 100% for many brittle polymers. Zinzow evaluated the error by replacing the broken half of an Izod specimen and finding the required energy to re-eject the broken half again. Callendar observed that the broken half of an ebonite specimen travelled a shorter distance when replaced and re-ejected. He therefore concluded that some fraction of the elastic energy restored in the specimen will be released at fracture and thus contribute to the kinetic energy of the broken pieces. However, the reason for this difference is not as postulated by Callendar, but rather is simply due to differences of restitution factors of broken and unbroken specimens (Williams & Birch (1977)). In fact, when unnotched or high impact resistant materials are tested, the estimated kinetic energy of re-ejected broken halves appears to be smaller than the energy absorbed in the main process. Burns & Werring (1938) used an Izod machine and measured the kinetic energies of some notched and unnotched specimens. They found that in the former specimens, the end was given a rotary motion whereas when the broken half was struck, the motion was translational. Hounsfield (1948) measured the kinetic energy of some dummy specimens which were short enough to pass through the supports. Also, he calculated the kinetic energy of the dummy specimens using the linear theory of collision, whereupon he found good agreement between the experimental and theoretical results. Hounsfield then calculated the energy for normal specimens broken by impact and showed that the rotational energy was $\frac{3}{4}$ of the linear kinetic energy.

As will be shown in Chapter 7, when some tougher grades of commercial HIPS were tested, a hinge break* was observed and specimens did not

---

* See footnote on next page.

separate away from the tup. In this case, there will be, therefore, a smaller contribution of kinetic energy to the total recorded energy.

From this discussion, it appears that, while an accurate estimation of the error arising from the kinetic energy of flying pieces cannot be achieved due to the uncertainty in departure conditions of the broken pieces from the tup, the experimental (or theoretical) evaluation of the kinetic energy of dummy specimens gives an upper limit for this error.

The energy absorbed in the initiation and propagation of the crack, and also the plastic deformation at the crack tip, were attributed to the mechanism involved in fracture of the specimens, and therefore were assumed to characterise the impact resistance itself. Since the introduction of the pendulum impact machine by Charpy at the beginning of the century, attempts were mostly concentrated on developing instrumentation in order to eliminate the errors arising from the experimental technique, and hence limited work was done in analysing the fracture mechanism. The first important contribution to theorise impact testing was made Ludwik in 1923. He postulated that materials fracture in two forms: ductile fracture associated with the shear components of the applied stress which cause shearing of the adjacent molecular planes; and brittle fracture associated with the tensile components of the applied stress which cause the breakage of the cohesive strength of the material. His theory was later extended by Haigh (1930), Kuntze (1932), and Lethersich (1946), who argued that brittle fracture must be attributed to hydrostatic components of the

---

* Footnote from previous page: In hinge breaks, the fractured parts of specimens are linked together by a narrow filament of the material and, if one part of the specimen is held vertically, the other part cannot support itself above the horizontal line.

applied stress (dilation) which produce a purely volumetric strain by increasing the distance between the molecules. Hence, Lethersich concluded that the fracture behaviour is determined by the "spatial stress ratio"*, shear and the dilation strengths of the material.

Moser (1925) postulated that the impact strength is a function of the ratio of the impact velocity to the strain propagation in the material. He therefore argued that, if the ratio exceeds unity, a transformation in fracture behaviour from ductile to brittle should be observed. Vitman & Stepanov (1939) and Nadi & Manjoine (1941) showed that viscous shear strain increases with impact velocity, whereas dilation strain is time-independent. Lethersich (1946) found experimentally that the impact strength increases with velocity and, at a critical speed, the fracture mode changes from ductile to brittle. Thereafter, as the velocity increases, the impact strength becomes smaller until it eventually approaches a constant value at higher velocities.

The effect of specimen geometry on the standard impact strength was observed by many investigators. Baumann (1912) and Moser (1925) measured the impact energy per unit area for steel and found that is decreases sharply at a critical specimen width. Wolstenholme et al (1964) studied the effect of changing the specimen width on Izod impact strengths for ten different polymers and found that, as the width is reduced from $\frac{1}{2}$ inch to $\frac{1}{8}$ inch, the impact strength of polycarbonate (PC) increased by a factor of 5.4 and that of PVC increased by a factor of 3.1. Moser (1925) measured the volume of the plastically deformed zone in steel specimens and showed that the impact energy per volume of deformed material remained independent of the specimen size and the type and depth of notch employed. However,

---

* The ratio of tri-axial tension to the shear stress.

Sauerwald & Wieland (1926) and Bauer et al (1928) showed that this assumption could not be applied for brass and other materials.

The effect of notch depth and radius on the standard impact strength were shown to be the most critical drawbacks of classical impact measurement. It is well known that the evaluated impact strength of notched specimens is generally much lower than unnotched ones, even if the ligament area for both specimens were assumed to be equal. The influence of the notch becomes more crucial when brittle materials are tested. On this basis, Moser (1937) recommended a method to distinguish between brittle and ductile materials. If the impact strength of a double width specimen was lower than twice the impact strength of a single width specimen, it must be considered to be brittle, otherwise it must be considered to be ductile.

The effect of notch radius was studied by many workers (e.g. Lethersich (1948); Adams et al (1956); Hulse & Taylor (1957)) and it has been generally agreed that the sharper notches produce lower impact strengths. Fillunger (1924) and Petrenko (1925) suggested some empirical relations which describe the standard impact strength (energy per unit cross-sectional area, I_{cs}) as a function of the specimen thickness and net width (B and D, respectively):

Petrenko:
$$I_{cs} = q_1 B \sqrt{(D - a)}\, \rho_c + q_2 B (D - a)^2 \qquad (4.2)$$

Fillunger:
$$I_{cs} = q_3 \left[B (D - a) \rho_c + B (D - a)^2/2 \right] + q_4 \qquad (4.3)$$

where ρ_c denotes the notch radius, and q_1, q_2, q_3 and q_4 are constants.

As Lethersich (1948) noted, these equations are derived for certain types of fracture, and therefore cannot be used for materials showing a

ductile to brittle transition as the notch tip radius varies.

Vincent (1971) argued that the effect of changing the notch tip radius, ρ_c, and notch depth, a, on the measured impact strength can be simultaneously analysed if the elastic stress concentration factor, S_K, is considered (when the crack tip radius is small, S_K is directly related to the intensity factor, K (equation (3.14))). For materials which obey the linear elastic theory, the stress concentration factor is approximately given by the following equation:

$$S_K = 1 + 2\,(a/\rho_c)^{\frac{1}{2}} \tag{4.4}$$

Vincent measured the impact strengths of a large number of acrylic specimens having various notch depths and tip radii, and plotted the impact data versus the calculated stress concentration factors. He found a satisfactory consistency in the results obtained for acrylic sheets. However, when PVC and other viscoelastic polymers were tested, the results were found to be far from satisfactory, and there seemed to be no hope of unifying the results using equation (4.4).

This brief review on the problems of standard impact testing has shown that the recorded impact energy is a composite quantity consisting of energy terms arising from various modes of fracture (initiation and propagation energies, plastic work, etc.), various energy losses through vibration and friction processes in the machine, and kinetic energy of flying pieces. Among these, the fracture energy is considered to be the true characteristic of the impact resistance of materials, while the other energy losses are assumed to be procedural errors. The error can be eliminated if a proper geometry of the specimen and an accurate design of the impact machine is chosen. Classical impact strengths were expressed

in various forms such as energy per unit area, energy per unit crack length, and energy per unit volume, etc. It has been shown that the impact strengths as such are not material properties and may vary significantly with changes in specimen size, crack length and tip radius, supporting span width and type of loading (Izod or Charpy). Hence, the results obtained at various test conditions will not rank a particular material in the same order of merit.

The problem of the geometrical dependence of impact energy can be solved in two ways:

1. Performing a large number of tests by systematic variations in notch depth and radius, specimen width, supporting configuration, etc., which is a time-consuming process and thus economically limited.

2. By unification of the results using fracture mechanics concepts on impact testing.

The latter has proved to be a promising technique, particularly for analysing brittle materials (Marshall et al (1973)), and it is the task of the present work to extend the application of the theory to a wider range of more intricate composite polymers such as HIPS.

4.3 INITIATION, PROPAGATION AND PLASTIC ENERGY LOSSES

The principal energies involved in the fracture mechanism comprise the reversible energy absorbed in crack initiation and the irreversible energies dissipated in crack propagation and plastic work at the tip of an initial notch. Some investigators (e.g. Callendar (1942)) argued that the impact strength should be based on the crack initiation energy only since, once the crack initiated, the material is useless. Other workers (e.g. Lavery & Southwell (1934)) disregarded the initiation energy and attempted to design the specimens in order to make the plastic work as small as possible, thereby the measured impact strength was assumed to consist of the propagation energy alone. However, in an impact test, the initiation, propagation and plastic energies are usually inseparable and hence the calculated impact strength will inevitably include the total energy dissipated in the process. Lethersich (1948) argued that, in the case of purely brittle fracture, the entire fraction of the energy is absorbed in initiating the crack since, once the crack starts, it expands throughout the material without any significant resistance. Conversely, with ductile materials, the major part of the energy is absorbed in propagating the crack, since the plastic formation causes a considerable resistance to crack expansion. Assuming St. Venant's maximum strain criterion (i.e. fracture occurs at a critical strain), Lethersich showed that the initiation energy is proportional to the volume of the specimen. Experimental work by Charpy (1912), Lavery & Southwell (1934), Charlton & Farmer (1947), and others, for relatively ductile materials, reveal that the impact strength is proportional to the net cross-sectional area (ligament area). In general, however, the fracture starts in a ductile manner but propagates in brittle form. Lethersich therefore suggests that the total energy dissipated in these materials should be expressed as:

$$I = \omega_1 v + \omega_2 s \tag{4.5}$$

where v and s are the volume and ligament area, respectively. ω_1 and ω_2 are assumed to be constants of the brittle and ductile modes of fracture.

Stephenson (1957) argued that, although equation (4.5) was found to hold experimentally, it does not justify Lethersich's assumption of separate initiation and propagation energies, since the elastic energy stored in a specimen at the initiation of a crack will be readily available to propagate fracture. Therefore, he suggested an alternative mechanism which gives a relationship similar to that given by Lethersich, but differing in the interpretation attributed to the coefficient ω_1. In his hypothesis, the product of ω_1 and the volume gives the amount of irreversible crack initiation energy.

Stephenson (1957) and Plati (1975) pointed out that, if similar specimens differing only in the notch tip radius are tested, the energy for crack propagation remains unvaried, while the initiation resistance decreases with the decrease in notch radius. Therefore, a critical notch tip radius can be defined above which the standard impact strength will increase with radius of the notch, since the crack initiation energy is involved, and below which there should be no significant dependence on crack radius since the initiation energy becomes negligible and the propagation energy is measured alone. Vincent's (1971) experimental results showed, however, that the standard impact strength of polyvinyl chloride (PVC), Nylon and acetal, acrylic and ABS sharply decreased with smaller notch tip radius*. It is the author's belief, therefore, that

---

* See footnote on next page.

the converse argument of Stephenson and Plati must be correct. Hence, the effect of notch radius on initiation and propagation energies can be explained as follows: the specimens, having blunt notches, are liable to larger plastic deformation prior to initiation of the crack and, when the crack starts, there is already a significant plastic zone which may even act as a resistance against rapid propagation of the crack. With sharp notches, however, the plastic deformation is at a minimum and rapid crack growth follows the crack initiation.

In the case of composite polymers (e.g. HIPS, ABS, etc.), craze growth similarly acts as a crack inhibitor, even if sharply notched specimens are used. Therefore, the propagation resistance of HIPS and ABS should be considered as an important factor in the impact process, as will be further described in Chapter 7.

---

* Footnote from previous page: Plati (1975), who refers to Vincent, mistakenly assumes an opposite trend for ABS. However, as Vincent noted "... The ABS sample was highest with sharp notches (i.e. compared to other materials, had a higher impact strength at sharper notches), but the proportional increase on blunting was least."

4.4 THE IMPACT STRENGTH OF BRITLLE MATERIALS

In the preceding sections, the disadvantages and inadequacies of classical methods of impact analysis were discussed and it was shown that the calculated impact strengths depend on the specimen geometry and loading configuration. However, the recent application of fracture mechanics in this field provided a promising method for the unification of impact results, using various types of pendulum impact machine.

In 1973, Marshall et al and Brown proved that, by assuming a linear elastic deformation, linear fracture mechanics theory (previously discussed in section 3.3 of Chapter 3) can be successfully applied to the impact results of brittle materials, such as Perspex (PMMA), polycarbonate and polyethyleneterephthalate (PET). In their analyses, the impact strength of sharply notched specimens were studied and, since it was assumed that the materials behave in a brittle manner, the crack propagation and plastic energies were not considered. Therefore, the impact strength deduced described the crack initiation resistance of the materials alone. By employing fracture mechanics principles, they related the impact strength of Charpy specimens to the critical energy release rate, G_c, which is an intrinsic material property. Plati & Williams (1975a,b) subsequently used a similar technique to analyse Izod impact data, and showed for the first time that the impact strength evaluated for Izod specimens is comparable to that obtained for Charpy specimens.

For linear elastic materials which break in a brittle manner, the load-deflection curve, generated by an impact pulse, forms a sharp triangle. The strain energy stored in the cracked specimen at the onset of instability, U_f, is therefore expressed in terms of the area under this triangle (Figure 4.4), that is:

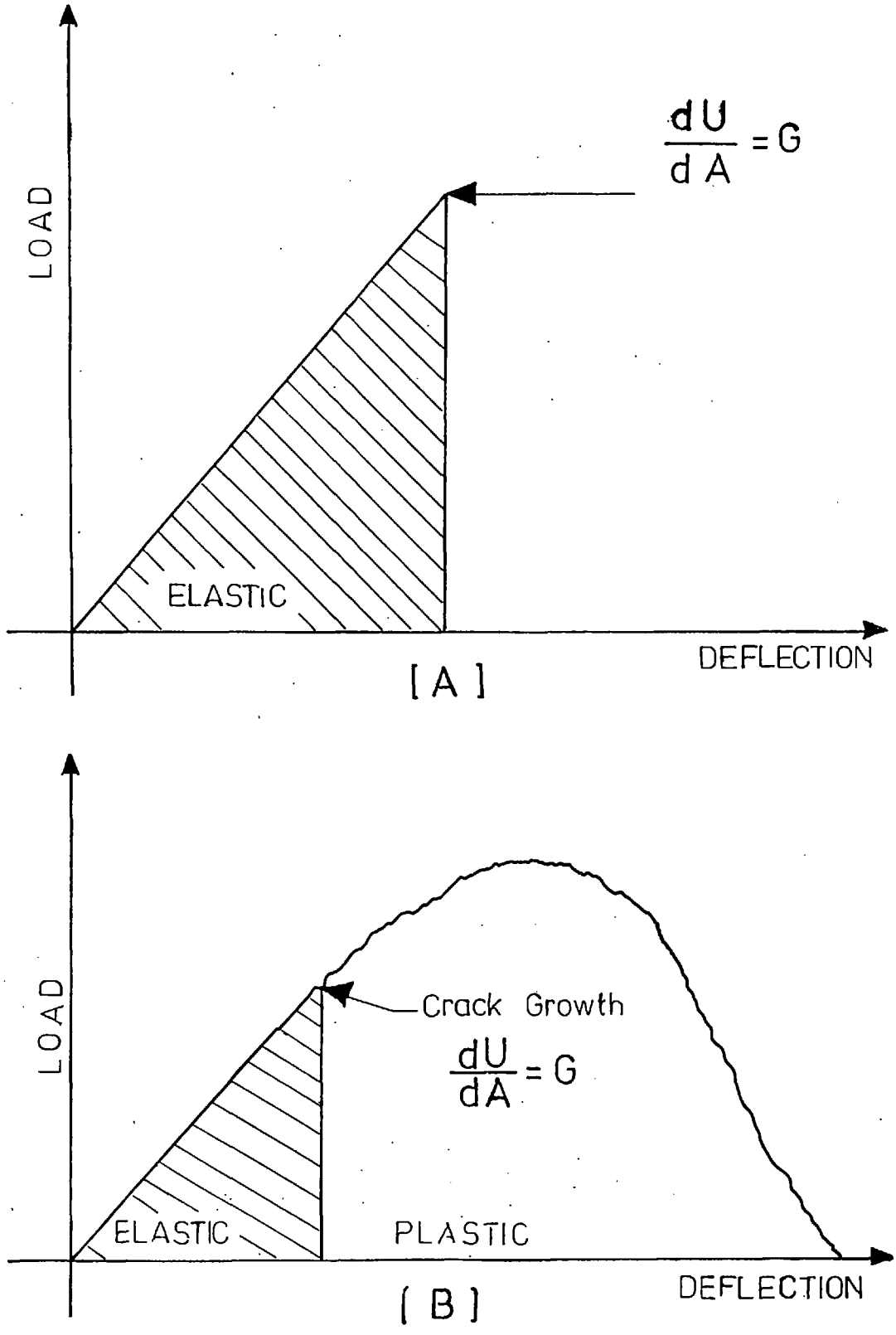


Figure 4.4: Load-deflection curves produced in an impact test

A = ideally brittle fracture

B = ductile fracture

$$U_f = \tfrac{1}{2} P_f X_f \tag{4.6}$$

where P_f is the load at fracture, and X_f is the deflection of the specimen at the point of application of the load. It is mathematically convenient to express equation (4.6) in terms of specimen compliance, C; thus:

$$U_f = \tfrac{1}{2} P_f^2 C \tag{4.7}$$

where:

$$C = \frac{X_f}{P_f} \tag{4.8}$$

From the Irwin-Griffith theory of linear elastic fracture, the critical energy release rate at fracture is given by:

$$\left(\frac{dU}{dA}\right)_{at\ fracture} = G_c \tag{4.9}$$

where A is the current crack surface (i.e. $A = B\,a$, where B and a are the specimen thickness and the crack length, respectively). Differentiating equations (4.6) and (4.8) with respect to A, we have:

$$G_c = \tfrac{1}{2}\left[X_f \frac{dP_f}{dA} + P_f \frac{dX_f}{dA}\right] \tag{4.10}$$

$$\frac{dC}{dA} = \frac{1}{P_f}\frac{dX_f}{dA} - \frac{X_f}{P_f^2}\frac{dP_f}{dA} \tag{4.11}$$

By eliminating the fracture deflection (X_f) from the above equations, the critical energy release rate, G_c, can be expressed as:

$$G_c = \frac{P_f^2}{2}\frac{dC}{dA} \tag{4.12}$$

which is known as the Irwin-Kies relationship (1952).

Combining expressions (4.12) and (4.7), we have:

$$U_f = G_c \frac{C}{dC/dA} \tag{4.13}$$

By assuming plane strain or plane stress conditions, the compliance remains unvaried through the thickness of the specimen, and therefore equation (4.13) becomes:

$$U_f = G_c \, B \, D \, \Phi(a/D, S_p/D) \tag{4.14}$$

where D and S_p are the specimen width along the crack and the supporting span, respectively, and Φ is given by:

$$\Phi = \frac{C\,(a/D, S_p/D)}{(dC\,(a/D, S_p/D))/(d\,(a/D))} \tag{4.15}$$

The function Φ can either be determined from experimental measurement of the relevant specimen compliance (Plati & Williams (1975a)) or calculated from a stress analysis of the specimen (Brown & Srawley (1966)).

For three-point bend (Charpy) and cantilever (Izod) beams, the maximum stresses are given by equations (4.16) and (4.17), respectively:

$$\sigma_{max} = \frac{3 \, P \, S_p}{2 \, B \, D^2} \tag{4.16}$$

$$\sigma_{max} = \frac{6 \, P \, S_p}{B \, D^2} \tag{4.17}$$

where B, D and S_p are the dimensions of the beam, as illustrated in Figures 4.1 and 4.2. In Chapter 3, it was shown that the critical strain energy release

rate, G_c, can be expressed in terms of the nominal applied stress, σ, crack length, a, and the geometry factor Y; that is:

$$G_c = \frac{Y^2 \sigma^2 a}{E_{red}} \tag{4.18}$$

where E_{red} is the reduced Young's modulus. The factor Y is a function of geometry and the loading system, and can be expanded in polynomial form for Izod and Charpy geometries (Plati (1975)). In Appendix B, these polynomials are given in terms of crack ratios, a/D, and for different span ratios, S_p/D.

The compliance, C, can then be obtained by integrating equation (4.12) and using equations (4.16), (4.17) and (4.18). Thus, for three-point bend specimens:

$$C = \frac{9 S_p^2}{2 B D^4 E_{red}} \int_o^D Y^2 (a/D, S_p/D) a \, da + C_o \tag{4.19}$$

and for cantilever specimens:

$$C = \frac{72 S_p^2}{B D^4 E_{red}} \int_o^D Y^2 (a/D, S_p/D) a \, da + C_o' \tag{4.20}$$

where C_o and C_o' are the compliances of the specimens at zero crack length and are given by the conventional theories of elasticity:

$$C_o = \frac{S_p^3}{4 E B D^3} \left[1 + 3 (1 + \frac{\nu}{2}) (\frac{D}{S_p})^2 \right] \tag{4.21}$$

$$C_o' = \frac{4 S_p^3}{E B D^3} \left[1 + \frac{3}{4} (1 + \nu) (\frac{D}{S_p})^2 \right] \tag{4.22}$$

The values of function Φ can be evaluated by substituting the relevant

compliances from equations (4.19) and (4.20) in equation (4.15). For short notches ($a/D \ll 1$), these solutions can be approximated as (assuming $Y^2 \approx \pi$):

$$\Phi_{Charpy} = \tfrac{1}{2} \left(\frac{a}{D}\right) + \frac{1}{18\,\pi} \left(\frac{D}{a}\right) \left(\frac{S_p}{D}\right) \tag{4.23}$$

$$\Phi_{Izod} = \tfrac{1}{2} \left(\frac{a}{D}\right) + \frac{1}{36\,\pi} \left(\frac{D}{a}\right) \left(\frac{2S_p}{D}\right) \tag{4.24}$$

It must be noted that, in the case of Izod specimens, the experimentally measured compliance differs from the theoretical values. This is due to the rotation of the specimen end in the clamp which was originally assumed to remain ideally rigid. Because of this consideration, Charpy impact testing is regarded as being preferable to that of Izod testing and the present work is essentially concentrated on the former specimens.

Equation (4.14) correlates the impact energy absorbed in the fracture process to the critical strain energy release rate, G_c, which is a material constant. The impact toughness of materials can therefore be calculated uniformly in terms of G_c values, using sharply notched specimens of various dimensions and crack lengths.

If the impact energy, I, comprises the crack initiation energy (which will eventually dissipate as fresh crack surfaces are generated) and the kinetic energy of the flying pieces alone, disregarding plastic work, propagation resistance and the other types of apparatus energy loss, we have:

$$I_b = G_b\, B\, D\, \Phi\, (a/D, S_p/D) + U_k \tag{4.25}$$

where U_k is the kinetic energy of the ejected specimens, and the suffix b implies that brittle fracture is considered. Equation (4.25) predicts that a graph of I_b versus $BD\Phi$ values should give a straight line, intercepting

the energy axis at a positive value relating to the kinetic energy of flying pieces. If brittle materials are studied, the determination of kinetic energy in a separate calibration is not of direct interest and the impact strength, G_b, can be simply obtained by measuring the slope of the data line in an energy-$BD\Phi$ plot. However, to avoid possible errors arising from the discrepancy of the impact data (which is usually intrinsic in the behaviour of brittle materials), it is usually useful to estimate the intercept of the data line with the energy axis by evaluating the kinetic energy theoretically or in a separate experiment.

If the linear kinetic energy of specimens is considered from classical mechanics, a mass M (pendulum), striking with velocity V_l a mass m (specimen) at rest, will impart to it a kinetic energy equal to:

$$U_k = (1 + e') \, m \, V_l^2 \left(\frac{M}{m + M}\right) \left[1 + \tfrac{1}{2} \frac{m}{M} (1 - e')\right] \qquad (4.26)$$

where e' is the restitution factor between the two masses and is found, experimentally, to be equal to about $(\pi/2 - 1)$ (Williams & Birch (1977)). As the pendulum mass is very much larger than that of the specimen ($m << M$), equation (4.26) reduces to:

$$U_k \simeq \frac{\pi}{2} m \, V_l^2 \qquad (4.27)$$

If hinge breaking occurs, the fractured halves of the specimen rotate about the supporting points, with the striking point attached to the pendulum and moving with the same speed, V_l. The kinetic energy of the broken halves is therefore of rotational form and can be evaluated as:

$$U_k' = \frac{1}{6} m \, V_l^2 \left[4 + \left(\frac{L}{S_p} - 1\right)\left(\frac{L}{S_p} - 2\right)\right] \qquad (4.28)$$

where L and S_p are the specimen length and supporting span, respectively*. Assuming $L \simeq S_p$, the rotational kinetic energy evaluated from equation (4.28) will be about $\frac{3}{4}\pi$ times smaller than the linear kinetic energy obtained from equation (4.27).

---

* A similar method for calculating the rotational kinetic energy of four-point bend specimens was employed by Frazer & Ward (1974).

4.5 MODIFICATION OF THE LINEAR THEORY OF IMPACT

When ductile polymers are tested, a considerable magnitude of impact energy is absorbed in the two mechanisms of plastic shear band formation and crazing. With sharply notched specimens, however, the extent of shear band formation is limited for two reasons (Bucknall (1977)): the introduction of triaxiality into the stress field around the notch tip, and the augmentation of the strain rate which tends to raise the yield stress relative to the fracture stress. Crazes are usually formed in planes perpendicular to the direction of applied tensile stress and propagate ahead of the moving crack. In toughened polymers, the crazing process is accelerated as a result of the existence of rubber particles, which, by absorbing a larger portion of impact energy, offer an appreciable resistance to crack propagation. If craze generation is limited to the surrounding region of the initial crack tip, resistance to crack propagation would be restricted to the inception of crack propagation and an unstable rapid fracture would soon follow the slow crack growth.

In Chapter 3, it was shown that the extent of the plastic zone, r_p, is proportional to fracture toughness, K_c (equation (3.15)). Using equation (3.13), the plastic radius can be expressed in terms of the modulus, E, the yield stress, σ_y, and the critical strain release rate, G_c, as follows:

$$r_p = \frac{1}{2\pi} \frac{E_{red}\, G_c}{\sigma_y^{\,2}} \tag{4.29}$$

As Irwin (1964) suggested, the effect of elastic field distortion due to the plastic deformation at the crack tip can be approximated by adding r_p to the original crack length. In impact testing, however, the plastic zone cannot easily be evaluated from equation (4.29) because the yield stress and the Young's modulus are unknown at high strain rates.

When unstable fracture is preceded by a limited slow crack growth, r_s, the linear impact theory can be similarly modified by adding r_s to the original crack length (Birch & Williams (1977)). The effective crack length to be substituted in equation (4.25) is therefore the summation of the original crack length, the plastic zone and slow crack growth; that is:

$$a_{eff} = a + r_s + r_p \tag{4.30}$$

As it will be shown in Chapter 7, there is some error in this approximation since the correction neglects the energies dissipated in the formation of a plastic zone and slow crack growth.

Williams & Birch schematically illustrated the effect of having an r_p or r_s error on the linear impact theory by plotting the I_b/BDG_b versus Φ for uncorrected impact data (the case considered was at $S_p/D = 3$, and $(r_p + r_s)/D = 0.2$). In this plot (Figure 4.5), the departure from the linear theory is displayed by the curvature of the data line and its intercept of $U_k + \frac{1}{2}(r_s + r_p)/D$. This illustration is of some importance since a similar trend of non-linearity is observed experimentally when toughened polymers are tested. However, when an appreciable plastic zone or unlimited slow crack growth occurs, the modification of linear impact theory by considering the effective crack length as defined in equation (4.30) can be shown to be no longer valid.

In ductile materials, the force-deflection curves show a smooth fall from the peak stress which is in contrast to the sharp drop observed in brittle materials. This type of failure cannot be studied by employing normal linear fracture mechanics theory and it was found necessary to seek a yielding fracture mechanics approach. Plati & Williams (1975a) and Brown (1973) have studied the impact strength of ductile materials using

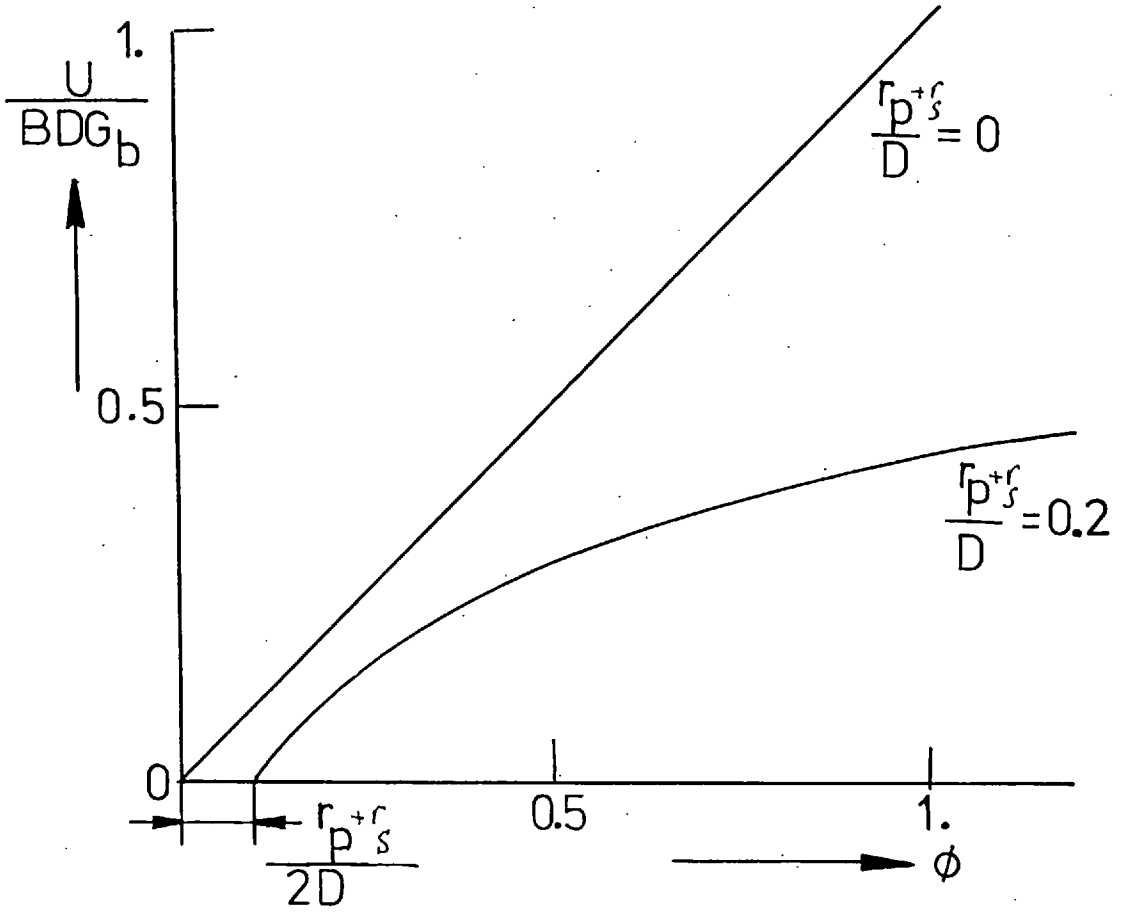


Figure 4.5: The effect of slow crack growth (or plastic zone) on the normalised energy-$BD\phi$ graphs (after Birch and Williams (1977))

the concept of Rice's path-independent integral, J_c. As discussed previously, Rice's integral concept is a more general fracture energy criterion and its value approaches the G_c value at elastic conditions.

If full yielding in bending is assumed, the impact specimen would have a solid body rotation and the energy absorbed can be defined by:

$$I_c = \frac{\delta_c}{2} \sigma_y B (D - a) + U_k \tag{4.31}$$

where δ_c is the crack tip displacement at fracture. Substituting equation (4.31) into equation (3.23), we have:

$$I_d = \tfrac{1}{2} G_c B (D - a) + U_k \tag{4.32}$$

The factor $\frac{1}{2}$ arises because of the assumption of an average displacement with regard to the hinging process in bending. The above equation predicts that the impact energy is proportional to the ligament area of a notched specimen. The experimental work on tough grades of HIPS and ABS by Plati (1975) and Brown (1973) have shown that the impact results obey the ductile theory when specimens with middling crack lengths are tested.

As discussed by Bucknall, however, the status of yielding fracture has not yet been clearly established and further work is required to ratify whether J_c is a satisfactory parameter for correlating the impact data of ductile materials. Theoretically, the general yielding and subsequent solid body rotation is unlikely to precede the crack initiation on sharply notched specimens and, therefore, the very first hypothesis in deriving equation (4.32) seems incorrect. In Chapter 7, the problem of the ductile failure of HIPS and similar toughened composite polymers will be theoretically analysed and formulated on a more realistic basis.

PART II

MECHANICAL BEHAVIOUR

OF RUBBER-MODIFIED POLYSTYRENE

CHAPTER 5

THE EFFECT OF RUBBER CONTENT ON THE VISCOELASTIC PROPERTIES OF HIPS

5.1 INTRODUCTION

Rubber modified polystyrene is a particulate-filled composite, consisting of a relatively rigid polystyrene matrix and dispersed rubbery particles. The stiffness and strength of the material is naturally determined by the properties of the matrix and by the presence of the rubber particles. In general, an increase in the ductility of these polymers due to rubber reinforcement is accompanied by a substantial reduction in their moduli and rupture strengths. Conversely, the elongation to break, as an immediate measure of fracture toughness, increases by ten to thirty-fold, depending on the rubber content. At low strain, both PS and HIPS can be treated as viscoelastic materials, since their moduli vary with time and strain rate, but are independent of strain and loading history. At large strains, however, the moduli of HIPS usually decrease sharply with strain and show little work-hardening. This effect can be construed as the result of a multiple craze generation emanating from the rubber particles (Bucknall & Smith (1965); Bucknall & Street (1967); Bucknall & Clayton (1972); Bucknall et al (1972); Bucknall (1977)).

The primary aim of the work to be described in this chapter is to study the effect of rubber content on the general bulk properties of HIPS. Thus, the modulus of elasticity and the yield stress of various special grades of HIPS were measured and collated with their rubber content. The rubber content in these materials varies from zero (plain polystyrene) to a maximum of 5.55%, while the amount of other processing additives is kept

constant. The materials were produced by blending a CPS with a parent HIPS (containing 5.55% rubber content) which use the same matrix base. Although there were some molecular weight changes, and the average size of the rubber particles was not precisely identical, these materials are a reasonable approximation to grades having 1.11%, 2.22%, 3.33% and 5.55% rubber content and are the same in all other respects. In particular, the structure and grafting percentage of the inclusion phase (consisting of about 80% occluded PS and 20% rubbery matrix) were consistent for all materials (US Steel Corporation, the Chemical Section (1976)). The significance of the particle structure on the mechanical properties of rubber modified plastics has been discussed by Bucknall (1967,1969,1977). On the other hand, as long as the dispersed inclusions in the matrix remain sufficiently small and perfect adhesion exists between the constituent phases of the composite, particle configuration and their dimensions will not play an important role in the overall behaviour of the material (Boldt (1973)). This assumption, however, cannot be generalised to the cases of rigid, gas or non-elastic particulate-filled polymers. It has been shown theoretically, and also by a number of experiments on glass-filled composites, that the moduli, final stress and maximum elongation may be significantly influenced by the size of the rigid glass beads (Leidner & Woodhams (1974)).

The results of the experiments which will be given show that the modulus of elasticity and yield stress of HIPS containing 5.55% rubber content reduces to about 60% of that of the parent polystyrene matrix. In principle, the assessment of the composite moduli should be possible prior to an experimental analysis if a suitable model is chosen. However, numerous theories based on different assumptions have been proposed for evaluating the modulus of elasticity of similar particulate-filled

composites. In the first theoretical part of this chapter, the validity of the application of these theories will be studied and discussed. As a result, an approximate method for predicting the modulus of rubber modified polymers will be introduced. The last part of this chapter provides a theoretical analysis on the effect of the arrangement and orientation of the rubber particles, and also the multiple craze production around these particles.

5.2 THE MORPHOLOGY OF HIPS

A direct observation of the morphology of particulate-filled composites is vital to determine the characterising micro-structural features of the constituent phases and hence to control and improve the rubber toughening process. Considerable information is sought from these studies; in particular, it is necessary to measure the size, shape, internal structure, fractional composition of each phase, and the degree of grafting, adhesion, and cross-linking at the interface of the constituent phases. There are three principal methods to acquire this information: light microscopy, conventional chemical analysis, and electron microscopy. In recent years, electron microscopy has been employed successfully for analysing the morphology of rubber-modified plastics (Matsuo (1969); Matsuo et al (1969); Moore (1971)), and therefore this technique was chosen to study the materials used in the present work.

The two main electron microscopic methods commonly used are transmission and scanning electron microscopy. The scanning electron microscope is usually employed to examine the surfaces of materials. The transmission electron microscope is mainly used to study the internal structure of materials.

The samples for scanning electron microscopy were sectioned from the specially prepared grades of HIPS and had dimensions of approximately 2 mm × 3 mm × 3 mm. They were washed in water in an ultrasonic bath in order to remove dust and residual polymer from the surfaces. Subsequently, the samples were placed on a suitable cylindrical stud and were vacuum-coated with about a 300 A layer of gold to prevent charging under the electron beam (see Figure 5.1(a)). Finally, the specimens were inserted in the microscope where photographs magnified to about 6×10^3 times were obtained. The results are shown in Figure 5.2 for a specially

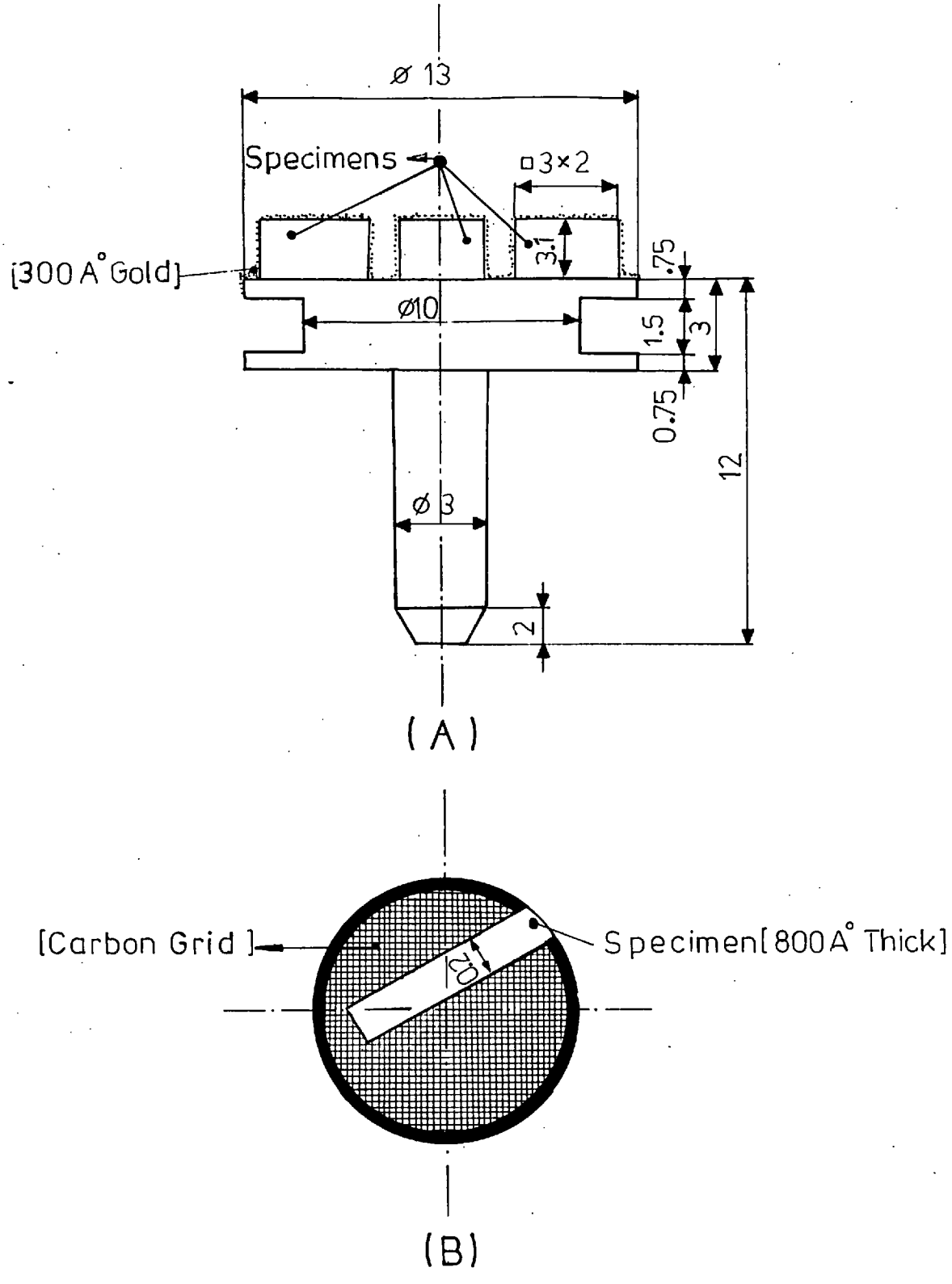


Figure 5.1: Specimens and supports used for:

A. Scanning electron microscopy; and

B. Transmission electron microscopy



Figure 5.2: The scanning electron micrograph of a specially prepared grade of HIPS, showing an ellipsoidal rubber particle in the PS matrix (magnification = ×6300)

prepared grade of HIPS. The contrast is poor since no chemical etching was used and the surfaces were not sufficiently cleaned.

Undoubtedly, the most informative pictures were obtained by the transmission electron microscope, and by using the osmium-staining method developed by Kato (1966,1967), following the method suggested by Andrews (1964) for staining synthetic rubbers. The samples were first trimmed to pyramid points and then carefully ultra microtomed to produce bevelled pyramids with perfectly smoothed tops about 0.5 mm across. Subsequently, they were exposed to osmium vapour at room temperature for several days. Extra care was taken in staining the specimens since osmium vapour is highly poisonous and generally harmful. By this method, the polybutadiene phases was selectively stained and hardened to a depth of about 10 to 30 microns. Ultra thin sections of approximately 1000 A were cut from the stained samples by an LKB Ultra Microtome. Finally, the samples were carefully placed on carbon-coated grids and inserted in the transmission electron microscope (Figure 5.1(b)). The photographs of some specially prepared samples of HIPS are presented in Figure 5.3, which reveal the morphology of these composites in excellent detail.

As shown in Figure 5.3(a), the particles are almost ellipsoidal in section and dispersed randomly in the crystal matrix. The average diameter of these particles vary from 1 to 10 microns with a mean value of about 3.5 to 6 microns, depending on the grade examined. The particles are shown to be grafts of occluded polystyrene surrounded by a polybutadiene matrix. The occluded polystyrene particles are similarly ellipsoidal in form, with average major and minor axes of about 0.25 and 0.15 microns, respectively. These particles are separated by thin layers of polybutadiene with an average thickness of about 0.07 microns. The grafting percentage of the composite particles is estimated at about 80% PS and 20% PBD.

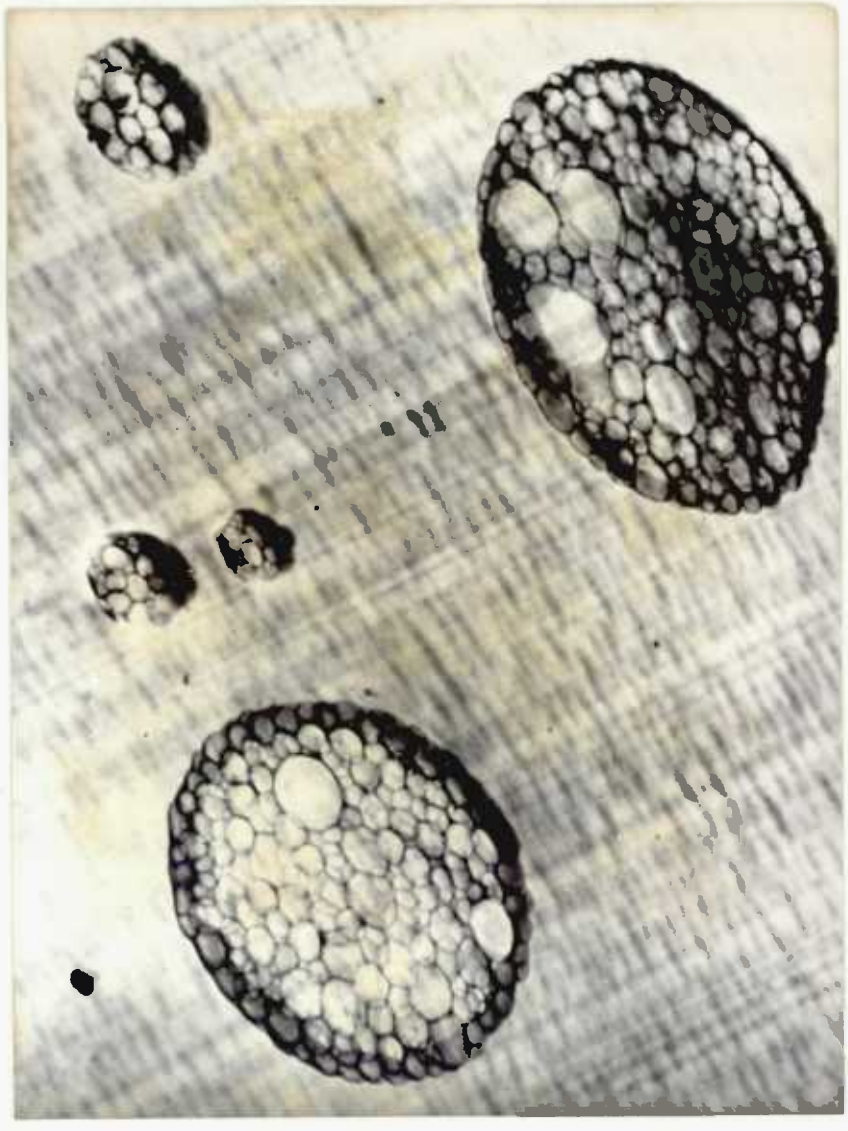


Figure 5.3(a): The transition electron micrograph of a specially prepared grade of HIPS, showing the dispersion of spheroidal rubber particles in the PS matrix (magnification = ×12000)

Figure 5.3(b) is a transmission electron micrograph of a crazed specimen under a tensile load. The dark lines emanating from the particles reveal the multiple craze production which is the principal contributor to the rubber toughening mechanism. Figure 5.3(c) shows the distribution of dispersed spherical particles in a commercial grade of HIPS.



Figure 5.3(b): The transition electron micrograph of a specially prepared grade of HIPS, showing the craze emanating from the rubber particle (magnification = ×41000)



Figure 5.3(c): Dispersion of spherical rubber particles in a commercial grade of HIPS. The micrograph was prepared by the Chemical Division of the US Steel Corporation (magnification = ×1500)

5.3 PREVIOUS STUDIES OF THE MECHANICAL PROPERTIES OF HIPS

Most studies on the viscoelastic nature of rubber modified plastics have employed a dynamic mechanical testing method by using a torsional damping apparatus. Turley (1963), Bucknall (1969), Cigna (1970), Keskkula et al (1971), and Dickie (1973) have measured the dynamic complex moduli and the mechanical damping of various commercial and experimental grades of particulate-filled polymers as a function of temperature.

Turley has pointed out that the comparison of various types of HIPS containing different rubber contents must be made only within a given method of processing and grafting procedure. Bucknall has shown that the rubber modified plastics are composite in character and the effect of their internal structure upon their mechanical properties is of great significance. Keskkula et al employed the dynamic mechanical properties as a basis for analysis of some important physical properties of modified polymers. They indicated that the damping peak (and hence the other mechanical properties) were influenced by composition, morphology, and method of polymer preparation.

Cigna studied the dynamic shear moduli of various grades of HIPS manufactured by both mechanical mixing and grafting methods. He found that the shear modulus does not directly depend upon the total butadiene content, but on the fractional volume of the rubbery dispersed phase. He also proved that the particle size and the molecular weight of the matrix had very little or no influence on the shear modulus. In a theoretical discussion, Cigna showed that the experimental data lay between Hashin's (1962,1964) bounds and somewhat closer to the values calculated from the Mackenzie (1950) model for a system containing empty holes in an elastic matrix (see Figure 5.4).

Boldt (1973) studied the effect of rubber content, particle size, and

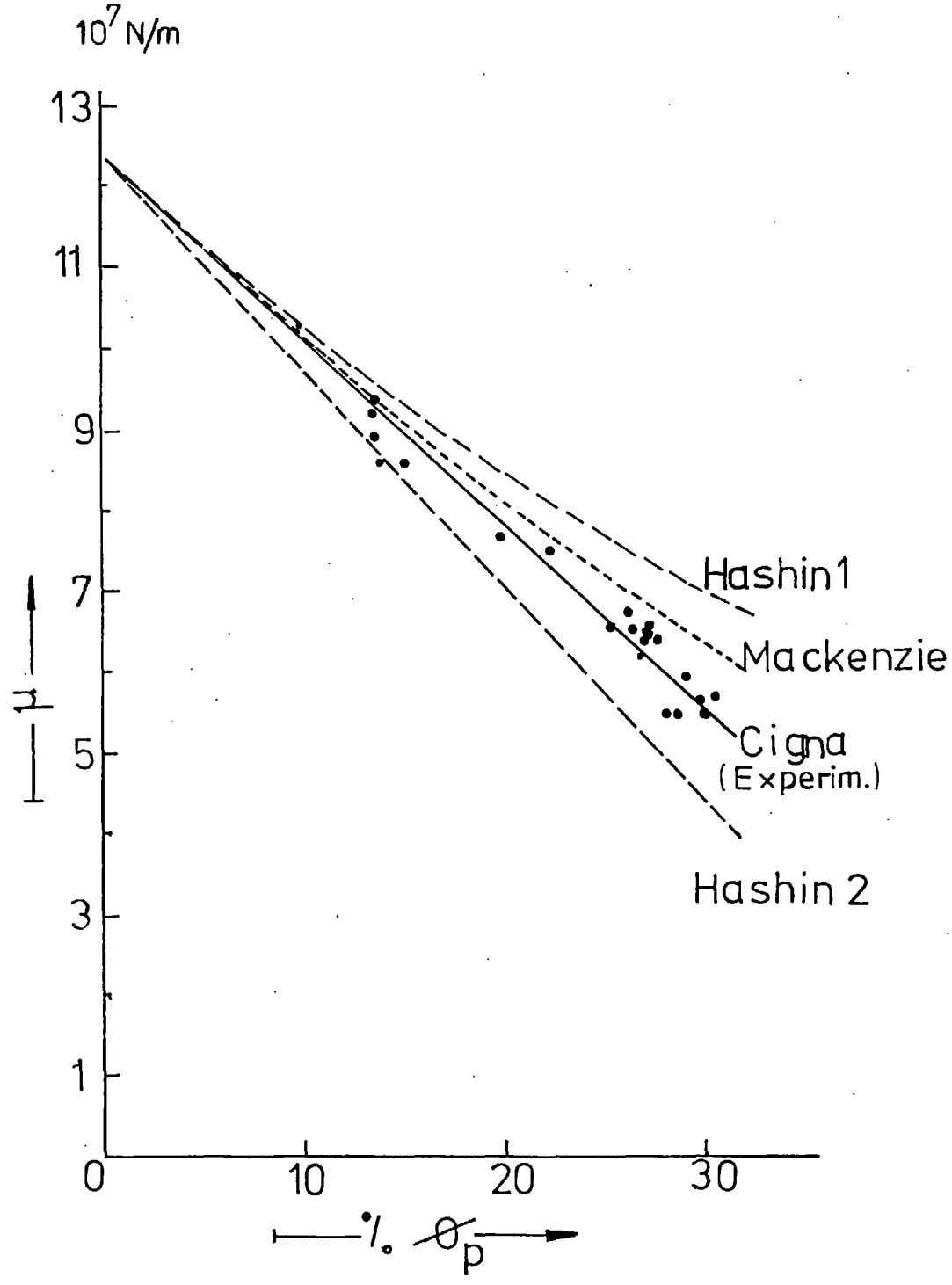


Figure 5.4: Shear modulus versus the dispersed phase content: comparison of Cigna's experimental data for a glass-filled composite resin with various theoretical models (after Cigna (1970))

mineral oil (added for processing purposes) on the elastic properties of several grades of HIPS, using the conventional tensile tests. He concluded that a definite dependence of physical properties on both mineral oil and rubber content existed, but no change was observed regarding the particle size variation. Figures 5.5, 5.6 and 5.7 show Boldt's experimental results for tensile stress, elongation to break, and Vicat temperature (the softening temperature, a parameter describing the flow properties of viscoelastic polymers) as functions of the mineral oil (for 2.7% rubber content), rubber content (for 3.06% mineral oil content), and particle size (for 0.8% mineral oil content and 3.3% rubber content). The tensile stress and the Vicat temperature can be seen to decrease almost linearly with increases in rubber and mineral oil content, but are independent of particle size. The elongation to break, which qualitatively manifests the toughness of a material, conversely increases with mineral oil and rubber content increasing, but the trend is not linear and, in some cases, the curves flatten off at higher oil and rubber contents.

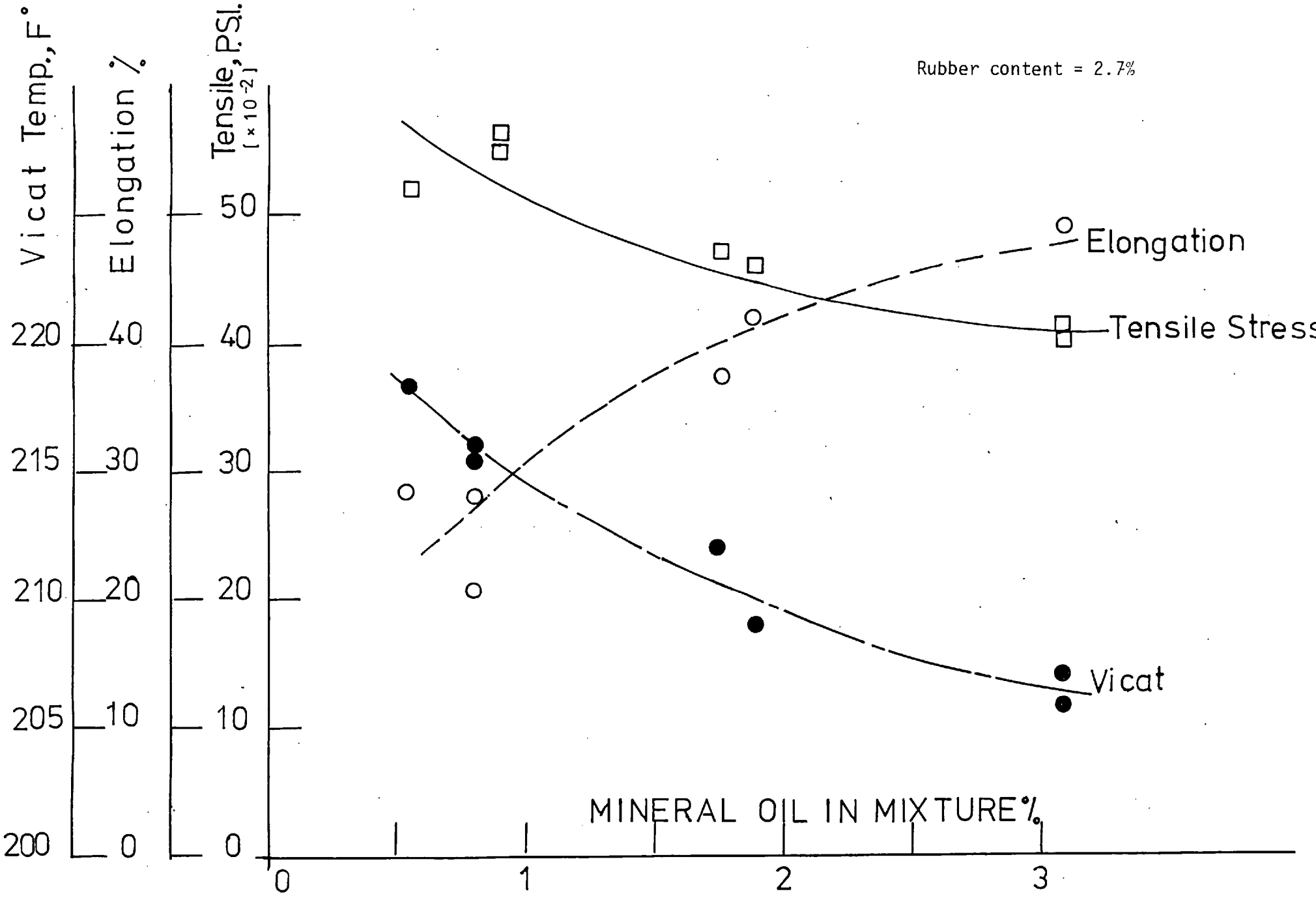


Figure 5.5: The effect of mineral oil on the mechanical properties of HIPS (after Boldt (1973))

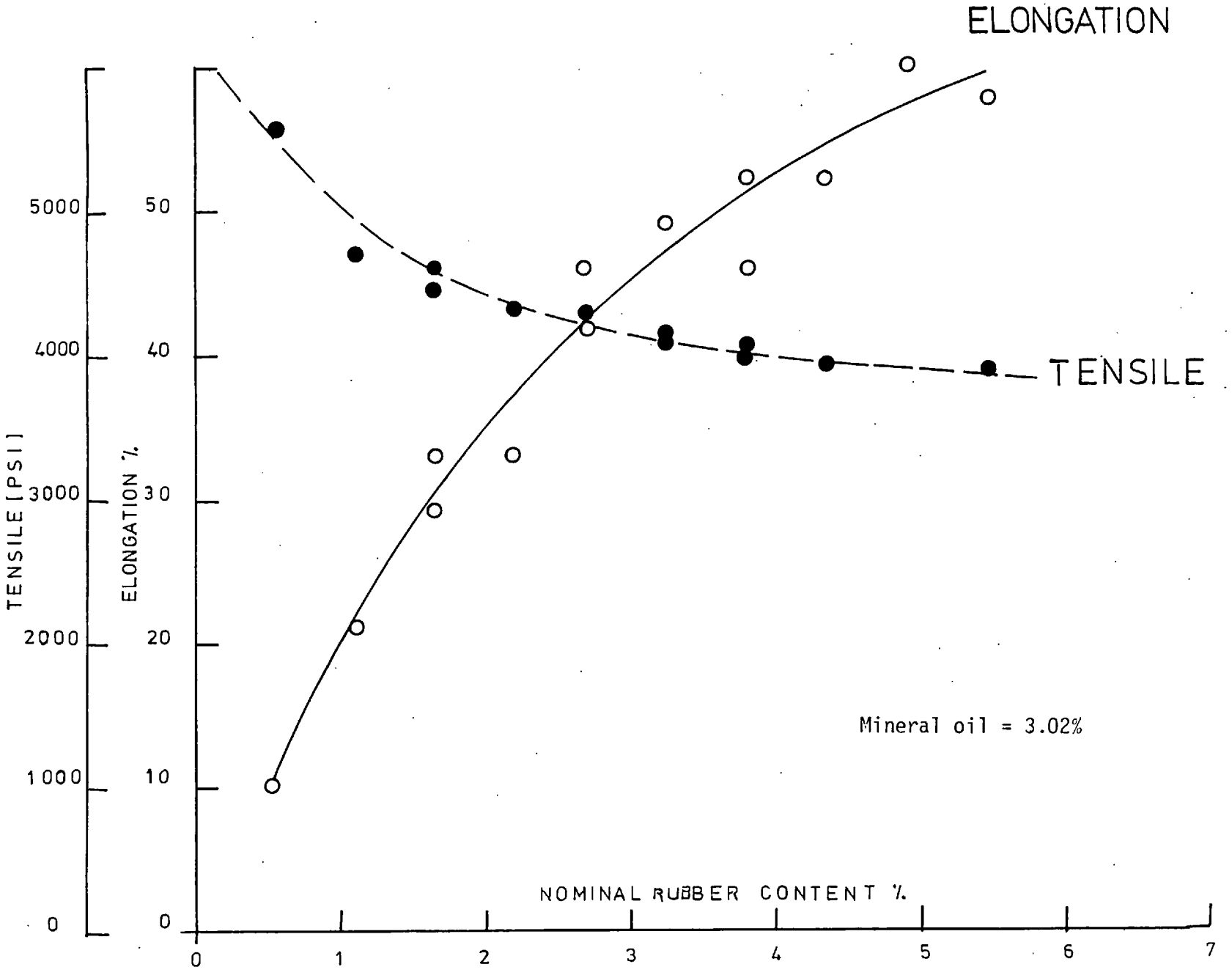


Figure 5.6: The effect of rubber content on the mechanical properties of HIPS (after Boldt (1973))

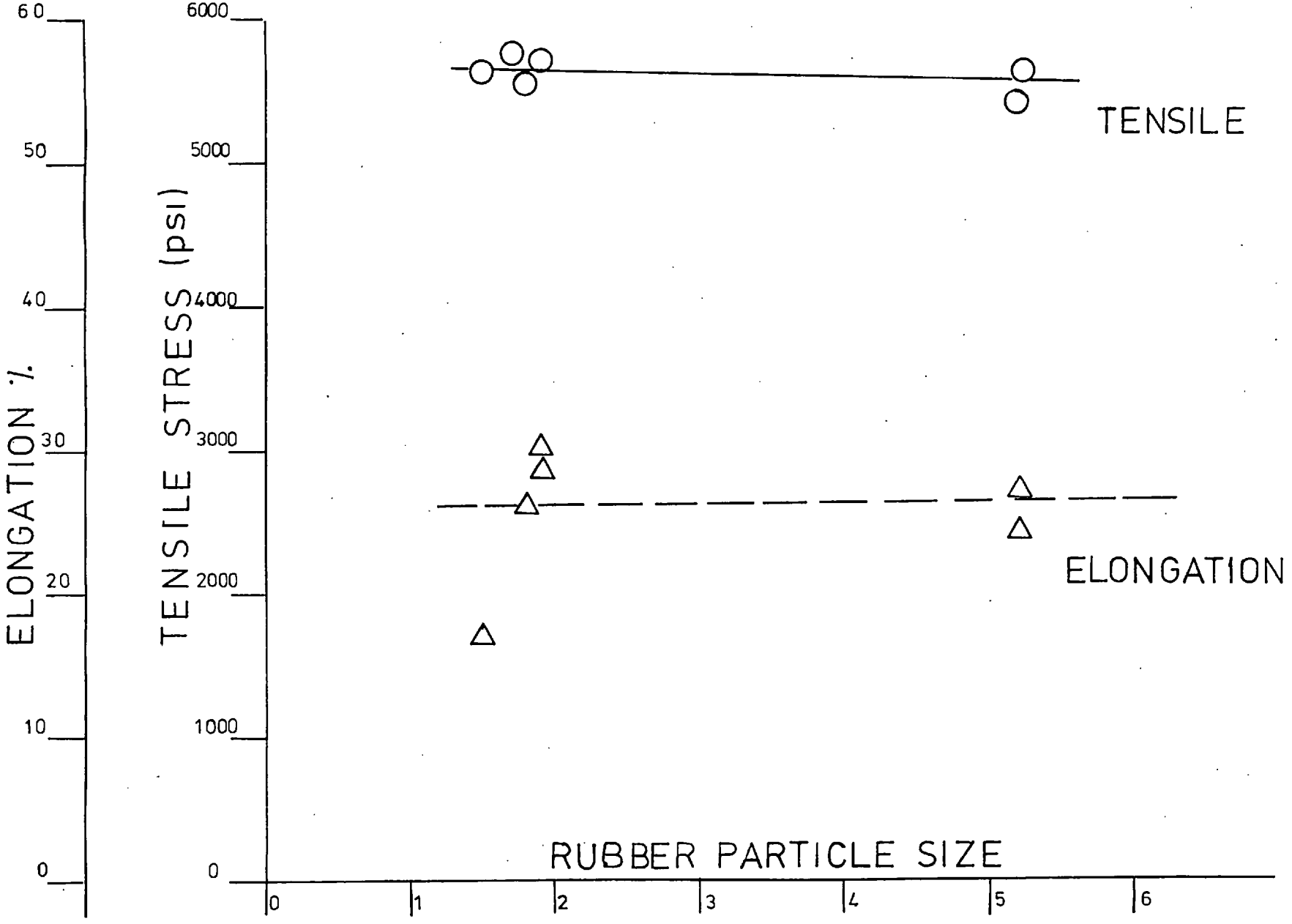


Figure 5.7: The effect of rubber particle size on the mechanical properties of HIPS (after Boldt (1973))

5.4 EXPERIMENTAL PROGRAMME

5.4.1 Test Conditions and Apparatus

A number of tensile tests were performed on dumbell-shaped specimens of thickness 3.17 mm with the appropriate dimensions suggested by ASTM D638 at three different Instron cross-head speeds (0.5, 5, and 50 mm/min). The specimens were manufactured from moulded sheets of experimental grades of HIPS and were normalised at about 20^{o}C and 50% humidity.

The experiments were carried out on an Instron Universal Testing Machine. The strain was measured and recorded by using a standard Instron extensometer (gauge length of 50 mm) and a chart drive amplifier. The elongation and stress were obtained directly from the Instron chart, on which the applied load was plotted versus the total cross-head movement.

5.4.2 Materials

Four grades of HIPS, along with their parent crystal polystyrene matrix, were tested in this work. The materials were supplied by the Chemical Section of the US Steel Corporation, and are hereafter denoted by U A0, U A1.11, U A2.22, U A3.33, and U A5.55. This conventional coding will be applied throughout this thesis, where the first two letters specify the manufacturer and type of material, respectively, and the subsequent digits specify the nominal fractional volume of the rubber. Some general specifications of these materials are given in Table 5.1.

5.4.3 Results

Typical stress-strain curves of crystal and impact PS are shown in Figure 5.8. At low strains, all grades of HIPS were found to be linear

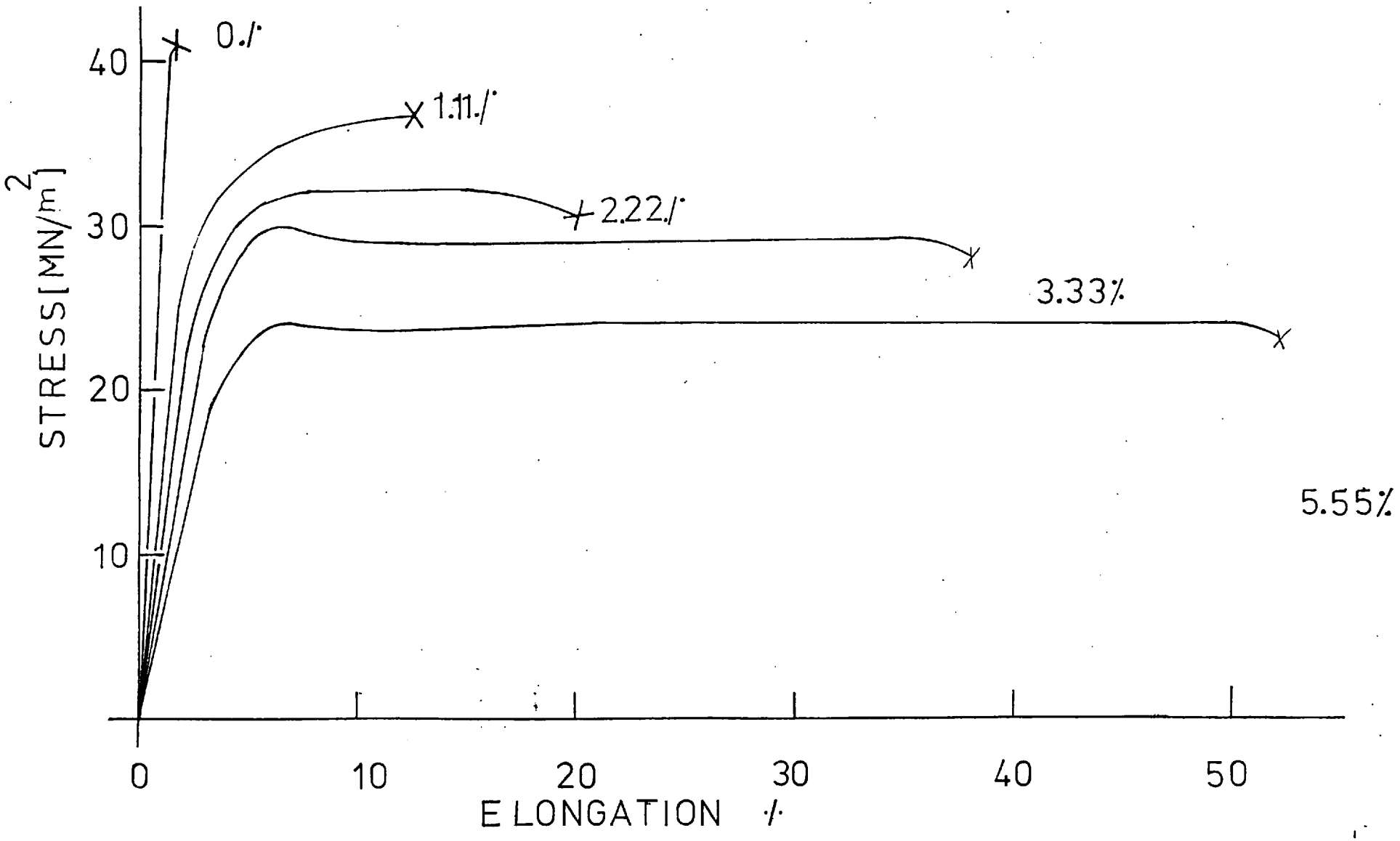


Figure 5.8: Typical stress-elongation curves for various grades of HIPS (numbers on the curves denote the percentage of rubber content)

TABLE 5.1

Specifications	U A0	U A1.11	U A2.22	U A3.33	U A5.55
Rubber content (%)	0	1.11	2.22	3.33	5.55
Mineral oil (%)	1.35	1.35	1.35	1.35	1.35
Residual monomer (%)	0.07	0.08	0.10	0.11	0.13
Ethyl benzene (%)	0.03	0.03	0.05	0.06	0.07
Particle size (μ)	-	5.5	3.3	3.4	3.4
No. average molecular weight	73004	76516	82022	80665	90311
Vicat temperature (^{o}C)	102.7	102.2	100.6	100	100
Solution viscosity (mm^2/sec)	9.65	10.84	12.5	14.7	22.9
Melt flow (g/10 min)	14.5	10.2	7.4	4.9	2.0
Rubber used	-	type 55 PBD	type 55 PBD	type 55 PBD	type 55 PBD
Particle composition	-	80%PS/20%PBD	80%PS/20%PBD	80%PS/20%PBD	80%PS/20%PBD

viscoelastic materials with their yield stress (or the maximum net stress) showing a strong dependence on strain rate. However, except for the case of crystal PS, all grades of materials showed a large non-linearity and some work-hardening at higher strains. The final failure occurred at 2% to 55% elongation, depending on the rubber contents. Figure 5.9 is an optical photograph of some typical brittle and ductile failures. The amount of craze growth, manifested by opacity and colour change in the fractured samples, was found to increase with rubber content. The modulus of elasticity, maximum fracture stress, and the elongation to break were measured at a strain rate of about 10^{-3} sec^{-1}. These parameters are given in Table 5.2.

TABLE 5.2

Mechanical Properties of the Type U A of the Specially Prepared HIPS

Material	Maximum tensile stress (MN/m^2)	Modulus (GN/m^2)	Elongation to break (%)
U A0	40	3.4	2
U A1.11	37	3.2	12
U A2.22	32	2.9	20
U A3.33	29	2.6	43
U A5.55	25	2.2	55

The rate dependence of the initial moduli of different grades of HIPS were expected to be the same as that of crystal polystyrene, and can be approximately described by:



U C0 U C1.11 U C2.22 U C3.33

Figure 5.9: Typical types of fracture in CPS and HIPS specimens subjected to a tensile load

$$(\Delta E/E_o) = 0.009\ (\Delta\dot{\varepsilon}/\dot{\varepsilon}_o) \tag{5.1}$$

where E_o denotes the modulus at a nominal strain rate, $\dot{\varepsilon}_o$, and ΔE and $\Delta\dot{\varepsilon}$ denote the changes in modulus and strain rate, respectively. Since this dependence is very small, any change in E_o would be within the experimental error and is therefore undetectable.

Figure 5.10 shows the effect of rubber content on the overall moduli of the rubber-modifed PS. Figure 5.11 reveals a similar effect on the overall yield stress of the same polymers. These results indicate that, at both low strains and large strains, the tensile stress and modulus values decrease sharply as the rubber content increases. The effect of strain rate on the yield stress of various grades of HIPS is also shown in these figures. From this, it can be concluded that the rate dependence of the yield stress is nearly identical for all grades of crystal and impact PS, regardless of their rubber content.

It is interesting to predict the overall elastic behaviour of modified PS if the nominal rubber content were to exceed 5.55% of the total composite weight. However, the extrapolation would only be valid if the composition of rubber particles remained unchanged. When a log-linear plot of yield stress and modulus of elasticity against rubber content is made, a straight line is obtained. Hence, if an exponential type of representation is introduced, the modulus and yield stress can be expressed as:

$$\tilde{\sigma}_y = \sigma\, e^{-B_o\phi} \tag{5.2}$$

$$\tilde{E} = E\, e^{-A_o\phi} \tag{5.3}$$

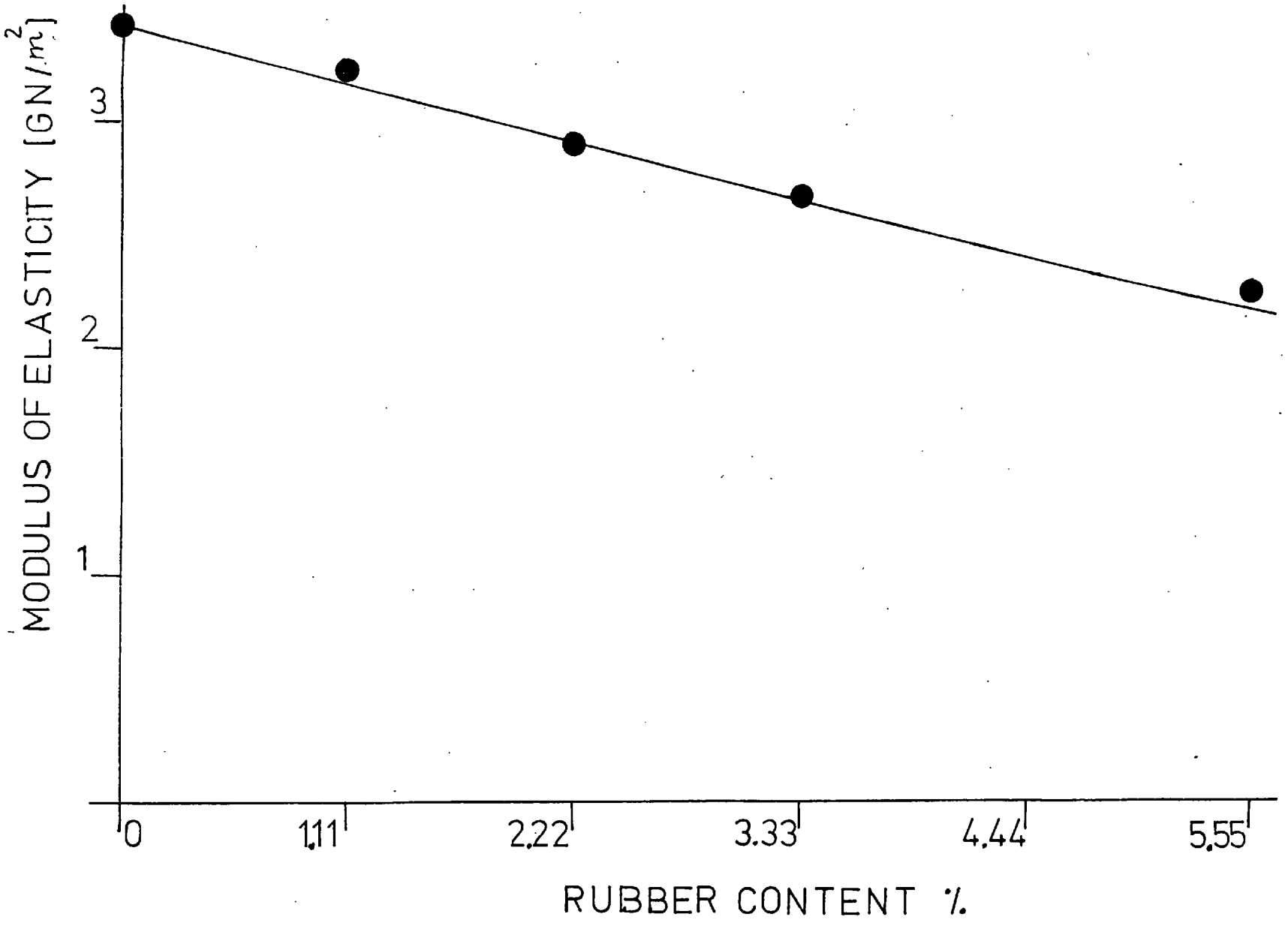


Figure 5.10: Modulus of elasticity versus rubber content

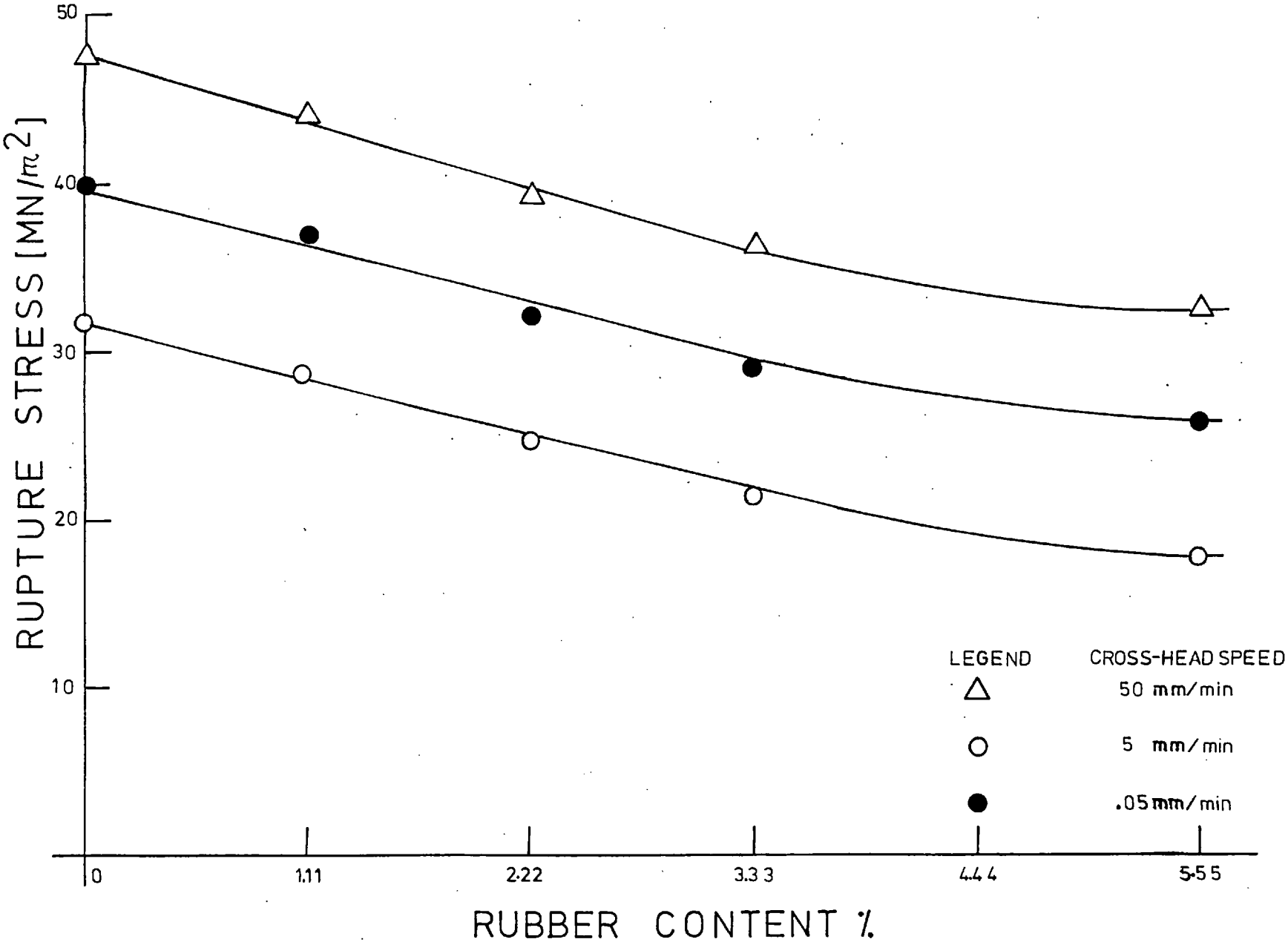


Figure 5.11: The effect of rubber content on the yield stress of HIPS. Each point on the curves represents the average value obtained for a batch of 10 to 15 specimens

where $\tilde{\sigma}_y$ and $\tilde{E}$ are the composite polymer yield stress and modulus, respectively, σ_y and E are those of the PS matrix, respectively, and ϕ is the nominal rubber content. A_o and B_o are constants which may be calculated by employing a least-squares method of fitting through the experimental data. From the experimental results, we get:

$$B_o = 6.8 \quad , \quad A_o = 6.7$$

Hence, approximately:

$$\frac{\tilde{\sigma}_y}{\tilde{E}} \simeq \frac{\sigma_y}{E} \tag{5.4}$$

This relationship implies that the variations in the modulus and yield stress of HIPS, due to rubber content, are nearly identical.

5.5 THEORETICAL PREDICTION OF MODULUS OF ELASTICITY OF COMPOSITE POLYMERS

The purpose of the following discussion is to ascertain an expedient theoretical basis on which accurate assessment of the elastic behaviour of certain composite polymers can be made prior to any experimental analysis. Numerous approximate theoretical models have been proposed to evaluate the moduli of composite polymers from the moduli of their phases and fractions. A literature survey of some widely used theories has been given in Chapter 2; however, there is no general agreement upon which is the most suitable approach.

In order to specify the elastic behaviour of a composite, it is necessary to define two independent stiffness parameters. In the present discussion, the expressions are formulated in terms of shear modulus, $\tilde{\mu}$, and the bulk modulus, $\tilde{k}$, of the composite. The problem is to calculate these moduli in terms of μ_s, k_s, μ_r and k_r (the moduli of the CPS matrix and the rubber inclusion, respectively). Young's modulus and the Poisson ratio can then be evaluated, using the standard elasticity relationships:

$$\tilde{E} = \frac{9\tilde{k}\,\tilde{\mu}}{3\tilde{k} + \tilde{\mu}} \tag{5.5}$$

$$\tilde{\nu} = \frac{3\tilde{k} - 2\tilde{\mu}}{6\tilde{k} + 2\tilde{\mu}} \tag{5.6}$$

5.5.1 Composite Model

Electron microscope studies, described in the preceding sections, provide some useful information about the structure and composition of composite constituent phases. On the basis of this information, the composite polymer is divided into the polystyrene matrix

(characterised by the moduli k_s and μ_s) and the dispersed composite particles (characterised by the moduli k' and μ'). The particle inclusions are, in themselves, subdivided into the rubber matrix (k_r and μ_r) and dispersed polystyrene particles (k_s and μ_s). The volume fraction of composite particles and the volume fraction of occluded polystyrene in these particles are denoted by ϕ_p and ϕ_s, respectively. The fractional volumes are related by:

$$\phi_p = \frac{\phi}{1 - \phi_s} \tag{5.7}$$

where ϕ is the nominal fractional volume of rubber.

On the basis of the above consideration, the moduli of HIPS have been calculated using the theoretical expressions derived by Dewey, Kerner, Hashin, Hill and others*. The properties of the constituent composite phases are assumed to be as follows:

k_s = 3.4 GPa $\qquad$ k_r = 1.9 GPa

μ_s = 1.25 GPa $\qquad$ μ_r = 0.7 MPa

ν_s = 0.335 $\qquad$ ν_r = 0.5

ϕ_s = 0.80 (the fractional volume of the occluded PS in composite particles)

The PS properties quoted above are mainly from the experimental analysis previously described in section 5.4. The moduli of PBD rubber are, however, approximate estimations based on the data from the conventional polymer and rubber handbooks (e.g. Brandrup & Immergut (1974)).

---

* See Chapter 2 (sections 2.3 to 2.5) for the method of derivation of the expressions used in this section and also for the corresponding references.

5.5.2 Bulk Modulus

The calculation of bulk modulus, $\tilde{k}$, of a composite polymer presents no difficulty since the difference between plastic and rubber bulk moduli is not very great. Also, the theoretical expressions derived for the lower and upper bounds of $\tilde{k}$ by Hashin (1962) and those proposed by Dewey (1947) and Kerner (1956b) yield an identical solution. The solution for the modulus of the composite particle is given by:

$$(k'/k_s) = 1 - \frac{(3k_s + 4\mu_r)(1 - k_r/k_s)(1 - \phi_s)}{\left((3k_s + 4\mu_r) - 3(k_s - k_r)\phi_s\right)} \tag{5.8}$$

Substituting for the moduli of the constituent phases, and by assuming $\phi_s = 0.8$, we have:

$$(k'/k_s) = 0.935 \tag{5.9}$$

A similar calculation for the bulk modulus of the overall composite polymer yields:

$$(\tilde{k}/k_s) = 1 - 0.34\phi/(1 + 0.23\phi) \tag{5.10}$$

For the special case of $\phi = 5.55\%$ (analogous to grade U A5.55), we have:

$$(\tilde{k}/k_s)_{\phi=5.55\%} = 0.98 \tag{5.11}$$

Because this fraction is very near to unity, any change in $\tilde{k}$ would be within experimental error and would be undetectable.

5.5.3 Shear Modulus Bounds

The calculation of shear modulus present more formidable difficulties since the shear moduli of the PS matrix is about three orders

of magnitude greater than that of the rubber phase. Moreover, the approximate theoretical expressions derived by various methods for the shear modulus of particulate-filled composites mostly differ greatly. In 1964, Hashin concluded that there is little hope of accurately predicting the elastic behaviour of composite polymers, because many interacting parameters are involved. Since then, numerous approximate theories were proposed to calculate the shear modulus of particulate-filled composites, which are only applicable to certain materials. Among these the more noteworthy theories will be mentioned.

By treating the composite as a set of plates in series and in parallel, the extreme bounds of modulus are defined as:

$$\text{Series (lower bound)} \quad : \quad \bar{\mu}/\mu_s = 1/\left((1-\phi) + \phi/\mu_o\right) \tag{5.12}$$

$$\text{Parallel (upper bound)} \quad : \quad \tilde{\mu}/\mu_s = 1 - (1-\mu_o)\,\phi \tag{5.13}$$

where $\mu_o = \mu_r/\mu_s \simeq 0.56 \times 10^{-3}$. As illustrated in Figure 5.12, these bounds are of very limited value because they are so far apart. Closer bounds for particulate-filled composites with arbitrary, spherical and elliptical particle geometries were obtained by Hashin (1959,1962) and Hashin & Shtrikman (1961,1962,1963). For two-phase particulate-filled composites containing spherical inclusions of a relatively softer material than the matrix, Hashin's lower bound coincides with the approximate equation proposed by Kerner (Hashin (1962)). Assuming an analogous two-stage composite model, as previously described, the shear bounds for modified PS were evaluated. This method was first proposed by Bucknall (1969), who calculated the upper shear bound of HIPS by feeding the upper bound values for the modulus of the composite particle into Hashin's upper

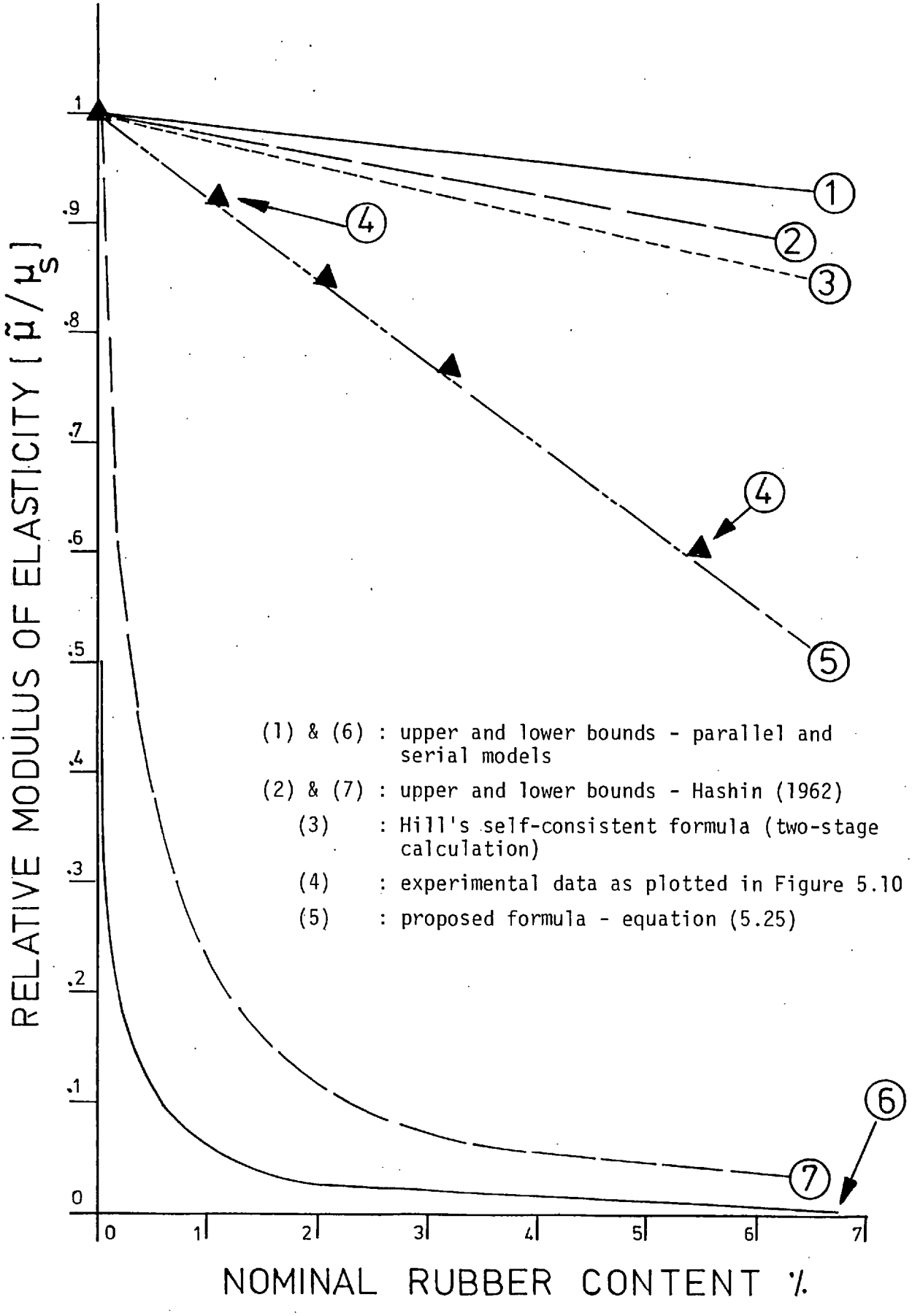


Figure 5.12: The dependence of shear modulus on the rubber content of HIPS

bound formula and, similarly, the lower bound values were fed into the lower bound expressions to evaluate the lower shear modulus. Bucknall's method does not, however, provide a better solution because, using Hashin's theory, a two-stage model calculation would yield the same results as those obtained for a one-stage model. This can be shown as follows:

The upper shear modulus bound for the composite particle is defined by:

$$\mu'/\mu_s = 1 - \frac{(1 - \phi_s)}{(1/(1 - \mu_o) - \alpha_o \phi_s)} \tag{5.14}$$

where:

$$\alpha_o = \frac{6}{5} \frac{k_s + 2\mu_s}{3k_s + 4\mu_s} \simeq 0.466$$

Since $\mu_o = \mu_r/\mu_s \ll 1$, equation (5.14) reduces to:

$$\mu'/\mu_s \simeq 1 - (1 - \phi_s)/(1 - \alpha_o \phi_s) \tag{5.15}$$

The lower shear bound of a composite polymer is obtained by feeding the results from equation (5.15) into Hashin's lower bound formula; hence:

$$\tilde{\mu}/\mu_s = 1 - \phi_p/\left((1 - \alpha_o)/(1 - \phi_s) + \alpha_o \phi_p\right) \tag{5.16}$$

By substituting for ϕ_p from equation (5.7), we have:

$$\tilde{\mu}/\mu_s = (1 - \phi)/(1 + 0.873\phi) \tag{5.17}$$

Similarly, the lower shear bound of the composite polymer is defined by:

$$\tilde{\mu}/\mu_s \simeq 11\ \mu_o \left[\frac{\mu_o + 1 - 3\phi}{\mu_o + 0.182\phi}\right] \tag{5.18}$$

and for $\mu_o << 1$:

$$\tilde{\mu}/\mu_s \simeq 0 \tag{5.19}$$

If a one-stage model is employed, the same results, as defined by equations (5.17) and (5.19), would be obtained. Figure 5.12 shows the Hashin bounds obtained for $\phi_s = 0.8$. Obviously, these bounds are widely separated, and cannot be effectively used for predicting the moduli of rubber-modified composites.

5.5.4 Approximate Expressions for Shear Modulus of Particulate-Filled Composites

There are several approximate theories proposed for the shear modulus of particulate-filled composites (e.g. Hill (1965); Laws (1973, 1974); Budiansky (1965,1970); Halpin (1969)). Among them, the self-consistent expression developed by Hill is mathematically the most acceptable of the available theories (Bucknall (1977)). The solution is known as self-consistent because it satisfies the upper and lower limits of the zero inclusion phase content ($\phi = 0$) and packed inclusions ($\phi = 1$). The main disadvantage of the self-consistent theory is that it generally ignores the possibility of phase inversion in the composite and hence does not distinguish between the dispersion of solid particles in a relatively soft matrix (the case of composite particles in HIPS where the occluded PS phase is floated in PBD), and the dispersion of rubbery particles in a relatively rigid matrix (the case of rubbery particles in HIPS).

Here, the moduli of the HIPS samples are evaluated by using Hill's self-consistent theory. The solution for the composite particle is given by:

$$\frac{\phi_s}{(1 + \mu_o' k_o)} + \frac{(1 - \phi_s)}{(1 + \mu_o' k_o')} + 5 \left[\frac{\phi_s \mu_o}{(\mu_o' - \mu_o)} - \frac{(1 - \phi_s)}{(1 - \mu_o')} \right] + 2 = 0 \qquad (5.20)$$

where:

$$\mu_o' = \frac{\mu'}{\mu_s} \quad , \quad k_o = \frac{4}{3} \left(\frac{\mu_s}{k_s}\right) \quad , \quad k_o' = \frac{4}{3} \left(\frac{\mu_r}{k_r}\right)$$

Substituting for values of μ_s, μ_r, k_s, k_r and ϕ_p in the above expression, and solving the equation by an iteration method, the modulus of a composite particle is obtained as:

$$\mu_o' = \mu'/\mu_s = 0.635 \qquad (5.21)$$

The overall shear modulus of an HIPS composite can then be obtained by substituting for shear and bulk moduli from equations (5.21) and (5.9) in Hill's main formula, thus:

$$\frac{1 - 5\phi}{1 + 0.49\ \mu_o''} + \frac{5\phi}{1 + 0.524\ \mu_o''} + \frac{5\ (1 - 5\phi)}{1.575\ \mu_o'' - 1} - \frac{-\ 25\phi}{1 - \mu_o''} + 2 = 0 \qquad (5.22)$$

where $\mu_o'' = \tilde{\mu}/\mu_s$.

Equation (5.22) can be solved by iteration for different values of ϕ. The solution is shown in Figure 5.12, where it apparently over-estimates the shear modulus of HIPS when compared with the experimental data.

5.5.5 Proposed Method to Evaluate the Modulus of Toughened Polymers

It has been shown that the Hashin and Hill self-consistent theories do not provide accurate expressions for predicting the modulus of rubber modified polymers. As previously noted, the discrepancy in results

is mainly due to the fact that neither of these theoretical approaches accounts for phase inversion within the composite polymer. However, the morphology of HIPS and similar rubber modified polymers clearly show the presence of two different phases within these materials:

1. Composite particles which are composed of relatively rigid PS phases floated in a rubbery media; and

2. The composite polymer aggregate which is composed of PS/PBD particles of a soft nature suspended in a relatively rigid PS matrix.

In order to accurately evaluate the overall composite modulus, the calculation technique should inevitably be based on differing models contrived for composites having rigid fillers (the case of the rubber particle) and soft fillers (the case of the polymer aggregate). The following method is proposed for the prediction of the moduli of rubber modified polymers, taking the above consideration into account.

In the first stage, the modulus of the composite particle is evaluated with the aid of the modified Kerner's theory, as proposed by Lewis & Nielsen (1970) for the dispersion of rigid spherical beads in an elastic matrix. The modified Kerner equation can be put in the form:

$$\left(\frac{\mu'}{\mu_s}\right) = \frac{(1 + \alpha\ \beta\ \phi_s)\ \mu_o}{(1 - \beta\ \psi\ \phi_s)} \qquad (5.23)$$

where:

$$\alpha = \frac{(7 - 5\nu_r)}{(8 - 10\nu_r)}\ ,\quad \beta = \frac{(1 - \mu_o)}{(1 + \alpha\ \mu_o)}$$

and the correction function, ψ, is defined by:

$$\psi = (1 - e^{-\phi_s/(1-\phi_s/\phi_m)})/\phi_s \qquad (5.24)$$

where ϕ_m is the maximum volumetric packing fraction of the spherical dispersed particles. In the case of random suspension of rigid spherical particles in an elastic body, ϕ_m was found to be 0.64 (Scott (1960), and McGeary (1961)). For the special case of PS particles surrounded by a rubbery matrix, ϕ_m can technically approach unity. This is because PS particles are elastic and irregular in shape and may therefore be packed together, separated by only a vanishing film of PBD rubber as the surrounding matrix.

The shear modulus of the composite particle is obtained by substituting for the moduli and fractional volumes of the constituent phases in equation (5.23). Assuming $\phi_m = 1$ and $\nu_r = \frac{1}{2}$:

$$\mu'/\mu_s = 0.0625 \qquad (5.25)$$

In the second stage, the modulus of the composite polymer is evaluated with the help of Hill's self-consistent expression for the suspension of soft particles in an elastic matrix. By inserting the solution (5.25) for the particle's shear modulus and the solution (5.9) for the particle's bulk modulus in Hill's formula, the HIPS shear modulus can be expressed explicitly in terms of the nominal rubber content (assuming $\phi_s = 0.8$) as follows:

$$\frac{1 - 5\phi}{1 + 0.49\ \mu''_o} + \frac{5\phi}{1 + 0.524\ \mu''_o} + 5\left(\frac{1 - 5\phi}{16\ \mu'' - 1} - \frac{5\phi}{1 - \mu''_o}\right) + 2 = 0 \qquad (5.26)$$

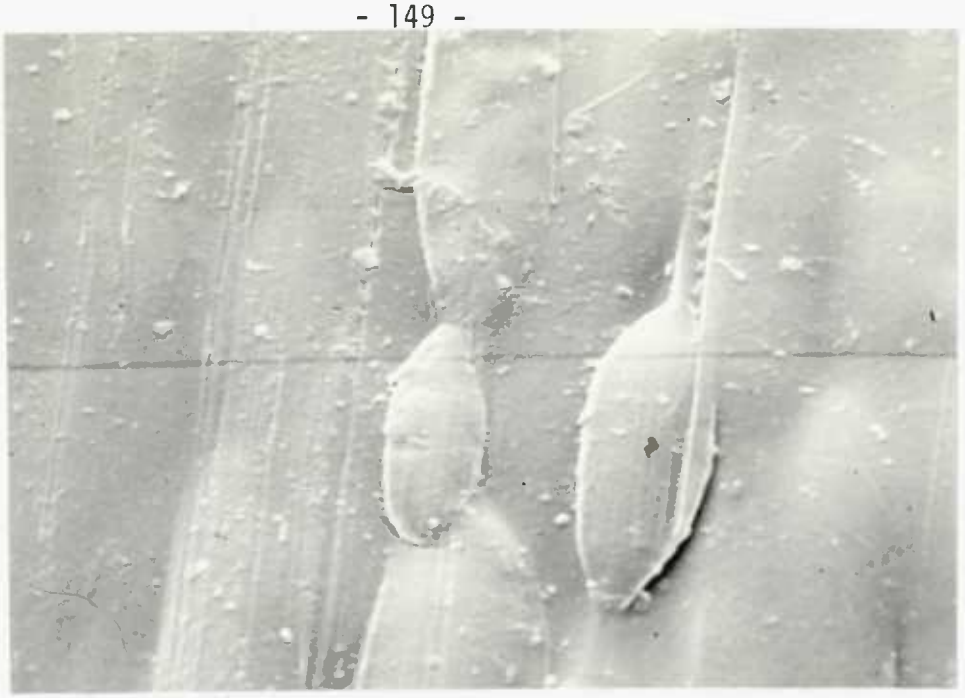
This equation can be solved graphically or by iterative methods. Figure 5.12 compares the experimental data for a specially prepared HIPS containing various rubber contents, the original Hill and Kerner equations, and the proposed theory, as defined by equation (5.26). As demonstrated, the experimental values lie very close to the values calculated by equation (5.26).

5.6 SOME PHYSICAL PARAMETERS AFFECTING THE OVERALL MECHANICAL BEHAVIOUR OF RUBBER MODIFIED POLYMERS

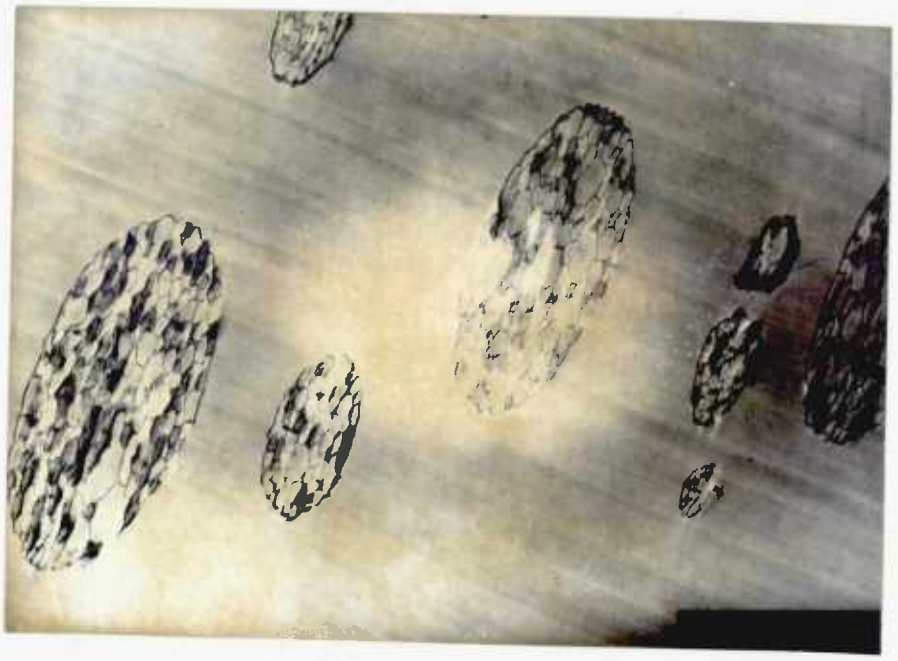
A substantial amount of the inconsistency associated with the physical behaviour of rubber modified polymers is believed to arise from the random variation in the structure of the constituting phases. The following factors are noteworthy:

(a) Adhesivity of rubber particles to the surrounding medium: An imperfect adhesion is usually observed when rubber modified polymers are produced by mechanical blending. The effect is manifested by the appearance of small cavities around the equators of the rubber particles which causes further crack growth. In particular, this is a dominant factor when the material is subjected to impact loads, as will be discussed in Chapter 7.

(b) Distribution and configuration of rubber particles: All the theoretical models neglect the probability of an uneven distribution of the particles in the composite polymer. The problem arises when the concentration of the composite phases differ from one region to another due to the coalescence of a series of neighbouring particles. In addition, to simplify the problem, these ordinary theories assume isotropic suspension of spherical particles in the matrix. However, electron microscope studies of HIPS does not always agree with this assumption, whereas other particle configurations are observed in various grades of the composite, depending on the processing technique. Figure 5.13 is an example of orientated ellipsoidal



A. Scanning electron micrograph (magnification = ×5000)



B. Transition electron micrograph (magnification = ×7500)

Figure 5.13: The dispersion and orientation of ellipsoidal particles in an anisotropic rubber-modified polystyrene

particle distribution in a PS matrix*.

(c) Microscopic craze and crack growth: Intrinsic flows, either produced during the processing of the polymer (due to differences in the thermal expansion coefficients of the composite phases) or as a result of loading, play an important rôle in the overall mechanical properties of the material. This will be studied in section 5.8.

(d) The presence of other additives (such as mineral oil and impurities): The effect of mineral oil on the mechanical and fracture properties of HIPS has been studied experimentally by Boldt (1973) and will not be further expounded in the present discussion (see also section 5.3).

---

* The electron micrographs are obtained by projecting the surfaces of the samples on an oblique plane and, therefore, the picture of the ellipsoidal particles obtained is, to some extent, attenuated in one direction.

5.7 THE DISTRIBUTION OF RUBBER PARTICLES

An accurate formulation of the effect of particle distribution and orientation on the rigidity of composite polymers requires a formidable statistical analysis. The simplified model presented in this section does not provide a precise prediction formula but may only serve as a basis for further discussion on anisotropic composites.

Let us first consider a hypothetical composite containing rectangular parallelepiped particles as shown in Figure 5.14. The particles are assumed to be distributed uniformly in the matrix, where l' and h' denote their horizontal and vertical inter-distances from each other. This model simply presents an anisotropic composite, since its properties depend on the direction chosen. The model can be sub-divided into equal rectangular parallelepiped particles of dimensions $l' \times h' \times h'$, each containing one rectangular parallelepiped particle of dimension $a' \times b' \times b'$. The following assumptions are necessary to develop the hypothesis:

1. Perfect adhesion should exist between constituent phases of the composite;

2. Stress concentration due to the presence of particles is insignificant;

3. The inter-effects between particles are negligible. Thereupon, the total displacement of the composite is simply the aggregate of the displacements of the constituting components.

To evaluate the elongation of each element i, we regard the element as a three-layer sandwich undergoing a uniform traction, σ. The displacement of the two top layers of the sandwich is given by:

$$\Delta_{top} = \frac{\sigma}{E_s} (h' - b') \tag{5.27}$$

The average displacement of the middle layer is determined by satisfying the equilibrium and compatability conditions; thus:

$$\Delta_{mid} = \frac{\sigma\, b'}{E_s} \Big/ \left[1 - (1 - \xi_o)\left(\frac{a'\, b'}{h'\, l'}\right)\right] \tag{5.28}$$

where $\xi_o = E_r/E_s$ (E_r and E_s denote the moduli of rubber and polystyrene, respectively).

If we assume the composite elongation per unit length is determined by the aggregation of the average displacements of each composite element divided by the total length of the sample, L, we have:

$$\tilde{X}_o = \frac{1}{L} \sum_{1}^{L/h'} (\Delta_{top} + \Delta_{mid}) \tag{5.29}$$

Thus, the apparent modulus of the composite model is given by:

$$\left(\tilde{E}/E_s\right) = \frac{1 - (1 - \xi_o)\, \phi_p}{\left(1 - (1 - \xi_o)(\beta_p - \phi_p)\right)} \tag{5.30}$$

where $\beta_p = (a'\, b')/(h'\, l')$, denoting the fractional surface of the particles perpendicular to the applied stress. The upper and lower limits of the relative [illegible] moduli are given by:

$$\text{At } \beta_p/\phi_p = 1 \text{ (upper limit)} \quad : \quad \tilde{E} = E_s\,(1 - \phi_p) + E_r\,\phi_p \tag{5.31}$$

$$\text{At } \beta_p = 1 \text{ (lower limit)} \quad : \quad \tilde{E} = 1/\left[(1 - \phi_p)/E_s + \phi_p\,E_r\right] \tag{5.32}$$

These equations are similar to those previously obtained for shear modulus by treating the composite as a set of parallel and serial plates.

In equation (5.30), the geometry factor β_p can also be construed as the degree of anisotropy of the composite material, since it is parallel to a number of smaller inclusions adhered together, forming orientated particle chains in the matrix (see Figure 5.15). As an approximate solution, the modulus of a composite material containing spherical inclusions can be obtained by substituting for $(\beta_p/\phi_p) = \left[9/16\ (\pi/\phi_p)\right]^{1/3}$ in equation (5.30). For grade U A5.55 of HIPS, we have:

$$d_o = \left(\frac{\beta_p}{\phi_p} - 1\right) = 0.85 \tag{5.33}$$

Figure 5.16 displays the modulus of anisotropic HIPS composites as a function of particle alignment, $d_o = (\beta_p - \phi_p)/\phi_p$ for $\xi_o = E_r/E_s \simeq 0$, and $\phi_p = 27.75\%$ (representing possible types of grade U A5.55 of HIPS). As illustrated in this figure, the composite modulus decreases hyperbolically as the concentration of particles along the planes perpendicular to the applied stress becomes greater. From experimental results, we have:

$$(d/d_o) = \frac{(\beta_p - \phi_p)}{\phi_p} = 1.02 \quad * \tag{5.34}$$

---

* The value of d_o is obtained from Figure 5.16 by substituting for $\tilde{E}/E_s = \xi_o' = 0.647$.

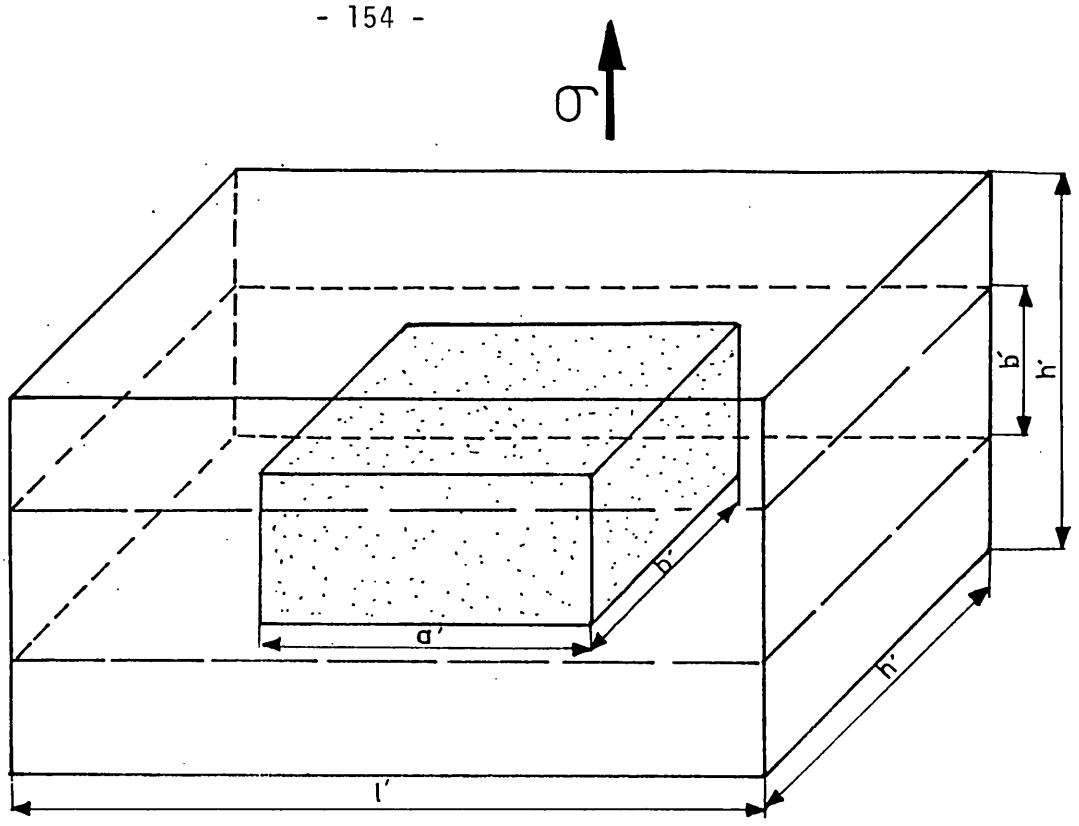


Figure 5.14: Rectangular parallelpiped composite model

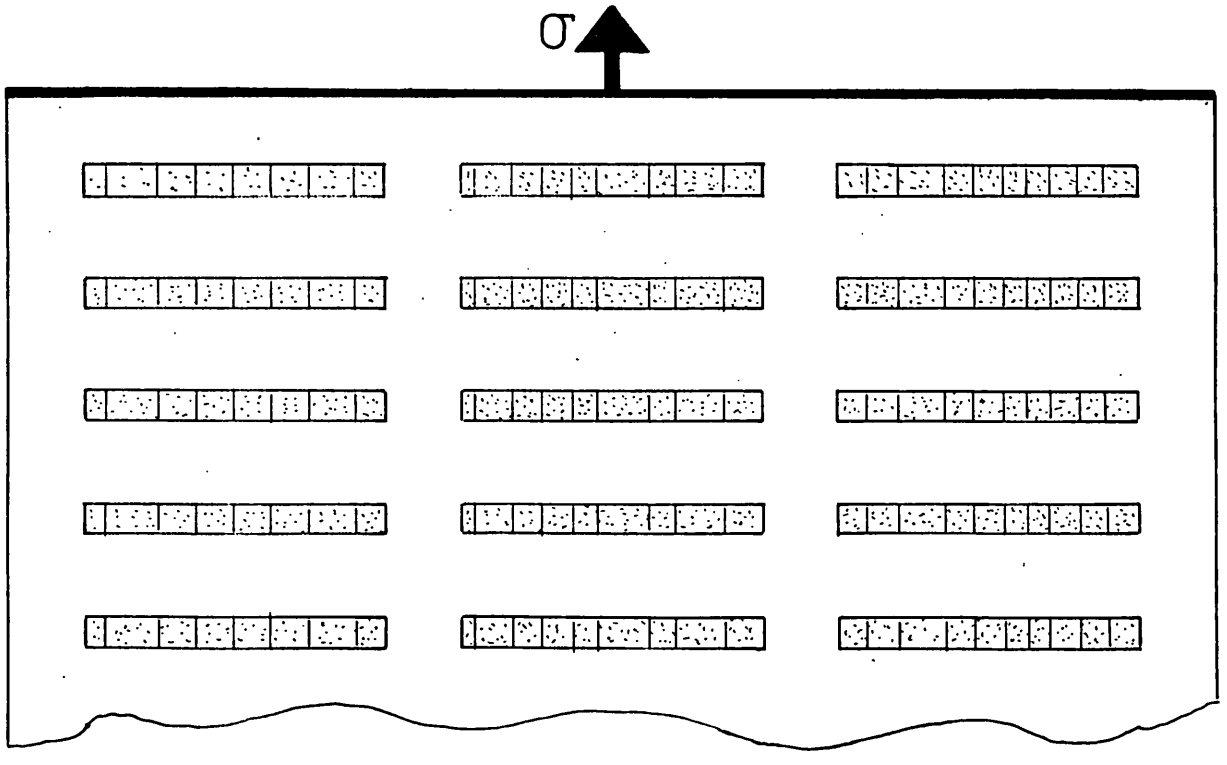


Figure 5.15: An anisotropic composite model containing aligned rectangular inclusion chains (b/a = 0.1)

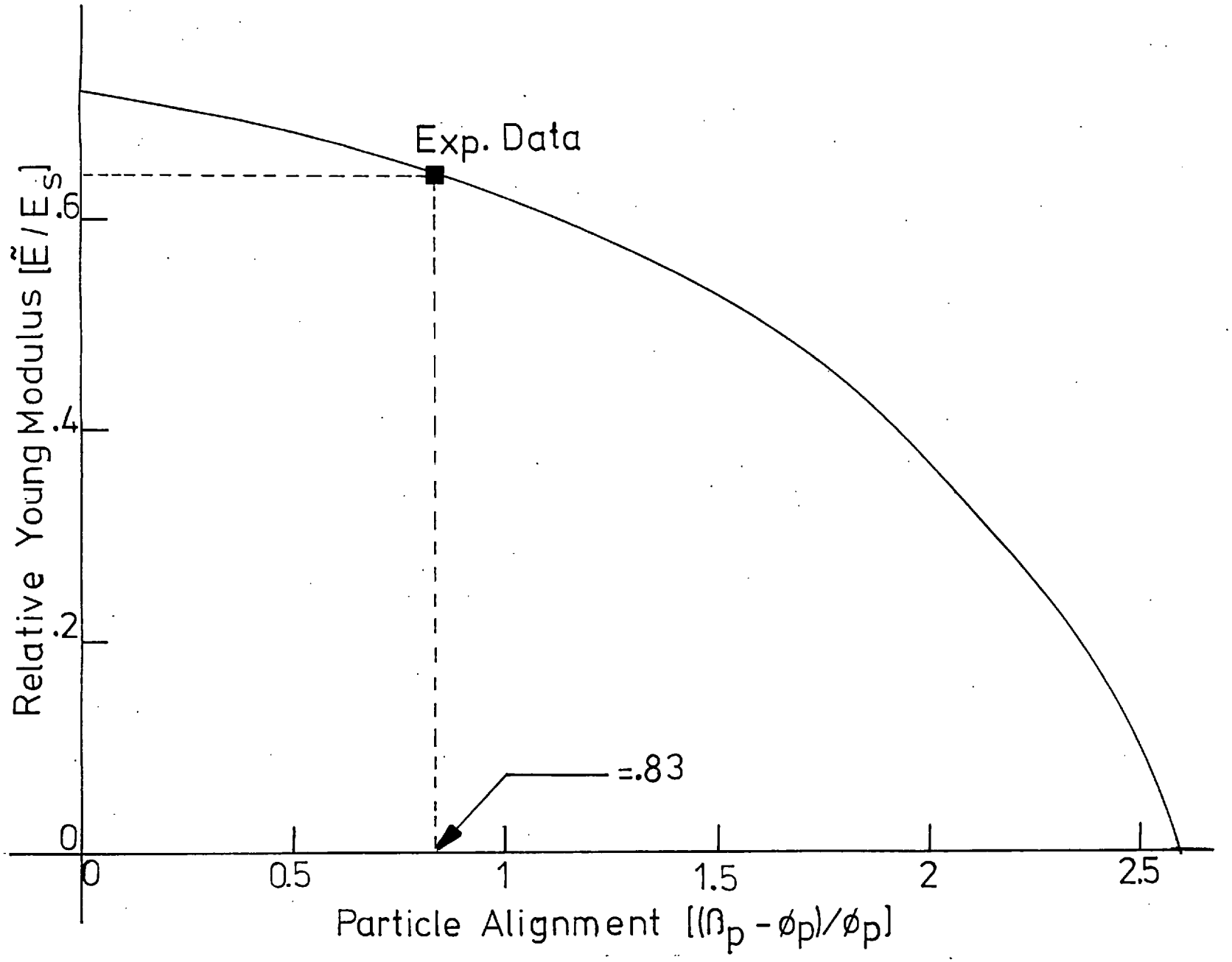


Figure 5.16: The effect of particle alignment on modulus of elasticity of HIPS. The square point corresponds to the experimental value for grade U A5.55 of HIPS

As this ratio is very close to unity, clearly no significant particle orientation should exist in these composite polymers. Therefore, macroscopically, these grades of HIPS may be considered as perfect isotropic materials.

5.8 THE CRAZE EFFECT

As previously discussed, in rubber modified plastics, rubber particles have a dual role of initiating crazes but preventing their propagation by the initiation of fresh crazes at neighbouring rubber particles. For this reason, the toughness of a modified polymer increases many times. To illustrate this phenomenon, the elongation to break (as a qualitative toughness criterion) of several grades of HIPS were measured and compared with that of crystal PS. Consequently, it was shown that the elongation to break of, for example, a grade of HIPS containing 5.55% rubber content was about 27 times greater than that of the parent crystal polymer. The theoretical model developed and discussed in this section provides a basis for the assessment of the composite toughness associated with craze formation around the rubber particles.

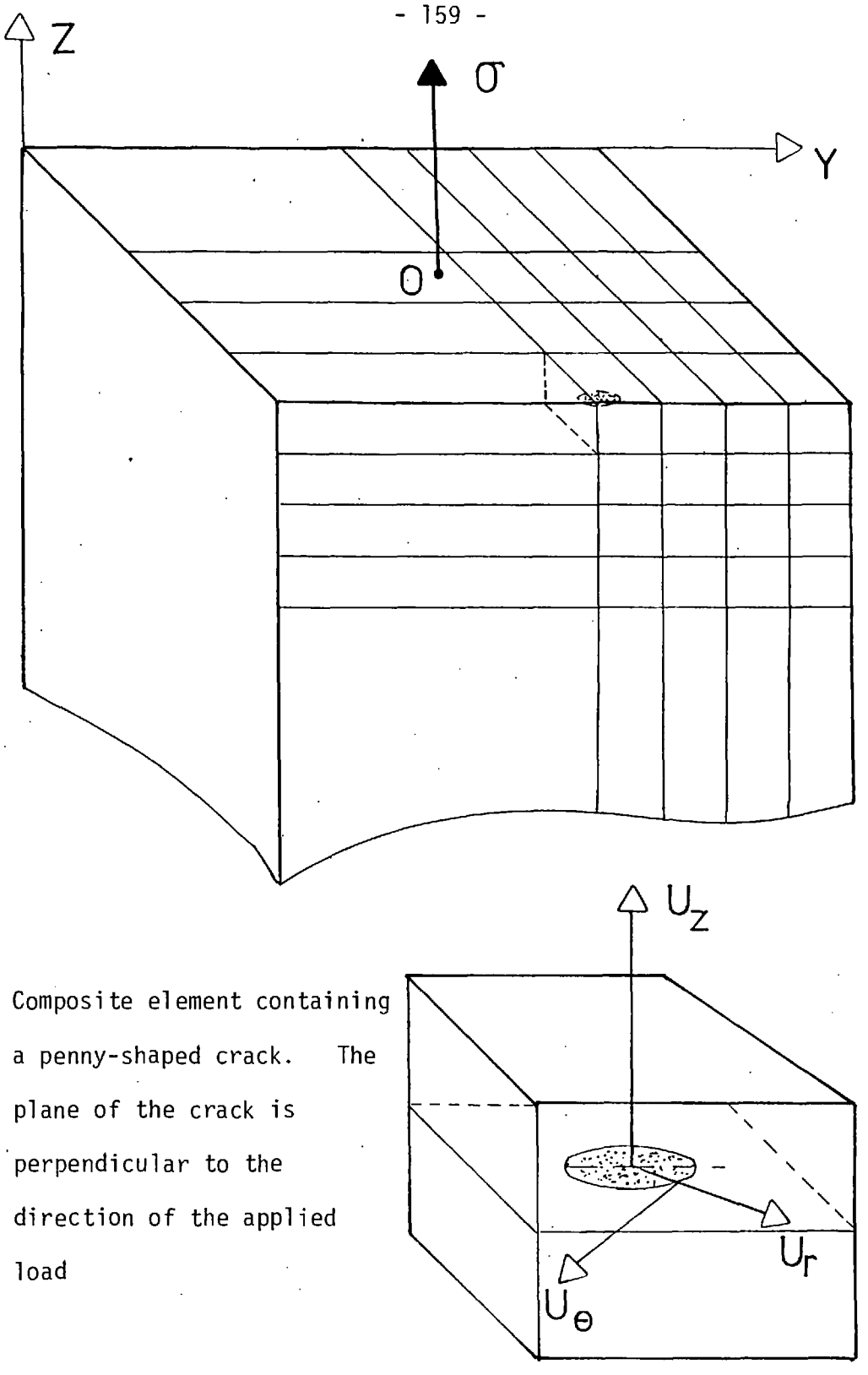
5.8.1 Craze Formation Model

Consider a composite sample subjected to a tensile stress, undergoing substantial craze growth. Electron micrographs of such a material show multiple craze growth perpendicular to the applied stress throughout the specimen (Figure 5.17). The theoretical model, shown in Figure 5.18, is based on a similar empirical concept.

As illustrated, the model contains infinite infinitesimal "penny-shaped" cracks of parallel equatorial planes perpendicular to the applied stress. On the other hand, the model may be regarded as an elastic body containing an infinite number of penny-shaped inclusions which are composed of relatively soft materials (analogous to a crazed media). Denoting δ_o and c as the thickness and the radius of these penny-shaped cracks, respectively, it is assumed that:



Figure 5.17: The scanning electron micrograph of a fully yielded HIPS specimen, showing the multiple craze formation perpendicular to the direction of the applied load



Composite element containing a penny-shaped crack. The plane of the crack is perpendicular to the direction of the applied load

Figure 5.18: Composite model for multiple craze formation in HIPS

$$\delta_o << c$$

In addition, the interaction between the cracks is neglected and therefore the properties of the composite is described by the aggregate of the effects of every isolated crack in an infinite elastic space.

5.8.2 A Single Penny-Shaped Crack in an Infinite Elastic Body

Sneddon (1946) has studied the effect of a single penny-shaped crack on the stress field of an elastic plate undergoing a uniform tensile stress. As a result, the conditions for the rupture of the plate has been deduced.

The cylindrical displacement coordinates, v_r, v_θ and v_z, in the interior of an infinite body due to the presence of a penny-shaped crack with an internal pressure, σ, are given by:

$$v_\theta = 0$$

$$v_r = \frac{2\sigma c}{\pi E}(1+\nu)\int_o^\infty (1 - 2\nu - \zeta\tau)\frac{d}{d\tau}\left(\frac{\sin\tau}{\tau}\right) e^{-\zeta\tau} J_1(\rho\tau)\, d\tau \qquad (5.35)$$

$$v_z = -\frac{4\sigma c}{\pi E}(1-\nu^2)\int_o^\infty \left(1 + \frac{\zeta\tau}{2(1-\nu)}\right)\frac{d}{d\tau}\left(\frac{\sin\tau}{\tau}\right) e^{-\zeta\tau} J_o(\rho\tau)\, d\tau$$

where $\rho = r/c$, $\zeta = z/c$, and r, θ and z are the cylindrical coordinates. E and ν denote the modulus of elasticity and Poisson's ratio of the elastic body, and J_o and J_1 denote the zero and first order Bessel functions of the J-type, respectively.

The boundary conditions in the vicinity of the crack surfaces

are described by*:

$$v_z = 0 \text{ at } z = 0 \ (r > c) \quad , \quad \sigma_z = \sigma \text{ at } z = 0 \ (r < c)$$

The stresses produced due to the presence of the internal crack pressure, σ, will die out in any direction at infinity.

The displacement vector of an infinite body subjected to a uniform stress, σ, can be deduced directly from equations (5.35) by superposing an additional solution due to a uniform tensile stress on the boundary of the elastic body. The boundary conditions will then be given by the following equations:

$$\sigma_z = \sigma \ , \ \sigma_r = \sigma_\theta = 0 \quad \text{at} \quad r = \infty$$
$$\sigma_z = 0 \ , \ \tau_{zr} = 0 \quad \text{at} \quad z = 0 \quad (r < c)$$

and the total displacement vector will be defined by:

$$\begin{aligned} u_\theta &= 0 \\ u_r &= v_r \\ u_z &= \frac{\sigma L}{E} + v_z \end{aligned} \tag{5.36}$$

where L denotes the specimen length.

---

* σ_z, σ_{rz}, σ_θ, and $\tau_{r\theta}$, τ_{rz}, $\tau_{z\theta}$ denote the orthogonal and shear stresses in the media.

5.8.3 An Infinite Number of Penny-Shaped Cracks in an Elastic Body

The composite model containing N ($N \to \infty$) penny-shaped cracks is subjected to a uniform stress perpendicular to the crack planes. The boundary conditions prescribed on the model are given by:

$$\sigma_z = \sigma \ , \ \sigma_r = \sigma_\theta = \tau_{zr} = 0 \quad \text{at} \quad r \to \infty$$

$$\sigma_z = \tau_{zr} = 0 \quad \text{at} \quad z = z_i \ , \ r_i < c \ , \ i = 1, 2, \ldots, N$$

where $z_i = z$ denotes the equatorial planes of the cracks, and r_i denotes the radial distance from the centre of each crack. Similar to the analysis performed by Sneddon, an internal pressure, σ, is first imposed within each crack and thereby the results are superposed on the solutions obtained for a uniformly stressed plate (Figure 5.19).

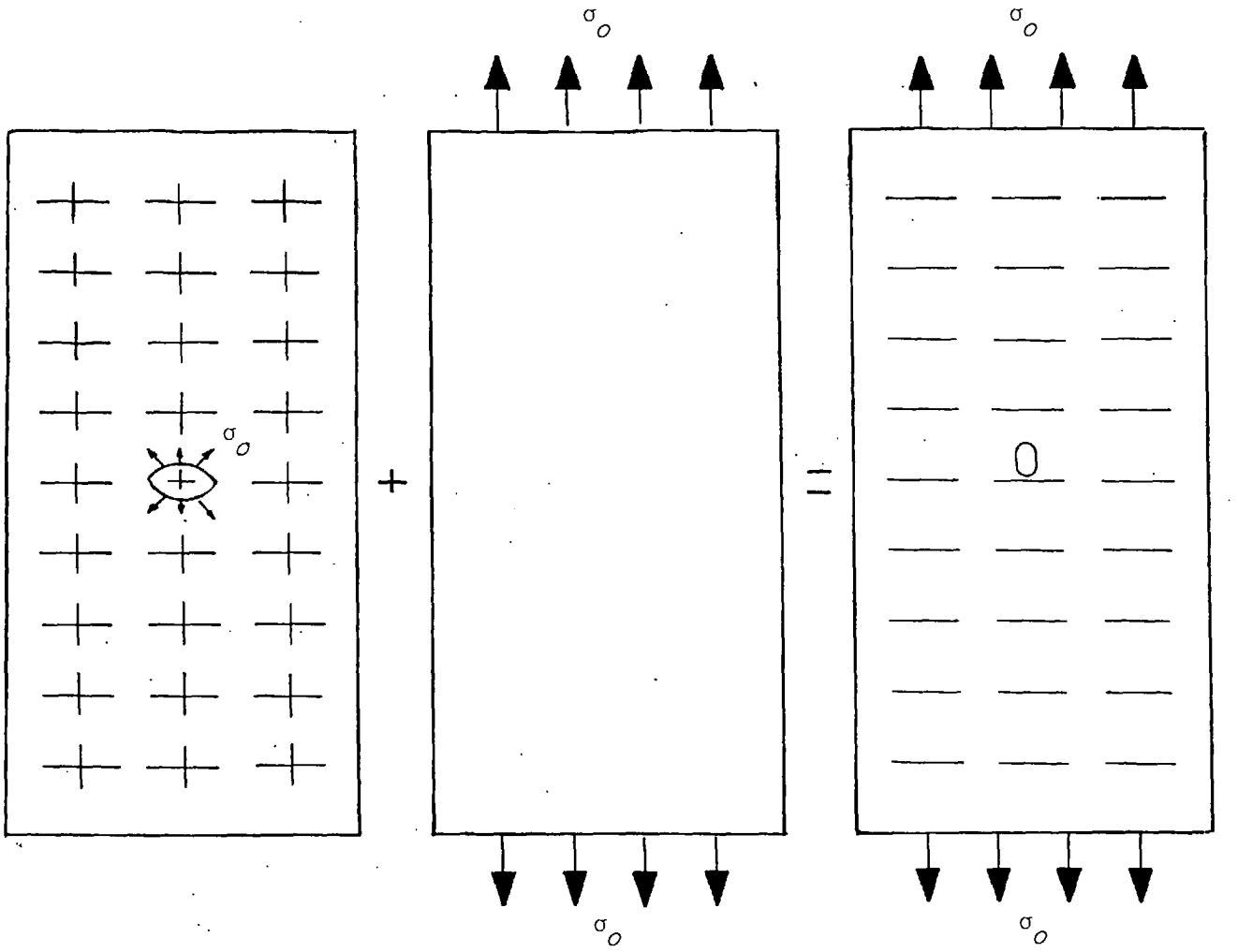
Let v_{zi} be the vertical displacement vector of the centre top point of the composite model (point 0 in Figure 5.18) due to the presence of the ith crack, where its centre is defined by the cylindrical coordinates z_i, r_i and θ_i. The total displacement of the model due to the presence of N particles is determined by the following equation:

$$v_z = \sum_{i=1}^{N} v_{zi}(r_i, z_i) \tag{5.37}$$

Since the cracks are symmetrically dispersed, the vector v_{zi} will remain independent of the angle θ. From the Sneddon analysis (equation (5.35)), we have:

$$v_{zi} = -\delta_o \int_o^\infty \left(1 + \frac{\zeta_i \tau}{2(1-\nu_s)}\right) \frac{d}{d\tau}\left(\frac{\sin \tau}{\tau}\right) e^{-\zeta_i \tau} J_o(\rho_i \tau)\, d\tau \tag{5.38}$$

where $\zeta_i = z_i/c$, $\rho_i = r_i/c$, and $\delta_o = (4\sigma c (1-\nu_s^2))/(\pi E_s)$ (denoting the



Cracks undergoing an internal pressure, σ_o

$v_{zi} = 0$ at $r > c$

$\sigma_{zi} = -\sigma_o$ at $r < c$

Simple tension

$\sigma_{ri} = \sigma_{\theta i} = 0$

$\sigma_{zi} = \sigma_o$

Multi-cracked specimen undergoing a tensile stress, σ_o

$\sigma_{ri} = \sigma_{\theta i} = 0$ at $r = \infty$

$\sigma_{zi} = 0$ at $r < c$

Figure 5.19: The superposition principle in a multi-cracked body

crack opening displacement).

Equation (5.38) can be rearranged in a more convenient form by introducing averaging principles; thus:

$$v_z = \frac{N}{V} \int_V v_z(r,z)\, dV \tag{5.39}$$

where the integration is performed over the volume, V, of the multi-cracked model. Combining equations (5.38) and (5.39), we have:

$$v_z = -\frac{\delta_o N}{V} c^3 \int_o^{\theta_m} \int_o^{\zeta_m} \int_o^{\rho_m} \int_o^{\infty} \rho \left(1 + \frac{\zeta\tau}{2(1-\nu_s)}\right) \frac{d}{d\tau}\left(\frac{\sin\tau}{\tau}\right) e^{-\zeta\tau} J_o(\rho\tau)\, d\tau\, d\rho\, d\zeta\, d\theta \tag{5.40}$$

where $\rho_m = \zeta_m \to \infty$, and $\theta_m = 2\pi$. Performing the integration for ζ and θ, we have:

$$v_z = -\frac{\delta_o c^3 (3 - 2\nu)\, \pi N}{V (1-\nu_s)} \int_o^{\rho_m} \int_o^{\infty} \rho \left(\frac{\tau \cos\tau - \sin\tau}{\tau^3}\right) J_o(\rho\tau)\, d\tau\, d\rho \tag{5.41}$$

To evaluate the above integration, we interchange the variables as:

$$\tau = X \quad , \quad \rho = (Y/X)$$

Hence:

$$v_z = -\frac{\delta_o c^3 (3 - 2\nu)\, \pi N}{V (1-\nu_s)} \int_o^{\infty} \int_{(Y/\rho_m)}^{\infty} Y \left(\frac{X \cos X - \sin X}{X^5}\right) J_o(Y)\, dY\, dX \tag{5.42}$$

The integral (5.42) can be solved analytically, assuming $c \ll 1$ and $\rho_m \to \infty$. After a long calculation, we have:

$$v_z = \frac{\delta_o c^2 (3 - 2\nu_s)\, \pi N}{4 s_o (1 - \nu_s)} \int_o^{\infty} J_o(Y)\, dY = \frac{\delta_o c^2 (3 - 2\nu_s)\, \pi N}{4 s_o (1 - \nu_s)} \tag{5.43}$$

where s_o is the gross cross-sectional area of the cracked model.

The total displacement of the composite model subjected to a uniform tensile stress, σ, is obtained by a simple superposition, as previously described, hence:

$$u_z = \frac{\sigma L}{E} \left(1 + (3 - 2\nu_s)(1 + \nu_s) \frac{N c^3}{V}\right) \tag{5.44}$$

where L denotes the composite dimension along the applied stress. Equation (5.44) gives the elastic deformation of a body containing N circular cracks of radius c subjected to a tensile stress, σ. If we assume that, on average, every rubber particle in the composite polymer causes M_c circular cracks (or crazes) around its equator, and expressing the number of cracks in terms of the true fractional rubber phase volume, we have:

$$u_z/u_o = \left[1 + \frac{3}{4\pi} (3 - 2\nu_s)(1 + \nu_s) \phi_p p M_c\right] \tag{5.45}$$

where $p = (c/o)^3$ denotes the ratio of the crack radius to the particle radius, and u_o denotes the displacement of an uncracked elastic body.

It is now appropriate to compare the experimental results for HIPS (for example, grade U A5.55) with those predicted by the model proposed. If we substitute the values of $\nu_s = 0.33$ and $\phi_p = \phi/(1 - \phi_s) = 0.2775$ in equation (5.45), we have:

$$u_z/u_o = 0.206\ p\ M_c + 1 \tag{5.46}$$

In discussing the craze formation theory in rubber modified polymers, it was stated that particles both initiate and control the craze growth (Bucknall & Smith (1965)). In a material subjected to a tensile

stress, the craze initiated from a particle propagates through the PS matrix and will finally be terminated when the next particle is encountered. In a fully yielded material (at rupture), the average craze length is therefore determined by the average distance between particles. Assuming a random distribution of particles in HIPS, the average distance between particles is approximately given by:

$$\bar{l}_c = 2\{(\tfrac{4}{3}\pi o^3/\phi_p)\}^{1/3} \qquad (5.47)$$

Assuming $\bar{l}_c = c$, equation (5.46) becomes:

$$u_z/u_o = 1 + 25\, M_c \qquad (5.48)$$

Equation (5.48) suggests that, if each particle causes a single circular craze on average, the final elongation at rupture of an HIPS material containing 5.55% nominal rubber content increases almost 26-fold compared to that of CPS. This is in excellent agreement with the experimental results reported in section 5.4.

5.9 CLOSURE

The study of the morphology of various experimental and commercial grades of HIPS reveals the random dispersion of the composite particles, consisting of occluded PS in a rubbery medium. The rubber particles are found to be almost spherical for commercial grades and ellipsoidal in some specially prepared samples.

The effect of rubber content on the mechanical properties of HIPS was studied experimentally. The theoretical discussion which followed has provided some theoretical methods to predict the modulus of rubber modified polymers. Subsequently, the effect of anisotropic dispersion of rubber particles on the overall behaviour of these materials was analysed. Finally, the theoretical model proposed for the determination of the effect of craze formation upon the material elongation to break may be used as a basis to assess the toughness of rubber modified polymers.

CHAPTER 6

THE FRACTURE OF HIPS AT ROOM TEMPERATURE

6.1 INTRODUCTION

The conventional design parameters, based on low strain elastic properties, elongation to failure, yield strength and buckling stress, are often accepted to be fundamental in the selection of materials. On the other hand, an accurate knowledge of the fracture behaviour of materials, especially when subjected to some sort of stress concentrator (e.g. intrinsic flaws) is indispensible to the safe design of any structural body. For rubber modified polymers in particular, the main interest is focused upon the fracture properties of these polymers since they are primarily formulated to overcome the poor fracture resistance encountered in their basic matrices.

In practice, different polymers fracture in a variety of ways because of the nature of the resistance of each of them to the initiation and propagation of the generated cracks. Some polymers (e.g. Perspex (PMMA) and CPS) exhibit a brittle behaviour in fracture, whereas some others fail in a ductile manner (e.g. PVC at room temperature). When materials fail in a brittle manner, the maximum stress is attained prior to yielding and failure occurs due to the propagation of cracks from weakening flaws in the material. The final strength is then predominantly determined by the size, sharpness and other conditions (e.g. environment) of those flaws contained within the material. These cracks usually grow almost instantly and so lead to the rapid rupture of parts below the design criteria based on net section or average stresses.

Ductile materials, however, normally fail at stresses above the yield point and are only slightly weakened by the presence of cracks. In

metallic materials, ductile failure is usually accompanied by work hardening and plasticity. In polymers, the phenomenon of work hardening is associated with the appearance of crazes. A craze is believed to consist of voided regions which always undergo work hardening (Bucknall & Smith (1965); Bucknall & Street (1967); Boyer et al (1970)). As the load increases, the craze will gradually grow around the crack tip and spread through the specimen. This crazing phenomenon blunts the crack tip and thus prevents the material breaking below the yield stress. When the fracture eventually begins, the crack propagation speed will be much smaller than that of brittle materials since a large amount of stressed void regions is produced which acts as a crack inhibitor. For example, when rubber modified PS breaks under ductile conditions, the crack propagation speed does not exceed 30 cm/min in the most unstable situations. On the other hand, when the same material fractures in a brittle manner, the crack speed is usually greater than 100,000 cm/min, which appears to be an instantaneous rupture.

In general, various grades of rubber modified PS behave differently depending on their rubber grafting percentage, particle configurations in the matrix, manufacturing procedure, etc. The main objective of the work to be described in this chapter is therefore to develop an accurate basis on which the ductility or brittleness of HIPS with differing rubber content can be assessed.

For HIPS, the material brittleness can be qualitatively estimated by direct inspection of the fracture surfaces of broken parts of a pre-notched specimen. As previously noted, the craze production in polymers is identified with work hardening and thereby denoting the extent of the material ductility. In HIPS, crazing is manifested by a whitening process and thus an estimate of the amount of work hardening can be obtained by

visual examination. To a first order of approximation, an exact measurement of the craze created ahead of the crack tip can therefore yield a quantitative basis on which to assess the fracture toughness. This can also be estimated theoretically by a hypothetical model (proposed by Dugdale (1960)) as will be shown later.

As stated, the fracture toughness of rubber modified polymers is easy to assess qualitatively by visual inspection as relatively weak materials have a smooth flat fracture with little crazing, whereas the tougher grades normally exhibit considerable plastic deformation. However, the difficulty remains of how to quantify it in a satisfactory manner. The reason for this is due to the fact that these toughened polymers cannot usually be defined clearly as either brittle or ductile, owing to their intricate fracture behaviour. In the case of HIPS, the fracture behaviour largely depends on the test conditions and also the validity of the plane strain assumptions applied to the specimen. Under normal laboratory conditions, successful grades of HIPS mostly break in a ductile manner even at the highest strain rates (Ferguson (1973)). In practice, however, it is occasionally observed that these materials fail in a brittle manner at low stresses.

Therefore, it is important, bearing in mind the uncertainty of fracture behaviour in HIPS, to attempt to forecast the brittle conditions of failure and thereby to determine a genuine estimate of the fracture toughness of different types of HIPS. Such an attempt should examine the effect of specimen geometry and crack configuration, notching technique, environmental conditions (e.g. the application of a constraining media, such as fragile but rigid glues on the initial cracks) and other specific conditions leading to a brittle fracture in HIPS. This should provide a consistent and appropriate method of measuring the fracture toughness by

maintaining the conditions for a brittle failure, which can be extended to appraise the effect of rubber content in HIPS.

6.2 BASIC LINEAR FRACTURE TOUGHNESS CRITERION

In linear fracture mechanics, the stress within a small region near the crack tip can be characterised by a single parameter, such as the stress intensity factor, K. This parameter is a function of the geometry of the cracked body and the applied stress alone, so that the stress field for different geometries varies only in the way K is defined. The linear fracture mechanics criterion postulates that there exists a critical value of the intensity factor at which unstable rupture occurs. This value (i.e. the fracture toughness, K_c) is independent of geometry and loading.

The intensity factor of a pin-loaded single-edge notched specimen is given by:

$$K = \sigma Y \sqrt{a} \tag{6.1}$$

where σ and a denote the current applied stress and crack length, respectively, and Y is the correction factor defined by:

$$Y = 1.99 - 0.41 \left(\frac{a}{D}\right) + 18.70 \left(\frac{a}{D}\right)^2 - 38.48 \left(\frac{a}{D}\right)^3 + 53.85 \left(\frac{a}{D}\right)^4 \tag{6.2}$$

where D is the specimen width along the crack (Brown & Srawley (1966)).

The intensity factor of a pin-loaded semi-elliptic surface notched specimen can be approximately evaluated as follows (Paris & Sih (1965); Smith (1966)):

$$K = \left(1 + 0.12 \left(1 - \frac{a}{b}\right)\right)\left(\frac{2B}{a} \tan \frac{\pi a}{2B}\right)^{\frac{1}{2}} \sigma \sqrt{a}/\Theta \tag{6.3}$$

where a and b are the crack depth and half width, respectively, B is the specimen thickness, σ is the applied gross stress, and the function Θ is given by:

$$\Theta = \left\{\left(\int_{o}^{\pi/2} \left(1 - \frac{b^2 - a^2}{b^2} \sin^2 \theta\right)^{\frac{1}{2}} d\theta\right)^2 - 0.212 \, (\sigma/\sigma_y)^2\right\}^{\frac{1}{2}} \qquad (6.4)$$

where σ_y is the effective yield stress of the material. The accuracy of this equation is about ± 5% if the crack geometry is limited by:

$$\frac{a}{B} \leqslant \frac{1}{2}$$

$$0.1 \leqslant \frac{a}{b} \leqslant 1 \qquad (6.5)$$

In principle, the linear fracture mechanics criterion is only a cogent hypothesis if the material tested behaves in a linear elastic manner and exhibits no more than small scale crazing (or yielding). The applicability of linear fracture mechanics should therefore be restricted by the following inequalities (Weiss & Yukawa (1965); Brown & Srawley (1966); ASTM (1973)):

$$\left(\frac{K_c}{\sigma_y}\right)^2 \leqslant 2.5 \, B \qquad (6.6)$$

$$\left(\frac{\sigma}{\sigma_y}\right) \leqslant 0.75 \qquad (6.7)$$

Expression (6.6) prescribes the plane strain conditions, where the minimum fracture toughness and maximum consistency in the experimental data will be achieved. To satisfy this inequality, the minimum required thickness for commercial types of HIPS must be in the range of 100 mm to 200 mm which is usually impractical. However, as will be shown in later sections of this chapter, the plane strain conditions can satisfactorily be maintained for much thinner materials if wider specimens ($D > a + 4.5$ cm for single-edge notched specimens) are employed.

The inequality (6.7) is, in effect, a prerequisite for brittle fracture in which the failure occurs below a certain stress level (i.e. 0.75 σ_y). On the other hand, if the material is subjected to stresses close to the yielding strength, the final fracture takes place in a ductile manner, and the use of linear fracture theory becomes inappropriate. If the conditions required for brittle fracture are maintained, the K_c criterion can accurately predict the failure of cracked bodies and therefore is a useful engineering tool for both the evaluation of stressed components and the selection of materials. Consequently, the main interest of this study centres upon the brittle fracture of HIPS and the attempt to ascertain the conditions which induce such catastrophic rupture in these materials.

6.3 PREVIOUS STUDIES OF THE FRACTURE OF HIPS

In recent decades, the application of fracture mechanics has been extensively investigated for a wide variety of thermoplastic polymers. In particular, the fracture properties of commercial grades of HIPS have been studied by many researchers, using both linear and yielding fracture criteria (Van den Boogart & Turner (1963); Ferguson et al (1973); Parvin & Williams (1976)). The first of these studies was not conclusive and failed to determine the fracture toughness of both blunt and sharp notched HIPS specimens due to an apparent ductile tearing of the materials.

As far as it is known, the most exhaustive research in this field was carried out by Ferguson (1973), who applied linear and yielding fracture criteria for a medium grade of HIPS. To evaluate the fracture toughness, K_c, Ferguson made use of 50 mm wide single-edge notched and four-point bend specimens. The notches were made using fresh razor blades to sharpen the saw-cuts to the approximately required crack lengths. Although attempts were made to minimise the craze bundle created at the crack tip (which will remove the severity of the notch), the quality of the notch sharpness and therefore the validity of the notching technique employed could not be ratified due to the opacity of HIPS. In his conclusion, Ferguson pointed out that the failure of HIPS cannot be characterised by a linear fracture theory. Consequently, the crack opening displacement (COD) and the Rice path-independent integral (J) criteria were used to obtain a reasonable fit to the experimental data. On the other hand, linear fracture mechanics was proven to be an adequate approach for predicting the initiation of cracking and crazing in these materials.

It is the author's belief that, although the comparison of materials can be done elegantly under ductile conditions using yielding fracture

criteria, the applicability of any fracture parameter obtained in ductile situations to predicting the brittle fracture of these polymers is unclear. In other words, tests on specimens fractured under ductile or brittle conditions may rank materials in different order of merit. As will be shown in later sections of this chapter, a predominantly brittle (or semi-brittle) fracture can be obtained if suitable specimen geometry, crack configuration and environmental conditions are employed. Consequently, the fracture phenomenon can simply be described by a linear fracture criterion and thus avoiding the more intricate parameters, such as COD and J_c.

The second relevant study is due to Parvin (1975) who used single-edge notched and surface notched specimens to investigate the effect of material thickness on the fracture toughness obtained, and found regions of both ductile and brittle failures with a distinct transition between them. He attributed this ductile-brittle fracture transition to a change in the constraint on the crack surfaces which consequently leads to a change in the mode of fracture from plane stress to plane strain. On this basis, two fracture toughnesses were defined for a commercial grade of HIPS, describing the resistance of the material at two extreme modes of fracture, corresponding to fully plane stress and plane strain conditions. Parvin's experimental analysis is based on a modified theoretical model first introduced by Bluhm (1961,1962). Apart from a need to perform a large number of tests for accurately describing the fracture behaviour of materials, the main disadvantage of Parvin's technique rests upon the unjustified modelling assumptions. Hence, the fracture toughnesses of extremes of plane strain and plane stress conditions were computed by extrapolating the experimental data obtained for single-edge notched and surface notched specimens, which are subject to composite plane stress and

plane strain conditions.

Parvin's hypothetical modelling can, however, be avoided if the fracture toughness at the critical plane strain conditions can be directly obtained from the experimental results for brittle fracture, and consequently an experimental programme was devised to attempt to induce failure under fully plane strain brittle conditions.

6.4 EXPERIMENTAL PROGRAMME

6.4.1 Materials

The materials selected in the first part of this work were commercial grades of medium impact PS which were supplied in compression moulded sheets of 1.6 mm, 3.2 mm and 6.4 mm nominal thicknesses. These materials were supplied by the Plastics Division of BP Chemicals Limited and were their grade CP40 (hereafter referred to as BCP) and grade 83CFT (hereafter referred to as BCF). BP quote a medium crack resistance and a medium impact strength for these polymers. Type BCF is, however, usually blended with other grades of HIPS before marketing.

In order to obtain the tensile properties of these materials, they were subjected to tension tests at 1.0 cm/min cross-head speed and the results, together with data quoted by BP (tested at 0.5 cm/min), are as follows:

Tensile Strength at Yield	Grade BCF = 15 MN/m^2 (against 16.2 MN/m^2 from BP) Grade BCP = 20.5 MN/m^2 (against 21.5 MN/m^2 from BP)
Elongation to Break	Grade BCF = 50% (from BP) Grade BCP = 40% (from BP)
Initial Modulus	Grade BCF = 1470 MN/m^2 (against 1560 MN/m^2 from BP) Grade BCP = 2070 MN/m^2 (against 2170 MN/m^2 from BP)
Izod Impact Strength (by BS 2782)	Grade BCP = 60 J/m (from BP) Grade BCF = 101 J/m (from BP)
Particle Size (for BCF)	1-7 microns (mean = 4 microns)
Rubber Type Used (for BCF)	High CIS polybutadiene (BPD)
Grafting Percentage of Particles	20-25% PBD & 75-80% occluded PS
Grafting Procedure (for BCF)	Free radical grafting

The second part of the present work was devoted to the study of the effect of rubber content on the fracture toughness of some specially prepared grades of HIPS (hereafter referred to as U A0, U A1.11, U A2.22, U A3.33, and U A5.55, where the digits following the alphabetical code denote the nominal rubber contents). These materials were supplied in extruded sheets of 3.2 mm nominal thickness by the Chemical Division of the US Steel Corporation. The mechanical and processing specifications of these materials have previously been given in Tables 5.1 and 5.2.

6.4.2 Specimens and Notching Techniques

Ferguson (1973) and Parvin (1975) employed different notching techniques and compared their fracture performance. In the first of these studies, a razor blade (mounted on a jig which was fitted to a Vickers Hardness Testing Machine in order to control the razor blade penetration) was slowly forced into a saw-cut in one edge of the specimen. Although the crack produced by this method was apparently square and sharp, considerable crazing and plastic deformation was observed at the crack tip. The most satisfactory results were later obtained by Parvin using a sharp fly-cutter for notching the specimens. In the present work, preliminary experiments on various types of HIPS have shown that the cracks produced by machining were sharp and, as material was gradually removed by the fly-cutter, no craze or plastic deformation was observed. Figure 6.1 shows the machining technique used.

Single-edge notched specimens were manufactured using a milling machine to the required dimensions (Figure 3.1). Slit gaps of different depths were then machined in one edge of the specimens and the final sharp notches were introduced into the slits using a fly-cutter of a radius of about 50 mm to 75 mm and a wedge angle of about 3^{o} to 4^{o}. The surface

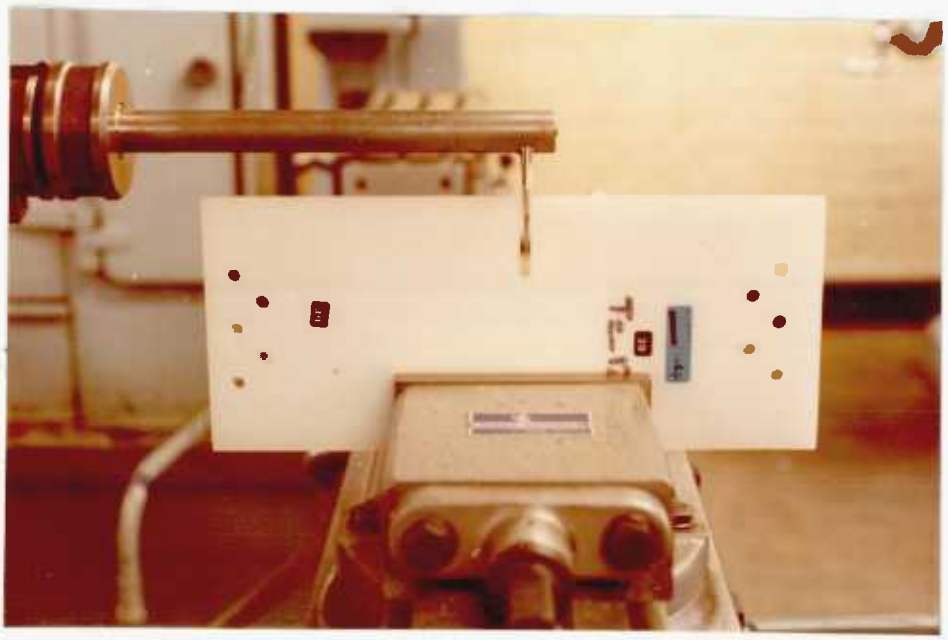


Figure 6.1: Notching technique for single-edge notched specimens

notches were similarly made using a fly-cutter of radius 15 mm to 25 mm and a wedge angle of about 2^{o} to 3^{o} (Figure 3.2).

6.4.3 Test Conditions and Apparatus

All experiments were carried out in an air-conditioned laboratory where the temperature was maintained at $20^{o}C \pm 1^{o}C$ and the relative humidity at about 50%. Specimens were carefully prepared to the required dimensions and notch lengths, and then allowed to normalise at ambient conditions for at least one week prior to performing the tests.

All specimens were loaded on an Instron Universal Testing Machine (capacity 100 KN) that was capable of cross-head speeds of between 0.005 cm/min and 50 cm/min. Initially, the process of craze and crack propagation was carefully observed by use of a travelling microscope and the initiation and propagation points were marked on the Instron chart using an event recorder. In later experiments, a closed circuit TV set and a Video recorder were used and the testing history was then recorded for further analysis. The timing of the TV recorder and the Instron plotter was synchronised by attaching an alarm light to the Instron chart event recorder. Consequently, by turning on a common switch, signals were recorded on both the Instron chart (by the event recorder) and the TV screen (by the alarm light) simultaneously at any required moment.

For measuring the craze and crack parameters (the starting time, the initial lengths, the critical lengths at instability), the results recorded were carefully analysed by replaying the Video tape recorder at one-fifth of the actual recording speed. The pertinent loads at the start of craze and crack growth and at crack instability could then be read directly from the Instron chart, which was synchronised with the TV recorder.

6.5 INDUCEMENT OF BRITTLE FRACTURE BY MEANS OF COVERING THE CRACK

Empirical observations have shown that polymeric structures, such as a pressure gas pipe made of HIPS, are liable to brittle failure when their intrinsic surface cracks come into contact with a fragile glue. This has been explained as follows:

When a crack is covered by a relatively rigid material (even if the crack comprises merely shallow surface scratches), plane strain conditions prevail. As a result, the fracture toughness of the material drops significantly leading to a premature brittle rupture of the article. This phenomenon is sometimes referred to as "sympathetic fracture" since it was believed that the sudden fracture of a relatively ductile polymer was followed by the brittle fracture of the overlaying fragile adhesive.

The aim of this preliminary work was therefore to gain an understanding of the fracture behaviour of a chosen grade of HIPS which was exposed to an Araldite glue.

6.5.1 Glueing Method

The tests were carried out on six batches of surface notched specimens made from a compression moulded sheet of BCP of a nominal thickness of 3.2 mm. The samples were machined in 150 mm × 50 mm dimensions and notches were then produced by using a fly-cutter of a constant radius of R_m = 17.2 mm. The experiments were performed at a medium Instron cross-head speed of e_s = 10 mm/min. In order to analyse the glue coating performance, cracks were covered by a layer of Araldite in six different ways (Figure 6.2):

Batch 1 : No glue was applied

Batch 2 : Two small bulbs of Araldite covered the crack tips only

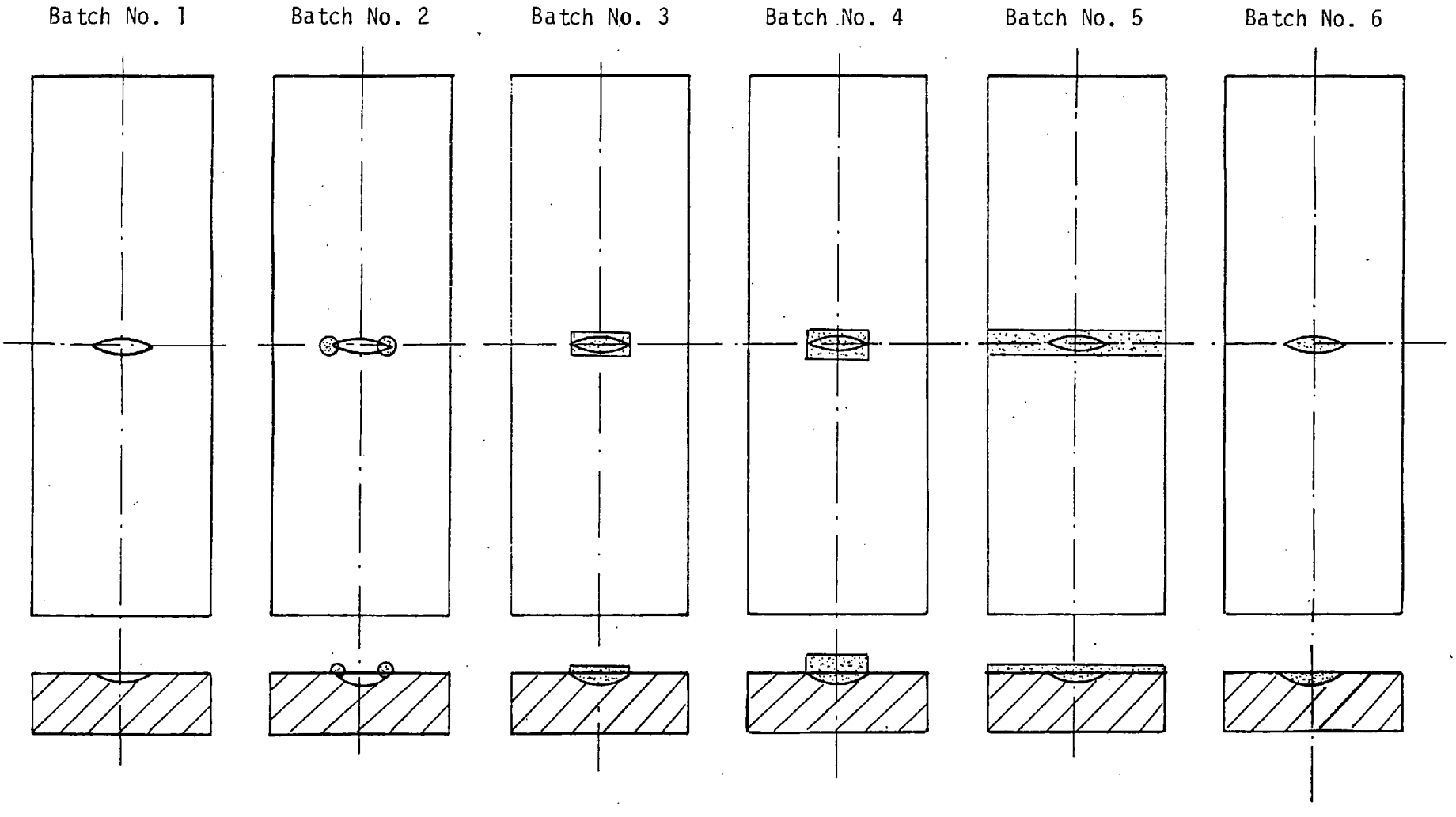


Figure 6.2: Methods of application of Araldite on surface notched specimens

Batch 3 : A thin layer of Araldite, 0.6 mm thick, covered the crack

Batch 4 : A thick layer of Araldite, 1.5 mm thick, covered the crack

Batch 5 : A thin layer of Araldite, 0.6 mm thick, covered the crack and extended to the edges of the specimens

Batch 6 : The crack cavity was filled with Araldite to the specimens' surface level

In order to speed up the Araldite hardening process, all specimens were then heated up in an oven at about $90^{o}C$ for a few hours.

6.5.2 Experimental Results

Taking the initial crack length and the maximum applied load, critical intensity factors were evaluated according to the theory described in the preceding sections. The initial crack dimensions were primarily measured using a scaled microscope. In the case of surface notched specimens, however, a direct assessment of the crack dimensions was sometimes difficult and could be erroneous, particularly for small notches. To overcome the problem, the crack depth, a, and the fly-cutter radius, R_m, were recorded during machining and subsequently the crack width was calculated from the geometry of the crack. The geometry equation is given by:

$$b^2 = R_m^2 - (R_m - a)^2 \qquad (6.8)$$

The experimental results are collated in Tables 6.1 to 6.6. As demonstrated, the scatter in the data obtained is considerable and the

TABLE 6.1: HIPS, Grade BCP

Surface notched specimens of nominal dimensions of 3.2 mm × 50 mm × 150 mm; Material yield stress = 20.5 MN/m^2; Cross-head speed = 10 mm/min; K_c values are evaluated, using the initial crack length and the maximum applied load; Batch No. 1: exposed surfaces.

NO	SPECIMEN WIDTH (CM.)	CRACK WIDTH (CM.)	CRACK DEPTH (CM.)	CRACK RADIUS (CM.)	CRACK AREA (SQ.CM.)	APPLIED LOAD (KG.F)	APPLIED STRESS (KGF/SQ.CM.)	INTENSITY FACTOR (MN/M.**1.5)
1	.320	1.210	.110	1.72	.089	300.	188.	1.32
2	.330	1.425	.155	1.72	.149	322.	195.	1.70
3	.320	1.579	.192	1.72	.204	295.	184.	1.94
4	.350	1.678	.215	1.74	.244	279.	159.	1.79
5	.316	1.816	.259	1.72	.319	265.	171.	2.90
6	.320	1.893	.287	1.70	.369	238.	149.	3.25

LOAD EXCEEDS 3/4 OF THE RELEVANT YIELD STRESS FOR SPECIMENS NO. 1, 2, 3, 5,

MAXIMUM STRESS INTENSITY FACTOR =3.25
MINIMUM STRESS INTENSITY FACTOR =1.32
MEAN STRESS INTENSITY FACTOR =2.15
VARIANCE OF THE STRESS INTENSITY FACTOR RESULTS = .569
STANDARD DEVIATION OF THE RESULTS = .755
STANDARD ERROR OF THE RESULTS = .308
SKEWNESS OF THE RESULTS = .402
KURTOSIS OF THE RESULTS =1.196

TABLE 6.2: HIPS, Grade BCP

Surface notched specimens of nominal dimensions of 3.2 mm × 50 mm × 150 mm; Material yield stress = 20.5 MN/m^2; Cross-head speed = 10 mm/min; K_c values are evaluated, using the initial crack length and the maximum applied load; Batch No. 2: two blobs of Araldite cover the crack tips.

NO	SPECIMEN WIDTH (CM.)	CRACK WIDTH (CM.)	CRACK DEPTH (CM.)	CRACK RADIUS (CM.)	CRACK AREA (SQ.CM.)	APPLIED LOAD (KG.F)	APPLIED STRESS (KGF/SQ.CM.)	INTENSITY FACTOR (MN/M.**1.5)
1	.330	1.245	.118	1.70	.099	338.	205.	1.94
2	.350	1.365	.136	1.83	.127	350.	200.	1.63
3	.340	1.550	.180	1.76	.188	321.	189.	1.83
4	.310	1.672	.212	1.75	.239	263.	165.	2.24
5	.350	1.835	.269	1.70	.335	283.	165.	2.55
6	.340	1.889	.285	1.71	.365	274.	161.	2.96

LOAD EXCEEDS 97% OF THE RELEVANT YIELD STRESS FOR SPECMENS NO. 1, 2, 3, 4, 5,

MAXIMUM STRESS INTENSITY FACTOR =2.96
MINIMUM STRESS INTENSITY FACTOR =1.54
MEAN STRESS INTENSITY FACTOR =2.13
VARIANCE OF THE STRESS INTENSITY FACTOR RESULTS = .309
STANDARD DEVIATION OF THE RESULTS = .556
STANDARD ERROR OF THE RESULTS = .227
SKEWNESS OF THE RESULTS = .275
KURTOSIS OF THE RESULTS =1.215

TABLE 6.3: HIPS, Grade BCP

Surface notched specimens of nominal dimensions of 3.2 mm × 50 mm × 150 mm; Material yield stress = 20.5 MN/m^2; Cross-head speed = 10 mm/min; K_c values are evaluated, using the initial crack length and the maximum applied load; Batch No. 3: a thin layer of Araldite of 0.6 mm thickness covers the crack (but not extended further to the specimen edges).

NO	SPECIMEN WIDTH (CM.)	CRACK WIDTH (CM.)	CRACK DEPTH (CM.)	CRACK RADIUS (CM.)	CRACK AREA (SQ.CM.)	APPLIED LOAD (KG.F)	APPLIED STRESS (KGF/SQ.CM.)	INTENSITY FACTOR (MN/M.**1.5)
1	.320	1.[illegible]2	.110	1.72	.089	343.	214.	1.52
2	.320	1.[illegible]4	.145	1.72	.135	337.	211.	1.79
3	.330	1.[illegible]50	.180	1.76	.168	353.	212.	1.99
4	.330	1.696	.213	1.76	.250	319.	193.	2.30
5	.320	1.795	.251	1.73	.305	265.	166.	2.50
6	.310	1.927	.291	1.74	.381	238.	154.	4.33

LOAD EXCEEDS 97% OF THE RELEVANT YIELD STRESS FOR SPECIMENS NO. 1, 2, 3, 4, 5,

MAXIMUM STRESS INTENSITY FACTOR =4.33
MINIMUM STRESS INTENSITY FACTOR =1.52
MEAN STRESS INTENSITY FACTOR =2.40
VARIANCE OF THE STRESS INTENSITY FACTOR RESULTS =1..15
STANDARD DEVIATION OF THE RESULTS =1.[illegible]7
STANDARD ERROR OF THE RESULTS = .411
SKEWNESS OF THE RESULTS =1.[illegible]
KURTOSIS OF THE RESULTS =2.360

TABLE 6.4: HIPS, Grade BCP

Surface notched specimen of nominal dimensions of 3.2 mm × 50 mm × 150 mm; Material yield stress = 20.5 MN/m^2; Cross-head speed = 10 mm/min; K_c values are evaluated, using the initial crack length and the maximum applied load; Batch No. 4: a relatively thick layer of Araldite, 1.5 mm thick, covers the crack but not extended across the specimen width to its edges .

NO	SPECIMEN WIDTH (CM.)	CRACK WIDTH (CM.)	CRACK DEPTH (CM.)	CRACK RADIUS (CM.)	CRACK AREA (SQ.CM.)	APPLIED LOAD (KG.F)	APPLIED STRESS (KGF/SQ.CM.)	INTENSITY FACTOR (MN/M.**1.5)
1	.320	1.230	.114	1.72	.094	347.	217.	1.55
2	.323	1.460	.165	1.76	.162	350.	219.	1.99
3	.320	1.530	.130	1.72	.106	338.	212.	2.09
4	.320	1.588	.218	1.74	.249	320.	200.	2.41
5	.340	1.800	.254	1.74	.306	337.	198.	2.74
6	.320	1.876	.270	1.76	.343	160.	100.	1.77

LOAD EXCEEDS 3/4 OF THE RELEVANT YIELD STRESS FOR SPECIMENS NO. 1, 2, 3, 4, 5,

MAXIMUM STRESS INTENSITY FACTOR =2.74
MINIMUM STRESS INTENSITY FACTOR =1.55
MEAN STRESS INTENSITY FACTOR =2.09
VARIANCE OF THE STRESS INTENSITY FACTOR RESULTS = .186
STANDARD DEVIATION OF THE RESULTS = .431
STANDARD ERROR OF THE RESULTS = .176
SKEWNESS OF THE RESULTS = .264
KURTOSIS OF THE RESULTS =1.374

TABLE 6.5: HIPS, Grade BCP

Surface notched specimen of nominal dimensions of 3.2 mm × 50 mm × 150 mm; Material yield stress = 20.5 MN/m^2; Cross-head speed = 10 mm/min; K_c values are evaluated, using the initial crack length and the maximum applied load; Batch No. 5: a thin layer of Araldite, 0.6 mm thick, covers the crack and extends further to the edges of the specimen).

NO	SPECIMEN WIDTH (CM.)	CRACK WIDTH (CM.)	CRACK DEPTH (CM.)	CRACK RADIUS (CM.)	CRACK AREA (SQ.CM.)	APPLIED LOAD (KG.F)	APPLIED STRESS (KGF/SQ.CM.)	INTENSITY FACTOR (MN/M.**1.5)
1	.320	1.205	.112	1.68	.091	316.	198.	1.44
2	.330	1.364	.151	1.81	.119	315.	191.	1.53
3	.330	1.595	.133	1.74	.192	300.	132.	1.65
4	.330	1.700	.226	1.71	.260	230.	170.	2.14
5	.340	1.830	.267	1.70	.331	150.	88.	1.40
6	.350	1.685	.277	1.74	.354	204.	117.	1.90

LOAD EXCEEDS 3/4 OF THE RELEVANT YIELD STRESS FOR SPECIMENS NO. 1, 2, 3, 4,

MAXIMUM STRESS INTENSITY FACTOR =2.14
MINIMUM STRESS INTENSITY FACTOR =1.40
MEAN STRESS INTENSITY FACTOR =1.72
VARIANCE OF THE STRESS INTENSITY FACTOR RESULTS = .090
STANDARD DEVIATION OF THE RESULTS = .300
STANDARD ERROR OF THE RESULTS = .123
SKEWNESS OF THE RESULTS = .215
KURTOSIS OF THE RESULTS =1.101

TABLE 6.6: HIPS, Grade BCP

Surface notched specimens of nominal dimensions of 3.2 mm × 50 mm × 150 mm; Material yield stress = 20.5 MN/m^2; Cross-head speed = 10 mm/min; K_c values are evaluated, using the initial crack length and the maximum applied load; Batch No. 6: the crack cavity is filled with Araldite to the specimen surface level.

NO	SPECIMEN WIDTH (CM.)	CRACK WIDTH (CM.)	CRACK DEPTH (CM.)	CRACK RADIUS (CM.)	CRACK AREA (SQ.CM.)	APPLIED LOAD (KG.F)	APPLIED STRESS (KGF/SQ.CM.)	INTENSITY FACTOR (MN/M.**1.5)
1	.330	1.212	.110	1.72	.089	333.	202.	1.42
2	.320	1.417	.148	1.77	.141	314.	196.	1.68
3	.370	1.618	.196	1.77	.214	310.	188.	2.00
4	.320	1.691	.217	1.76	.248	263.	177.	2.13
5	.340	1.791	.252	1.72	.306	286.	168.	2.36
6	.331	1.388	.232	1.72	.361	260.	158.	2.95

LOAD EXCEEDS 3/4 OF THE RELEVANT YIELD STRESS FOR SPECMENS NO. 1, 2, 3, 4, 5,

MAXIMUM STRESS INTENSITY FACTOR =2.95
MINIMUM STRESS INTENSITY FACTOR =1.42
MEAN STRESS INTENSITY FACTOR =2.09
VARIANCE OF THE STRESS INTENSITY FACTOR RESULTS = .288
STANDARD DEVIATION OF THE RESULTS = .537
STANDARD ERROR OF THE RESULTS = .219
SKEWNESS OF THE RESULTS = .302
KURTOSIS OF THE RESULTS =1.571

apparent fracture toughnesses show a strong dependence on the initial cracks whereas, if the theory is valid, fracture toughness should be independent of notch configuration. As the matter stands, a statistical analysis of the results can provide a comparative basis upon which the consistency of the data obtained can be verified. Hence, the mean value, standard error, skewness and the Kurtosis of the results were evaluated and noted below the tables.

When no glue was applied, all specimens failed in a ductile manner with a large amount of crazing produced prior to final fracture. In the best cases, when the glue was spread over the crack and extended to the specimen edges (Case 5), the fracture occurred in a semi-brittle manner with a limited amount of observable craze and slow crack growth.

In Figure 6.3, the applied stress at fracture is plotted versus the initial crack lengths for specimens having different glue coating procedures. As shown, the data are scattered between the line of yield stress (i.e. the net stress with reference to the material ultimate stress) and the fracture mechanics criterion (i.e. the fracture toughness with reference to the mean experimental value). However, when no glue was used, the values of the maximum applied stresses were closer to the yield stress line whereas, in Case 5, the results indicate a relative accuracy of the linear fracture mechanics criterion, particularly for specimens with longer cracks. Moreover, the lowest fracture toughness (K_c = 1.7 MN/m$^{3/2}$) and minimum standard error (S_e = 0.123 MN/m$^{3/2}$) were obtained when the crack was covered by Araldite, as in Case 5.

As a conclusion to the work described, it can be noted that, even if a thin layer of a relatively hard material properly covers the crack surfaces of an ostensibly ductile polymer, plane strain conditions would prevail, thereby leading to a brittle (or semi-brittle) fracture of

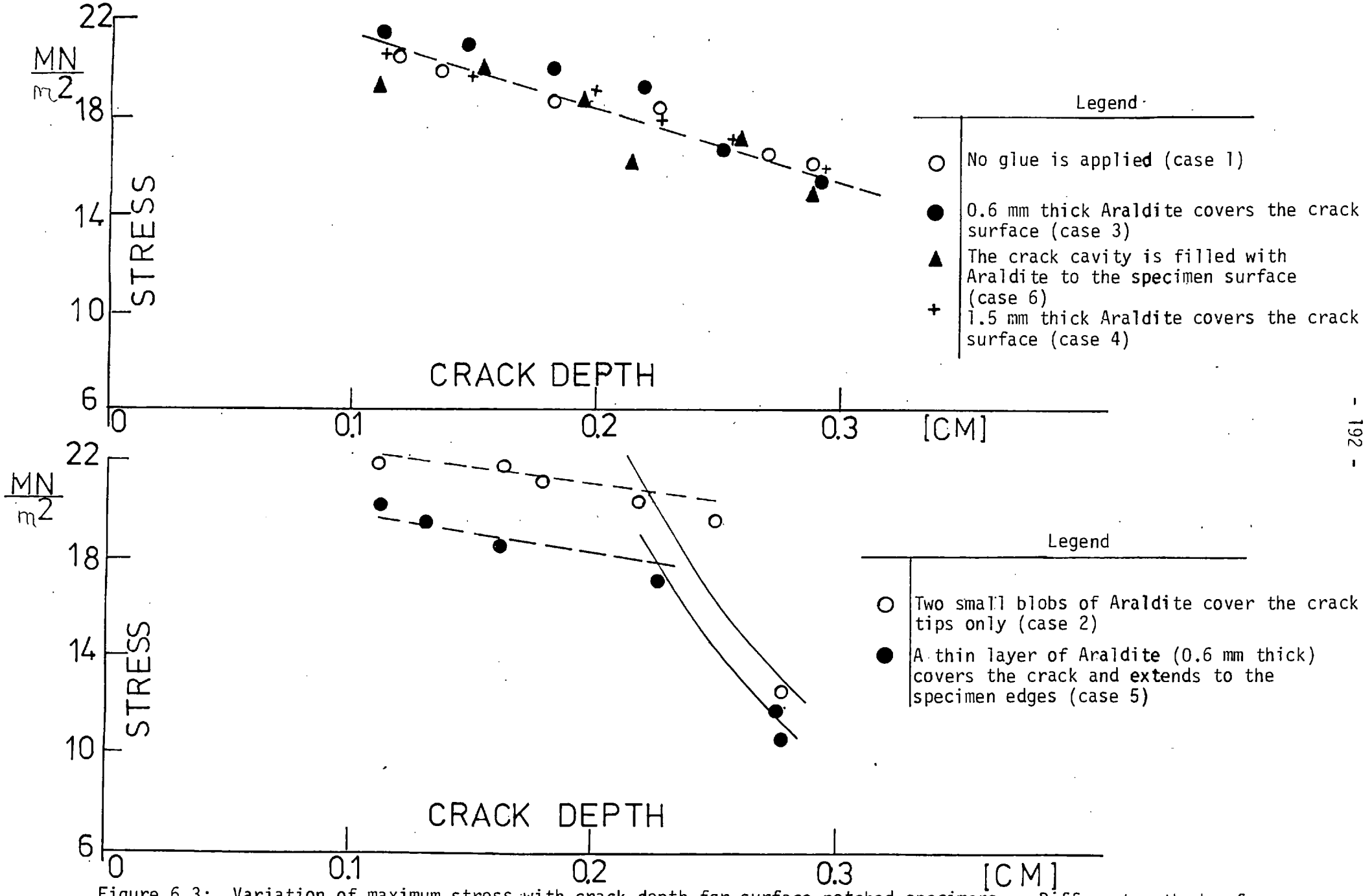


Figure 6.3: Variation of maximum stress with crack depth for surface notched specimens. Different methods of crack constraint by Araldite glue are compared.

the article. However, the poor consistency of the data presented prevents an accurate assessment of the fracture toughness of the materials tested.

6.6 THE EFFECT OF NOTCH GEOMETRY

As previously discussed, the plane strain mode of fracture requires the least energy to cause failure and, to maintain the plane strain conditions, the strength of the constraint on plastic flow at the crack tip must be enhanced. Since, in a relatively thin material, plane strain conditions do not exist across the whole thickness, a layer of fragile and rigid adhesive was applied on the specimen surfaces to strengthen the overall rigidity of the material through the thickness. Nevertheless, if the fracture toughness has to be evaluated, the reinforcement method does not provide a satisfactory solution since the normal stress field around the crack tip will be affected by the presence of the hardener.

On the other hand, in Chapter 3 it was shown that the extent to which the plane stress effect penetrates the thickness is determined by the plastic radius, $r_p = 1/2\pi\ (K_c/\sigma_y)^2$. If this constitutes a considerable proportion of the thickness, the apparent K_c evaluated is a composite quantity made up of contributions from the plane strain fracture toughness, K_{1c}, relevant to the brittle mode of fracture in the mid-thickness layer and the plane strain fracture toughness, K_{2c}, relevant to the ductile mode of fracture in the outer layers of the specimen. The apparent fracture toughness obtained is therefore a function of K_{1c} and K_{2c} and is strongly influenced by the effective thickness of the material. In the extremes, K_{1c} and K_{2c} are measurable for infinitely thick and infinitely thin materials. Otherwise, as discussed by Parvin (1975), these values can be calculated indirectly from two sets of data collected from specimens containing different crack geometries using equations (3.30) and (3.31).

The subsequent experiments to be described in this section form an attempt to investigate the effect of crack geometry on the fracture mode of HIPS, using single-edge notched and surface notched specimens. The

thickness effect will then be analysed by the comparison of the results obtained for different crack geometries.

6.6.1 Surface Notched Specimens

Surface notched specimens were manufactured to the dimensions of 150 mm × 50 mm from compression moulded sheets of 3.2 mm nominal thickness. Notches were produced using a fly-cutter of radius 22.64 mm. Observation of the crack tip was found difficult because of the opacity of the material and the particular crack configuration thus making it impossible to decide when crazing or slow crack growth initiated.

In general, the fracture behaviour can be classified as nearly ductile in which the final failure was abrupt, but large scale crazing and limited slow crack growth took place. The experimental results are collated in Table 6.7 which again displays a large discrepancy from the K_c criterion. In contrast, with few exceptions, the net stress at rupture approximately coincides with the yield stress of the material.

If an apparent fracture toughness is computed from the data, then the average value is found to be about 1.9 $MN/m^{3/2}$. Figure 6.4 shows the experimental results on a plot of the maximum stress versus the initial crack length. The large devivation from the average K_c curve clearly indicates the inadequacy of the K_c criterion employed.

6.6.2 Single-Edge Notched Specimens

Thirty five specimens of approximate dimensions of 150 mm × 50 mm were machined from 3.4 mm thick compression moulded sheets and the notches were produced using a sharp fly-cutter of radius 50 mm. Tests were carried out at 1 cm/min Instron cross-head speed and the fracture process was carefully observed using a travelling microscope and

TABLE 6.7: HIPS, Grade BCP

Glue-free surface notched specimens of nominal dimensions of 3.2 mm × 50 mm × 150 mm; Material yield stress = 20.5 MN/m^2; Cross-head speed = 10 mm/min; K_c values are evaluated, using the initial crack length and the maximum applied load.

NO	SPEC. THICK. (CM.)	CRACK LENGTH (CM.)	SP. WIDTH (CM.)	SP. RADIUS (CM)	C.S. AREA (SQ. CENTIMS)	APPL. LOAD (KGF.)	GROSS STRESS (KGF./SQ.CM)	NET STRESS (KGF/SQCM)	INTENS. FACT. (MN/M**3/2) (S/ZI)
1	.339	.067	1.234	2.15	4.24	282.	169.	177.	1.875
2	.337	.088	1.285	2.19	5.13	253.	153.	161.	1.637
3	.356	.115	1.304	2.17	6.14	277.	153.	169.	1.172
4	.326	.115	1.417	2.24	6.62	235.	239.	224.	1.563
5	.316	.118	1.429	2.22	7.28	335.	216.	233.	1.645
6	.335	.125	1.452	2.26	7.09	351.	213.	229.	1.625
7	.320	.128	1.510	2.29	8.24	336.	210.	228.	1.662
8	.344	.130	1.503	2.23	7.73	347.	205.	222.	1.643
9	.311	.133	1.498	2.18	8.74	300.	196.	215.	1.626
10	.308	.133	1.505	2.20	8.37	310.	205.	225.	1.694
11	.364	.143	1.569	2.21	8.82	355.	195.	218.	1.709
12	.355	.154	1.615	2.19	9.57	300.	172.	190.	1.527
13	.338	.158	1.683	2.32	10.79	317.	191.	214.	1.746
14	.330	.155	1.624	2.32	12.01	316.	195.	219.	1.793
15	.349	.168	1.732	2.32	11.39	355.	207.	234.	1.964
16	.338	.170	1.721	2.26	11.83	334.	201.	225.	1.943
17	.327	.175	1.799	2.32	12.94	280.	174.	200.	1.748
18	.318	.178	1.791	2.34	14.15	298.	182.	223.	1.988
19	.318	.184	1.800	2.29	14.24	275.	176.	205.	1.855
20	.337	.187	1.805	2.27	13.70	265.	163.	185.	1.671
21	.323	.200	1.804	2.27	15.30	275.	175.	208.	1.986
22	.324	.205	1.893	2.29	16.46	285.	179.	214.	2.079
23	.329	.208	1.858	2.29	16.52	285.	176.	211.	2.061
24	.332	.212	1.936	2.30	16.83	310.	190.	229.	2.255
25	.346	.218	1.862	2.10	16.89	283.	169.	202.	2.016
26	.343	.223	1.957	2.26	17.44	312.	184.	223.	2.266
27	.348	.225	1.961	2.25	17.39	309.	179.	216.	2.192
28	.342	.229	2.025	2.35	18.58	269.	157.	195.	2.117
29	.329	.231	2.022	2.34	19.76	282.	177.	220.	2.365
30	.343	.233	2.063	2.32	19.69	309.	178.	220.	2.329
31	.345	.238	2.043	2.31	19.32	290.	171.	214.	2.254
32	.347	.247	2.083	2.32	20.34	293.	172.	216.	2.378
33	.327	.249	2.031	2.32	21.84	280.	174.	225.	2.602
34	.347	.253	2.124	2.31	21.05	303.	177.	224.	2.537
35	.330	.273	2.169	2.24	25.02	267.	155.	220.	3.058

Maximum evaluated K_c = 3.07 MN/m$^{3/2}$; Minimum evaluated K_c = 1.04 MN/m$^{3/2}$; Mean evaluated K_c = 1.92 MN/m$^{3/2}$; Variance of results = 0.183 (MN)^2/m^3; Standard deviation = 0.428 MN/m$^{3/2}$; Standard error = 0.072 MN/m$^{3/2}$; Skewness of the results = 0.181 (MN)^3/m$^{9/2}$; Kurtosis of the results = 3.216 (MN)^4/m^6.

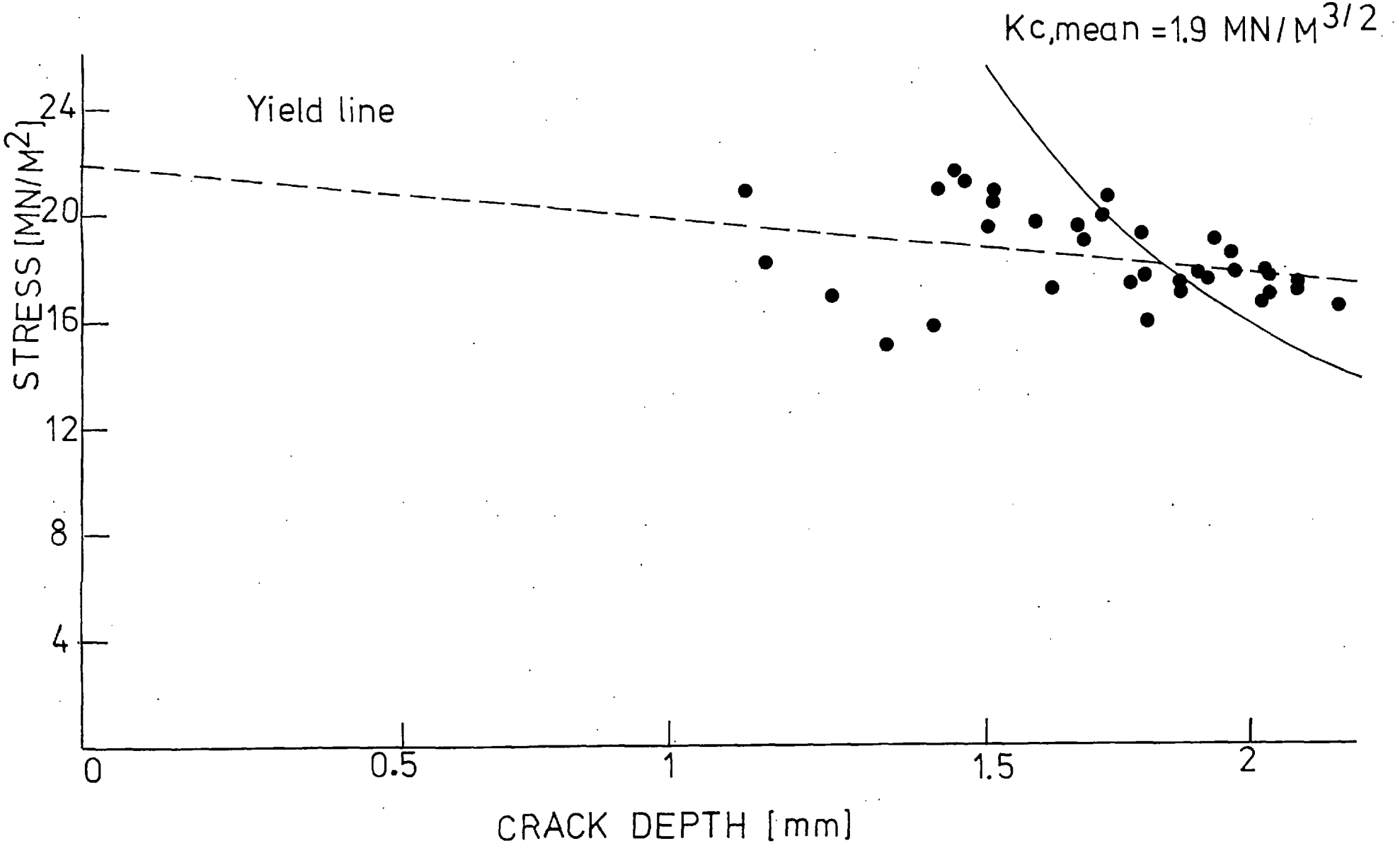


Figure 6.4: Variation of the applied stress with notch depth for 50 mm wide surface notched specimens

a closed circuit TV recorder. It was then possible to determine the load at craze initiation, crack initiation and the onset of rapid crack growth. All specimens exhibited a ductile failure with gross yielding.

The stress intensity factors were evaluated at the maximum applied stress, crack initiation and craze initiation. The results are collated in Tables 6.8 to 6.10. From these tables, it is clear that the K_c criterion cannot be applied at either crack initiation or final fracture since the derived values of K_c are not consistent. Moreover, the mean apparent fracture toughness computed from the data at maximum applied load is found to be considerably larger than that evaluated for surface notched specimens, having a mean value of K_c = 3.5 MN/m$^{3/2}$ (against a mean value of K_c = 1.9 MN/m$^{3/2}$ for surface notched specimens). On the other hand, linear fracture mechanics theory provides an approximately accurate criterion for craze initiation ($K_{c_{craze}}$ = 1.27 ± 0.06 MN/m$^{3/2}$).

The net stress at failure against the initial crack length is shown in Figure 6.5 and, since the results are scattered between the mean fracture toughness curve and the yield stress line, the failure cannot be considered to be either brittle or ductile but it rather demonstrates a composite mode of fracture.

TABLE 6.8: HIPS, Grade BCP

Glue-free single-edge notched specimens of nominal dimensions of 3.2 mm × 50 mm × 150 mm
Material yield stress = 20.5 MN/m^2; Cross-head speed = 10 mm/min; K_c values are evaluated, using the initial crack length and the maximum applied load.

NO	SPECIMEN THICK (CM)	CRACK LENGTH (CM)	CRACKED AREA PROPORTION (PER CENTAGE)	APPLIED LOAD (KGF.)	GROSS STRESS (KGF./SQ.CM)	NET STRESS (KGF/SQ.CM)	INTENSITY FACTOR (M.N/M.**(3/2))
1	.340	.207	4.22	343.	206.	215.	1.84
2	.333	.307	6.27	343.	208.	222.	2.30
3	.315	.355	7.27	305.	191.	206.	2.29
4	.333	.405	8.27	315.	191.	200.	2.46
5	.339	.469	9.57	295.	173.	196.	2.58
6	.340	.537	10.35	325.	191.	213.	2.81
7	.350	.555	11.35	318.	185.	209.	2.96
8	.346	.611	12.47	304.	173.	205.	2.95
9	.353	.661	13.49	297.	173.	200.	3.04
10	.347	.710	14.49	299.	176.	206.	3.24
11	.336	.746	15.22	284.	170.	207.	3.35
12	.338	.767	15.65	274.	165.	196.	3.22
13	.344	.787	16.06	265.	157.	187.	3.12
14	.335	.811	16.55	287.	175.	210.	3.55
15	.322	.841	17.16	265.	163.	203.	3.51
16	.337	.769	15.69	276.	168.	200.	3.23
17	.330	.913	18.57	282.	174.	214.	3.59
18	.353	.925	18.88	287.	167.	206.	3.77
19	.336	.941	19.20	249.	154.	191.	3.52
20	.348	.959	19.76	295.	175.	219.	4.10
21	.340	.984	20.09	257.	154.	193.	3.66
22	.326	1.013	20.67	245.	153.	193.	3.73
23	.322	1.043	21.35	242.	153.	195.	3.83
24	.336	1.053	21.30	240.	145.	185.	3.63
25	.352	.934	20.29	275.	159.	200.	3.81
26	.355	1.134	23.14	257.	146.	190.	3.93
27	.349	1.044	21.33	208.	168.	214.	4.22
28	.339	1.170	24.14	261.	159.	205.	4.41
29	.323	1.133	22.14	250.	159.	205.	4.12
30	.322	1.234	24.53	223.	133.	185.	4.01
31	.342	1.257	25.86	205.	133.	187.	4.14
32	.333	1.315	26.64	237.	145.	195.	4.51
33	.330	1.352	27.83	230.	139.	193.	4.58
34	.339	1.414	28.96	207.	129.	179.	4.15
35	.336	1.513	29.73	233.	141.	197.	4.84

Maximum evaluated K_c = 4.51 $MN/m^{3/2}$; Minimum evaluated K_c = 1.84 $MN/m^{3/2}$; Mean evaluated K_c = 3.48 $MN/m^{3/2}$; Variance of results = 0.455 $(MN)^2/m^3$; Standard deviation = 0.675 $MN/m^{3/2}$; Standard error = 0.114 $MN/m^{3/2}$; Skewness of results = - 0.602 $(MN)^3/m^{9/2}$; Kurtosis of results = 2.470 $(MN)^4/m^6$.

TABLE 6.9: HIPS, Grade BCP

Glue-free single-edge notched specimens of nominal dimensions of 3.2 mm × 50 mm × 150 mm; Material yield stress = 20.5 MN/m^2; Cross-head speed = 10 mm/min; K_c values are evaluated, using the initial crack length and the maximum applied load at crack growth.

NO	SPECIMEN THICK (CM)	CRACK LENGTH (CM)	CRACKED AREA PROPORTION (PER CENTAGE)	APPLIED LOAD (KGF.)	GROSS STRESS (KGF./SQ.CM)	NET STRESS (KGF/SQ.CM)	INTENSITY FACTOR (N.M**-3/2)
1	.340	.287	6.22	340.	204.	213.	1.92
2	.333	.[illegible]	6.27	320.	196.	209.	2.16
3	.315	.335	7.27	245	159.	171.	1.9[illegible]
4	.333	.435	8.27	275.	163.	184.	2.17
5	.339	.469	9.57	290.	175.	193.	2.45
6	.348	.537	11.35	32[illegible].	188.	2[illegible]9.	2.77
7	.350	.556	11.35	285.	166.	187.	2.68
8	.346	.611	12.47	245.	145.	165.	2.40
9	.350	.631	13.49	275.	167.	185.	2.81
10	.347	.715	14.49	262.	154.	150.	2.64
11	.330	.745	15.22	240.	149.	175.	2.83
12	.333	.767	15.65	232.	139.	165.	2.71
13	.344	.787	16.56	220.	131.	155.	2.59
14	.336	.811	16.65	219.	127.	152.	2.57
15	.322	.841	17.15	222.	141.	170.	2.94
16	.327	.759	15.69	207.	125.	149.	2.45
17	.330	.[illegible]	18.57	203.	126.	154.	2.79
18	.350	.[illegible]	18.98	210.	122.	151.	2.76
19	.330	.941	19.21	200.	124.	153.	2.87
20	.348	.[illegible]	19.76	230.	136.	168.	3.15
21	.349	.804	20.03	190.	114.	143.	2.70
22	.326	1.017	20.67	185.	116.	146.	2.82
23	.322	1.046	21.35	185.	117.	149.	2.93
24	.336	1.069	21.39	160.	97.	124.	2.46
25	.352	.[illegible]	20.29	205.	119.	145.	2.77
26	.359	1.136	23.14	215.	122.	159.	3.23
27	.349	1.[illegible]	21.39	235.	137.	176.	3.44
28	.339	1.17[illegible]	24.[illegible]4	202.	122.	163.	3.39
29	.321	1.[illegible]	22.14	205.	131.	168.	3.73
30	.[illegible]	1.[illegible]	24.53	175.	103.	145.	3.15
31	.332	1.267	25.86	165.	[illegible]	140.	3.03
32	.338	1.[illegible]	26.84	170.	107.	102.	3.39
33	.[illegible]	1.[illegible]	27.39	175.	108.	150.	3.49
34	.339	1.[illegible]	26.[illegible]5	150.	[illegible].	127.	3.03
35	.[illegible]	1.[illegible]	24.73	170.	104.	138.	2.[illegible]

Maximum evaluated K_c = 3.49 MN/m$^{3/2}$; Minimum evaluated K_c = 1.82 MN/m$^{3/2}$; Mean evaluated K_c = 2.73 MN/m$^{3/2}$; Variance of results = 0.190 (MN)^2/m^3; Standard deviation = 0.436 MN/m$^{3/2}$; Standard error = 0.075 MN/m$^{3/2}$; Skewness of results = - 0.251 (MN)^3/m$^{9/2}$; Kurtosis of results = 2.413 (MN)^4/m^6.

TABLE 6.10: HIPS, Grade BCP

Glue-free single-edge notched specimens of nominal dimensions of 3.2 mm × 50 mm × 150 mm: Material yield stress = 20.5 MN/m^2; Cross-head speed = 10 mm/min; K_c values are evaluated, using the initial crack length and the maximum applied load at craze growth.

NO	SPECIMEN THICK (CM)	CRACK LENGTH (CM)	CRACKED AREA PROPORTION (PER CENTAGE)	APPLIED LOAD (KGF.)	GROSS STRESS (KGF./SQ.CM)	NET STRESS (KGF/SQ.CM)	INTENSITY FACT (M.N./M.**(1/
1	.340	.717	4.22	165.	39.	103.	.89
2	.337	.737	6.27	90.	55.	59.	.61
3	.315	.755	7.27	145.	94.	101.	1.12
4	.333	.413	8.27	100.	61.	67.	.79
5	.339	.463	9.57	85.	51.	57.	.72
6	.348	.537	10.35	170.	76.	85.	1.12
7	.350	.575	11.35	190.	105.	119.	1.64
8	.346	.611	12.47	60.	35.	40.	.59
9	.353	.651	13.49	165.	96.	111.	1.69
10	.347	.715	14.49	85.	50.	58.	.92
11	.330	.745	15.22	75.	46.	55.	.89
12	.339	.787	15.65	103.	60.	72.	1.18
13	.344	.797	16.06	105.	62.	74.	1.24
14	.335	.811	16.55	61.	43.	58.	.99
15	.322	.841	17.15	102.	65.	78.	1.35
16	.337	.759	15.69	107.	65.	77.	1.27
17	.331	.910	18.57	107.	62.	76.	1.37
18	.359	.925	18.88	102.	59.	73.	1.34
19	.331	.941	19.20	100.	62.	77.	1.41
20	.342	.963	19.75	85.	50.	62.	1.17
21	.340	.984	20.08	112.	67.	84.	1.59
22	.326	1.013	20.67	113.	71.	89.	1.72
23	.339	1.045	21.35	105.	67.	85.	1.66
24	.335	1.068	21.81	92.	56.	71.	1.41
25	.352	.994	20.29	92.	53.	67.	1.28
26	.359	1.134	23.14	95.	54.	71.	1.45
27	.349	1.043	21.39	110.	64.	82.	1.61
28	.339	1.179	24.14	85.	51.	67.	1.43
29	.320	1.085	22.14	104.	66.	85.	1.71
30	.326	1.224	24.88	95.	63.	79.	1.71
31	.332	1.267	25.86	90.	55.	75.	1.65
32	.333	1.315	26.84	65.	40.	54.	1.24
33	.330	1.362	27.81	67.	35.	49.	1.14
34	.333	1.414	28.85	61.	36.	51.	1.21
35	.332	1.212	24.73	70.	43.	57.	1.23

Maximum evaluated K_c = 1.72 $MN/m^{3/2}$; Minimum evaluated K_c = 0.6 $MN/m^{3/2}$; Mean evaluated K_c = 1.27 $MN/m^{3/2}$; Variance of results = 0.105 $(MN)^2/m^3$; Standard deviation = 0.324 $MN/m^{3/2}$; Standard error = 0.055 $MN/m^{3/2}$; Skewness of results = - 0.372 $(MN)^3/m^{9/2}$; Kurtosis of results = 2.212 $(MN)^4/m^6$.

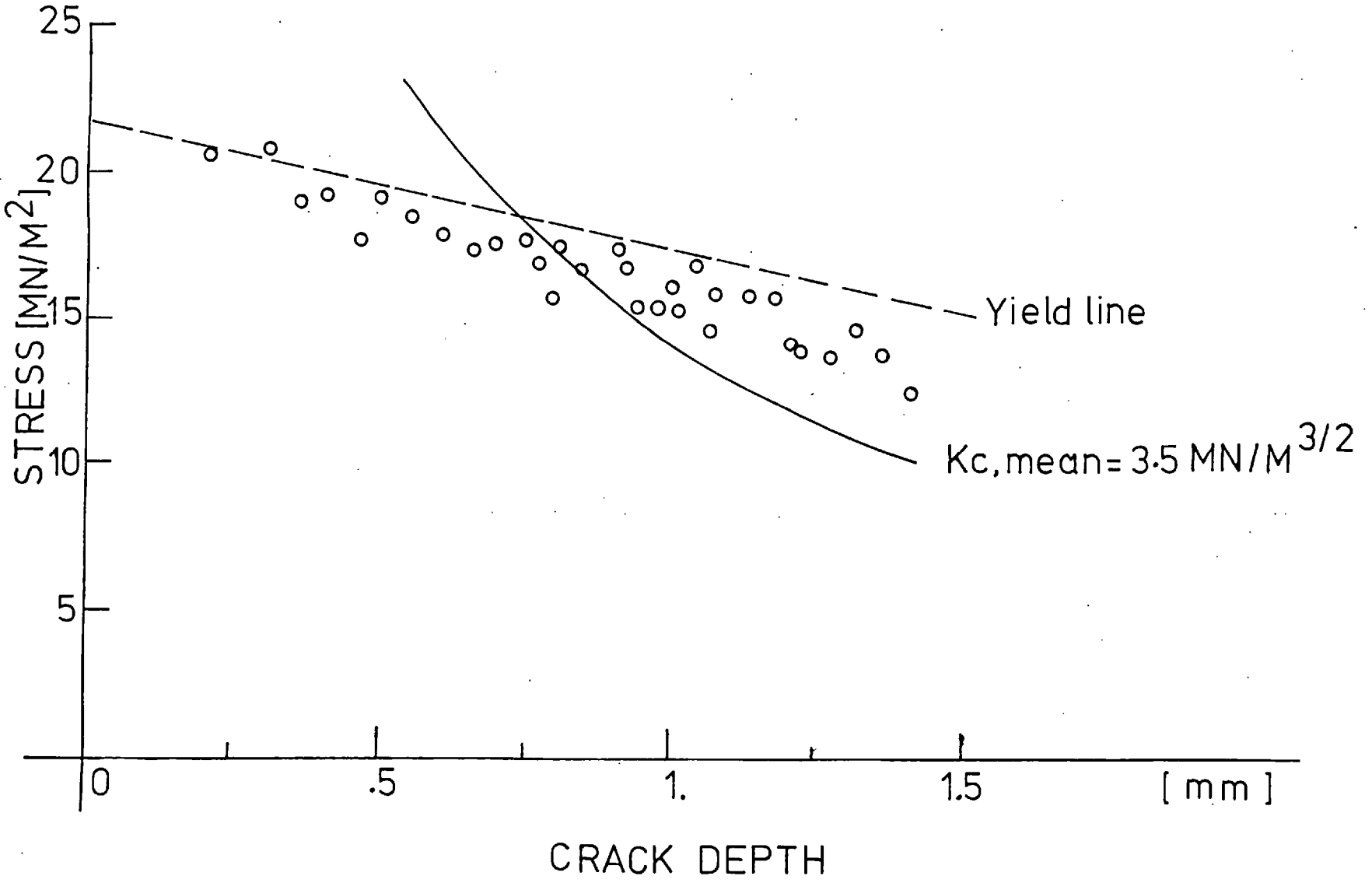


Figure 6.5: Variation of the maximum applied stress with notch depth for 50 mm wide single-edge notched specimens

6.7 INFLUENCE OF SPECIMEN DIMENSIONS ON THE MODE OF FRACTURE

In the preceding sections, the effect of notch geometry and the application of a constraining material over the crack surfaces on fracture behaviour were reported. As was shown, the mode of failure ranged from a ductile to a composite ductile-brittle fracture, depending on the crack shape or the constraining method used. The experimental work to be described in this section was carried out in order to study the fracture behaviour of a commercial grade of HIPS apropos of a change in the specimen dimensions.

The original Grade BCP of HIPS, which was supplied by BP Chemicals, was not available for the present work to be described and thus the Grade BCF, which is a basic commercial grade of medium impact PS, has been used. The mechanical and grafting properties of BCF were previously quoted in section 6.4.1 of this chapter.

6.7.1 Thickness Effect

Theoretically, very thick specimens fracture under plane strain conditions. The thickness of the specimens studied in this work cannot, however, be taken to be as large as the theory requires (i.e. greater than $2.5\ K_c^2/\sigma_y^2$) for plane strain conditions. Nevertheless, to investigate the effect of thickness, a series of tests was carried out on 50 mm wide single-edge notched specimens of 1.6 mm, 3.2 mm and 6.4 mm nominal thickness. The fracture toughnesses were calculated based on craze initiation, crack initiation and maximum applied load, together with the initial and current crack lengths at maximum load. All the specimens tested failed in a ductile manner displaying large crazing even prior to the onset of slow crack growth. It was to be therefore expected that the K_c criterion would be unable to characterise the fracture and thus

TABLE 6.11: HIPS, Grade BCF

Glue-free single-edge notched specimens of nominal dimensions of 6.35 mm × 50 mm × 150 mm; Material yield stress = 150 MN/m^2; Cross-head speed = 10 mm/min; K_c values are evaluated, using the initial crack length and the maximum applied load.

NO	SPECIMEN THICK (CM)	CRACK LENGTH (CM)	CRACKED AREA PROPORTION (PER CENT(AGE))	APPLIED LOAD (KGF.)	GROSS STRESS (KGF./SQ.CM)	NET STRESS (KGF/SQ.CM)	INTENSITY FACTOR (M.N/M.**(3/2))	FRACTURE MANNER
1	.616	.711	8.20	350.	117.	125.	1.38	DUCTILE
2	.617	.[illegible]	12.98	335.	108.	126.	2.89	DUCTILE
3	.[illegible]	.[illegible]	17.76	315.	139.	127.	2.27	DUCTILE
4	.[illegible]	1.[illegible]	22.96	253.	82.	105.	2.21	DUCTILE
5	.612	1.236	20.20	254.	84.	112.	2.62	DUCTILE
6	.[illegible]	2.[illegible]	20.98	252.	82.	115.	2.76	DUCTILE
7	.627	1.772	30.47	217.	70.	108.	3.63	DUCTILE
8	.[illegible]	1.[illegible]	37.09	194.	64.	104.	3.15	DUCTILE
9	.[illegible]	2.[illegible]	43.35	186.	61.	108.	3.59	DUCTILE
10	.624	2.278	45.72	173.	56.	103.	3.64	DUCTILE
11	.617	2.[illegible]	47.75	168.	52.	99.	3.67	DUCTILE
12	.[illegible]	2.502	50.10	153.	50.	100.	3.80	DUCTILE
13	.[illegible]	2.[illegible]	51.38	152.	48.	107.	4.20	SEMI-DUCTILE
14	.[illegible]	2.[illegible]	54.15	147.	48.	104.	4.45	SEMI-DUCTILE
15	.628	2.[illegible]	53.45	148.	48.	103.	4.79	DUCTILE
16	.[illegible]	2.[illegible]	53.58	140.	45.	111.	5.34	DUCTILE

$K_{c,max}$ = 5.34 MN/m$^{3/2}$; $K_{c,min}$ = 1.30 MN/m$^{3/2}$; $K_{c,mean}$ = 3.30 MN/m$^{3/2}$; Variance of the results = 1.237 (MN)^2/m^3; Standard deviation = 1.112 MN/m$^{3/2}$; Standard error = 0.278 MN/m$^{3/2}$; Skewness = 0.024 (MN)^3/m$^{9/2}$; Kurtosis = 1.958 (MN)^4/m^6.

correlate the experimental results.

The results for the 6.4 mm thick specimens are collated in Table 6.11 and the corresponding statistical terms (mean, standard deviation, standard error, skewness and Kurtosis) are noted. It is clearly seen that the K_c values evaluated are comparatively small for specimens containing shallow cracks but increase rapidly as the initial crack becomes greater. Similar effects were observed for specimens of other thicknesses.

The results are therefore identical to those obtained before for the Grade BCP of HIPS, indicating a prevailing ductile fracture behaviour. As far as the effect of thickness is concerned, no significant improvement in the consistency of the experimental data was achieved, even for the thickest material examined.

6.7.2 Width Effect

From the experimental work previously described, it is clear that the 50 mm wide specimens of various practical thicknesses and crack geometries (single-edge notched and surface notched specimens with varying initial crack lengths) fail in an almost ductile manner and therefore the fracture toughness of the materials tested cannot be correctly calculated. Since the stress field produced at the crack tip is triaxial, then it is reasonable to suggest that the ductile failure mechanism (associated with shear effects) is not only dependent on specimen thickness but also on specimen width, leading to a mechanism controlled by the net cross-section of the specimen. This postulate is further supported by considering the length of craze growth at the crack tip prior to final fracture. Direct observation of the notched specimens shows that the craze length is nearly constant at the onset of crack unstable

growth, regardless of the initial crack length*. For the Grade BCF of HIPS, this is estimated to be 1.15 cm. It is worth mentioning that this length for Perspex (PMMA), which is a very brittle material, does not exceed 10 μm (Marshall et al (1974)). If this crazed cross-sectional area is of the same order of magnitude as the net cross-sectional area of the specimen, the failure occurs by a predominantly shearing mechanism and the K_c criterion is invalid. On the basis of this argument, a predominantly brittle fracture should result when the specimen width is very much greater than the craze length created at the onset of crack growth.

To examine further this hypothesis, experiments were conducted for single-edge notched and surface notched specimens having a width of 100 mm. For the completeness of this analysis, the effect of constraining adhesives on the crack surfaces was also studied.

6.7.3 100 mm Wide Surface Notched Specimens

Two series of tests were performed on surface notched specimens, the first series having no glue applied to the crack surfaces and the second series having a 0.24 mm thick layer of Araldite covering the cracks, so that plane strain conditions could be induced through the thickness.

Having recorded the applied load at craze and crack initiation, it is possible to calculate the intensity factors of these loads and also at the maximum applied load. These values have been calculated by the methods previously described in section 6.2 of this chapter.

The initial dimensions of the specimen and crack, and the results (net stress, gross stress, and intensity factor), are shown in

---

* This observation is only valid for specimens containing relatively long cracks (that is, $a/D > 1/5$).

Tables 6.12 to 6.16, and the statistical terms regarding the fracture toughnesses obtained are noted below these tables.

Using the maximum applied load and the initial crack length, the calculated K_c values for both series of tests show inconsistencies and tend to increase as the crack length becomes larger. The yielding theory, however, seems to be sufficiently reliable to imply a ductile fracture condition.

For surface-free specimens, the evaluated critical intensity factor at the instant of crack initiation does not show any better consistency, but as long as the crack length remains smaller than one third of the specimen width, the fracture toughness values at craze initiation fluctuate around a constant mean value. Moreover, when the crack is covered, the critical intensity factor values at crack initiation obey a constant fracture toughness criterion within the range of $0.15 < a/D < 0.5$. The reason for this must be sought in the comparative through thickness strength of the material which was reinforced by the constraining layers of Araldite on the free surfaces of the specimen. For smaller cracks, $a/D < 0.15$, however, the specific elastic energy stored in the vicinity of the crack is very close to the yielding energy, thereby making the material pliant in the stress concentrated regions. This leads to a subsequent ductile rupture of the specimen, complying with the rules of yielding theory. In the case of longer cracks, $a/D > 0.5$, the restriction is due to the inaccuracy of the approximate expressions used for evaluating the intensity factors (see section 6.2 of this chapter).

6.7.4 100 mm Wide Single-Edge Notched Specimens

These tests were carried out on two sets of fifteen single-edge notched specimens containing different initial crack lengths, the first

TABLE 6.12: HIPS, Grade BCF

Wide glue-free surface notched specimen of nominal dimensions of 6.35 mm × 100mm × 300 mm; Material yield stress = 15 MN/m^2; Cross-head speed = 10 mm/min; K_c values are evaluated, using the initial crack length and the maximum applied load.

NO	SPEC. THICK. (CM.)	CRACK DEPTH (CM.)	GR. WIDTH (CM.)	GR. SIDING (CM)	GR. AREA SPC. (PER CENTAGE)	APPL. LOAD (KGF.)	GROSS STRESS (KGF./SQ.CM)	NET STRESS (KGF/SQCM)	INTENS. FACT. (MN/M**(3/2))	FRAC. MANNER
1	.611	.1 .	1.322	2.20	1.48	91[illegible].	137.	139.	.925	DUCTILE
2	.612	.133	1.478	2.17	2.17	905.	136.	139.	1.044	SEMI-DUCTILE
3	.623	.193	1.653	2.15	3.61	835.	139.	142.	1.213	SEMI-DUCTILE
4	.619	.194	1.824	2.25	3.98	8[illegible].	133.	139.	1.266	SEMI-DUCTILE
5	.619	.223	1.940	2.22	4.68	819.	137.	144.	1.424	SEMI-DUCTILE
6	.616	.274	2.122	2.19	6.57	8[illegible].	135.	144.	1.586	SEMI-DUCTILE
7	.627	.326	2.3[illegible]	2.21	8.38	783.	125.	137.	1.646	SEMI-DUCTILE
8	.616	.348	2.365	2.25	9.40	751.	126.	135.	1.748	SEMI-DUCTILE
9	.627	.393	2.537	2.20	10.64	785.	127.	142.	1.956	SEMI-DUCTILE
10	.6[illegible]5	.425	2.60[illegible]	2.25	12.67	7[illegible].	115.	136.	2.035	SEMI-DUCTILE
11	.615	.460	2.712	2.23	14.47	705.	115.	139.	2.3[illegible]5	SEMI-DUCTILE
12	.617	.464	2.738	2.26	15.44	655.	116.	[illegible]37.	2.4[illegible]3	SEMI-DUCTILE
13	.618	.5[illegible]5	2.819	2.22	16.23	69[illegible].	11[illegible].	137.	2.592	SEMI-DUCTILE
14	.622	.520	2.846	2.21	16.76	6[illegible].	114.	137.	2.715	SEMI-DUCTILE

$K_{c,max}$ = 2.72 MN/m$^{3/2}$; $K_{c,min}$ = 0.92 MN/m$^{3/2}$; $K_{c,mean}$ = 1.7 MN/m$^{3/2}$; Variance of the results = 0.335 (MN)^2/m^3; Standard deviation = 0.578 MN/m$^{3/2}$; Standard error = 0.155 MN/m$^{3/2}$; Skewness = 0.157 (MN)^3/m$^{9/2}$; Kurtosis = 1.58 (MN)^4/m^6.

TABLE 6.13: HIPS, Grade BCF

Wide glue-free surface notched specimens of nominal dimensions of 6.35 mm × 100mm × 300 mm; Material yield stress = 15 MN/m^2; Cross-head speed = 10 mm/min; K_c values are evaluated, using the initial crack length and the load at crack initiation.

NO	SPEC. THICK. (m)	NOTCH DEPTH (m)	GR. WIDTH (m)	AV. WIDTH (m)	MAXIMUM FIL. (MN/m**(3/2))	FAILURE LOAD (KGF.)	GROSS STRESS (MGF/m2.DA)	NET STRESS (KGF/CM2)	INTENS. FACT. (MN/M**(3/2))	FRAC. MANNER
1	.010	.003	2.452	2.23	1.46	840.	213.	117.	.712	DUCTILE
2	.010	.003	2.472	2.17	2.17	840.	211.	116.	.745	SEMI-DUCTILE
3	.010	.003	2.483	2.18	3.09	720.	184.	101.	1.120	DUCTILE
4	.010	.003	2.488	2.23	3.96	770.	195.	134.	1.220	SEMI-DUCTILE
5	.010	.003	2.496	2.22	4.66	800.	134.	141.	1.400	SEMI-DUCTILE
6	.010	.003	2.522	2.19	5.67	900.	228.	146.	1.595	SEMI-DUCTILE
7	.010	.003	2.497	2.23	6.58	710.	115.	127.	1.517	SEMI-DUCTILE
8	.007	.003	2.507	2.21	10.64	710.	185.	142.	1.661	SEMI-DUCTILE
9	.010	.003	2.519	2.21	12.28	560.	113.	105.	2.069	SEMI-DUCTILE
10	.010	.003	2.510	2.23	12.87	700.	112.	130.	2.052	SEMI-DUCTILE
11	.010	.003	2.712	2.23	14.40	670.	113.	132.	2.193	SEMI-DUCTILE
12	.010	.003	2.708	2.23	15.48	640.	104.	119.	2.253	SEMI-DUCTILE
13	.010	.003	2.516	2.23	16.78	631.	104.	125.	2.480	SEMI-DUCTILE

$K_{c,max}$ = 2.57 MN/m$^{3/2}$; $K_{c,min}$ = 0.75 MN/m$^{3/2}$; $K_{c,mean}$ = 1.69 MN/m$^{3/2}$; Variance of the results = 0.40 (MN)^2/m^3; Standard deviation = 0.63 MN/m$^{3/2}$; Standard error = 0.174 MN/m$^{3/2}$; Skewness = - 0.89 (MN)^3/m$^{9/2}$; Kurtosis = 1.47 (MN)^4/m^6.

TABLE 6.14: HIPS, Grade BCF

Wide glue-free surface notched specimens of nominal dimensions of 6.35 mm × 100mm × 300 mm; Material yield stress = 15 MN/m^2; Cross-head speed = 10 mm/min; K_c values are evaluated, using the initial crack length and the load at the craze initiation.

NO										
1	.[illegible]	.[illegible]	[illegible]	2.23	[illegible]	79.	[illegible]	184.	[illegible]	DUCTILE
2	.[illegible]	.[illegible]	1.[illegible]	2.17	2.17	660.	180.	180.	1.049	SEMI-DUCTILE
3	.[illegible]	.[illegible]	[illegible]	[illegible]	3.00	730.	[illegible]	120.	1.039	DUCTILE
4	.[illegible]	.[illegible]	[illegible]	2.23	3.96	[illegible]	107.	111.	.987	SEMI-DUCTILE
5	.[illegible]	.223	[illegible]	2.27	4.64	564.	107.	[illegible]	1.077	SEMI-DUCTILE
6	.[illegible]	.[illegible]	[illegible]	[illegible]	5.57	379.	[illegible]	[illegible]	[illegible]	SEMI-DUCTILE
7	.[illegible]	.[illegible]	[illegible]	[illegible]	[illegible]	479.	76.	83.	.988	SEMI-DUCTILE
8	.[illegible]	.[illegible]	[illegible]	[illegible]	10.94	260.	61.	76.	1.191	SEMI-DUCTILE
9	.[illegible]	.[illegible]	[illegible]	[illegible]	16.24	169.	[illegible]	63.	1.000	SEMI-DUCTILE
10	.[illegible]	.[illegible]	[illegible]	2.25	12.37	250.	83.	107.	1.[illegible]	SEMI-DUCTILE
11	.[illegible]	.[illegible]	2.712	2.23	[illegible]	390.	66.	77.	1.217	SEMI-DUCTILE
12	.[illegible]	.[illegible]	[illegible]	2.20	[illegible]	420.	78.	93.	1.097	SEMI-DUCTILE
13	.[illegible]	.[illegible]	[illegible]	2.21	11.78	350.	55.	78.	1.491	SEMI-DUCTILE

$K_{c,max}$ = 1.56 MN/m$^{3/2}$; $K_{c,min}$ = 0.90 MN/m$^{3/2}$; $K_{c,mean}$ = 1.19 MN/m$^{3/2}$; Variance of the results = 0.05 (MN)^2/m^3; Standard deviation = 0.226 MN/m$^{3/2}$; Standard error = 0.063 MN/m$^{3/2}$; Skewness = 0.44 (MN)^3/m$^{9/2}$; Kurtosis = 1.52 (MN)^4/m^6.

TABLE 6.15: HIPS, Grade BCF

Wide glued surface notched specimens of nominal dimensions of 6.35 mm × 100mm × 300 mm; Material yield stress = 15 MN/m^3; Cross-head speed = 10 mm/min; K_c values are evaluated, using the initial crack length and the maximum applied load.

S.NO	SPEC. THICK. (B)	GROOV DEPTH (D)	SP. WIDTH (2W)	SP. RADIUS (2R)	SP. AREA PRO. (PER CENTAGE)	APPL. LOAD (KGF.)	GROSS STRESS (KGF./SQ.CM)	NET STRESS (KGF/SQCM)	INTENS. FACT. (MN/M**(3/2))	FRAC. MANNER
1	.[illegible]	.[illegible]	1.322	2.23	1.48	705.	119.	120.	.776	DUCTILE
2	.613	.142	1.590	2.30	2.55	704.	118.	122.	.933	DUCTILE
3	.[illegible]	.[illegible]	1.671	2.20	3.02	699.	114.	117.	.952	DUCTILE
4	.597	.240	1.814	2.20	3.75	739.	120.	124.	1.101	DUCTILE
5	.[illegible]	.256	2.070	2.27	5.68	714.	115.	123.	1.254	SEMI-DUCTILE
6	.621	.[illegible]	2.160	2.17	6.96	698.	116.	125.	1.370	SEMI-DUCTILE
7	.[illegible]	.[illegible]	2.270	2.25	8.01	699.	117.	127.	1.465	SEMI-DUCTILE
8	.[illegible]	.340	2.350	2.25	9.11	677.	113.	124.	1.512	SEMI-DUCTILE
9	.[illegible]	.384	2.435	2.22	9.98	672.	112.	124.	1.556	SEMI-DUCTILE
10	.[illegible]	.[illegible]	2.534	2.25	11.00	659.	110.	121.	1.627	SEMI-DUCTILE
11	.623	.454	2.674	2.15	13.76	647.	107.	124.	1.955	SEMI-DUCTILE
12	.[illegible]	.[illegible]	2.717	2.22	13.99	647.	105.	122.	1.963	SEMI-DUCTILE
13	.[illegible]	.411	2.766	2.23	14.86	648.	106.	124.	2.075	SEMI-DUCTILE
14	.630	.536	2.933	2.22	17.37	612.	100.	121.	2.484	SEMI-DUCTILE

$K_{c,max}$ = 2.48 MN/m$^{3/2}$; $K_{c,min}$ = 0.78 MN/m$^{3/2}$; $K_{c,mean}$ = 1.50 MN/m$^{3/2}$; Variance of the results = 0.24 (MN)^2/m^3; Standard deviation = 0.49 MN/m$^{3/2}$; Standard error = 0.13 MN/m$^{3/2}$; Skewness = 0.31 (MN)^3/m$^{9/2}$; Kurtosis = 2.04 (MN)^4/m^6.

TABLE 6.16: HIPS, Grade BCF

Wide glued surface notched specimens of nominal dimensions of 6.35 mm × 100mm × 300 mm; Material yield stress = 15 MN/m^2; Cross-head speed = 10 mm/min; K_c values are evaluated, using the initial crack length and the load at crack initiation.

NO	SPEC. THICK. (in)	CRACK DEPTH (in)	SPEC. WIDTH (in)	K_c RADIUS (in)	MAX. ITER. PRES. (psi)	PEAK LOAD (lbf)	GROSS STRESS (lbf/in^2)	NET STRESS (lbf/in^2)	K_c (psi$\sqrt{in}$)	FRAC. MANNER
1	.248	.060	1.062	2.23	1.46	154.	134.	136.	.910	DUCTILE
2	.248	.062	1.598	2.31	2.55	264.	166.	166.	1.036	DUCTILE
3	.248	.065	1.671	2.29	3.02	257.	155.	167.	1.067	SEMI-DUCTILE
4	.247	.060	1.614	2.26	3.45	294.	182.	194.	1.221	SEMI-DUCTILE
5	.245	.065	2.070	2.27	5.65	417.	203.	217.	1.371	SEMI-DUCTILE
6	.251	.068	2.106	2.17	6.56	442.	215.	166.	1.379	SEMI-DUCTILE
7	.248	.065	2.270	2.25	6.61	426.	185.	115.	1.325	SEMI-DUCTILE
8	.248	.060	2.089	2.25	5.12	449.	78.	82.	.970	SEMI-DUCTILE
9	.247	.064	2.095	2.20	6.59	426.	194.	116.	1.278	SEMI-DUCTILE
10	.250	.060	2.054	2.25	11.66	573.	93.	105.	1.063	SEMI-DUCTILE
11	.247	.056	2.074	2.19	13.76	469.	78.	86.	1.084	SEMI-DUCTILE
12	.251	.065	2.717	2.27	13.59	412.	68.	76.	1.180	SEMI-DUCTILE
13	.250	.061	2.756	2.23	14.66	561.	92.	106.	1.767	SEMI-DUCTILE
14	.253	.066	2.793	2.22	17.37	538.	87.	1 6.	2.[illegible]	SEMI-DUCTILE

$K_{c,max}$ = 2.15 MN/m$^{3/2}$; $K_{c,min}$ = 0.91 MN/m$^{3/2}$; $K_{c,mean}$ = 1.31 MN/m$^{3/2}$; Variance of the results = 0.11 (MN)^2/m^3; Standard deviation = 0.34 MN/m$^{3/2}$; Standard error = 0.09 MN/m$^{3/2}$; Skewness = 1.07 (MN)^3/m$^{9/2}$; Kurtosis = 3.40 (MN)^4/m^6.

being glue-free and the second being covered with a layer of Araldite, 0.24 mm thick, in order to induce plane strain conditions at the crack tip and along the surfaces of the specimens in the crack plane, where the maximum through-thickness deflection takes place.

The critical intensity factors at maximum load were calculated for both tests using the initial crack lengths in equation (6.2). Tables 6.17 and 6.18 show the calculated K_c values versus the applied loads. The results show that a critical net stress criterion at fracture (the yield theory) does not describe the behaviour, whereas they ratify the constant critical intensity factor approach. Although there appeared to be a slight work hardening and considerable craze growth before complete fracture, it is clear that the linear fracture mechanics theory holds true even at the instability situation (i.e. at the maximum applied load). This is in contrast to the results previously described for surface notched specimens where only the initiation of crazes could be characterised by the linear fracture mechanics theory, while the crack initiation and instability were predominantly governed by the yielding theory.

Similarly, when a layer of Araldite is used to cover the crack, the results obey the theory of a constant fracture toughness exactly, while the gross stress and net stress values decrease sharply as the crack lengths become larger.

Statistical values, noted below Tables 6.17 and 6.18, are in very good agreement with the previously mentioned conclusions, since the standard error in both tests is less than 1%.

It is worth mentioning that, regardless of the use of glue in Tests 1 and 2, the results are identical and the same values for fracture toughness are obtained ($K_c \simeq 2.6$ MN/m$^{3/2}$). However, there still exists an important difference in the fracturing process since the crack

TABLE 6.17: HIPS, Grade BCF

Wide glue-free single-edge notched specimens of nominal dimensions of 6.35 mm × 10 mm × 300 mm; Material yield stress = 15 MN/m^2; Cross-head speed = 10 mm/min; K_c values are evaluated, using the initial crack length and the maximum applied load.

NO	SPECIMEN THICK (CM)	CRACK LENGTH (CM)	CRACKED AREA PROPORTION (PERCENTAGE)	APPLIED LOAD (KGF.)	GROSS STRESS (KGF./SQ CM)	NET STRESS (KGF/SQ.CM)	INTENSITY FACTOR (M.N./M.**(3/2))	FRACTURE MANNER
1	.605	2.210	22.78	420.	72.	93.	2.67	SEMI_BRITTE
2	.625	2.310	23.81	395.	65.	85.	2.52	
3	.622	2.548	26.27	383.	63.	86.	2.71	
4	.641	2.755	28.51	354.	57.	80.	2.65	
5	.612	2.878	29.67	283.	49.	70.	2.40	
6	.635	3.120	32.16	313.	51.	75.	2.71	
7	.614	3.322	34.25	267.	45.	66.	2.59	
8	.637	3.625	37.33	255.	41.	66.	2.69	
9	.617	3.965	40.88	212.	35.	60.	2.64	
10	.623	4.275	44.05	189.	31.	56.	2.65	
11	.630	4.670	48.14	157.	26.	50.	2.57	
12	.620	4.990	51.44	134.	22.	46.	2.57	
13	.620	5.255	53.97	116.	19.	42.	2.48	
14	.603	5.554	57.26	105.	18.	42.	2.68	

$K_{c,max}$ = 2.71 MN/m$^{3/2}$; $K_{c,min}$ = 2.40 MN/m$^{3/2}$; $K_{c,mean}$ = 2.61 MN/m$^{3/2}$; Variance of the results = 0.008 (MN)^2/m^3; Standard deviation = 0.092 MN/m$^{3/2}$; Standard error = 0.025 MN/m$^{3/2}$; Skewness = 0.794 (MN)^3/m$^{9/2}$; Kurtosis = 2.465 (MN)^4/m^6.

TABLE 6.18: HIPS, Grade BCF

Wide glued single-edge notched specimens of nominal dimensions of 6.35 mm × 10 mm × 300 mm; Material yield stress = 15 MN/m^2; Cross-head speed = 10 mm/min; K_c values are evaluated, using the initial crack length and the maximum applied load.

NO	SPECIMEN THICK (CM)	CRACK LENGTH (CM)	CRACKED AREA PROPORTION (PER CENT.AGE)	APPLIED LOAD (KGF.)	GROSS STRESS (KGF./SQ.CM)	NET STRESS (KGF/SQ.CM)	INTENSITY FACTOR (M.N./M.**(3/2))	FRACTURE MANNER
1	.635	2.622	42.57	418.	69.	97.	2.59	BRITTLE
2	.631	2.561	25.40	353.	58.	75.	2.48	
3	.617	2.605	26.76	371.	62.	85.	2.71	
4	.629	2.322	23.21	316.	52.	74.	2.49	
5	.636	3.019	31.03	297.	48.	70.	2.48	
6	.646	3.117	32.26	293.	47.	73.	2.57	
7	.621	3.409	35.35	269.	45.	69.	2.66	
8	.615	3.631	37.11	243.	41.	65.	2.53	
9	.637	3.783	38.97	226.	38.	58.	2.47	
10	.655	3.999	41.13	215.	35.	59.	2.62	
11	.613	4.409	45.41	178.	30.	55.	2.67	
12	.621	4.762	48.73	151.	25.	49.	2.61	
13	.632	4.976	51.32	136.	22.	46.	2.55	
14	.615	5.257	54.23	117.	20.	43.	2.54	
15	.647	5.585	57.53	107.	17.	42.	2.55	

$K_{c,max}$ = 2.71 MN/m$^{3/2}$; $K_{c,min}$ = 2.47 MN/m$^{3/2}$; $K_{c,mean}$ = 2.58 MN/m$^{3/2}$; Variance of the results = 0.006 (MN)^2/m^3; Standard deviation = 0.076 MN/m$^{3/2}$; Standard error = 0.020 MN/m$^{3/2}$; Skewness = 0.056 (MN)^3/m$^{9/2}$; Kurtosis = 1.67 (MN)^4/m^6.

propagation speeds differ greatly. In this respect, the effect of Araldite covering the free surfaces of the specimen is to increase the cracking speed (10^5 times faster), thus causing an ostensibly brittle fracture. This, of course, is vital to the design of components made of HIPS and will be discussed in the next section.

6.8 DUCTILITY AND BRITTLENESS

The fracture behaviour of a polymer can be judged by directly scanning the fracture surfaces and analysing the load-deflection curves. Figure 6.6 shows some typical fracture surfaces of HIPS samples, demonstrating failure occurring in a mode varying from brittle to ductile. As shown, the size of the craze zone and plasticity at the fracture surfaces display the degree of ductility of the materials tested. The relative amount of transparent and opaque regions on the fracture surfaces indicate whether the mode of failure is predominantly brittle or ductile. Figure 6.7 shows the history of craze growth in a single-edge notched specimen. It can be seen that the craze can be regarded as a narrow strip of stressed material of a thickness of less than 1 mm.

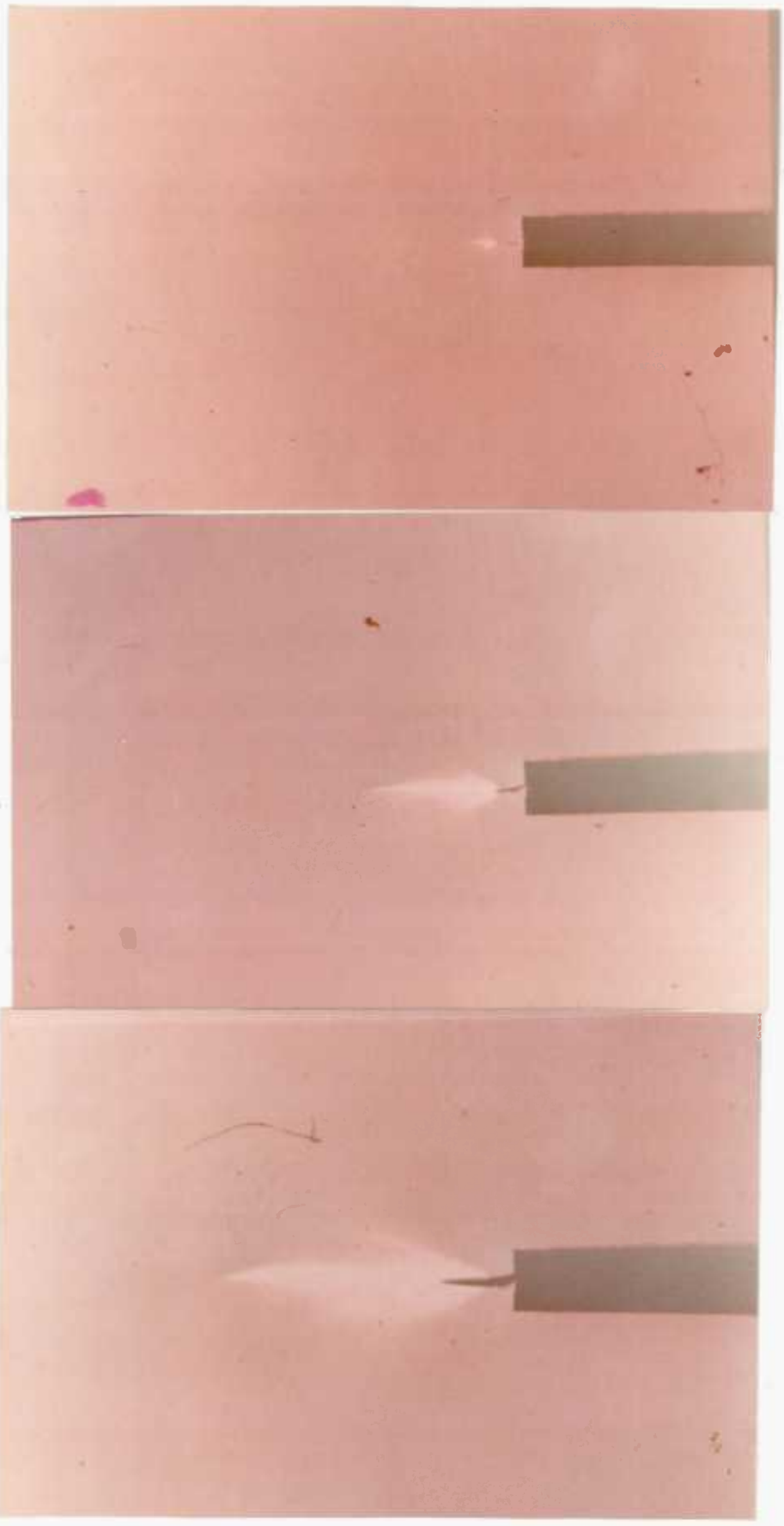
From an analysis of the fracture surfaces and the load-deflection curves, the apparent fracture behaviour of the specimens are characterised as follows:

A. Brittle Fracture: There is no significant craze or crack growth prior to the sudden rupture of the specimen. The corresponding stress-deflection curve is shown schematically in Figure 6.8(a).

B. Semi-Brittle Fracture: At a certain load, a narrow craze zone (usually less than 1 mm thick) propagates ahead of the initial crack and, as the load increases, it grows in length but remains in the crack plane. At higher loads, the crack initiates and propagates slowly through the craze zone and, finally, at a critical crack length, accelerates leading to an almost instant rupture of the material. An analysis of the fracture surfaces shows the regions of slow and rapid crack growth. The load-



Figure 6.6: Typical fracture surfaces of some brittle to ductile HIPS samples



1. Craze initiation from the tip of the original crack in a direction perpendicular to the applied load

2. Crack initiation through the propagating craze

3. Crack propagation through highly crazed media

Figure 6.7 Fracture in a single-edge notched specimen subjected to a uniform tensile stress

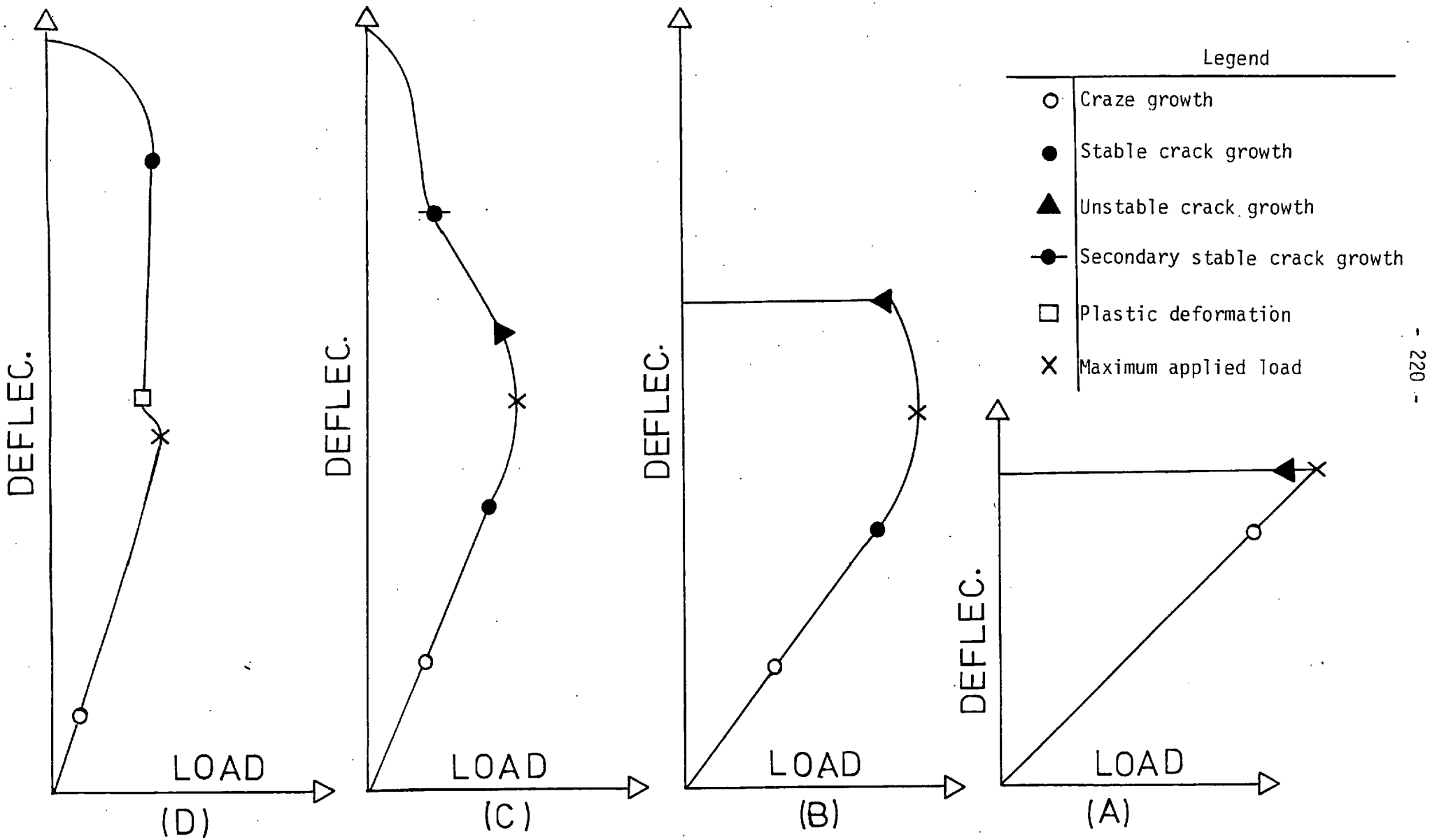


Figure 6.8: Load-deflection diagrams for various types of fracture: A. Brittle; B. Semi-brittle; C. Semi-ductile; D. Ductile

deflection diagram of a semi-brittle failure is shown schematically in Figure 6.8(b).

C. Semi-Ductile Fracture: As described for semi-brittle materials, slow crack growth can be seen prior to maximum loading. However, crack instability does not take place and, instead, a limited fast, but not instantaneous, crack growth follows stable cracking until it is finally trapped in fully grown crazed media. The final failure occurs after a large amount of a subsequent slow crack growth through the craze which will simultaneously travel ahead of the moving crack. The typical load-deflection curve is shown in Figure 6.8(c).

D. Ductile Fracture: A line craze growth may appear at first but, as the load increases, it will be divided and diverged into an irregular craze band which no longer travels on the plane of the initial crack. The crack initiates and propagates at a very slow speed through highly yielded material and failure usually takes place after maximum load is reached (Figure 6.8(d)).

In a brittle (or semi-brittle) fracture, the craze created at the crack tip prior to crack initiation may provide a quantitative basis on which to assess the fracture toughness of the material. This can be either estimated theoretically or may be directly measured from experiment. Assuming a Dugdale line craze zone at the crack tip, the craze zone length, r_c, can be approximately determined by:

$$r_c = \frac{\pi}{8} (K_c^2/\sigma_y^2) \qquad (6.9)^*$$

This equation suggests that r_c can be regarded as the material property, if K_c and σ_y are presumed to be so. The Dugdale mode, however, is valid only when the craze band ahead of the crack tip remains narrow (approximately less than $1/(4B)$) on a plane perpendicular to the applied stress. The experimental results ratify the above solution for HIPS as long as the craze zone is shorter than the remaining space between the craze tip and the opposite specimen edge. Furthermore, the previous experimental work for measuring the critical intensity factor of a pre-notched specimen confirms that this is also an essential prerequisite to obtaining a consistent value for the fracture toughness of the material, K_c.

Equation (6.9) can be rearranged to evaluate the fracture toughness, taking into account that the craze length at instability is a material property and is only a function of temperature, strain rate and environmental conditions. For BCF, the following properties are measured from experiments:

$$\sigma_y = 15 \text{ MN/m}^2$$

r_c = 11.5 mm (for specimens with cracks longer than 20 mm)

Thus, substituting for σ_y and r_c in equation (6.9), we have:

---

* This equation is an approximate solution for low stress failure. The domain of its validity is therefore confined to brittle (or semi-brittle) fractures and particularly for specimens which contain relatively longer cracks (i.e. $a/D > 1/5$).

$$K_c = (\sigma_y^2 \frac{8r_c}{\pi})^{\frac{1}{2}} \simeq 2.6 \text{ MN/m}^{3/2} \qquad (6.10)$$

The excellent agreement between the two methods of obtaining K_c is an important conclusion which verifies the simple assumption of line craze growth originally put forward by Dugdale. However, the evaluation of K_c from equation (6.10) has certain drawbacks since, firstly, it requires an accurate knowledge of the material yield stress and, secondly, it assumes line craze growth which is not a valid criterion for many other polymers (e.g. ABS, where the craze growth occurs with an almost spherical front*).

The crack speed is also a useful quantity to compare the ductility or brittleness of materials. As previously demonstrated, the fracture toughnesses of identical specimens containing free and glue-coated single-edge notches were identical, regardless of different glue applications. This is, however, valid only if the fracture occurs in a brittle (or semi-brittle) manner. Moreover, although both tests yield the same value for the critical intensity factor, there is a strikingly large difference in crack speed if one is compared with the other.

Figure 6.9 shows the crack propagation speed from the crack instability point (or the instant of crack initiation) to the point of complete fracture. It is seen that, although an equal fracture toughness is obtained for specimens having glue-covered and exposed cracks, the fracture speed ratios of these specimens vary significantly. Mathematically, the cracking history diagram is a smooth function if the materials has an exposed crack but is a series of step functions if the

---

* For further discussion on the limitation of the craze zone length as a fracture criterion, see section 9.5 of Chapter 9.

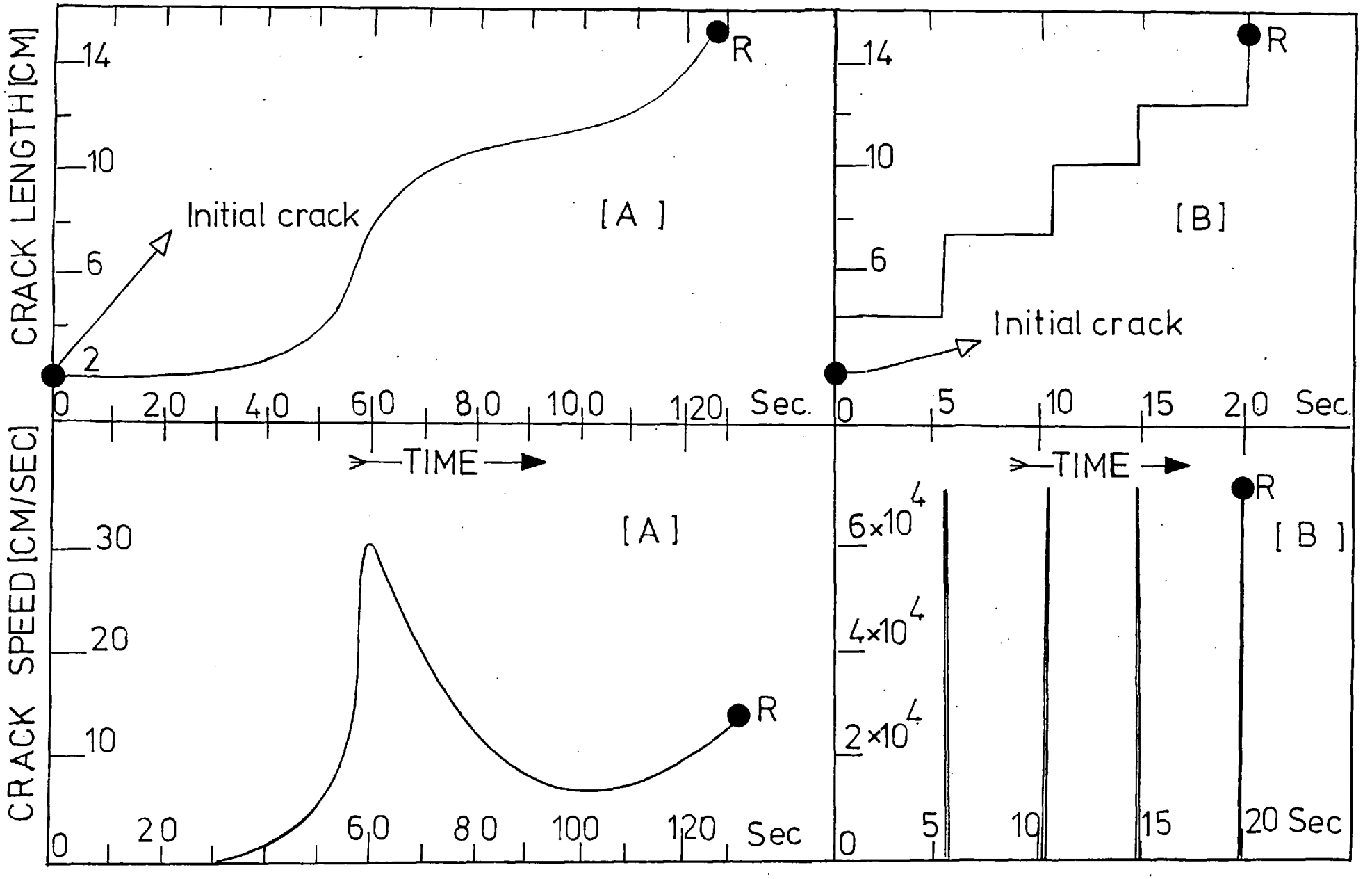


Figure 6.9: Comparison of crack propagation speeds in single-edge notched specimens having (A) exposed and (B) glue-covered cracks

crack is covered (in the latter case, the cracking history consists of alternate periods of instantaneous crack growth followed by a period of crack arrest).

Rapid crack extension in glued notched specimens has sometimes been regarded as sympathetic fracture. This idea describes the phenomenon as an inter-molecular sympathy between two molecules, one with a broken and the other with an intact bond (the polymer molecule), and thus damage in the fragile glue molecules will be sympathetically transferred to the relatively ductile polymer molecule causing a rapid brittle fracture.

The viewpoint presented here is that the apparent brittle failure of a glued specimen is caused by sustaining the plane strain conditions at the near-to-surface layers of the specimen which are normally liable to a larger through-thickness deflection. This aspect of fracture has a greater influence on the apparent fracture toughness obtained for specimens exhibiting a comparatively large craze growth (for HIPS, this is identical to assuming that the ratio $r_c/(D - a)$ approaches unity). On the other hand, if the plane strain condition is predominant due to using wider specimens, the fracture toughness value is not significantly affected by the relatively small craze formation at the crack tip.

The reason for alternate unstable crack extension in glue-covered specimens with relatively wider dimensions cannot merely be explained on the basis of the previously mentioned hypothesis since the plane strain conditions prevail, even prior to using a constraint. The underlying mechanism of this phenomenon can be put forward as follows:

The tensile energy exerted on the specimen is shared in the main polymer and the covering constraining glue layers according to the simple rule of parallel plates. At the critical intensity factor of the glue, it fractures locally in a brittle manner and thus releases an impact load

on the main polymer. The concurrence of this phenomenon and the crack initiation within the polymer at its critical intensity factor produces an instability situation which leads to an abrupt rupture of the two-phase system. The unstable crack growth can later be arrested because the burden of the impact is disencumbered as a result of the unloading mechanism. The alternate fracturing will occur at subsequent instability points of the two-phase system.

A correct knowledge of the cracking phenomenon in polymeric materials is therefore a vital factor in designing the components which are exposed to some sort of glue or any fragile constraining media, since it may cause a sudden catastrophic failure without a preceding slow cracking. The critical fracture toughness will not, however, be influenced by the presence of this constraint.

6.9 DISCUSSION ON THE VALIDITY OF THE LINEAR FRACTURE MECHANICS CRITERION IN HIPS

In order to study the extent to which the linear fracture mechanics criterion can be applied to describe the fracture of HIPS, the experimental results previously reported in section 6.7 of this chapter are rearranged graphically and the results are illustrated in Figures 6.10 to 6.17. Each figure contains four graphs which are produced using a computer plotter*. These graphs are as follows:

Graph 1: The maximum applied stress is plotted versus the initial crack length and the percentage of the crack area with reference to the specimen gross cross-sectional area (i.e. $P_c = a/D$ for single-edge notched specimens, and $P_c = R_m^2\ (2\alpha_s - sin\ 2\alpha_s)/2$ for surface notched specimens, where $\alpha_s = sin^{-1}\ (b/\ R_m)$ and R_m is the cutter radius). These plots are shown in the first graph of Figures 6.10, 6.11, 6.14, 6.16 and 6.17 for 50 mm wide single-edge notched specimens, 100 mm wide surface notched specimens (with free and glue-exposed surfaces) and 100 mm wide single-edge notched specimens (with free and glued surfaces), respectively. Similarly, the critical stress at craze initiation (Figure 6.13) and the critical stress at crack initiation (Figures 6.12 and 6.15 for surface notched specimens having free and glued surfaces, respectively) are plotted. In these graphs, the two theoretical lines, solid and dashed, show the constant

---

* The programme list is given in Appendix C.

critical net stress and the mean critical stress intensity factor, respectively. The experimental points, shown by asterisks, represent the gross stress at critical loads.

Graph 2: In this graph, the product of $\sigma.Y$ is plotted against the inverse square root of the crack length (Y denotes the geometry factor in equation (6.1), and σ is the applied gross stress). If the experimental results obey $\overset{\alpha}{\lambda}$ linear fracture criterion, the data points should be covered by a straight line. The slope of this line presents the mean fracture toughness of the material.

Graph 3: The intensity factors evaluated from the slope of the previously mentioned graphs are plotted versus the initial crack length and the percentage of cracked area, P_c. The solid line, which is drawn through the experimental data, denotes the mean fracture toughness.

Graph 4: A statistical analysis assessing the validity and accuracy of the fracture toughness approach to describing the experimental results is shown in this graph. The computed K_c values are plotted against the percentage of specimens having a value equal to or greater than any given value. This plot describes graphically the following analysis which has been developed to study an individual experimental result in relation to a group of results obtained from a series of experiments.

Assuming that the variation in fracture toughness

values are described in terms of the Poisson distribution function, we have:

$$X_n = 100\, e^{-(K_c - K_{0c})/\Delta K_c} \qquad (6.11)$$

where X_n = the fraction of specimens having a value equal to or greater than an arbitrary value for K_c (%)

K_{0c} = minimum value of K_c in a series of experimental analysis

ΔK_c = the estimated spread from $K_{c,mean}$

Equation (6.11) can be rearranged as follows:

$$K_c = -(\Delta K_c / \log e)\, \log X_n + (2\Delta K_c / \log e) + K_{0c} \qquad (6.12)$$

If K_c values are plotted against $\log X_n$, all the points should be covered by a straight line with a slope of the total estimated spread divided by $\log e$. If the deviation from the linear fracture criterion is of a random character, the slope of the line produced yields an implicit value of the error involved. However, if the points cannot be covered by a single line and it is necessary to draw two or more lines through them, then that set of experimental data does not obey the constant K_c criterion.

This is an important conclusion reached in the present work when the scatter in the results are significantly large and it is often difficult to clarify the nature of the fracture phenomenon. In view of the random

Figure 6.10

SINGLE EDGE-NOTCHED SPECIMENS(PRODUCED BY A FLY CUTTER. R=22.6 MM)

MATERIAL SPECIFICATIONS = HIGH IMPACT POLYSTYRENE GRADE BCF , MADE BY BP CHEMICAL .

SPECIMENS DIMENSIONS=15.*5.000*.635 CM.. CROSS-HEAD SPEED=1.0 CM./MIN.

NO GLUE COVERS THE INITIAL CRACK

KC-VALUES WERE EVALUATED . USING THE INITIAL CRACK LENGTH & MAXIMUM APPLIED LOAD .

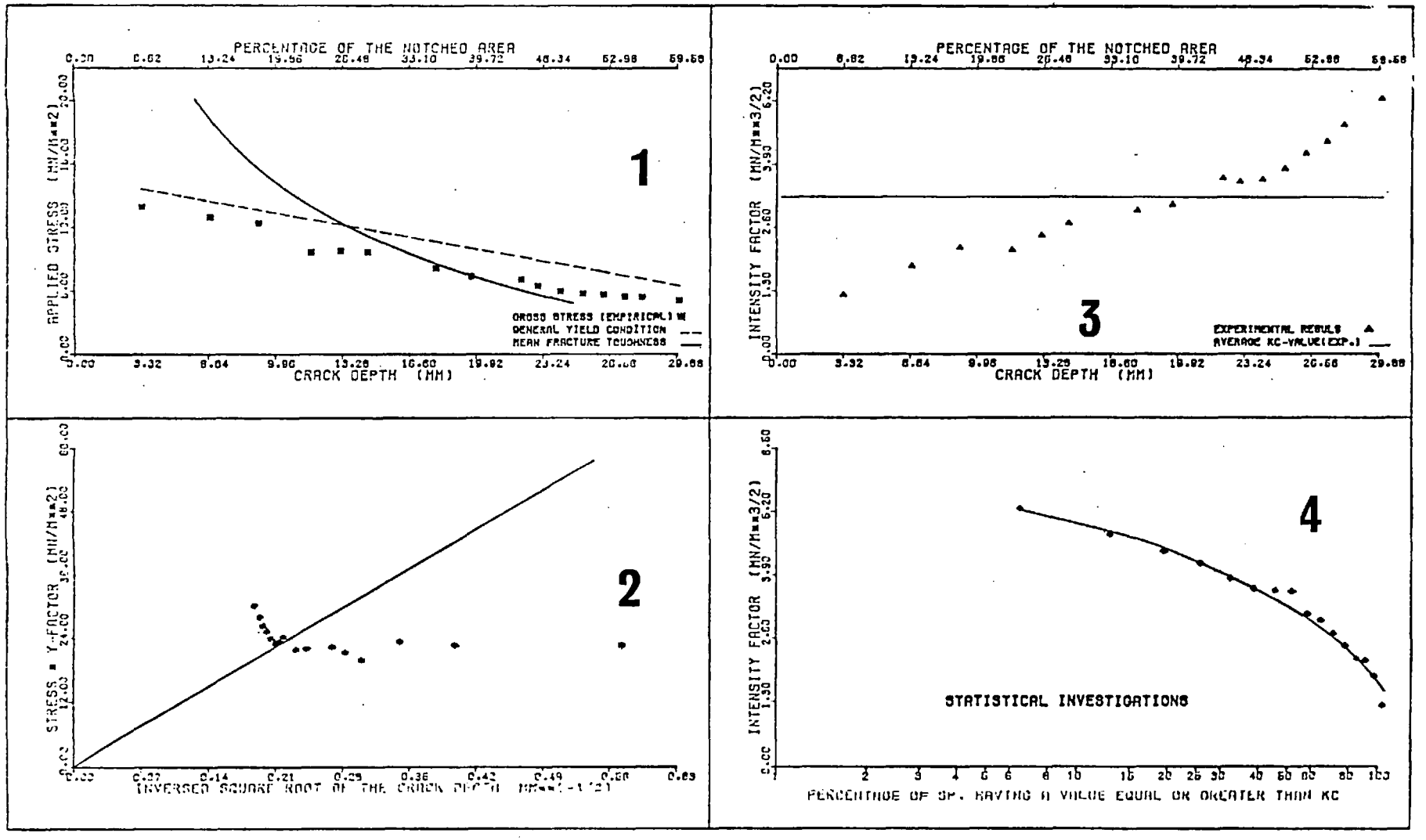


Figure 6.11

CIRCULAR SURFACE NOTCHED SPECIMENS(PRODUCED BY A FLY CUTTER, R=22.6 MM)

MATERIAL SPECIFICATIONS = HIGH IMPACT POLYSTYRENE GRADE BCF , MADE BY BP CHEMICAL .

SPECIMENS DIMENSIONS=20.0*9.7*.635 CM., CROSS-HEAD SPEED=1.0 CM./MIN.

NO GLUE COVERS THE INITIAL CRACK .

KC-VALUES WERE EVALUATED , USING THE INITIAL CRACK LENGTH & MAXIMUM APPLIED LOAD .

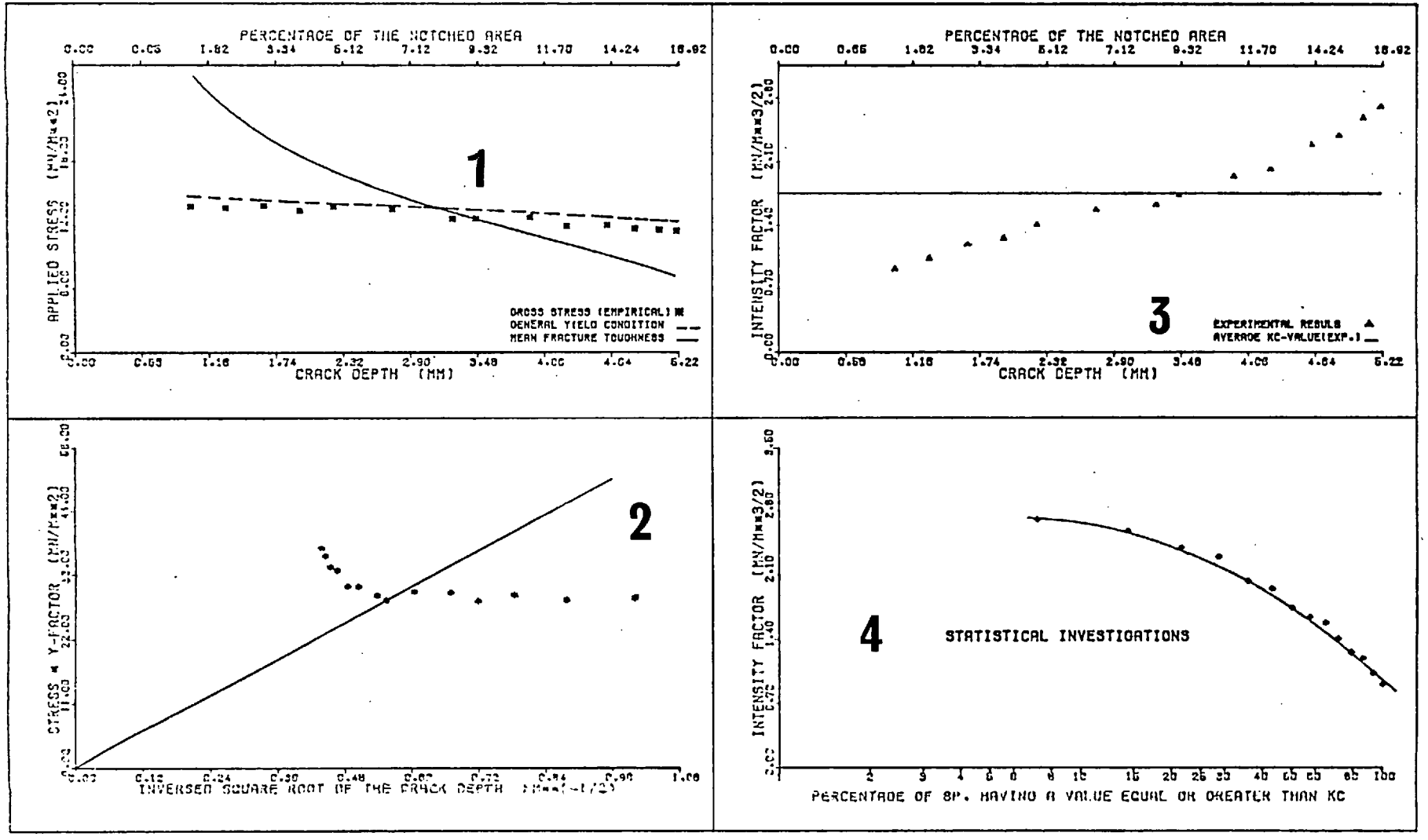


Figure 6.12

CIRCULAR SURFACE NOTCHED SPECIMENS(PRODUCED BY A FLY CUTTER, R=22.6 MM)

MATERIAL SPECIFICATIONS = HIGH IMPACT POLYSTYRENE GRADE BCF , MADE BY BP CHEMICAL .

SPECIMENS DIMENSIONS=29.0=9.7=.635 CM., CROSS-HEAD SPEED=1.0 CM./MIN.

NO GLUE COVERS THE CRACK.

THE FRACTURE TOUGHNESS VALUES ARE EVALUATED BY USING THE APPLIED LOAD AT THE CRACK GROWTH APPEARANCE

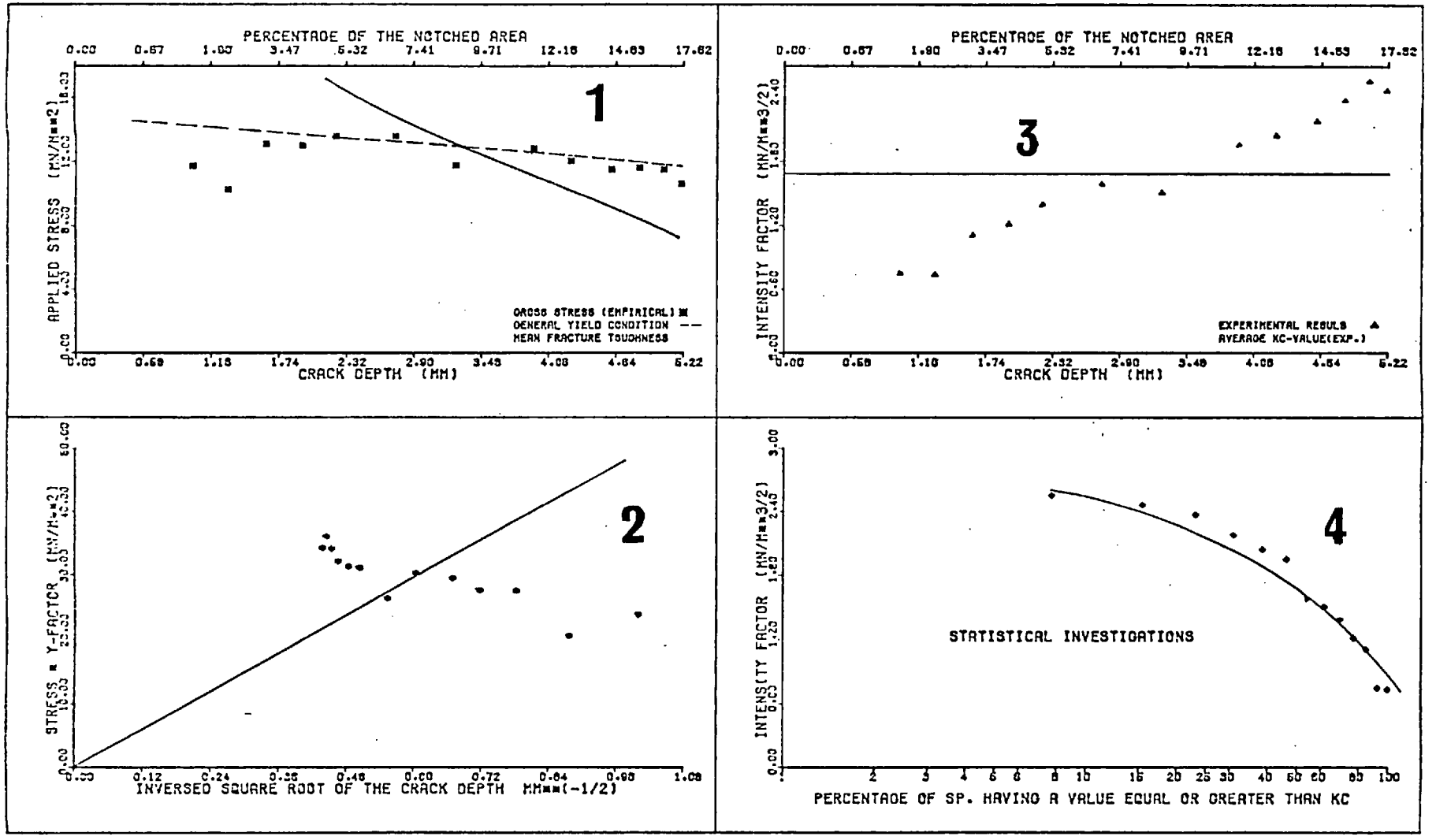


Figure 6.13

CIRCULAR SURFACE NOTCHED SPECIMENS(PRODUCED BY A FLY CUTTER. R=22.6 MM)

MATERIAL SPECIFICATIONS.= HIGH IMPACT POLYSTYRENE GRADE BCF . MADE BY BP CHEMICAL .

SPECIMENS DIMENSIONS=28.0*9.7*.635 CM.. CROSS-HEAD SPEED=1.0 CM./MIN.

NO GLUE COVERS THE CRACK.

THE FRACTURE TOUGHNESS VALUES ARE EVALUATED BY USING THE APPLIED LOAD AT THE CRAZE APPEARANCE

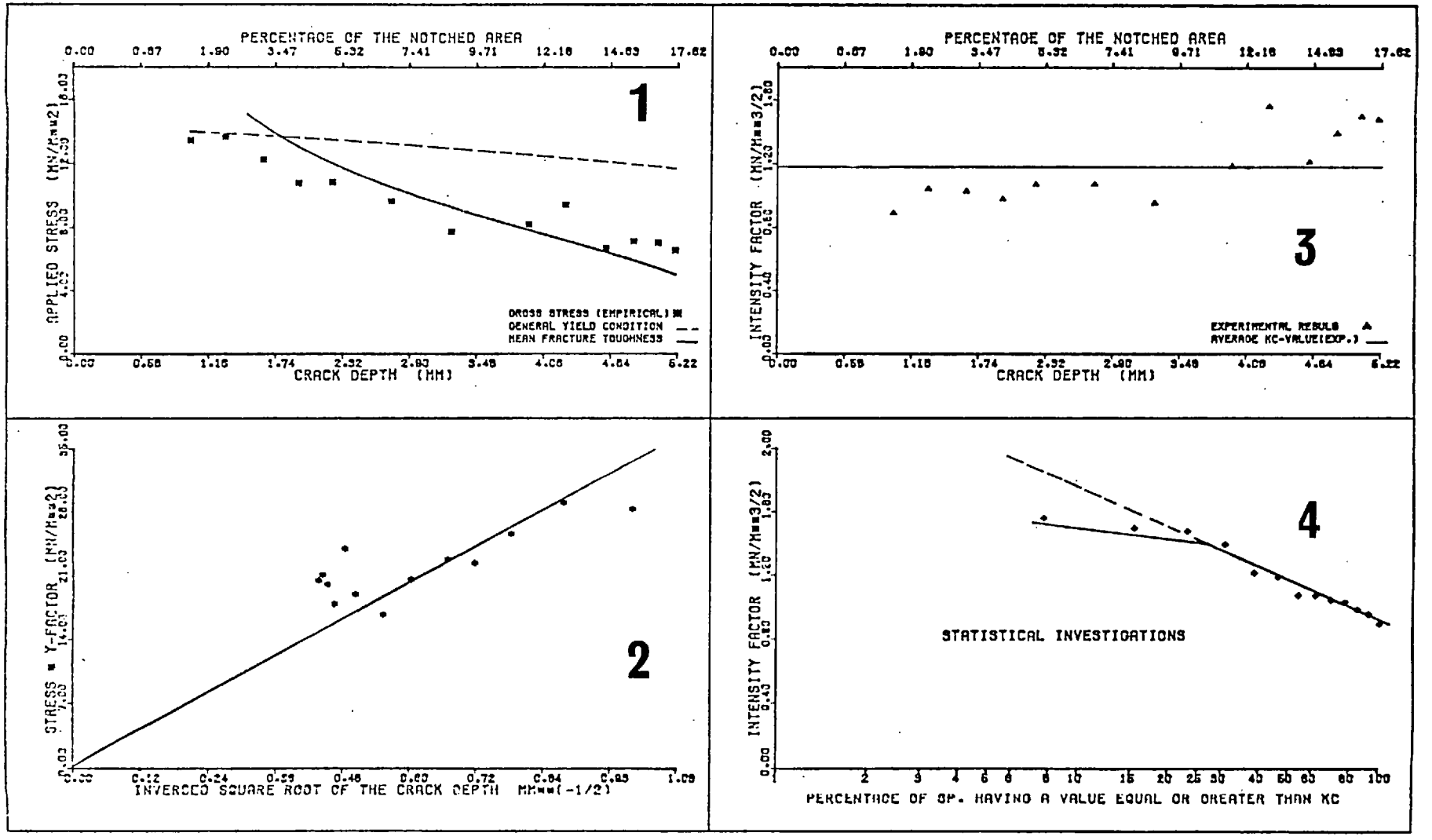


Figure 6.14

CIRCULAR SURFACE NOTCHED SPECIMENS(PRODUCED BY A FLY CUTTER. R=22.6 MM)

MATERIAL SPECIFICATIONS = HIGH IMPACT POLYSTYRENE GRADE BCF . MADE BY BP CHEMICAL .

SPECIMENS DIMENSIONS=29.0*9.7*.635 CM.. CROSS-HEAD SPEED=1.0 CM./MIN.

A LAYER OF ARALDITE 24 MM. THICK IS SPRED OVER THE BOTH SIDEHE SPECIMENS CRACKS AND EXTENDED TO ITS EDGES .

KC-VALUES WERE EVALUATED . USING THE INITIAL CRACK LENGTH & MAXIMUM APPLIED LOAD .

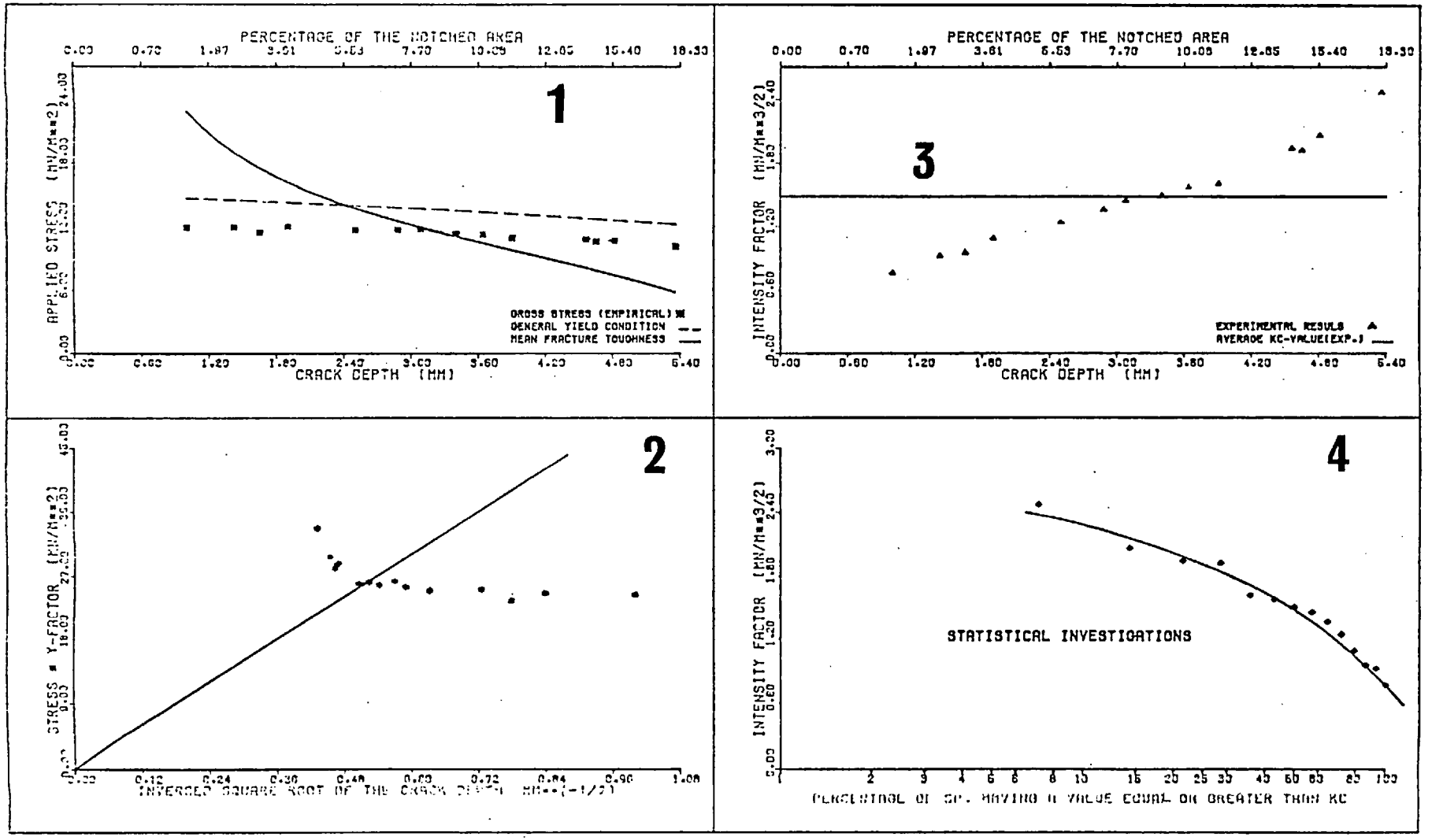


Figure 6.15

CIRCULAR SURFACE NOTCHED SPECIMENS(PRODUCED BY A FLY CUTTER. R=22.6 MM)

MATERIAL SPECIFICATIONS = HIGH IMPACT POLYSTYRENE GRADE BCF . MADE BY BP CHEMICAL .

SPECIMENS DIMENSIONS=29.0*9.7*.635 CM.. CROSS-HEAD SPEED=1.0 CM./MIN.

A LAYER OF ARALDITE .24MM. THICK COVERS THE CRACK LENGTH ADDED TO THE SPECIMENS EDGES

THE FRACTURE TOUGHNESS VALUES ARE EVALUATED BY USING THE APPLIED LOAD AT THE CRACK GROWTH APPEARANCE

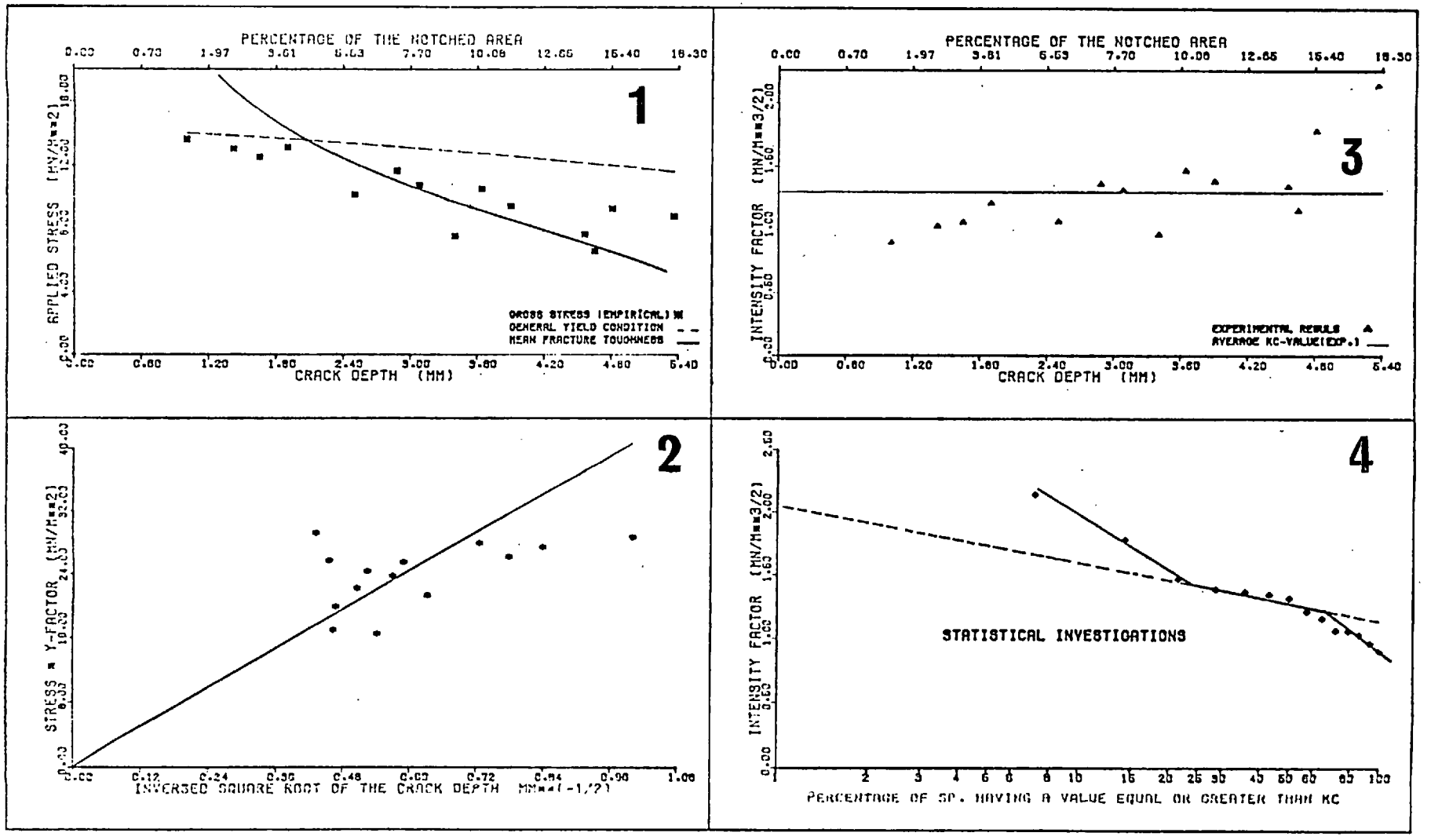


Figure 6.16

SINGLE EDGE-NOTCHED SPECIMENS(PRODUCED BY A FLY CUTTER, R=22.6 MM)

MATERIAL SPECIFICATIONS = HIGH IMPACT POLYSTYRENE GRADE HCF , MADE BY BP CHEMICAL .

SPECIMENS DIMENSIONS=20.0=0.7=.635 CM., CROSS-HEAD SPEED=1.0 CM./MIN.

NO GLUE COVERS THE CRACK.

KC-VALUES WERE EVALUATED , USING THE INITIAL CRACK LENGTH & MAXIMUM APPLIED LOAD .

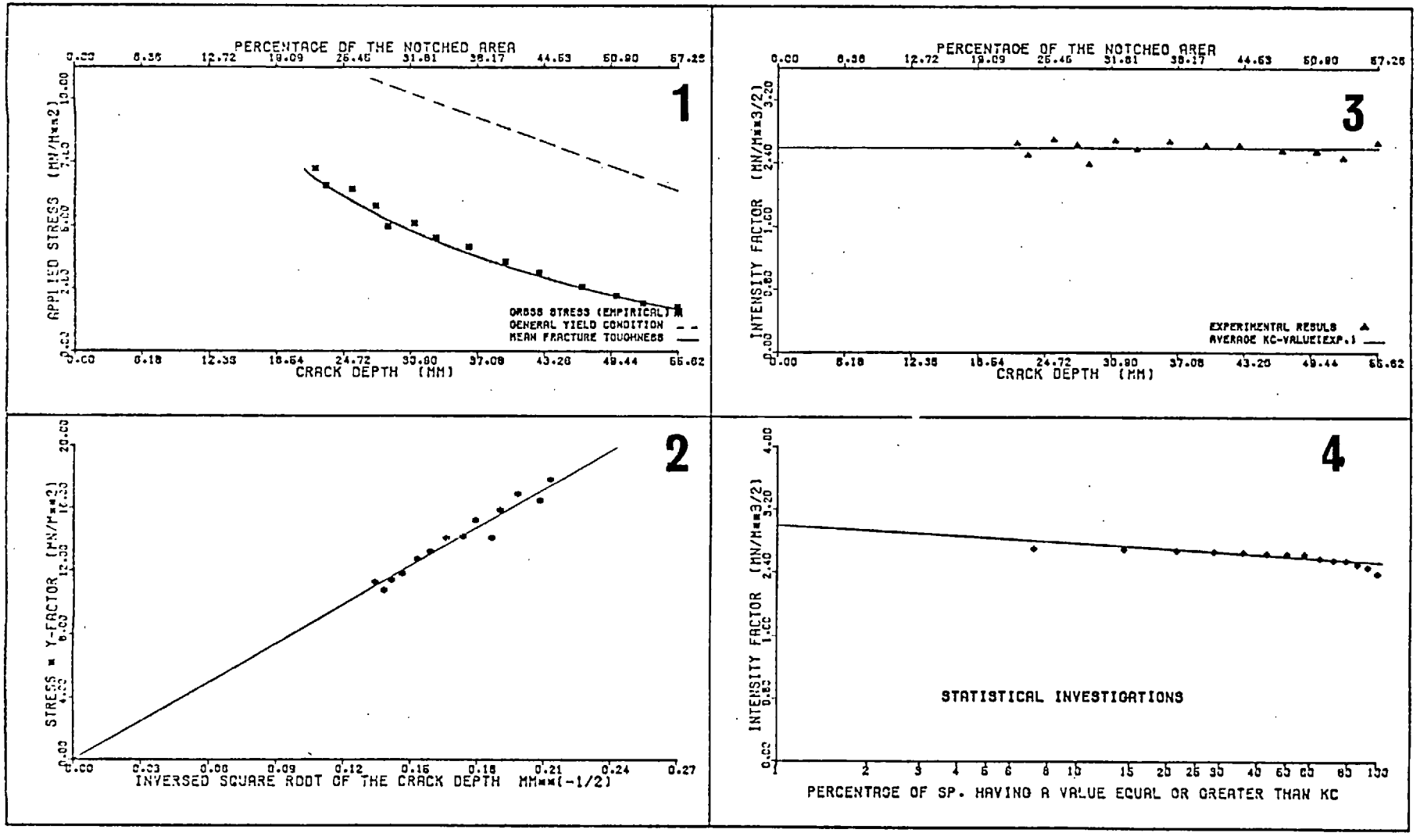


Figure 6.17

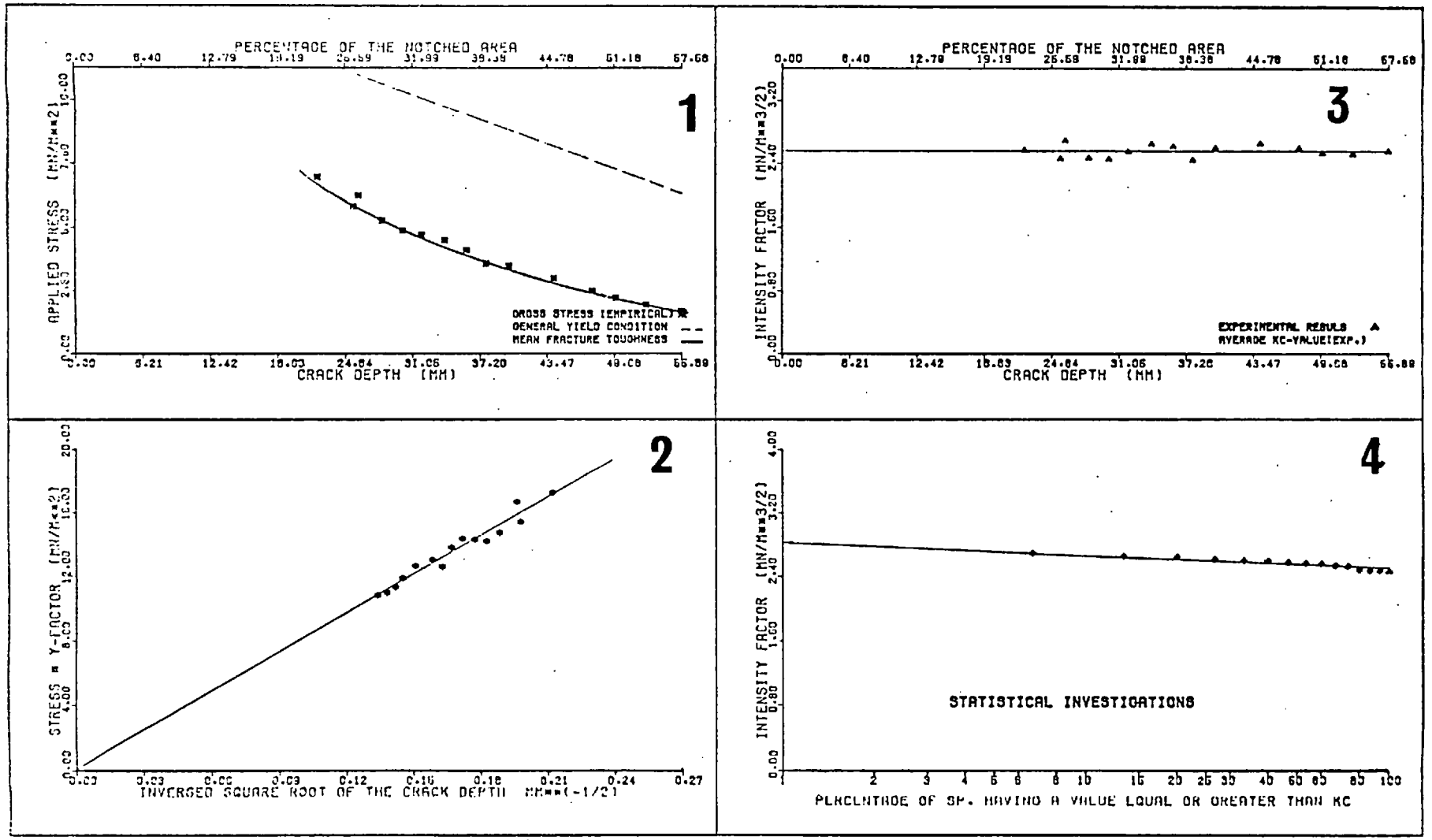
SINGLE EDGE-NOTCHED SPECIMENS(PRODUCED BY A FLY CUTTER, R=22.8 MM)

MATERIAL SPECIFICATIONS = HIGH IMPACT POLYSTYRENE GRADE BCF , MADE BY BP CHEMICAL ,

SPECIMENS DIMENSIONS=29.0=8.7=.635 CM., CROSS-HEAD SPEED=1.0 CM./MIN.

A LAYER OF ARALDITE 24 MM. THICK IS SPRED OVER THE BOTH SIDEHE SPECIMENS CRACKS AND EXTENDED TO ITS EDGES .

KC-VALUES WERE EVALUATED , USING THE INITIAL CRACK LENGTH & MAXIMUM APPLIED LOAD .



characteristics observed in the fracture of polymers, it is therefore clear that the statistical analysis described is indispensible for the understanding of the assumptions and limitations of the fracture criterion employed. If the fracture takes place in a brittle manner, obeying the linear fracture mechanics assumptions, the experimental results are randomly scattered around a constant fracture toughness value. Assuming a Poisson distribution function, the results are represented by equation (6.11). On the other hand, in a ductile failure, the yielding fracture criterion prevails and the data are spread randomly around a constant critical stress. A similar random distribution function, as formulated for K_c, can be obtained to describe the ductile failure on the basis of a constant σ_y. If a transition from ductile to brittle failure occurs, the results will similarly be reflected in the statistical graphs previously denoted.

Figures 6.10 to 6.17 illustrate the results of all the experiments reported in section 6.7 of this chapter. Taking the maximum applied stress and the initial crack length, the results for the 150 mm wide surface notched specimens show that a critical net section stress theory is appropriate. The experimental data are, therefore, randomly scattered around the yield line, as demonstrated in Figures 6.11 and 6.14 for glue-coated and exposed specimens, respectively. The statistical graphs based on a critical intensity factor clearly support the fact that the fracture phenomenon for these specimens cannot be described by linear fracture mechanics theories.

For the narrow single-edge notched specimens (50 mm wide), fracture is similarly governed by a constant net stress theory. The apparent fracture toughness is therefore a strong function of the crack length (Figure 6.10). In contrast, the results for 100 mm wide specimens show

that the fracture toughness evaluated is independent of the crack geometry and therefore the fracture is described by a constant critical intensity factor, K_c (Figures 6.16 and 6.17 for glued and exposed specimens). As shown, the statistical plots of K_c versus $log\ X_n$ produce straight lines through all data for both exposed and glue-coated specimens. ΔK and K_c may be estimated by taking the slopes of the lines and their intercepts on the K axis, so that:

$$\text{Exposed specimens} \begin{cases} \Delta K = 0.11\ MN/m^{3/2} \\ K_{0c} = 2.40\ MN/m^{3/2} \end{cases}$$

$$\text{Glue-coated specimens} \begin{cases} \Delta K = 0.08\ MN/m^{2} \\ K_{0c} = 2.47\ MN/m^{3/2} \end{cases} \qquad (6.13)$$

A measure of the scatter in the distribution may be found from $\Delta K/K_{0c}$, that is:

Scatter for exposed specimens = 4.5%

Scatter for glue-coated specimens = 3.2%

The mean value of K_c will be given approximately by $K_{0c} + \Delta K$, thus:

K_c (exposed) = 2.51 $MN/m^{3/2}$

and K_c (glue-coated) = 2.55 $MN/m^{3/2}$

The results above show that the spread in the experimental results for both glue-coated and exposed single-edge notched specimens are decidedly small. This is, of course, achieved when wider specimens (100 mm) are tested. (The results for narrow specimens can be compared with the previously mentioned data, which shows ΔK = 1.1 $MN/m^{3/2}$, that is,

almost 90% scatter.)

Although, owing to a comparatively large craze formation, linear fracture mechanics fails to describe the fracture of surface notched specimens*, the inception of craze production can be adequately determined by considering the fracture toughness at craze initiation. The experimental results illustrated in Figure 6.13 show the fracture toughness at craze initiation for exposed surface notched specimens (100 mm wide). The fracture toughness evaluated is reasonably independent of the crack length (except for $a/B > 0.5$†), although the scatter in the results is considerably large. From the statistical analysis (graph 4), we have:

$$\begin{aligned} \Delta K &= 0.25 \text{ MN/m}^{3\ 2} \\ K_c &= K_{0c} + \Delta K = 1.15 \text{ MN/m}^{3/2} \text{ (at craze initiation)} \end{aligned} \tag{6.14}$$

For exposed surface notched specimens (100 mm wide), the crack initiation is again preceded by a considerable amount of craze growth and, therefore, cannot be accurately described by linear fracture mechanics theories (Figure 6.12). On the other hand, when the specimens are coated by a thin layer of Araldite, the crack initiation occurs at an almost constant intensity factor, K_c (except for $a/B > 0.5$). From the statistical graph (Figure 6.15), we have:

---

* In contrast to single-edge notched specimens, the application of wider specimens did not provide a better consistency in fracture toughness values evaluated at crack instability.

† This is due to the limitation of the approximate solution (equation (6.4)) which was used to evaluate the intensity factor.

$$\Delta K = 0.3 \text{ MN/m}^{3/2}$$
$$K_c = K_{0c} + \Delta K = 1.45 \text{ MN/m}^{3/2} \text{ (at crack initiation)} \qquad (6.15)$$

6.10 STRAIN RATE EFFECT

The experiments described in the preceding sections showed that the failure of HIPS can be characterised by fracture mechanics theories, provided that appropriate specimen geometries and crack configurations were employed. The fracture toughness evaluated is, however, a function of strain rate, temperature, and environmental conditions. The strain rate effect on the yield stress and modulus of HIPS has been discussed in Chapter 5. It was shown that, while the yield stress increased smoothly with strain rate, the modulus of elasticity remained almost unvaried. This section describes tests carried out over a wide range of Instron cross-head speeds (from 0.005 cm/min to 5 cm/min) with the aim of studying the strain rate effect on the fracture toughness of the same commercial grade of HIPS previously used.

The method of specimen preparation and the test procedure were similar to that described in the earlier sections, but only wide specimens were used in order to induce a more brittle fracture. Batches of 10 to 15 single-edge notched specimens of dimensions 300 mm × 100 mm × 6.4 mm made from compression moulded sheets of the BCF grade of HIPS were tested to failure at different Instron cross-head speeds. In all cases, fracture occurred in a semi-brittle to brittle manner and therefore the K_c criterion could validly be applied at crack instability. The results are shown in Figure 6.18, where the fracture toughness evaluated at the maximum load is plotted versus the Instron cross-head speed. It can be seen that the fracture toughness increases smoothly with the strain rate in a similar manner previously observed for the yield strength of identical materials.

It is interesting to evaluate the fracture toughness of HIPS at higher cross-head speeds by extrapolating the experimental data obtained at a lower range of testing speeds. The results can then be compared with

Machined Single-Edge Notched Specimens

Effect of Strain Rate on the Fracture Toughness

Material specifications = high impact polystyrene, grade BCF, made by BP Chemicals Limited. No Araldite is used to cover the initial crack. The initial crack length and the maximum applied load are used to evaluate the fracture toughness values.

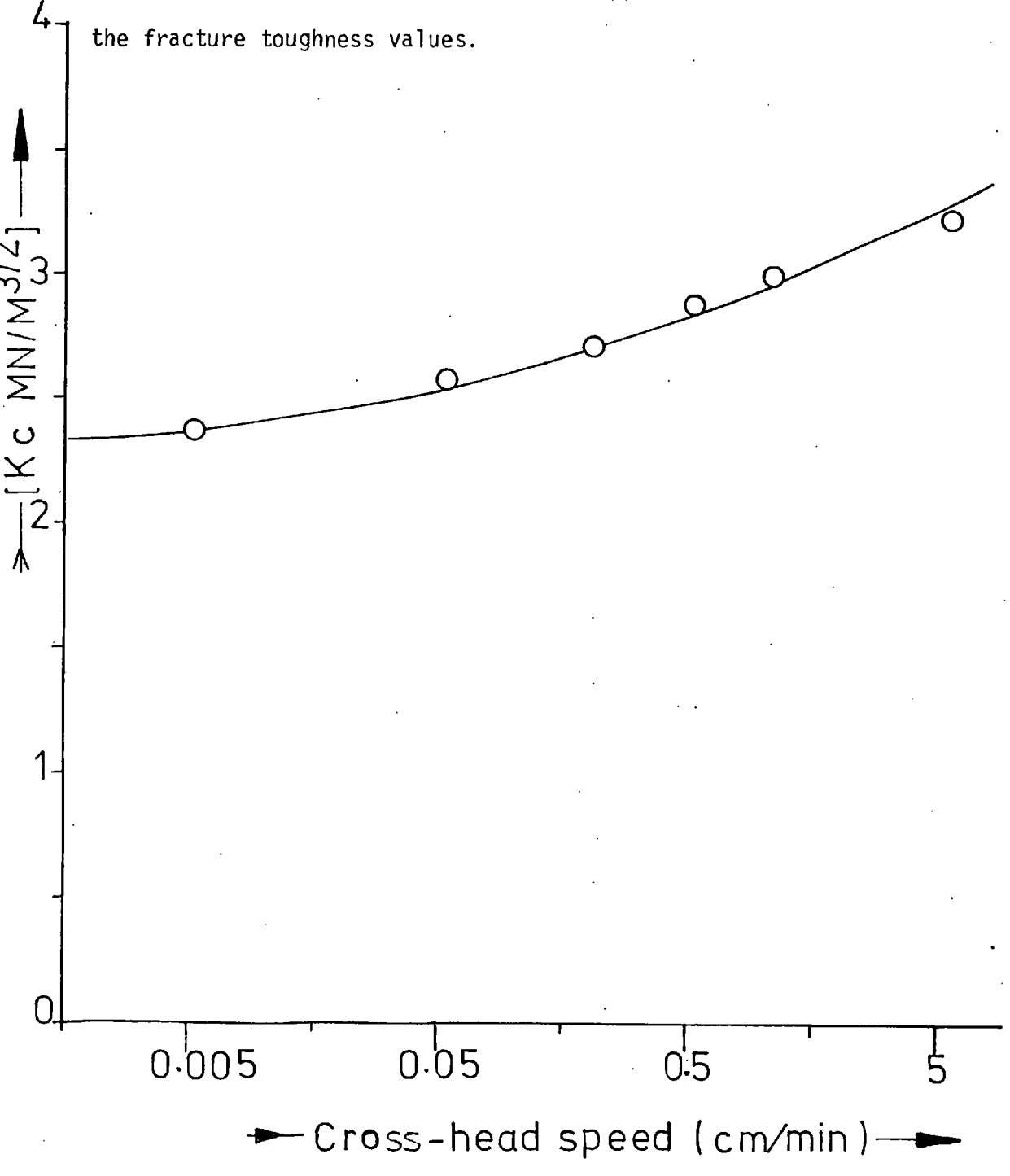


Figure 6.18: Variation of K_c versus cross-head speed

those obtained from impact testing. This must, however, be done with some reservations, since it is reported that the fracture toughness may decrease at higher strain rates (Ferguson (1973)).

The extrapolation of the results to a cross-head speed of about 15×10^3 cm/min, equivalent to the striker speed in a standard impact test, predicts a value of about 3.75 $MN/m^{3/2}$ for the fracture toughness of the BCF grade of HIPS. The equivalent critical strain rate release, G_c, can then be calculated using equation (3.12). Thus:

$$G_c = K_c^2 (1 - \nu^2)/E \simeq 8.5 \text{ kJ/m}^2 \qquad (6.16)$$

where the modulus and Poisson ratio are assumed to be independent of the strain rate and their values are given in section 6.4 of this chapter. The G_c value obtained in the standard test is, however, significantly smaller due to the reason previously explained
(G_c (standard test) = 4.5 kJ/m^2).

6.11 FRACTURE TOUGHNESS AS A FUNCTION OF RUBBER CONTENT

In the preceding chapter, it was shown that the modulus and yield stress dropped markedly with increasing rubber content, having values of 40% to 50% of those for crystal PS at 5.55% nominal rubber fraction. On the other hand, the elongation to break (as an immediate measure of the material toughness) was shown to increase about 23-fold at the 5.55% rubber level. The only reasonable explanation to this is the presence of flaws and crazes near each particle which make the material very compliant.

It is these same flaws which result in an increase in energy absorption in toughness testing and this suggests that there should be a significant increase in K_c with increasing rubber volume fraction. It is therefore of prime importance to any designer working with HIPS to have a clear understanding of the effect of rubber content on the toughness of the article being utilised.

The preliminary experiments on some commercial HIPS have proved that the fracture toughness can be accurately evaluated at critical loads (the instants of craze and crack growth and at maximum applied load) if the appropriate specimen geometry (i.e. wider and thicker specimens), notching technique and application of constraining fragile materials at crack environment are chosen. Therefore, the fracture toughnesses of some specially prepared HIPS containing different rubber contents were measured on a similar basis as previously described for commercial grades of these materials*.

---

* See footnote on next page.

6.11.1 Testing Procedure and Results

Single-edge notched specimens of 300 mm × 100 mm were machined from 3.2 mm thick extruded sheets of HIPS (grades U A0, U A1.11, U A2.22, U A3.33, U A5.55) which contained 0, 1.11%, 2.22%, 3.33% and 5.55% nominal rubber content†. Notches were produced in one edge with a sharp fly-cutter. The specimens were then fractured at 0.05 cm/min in an Instron testing machine and the fracture process was observed using a travelling microscope. The slow cross-head speed was particularly chosen because, firstly, the minimum and therefore the most critical fracture toughness values are obtained at the lowest strain rates (see section 6.10 of this chapter), and secondly, the recording of the fracturing process can be achieved with sufficient accuracy using simpler equipment. Consequently, it was possible to determine the load at both crack initiation and at the onset of rapid crack growth (i.e. instability).

The analysis of the data for toughened materials has always presented a problem because the fracture, by design, is never truly brittle and the K_c criterion is difficult to apply. In these tests, a varying degree of ductility was observed, ranging from brittle through semi-brittle to ductile. However, the use of 100 mm wide specimens does overcome many of the analytical problems. The experimental results were analysed in

---

* Footnote from previous page: Some preliminary tests were carried out on 50 mm wide single-edge notched specimens made of identical grades of specially prepared HIPS. As was expected, the results were similar to those previously described for the commercial grades of HIPS, indicating a large scatter in the K_c evaluated.

† The mechanical properties of these materials have been previously described in Tables 5.1 and 5.2 of Chapter 5.

three ways:

1. The initiation conditions using the crack initiation load and the original crack length;

2. The final, instability, load using the original crack length;

3. The maximum load and crack length at instability.

Figures 6.19 to 6.23 (method 1), 6.24 to 6.27 (method 2) and 6.28 to 6.31 (method 3) show the experimental data for all the materials. The initiation data is notable for being quite accurately described by K_c and this is due to the use of wider specimens. The instability values are not particularly well described if the final crack length is used (method 3) and should only be regarded as apparent K_c values. However, when the fracture toughness at instability is considered, a more consistent result will be obtained if the initial crack length is chosen.

The accuracy of the results are further assessed by evaluating the statistical terms (standard error, skewness, and Kurtosis) which are noted in Table 6.19. In particular, the deviation from the linear theory of fracture can be defined by the slope of the line passing through the data points in a plot of K_c versus the initial crack lengths, that is:

$$\frac{K_c}{K_{cm}} = \Pi_1 + \Pi_2 \, (a/D) \qquad (6.17)$$

where K_{cm} denotes the average K_c value for specimens containing different crack lengths. In this equation, Π_2 illustrates the deviation from the

Figure 6.19

SINGLE EDGE-NOTCHED SPECIMENS(PRODUCED BY A FLY CUTTER. R=60.0 MM)

MATERIAL SPECIFICATIONS = HIGH IMPACT POLYSTYRENE GRADE UAO . MADE BY US STEEL CORPORATION

SPECIMEN DIMENSIONS=30.0*10.0*.316 CM.. CROSS-HEAD SPEED=0.05 CM./MIN.

THE FRACTURE TOUGHNESS IS CALCULATED ON THE BASIS OF THE INITIAL CRACK LENGTH AND MAXIMUM APPLIED LOAD .

NO GLUE COVERS THE INITIAL CRACK OR ANY PART OF SPECIMEN .

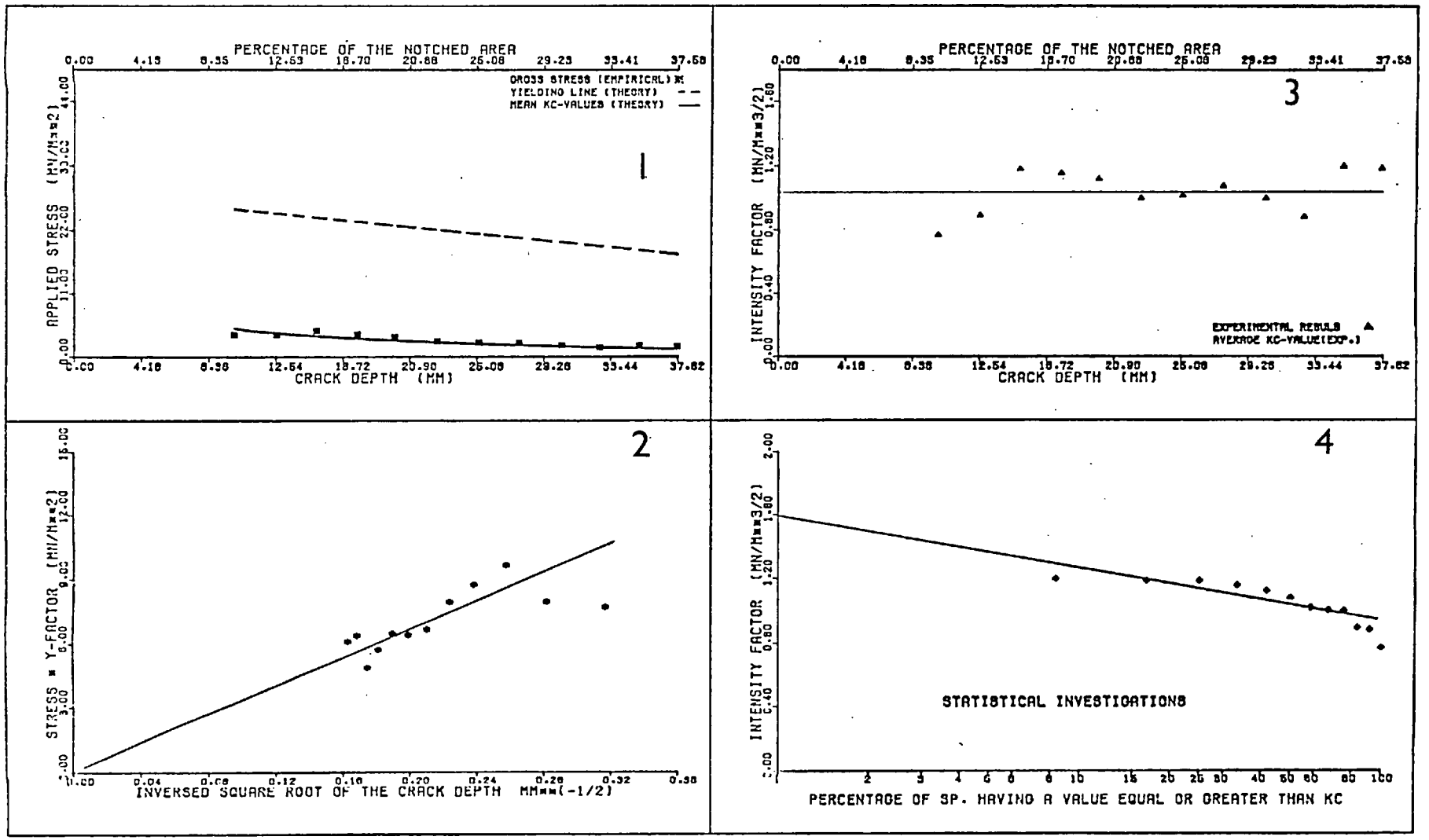


Figure 6.20

SINGLE EDGE-NOTCHED SPECIMENS(PRODUCED BY A FLY CUTTER. R=60.0 MM)

MATERIAL SPECIFICATIONS = HIGH IMPACT POLYSTYRENE GRADE UA1.11 , MADE BY US STEEL CORPORATION

SPECIMEN DIMENSIONS=30.0*10.0*.318 CM.. CROSS-HEAD SPEED=0.05 CM./MIN.

THE FRACTURE TOUGHNESS IS CALCULATED ON THE BASIS OF THE INITIAL CRACK LENGTH AND THE LOAD AT CRACK GROWTH .

NO GLUE COVERS THE INITIAL CRACK OR ANY PART OF SPECIMEN .

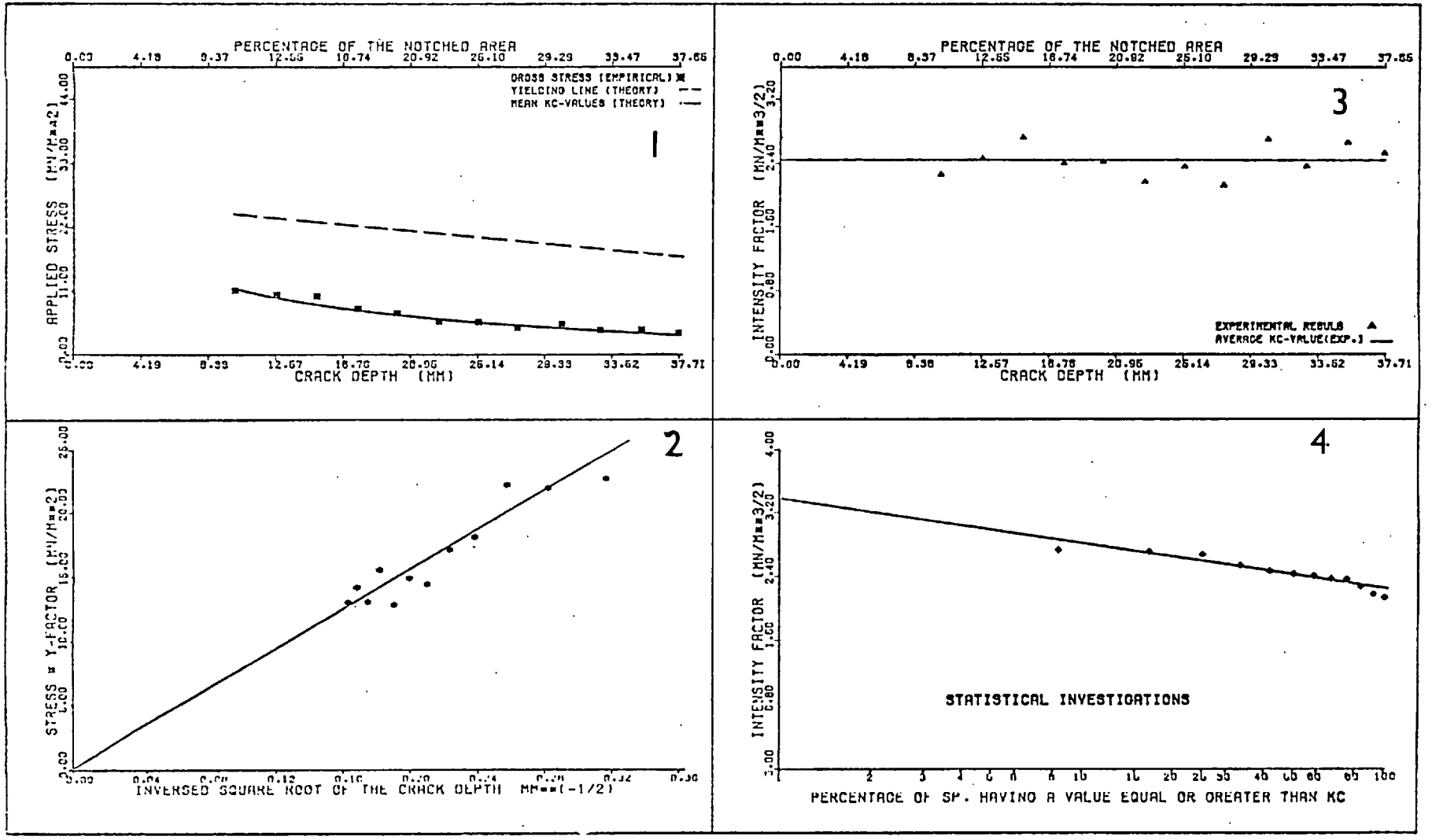


Figure 6.21

SINGLE EDGE-NOTCHED SPECIMENS(PRODUCED BY A FLY CUTTER. R=80.0 MM)

MATERIAL SPECIFICATIONS = HIGH IMPACT POLYSTYRENE GRADE UA 222, MADE BY US STEEL CORPORATION

SPECIMEN DIMENSIONS=30.0*10.0*.318 CM.. CROSS-HEAD SPEED=0.05 CM./MIN.

THE FRACTURE TOUGHNESS IS CALCULATED ON THE BASIS OF THE INITIAL CRACK LENGTH AND THE LOAD AT CRACK GROWTH .

NO GLUE COVERS THE INITIAL CRACK OR ANY PART OF SPECIMEN .

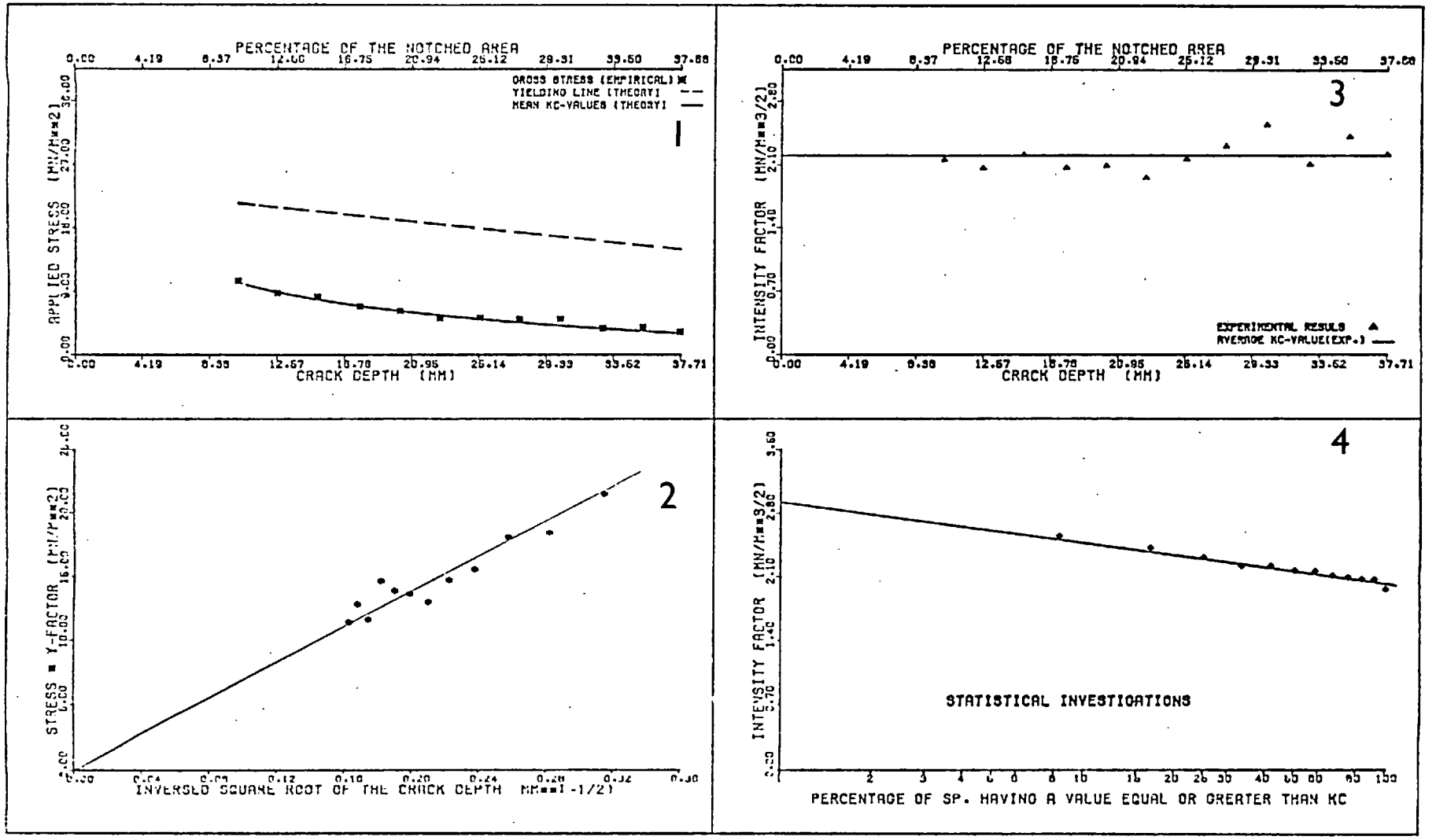


Figure 6.22

SINGLE EDGE-NOTCHED SPECIMENS(PRODUCED BY A FLY CUTTER, R=60.0 MM)

MATERIAL SPECIFICATIONS = HIGH IMPACT POLYSTYRENE GRADE UA 3,33 . MADE BY US STEEL CORPORATION

SPECIMEN DIMENSIONS=30.0*10.0*.316 CM.. CROSS-HEAD SPEED=0.05 CM./MIN.

THE FRACTURE TOUGHNESS IS CALCULATED ON THE BASIS OF THE INITIAL CRACK LENGTH AND THE LOAD AT CRACK GROWTH .

NO GLUE COVERS THE INITIAL CRACK OR ANY PART OF SPECIMEN .

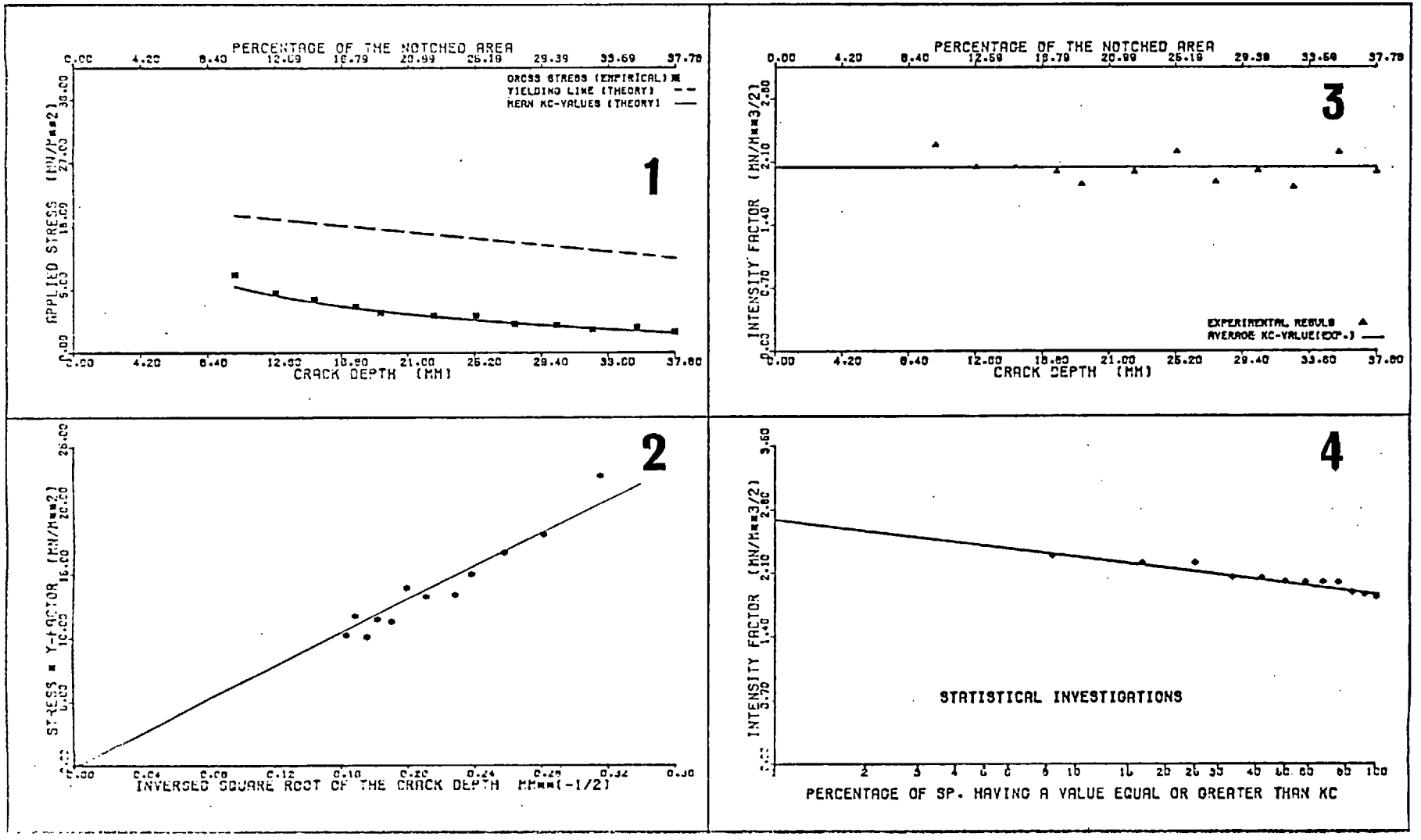


Figure 6.23

SINGLE EDGE-NOTCHED SPECIMENS(PRODUCED BY A FLY CUTTER. R=60.0 MM)

MATERIAL SPECIFICATIONS = HIGH IMPACT POLYSTYRENE GRADE UA 5,55. MADE BY US STEEL CORPORATION

SPECIMEN DIMENSIONS=30.0*10.0*.915 CM.. CROSS-HEAD SPEED=0.05 CM./MIN.

THE FRACTURE TOUGHNESS IS CALCULATED ON THE BASIS OF THE INITIAL CRACK LENGTH AND THE LOAD AT CRACK GROWTH .

NO GLUE COVERS THE INITIAL CRACK OR ANY PART OF SPECIMEN .

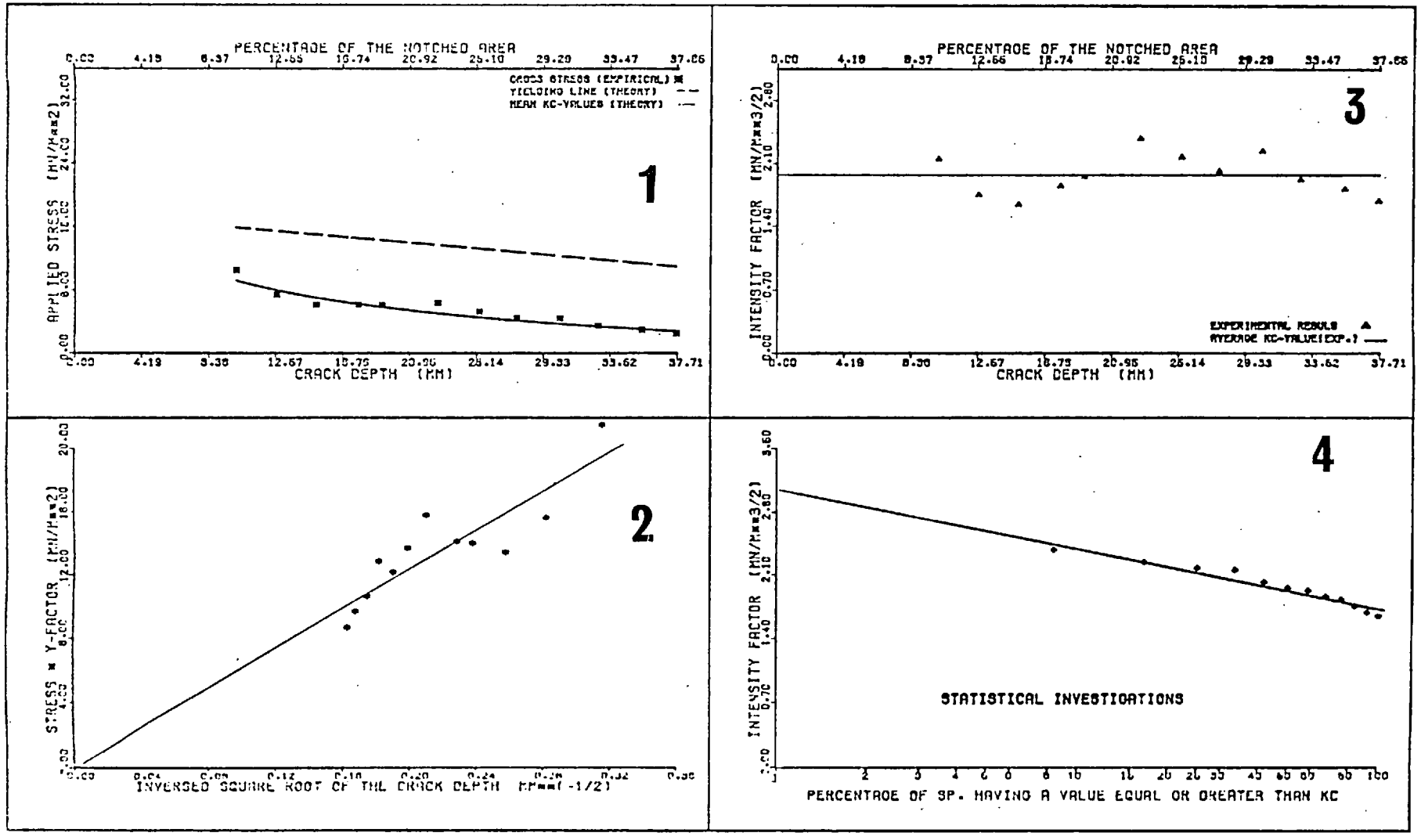


Figure 6.24

SINGLE-EDGE-NOTCHED SPECIMENS [Fly cutter radius, R = 60 mm]

MATERIAL • HIGH IMPACT POLYSTYRENE, GRADE UA 1.11 . CROSS-HEAD SPEED • 0.05 CM/MIN.

SPECIMEN DIMENSIONS•90.0=10.0=.318 CM.. CROSS-HEAD SPEED=0.05 CM./MIN.

THE FRACTURE TOUGHNESS IS CALCULATED ON THE BASIS OF THE INITIAL CRACK LENGTH AND MAXIMUM APPLIED LOAD .

NO GLUE COVERS THE INITIAL CRACK OR ANY PART OF SPECIMEN .

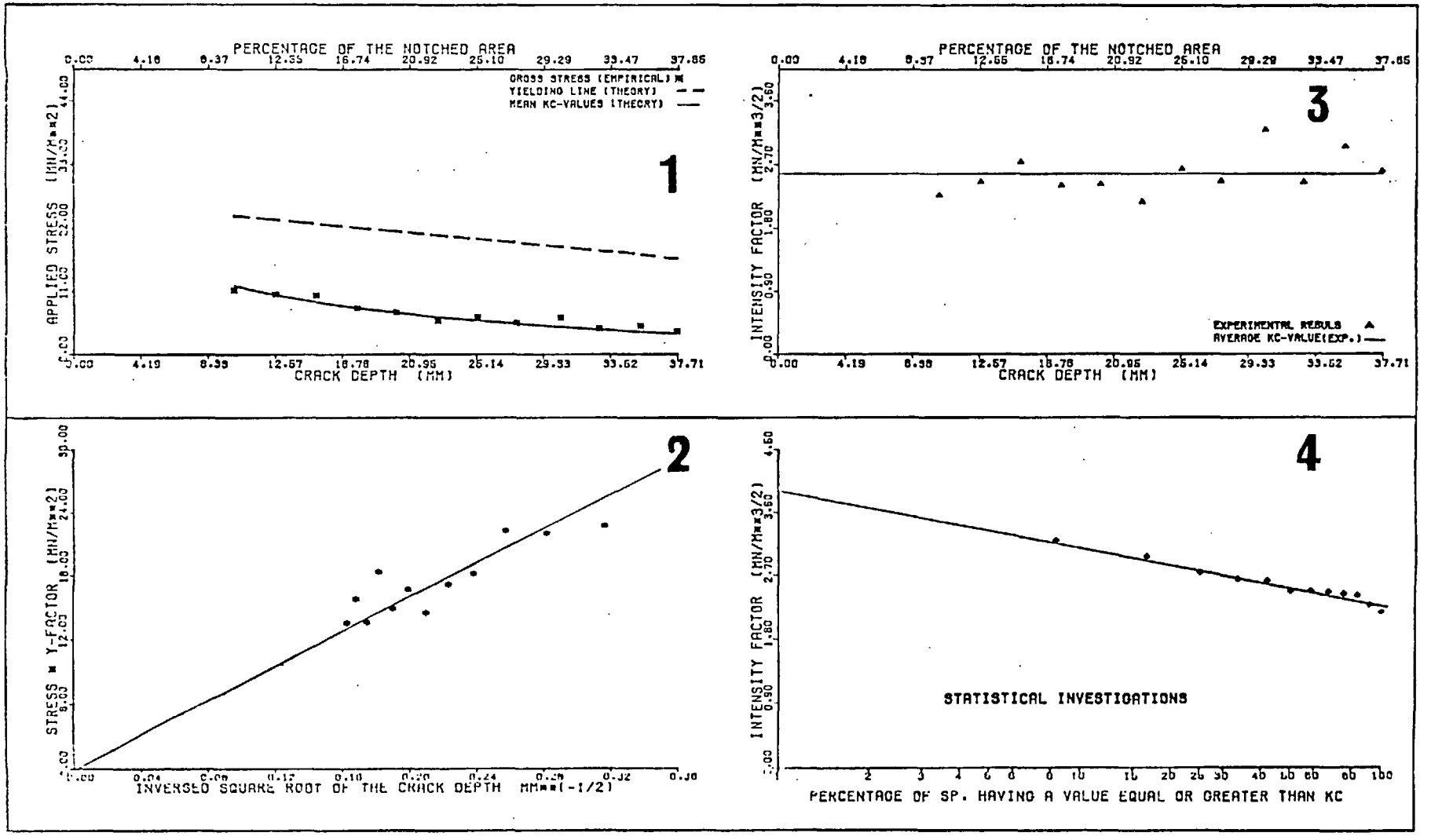


Figure 6.25

SINGLE EDGE-NOTCHED SPECIMENS(PRODUCED BY A FLY CUTTER. R=60.0 MM)

MATERIAL SPECIFICATIONS = HIGH IMPACT POLYSTYRENE GRADE UA222 , MADE BY US STEEL CORPORATION

SPECIMEN DIMENSIONS=30.0*10.0*.318 CM., CROSS-HEAD SPEED=0.05 CM./MIN.

THE FRACTURE TOUGHNESS IS CALCULATED ON THE BASIS OF THE INITIAL CRACK LENGTH AND MAXIMUM APPLIED LOAD .

NO GLUE COVERS THE INITIAL CRACK OR ANY PART OF SPECIMEN .

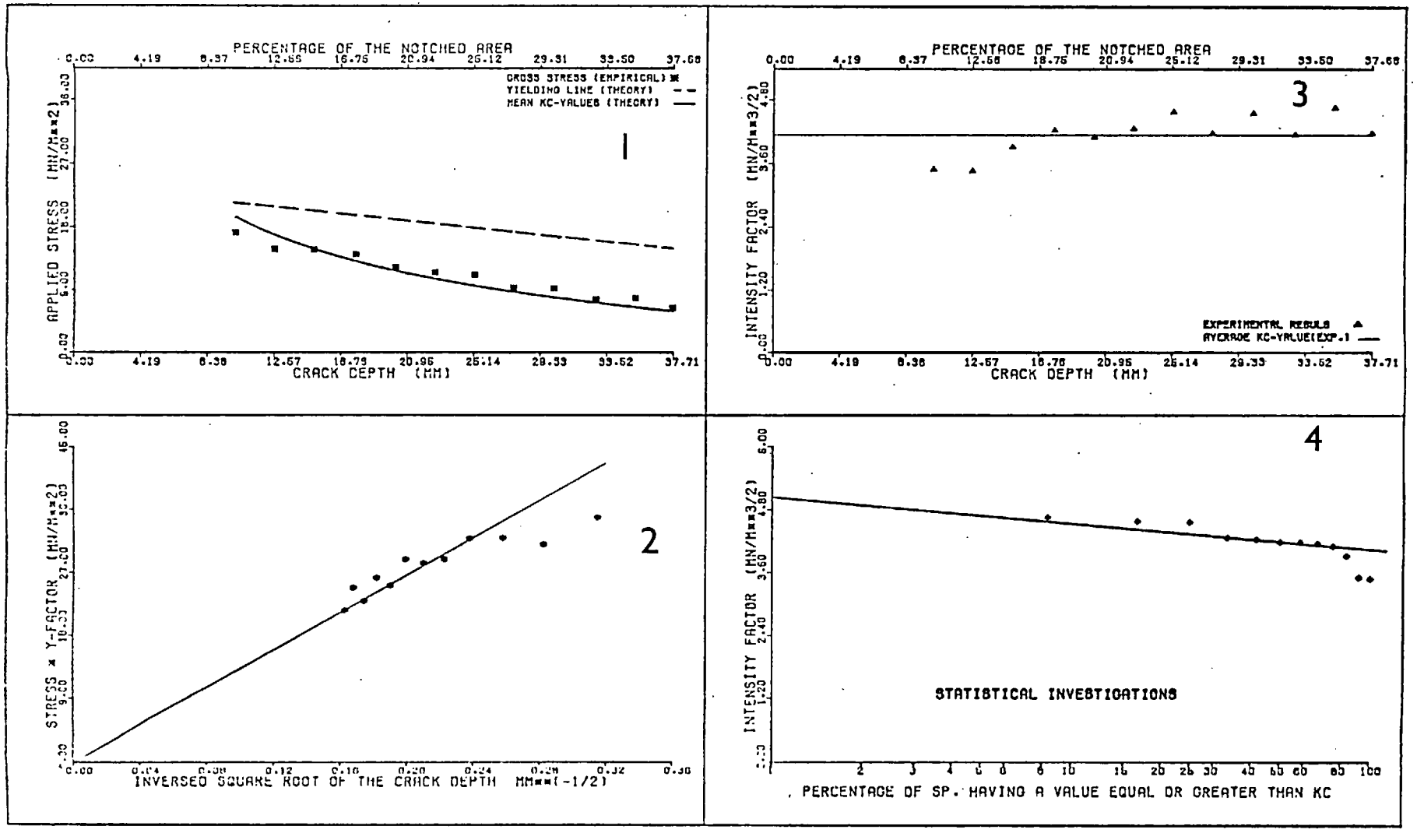


Figure 6.26

SINGLE EDGE-NOTCHED SPECIMENS(PRODUCED BY A FLY CUTTER. R=60.0 MM)

MATERIAL SPECIFICATIONS = HIGH IMPACT POLYSTYRENE ORADE UA 3,33. MADE BY US STEEL CORPORATION

SPECIMEN DIMENSIONS=80.0*10.0*.318 CM.. CROSS-HEAD SPEED=0.05 CM./MIN.

THE FRACTURE TOUGHNESS IS CALCULATED ON THE BASIS OF THE INITIAL CRACK LENGTH AND MAXIMUM APPLIED LOAD .

NO GLUE COVERS THE INITIAL CRACK OR ANY PART OF SPECIMEN .

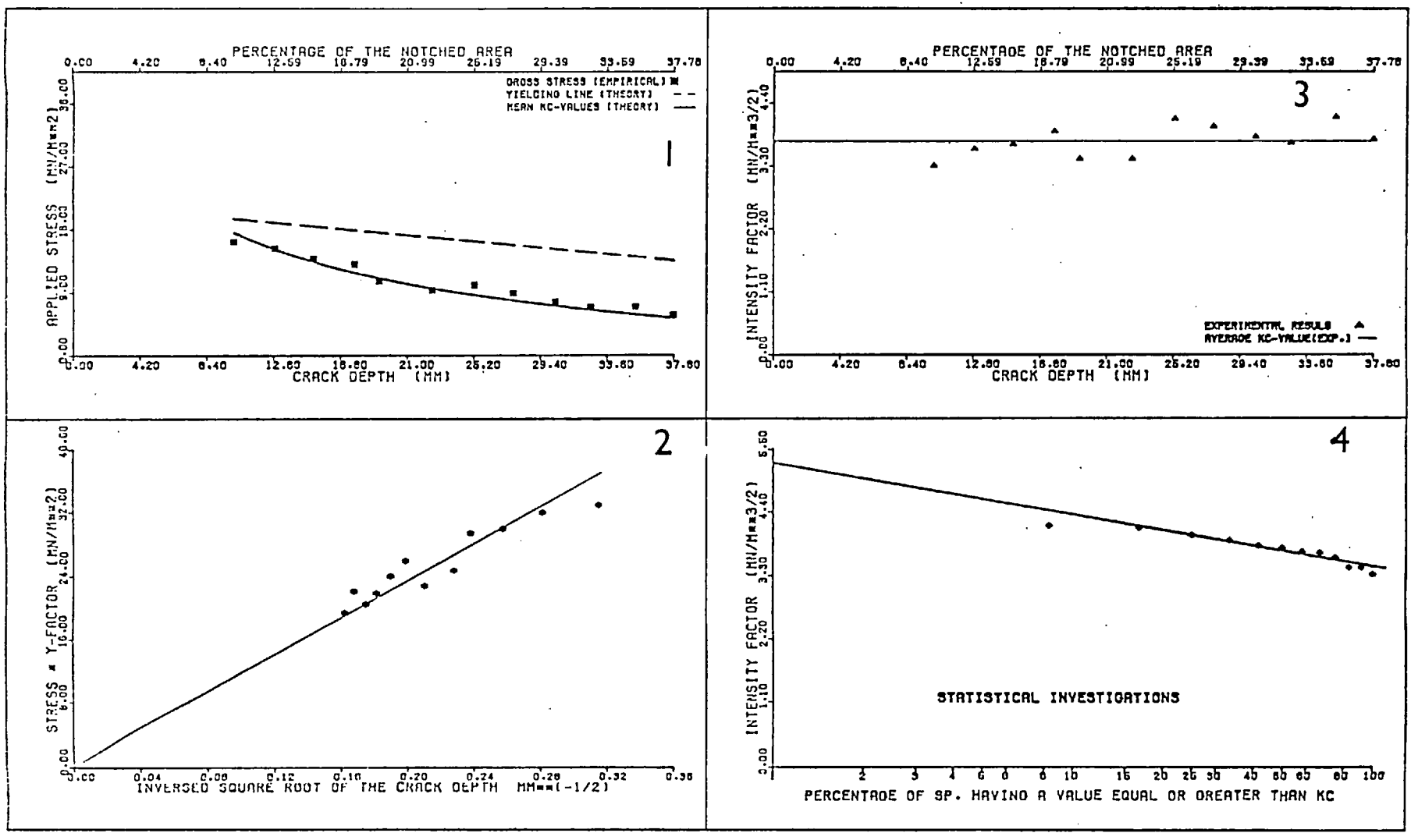


Figure 6.27

SINGLE - EDGE - NOTCHED SPECIMEN S (PRODUCED BY A FLY CUTTER. R=60.0 MM)

MATERIAL SPECIFICATIONS = HIGH IMPACT POLYSTYRENE GRADE UA555 MADE BY US STEEL CORPORATION

SPECIMEN DIMENSIONS=30.0=10.0=.318 CM., CROSS-HEAD SPEED=0.05 CM./MIN.

THE FRACTURE TOUGHNESS IS CALCULATED ON THE BASIS OF THE INITIAL CRACK LENGTH AND MAXIMUM APPLIED LOAD .

NO GLUE COVERS THE INITIAL CRACK OR ANY PART OF SPECIMEN .

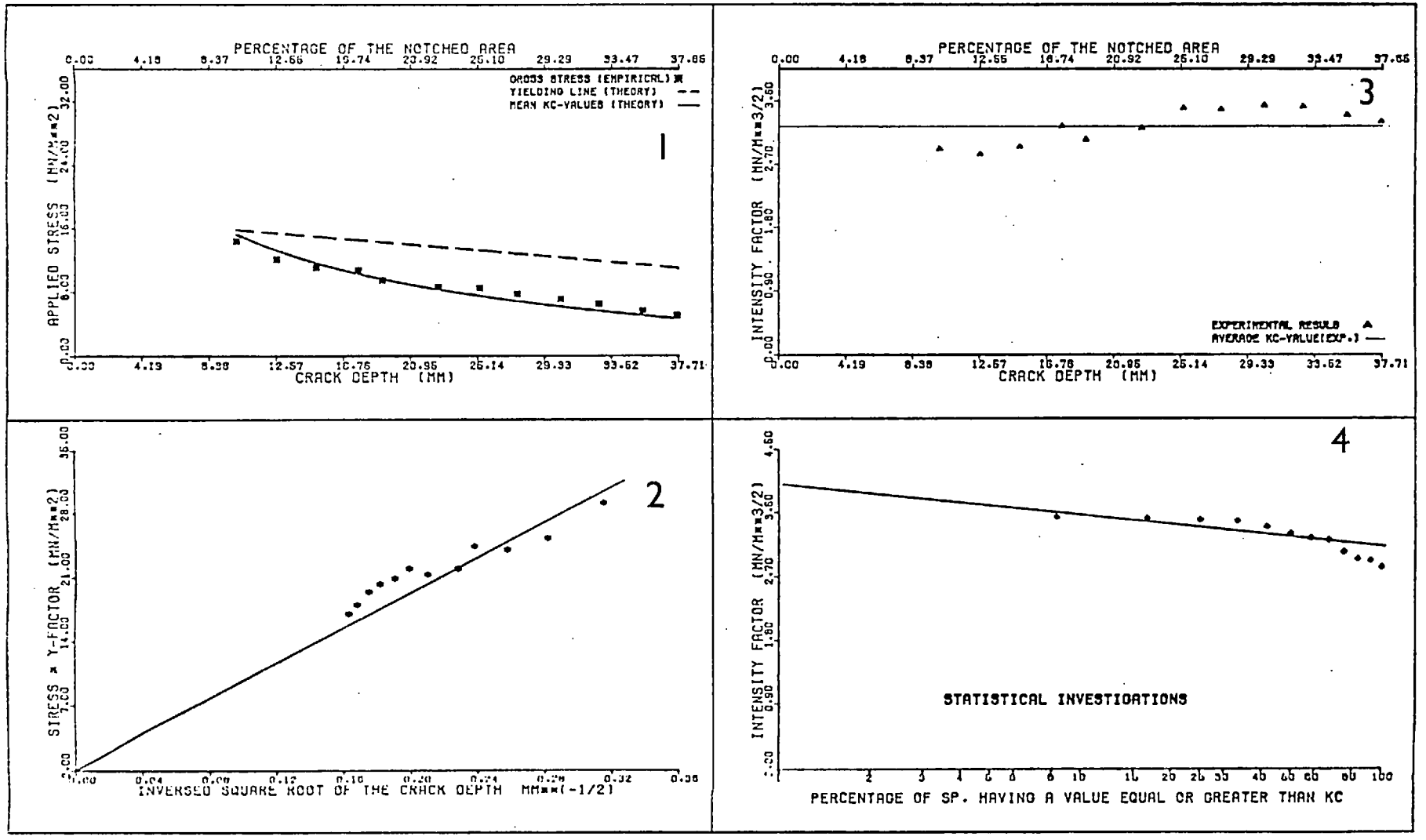


Figure 6.28

SINGLE EDGE-NOTCHED SPECIMENS(PRODUCED BY A FLY CUTTER, R=60.0 MM)

MATERIAL SPECIFICATIONS = HIGH IMPACT POLYSTYRENE GRADE UA 1.11 , MADE BY US STEEL CORPORATION

SPECIMEN DIMENSIONS=30.0*10.0*.318 CM., CROSS-HEAD SPEED=0.05 CM./MIN.

THE FRACTURE TOUGHNESS IS CALCULATED BY TAKING THE CRACK LENGTH AND THE APPLIED LOAD AT RUPTURE.

NO GLUE COVERS THE INITIAL CRACK OR ANY PART OF SPECIMEN .

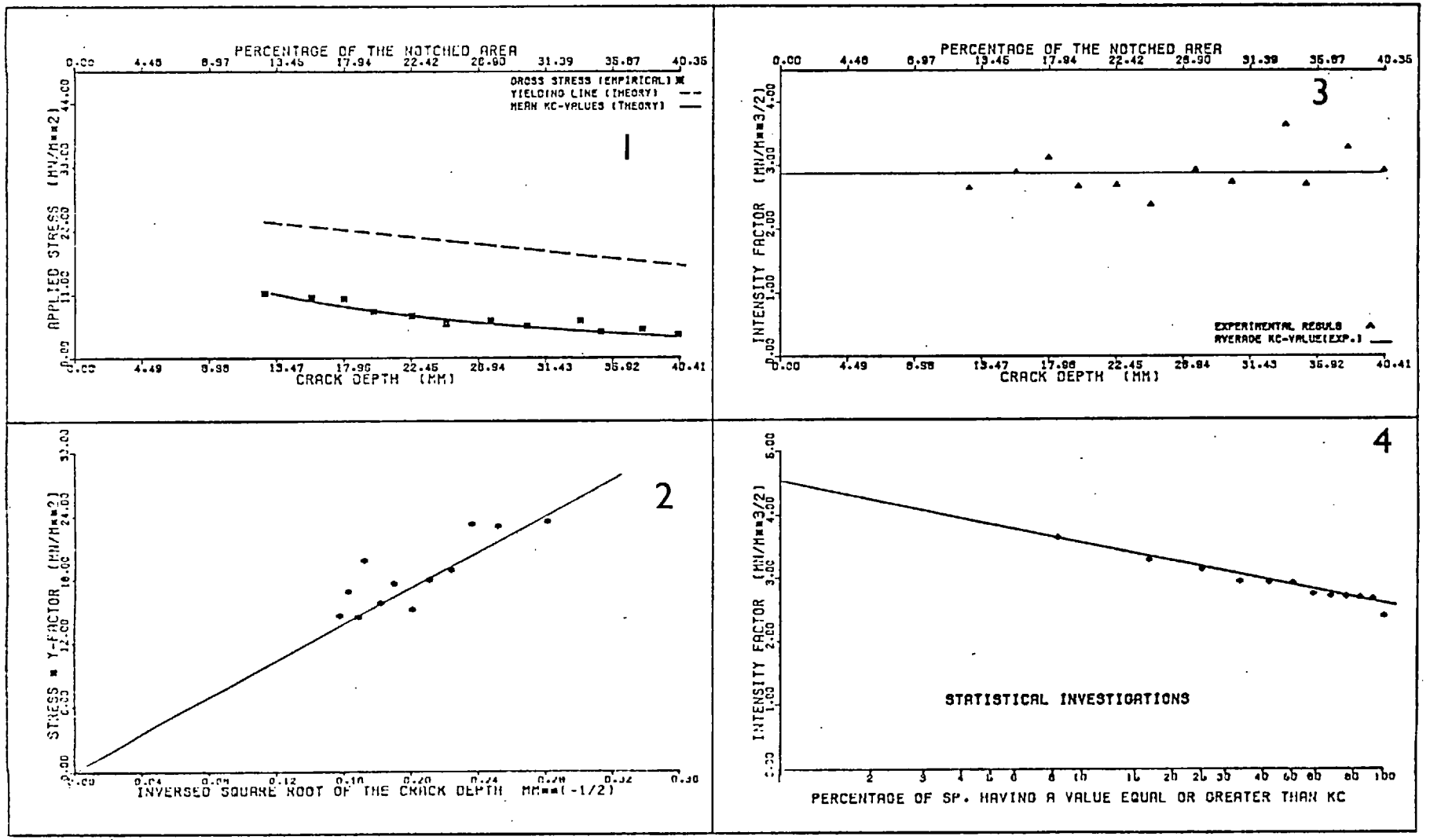


Figure 6.29

SINGLE EDGE-NOTCHED SPECIMENS(PRODUCED BY A FLY CUTTER, R=60.0 MM)

MATERIAL SPECIFICATIONS = HIGH IMPACT POLYSTYRENE GRADE UA 2,2,2, MADE BY US STEEL CORPORATION

SPECIMEN DIMENSIONS=30.0*10.0*.318 CM., CROSS-HEAD SPEED=0.05 CM./MIN.

THE FRACTURE TOUGHNESS IS CALCULATED BY TAKING THE CRACK LENGTH AT MAXIMUM LOAD AND THE MAXIMUM LOAD.

NO GLUE COVERS THE INITIAL CRACK OR ANY PART OF SPECIMEN .

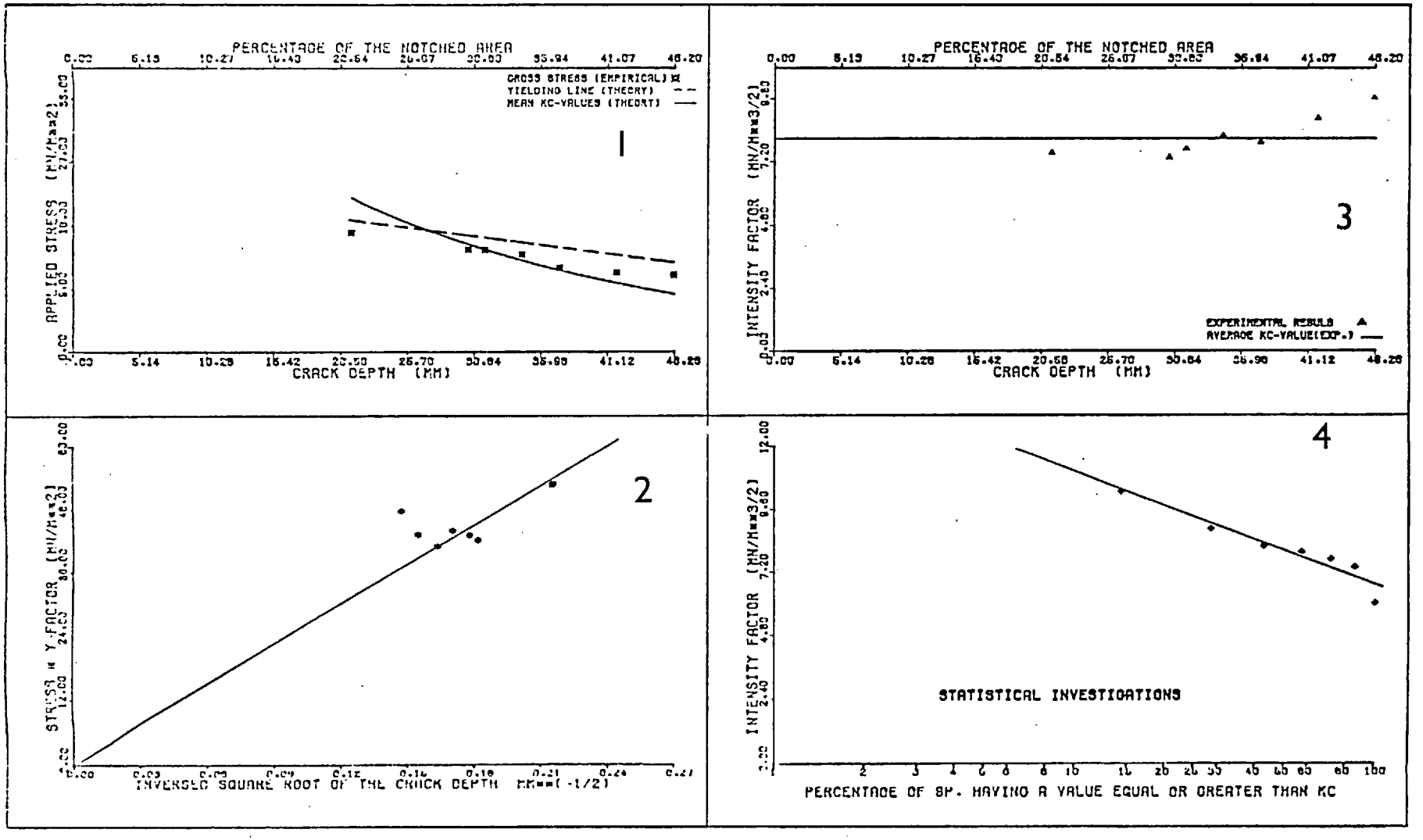


Figure 6.30

SINGLE EDGE-NOTCHED SPECIMENS(PRODUCED BY A FLY CUTTER. R=60.0 MM)

MATERIAL SPECIFICATIONS = HIGH IMPACT POLYSTYRENE GRADE UA 333 , MADE BY US STEEL CORPORATION

SPECIMEN DIMENSIONS = 30*10*.315 CM

THE FRACTURE TOUGHNESS IS CALCULATED BY TAKING THE CRACK LENGTH AT MAXIMUM LOAD AND THE MAXIMUM LOAD.

NO GLUE COVERS THE INITIAL CRACK OR ANY PART OF SPECIMEN .

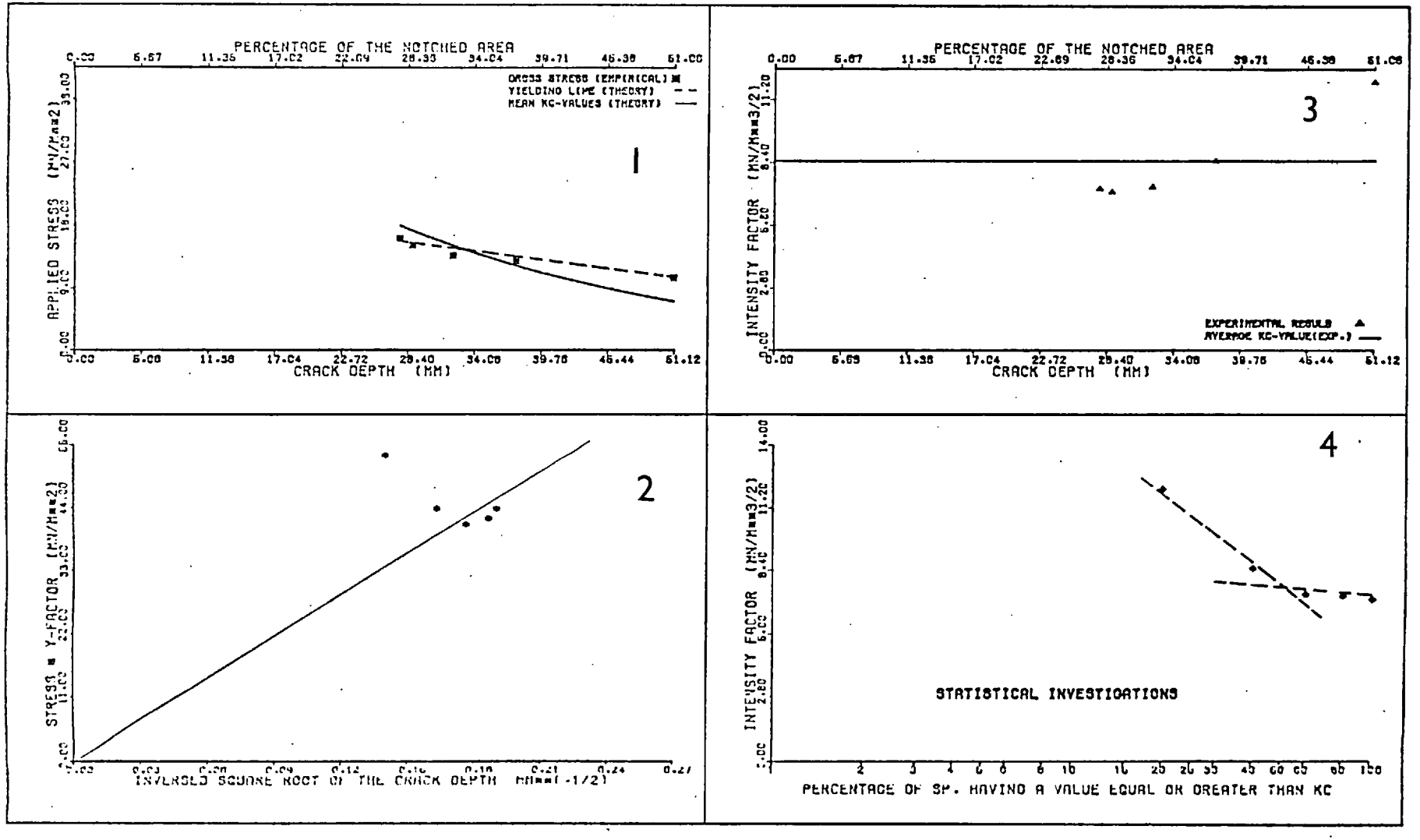


Figure 6.31

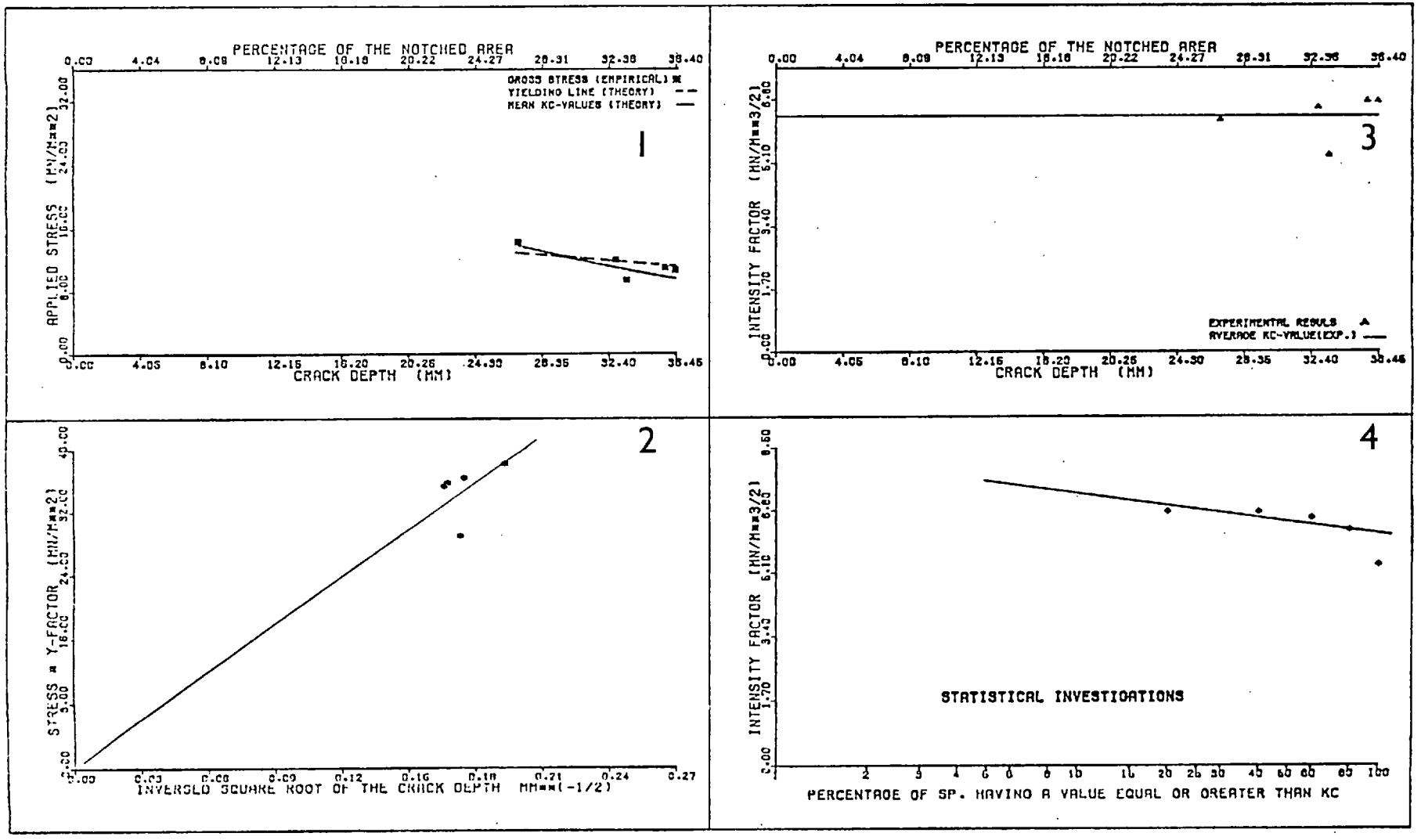
SINGLE EDGE-NOTCHED SPECIMENS(PRODUCED BY A FLY CUTTER, R=60.0 MM)

MATERIAL SPECIFICATIONS = HIGH IMPACT POLYSTYRENE GRADE UA 5.55, MADE BY US STEEL CORPORATION

SPECIMEN DIMENSIONS=30.0*10.0*.318 CM., CROSS-HEAD SPEED=0.05 CM./MIN.

THE FRACTURE TOUGHNESS IS CALCULATED BY TAKING THE CRACK LENGTH AT MAXIMUM LOAD AND THE MAXIMUM LOAD.

NO GLUE COVERS THE INITIAL CRACK OR ANY PART OF SPECIMEN .



linear fracture mechanics criterion. Figure 6.32 shows the deviation from the K_c criterion, using the three methods previously described in evaluating the fracture toughness for different grades of HIPS.

The final plot (Figure 6.33) shows the initiation K_c as a function of rubber content and the striking feature is that K_c maximises at around 1% to 2% rubber content and then remains fairly constant at about twice the crystal value. This result is also obtained using K_c based on the instability values of stress and original crack length (method 2).

On a similar basis, described in section 6.9 of this chapter, the apparent fracture behaviour of these materials are shown in Table 6.19. As demonstrated, the fracture behaviour changes from 100% brittle fracture for CPS to almost 50% semi-brittle and 50% semi-ductile for all other grades of HIPS containing from 1.11% to 5.55% rubber contents.

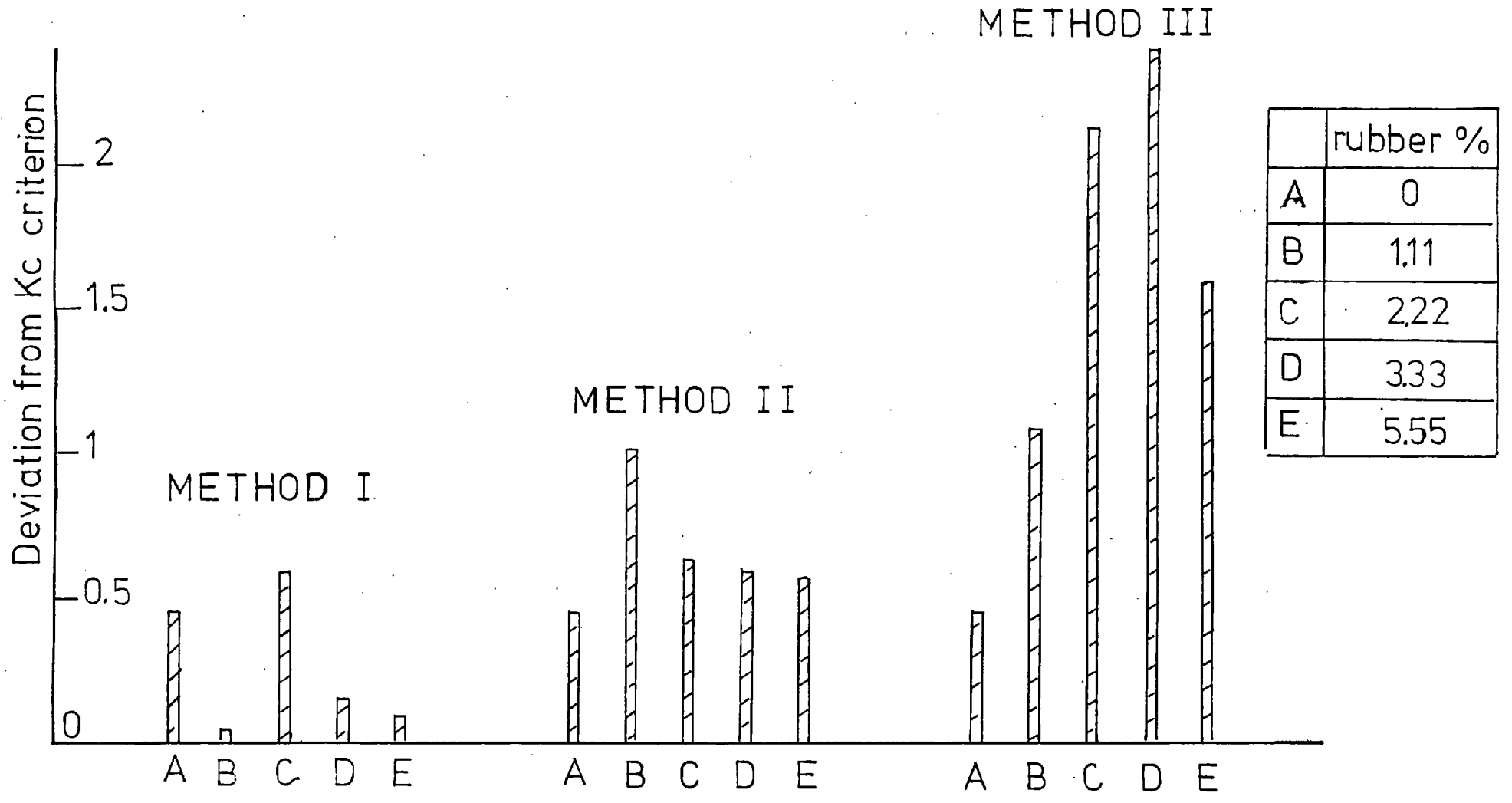


Figure 6.32: Comparison of the computation errors encountered in determining the fracture toughness of HIPS using: I. The original crack length and the crack initiation load; II. The original crack length and the load at instability; III. The crack length at instability and the maximum applied load.

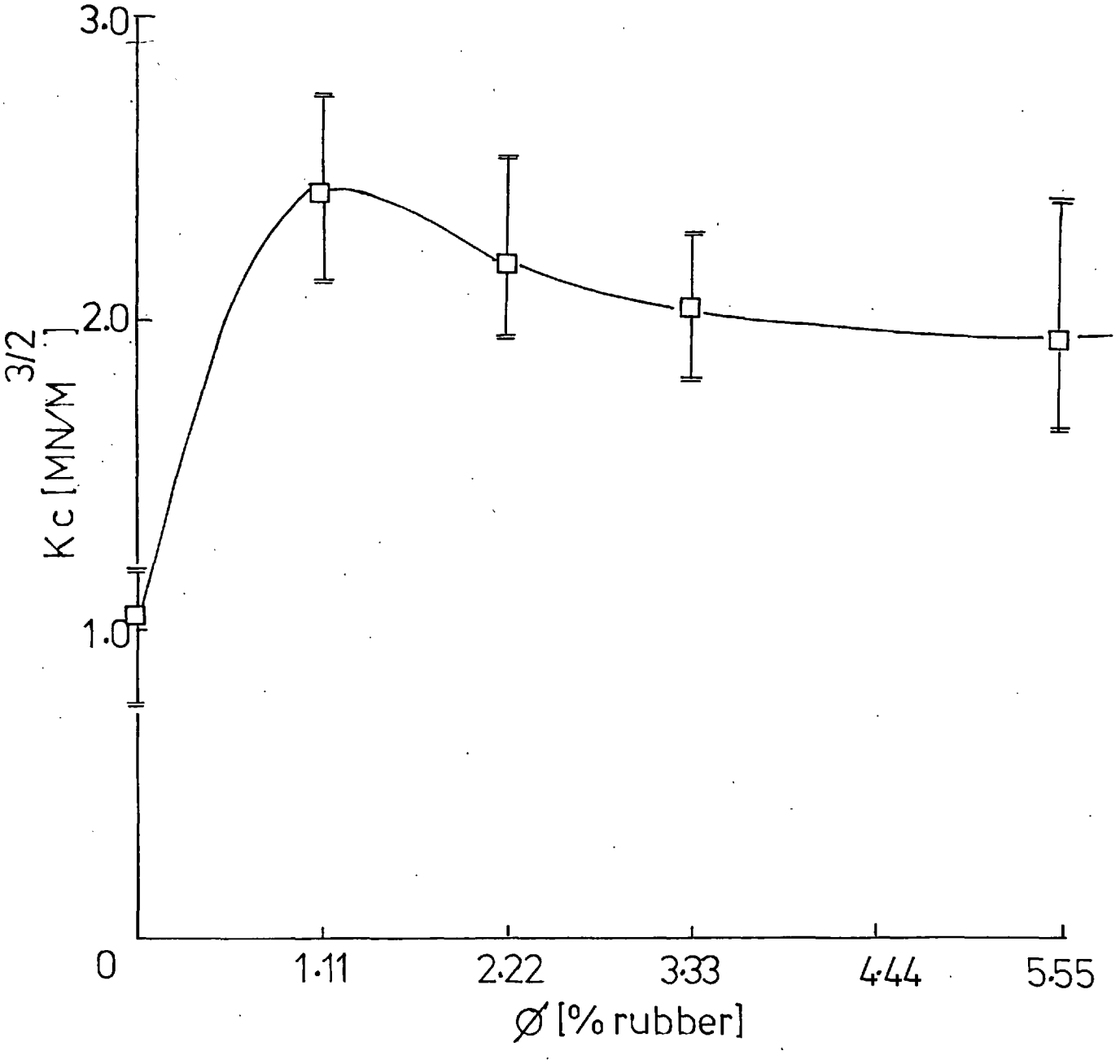


Figure 6.33: Variation of the crack initiation fracture toughness with rubber

TABLE 6.19

Material	U A0	U A1.11	U A2.22	U A3.33	U A5.55
I. Fracture Behaviour:					
1. Brittle	100%	-	-	-	-
2. Semi-brittle	-	100%	50%	45%	48%
3. Semi-ductile	-	-	50%	55%	52%
4. Ductile	-	-	-	-	-
II. Results (Method 1):					
1. Fracture toughness ($MN/m^{3/2}$)	1.04	2.57	4.15	3.74	3.24
2. Plastic radius (mm)	0.23	1.5	5.2	5.1	5.8
3. Variance of results	0.019	0.082	0.141	0.075	0.063
4. Standard error ($MN/m^{3/2}$)	0.040	0.082	0.109	0.079	0.073
5. Skewness	- 0.471	0.760	- 0.480	0.006	- 0.300
6. Kurtosis	1.838	2.613	2.125	1.645	1.393
7. Deviation, ΔK_c	0.469	1.073	0.676	0.604	0.572
III. Results (Method 1):					
1. Fracture toughness ($MN/m^{3/2}$)	-	2.45	2.20	2.04	1.98
2. Plastic radius (mm)	-	1.4	1.4	1.5	2.1
3. Variance of results	-	0.038	0.027	0.021	0.053
4. Standard error ($MN/m^{3/2}$)	-	0.057	0.047	0.042	0.067
5. Skewness	-	0.080	0.718	0.354	0.237
6. Kurtosis	-	1.675	2.531	1.843	1.665
7. Deviation, ΔK_c	-	- 0.056	0.663	- 0.157	0.087

TABLE 6.19 (continued)

Material	U A0	U A1.11	U A2.22	U A3.33	U A5.55
IV. Results (Method 3):					
1. Fracture toughness ($MN/m^{3/2}$)	-	2.88	8.07	8.49	6.35
2. Plastic radius (mm)	-	2.0	1.9	2.6	2.2
3. Variance of results	-	0.113	1.744	4.268	0.369
4. Standard error ($MN/m^{3/2}$)	-	0.097	0.499	0.924	0.272
5. Skewness	-	0.742	0.179	0.908	- 0.809
6. Kurtosis	-	2.808	2.026	1.845	1.714
7. Deviation, ΔK_e ($MN/m^{3/2}$)	-	1.076	2.135	2.390	0.899

6.12 CONCLUSION

Subject to the prerequisite conditions for brittle fracture in HIPS, these materials will break at a constant critical stress intensity factor known as the material fracture toughness. The wide single-edge notched specimens, generally, exhibit a more severe brittle failure compared to narrow specimens or surface notched specimens of the same dimensions. The error and deviation from the linear fracture mechanics for wide single-edge notched specimens will not exceed ± 0.5% of the mean evaluated K_c even for the most ductile materials.

The prerequisite conditions for producing a brittle fracture are summarised for the grade BCF of commercial HIPS as follows*:

A. Single-Edge Notched Specimens: If fracture is considered at the maximum applied load, the gross stress produced must be roughly less than 85% of the material yield stress. Therefore, small cracks do not cause a brittle fracture since they induce a highly stressed medium at the vicinity of the crack plane. On a similar basis, it can be argued that, in order to produce a brittle fracture, the percentage of cracked area must not be less than 15% of the specimen cross-sectional area.

The specimen dimensions must be chosen such that the craze length created at the crack tip remains smaller than at least half the distance between the craze tip and the opposite side of the specimen. The craze length at the final load is estimated

---

* A similar argument is right for the specially prepared HIPS with various rubber contents, although the dimensional conditions prescribed may slightly differ in magnitude but not in form.

at about 1.5 cm for the grade BCF of HIPS. Hence, the conditions for the brittle fracture of this polymer can be approximately formulated by:

$$a + 2.5 \text{ cm} < D < 6.67\, a \qquad (6.18)$$

B. Surface Notched Specimens: The fracture toughness at maximum applied stress cannot be estimated if surface notched specimens are employed. However, the fracture toughness at craze initiation can be evaluated if $a < 0.5\, B$. The fracture toughness of the grade BCF of HIPS at craze initiation is estimated at about 1.15 $MN/m^{3/2}$. If a layer of glue covers the initial crack of a surface notched specimen, the overall ductility of the specimen decreases and thus the fracture toughness at crack initiation may also be obtained with the proviso that:

$$1.8 \text{ cm} < a < 4 \text{ cm} \qquad (6.19)$$

and for this situation:

$$K_c = 1.45 \text{ } MN/m^{3/2} \text{ (at crack initiation)}$$

It is interesting to compare the fracture toughnesses obtained at craze and crack initiation, using surface notched specimens with the

instability fracture toughness evaluated at maximum load utilising wide single-edge notched specimens. As shown, the K_c at crack initiation is almost a half of the estimated K_c at the maximum load suffered by the material. This is an important safety factor in the design of polymeric structures since the load bearing capacity of these materials will not immediately be exhausted after the appearance of the first incipient cracks and thus the damaged articles can be observed and replaced, even if the loading may increase in the meantime to much higher levels.

The second part of the work described in this chapter was to analyse the effect of rubber content on the toughness of some specially prepared HIPS containing different nominal rubber fractions. The picture which emerges is that the fracture toughness increases quite significantly with rubber content up to 2% nominal rubber fractional volume. However, there appears to be no further improvement with increasing the rubber fraction. It seems likely that there are two toughening processes involved here. There is the initiation of crazes by the rubber particles, and the toughening effect of the damping characteristics of the rubber. In slow rate tests, the particles normally initiate large volumes of crazes (as reflected in the modulus of elasticity) and the energy absorbing capacity of the material will soon be exhausted. The presence of a large number of particles may eventually inhibit craze formation, resulting in a gradual fall-off in fracture properties.

The choice of an optimum rubber content is clearly complex and will depend on the desired properties. This aspect will be the subject of the study in Chapter 9, where the effect of temperature on the fracture behaviour of identical specially prepared types of HIPS will be investigated.

CHAPTER 7

THE IMPACT STRENGTH OF RUBBER-MODIFIED POLYMERS

7.1 INTRODUCTION

In many applications of plastics, such as valves, fan blades, motor components and pipes, where dynamic and sudden loads are expected, a precise knowledge of the impact resistance is of major importance. In other applications, such as optical instruments, the impact properties may not be of immediate interest to designers; however, it cannot usually be entirely ignored with confidence. This is an even more significant parameter for plastics since many of these materials exhibit ductile behaviour under low or moderate strain rate conditions but show brittle behaviour when subjected to impact loading.

Many would consider plastics to be tough if they could withstand a hammer blow or similar impact treatment without a shattering fracture. However, when the impact behaviour of a component is a crucial engineering parameter, the classification of materials as such does not obviously provide an accurate and scientific basis for designers. This is particularly important when the components concerned contain artificial stress concentrators or a probability of intrinsic flaws and manufacturing defects, since it is found that these have a greater weakening effect under impact conditions. To cite an example, an unnotched HIPS specimen which can be bent back and forth through an arc of 180^{o} in a slow laboratory experiment, fails in a brittle manner at considerably lower stresses if tested under impact loads.

Since the introduction of plastics on the market as a substitute for metallic substances, several impact machines and various data analysis techniques have been devised to study the ability of these materials to

absorb impact energies required for fracturing. Previous knowledge on the impact testing of metals was considered to be a useful basis on which to assess the impact resistance of ductile polymers, but was found to be insufficient and erroneous when employed for brittle and quasi-brittle polymers. The principal requirements of any impact analysis of such polymers are, briefly, as follows:

1. The experimental data must be lucid and scientifically construable.

2. The impact strength defined for a particular material must be reproducable in other laboratories.

3. The testing technique must minimise the volume of work necessary to obtain the required information.

4. The analysis of an entire spectrum of a definite family of polymers (and possibly other types of materials) must be made uniquely and the numerical scale on which the results are placed must be consistent and reflect the differences between the impact strengths of these materials.

As shown in the preceding chapter, HIPS behaves in a dual brittle-ductile manner under low strain rate conditions. A similar process occurs when these polymers are tested at comparatively high strain rates. The aim of the present chapter is, therefore, to arrive at a universal solution which can genuinely represent the composite impact behaviour of rubber-modified polymers and to assess the effect of rubber content on the impact strength of various grades of HIPS.

7.2 PREVIOUS WORK ON THE IMPACT TESTING OF TOUGHENED POLYMERS

A comprehensive literature survey and discussion on the impact testing of polymers has previously been given in Chapter 4, and here only specific experimental work on rubber-modified polymers will be reviewed. The preliminary fracture studies of toughened plastics have employed standard impact test methods and have examined the change in impact energy with specimen and notch dimensions, fabrication conditions, testing temperature, etc., (Hulse & Taylor (1957); Bobalek & Evans (1961); Bucknall & Street (1967); Vincent (1971)). The experimental results of these conventional impact tests are mostly expressed in terms of specific impact energies (e.g. energy per unit length of notch, energy per unit ligament area, and energy per unit volume of the plastically deformed zone at the crack tip). As previously discussed (section 4.2 of Chapter 4), the standard analysis of impact data does not provide a reliable basis on which to assess the fracture strengths of materials, since the specific impact energies evaluated are a strong function of the specimen dimensions, notch radius and the impact machine employed. Hence, the comparison of the impact strengths of various types of HIPS cannot satisfactorily be made if standard impact testing is used. This is because tests on differing specimen dimensions often rank the material in a different order of impact strength.

As far as it is known, the first attempt to determine the impact strength of rubber-modified polymers on a scientific basis was due to Plati (1975). In trying to analyse the data obtained from a commercial grade of HIPS (equivalent to Grade BCF), Plati employed linear fracture mechanics theory which was previously formulated by Marshall et al (1973). The results did not agree with the theory and thus she concluded that the linear fracture mechanics criterion cannot be validly applied to toughened

polymers due to considerable craze and plastic deformation prior to break. To overcome the problem, Plati suggested either modifying the linear theory by using the effective crack length (which comprised the initial crack length and the plastic zone length created at the crack tip) or by using Rice's contour integral which assumes a full yielding in bending instead of a brittle fracture. As will be shown, neither approach provides a unique solution, especially when a wide spectrum of brittle to ductile HIPS is to be analysed. It is worth mentioning that the results obtained from Charpy and Izod tests by Plati predicted different values for the impact strength of the materials tested, whereas a genuine impact resistance should be a material constant, being independent of the method applied.

7.3 FUNDAMENTALS OF LINEAR AND YIELDING FRACTURE MECHANICS APPROACHES TO IMPACT

The impact strength can be obtained by evaluating the rate of strain energy release due to the extension of the initial crack in a pre-notched impact specimen. Since a comprehensive theoretical discussion on impact testing is given in Chapter 4, only the outline will be presented here.

If a material behaves elastically and the final fracture occurs in a brittle manner with no significant craze or plastic zone ahead of the cracks, the rate of strain energy release at fracture will be defined as the impact toughness, G_b, and can be obtained by applying linear fracture mechanics theories. Hence, by denoting the energy absorbed in impact by I_b, the specimen dimensions by D and B (along and perpendicular to the initial crack, respectively), the initial crack length by a, and the kinetic energy of the flying pieces by U_k, and assuming that the fracture energy only comprises the energy dissipated in crack initiation (that is, the other forms of fracture energies are negligible), we have:

$$G_b = \frac{I_b - U_k}{B\ D\ \Phi\ (a)} \tag{7.1}$$

where Φ is a calibration factor which is a function of the crack length and the supporting span. The values of Φ can be obtained theoretically and experimentally for different geometries of the specimen. In Appendix B, the values of Φ for Charpy specimens are given in polynomial forms in terms of the crack ratios, a/D, and the span ratios, S_p/D.

In ductile materials where an appreciable craze and plastic zone is produced prior to the final fracture, elastic fracture mechanics does not apply and yielding fracture mechanics techniques must be invoked. In this case, when full yielding occurs, the impact strength is defined as

the ratio of the applied energy to the ligament cross-sectional area of a pre-notched sample. That is:

$$G_d = \chi \frac{I_d - U'_k}{B\ D\ (1 - a/D)} \tag{7.2}$$

where I_d denotes the ductile impact energy, and U'_k denotes the rotational kinetic energy. The coefficient χ is numerically equal to unity when no hinging occurs and is taken as equal to 2 when the specimen breaks in a hinge bending mode rather than in shear.

Between the two extremes of perfect ductility and brittleness, there are some plastics which behave in a complex manner. In these cases, the short cracked specimens mostly break in a brittle manner, showing only partial crazing and plasticity. On the other hand, specimens with longer cracks exhibit a ductile failure and thus the results tend to comply with the ductile fracture theory. If the material displays slight crazing or a limited slow crack growth, the modified linear fracture mechanics approach provides a reasonable approximation to the value of impact strength. G_b values can then be obtained by substituting the effective crack length, a_{eff}, in equation (7.1). Assuming a limited plastic zone length, r_p, and a limited slow crack growth, r_s, the effective crack length is defined as:

$$a_{eff} = r_p + r_s + a_o \tag{7.3}$$

where a_o denotes the initial crack length. Generally, a_{eff}, being a function of the specimen geometry and the fracture toughness, cannot be estimated theoretically. The problem can, however, be overcome if adequate experimental data are collected and analysed by trial and error; that is, by adding increasing $(r_p + r_s)$ values to a_o until the best line-

fit is obtained for equation (7.1).

As previously mentioned in Chapter 4, the modified linear fracture theory, as such, ignores the energy dissipated during the formation of r_s. However, if the creation of plastic and craze zones does not disturb the elastic stress field, the energy due to the formation of r_s can be estimated by ductile fracture theory. That is:

$$U_s = G_d B r_s \tag{7.4}$$

The brittle impact strength is then determined by:

$$G_b = \frac{(I_b - U_s - U_k)}{B D \Phi (a_{eff})} \tag{7.5}$$

Hence, if $BD\Phi(a_{eff})$ is plotted versus the total impact energy, I_b, a straight line of slope G_b is produced which intercepts the I_b axis at $U_k + U_s$.

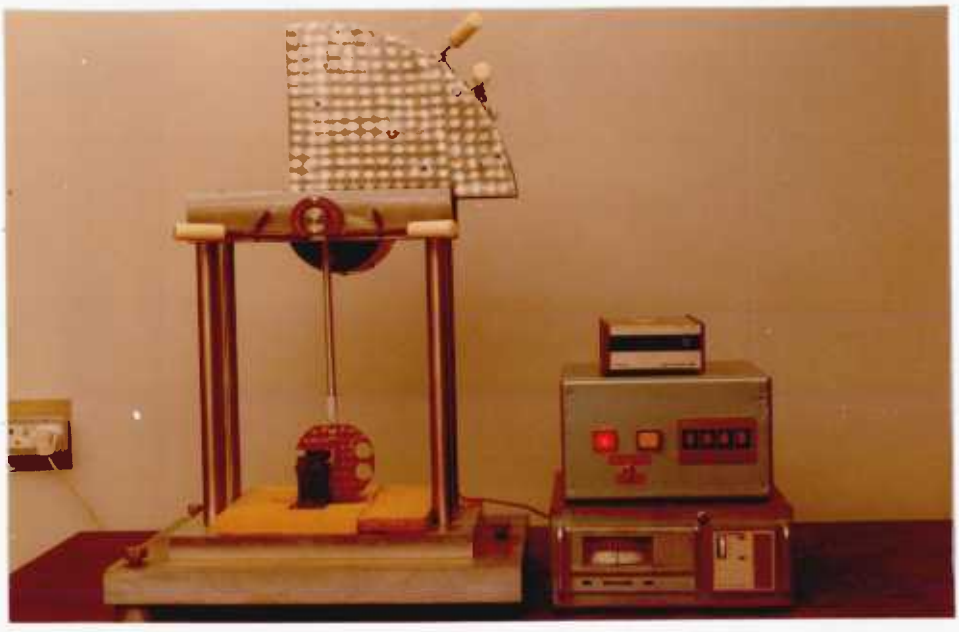


Figure 7.1: Impact apparatus set up for the Charpy test

7.4 IMPACT TEST INSTRUMENTATION

The Charpy impact strength of CPS and HIPS polymers was measured on a conventional pendulum-type impact machine. The apparatus was originally designed by BP Chemicals (UK) Limited and its outline is illustrated in Figure 7.1. Izod and tensile impact tests could also be conducted on this machine, although these were not attempted since, firstly, an accurate stress analysis of Izod specimens is more difficult to achieve than that obtained for Charpy tests. This is because the clamping of the Izod specimens produces complex stresses around the notch tip, and the variation in clamping force may cause significant differences in the impact energy obtained. Secondly, the tensile impact tests are not so popular in the plastics industry.

The impact machine used consists of a massive base on which the Charpy vice was mounted for holding the specimen, a rigid frame to which the pendulum-type hammer (tup) was attached through an anti-friction bearing, a release mechanism and a recording system which made it possible to measure the kinetic energy absorbed from the pendulum during impact. A set of four pendulum hammers (tups) of varying mass was available which could be released at four different heights onto the specimen. The velocity variations of the pendulums were rather small ($V_l \simeq 2.5$ m/sec) and, therefore, within the experimental error in an impact test, a constant strain rate was obtained for specimens of identical dimensions. The striking edge of each tup had a single rounded nose, so that the test specimens were all loaded in three-point bending. Although a large proportion of the mass of the tup was concentrated in the head, its arm was sufficiently rigid to minimise vibrational energy losses during impact. The contact line of the striking nose was located at the centre of percussion of the pendulum. This was carefully aligned along the

specimen crack during experiments using an optical magnifier.

By choosing the appropriate pendulum and altering the release position, the potential energy of the striking tup could be adjusted as closely as possible to the values just adequate to break the HIPS specimens. The energy absorbed in impact was then obtained by subtracting the excess energy remaining in the pendulum after impact from the maximum effective potential energy. This was made possible by recording the angular swing of the tup using a photoelectric device and a marked transparent disc attached to the pendulum pending point. The angular displacements of the pendulum were displayed as a number on a digital counter, which reflected the impact energy absorbed by the specimen .

7.5 CALIBRATION OF THE IMPACT MACHINE

The calibration method used has been given in detail elsewhere (Plati (1975)) and will be described only in outline here. The energy absorbed to fracture a specimen (crack initiation and propagation energies, plastic work, etc.), is equivalent to the potential energy lost by the pendulum during impact. The equivalent energy loss recorded by the digital counter, however, contains other energy losses which must be considered as errors and thus are to be subtracted from the values recorded. These errors are mainly as follows:

1. Energy losses due to vibration of the pendulum and horizontal movement of the impact machine.

2. Energy losses due to windage and bearing friction.

3. Kinetic energy of the broken specimens.

The first factor is associated with the design of the impact machine and is considered to be insignificant, since the impact energies required to fracture the HIPS specimens were in all cases much smaller than the maximum limit permitted in the design specifications.

The energy losses due to windage and friction is often considerable but may be accurately estimated experimentally. This is done by releasing the tups at different positions and allowing them to swing freely while noting the potential energy losses during each complete oscillation. The measurements were performed using a closed circuit TV set and a tape recorder in order to facilitate the interpretation of the readings. Using this technique, the counts displayed on the digital

counter during 20 to 30 alternate free swings of the pendulum were recorded on the tape. The differences between each count thus reflected the energy losses due to the friction and windage in the system for varying positions of the tup. These differential losses were then plotted versus the current potential energy of the pendulum which was denoted by the digital counter. The relationship between the current potential energy and the windage and friction energy losses was, consequently, expressed in a polynomial form by means of a curve fitting program. The corrected impact energies were then evaluated by subtracting the windage/friction energy from the total potential energy loss.

The impact energy evaluated as described above comprises the fracture energy (due to initiation and propagation of the crack and the possible plastic work involved) and the kinetic energy of the broken pieces. If a realistic estimate of the impact resistance of a material is to be made, then it must be possible to separate the fracture energy from the kinetic energy since the latter parameter is a function of the specimen geometry, and thus should not be considered as an intrinsic material property. The corresponding experimental error will be especially significant if the material breaks in a brittle manner, in which the fracture energy may even be less than the kinetic energy of the broken parts.

The estimate of the kinetic energy of the broken pieces is not usually a simple matter, since it is difficult to compute or measure it with precision. Some useful results may, however, be obtained by measuring the energy loss due to ejecting an identical impact specimen freely supported on the Charpy vice. The kinetic energy evaluated as such is an approximate estimation of the energy loss of the broken pieces in an actual test. Assuming a linear flight of the broken parts, it is also possible to evaluate the corresponding kinetic energy analytically,

using equation (4.26) or equation (4.27), as previously described in section 4.4 of Chapter 4.

If specimens break in a ductile manner, the linear kinetic energy evaluated by the above procedure does not truly represent the real energy losses of the broken pieces in an impact test. This is because the specimens plastically deform in a ductile fracture and usually stick to the impact pendulum, and thus the kinetic energy absorbed will only be of a rotational form. This energy can be theoretically estimated from equation (4.28) of Chapter 4.

The greater problem which arises here is due to semi-brittle or semi-ductile fracture in which the kinetic energy loss will be of a composite form. In this case, the exact value of the kinetic energy of the broken pieces is uncertain, being somewhere between the two limits of linear and rotational kinetic energies. Fortunately, the kinetic energies of semi-ductile materials tested in the present research were found to be small so their effects were reduced in significance and it is reasonable, therefore, to consider the mean of the linear and rotational kinetic energies described by equations (4.27) and (4.28) of Chapter 4 as the approximate loss due to the ejection of the broken pieces.

7.6 EXPERIMENTAL PROGRAMME

The experimental work to be described in this chapter was mainly devoted to the two samples of specially prepared HIPS, each containing from 0% to 5.55% nominal rubber inclusion, and the discussion of the experimental technique will be limited to these materials; that is, the effect of rubber content on the impact strengths of these materials.

Confirmative tests were also carried out on some Super, Standard and Medium impact polystyrene in order to verify the theoretical assumptions, and are treated in the same manner as the former materials, except where noted.

7.6.1 Test Conditions

All experiments were carried out at room temperature ($20^{o}C$) and 50% relative humidity, and the specimens were normalised at these conditions for a month before use. The values of the impact energies were obtained using the 0.152 kg Charpy tup at position 4 (with an effective speed of 2.912 m/sec) for special HIPS and the 0.28 kg Charpy tup at position 3 (with an effective speed of 2.448 m/sec) for commercial grades of HIPS.

Specimens having dimensions of approximately 6.3 mm × 3.15 mm × 50 mm were manufactured from moulded sheets of material and were supported on the Charpy stand with a span of 41 mm wide.

7.6.2 Materials

The following injection moulded 3.15 mm sheet samples of HIPS, which were supplied by the US Steel Corporation, were tested in the present work:

A. The specially prepared HIPS (Sample 1) containing from 0% to 5.55% rubber inclusion: these materials are, hereafter, denoted by U B0, U B1.11, U B2.22, U B3.33, and U B5.55. The numbers following the alphabetical codes indicate the nominal rubber content of the materials.

B. The specially prepared HIPS (Sample 2) containing from 0% to 3.33% nominal rubber content: the materials are hereafter labelled as U C0, U C1.11, U C2.22, and U C3.33.

C. Standard HIPS*: USSA, USSB, USSC, USSD, USSE, and USSF.

D. Super HIPS: USTA, and USTB.

E. Medium HIPS: USMA, and USMB.

F. Experimental HIPS: USEA, USEB, and USEC.

The grafting and mechanical properties of the U B grade of the specially prepared HIPS are shown in Table 7.1.

The U B grades of specially prepared HIPS were nominally duplications of the materials (Grade U A) previously used for the fracture toughness experiments and their mechanical properties were fairly consistent with those described before (Table 5.1 of Chapter 5) with a few

---

* The codings used here are conventional for this thesis and do not represent the trade names.

TABLE 7.1

Grafting and mechanical properties of the grade U B of the specially prepared HIPS

Properties	U B0	U B1.11	U B2.22	U B3.33	U B5.55
Nominal rubber content (%)	0	1.11	2.22	3.33	5.55
Nominal mineral oil (%)	1.35	1.35	1.35	1.35	1.35
Residual monomer (%)	0.10	0.11	0.11	0.12	0.15
Ethyl benzene (%)	< 0.07	< 0.07	< 0.07	< 0.07	< 0.07
No. average molecular weight	73000	80000	79000	85000	88000
Vicat temperature (^{o}C)	102.7	102.7	102.2	102.2	101.5
Solution viscosity (mm^2/s)	9.3	10.8	12.2	13.8	18.4
Melt flow (g/10 min)	15.4	11.0	7.8	5.3	2.4
Rubber used	PBD	PBD	PBD	PBD	PBD
Maximum tensile stress (MN/m^2)	49	42	38.5	35	30
Modulus of elasticity (GN/m^2)	3.1	2.8	2.6	2.3	1.8
Elongation to break	2	9	19	37	58

TABLE 7.2

Grafting and mechanical properties of the grade U C of the specially prepared HIPS

Properties	U C0	U C1.11	U C2.22	U C3.33
Nominal rubber content (%)	0	1.11	2.22	3.33
Nominal mineral oil (%)	1.35	1.35	1.35	1.35
Residual monomer (%)	0.11	0.11	0.11	0.14
Ethyl benzene (%)	< 0.05	< 0.05	< 0.05	< 0.05
No. average molecular weight	100000	98000	95000	94000
Vicat temperature (^{o}C)	102.7	102.2	102.2	102.2
Solution viscosity (mm^2/s)	16	16.8	17.1	17.6
Melt flow (g/10 min)	4.2	3.8	3.9	2.8
Rubber used	-	PBD	PBD	PBD
Maximum tensile stress (MN/m^2)	56	48	42	36.5
Modulus of elasticity (GN/m^2)	3.0	2.8	2.5	2.3
Elongation to break	2	14	32	40

exceptions. In particular, the solution viscosity of U-A5.55 and U-B5.55 showed significant disparity. The tensile properties of U-A and U-B are also somewhat different, although this may mainly be due to the dissimilar testing conditions employed*.

The U-C grades of specially prepared HIPS consisted of blends containing identical mineral oil and rubber levels to that of U-A and U-B. However, here the solution viscosities were kept constant at around 17.0 mm^2/sec (this was done by tailor-making some crystal resins in the reactors to match the viscosity of HIPS). As a result, the size and shape of the rubber particles were nearly consistent for the various blends of type U-C of HIPS. Bearing this in mind, these blends are therefore considered to be a better representation of HIPS composites than the previous blends, U-A and U-B, having identical grafting properties but varying only in the quantity of the rubber used. The mechanical properties of the U-C series of HIPS are shown in Table 7.2.

All series of specially prepared samples of HIPS employed Diene 55 as the rubber in the massing stage. Diene 55 is produced by Firestone, using an anionic polymerisation of butadiene in solvent. Diene 55's micro-structure is predominantly transparent. The properties of the rubber in the HIPS used here are described in Table 7.3.

The ingredient properties of the commercial HIPS were not available; however, it is believed that the PS matrices and PBD rubbers of these polymers were identical (with the exception of the Super HIPS series which employs a tougher PS matrix).

---

* The mechanical properties quoted for the U B type of HIPS are provided by the manufacturer, in which the test conditions (e.g. strain rate) has not been specified.

TABLE 7.3

The Properties of Polybutadiene Rubber, Type 55

Properties	Limits	
	Minimum	Maximum
Volatile Matter (%)	-	0.20
Ash (%)	-	0.05
Solution Viscosity (mm^2/s)	176	196
Gel	Nil	Nil
Antioxidant (BHT) (%)	-	0.25

7.6.3 Notching Technique

The notches were made using a sharp single point fly-cutter mounted in a notching instrument, as shown in Figure 7.2. The cutting angle was around 60^{o} and the crack tip radius was estimated to be around 0.03 mm. Particular care was taken in notching the specimens to avoid the creation of craze bundles around the crack tip.

As previously discussed in Chapter 6, the machine notching technique has considerable advantages over razor notching. This has been shown by Plati (1975), who made use of the two notching methods and found more consistent results when using the machine notches.

The initial cracks were inserted in one edge of the specimens varying from 0.015 D to 0.5 D (where D denotes the specimen width along the crack). The use of shorter cracks was found to be vital in evaluating the impact strength of quasi-ductile polymers as they often induce a more brittle fracture under impact loads than longer cracks.



Figure 7.2: Notching apparatus for impact specimens

The initial crack lengths were accurately measured after fracture, using a scaled travelling microscope, as shown in Figure 7.3.

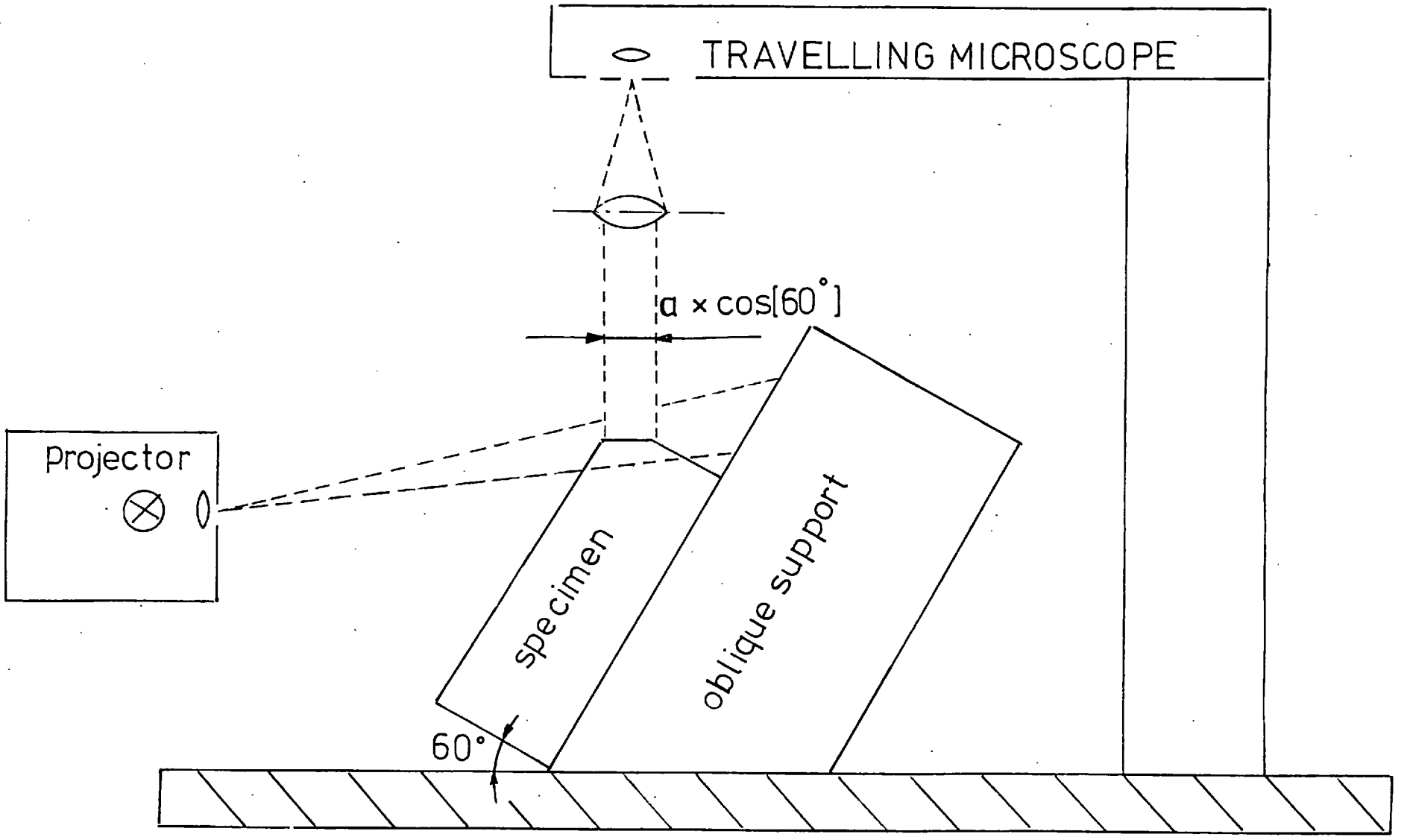


Figure 7.3: The optical arrangment for the analysis of the fracture surfaces of impact specimens

7.7 ANALYSIS OF THE EXPERIMENTAL DATA

There emerged a variety in the appearance of the fracture surfaces of the crystal and impact polystyrene specimens, corresponding to the nature of the material resistance to fracture. The general impact behaviour of polymers is described elsewhere (Vincent (1971); Nikpur & Williams (1977)*). On a similar basis, different types of fracture of HIPS samples, tested in the present work, are classified as follows:

1. Brittle Polymers (e.g. the crystal polystyrenes): An analysis of the fracture surfaces indicated no trace of craze growth or stress-whitening. This is due to insignificant resistance to crack propagation and so a rapid unstable crack growth follows the initiation.

2. Semi-Brittle Polymers (e.g. low-level impact polystyrenes): A small craze zone and limited stable crack growth could be detected in these materials. Unstable crack growth finally takes place after the slow cracking.

3. Semi-Ductile Polymers (e.g. standard impact polystyrenes): Opaque surfaces of fracture pieces indicated a stable crack propagation throughout the specimens. It can be concluded that, although these materials display a low resistance for crack initiation, there must be a relatively significant propagation resistance which inhibits the free travel of the initiated crack. This is due to rubber particles which impede the rapid extension

---

* This paper is appended at the end of this thesis.

of a crack by absorbing a significant portion of the impact energy as a result of craze generation.

4. Ductile Polymers (e.g. super HIPS): The fracture occurs after nearly full yielding. A large region of crazing and stress-whitening could be detected around the propagated crack.

The fracture surfaces of different types of HIPS are shown in Figure 7.4.

7.7.1 Fracture of Crystal Polystyrene (CPS)

Plots of the fracture energy, I_b, versus $BD\Phi$ for the two grades of CPS (U BO and U CO) are shown in Figures 7.5 and 7.6 (graphs A). The impact strengths, G_b, were determined from the slopes of the best straight line through the data points. As expected, these lines intercept the energy axes at 0.010 J which is the kinetic energy of the flying pieces. The scatter of the points is conspicuous for both materials. This was predictable owing to the great sensitivity of brittle materiasl to small variations that may occur during the experiment. The results are also shown in the energy-ligament area plots (Figures 7.5 and 7.6, graphs B) and, if compared with the energy-$BD\Phi$ plots, it is clear that the linear fracture mechanics provides a better fit to the experimental data.

The grade U CO of CPS, which is a tougher material, according to the manufacturers, displayed a slight deviation from the brittle theory at shorter cracks. A crack length correction, r_s, of approximately 0.01 mm was found necessary to produce the best line-fit through the data (Figure 7.6, graph C). The corresponding impact strengths obtained for U BO and U AO were about 0.4 kJ/m^2 and 1.1 kJ/m^2, respectively.



Figure 7.4: Typical fracture surfaces of Charpy impact specimens:

1 (top left) : Brittle fracture in U B0;

2 (top centre) : Semi-brittle fracture in U B1.11;

3 (top right) : Semi-ductile fracture in U B2.22;

4 (bottom left) : Semi-ductile fracture in U B3.33;

5 (bottom right) : Ductile fracture in U B5.55.

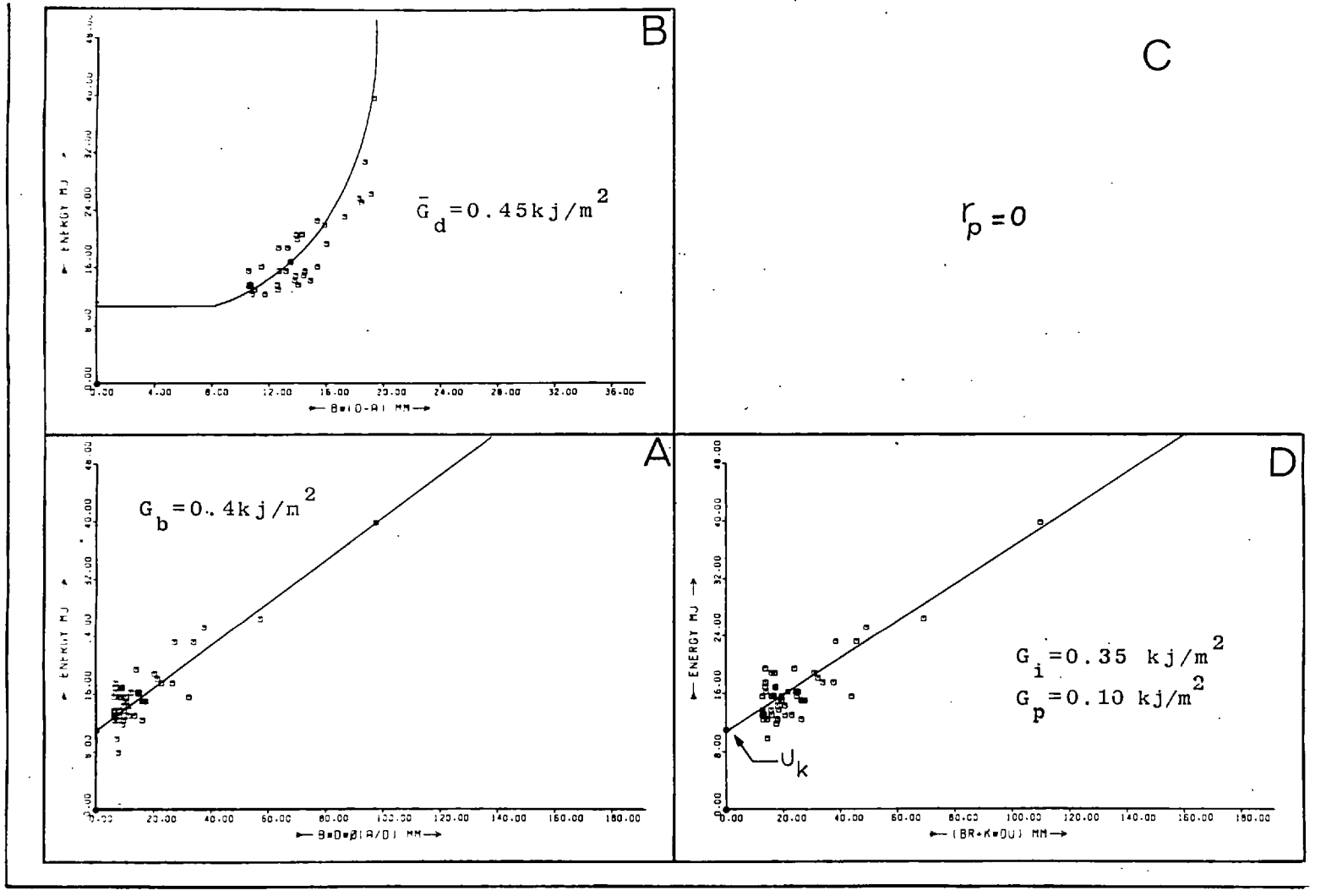


Figure 7.5: Comparison of the impact results for CPS, using linear (A), yielding (B), modified linear (C) and composite (D) fracture mechanics theories

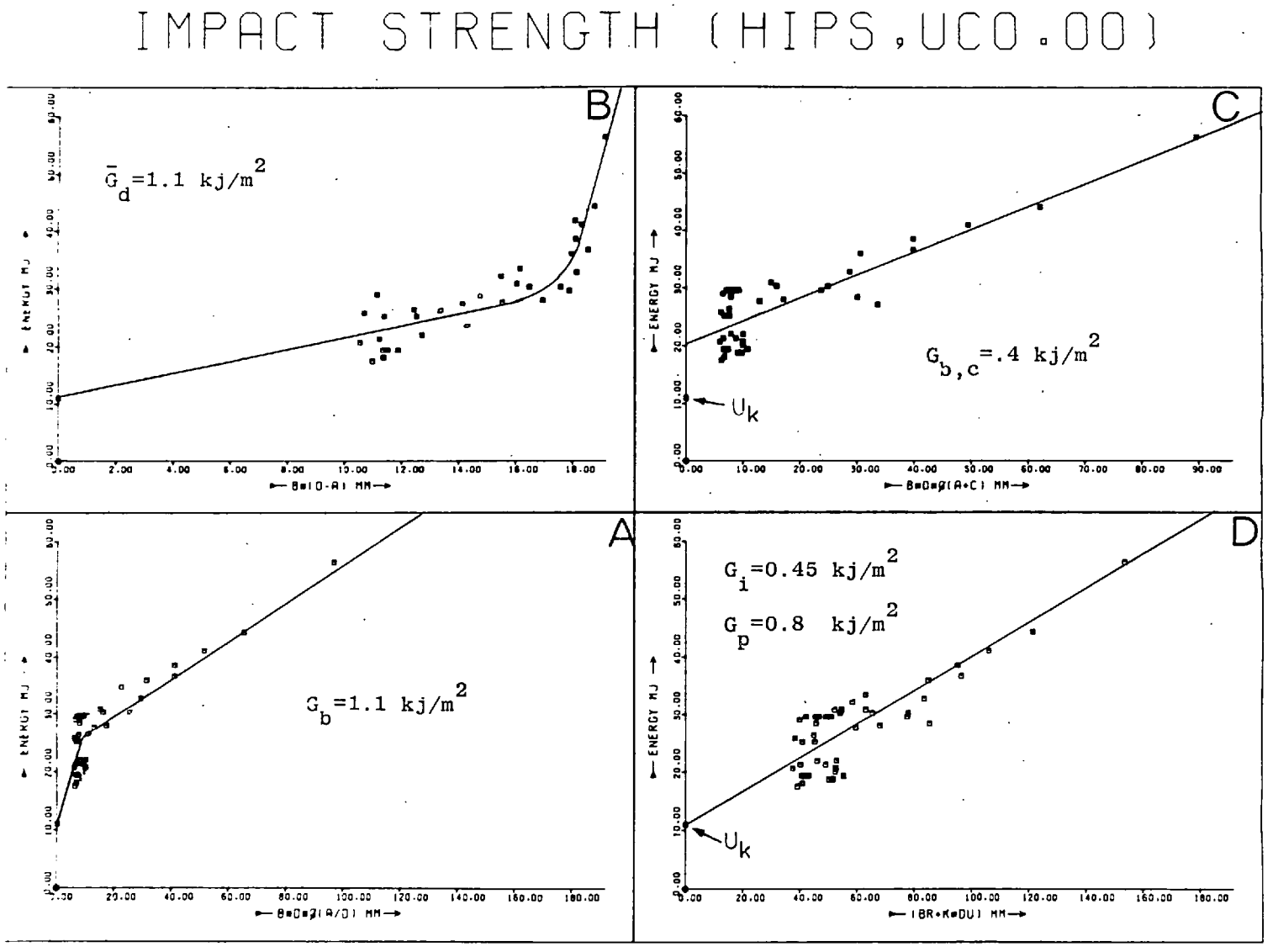


Figure 7.6: Comparison of impact results for CPS, using linear (A), yielding (B), modified linear (C) and composite (D) fracture mechanics theories

7.7.2 Low-Level Impact Polystyrene

The grades of HIPS having low-level rubber contents behaved in a semi-brittle manner and only a very small region of stable crack growth was detected on the surfaces of the broken specimens. The grade U Bl.11 was a typical example of such materials.

Figure 7.7, graphs A and B, show the experimental data on energy-$BD\phi$ and energy-ligament area planes. Apparently, the scatter of the results is significantly smaller than that obtained for brittle CPS.

Conclusively, it can be noted that, as the rubber content in HIPS increases, the fracture toughness of the material becomes greater and, therefore, its sensitivity to the initial test conditions reduces and thus smaller scatter in the impact data will be obtained.

Although the results are less scattered for U Bl.11, neither the linear nor the yielding fracture mechanics theories provides an accurate representation of the experimental impact data obtained. However, the deviation from the linear theory in the energy-$BD\phi$ plot is small and only becomes apparent at smaller crack lengths. This can be overcome by reconsidering the distortions caused by a limited plastic zone and stable crack growth prior to final fracture. Graph C of Figure 7.7 shows the corrected data using the modified linear fracture mechanics theory. The best line-fit on the data points is produced by assuming $r_s + r_p = 0.35$ mm. The slope of the fitted line implies an impact strength of about 2.3 kJ/m^2 for U Bl.11. The intercept of this line with the energy axis at about 10 m coincides with the theoretical value predicted for the kinetic energy of the fractured specimens.

7.7.3 Medium- and High-Level HIPS

The grades of HIPS containing sufficient quantities of rubber

phase generally showed a composite behaviour in fracture. The impact energies recorded in a complete fracture, however, substantially increased with increasing rubber contents. In accordance with this, the amount of plastic stress whitening and crazing was also increased significantly. The corresponding plots of energy versus $BD\phi$ and also the energy versus ligament area for the specially prepared HIPS containing various rubber contents are shown in Figures 7.7 to 7.13. It seems that, while the linear fracture theory does not describe the impact behaviour of the tougher grades of these materials, a reasonable approximation can be made if the yielding fracture criterion is employed. However, the data for shorter notches indicate a clear deviation from the yielding theory, espectially when medium HIPS grades are studied.

Except in the case of U B1.11, which was discussed before, the modified linear theory does not provide any better solution. For example, the correction method for U B2.22 converges at r_s = 0.22 mm, and the best straight line through the corrected data gives an apparent impact strength of about 0.76 kJ/m^2. This is noticeably lower than the value obtained for U B1.11 which contained a small rubber content, thereby indicating the inefficien cy of the modified linear theory to describe the impact behaviour of composite polymers. Moreover, the intercept of the fitted line through the corrected data points with the energy axis was found to be around 31 mJ which is significantly higher than the theoretical value predicted for the kinetic energy of the flying pieces (U_k = 10 mJ). As discussed in the preceding theoretical section, this difference could be accounted for partially due to the dissipation of energy during the stable crack growth. However, the energy difference is too great to be wholly considered as the result of merely 0.22 mm ductile crack propagation in the specimen.

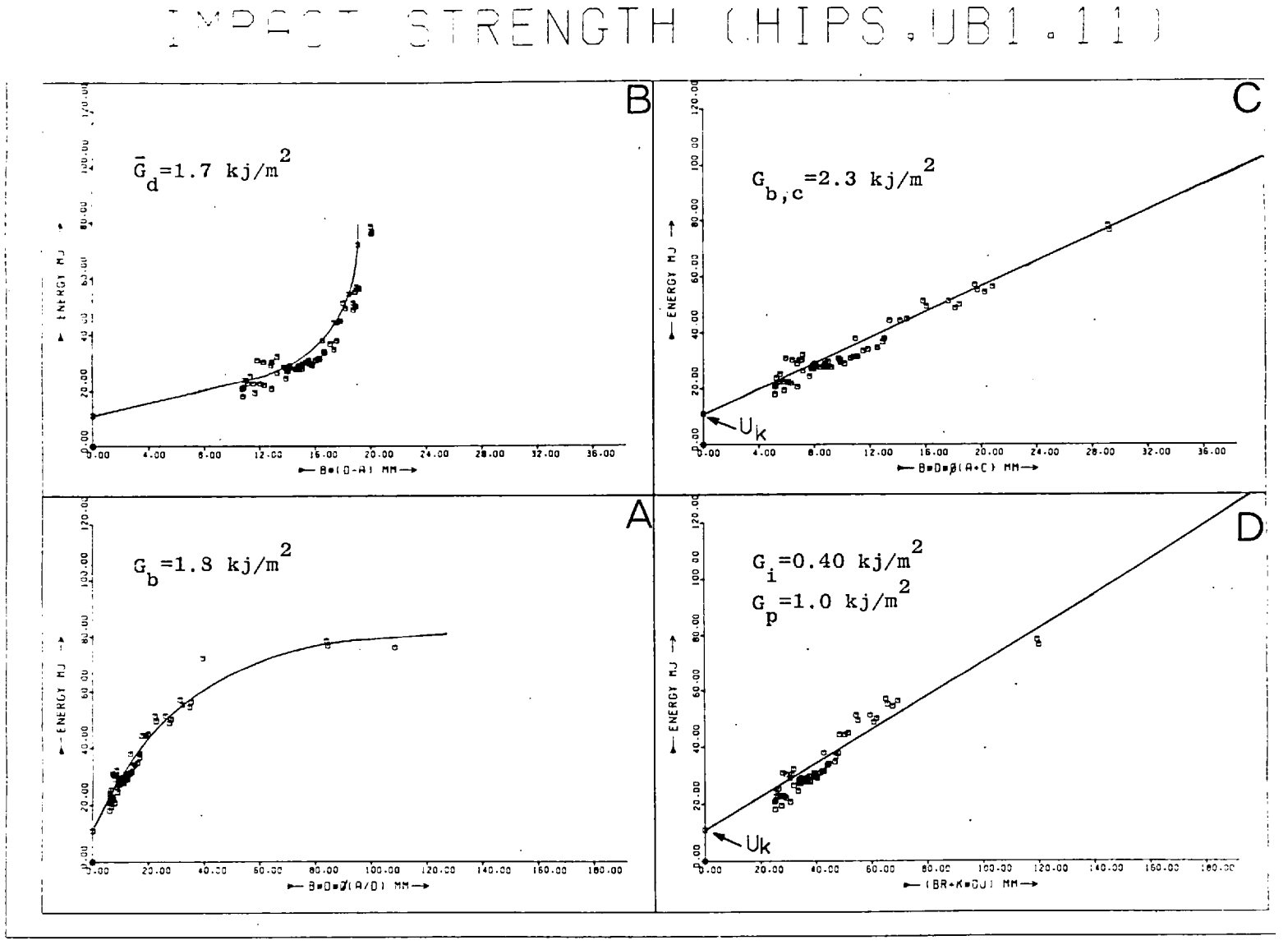


Figure 7.7: Comparison of impact results for specially prepared HIPS, using linear (A), yielding (B), modified linear (C) and composite (D) fracture mechanics theories

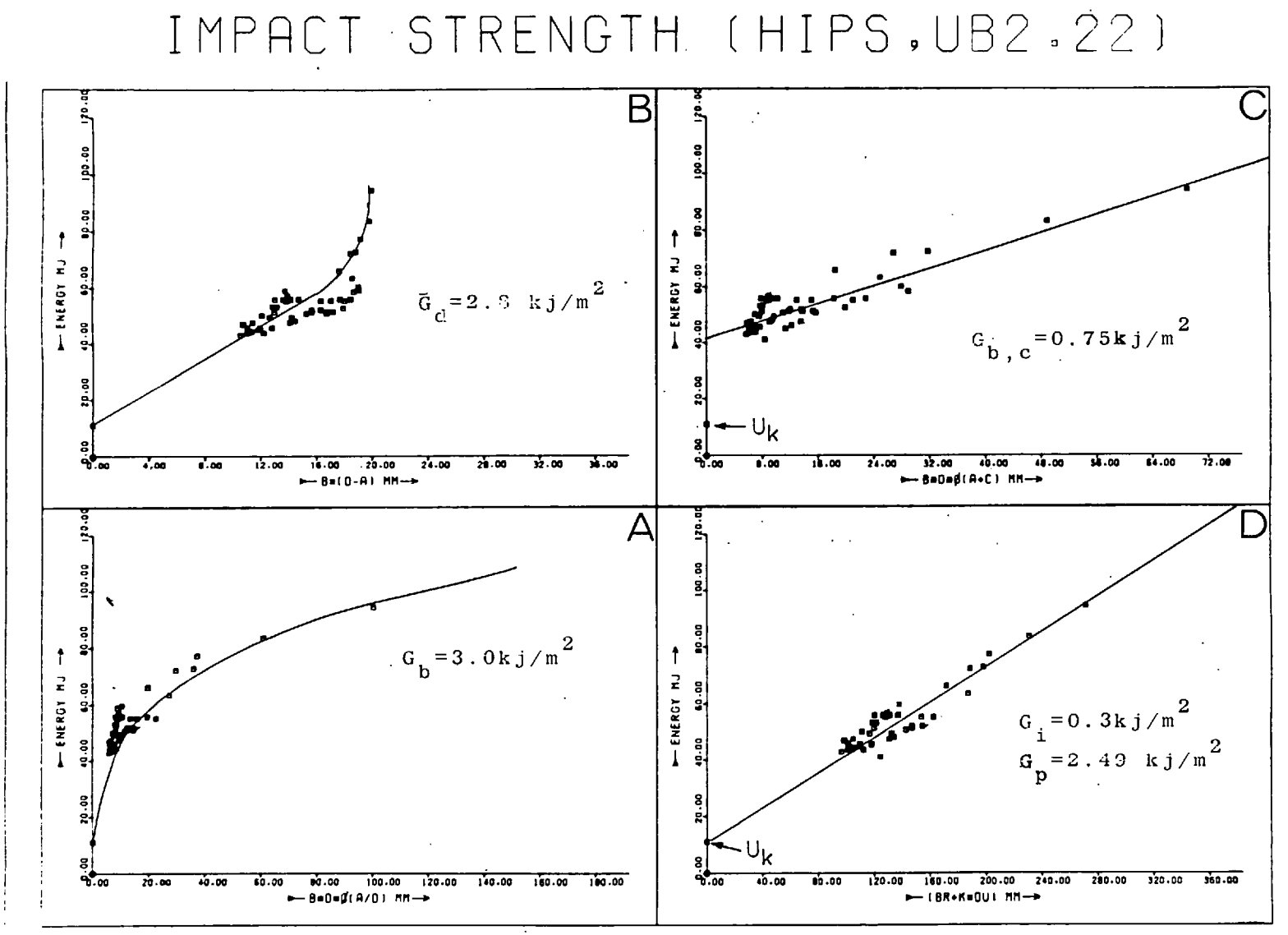


Figure 7.8: Comparison of impact results for specially prepared HIPS, using linear (A), yielding (B), modified linear (C) and composite (D) fracture mechanics theories

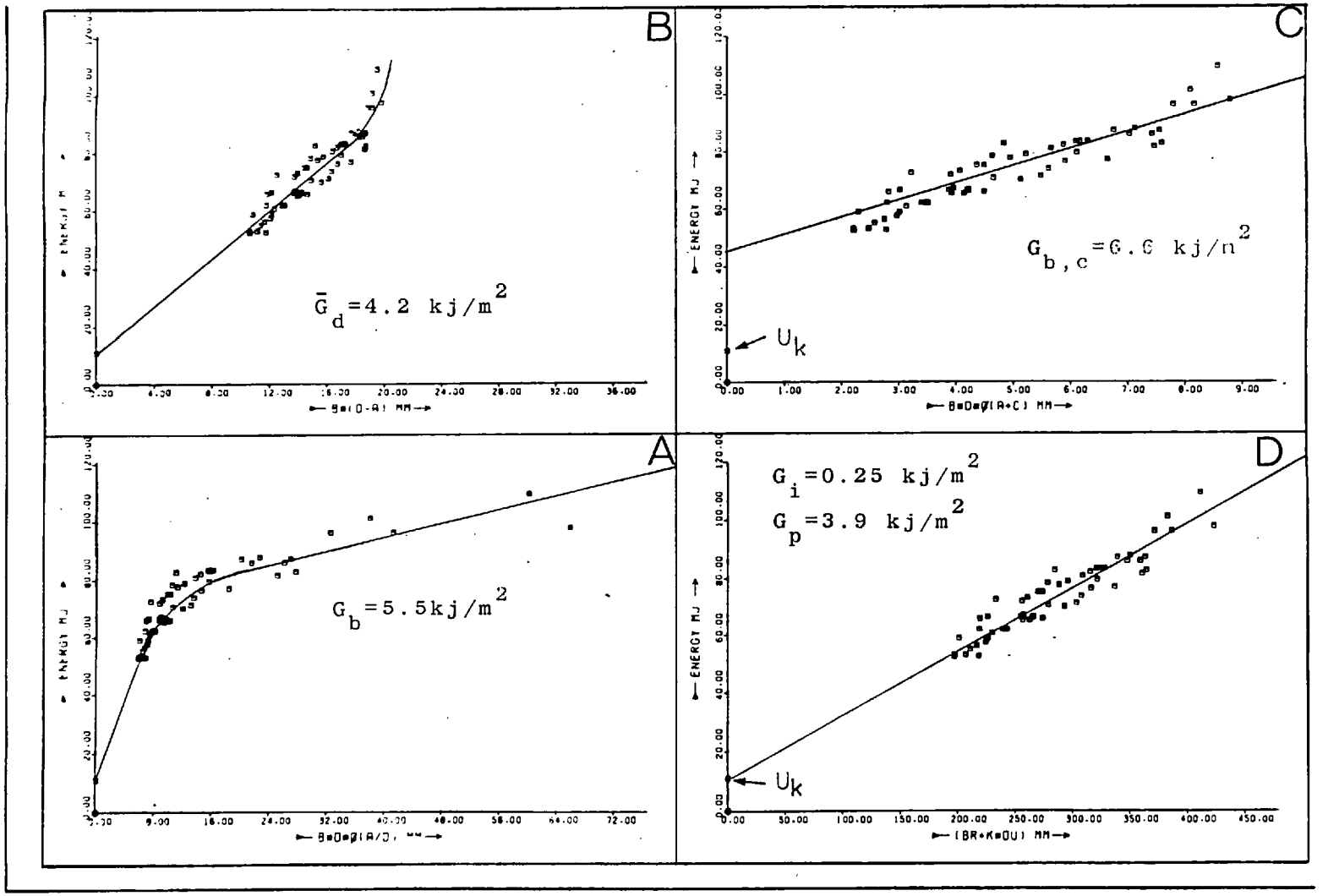


Figure 7.9: Comparison of impact results for specially prepared HIPS, using linear (A), yielding (B), modified linear (C) and composite (D) fracture mechanics theories

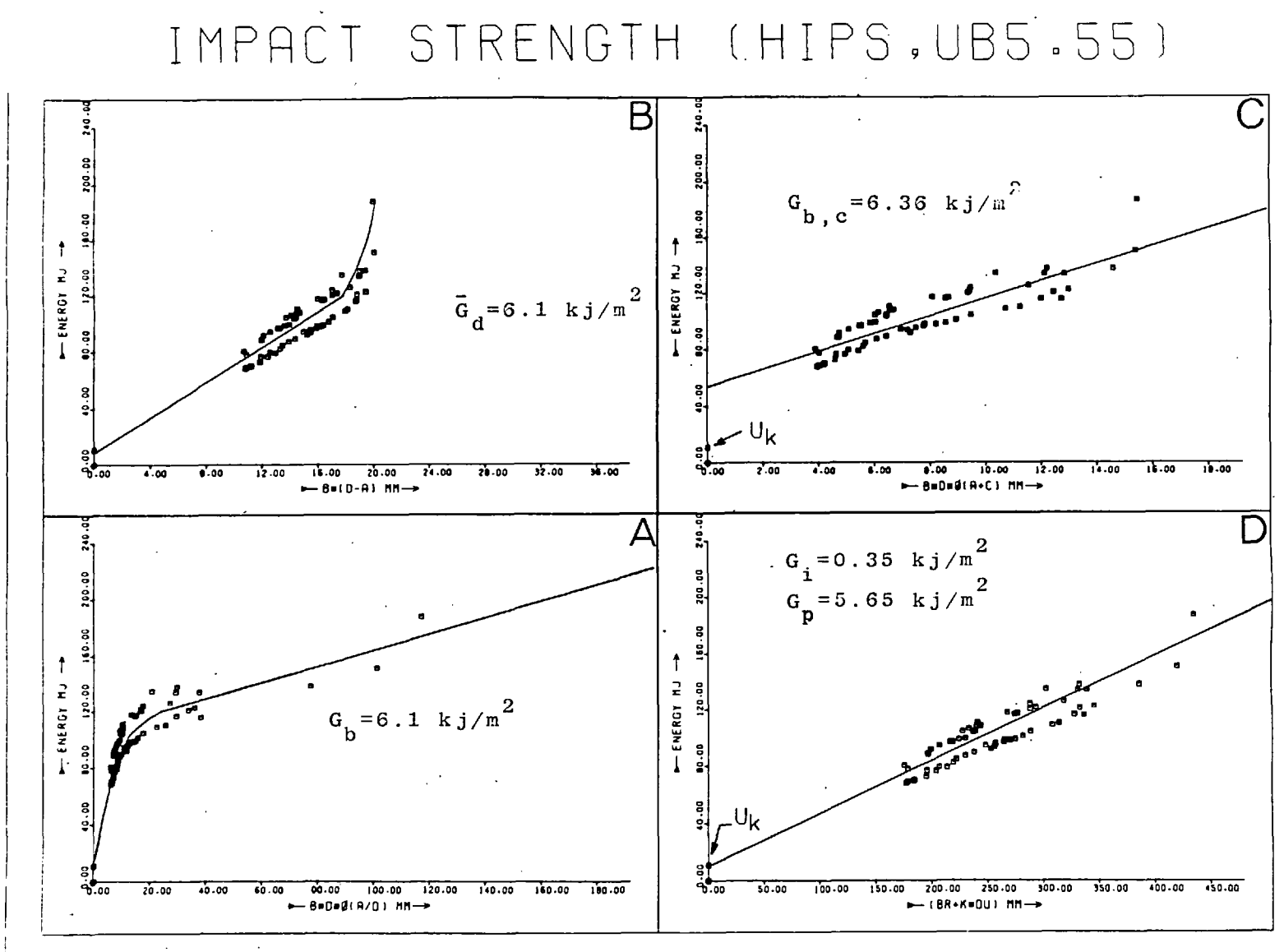


Figure 7.10: Comparison of impact results for specially prepared HIPS, using linear (A), yielding (B), modified linear (C) and composite (D) fracture mechanics theories

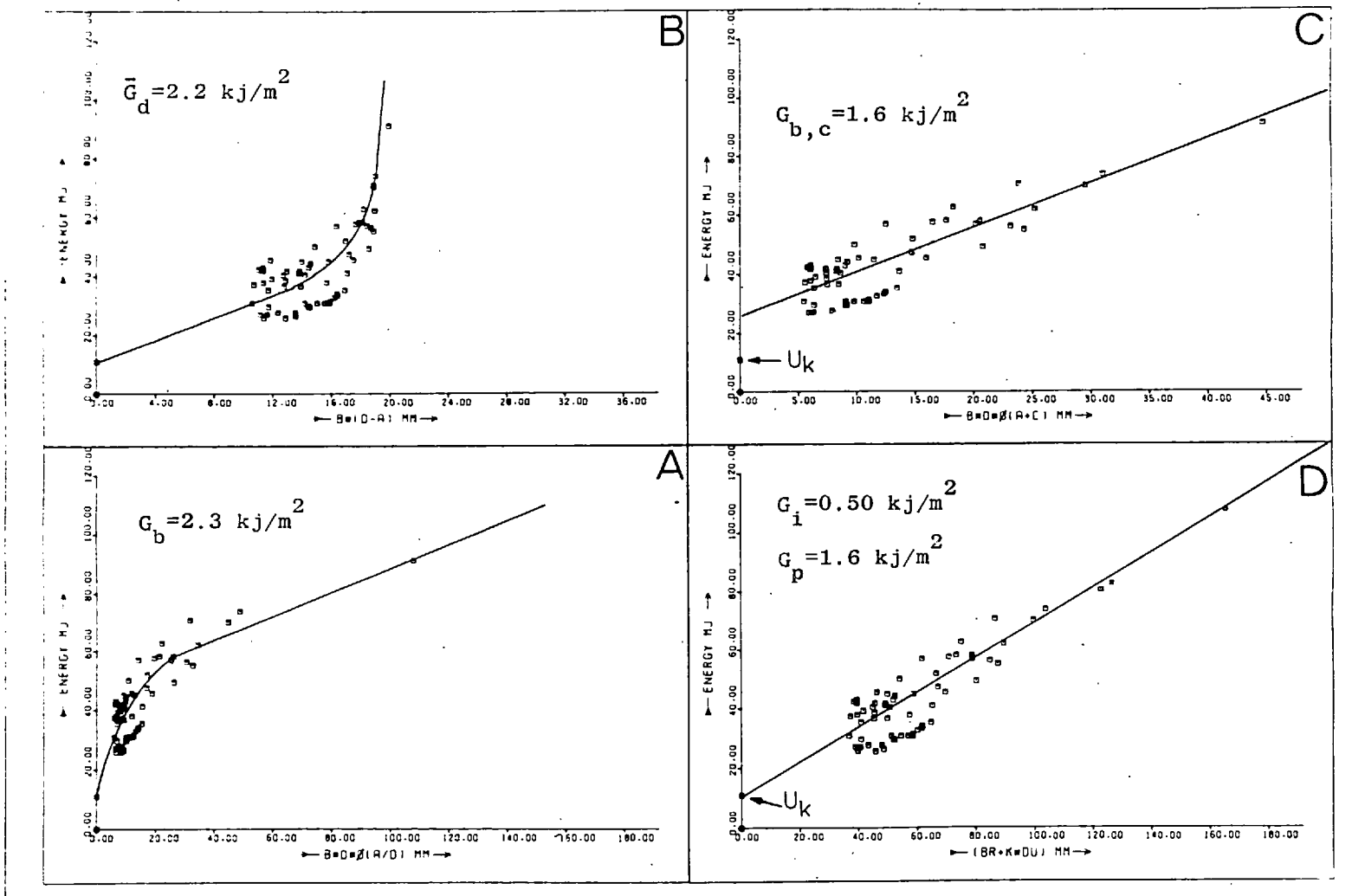


Figure 7.11: Comparison of impact results for specially prepared HIPS, using linear (A), yielding (B), modified linear (C) and composite (D) fracture mechanics theories

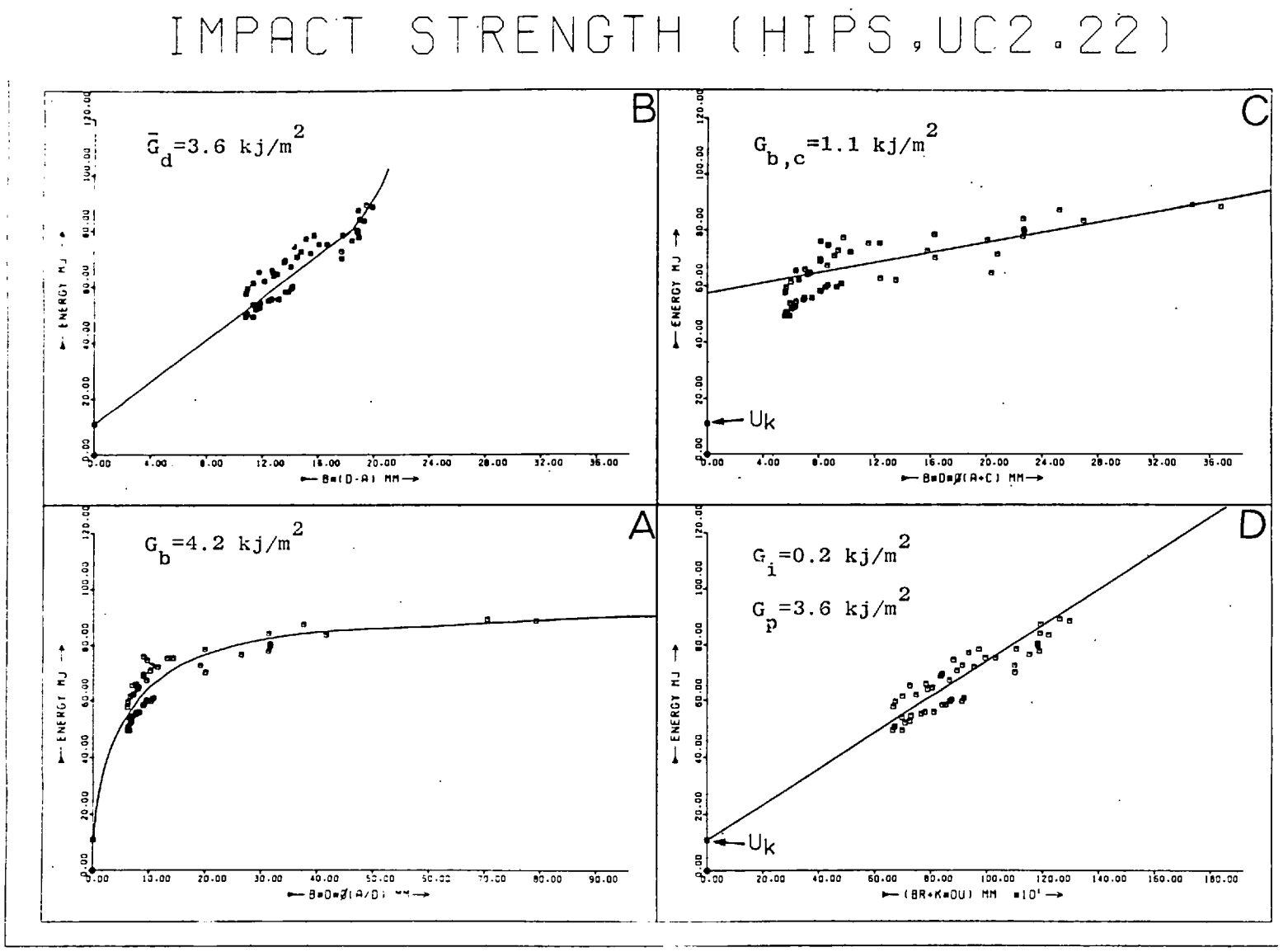


Figure 7.12: Comparison of impact results for specially prepared HIPS, using linear (A), yielding (B), modified linear (C) and composite (D) fracture mechanics theories

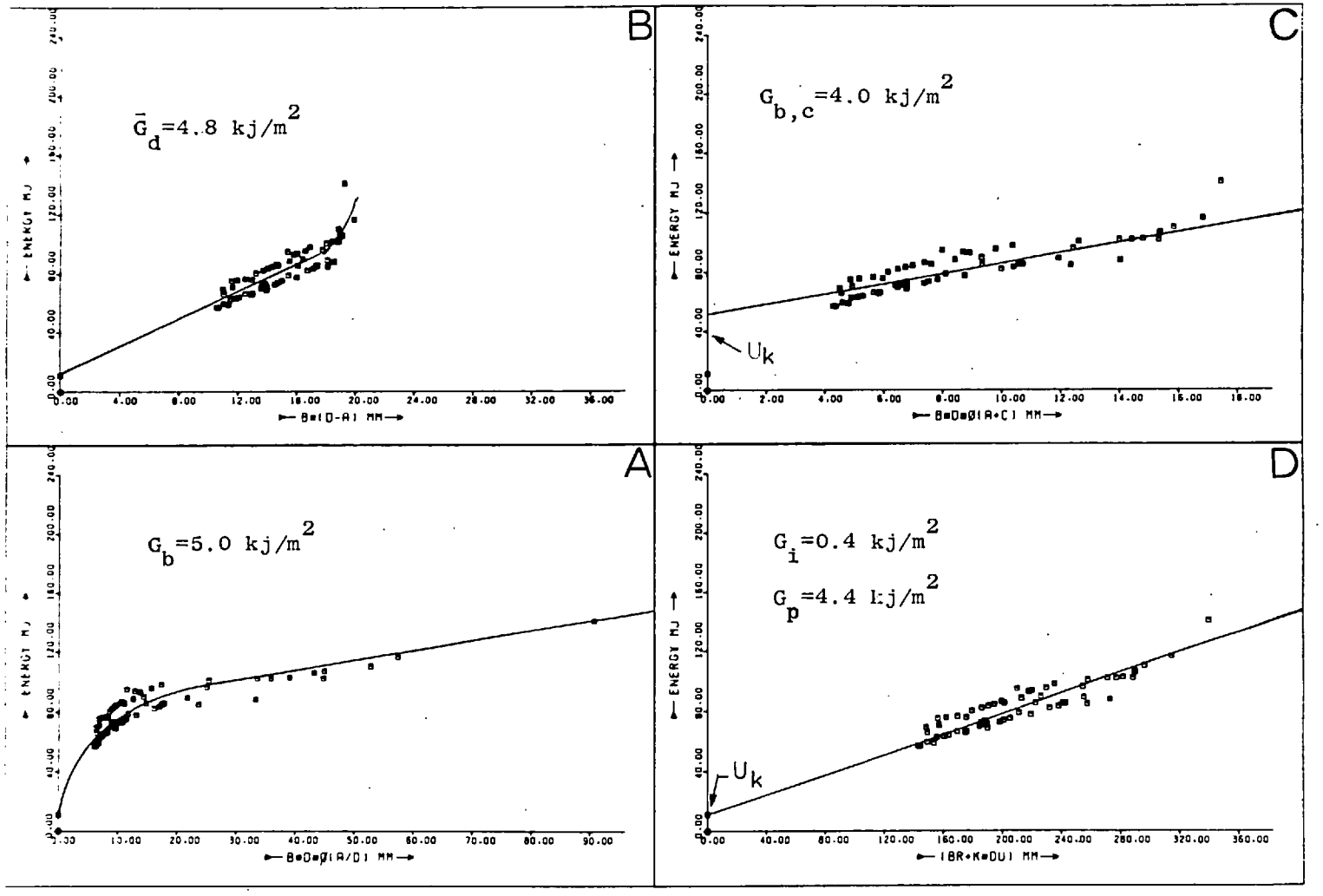


Figure 7.13: Comparison of impact results for specially prepared HIPS, using linear (A), yielding (B), modified linear (C) and composite (D) fracture mechanics theories

The inadequacy of the linear fracture mechanics (modified or unmodified) in predicting the impact behaviour of composite polymers is better shown when comparing the impact strengths evaluated on this basis for different grades of HIPS (see Table 7.4). Obviously, no consistent relationship exists between the impact strengths of these polymers and their rubber contents. In particular, when medium grades of HIPS are studied, the results largely deviated from both modified linear fracture mechanics and yielding fracture criteria. For example, as shown in Figures 7.11 and 7.12, the impact data for U C1.11 and U C2.22 indicate a clear upward trend on the energy-ligament area plot and a sharp downward incline on the energy-$BD\phi$ plot. Notably, the appreciable curvatures of the data obtained for medium HIPS require a substantial correction of the initial crack lengths. However, the modified fracture mechanics hypothesis only applies when the distortion due to the plastic zone or stable crack growth is small and thus the theory must be considered inaccurate when analysing materials showing a large slow crack growth.

7.7.4 Application of the Composite Impact Theory

The basic theories derived for homogeneous brittle or ductile materials were shown to be inaccurate for predicting the impact resistances of rubber-modified polymers. In the paper appended at the end of this thesis, a universal theory is developed which attempts to study the impact strength of composite materials in terms of the resistances due to the initiation and propagation of a crack. The total energy dissipated during impact can then be obtained by considering the initiation impact resistance, G_i, and the propagation impact resistance, G_p. Thus:

$$I_c = B\,D\left[G_p\,(1 - a/D) + G_i\,\phi\,(a)\right] + U_k \qquad (7.6)$$

TABLE 7.4

Impact strength of specially prepared HIPS

Material	U B0	U B1.11	U B2.22	U B3.33	U B5.55	U C0	U C1.11	U C2.22	U C3.33
G_b (initial slope) kJ/m^2	0.4	1.8	3.0	5.5	6.1	1.1	2.3	4.2	5.0
G_d (mean value) kJ/m^2	0.45	1.7	2.8	4.2	6.1	1.1	2.2	3.6	4.8
G_e (modified) kJ/m^2	-	2.3	0.8	6.6	6.4	0.4	1.6	1.1	4.0
G_i (composite theory) kJ/m^2	0.35	0.40	0.3	0.25	0.35	0.45	0.5	0.2	0.4
G_p (composite theory kJ/m^2	0.1	1.0	2.5	3.9	5.6	0.8	1.6	3.6	4.4

The impact strengths G_i and G_p can be determined by performing at least two impact tests on specimens containing different crack lengths. However, in an impact test there exists considerable scatter owing to the nature of the experimental conditions. To cope with the inconsistency due to this problem, a sufficient number of tests must therefore be carried out for specimens containing a wide range of initial crack lengths. The experimental data can then be analysed using a statistical program.

The experimental data for the various grades of CPS and HIPS were re-analysed using the composite impact theory described by equation (7.6). A computer program was written to evaluate the impact resistances associated with initiation, G_i, and propagation, G_p. The program list is given in Appendix D which can be used for further research on the impact strength of composite polymers. The program generates the best surface-fit on the data described by equation (7.6). The basic impact theories (equations (7.1), (7.2) and (7.5)) are similarly studied and the statistical errors of the results are compared.

Plots of the energy versus $BD\ (\phi + G_p/G_i\ (1 - a/D))$ for the various CPS and HIPS, are shown in the fourth graphs of Figures 7.5 to 7.13. As shown, a straight line can be drawn through the data which intercepts the energy axis at around 10 mJ, equal to the predicted kinetic energy of the broken pieces. The corresponding slopes of these lines give the initiation impact strength, G_i.

Equation (7.6) can be re-written as:

$$I_r = G_i + G_p\ (1 - a/D)/\Phi(a/D) \qquad (7.7)$$

where I_r denotes the reduced impact energy and is given by:

$$I_r = \frac{(I_c - U_k)}{(B\ D\ \phi\ (a))} \tag{7.8}$$

If the composite impact theory genuinely describes the impact resistance of a rubber-modified polymer, a plot of I_r versus the ratio $(1 - a/D)/\Phi$ should produce a straight line with a slope of G_p and an intercept of G_i. The experimental data for U C3.33 is re-illustrated in I_r-ligament area ratio plots (Figure 7.14). These results demonstrate the self-consistency of the composite impact theory when applied to a wide range of brittle to ductile polymers.

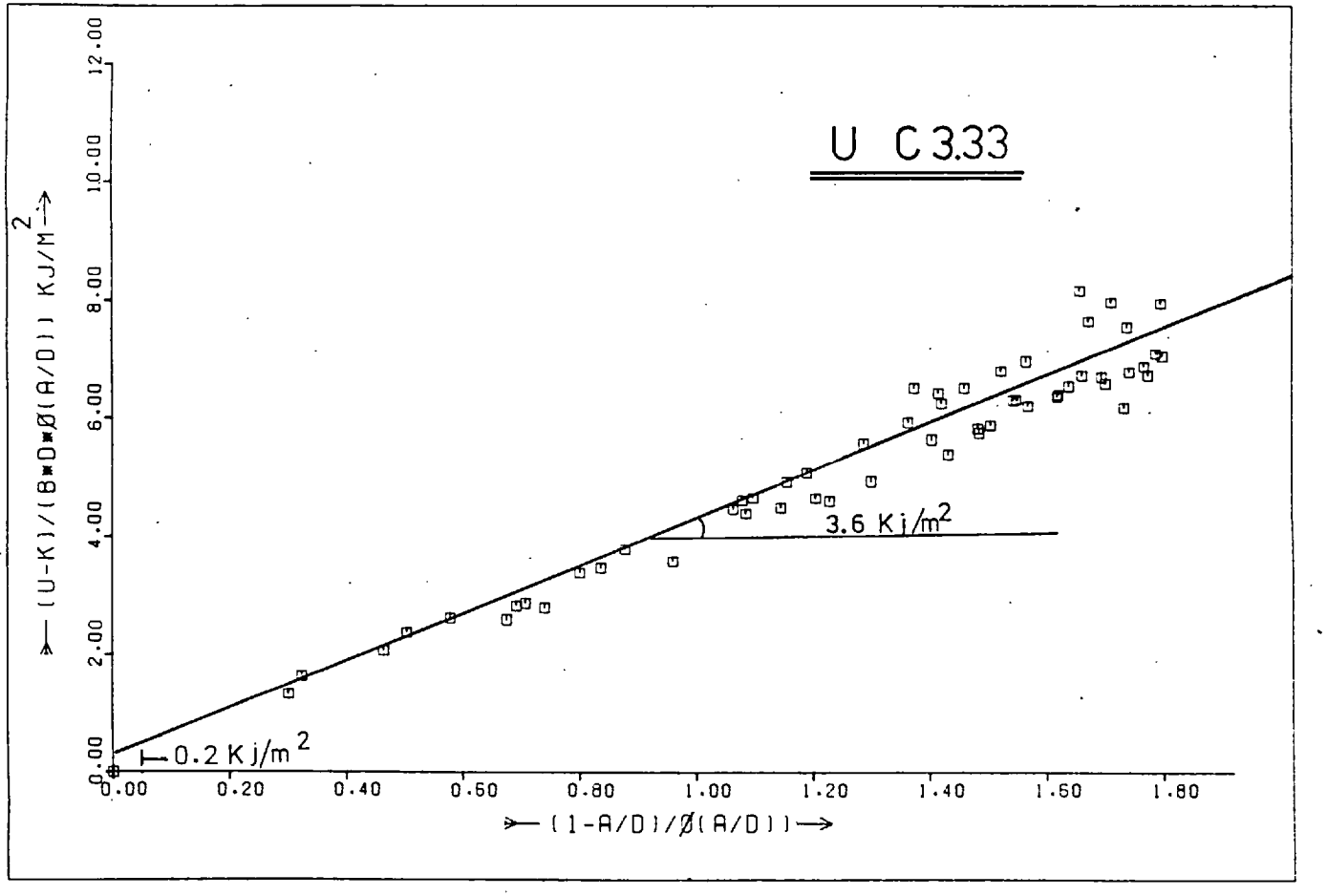


Figure 7.14: Application of composite impact theory for a specially prepared grade of HIPS

7.8 EFFECT OF RUBBER CONTENT ON THE IMPACT STRENGTH OF HIPS

In the preceding section, two HIPS samples, each containing different rubber contents, were tested and their impact resistances to crack initiation, G_i, and crack propagation, G_p, were evaluated using the composite theory of fracture. Figure 7.15 shows G_i and G_p versus the nominal rubber content for the two HIPS samples. It is clear that, within the experimental errors, the initiation resistance remains almost unvaried with increasing rubber content. The propagation resistance, however, increases linearly as the rubber content becomes greater.

The question to be asked then is whether a theoretical limit exists beyond which the impact strength will not be affected by increasing the nominal rubber content. It is worth recollecting that the fracture toughness of identical HIPS samples maximised at 1% to 2% rubber content and then showed no improvement with increasing rubber. The empirical picture which is emerging is that the toughness of rubber-modified polymers is the reciprocal function of the testing speed. Hypothetically, at the extreme of zero strain rate, the fracture toughness improvement due to the presence of rubber particles is a minimum and takes its optimum effect with the introduction of only a small quantity of rubber. On the other hand, when an infinitely fast strain rate test is performed, the toughness increases significantly with increasing rubber content and may only maximise at a large rubber fractional volume. This can be theoretically explained as follows:

The introduction of viscoelastic rubber particles in a brittle elastic matrix initiates the production of craze bands emanating from each rubber particle. The energy absorption during the craze formation will therefore enhance the fracture strength of the material. In contrast, the expansion of the craze bands weakens the material (as reflected in the modulus

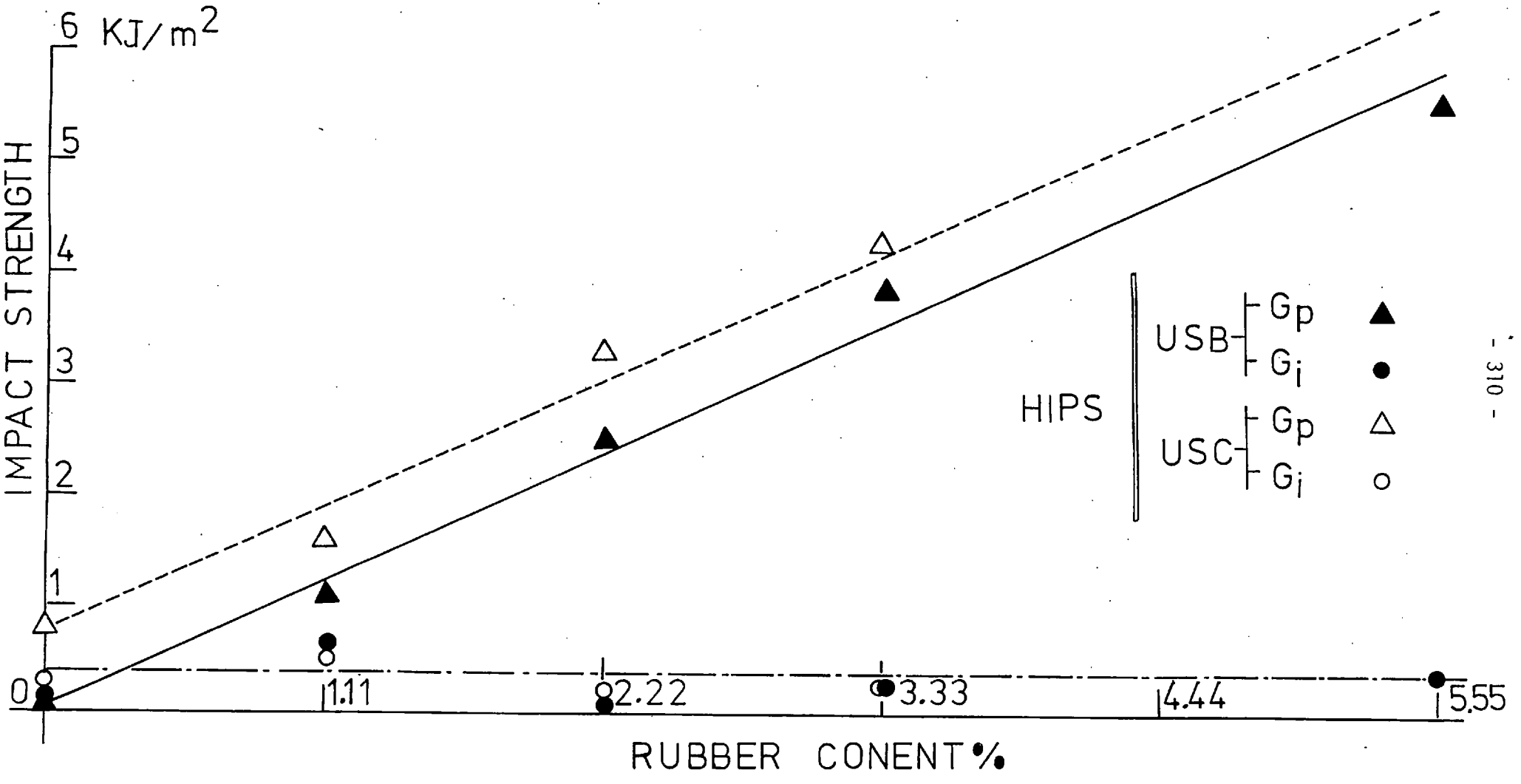


Figure 7.15: The effect of rubber content on the initiation resistance, G_i, and propagation resistance, G_p, of HIPS

reduction due to the presence of rubber particles) since the crazed regions will act as the nuclei of subsequent microscopic cracks. Craze formation, therefore, has a dialectic effect since there are dual opposing influences of strengthening and weakening. In a slow rate test, each particle forms a craze band which will grow with time. The craze bands emanating from particles will then interlink, forming a weak stressed plane perpendicular to the applied load. At this stage, when the energy absorbing capacity due to crazing is exhausted, the material fractures at the weakest stressed region. On the other hand, in impact failure, the growth of crazes is difficult in the short period of loading so that any addition of rubber results in proportionally more crazing with comparatively shorter lengths. Hence, the inter-effect of craze bands is minimised, while the impact strength increases due to a relatively unlimited energy absorption capacity of multiple infinitesimal craze formation.

7.9 AN ANALYSIS OF THE COMMERCIAL GRADES OF HIPS

Commercial grades of Medium, Standard and Super HIPS supplied by the US Steel Corporation were tested in the present work. The values of impact energies were obtained using a 0.28 kg Charpy tup at position 4 (effective speed = 2.45 m/sec). The experimental procedure was similar to that used for specially prepared grades of HIPS.

The Standard and Super HIPS all failed in an apparently semi-ductile to ductile manner with a significant stress whitening visible from the surfaces of the broken specimens. The two medium grades of impact polystyrene failed in a complex manner where the local stable and unstable crack growth could be found on the fracture surfaces of the specimens with small initial cracks.

The experimental results for the Super, Standard and Medium HIPS are illustrated in Figures 7.16 to 7.25, where the applied impact energies are plotted against $BD\phi$ (graph A), ligament area (graph B), modified $BD\phi$ (graph C), and $BD\left(\phi + G_p/G_i\ (1 - a/D)\right)$ (graph D). Except for specimens containing small notches, the experimental data for Super HIPS and to some extent for the tougher grades of Standard HIPS give a straight line on energy-ligament area plots. The slope of these lines can therefore be regarded as an upper limit to the propagation strength, G_p, of the materials. The impact behaviour of Medium grades of HIPS, containing relatively smaller rubber contents, cannot, however, be analysed using the classical impact theories. Although, as previously observed for the specially prepared grades of these polymers, short crack samples tend to obey the linear fracture mechanics theory, thus the impact toughness for the brittle mode of fracture can be approximately estimated. The data for long crack samples, conversely, comply with the yielding impact theory so that the propagation impact resistance can be deduced. Nevertheless,

when a wide spectrum of impact data for specimens containing various crack lengths is considered, the results are inconsistent with the linear and yielding fracture theories.

The theory derived for the composite polymers was found to be in excellent agreement with the impact data obtained for the whole range of brittle to ductile HIPS. As shown in graphs D of Figures 7.16 to 7.25, the best line-fits on the experimental points intercept the energy axis at about 10 mJ without exception, equal to the predicted kinetic energy of the flying pieces. The slopes of these lines demonstrate the brittle impact resistances (initiation values) which were found to be almost constant for all materials (except for Super HIPS which had a tougher PS matrix). Figures 7.26 to 7.35 show the impact data for the commercial grades of HIPS on the reduced impact energy, I_r, and normalised ligament area plots. An excellent line-fit through the data can be produced on these graphs, thereby verifying the accuracy of the composite theory in a clear manner. The slope of these lines are the propagation impact resistances of these materials. The results are summarised in Table 7.5 in which the materials are collated against their propagation impact resistances.

The conclusion to be made here is that the impact strengths of rubber-modified polymers are to be defined as their impact resistances in crack propagation and crack initiation combined. These variables are not, however, to be considered as separate material properties since they are simply mathematical factors which describe the impact behaviour in a combined manner. As the initiation resistances remain almost constant for different polymers having identical matrices, the impact improvement can therefore be assessed by comparing their propagation impact resistances alone. When a wider spectrum of materials is studied, the initiation resistances and propagation resistances should both be considered, where

IMPACT STRENGTH (HIPS, USMA)

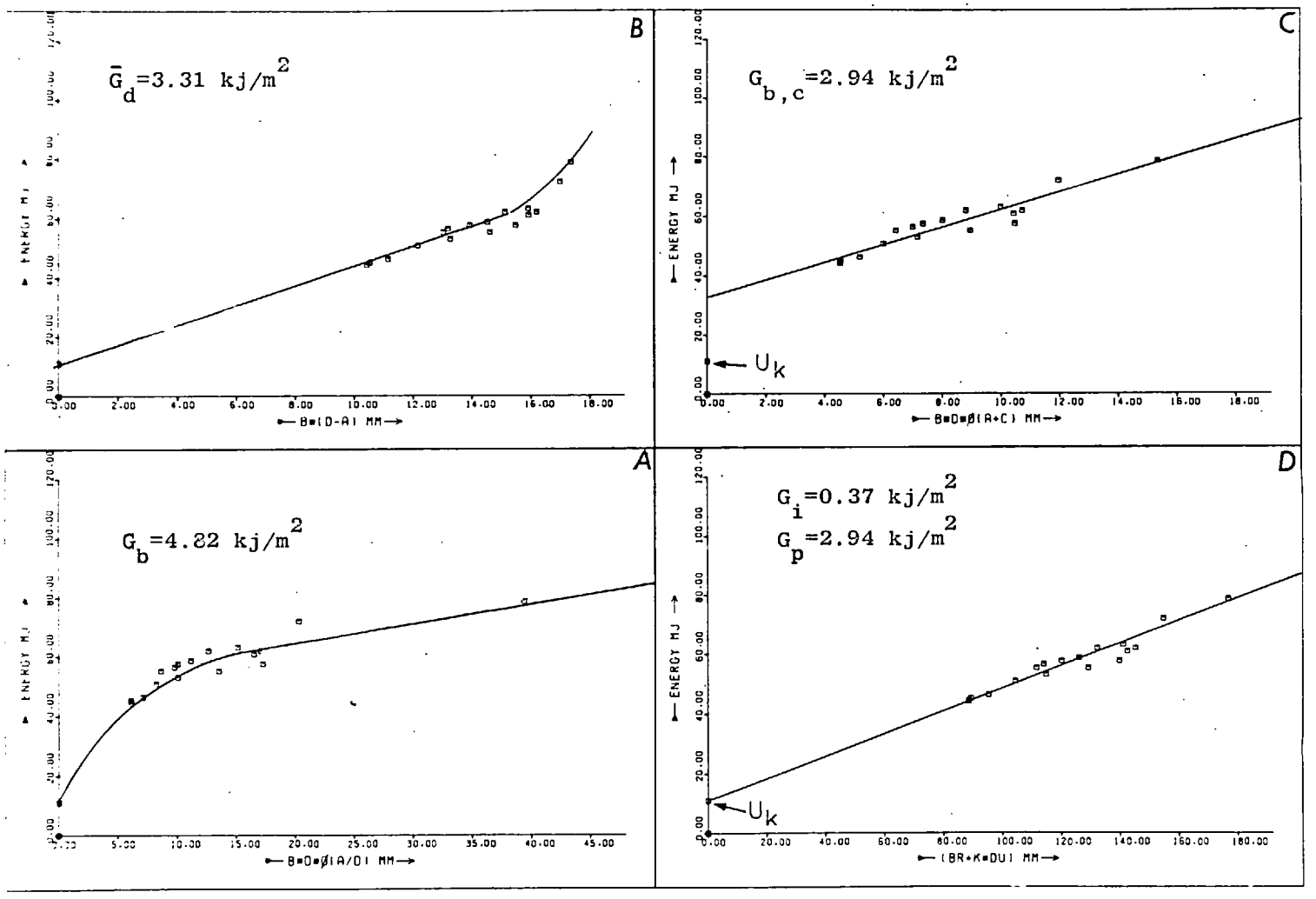


Figure 7.16

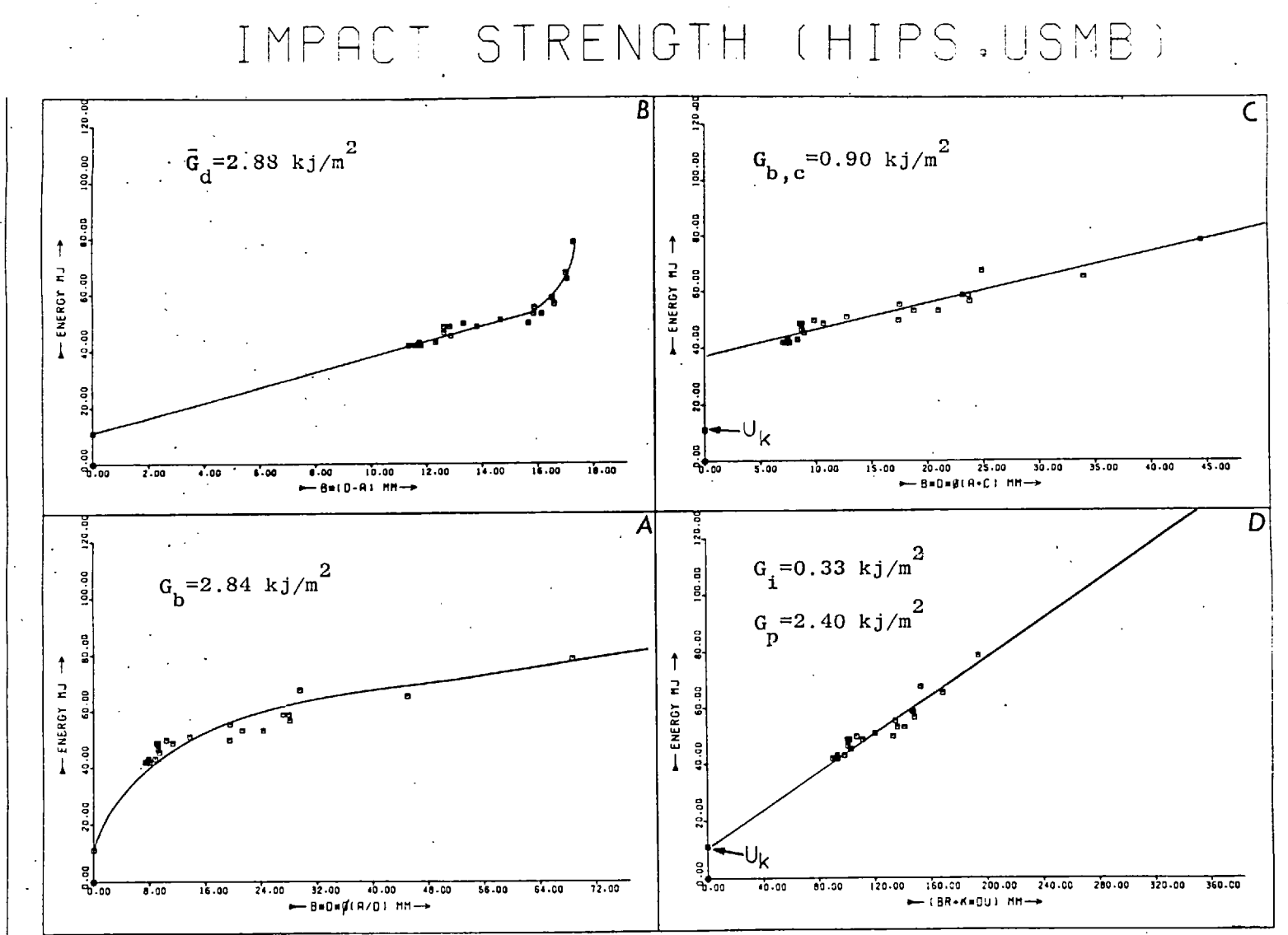

IMPACT STRENGTH (HIPS.USMB)
B
$\bar{G}_d$=2.88 kj/m^2
ENERGY MJ
B=(D-A) MM
C
$G_{b,c}$=0.90 kj/m^2
U_k
B=D=(A+C) MM
A
G_b=2.84 kj/m^2
B=D=(A/D) MM
D
G_i=0.33 kj/m^2
G_p=2.40 kj/m^2
(BR+K=DU) MM

Figure 7.17

IMPACT STRENGTH (HIPS, USSA)

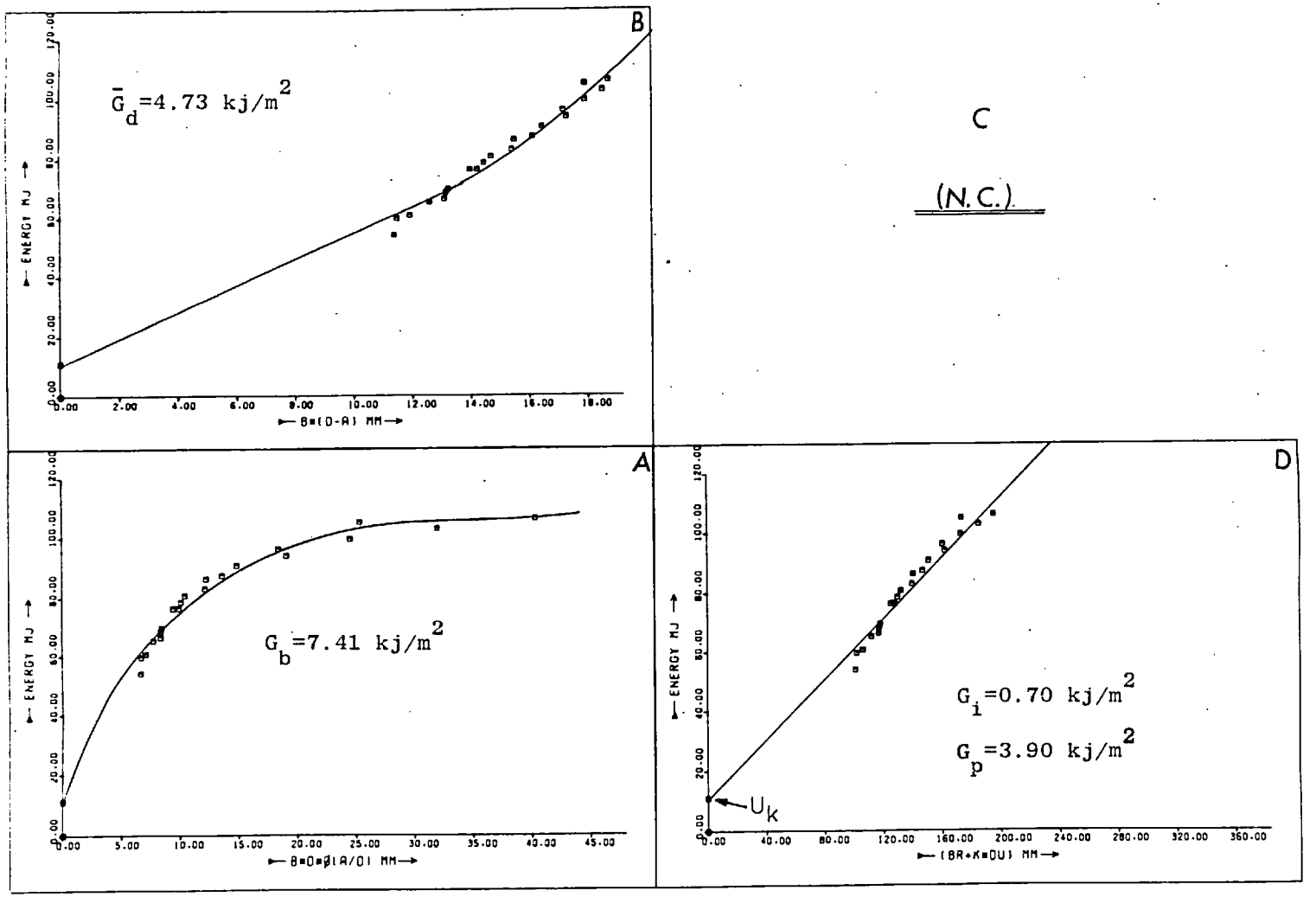


Figure 7.18

IMPACT STRENGTH (HIPS, USSB)

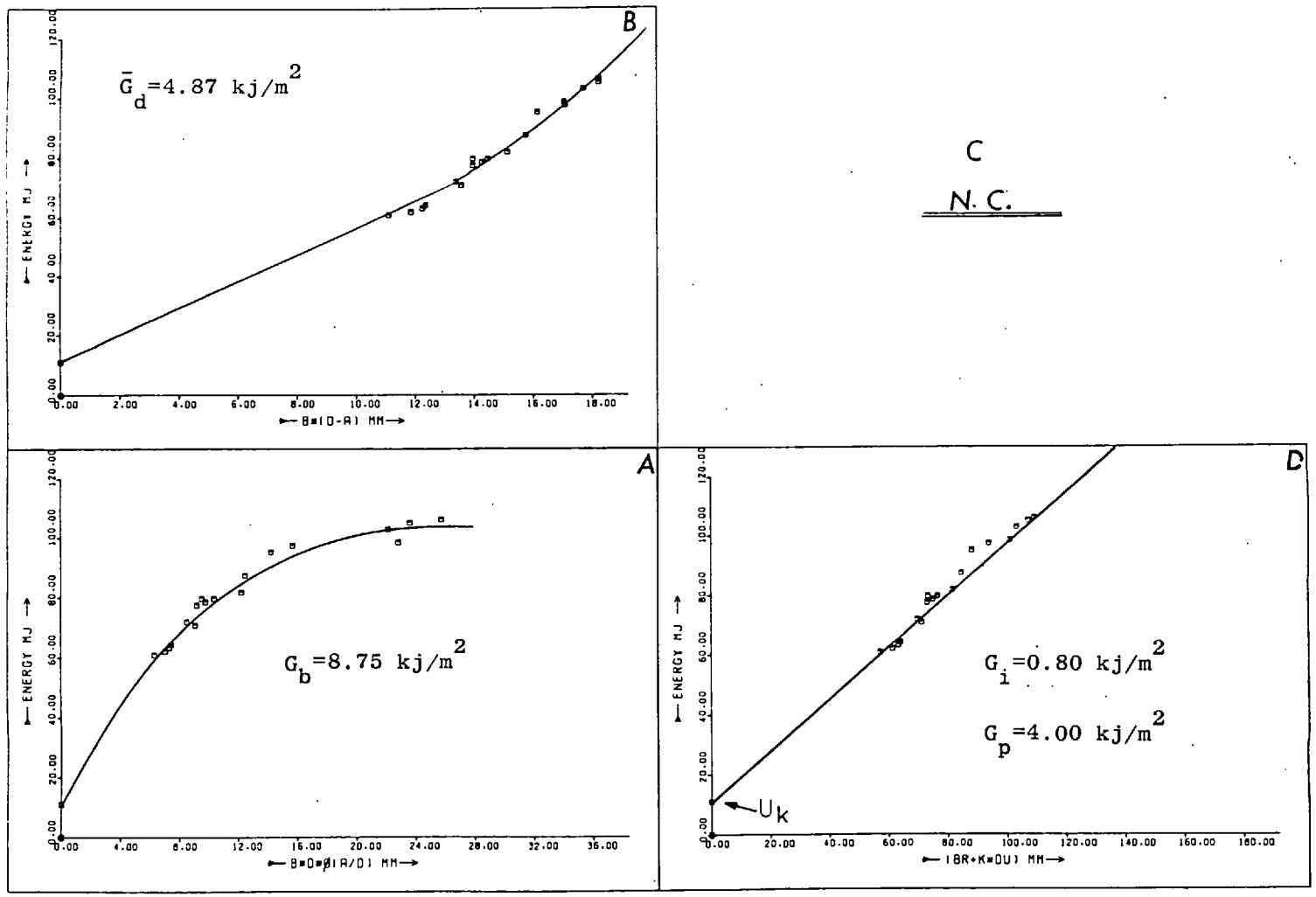


Figure 7.19

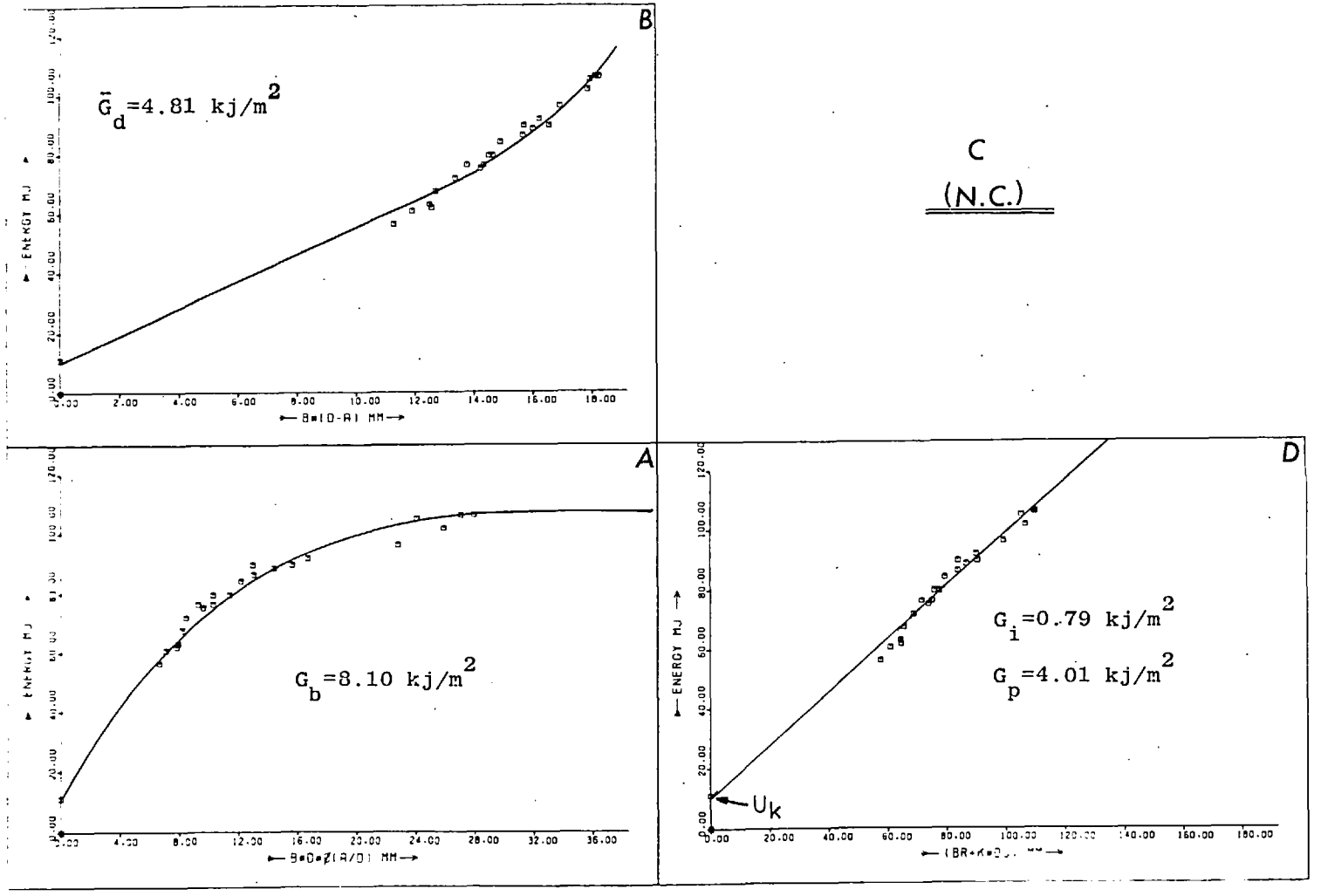

IMPACT STRENGTH (HIPS, USSC)
B
$\bar{G}_d$=4.81 kj/m^2
C
(N.C.)
A
G_b=8.10 kj/m^2
D
G_i=0.79 kj/m^2
G_p=4.01 kj/m^2
U_k

Figure 7.20

IMPACT STRENGTH (HIPS, USSD)

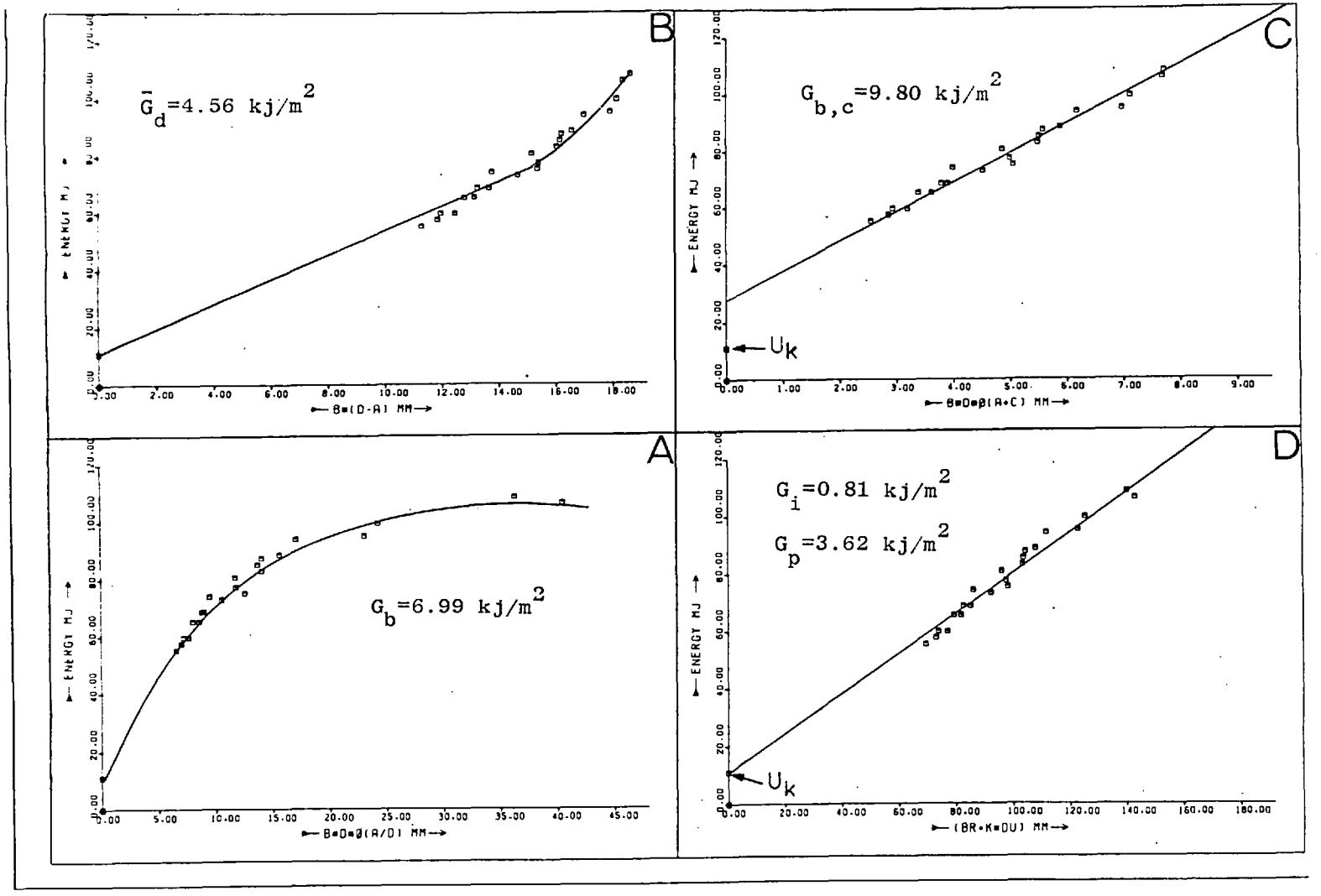


Figure 7.21

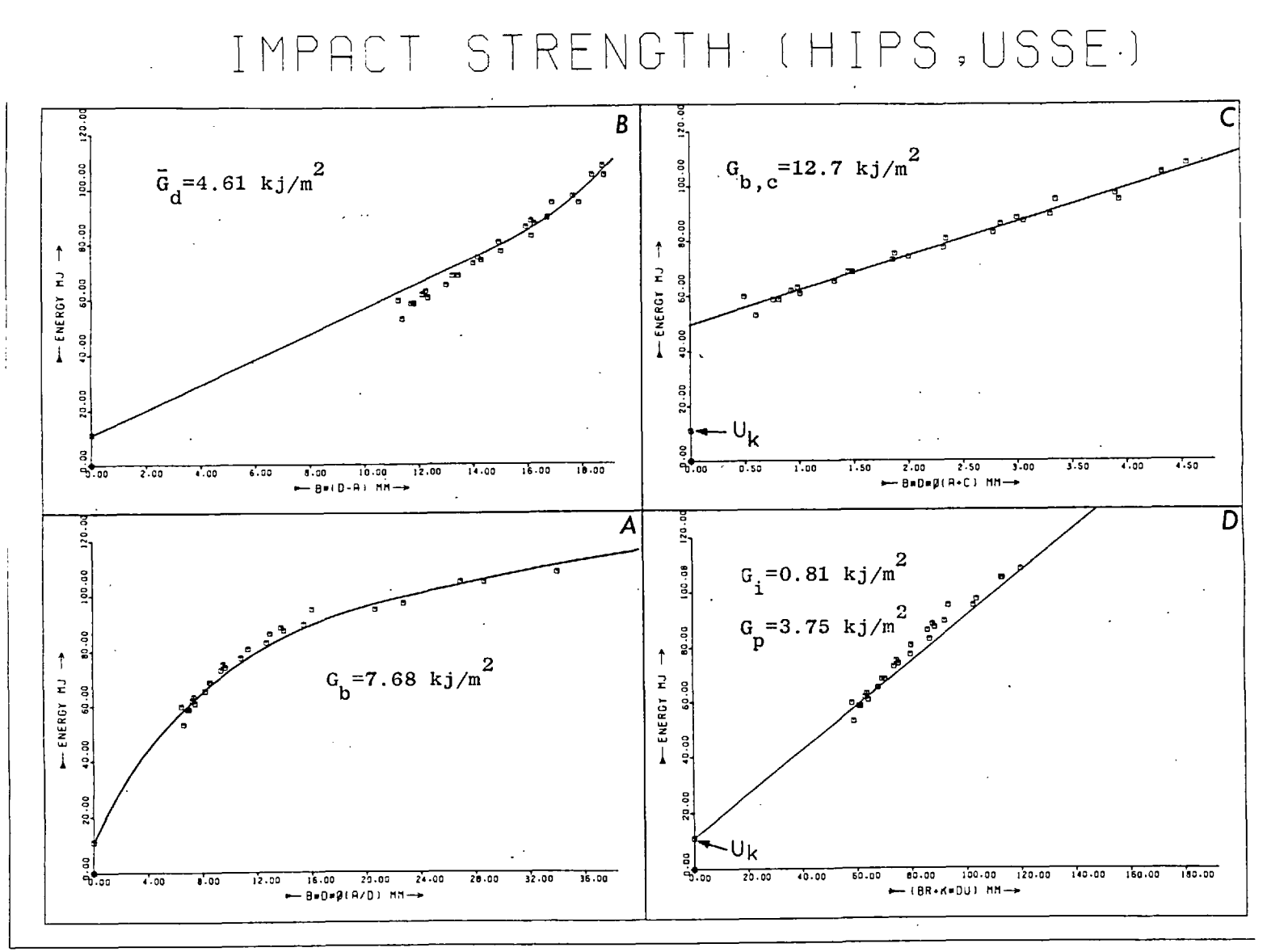

IMPACT STRENGTH (HIPS, USSE)
B
$\bar{G}_d$=4.61 kj/m^2
ENERGY MJ
B=(D-A) MM
C
$G_{b,c}$=12.7 kj/m^2
U_k
B=D=β(A+C) MM
A
G_b=7.68 kj/m^2
B=D=β(A/D) MM
D
G_i=0.81 kj/m^2
G_p=3.75 kj/m^2
U_k
(BR+K=DU) MM

Figure 7.22

IMPACT STRENGTH (HIPS, USSF)

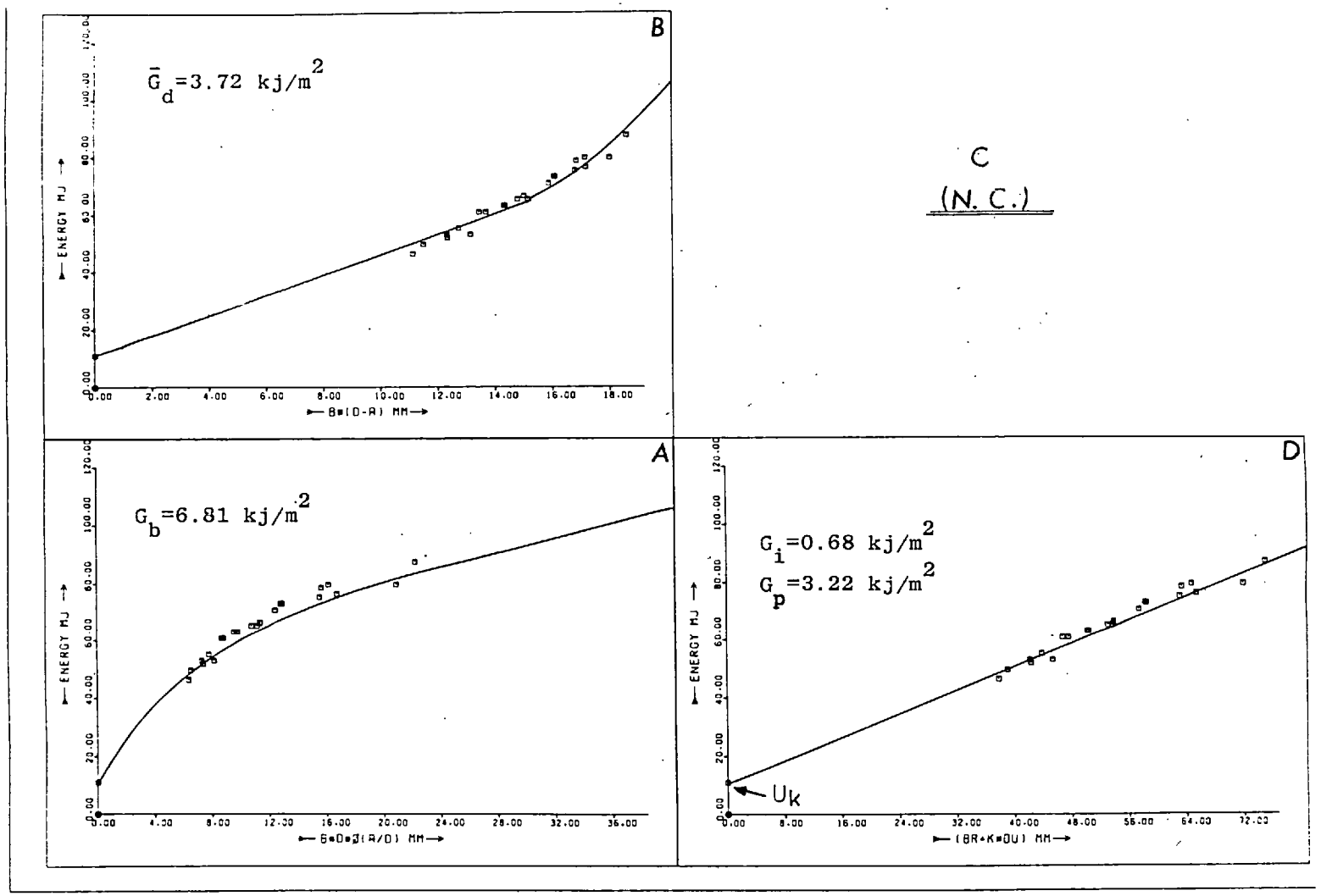


Figure 7.23

IMPACT STRENGTH (HIPS, USTA)

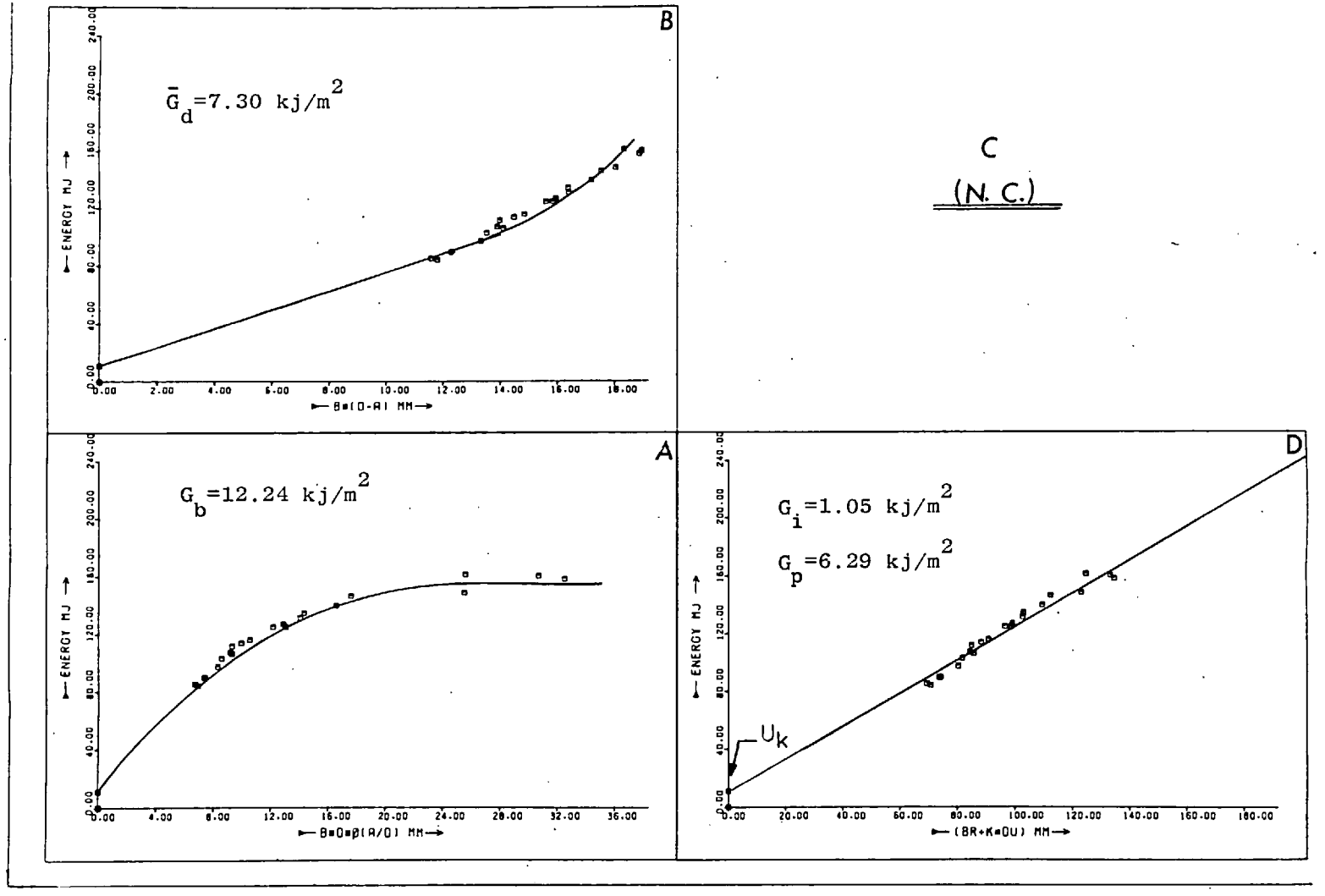


Figure 7.24

IMPACT STRENGTH (HIPS, USTB)

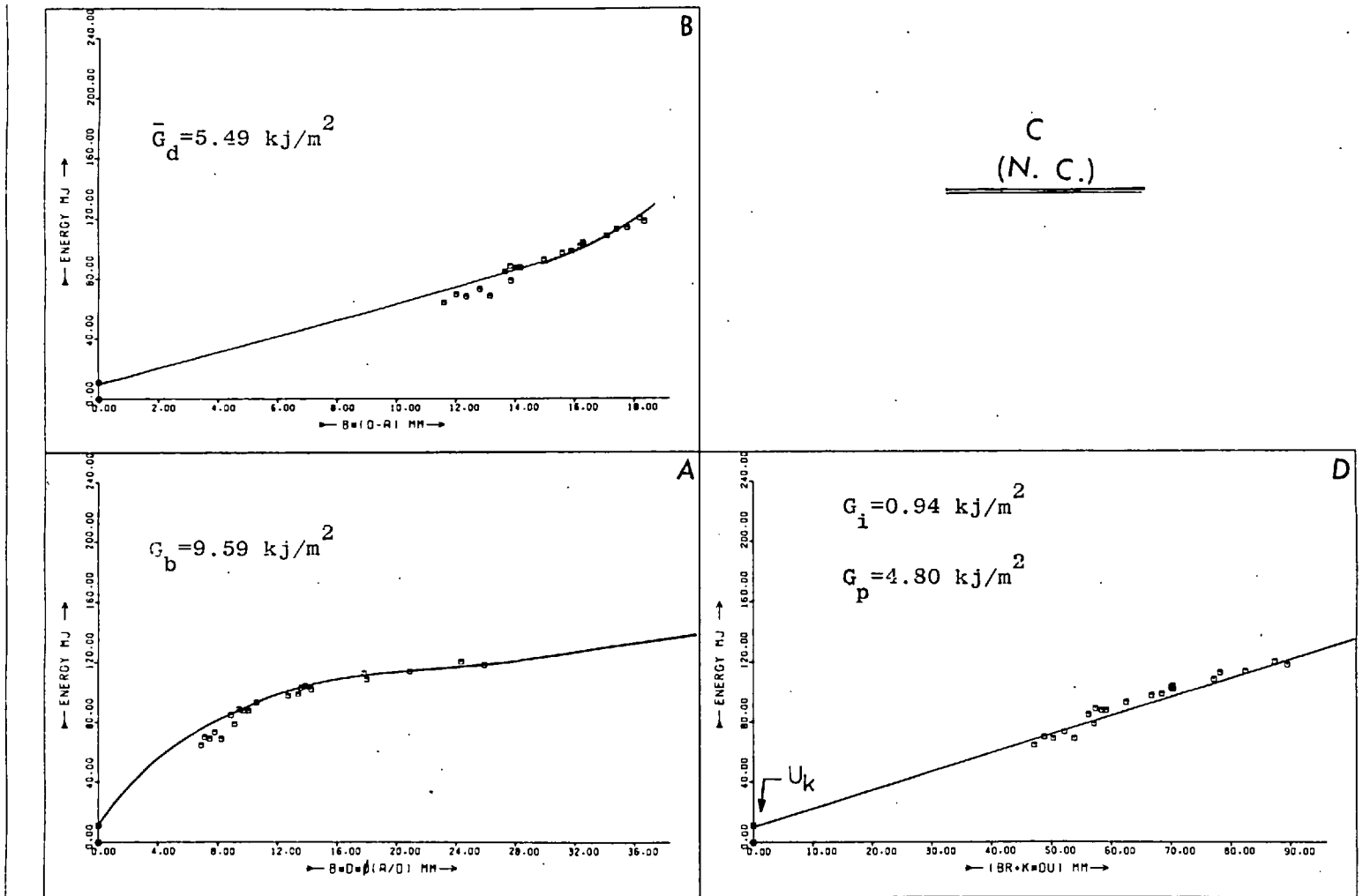


Figure 7.25

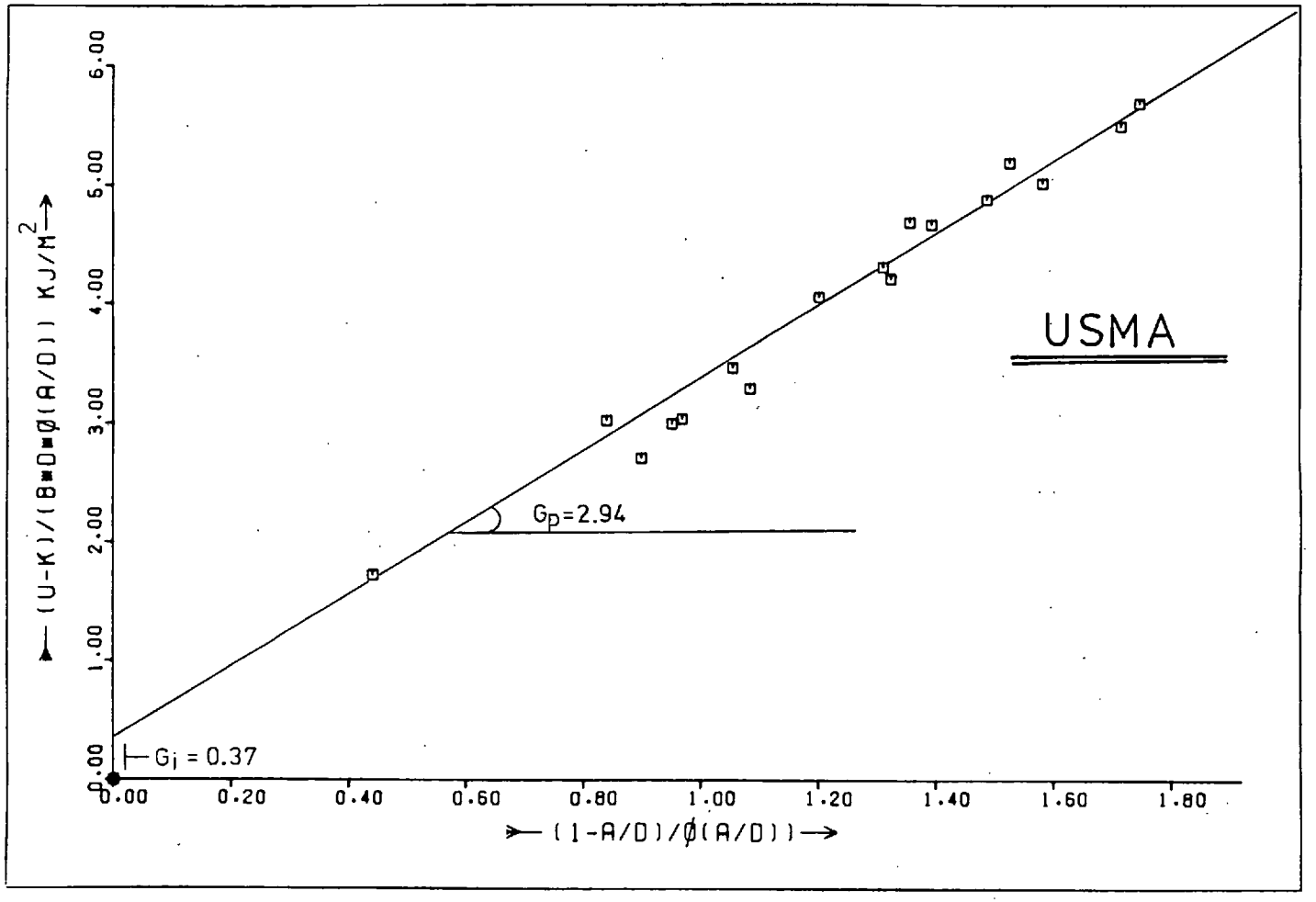


Figure 7.26: Initiation and propagation impact resistances for Medium HIPS

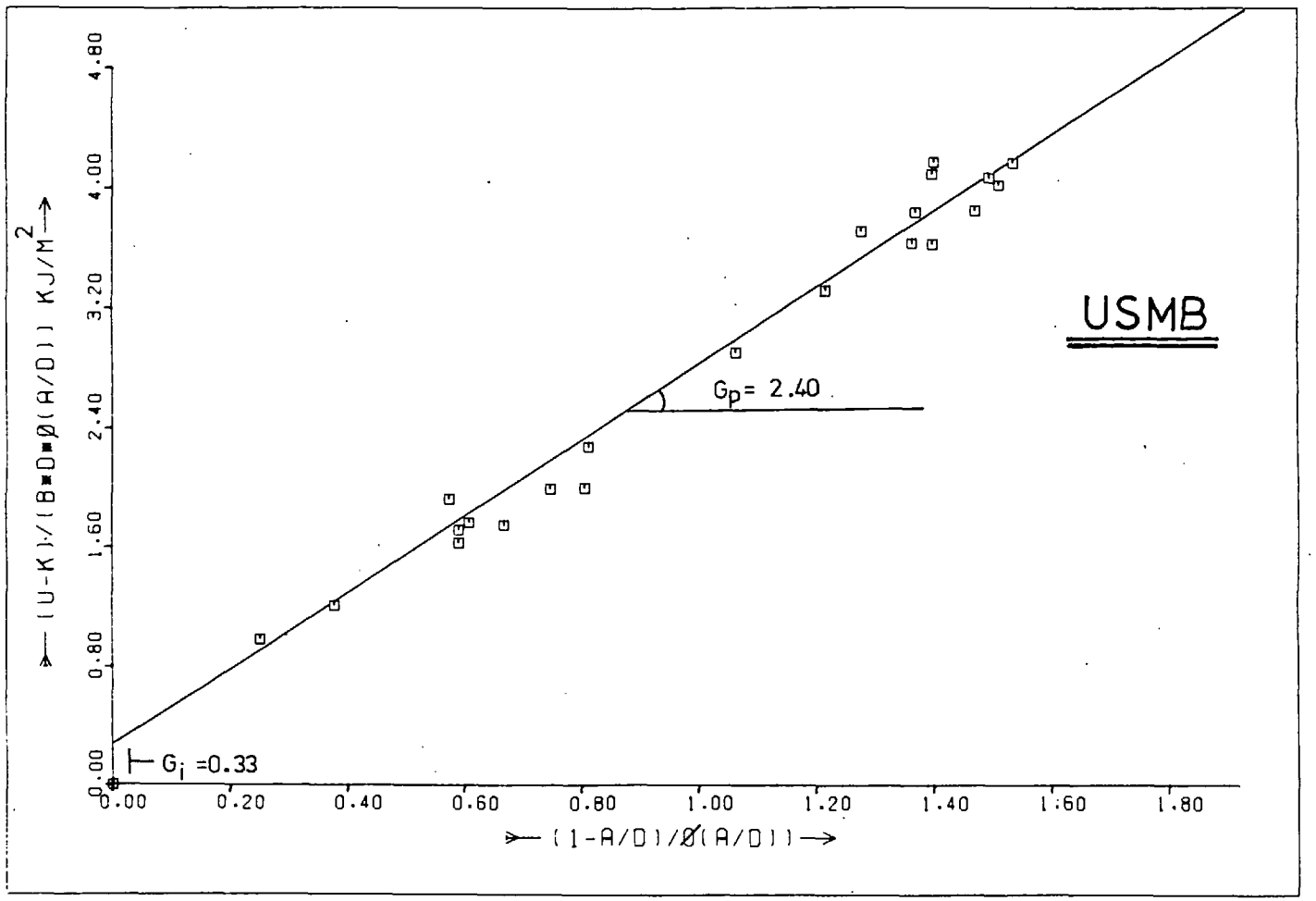


Figure 7.27: Initiation and propagation impact resistances for Medium HIPS

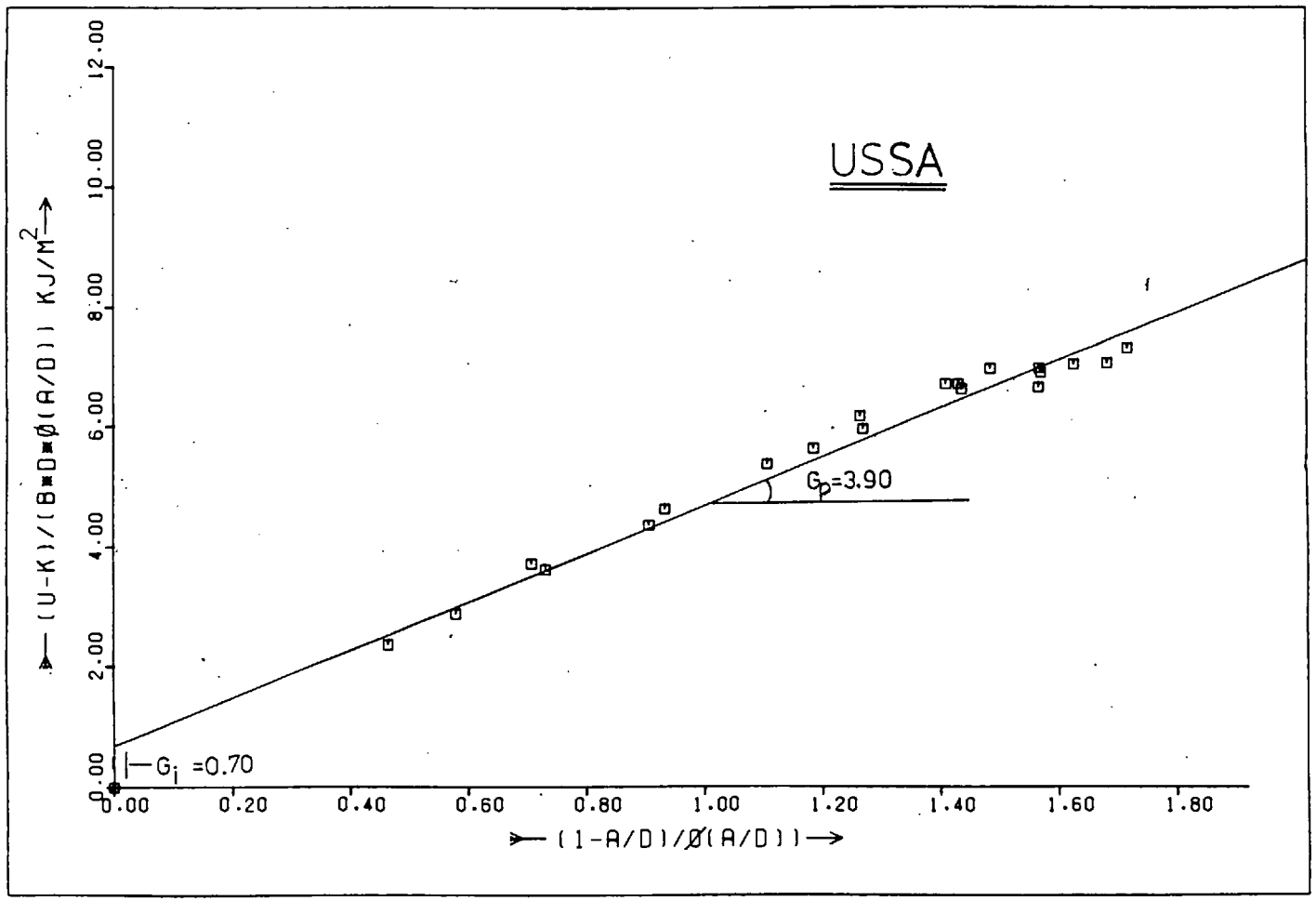


Figure 7.28: Initiation and propagation impact resistances for Standard HIPS

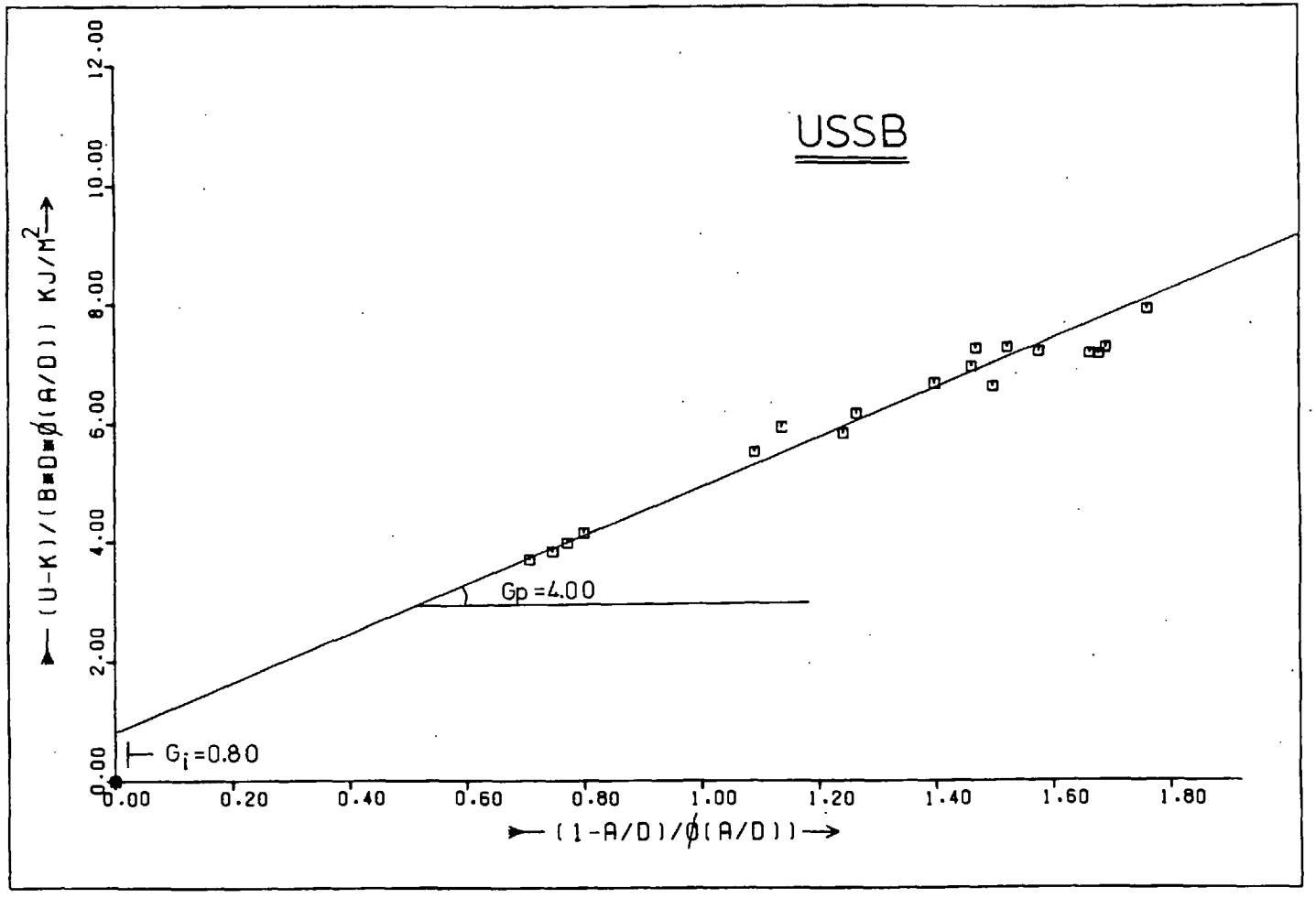


Figure 7.29: Initiation and propagation impact resistances for Standard HIPS

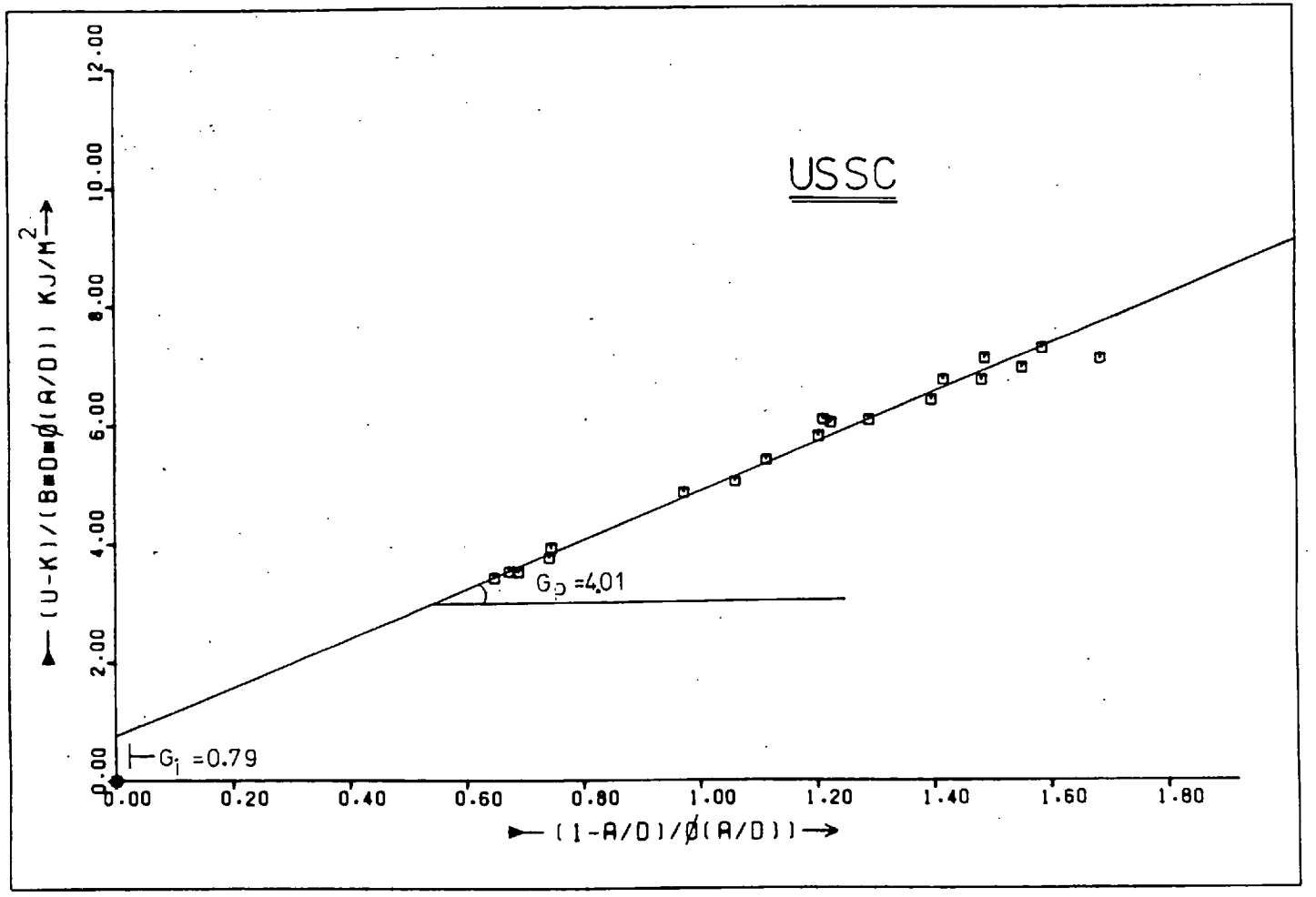


Figure 7.30: Initiation and propagation impact resistances for Standard HIPS

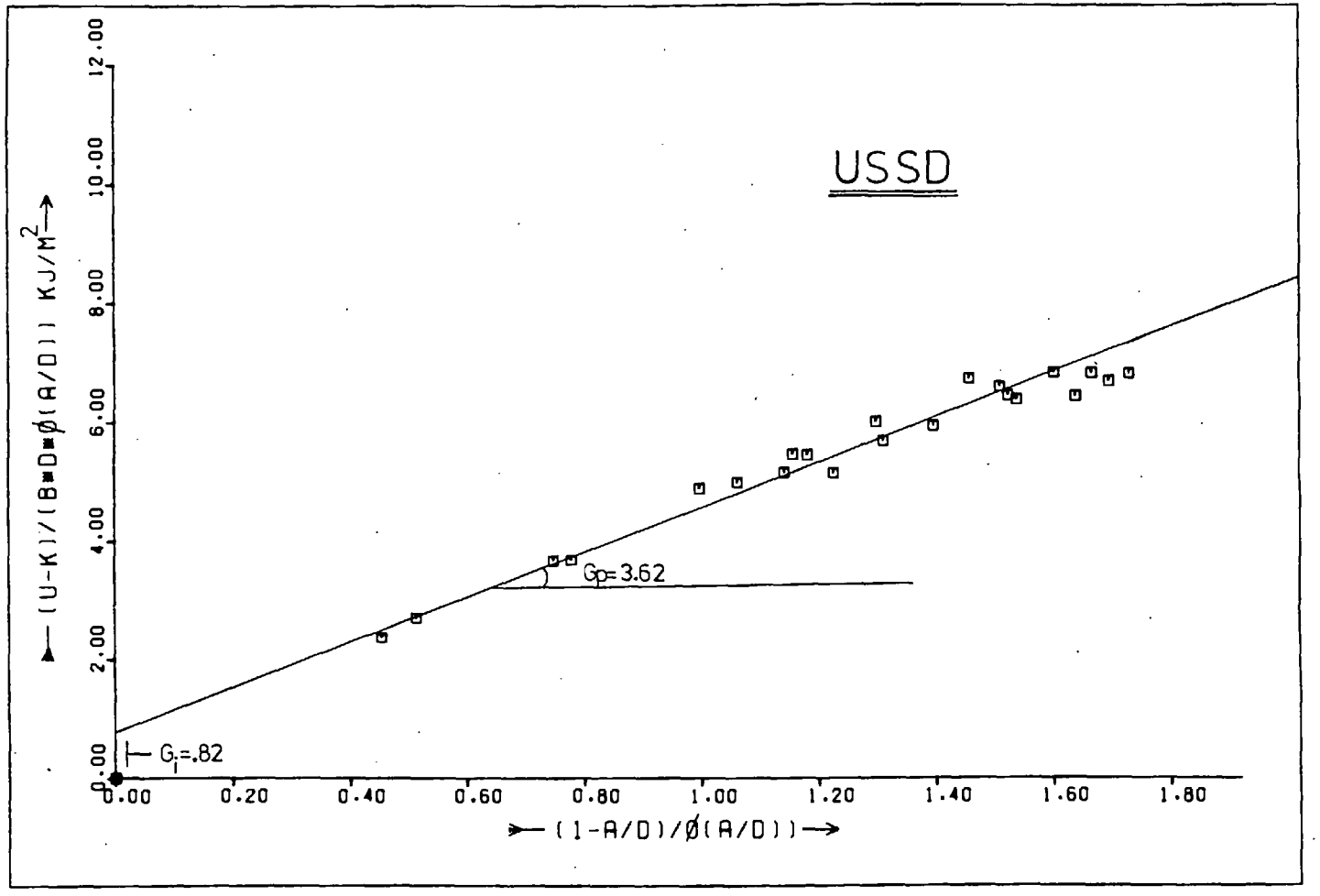


Figure 7.31: Initiation and propagation impact resistances for Standard HIPS

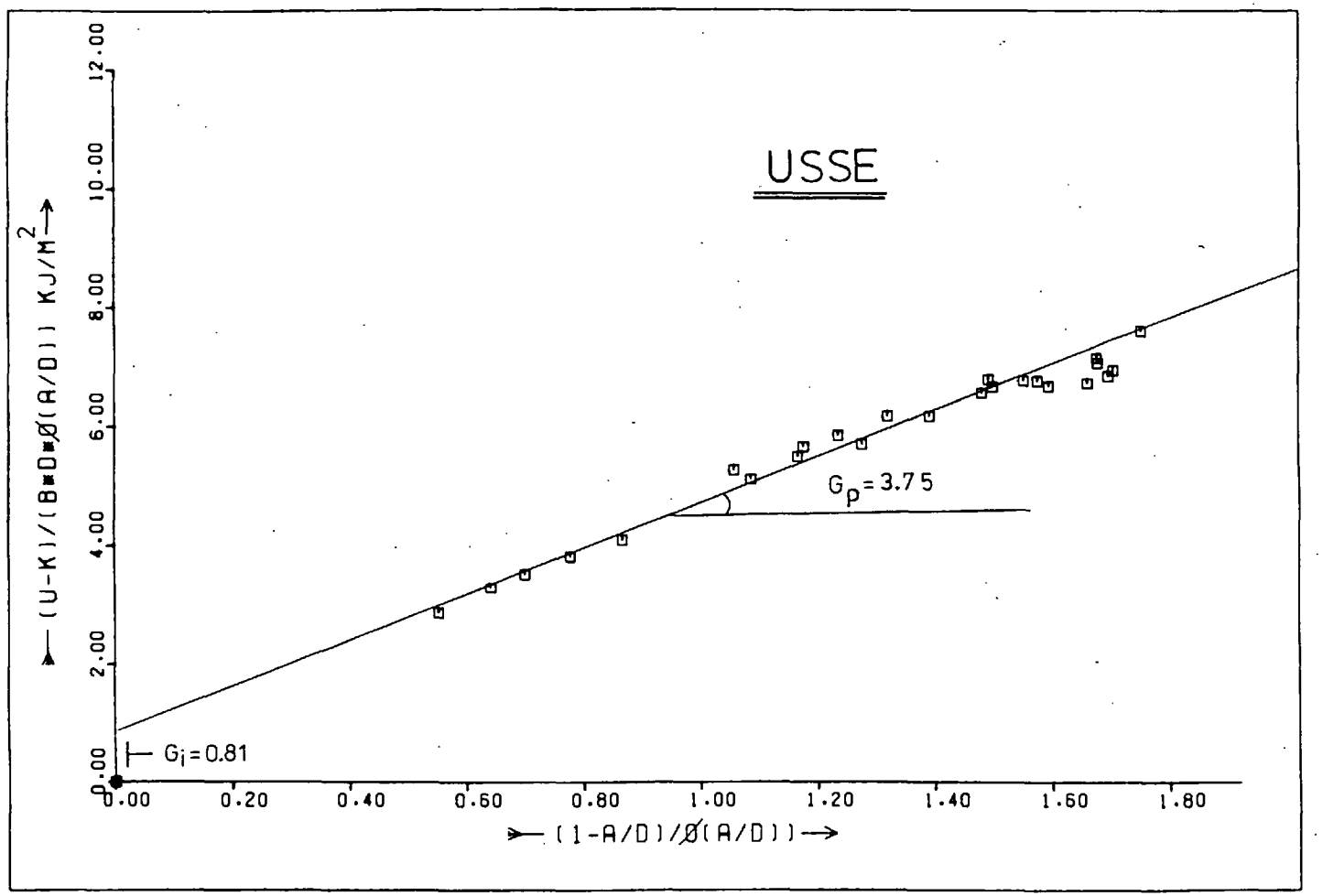


Figure 7.32: Initiation and propagation impact resistances for Standard HIPS

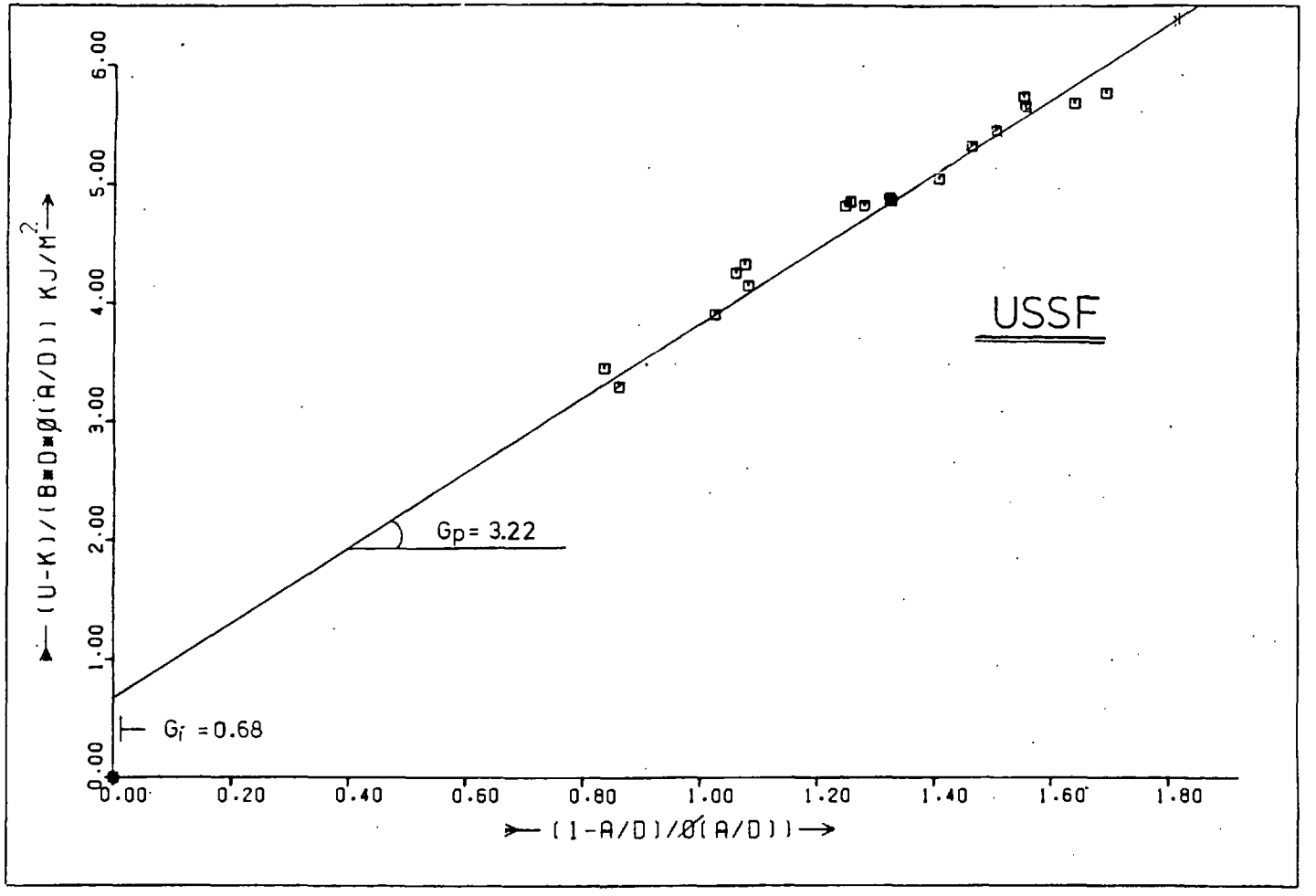


Figure 7.33: Initiation and propagation impact resistances for Standard HIPS

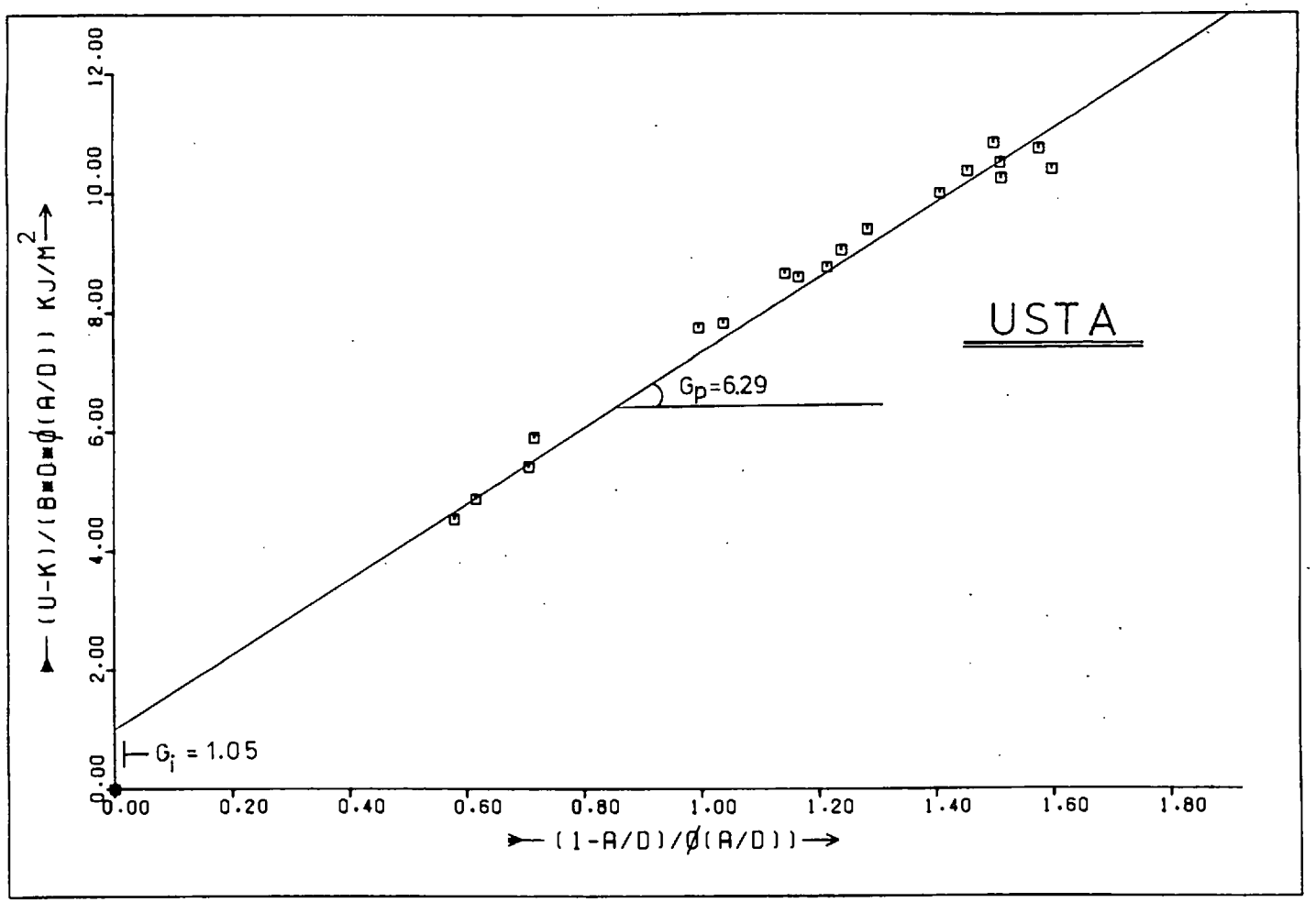


Figure 7.34: Initiation and propagation impact resistances for Super HIPS

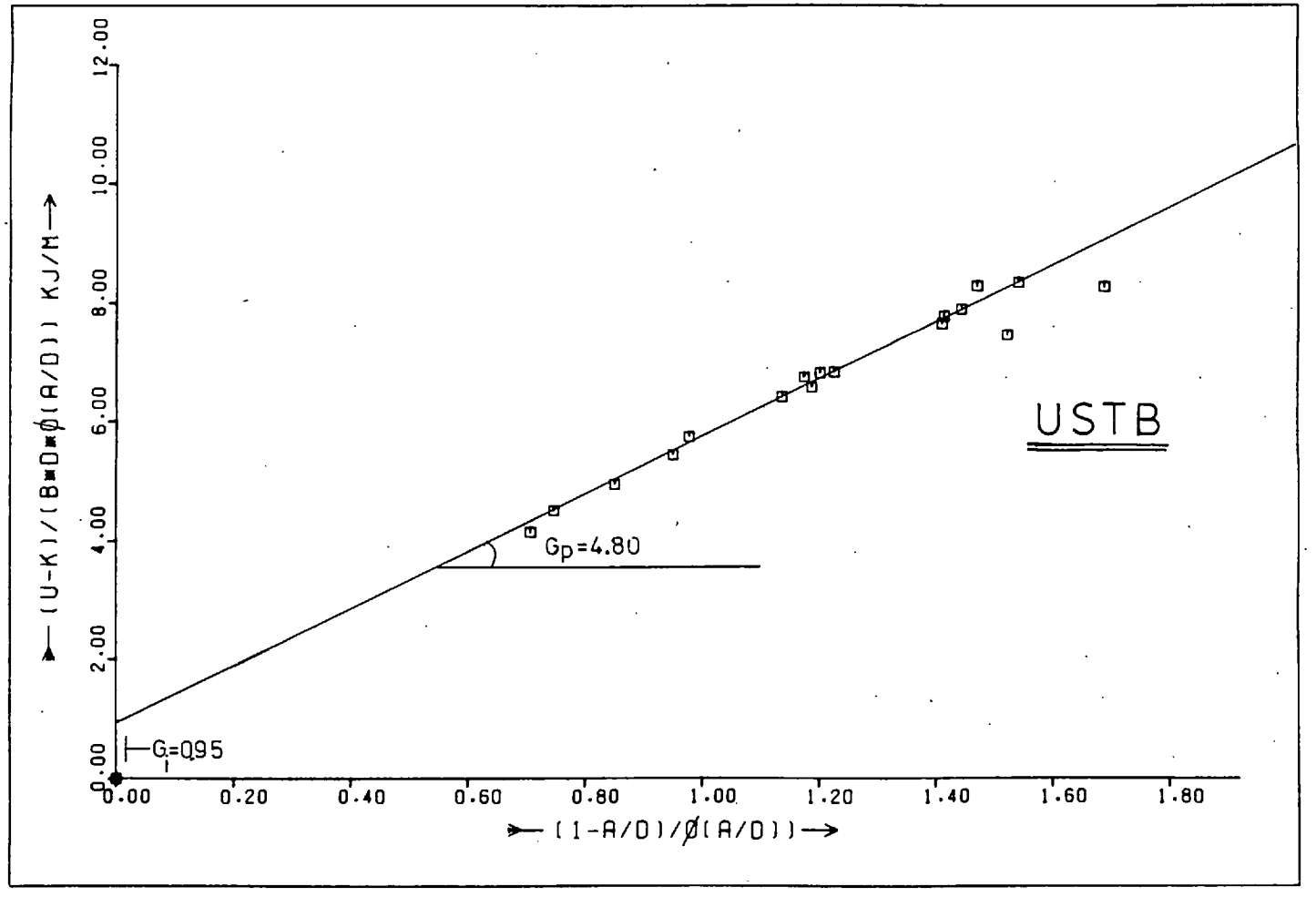


Figure 7.35: Initiation and propagation impact resistances for Super HIPS

TABLE 7.5

The Impact Strength of Commercial HIPS

Material		Initiation Resistance (kJ/m^2)	Propagation Resistance (kJ/m^2)
Type	Code		
Medium HIPS	USMB	0.33	2.40
	USMA	0.37	2.94
Standard HIPS	USSF	0.68	3.20
	USSD	0.82	3.62
	USSE	0.81	3.75
	USSA	0.70	3.90
	USSB	0.80	4.00
	USSC	0.79	4.01
Super HIPS	USTA	0.94	4.80
	USTB	1.05	6.29

the first parameter represents the toughness at low strain rates, while the latter determines the toughness in an impact test.

7.10 EFFECT OF RUBBER-MATRIX INTERFACE ON IMPACT STRENGTH

Three experimental grades of HIPS (USEA, USEB and USEC) were tested for their impact strengths and the results were similarly analysed. The manufacturer especially noted that these experimental materials were mal-processed and unexpected shattering fracture of the parts were often reported.

An analysis of fracture surfaces of impact specimens made from extruded sheets of these polymers was studied and two distinguishable modes of brittle and ductile fractures were observed. The specimens having shorter notches showed insignificant stress whitening and slow crack growth, while a large plastic flow was detected from the surfaces of those specimens containing longer crack lengths.

The experimental data for USEA, USEB and USEC are demonstrated in Figures 7.36 to 7.38, where the impact energies were plotted versus the ligament area. Two separate regions depending on the initial crack lengths can be detected in these plots. The specimens containing longer crack lengths are described by a straight line intercepting the energy axis at about 10 mJ, equal to the predicted kinetic energy of the fractured parts. As the initial crack length decreases at a critical crack length (about 0.2 D), the impact energy abruptly falls off to a level around half the value theoretically expected. At shorter cracks below this critical point, the impact data will be scattered on a low energy level, indicating a brittle mode of failure.

The precipitant ductile to brittle transition of mal-processed modified polymers can be explained as follows. As previously discussed, rubber particles act as stress concentrator elements, since they have much lower moduli than the surrounding polystyrene matrix. Goodier's equations (see Appendix A) show that the maximum stress concentration occurs at the

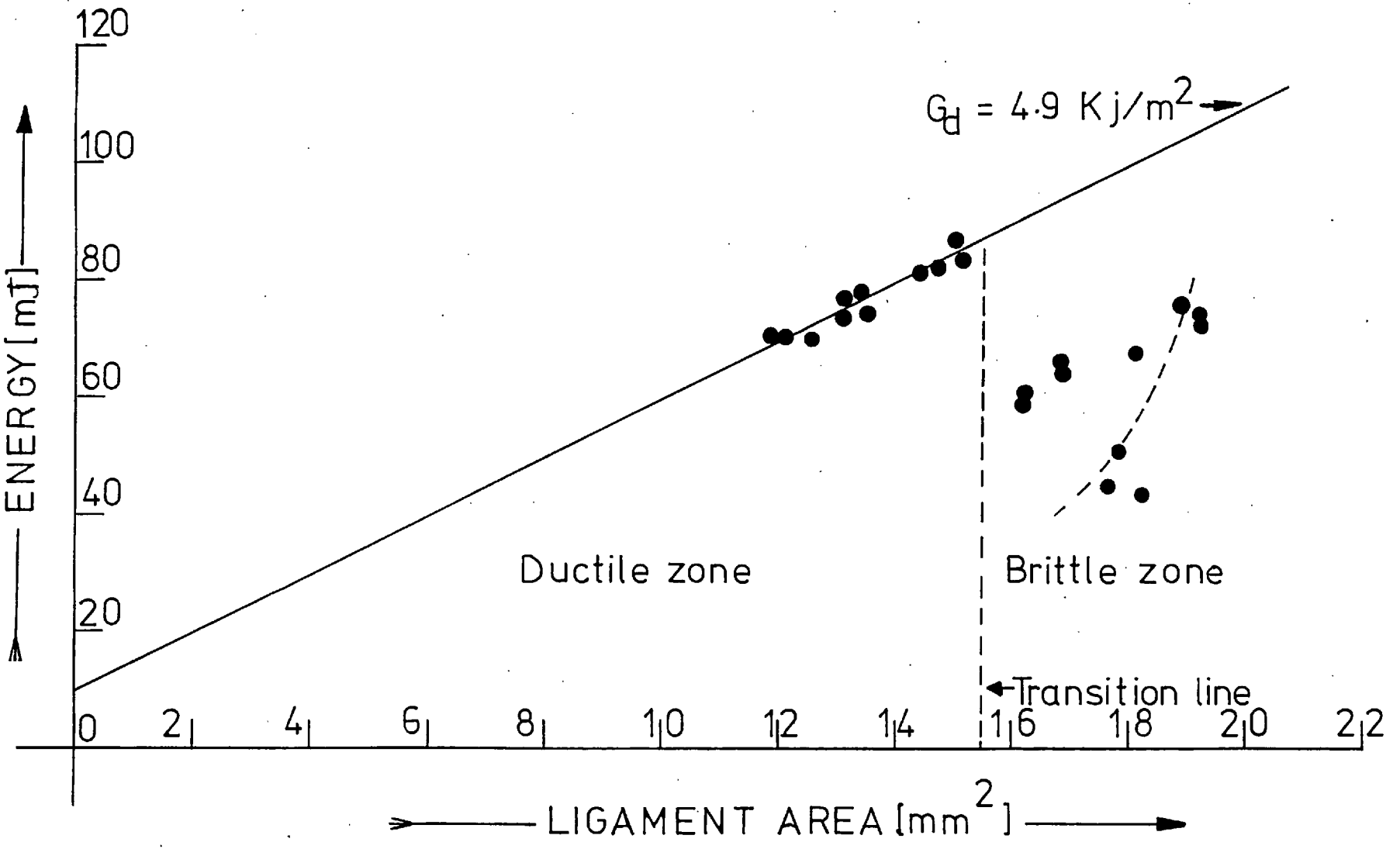


Figure 7.36: Ductile-brittle transition in a mal-processed HIPS (grade USEA)

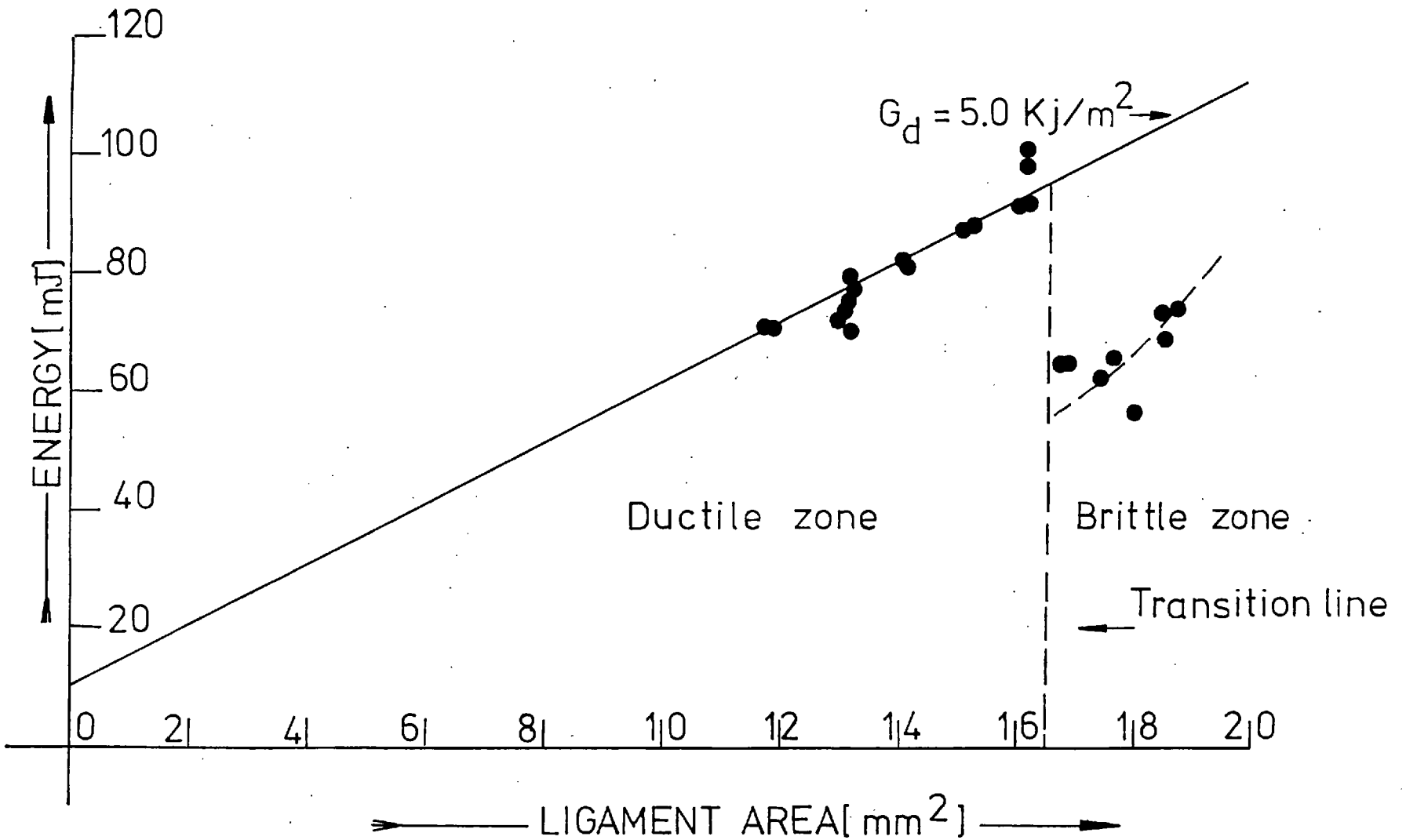


Figure 7.37: Ductile-brittle transition in a mal-processed HIPS (grade USEB)

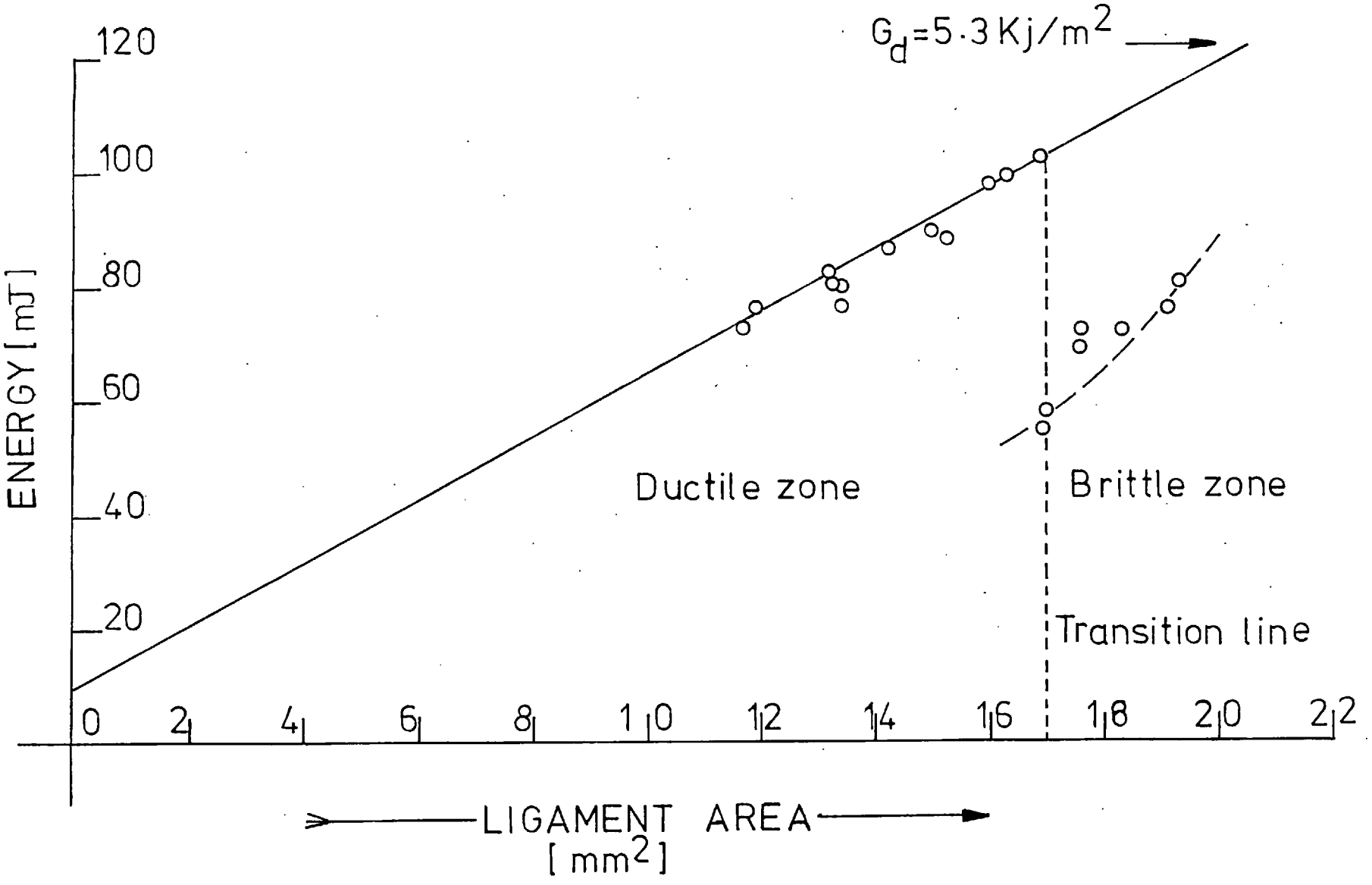


Figure 7.38: Ductile-brittle transition in a mal-processed HIPS (grade USEC)

equator of the rubber particles. If the particles are elastomeric and perfectly bonded to the matrix, the crazes initiate at points of maximum principal strain and propagate outward through the matrix. The result is the generation of a large number of short craze bands, in contrast with the small number of long crazes formed in the same matrix in the absence of these particles. On the other hand, if the particles are only loosely bonded to the matrix, the application of tensile loads preduces "penny-shaped" cavities around the equators of these particles, forming the nuclei for subsequent crack propagation. The result will then be manifested by a sudden brittle fracture. Now, an initial crack induces a larger stress concentration in the vicinity of the crack tip. The stress concentration is more critical when shorter notches are produced in specimens, since the average stress level will be higher in the media (that is, the applied stress prior to rupture would be nearer to the yield stress than the case of a specimen with longer initial cracks). Therefore, at a critical crack length, the applied stresses transgress the strength of the matrix-rubber bonds so that these bonds break and, through a cavity mechanism, incipient cracks initiate causing a brittle fracture.

7.11 CLOSURE

The basic theories derived for homogeneous brittle or ductile materials were found to be inaccurate to describe the impact strength of rubber-modified polymers. The composite theory, however, could clearly determine the effect of rubber content on the impact strength of these materials. The impact resistances were then defined in terms of initiation (G_i) and propagation (G_p) impact strengths. The values for G_i and G_p can be evaluated by performing two experiments on specimens containing different crack lengths. It was found that G_i was nearly constant, while G_p increased linearly with increasing rubber percentage. Moreover, it was shown that the matrix-particle interface cohesion plays a dominant rôle in the processing of rubber-modified polymers.

CHAPTER 8

DYNAMIC MECHANICAL PROPERTIES

8.1 INTRODUCTION

A knowledge of the viscoelastic nature of multi-phase polymers and its relationship to temperature provides a basis for relating the macroscopic physical characteristics to the micro-structure of the constitutive components. An understanding of the time-dependent behaviour of these polymers when subjected to constant load (as in a creep test) or constant deformation (as in a stress-relaxation test) yields useful information about their viscoelastic properties, but greater insight and an intrinsic understanding of the general behaviour of the polymer can be obtained more rapidly by the study of dynamic mechanical properties. These are ascertained by measuring the response to a dynamic stimulus.

In general, a careful and systematic analysis of the dynamic mechanical experimental data provides a powerful basis for examining the effect of cross-linking, crystallinity, plasticisation and the grafting procedure on the mechanical and fracture behaviour of polymers (Ball (1971); Bucknall (1967)). The experimental work to be presented in this chapter is, however, restricted to the study of the influence of rubber content on the viscoelastic properties of HIPS, since it is considered to be the most important parameter in the toughening process. The effects of crystallinity, rubber-polystyrene cross-linking and the grafting characteristics of the rubber particle have been examined elsewhere (e.g. Turley (1963); Cigna (1970); Koo (1974); Nielsen (1974); Bucknall (1977)). These aspects have been previously discussed in Chapter 5 and will not be expounded further.

Generally, dynamic mechanical tests can be classified in two ways,

one measuring the torsional response (stress of a specimen subjected to a free periodic stimulus (strain) using a torsion pendulum apparatus, and the other measuring the forced oscillations of a tensile specimen using a Rheovibron apparatus. Both instruments have been widely accepted and used in polymer technology. The torsion pendulum machine was developed in the early 1950s by Wolf & Schmieder (Germany) and Buchdahl & Nielsen (USA) (Koo (1974)), and a standard method for testing was later drafted and approved by the ASTM section on dynamic mechanical properties (ASTM (1972d)). The torsion pendulum machine is relatively simple to construct and to operate, but it has certain limitations. The main disadvantage is that the frequency is not an independent test parameter and its influence on the dynamic response cannot be easily ascertained.

Non-resonant forced-vibration instruments were originally employed for testing rubbers (Roelig (1945); Wilkinson & Gehman (1950)), and this apparatus, commercially known as the "Rheovibron", was later developed and successfully used for polymeric materials by Takayanagi in Japan (Yoshino & Takayanagi (1959); Takayanagi (1963); Takayanagi et al (1963)). The Rheovibron is so designed that the frequency of the oscillation can be altered as an independent variable and the resultant stress and strain responses are simultaneously measured. Consequently, the differential phase angle between stress and strain are read directly from an oscilloscope display or from some other electronic device. The damping coefficient and the moduli of the materials tested can then be evaluated using standard vibration theories. Rheovibron specimens are normally very thin (less than 1 mm) and this gives an advantage over the torsion pendulum since it is possible to vary the temperature continuously over a relatively short period of time while taking the response measurements simultaneously. The main drawback of Rheovibrons lie with their limited loading capacity

over a wide range of temperatures. This is because a polymeric specimen with the appropriate dimensions at lower temperatures, where it is sufficiently rigid, can become too soft at higher temperatures. If a compromise thickness cannot be chosen, two specimens of different thickness must therefore be employed to cover the whole temperature spectrum.

8.2 THEORETICAL APPROACH

The mathematical analysis of a dynamic mechanical test can be found in most common texts (e.g. Nielsen (1974)). The outlines of the main concepts employed in the present work are described as follows:

Assume an ideally elastic material undergoes a sinusoidal elongation described by:

$$\bar{\varepsilon} = \bar{\varepsilon}_o \sin \psi_o t \tag{8.1}$$

where t = time, and $\bar{\varepsilon}_o$ and ψ_o denote the amplitude of elongation and angular frequency, respectively.

Since an elastic material responds instantaneously to the applied strain, the resultant stress is given by:

$$\sigma = \sigma_o \sin \psi_o t \tag{8.2}$$

where σ_o denotes the amplitude of applied stress.

Here, the material is mathematically analogous to a system consisting of a mass and a spring. The maximum energy per unit volume stored in the system is given by:

$$U_o = \tfrac{1}{2} E \varepsilon_o^2 \tag{8.3}$$

where E is the modulus of elasticity equivalent to the spring constants, and ε_o is the amplitude of the applied strain.

Polymers are, however, viscoelastic materials in which a portion of the excitation energy fed to the system will not be stored elastically but rather dissipated through friction and heat release. A linear viscoelastic material can be paralleled by a system comprising a mass, a spring and a dash-pot. If a sinusoidal elongation is applied to a linear viscoelastic

specimen, the stress also varies sinusoidally but lags the elongation by a phase angle Ω, that is:

$$\sigma = \sigma_o \sin (\psi_o t - \Omega) \tag{8.4}$$

The peak stress can be resolved into the in-phase and out-of-phase components, and the ratio of the two, $\tan \Omega$, is the damping factor which represents the relative importance of viscous as compared to elastic component of the material. The two corresponding moduli can be defined as:

$$E_1 = (\sigma_o/\varepsilon_o) \cos \Omega = E^* \cos \Omega \tag{8.5}$$

$$E_2 = (\sigma_o/\varepsilon_o) \sin \Omega = E^* \sin \Omega \tag{8.6}$$

$$E^* = (E_1^2 + E_2^2)^{\frac{1}{2}} \tag{8.7}$$

where E_1, E_2 and E^* are the in-phase, out-of-phase and complex moduli, respectively. The complex modulus for a flat-strip specimen subjected to a tensile strain is given by:

$$E^* = \frac{F_o}{\bar{\varepsilon}_o} \frac{L}{s_o} \tag{8.8}$$

where F_o = amplitude of the tensile force, L = specimen length, s_o = cross-sectional area of specimen, and $\bar{\varepsilon}_o$ = amplitude of elongation, and the phase angle is defined by:

$$\Omega = \tan^{-1} (E_1/E_2) \tag{8.9}$$

The physical importance of Ω becomes clearer when the damping energy dissipated per cycle is considered for a linear viscoelastic material. The dissipation loss is obtained from:

$$W_d = \oint \sigma \, (d\varepsilon_o/dt) \, dt \tag{8.10}$$

where ε_o denotes the amplitude of the strain sufferred by the specimen. From equations (8.1) and (8.2), we have:

$$W_d = \pi \sigma_o \varepsilon_o \sin \Omega \tag{8.11}$$

and the elastic energy is given by equation (8.3), except in this case $E = E_1$ is the elastic in-phase modulus. The ratio of the maximum energy stored and the damping energy dissipated per cycle is then obtained from:

$$2\Delta = \frac{W_d}{U_o} = 2\pi \tan \Omega \tag{8.12}$$

The above relationship of $\tan \Omega$ to energy dissipation is the principal basis on which the dynamic mechanical data are interpreted. A polymer which exhibits high energy dissipation with a high value of Δ is known as a high damping or viscous material and, conversely, a purely elastic polymer is defined by a zero damping energy ratio.

8.3 EXPERIMENTS

8.3.1 Apparatus

The non-resonant, forced viscoelastometer used in this study was a commercial apparatus (Type DDV-II, Rheovibron) made by the Toyo Baldwin Company Limited in Japan. A photograph of this apparatus is shown in Figure 8.1. In addition to the Rheovibron, the stabilised power source, *tan* δ indicator, operating switches and oscilloscope display are also shown in this figure.

For simplicity, the apparatus will be described using the schematic diagrams presented in Figure 8.2. As shown in diagrams 8.2(a) and 8.2(b), the specimen is fixed between two wire strain gauges of the unbound type, one being designed for stress detection (T1) and the other for strain detection (T2). The specimen is excited at definite frequencies (3.5, 11, 35 and 110 Hz) by means of a magnetic coil. The temperature of the sample is regulated by use of an electric furnace over a temperature range from room temperature to 250^{o}C and a cooling system, which utilises liquid nitrogen, over a temperature range from -170^{o}C to room temperature. To prevent ice forming and also to reduce the ambient humidity, dry air was pumped into the specimen chamber.

A simple block diagram of the instrument circuit is shown in Figure 8.2(c). As illustrated, the signals provided by the oscillation generator at a definite frequency (e.g. ψ_o = 11 Hz) are fed to the main driver through a phase adjusting unit, an amplitude adjusting unit and selective power amplifiers. Via another circuit, these signals are supplied through a phase corrector unit to the synchronous rectifier as a reference voltage. The output signals from the stress and strain transducers can be detected by a vacuum voltmeter after being amplified through the potentiometer VR1 and VR2. If the absolute values of the electrical

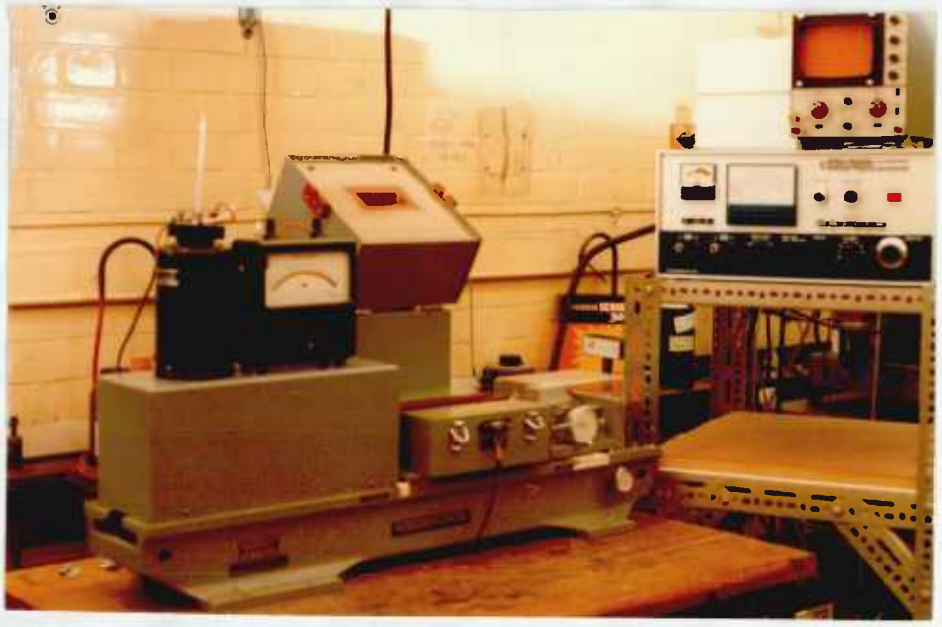
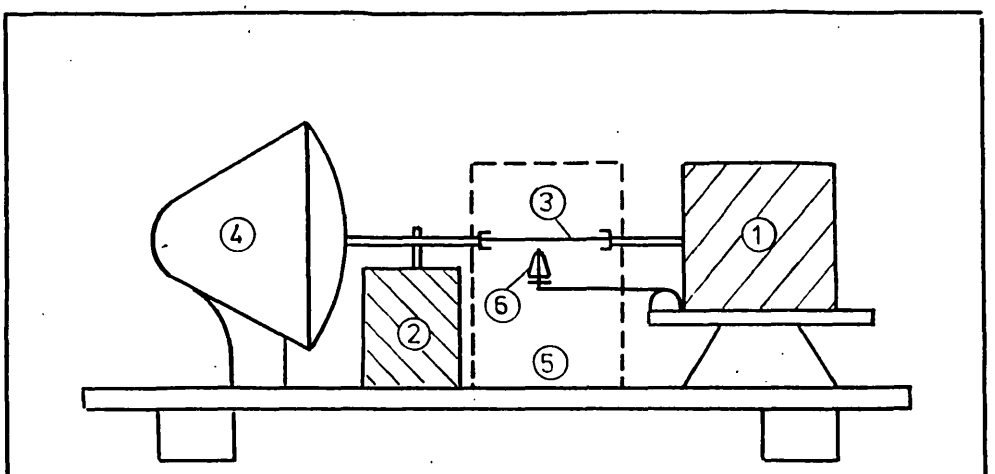
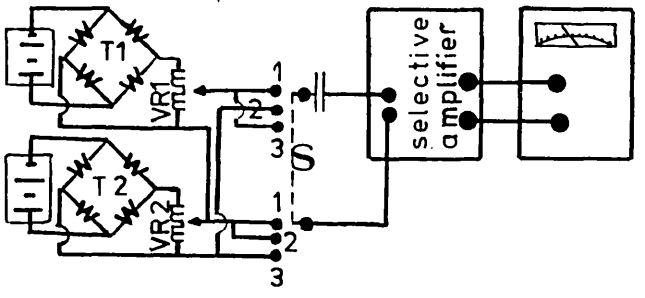


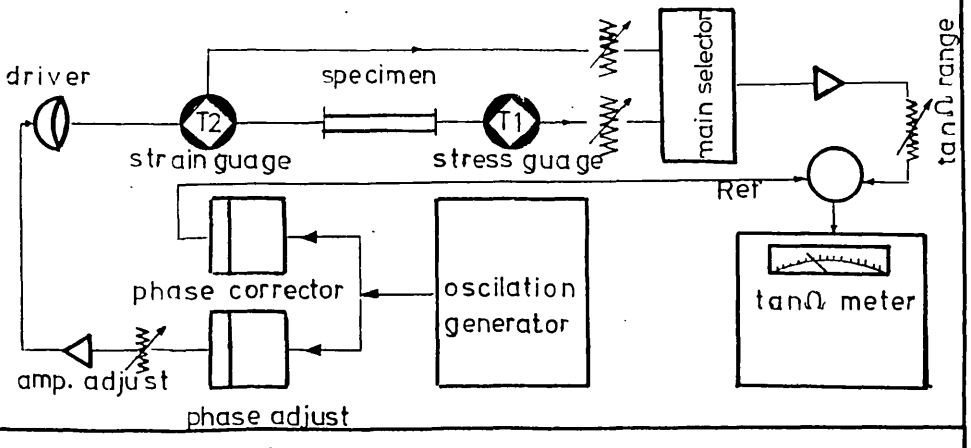
Figure 8.1: The Rheovibron testing apparatus



(a) Arrangement of apparatus: 1. stress transducer; 2. strain transducer; 3. specimen; 4. driver; 5. temperature box; 6. thermocouple.



(b) Circuit for detection of stress, strain and *tan* Ω



(c) Block diagram of Rheovibron

Figure 8.2: Schematic arrangement of the dynamic mechanical testing apparatus

stress and strain vectors are adjusted to unity, the phase angle, $tan\ \Omega$, is obtained by vector subtraction and the resultant is compared with the reference voltage from the synchronous rectifier. This can be performed by the following procedure, using the main operating switch, S.

8.3.2 Operating Procedure

Turning the switch S into position 2 (Figure 8.2(b)) and regulating the potentiometer VR1, the indication of the vacuum voltmeter is set to unity. The potentiometer ratio in this case is measured (G_1). Subsequently, the switch is turned to position 1 and the voltmeter indicator is similarly adjusted to unity. The potentiometer ratio is also measured (G_2). Turning the switch S to position 3, a subtraction of the normalised stress and strain vectors is made and the absolute value of the resultant vector, being equal to $2\ sin\ \Omega/2$, is indicated on the voltmeter. By transforming the scale of the voltmeter, however, the corresponding phase angle, $tan\ \delta$, can be read directly on this voltmeter.

If the ratios G_1 and G_2 are recorded, the complex modulus E^* can be calculated as follows: representing the output voltage of the stress and strain transducers by e_1 and e_2, respectively, and the input voltages of these transducers by g_1 and g_2, respectively, the amplitude of stress, σ_o, and strain, ε_o, are given by:

$$\sigma_o = \frac{e_1}{g_1 f_1} \frac{1}{s_o} \tag{8.13}$$

$$\varepsilon_o = \frac{e_2}{g_2 f_2} \frac{1}{L} \tag{8.14}$$

where f_1 and f_2 are the calibration factors of the stress and strain transducers, respectively. From equations (8.7), (8.13) and (8.14), the

following relationship is obtained:

$$E^* = \frac{(f_2\ e_1\ g_2\ L)}{(f_1\ e_2\ g_1\ s_o)} \tag{8.15}$$

As the ratio e_1/e_2 is set equal to the ratio G_1/G_2 whilst measuring *tan* δ, equation (8.15) becomes:

$$E^* = \frac{f_2}{f_1}\frac{g_2}{g_1}\frac{L}{s_o}\frac{G_2}{G_1} \tag{8.16}$$

In equation (8.16), f_2L/f_1s_o is a constant for the specimen and the transducers employed, and if the ratios g_2/g_1 and G_2/G_1 are recorded, E_1 and E_2 can be evaluated from equations (8.5) and (8.6).

For the Rheovibron, Type DDV-II, equation (8.16) can be simplified as follows*:

$$E^* = 2\frac{L}{s_o}\frac{1}{P_o\ N_o - \beta_o} \times 10^8\ \text{N/m}^2 \tag{8.17}$$

where P_o denotes the value of the dynamic force dial, N_o is a proportional constant specified by the manufacturer as a function of the *tan* δ dial range, and β_o is the strain error†. This error arises due to the parasitic oscillation of the specimen grips, stress and strain gauge rods.

8.3.3 Specimen Preparation and Experimental Procedure

The materials selected were the specially prepared samples of

---

* This is according to the instruction manual published by the manufacturer (Rheovibron (1973)).

† The values in equation (8.17) are expressed in metric units.

HIPS which were supplied in compression moulded sheets of 3.2 mm nominal thickness. The type U B of these polymers comprised five different grades of HIPS containing from zero to 5.55% rubber and their general properties are shown in Table 7.1 of Chapter 7. The type U C, having a different PS matrix and different processing additives, contained from zero to 3.33% rubber (Table 7.2 of Chapter 7).

To prepare the specimens for the Rheovibron, the thickness of moulded sheets of HIPS used had to be reduced to less than 1 mm. This was done by using a vertical fly-cutter. The specimens were cut to the required dimensions of 0.90 mm × 3.35 mm × 7 mm and were subsequently cleaned in an ultrasonic bath.

The viscoelastic properties of HIPS samples were obtained at a constant frequency (ψ_o = 11 Hz) as a function of temperature. Sinusoidal tensile strain was applied with an almost constant amplitude to the samples, and the phase angle, δ, and the pertaining moduli parameters were measured by the direct reading method previously described. The in-phase and out-of-phase moduli were then evaluated using the standard theory described in the preceding section.

8.4 RESULTS

The damping parameter, *tan* Ω, was measured as a function of temperature at intervals varying from 1°C to 5°C within the range of -140°C to 135°C. Figures 8.3 and 8.4 show the damping curves for two types of crystal polystyrene (U CO and U BO). At lower temperatures (-150°C to 50°C), both polymers show very little damping and this gradually increases as the testing temperature approaches the glass transition temperature (about 120°C). The glass transition temperature can be defined as the temperature below which the material is predominantly in its *glassy* state and above which it is in a rubbery state. In the glass transition region (50°C to 150°C), the damping factor, *tan* Ω, increases rapidly, reaching a maximum (3.5 to 3.75) at about 120°C to 130°C. In general, the material is brittle with a relatively high modulus on the low temperature side of the damping peak, while in the glass transition region it behaves in a ductile manner with a significantly lower modulus.

The damping curve for CPS (type U CO) shows a very small secondary peak at about -40°C. This may be due to the glass transition of the processing additives (presumably, the mineral oil which is the predominant additive and has a glass transition temperature of about -40°C) contained in this polymer, although the secondary peak was not observed in grade U BO which contained the same amount of mineral oil*.

Figures 8.5 to 8.11 show the damping coefficient as a function of temperature for various grades of specially prepared high impact polystyrene. The large increase in damping above 50°C to 60°C is again due to the onset of the glass transition of the CPS matrix which takes place at slightly

---

* It is interesting to note that there is a small β-peak in this region for CPS (McCrum et al (1967)).

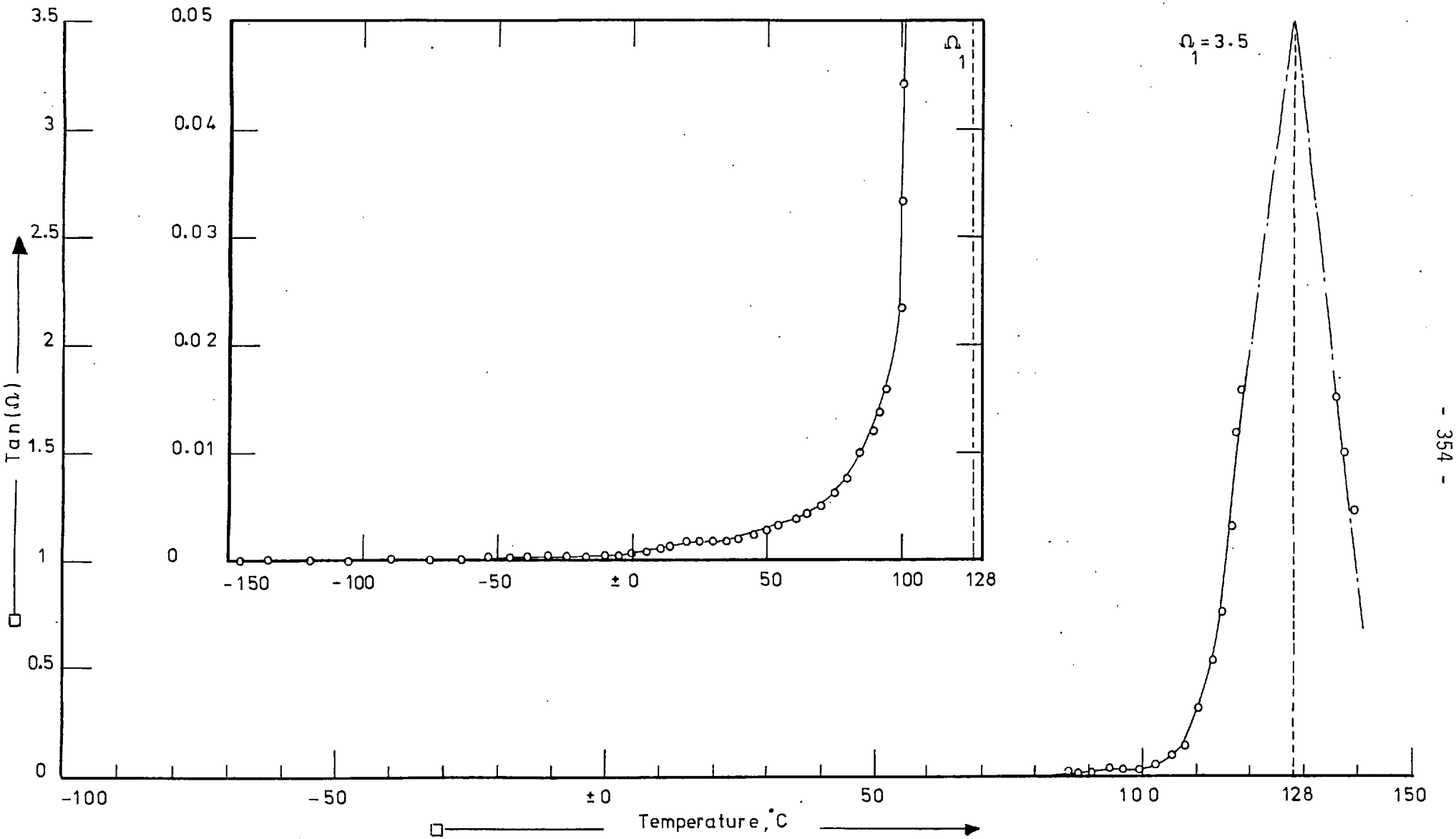


Figure 8.3: Dynamic mechanical loss diagram for CPS (type U BO) showing a peak at about 128°C due to the polystyrene glass transition temperature

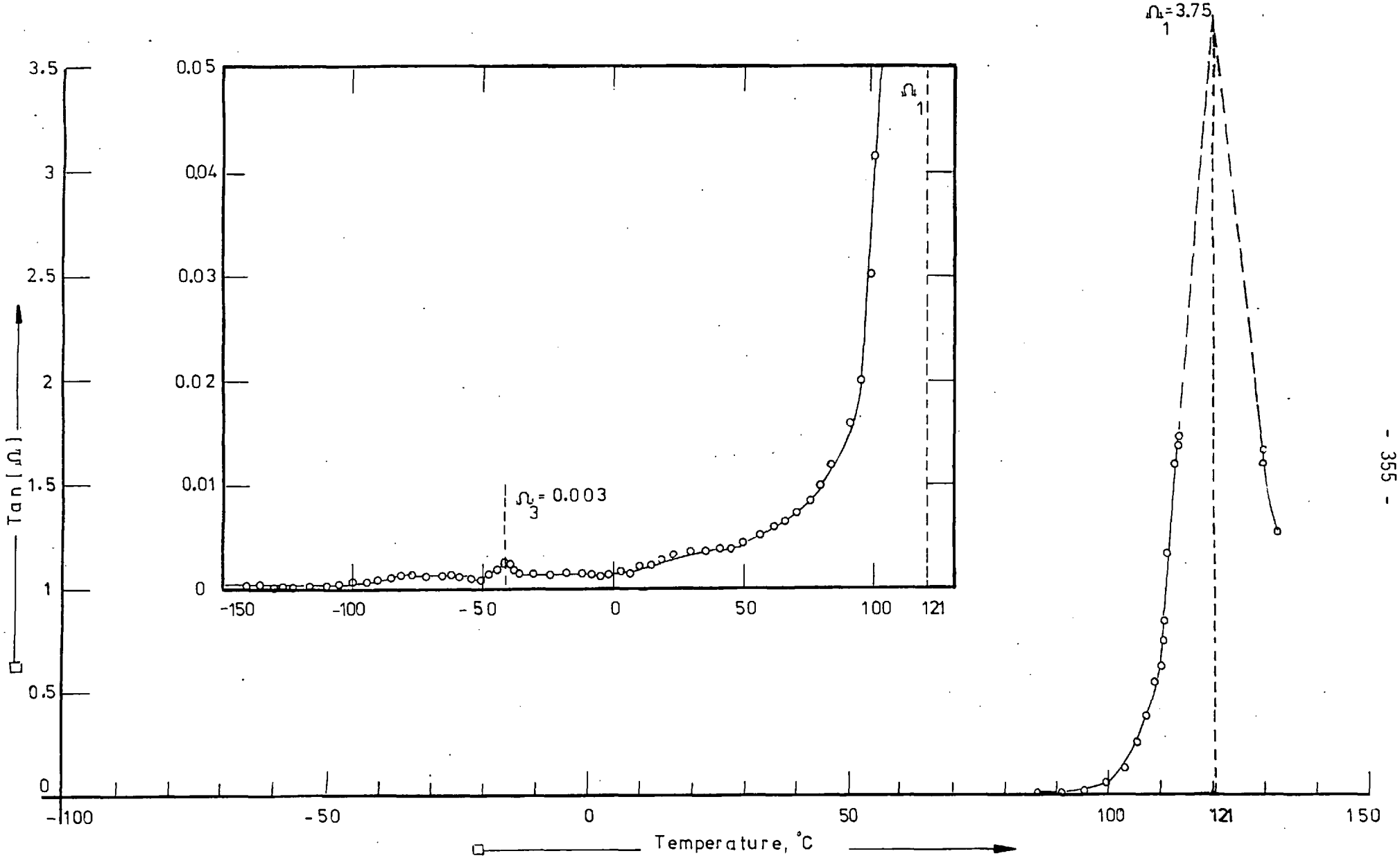


Figure 8.4: Dynamic mechanical loss diagram for CPS (type U CO) showing a small secondary loss peak at -40°C due to the glass transition of certain processing additives. The steep *tan* Ω peak occurring at +121°C Coincides approximately with the glass transition temperature of CPS

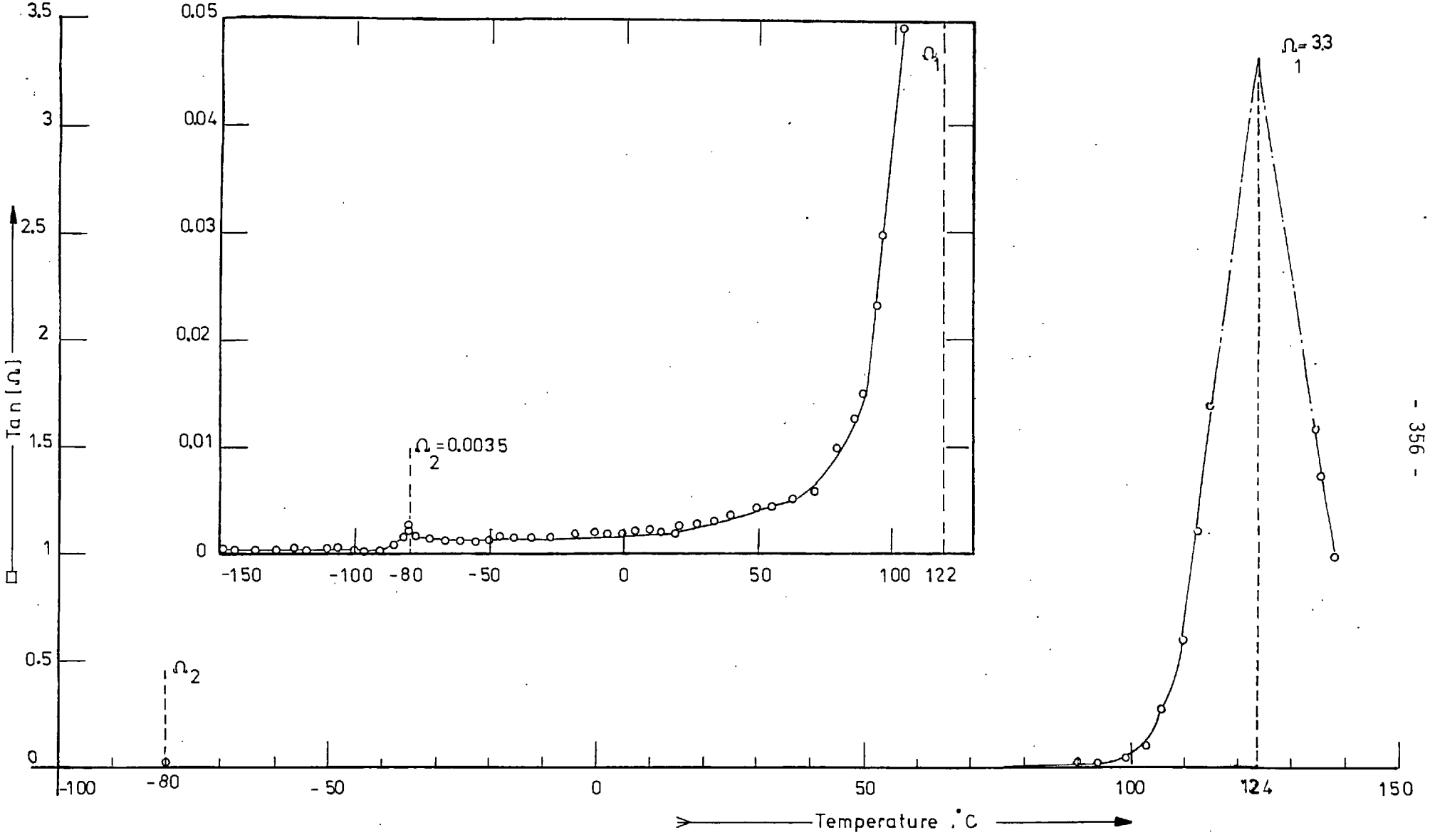


Figure 8.5: Dynamic mechanical loss diagram for U B1.11 showing a secondary loss peak at -80°C due to the presence of rubber particles

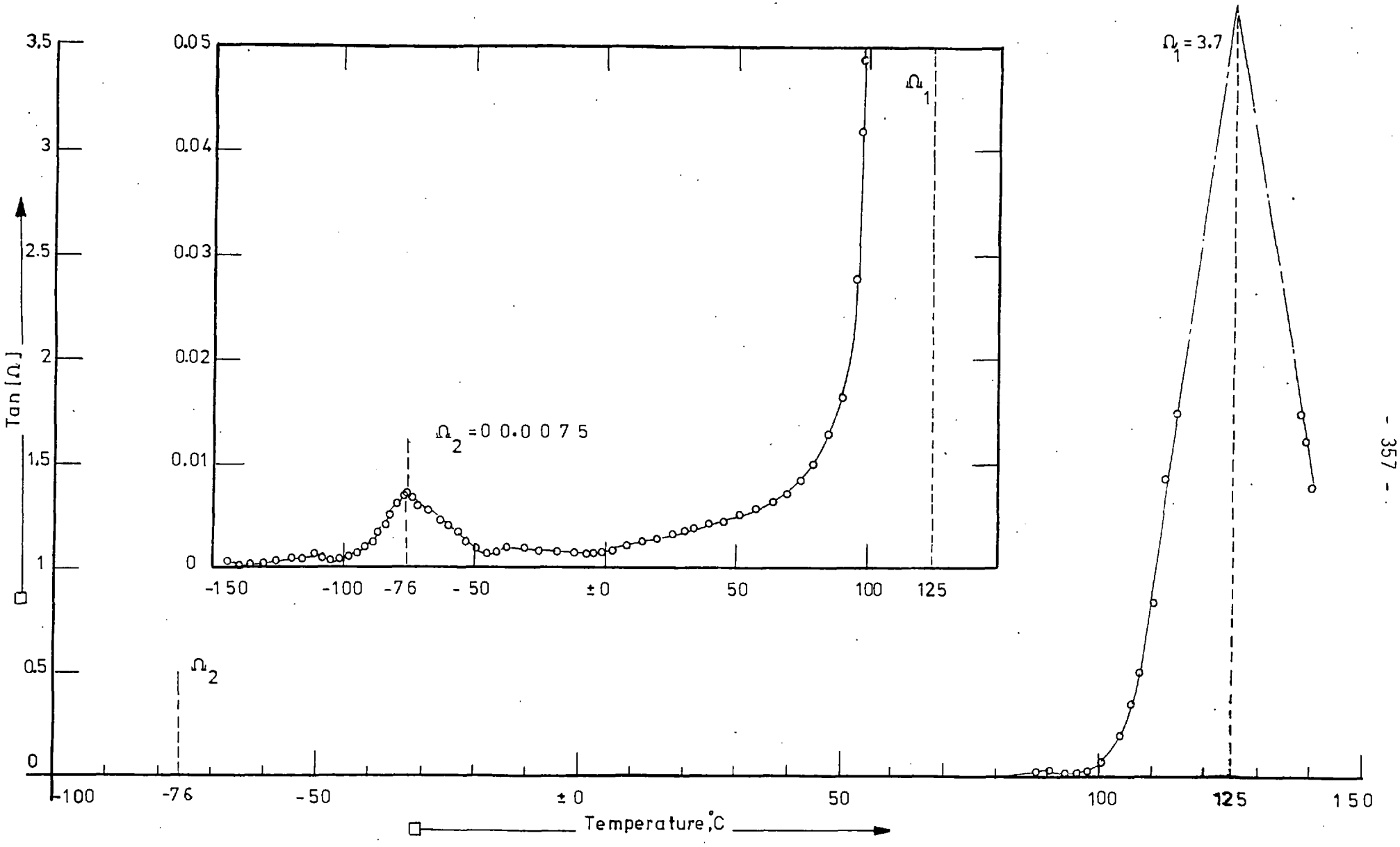


Figure 8.6: Dynamic mechanical loss diagram for U B2.22 showing a secondary loss peak at -76°C due to the presence of rubber particles

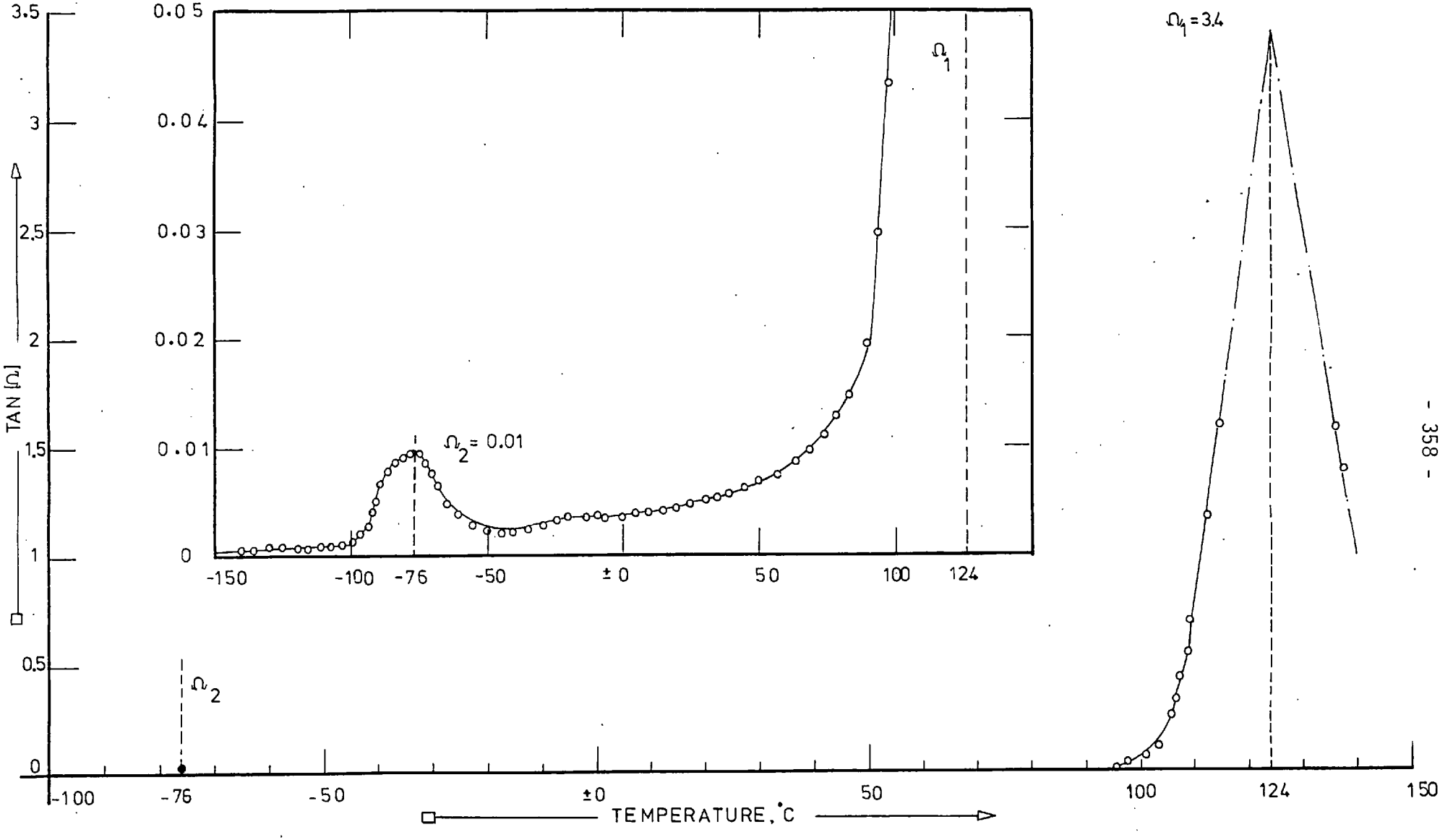


Figure 8.7: Dynamic mechanical loss diagram for U B3.33 showing a secondary loss peak at -76°C due to the presence of rubber particles

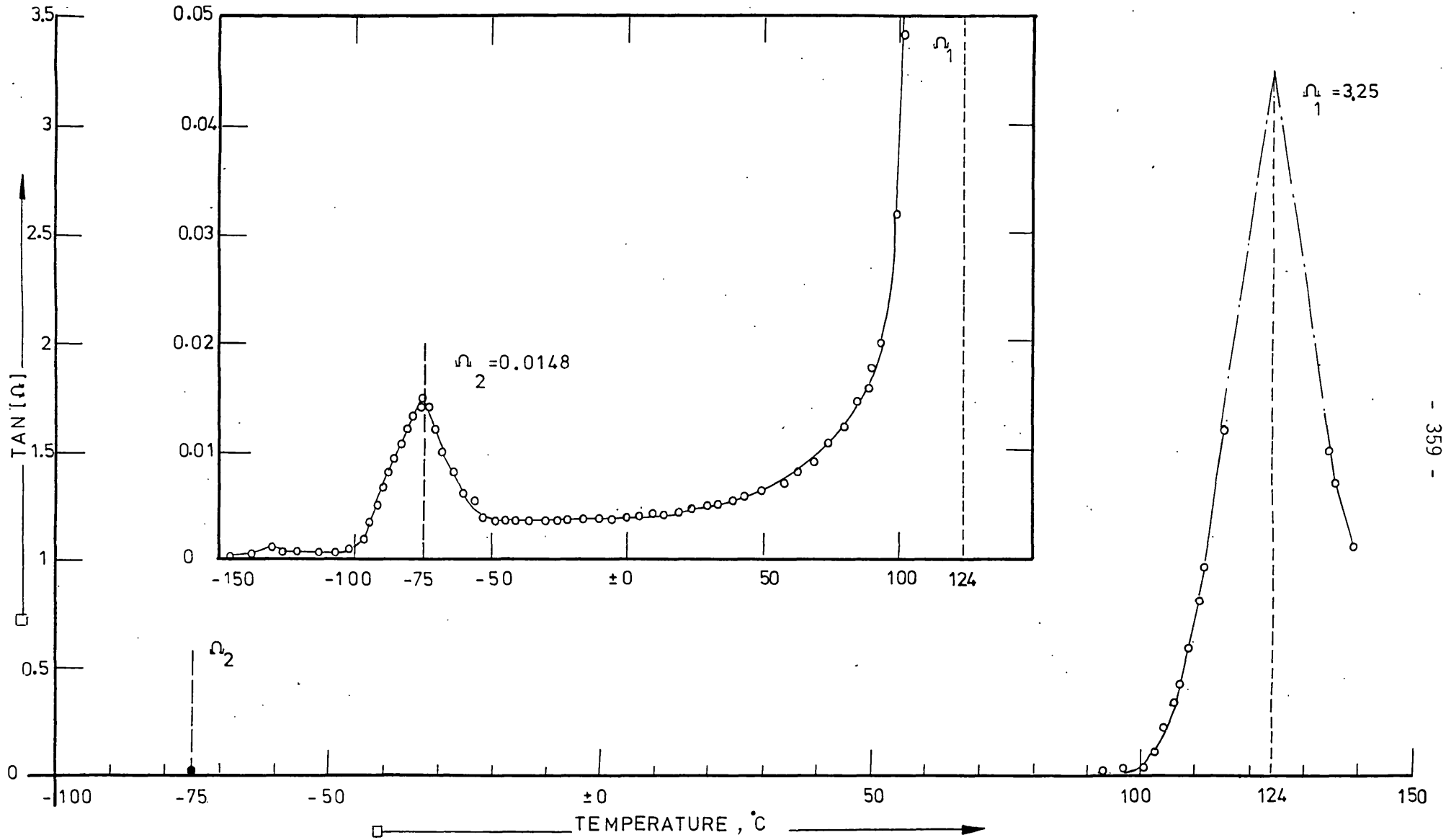


Figure 8.8: Dynamic mechanical loss diagram for U B5.55 showing a secondary loss peak at -75°C due to the presence of rubber particles

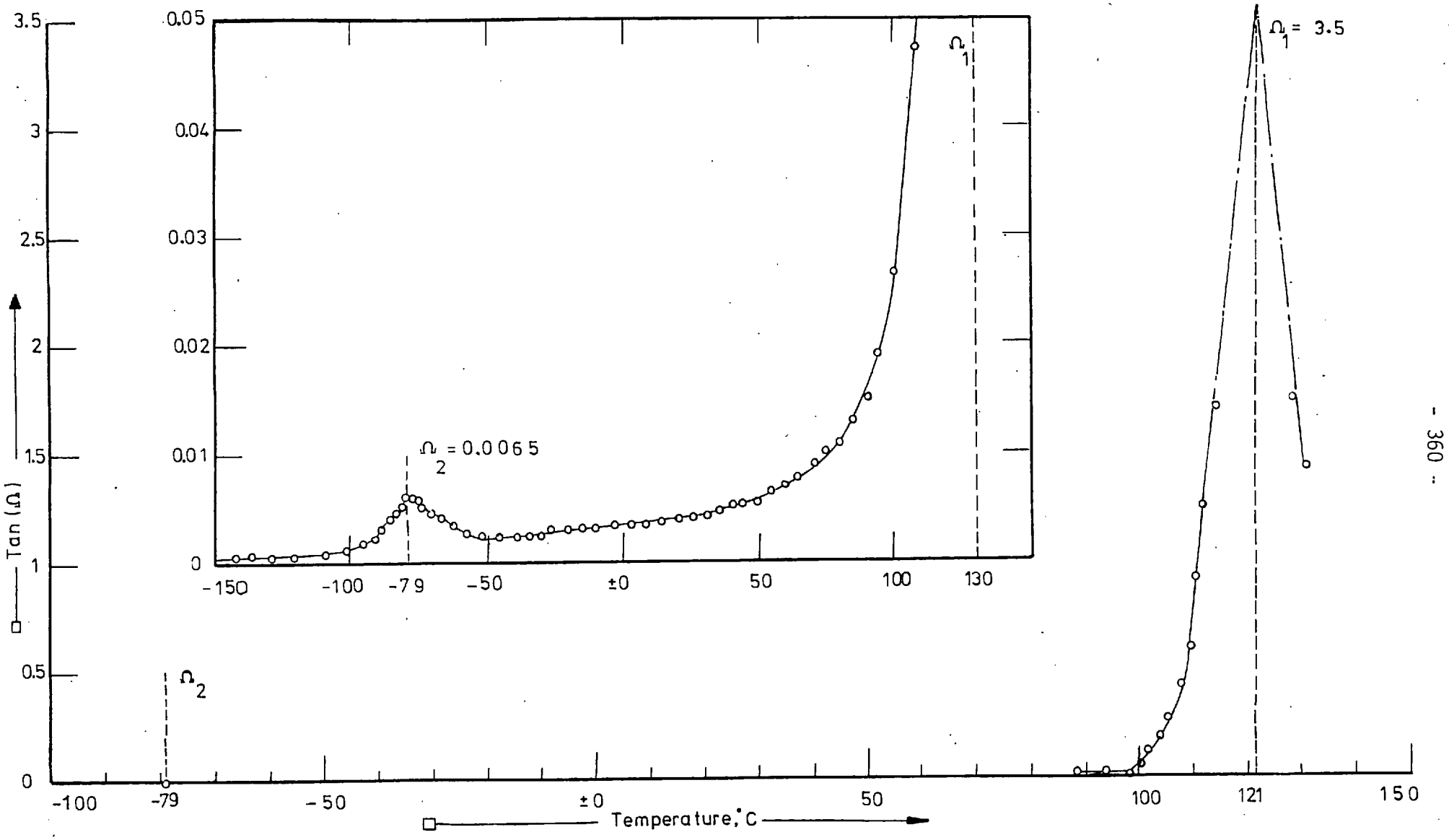


Figure 8.9: Dynamic mechanical loss diagram for U C1.11 showing a secondary loss peak at -79°C due to the presence of rubber particles

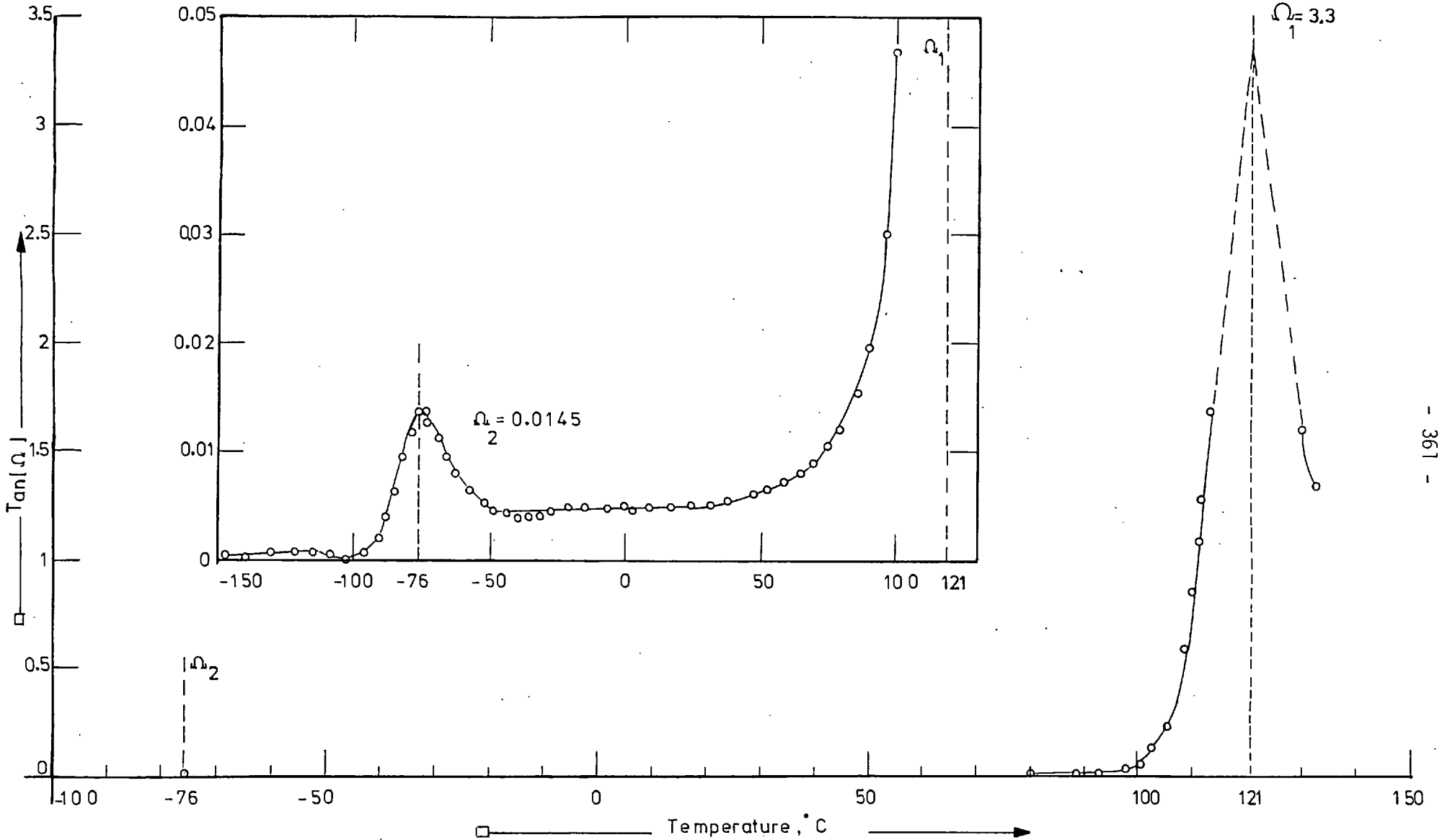


Figure 8.10: Dynamic mechanical loss diagram for U C2.22 showing a secondary loss peak at -76°C due to the presence of rubber particles

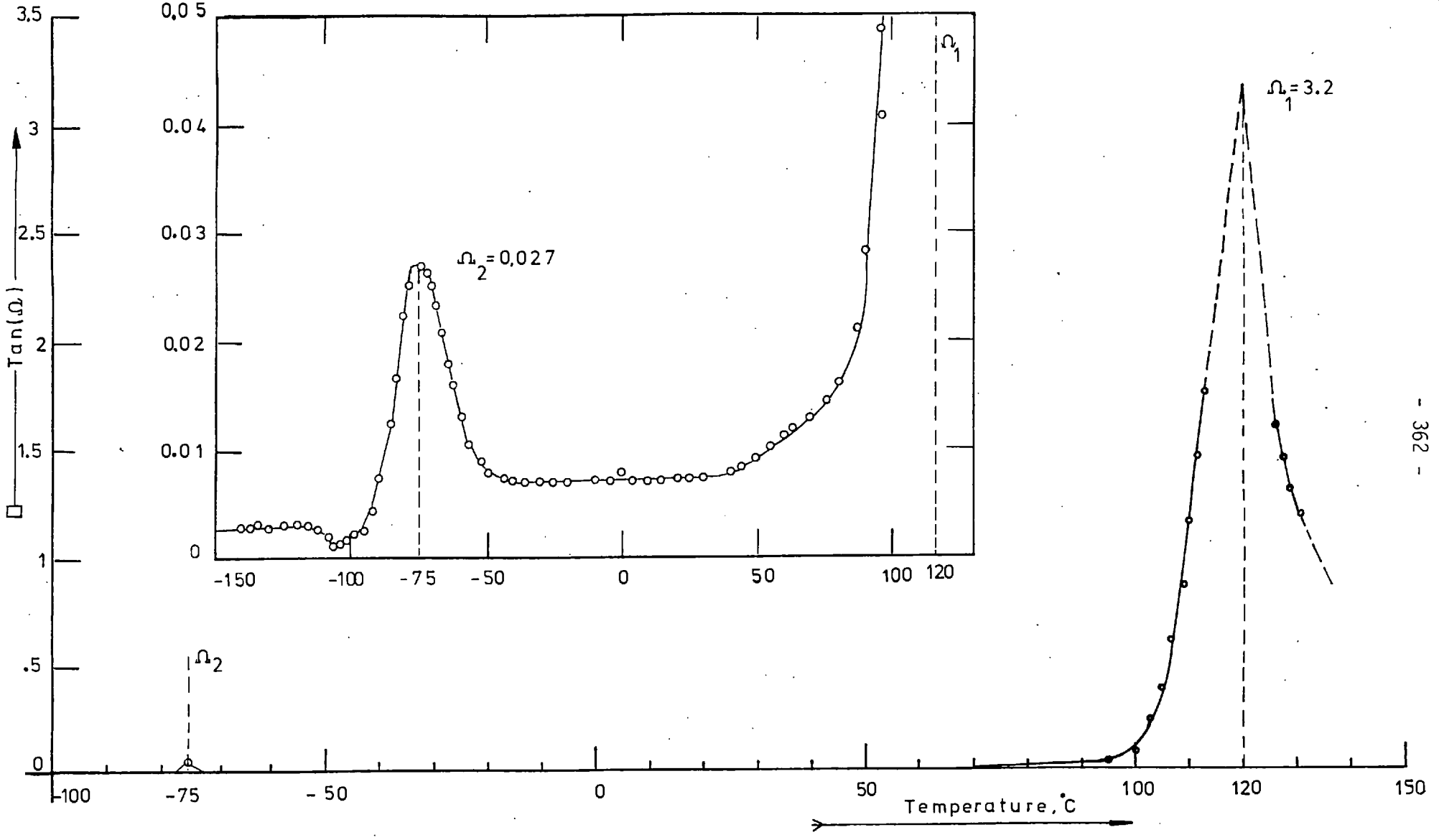


Figure 8.11: Dynamic mechanical loss diagram for U C3.33 showing a secondary loss peak at -75°C due to the presence of rubber particles

lower temperatures than for the unmodified polymer. This is believed to be due to the softening effect of the rubber.

The curves for the HIPS materials show that the effect of adding rubber is to increase the amount of damping parameter, *tan* Ω. This is more noticeable when the results are compared in regions at about -75°C to -80°C where there is a secondary peak in the *tan* Ω curve for HIPS and this corresponds approximately to the glass transition temperature of the rubber additive. It is also apparent that the rubber relaxation commences well below -100°C.

Figure 8.12 demonstrates the magnitude of the secondary loss peak as a function of rubber content for the two types of HIPS (U B and U C). The curves through the experimental points clearly indicate a uniform increase in the secondary damping peak values with increasing rubber content. It is therefore evident that an incremental addition of rubber in HIPS effectively enhances the energy absorption capacity of these polymers.

The complex modulus E^* and the out-of-phase modulus E_1 for various grades of CPS and HIPS samples were evaluated using equation (8.17) and (8.6). The strain error coefficient, β_o, which is due to the parasitic oscillations of the Rheovibron connecting rods was neglected in the present work*. However, this error may become significant when working

---

* The technique for assessing the strain error encountered when evaluating the dynamic elastic moduli from the Rheovibron experimental data is still in an evolutionary stage and a rough estimation of which requires a considerable volume of experimental work and computer programming. This analysis is being conducted on PTFE by Mr J.M. Hodgkinson at the Department of Mechanical Engineering, Imperial College, London.

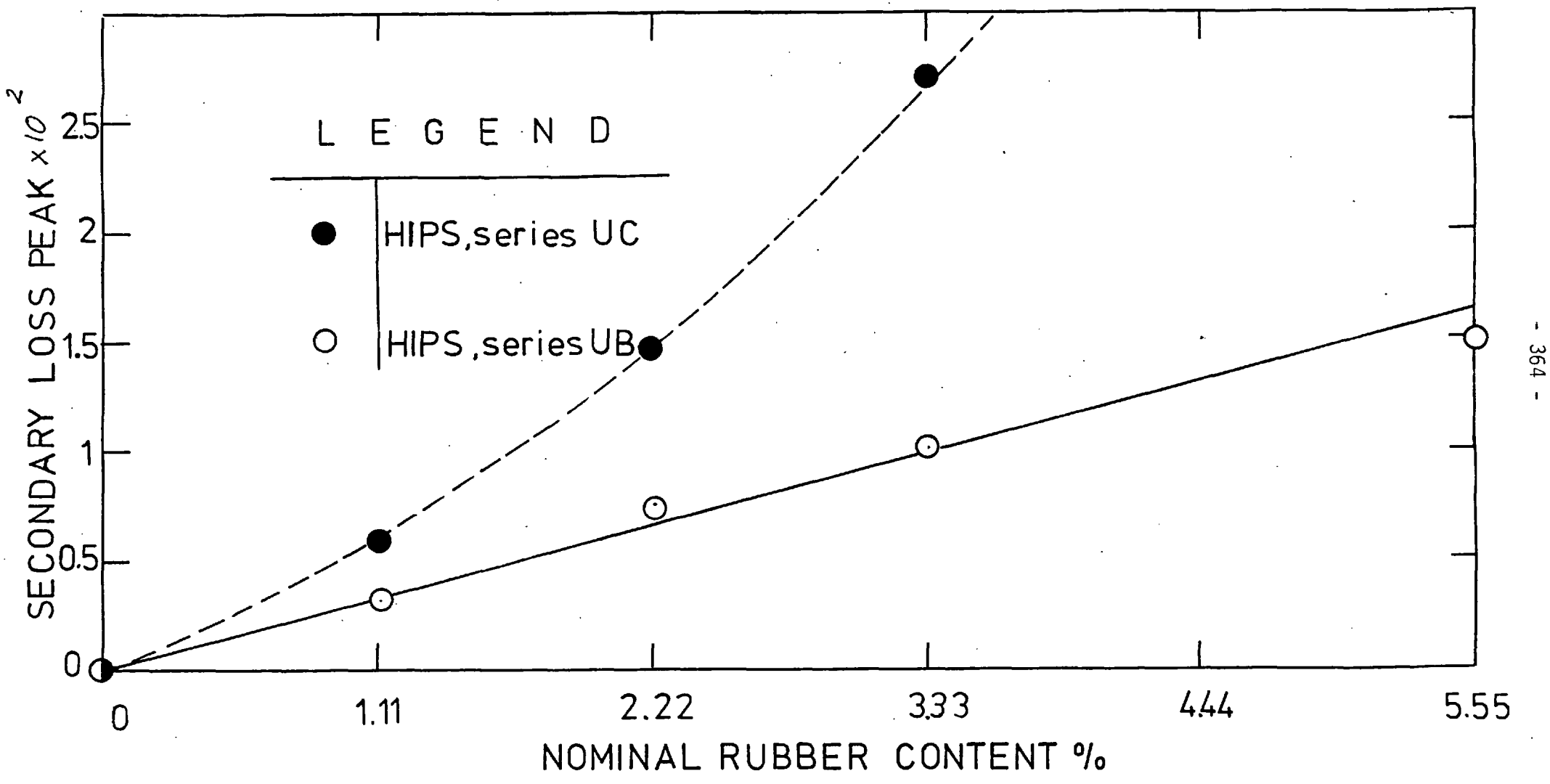


Figure 8.12: The magnitude of the secondary loss peak in *tan* Ω-temperature plots as a function of the nominal rubber fractions in the U B and U C grades of specially prepared HIPS

in the lower temperature region. Figure 8.13 illustrates the variation of the complex and out-of-phase components of the dynamic moduli against temperature for the different polymers tested. The in-phase modulus was also calculated (using equation (8.5)) but these are not shown as they are approximately identical to those of the complex modulus*, except in the vicinity of the PS glass transition temperature, where the E_1 curves show a more precipitious downward trend. The out-of-phase modulus versus temperature plots manifest a similar behaviour to the $tan\ \Omega$ plots over the whole temperature spectrum. In view of the low values obtained for E_2 and $tan\ \Omega$ below the CPS glass transition temperature, it can be seen that HIPS, in general, behaves in a similar manner to linear elastic materials. The complex modulus curves (and also those of the in-phase modulus which are similar as stated above) show a slight but distinct drop near the rubber glass transition temperature ($-80^{o}C$ to $-75^{o}C$) and therefore gradually decrease with increasing temperature. Finally, it can be concluded from the family of E^* curves obtained for various grades of HIPS that the complex modulus (which is equivalent to the elastic modulus in a standard tensile test for $tan\ \Omega << 1$) significantly decrease with increasing rubber content.

---

* This is simply because $\Omega << 1$ for HIPS, except near the glass transition temperature of PS, and therefore $E^* = E_1\ cos\ \Omega \simeq E_1$.

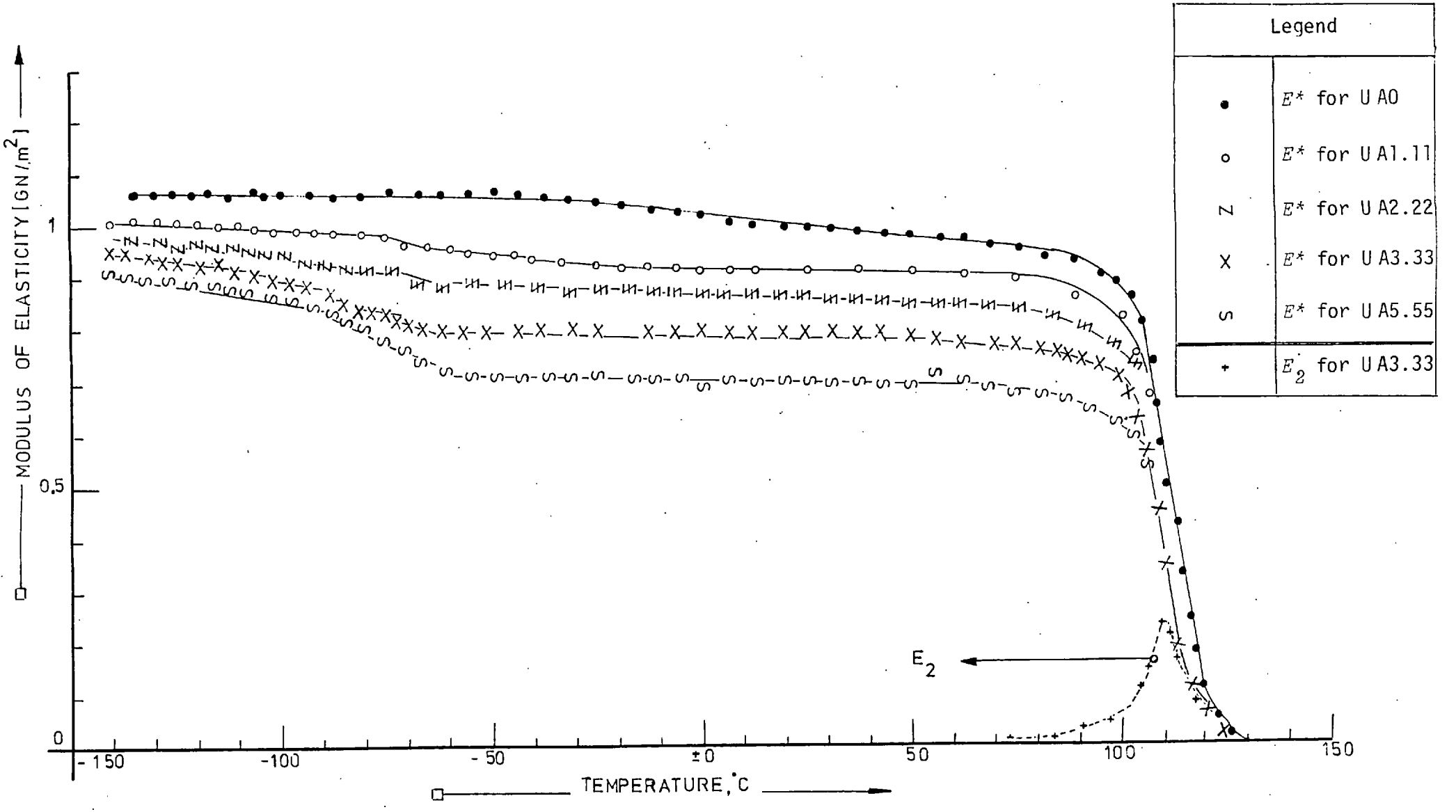


Figure 8.13: Dynamic mechanical moduli for different grades of CPS and HIPS containing from zero to 5.55% rubber content

8.5 DISCUSSION AND CONCLUSIONS

The dynamic mechanical analysis of various HIPS samples has been shown to be informative when the overall bulk properties of these polymers over a wide range of temperatures are required. An increase in the maximum *tan* Ω values at the rubber glass transition generally indicates a reduction in the moduli and yield stress. It may be feasible to conclude that the presence of a secondary peak at low temperatures forecasts an improvement in fracture toughness and the impact behaviour of these materials. This leads to a more searching question, whether the size of this secondary peak coinciding with the onset of the rubber glass transition temperature provides quantitative information with regard to the fracture toughness and impact resistance of rubber-modified polymers? In retrospect, considering the results obtained for the fracture toughness of various grades of HIPS, it seems that this is not so. The fracture toughness was shown to maximise at about 1% to 2% rubber content, while the secondary peak of *tan* Ω increases monotonically with increasing rubber content. On the other hand, the initiation impact resistance was shown to be nearly independent of the rubber content, while the propagation resistance manifested a linear increase with increasing rubber content.

The value obtained for the complex modulus shows the general elastic behaviour of various HIPS over a wide range of temperatures. If we compare the results with those obtained by employing standard tensile tests at room temperature (section 5.4.3 of Chapter 5), it is clear that the dynamic in-phase modulus is considerably smaller than that of the standard static test. This is, firstly, due to the fact that these experiments are different in nature, since different loading systems and strain rates are employed. Secondly, it is believed that the strain error, β_o, which was neglected in the present work, contributes largely to these discrepancies.

It was shown by Hodgkinson (1977) that, if β_o is considered for PTFE, the ratio of the corrected modulus to uncorrected modulus could reach as high as 3 to 10-fold, depending on the temperature employed. However, the Hodgkinson correction method was not attempted in the present work, since considerable difficulty is involved in finding the strain error, β_o. The effect of temperature on the fracture properties (such as yield stress and fracture toughness) of similar types of specially prepared HIPS will be described in the following chapter. The previous experimental analysis on low strain (e.g. modulus of elasticity) and high strain (e.g. yield stress) properties of different grades of HIPS has shown that a linear relationship exists between these parameters, independent of the material rubber content (equation (5.4) of Chapter 5). An analysis of the fracture stresses at various temperatures will therefore provide a common basis as regards predicting the effect of temperature on low strain properties of HIPS.

CHAPTER 9

THE EFFECT OF TEMPERATURE ON THE STRENGTH OF HIPS

9.1 INTRODUCTION

An important factor limiting the application of polymers is the high dependence of their properties on temperature and test speed. In effect, the elastic and fracture characteristics of polymers are not inherently invariable in these materials but are to be treated as relative parameters which may vary with temperature and strain history. The commonly accepted superposition rule, inferred from the experimental analysis of some time-dependent material, provides methods with which to correlate the moduli and yield strengths obtained at different temperatures and strain rates by using some shift factor along the speed of testing scale (Smith (1963,1964); Halpin (1964)). The effect of strain rate on the moduli, yield strengths and fracture toughnesses of some commercial grades of HIPS have already been studied in the foregoing chapters of this thesis (section 5.4 of Chapter 5, and section 6.10 of Chapter 6) and will not be discussed further here.

The dynamic mechanical test, which was described in the preceding chapter, serves to illustrate how the low strain elastic properties (e.g. modulus of elasticity and loss factor) of various types of HIPS are a function of temperature. Although the measurement of the dynamic loss factor, which reflects the molecular activation energy of the material, furnishes a qualitative basis on which to assess the fracture behaviour of HIPS composites, a direct study of the mechanical behaviour of polymers at various temperatures is vital when an accurate and safe design of polymeric structures in different climates and for versatile applications is required.

It is generally conjectured that most polymers which exhibit a ductile failure at relatively high temperatures may break in a more brittle manner as the temperature decreases. This assumption is supported by visual examination of broken materials which show comparatively small craze growth and plastic work hardening at lower temperatures. However, the fact that the material breaks in an apparently brittle manner does not necessarily imply that a smaller fracture toughness is obtained.

In the present work, two fundamental aspects of HIPS fracture behaviour in connection with temperature variations will be studied. The first, which is the fracture strength (ultimate stress at fracture) of an unnotched specimen, serves as an upper limit in the design of HIPS components. The effect of rubber toughening on the fracture strength will subsequently be analysed at different temperatures, using some specially prepared HIPS materials which contain different rubber contents. Secondly, the fracture toughness, a parameter associated with the lowest fracture resistance of a notched material, will be studied at various temperatures employing similar grades of HIPS.

9.2 EXPERIMENTAL PROGRAMME

Uniaxial tensile tests on both unnotched dumbell and single-edge notched specimens were performed on an Instron testing machine in the temperature range from +60°C to -140°C. The dumbell specimens were moulded into the required dimensions specified by ASTM (1972c) - the nominal thickness, width and effective gauge length are 3.2 mm, 12.7 mm and 100 mm, respectively. Rectangular specimens manufactured from moulded sheets of HIPS 300 mm × 120 mm and of 3.2 mm nominal thickness, were used for fracture toughness tests. Single-edge notches were induced by machining with a very sharp fly-cutter, having a cutting radius of 70 mm.

The materials used for all specimens were the specially prepared grades of HIPS (type U B and U C) which contained from zero to 5.55% nominal rubber content. The mechanical properties of these materials have previously been shown in Tables 7.1 and 7.2 of Chapter 7.

9.2.1 Cooling and Heating Apparatus

All experiments were carried out in a temperature cabinet which was fitted to the Instron testing machine. The temperature cabinet contained electrical heating elements to maintain temperatures greater than ambient. For performing low temperature experiments, liquid nitrogen was vaporised and circulated inside the chamber by an electric fan which was installed on the temperature cabinet. Temperature control was achieved by an Eurotherm Control Unit giving the required temperature with an accuracy of ± 1°C over the full range of +60°C to -140°C. The chamber contained a double-glazed window through which the initiation and propagation of cracks could be observed by utilising a travelling monocular microscope and recorded on the Instron chart using an event recorder. Figure 9.1 shows a photograph of the experimental set-up and the details of the heating and



Figure 9.1: Experimental arrangement for temperature controlled tests on an Instron testing machine

cooling system are further illustrated in Figure 9.2.

As shown, liquid nitrogen is first sucked through the capillary centre pipe (14) from the nitrogen dewar with the help of a high vacuum vaned pump (2). The blades of this pump were originally made from carbon graphite but, however, they were found to be soluble in liquid nitrogen and were, therefore, replaced by PTFE blades. The liquid nitrogen drawn from the dewar vaporised in a helical brass tube (6) and re-entered the dewar as a pressurising agent. The pressure inside the dewar was maintained at about 1 to 1.5 atm by a variable reset pressure switch (11) in the system. The pressure generated in the nitrogen dewar drove the liquid nitrogen through a peripheral outer tube (15) to the temperature cabinet (21) via a solenoid valve (35) whichwas controlled by the Eurotherm output (29). The temperature inside the chamber was measured by a Chromel/Alumel (23) thermocouple and the output signals were conducted to the Eurotherm servo-mechanism (34).

The amount of heating or cooling required could then be supplied in the temperature cabinet in order to maintain the temperature at a specific level. The temperature of the cabinet was further checked by a Copper/Constantan thermocouple (27) connected to a digital display, Comark (16).

In order to reduce the heat transfer to or from the cabinet, additional low density polystyrene insulating material was used to cover the internal wall of the chamber.

9.2.2 Test Procedure

The dumbell and single-edge notched specimens were all normalised at specific ambient conditions in the temperature cabinet for at least one hour prior to performance of the test. The dumbell specimens

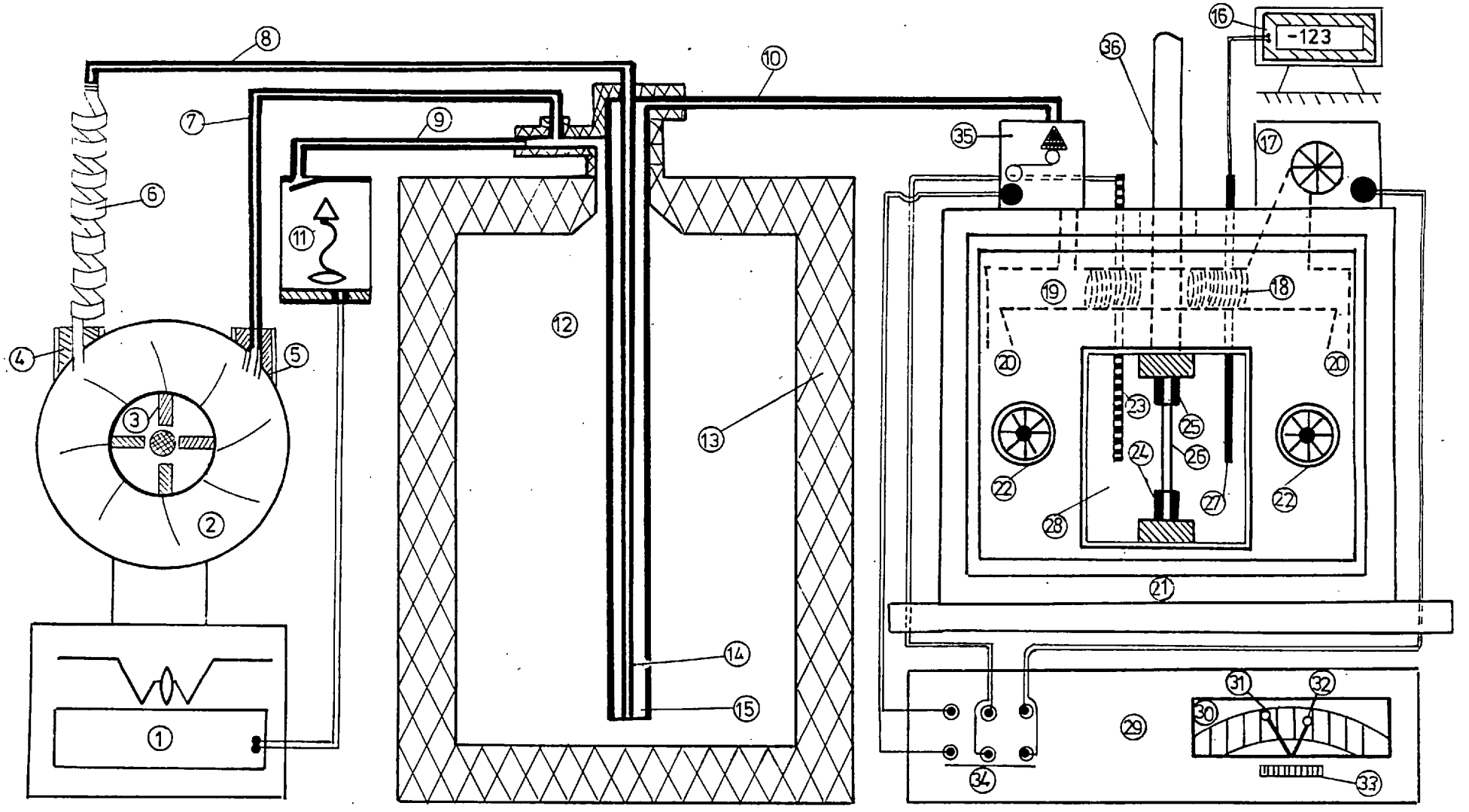


Figure 9.2: Heating and cooling systems

1. Electric motor
2. High vacuum vaned pump
3. PTFE blades of the pump
4. Pump inlet
5. Pump outlet
6. Vaporising coil
7. Pressurised dewar duct
8. Suction dewar duct
9. Pressure switch duct
10. Dewar feeder to temperature box duct
11. Variable reset pressure switch
12. Dewar
13. Dewar insulation
14. Capillary centre tube
15. Peripheral tube
16. Digital temperature display (Comark)
17. Air fan
18. Electric heating elements
19. Air/nitrogen duct
20. Air/nitrogen diffusion
21. Temperature box
22. Temperature box cap doors
23. Chromel/Alumel thermocouples
24. Lower grips
25. Upper grips
26. Specimen
27. Copper/Constantan thermocouples
28. Temperature box window
29. Eurotherm differential amplifier
30. Temperature scale window
31. Temperature indicator
32. Fixed temperature pointer
33. Temperature controlling knob
34. Eurotherm connections
35. Solenoid valve
36. Instron shaft

were then clamped in a pair of sliding wedge grips, one of which was fixed and the other moving at a constant cross-head speed. The rectangular notched specimens were clamped between two steel plattens by six (or eight) screws, $\frac{1}{4}$" in diameter. This method was found preferable to using the sliding wedge grips because slippage at high loadings was prevented. Nevertheless, some difficulty was experienced during tests at very low temperature where the specimens suffered some stress concentration between the clamps and thus fractured in that region. Stress concentration was mainly due to the discontinuity in the clamping pressure. This was further aggravated by the formation of ice which enhanced the localised pressure between the clamps, leading to the initiation of multiple cracks in the stress concentrated regions. The problem was partially solved by wrapping the ends of the specimens in emery paper which mitigated the severity of the localised clamping pressure. An efficient solution to the problem was not, however, found and whenever a specimen broke in the clamps, the test had to be repeated.

Dumbbell tensile specimens and rectangular single-edge notched specimens were all tested at constant cross-head speeds (0.1 cm/min for unnotched and 0.01 cm/min for notched specimens) and the ultimate strengths and fracture toughnesses were evaluated for the different grades of HIPS at different temperatures. A low cross-head speed was selected for the fracture toughness measurement to allow sufficient time for craze formation and crack initiation to be carefully observed and recorded.

9.3 RESULTS AND DISCUSSION*

9.3.1 Effect of Temperature on the Ultimate Stress of HIPS

Typical force-deflection records for brittle materials (such as grades U BO and U CO of CPS with zero rubber contents) and ductile materials (such as grade U B5.55 of HIPS with 5.55% rubber content) are shown in Figure 9.3. For both types of fracture, the ultimate fracture stress is defined by the ratio of the maximum force to the original cross-sectional area. The yield point was not always as distinct as illustrated for grade U B5.55 in Figure 9.3(b). A common phenomenon was, however, the premature fracture of the more brittle materials below the yield point which was due to the presence of intrinsic cracks†. It is therefore essential to appreciate that, whereas in the case of metals one carefully conducted test provides reasonable meaningful values of tensile data, plastics on the other hand exhibit considerable scatter in the results. Bearing this in mind, it was found necessary to perform two or more tests under nominally identical conditions and to take the average of the results

---

* The testing of dumbbell specimens was performed with the assistance of Mr G. Campaner as part of his third year mini-project at the Mechanical Engineering Department, Imperial College, London.

† Below its glass transition, CPS is by nature a brittle material. The fracture strength of these polymers is therefore to be viewed as the brittle strength rather than the yield strength. The hypothetical yield stress of these materials, compared to that obtained for their rubber-modified derivatives, is somewhat greater than the measured fracture stress (Andrews (1968)). A similar problem may arise for HIPS materials at low temperatures, whereby the fracture takes place below yielding.

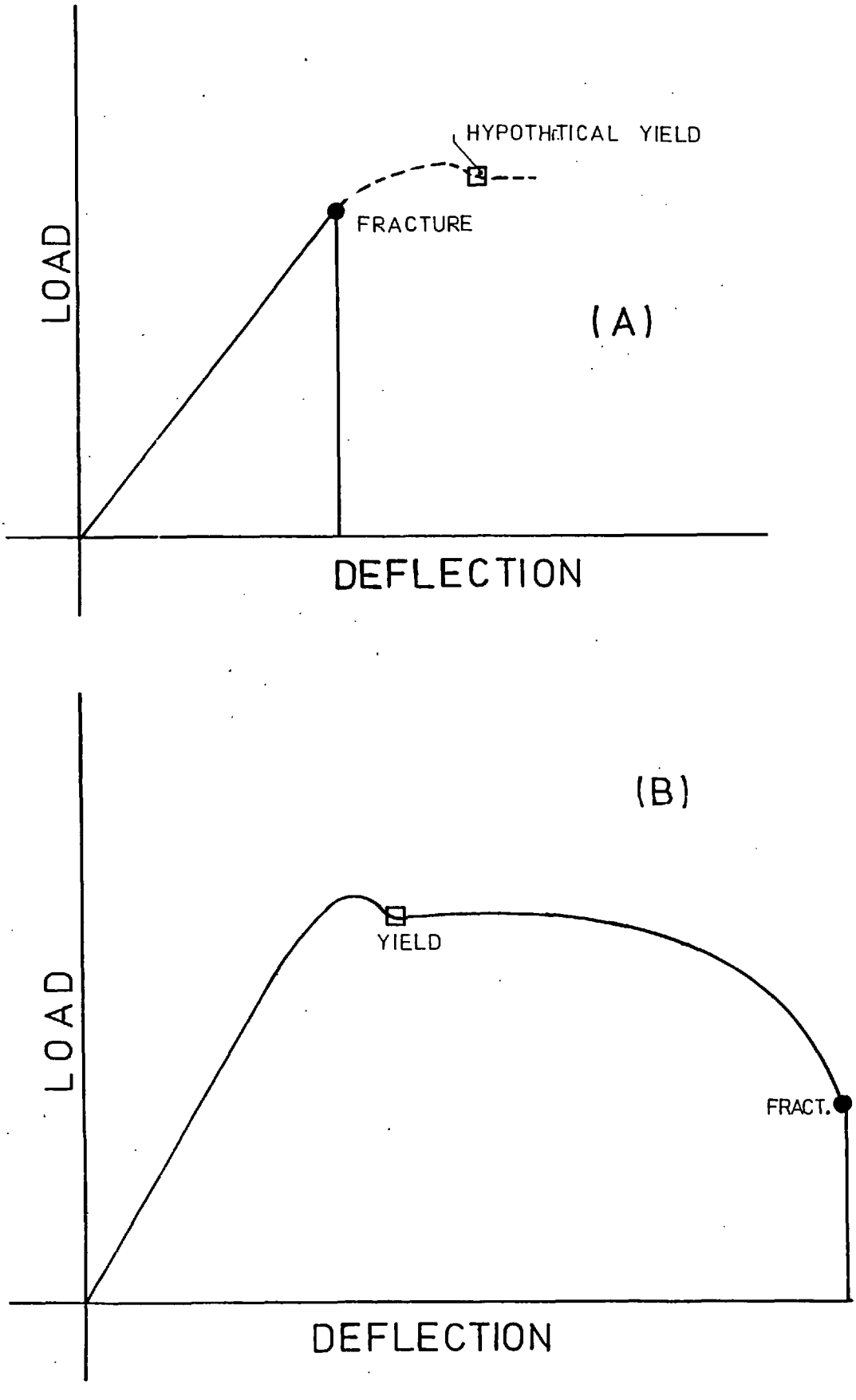


Figure 9.3: Typical force-deflection curves for brittle (A) and ductile (B) failure in a tensile test

in the case of ductile failure and the maximum value obtained in the case of brittle failure, in order to acquire more reliable information. The error arising from the use of the original cross-sectional area as a basis for calculating the stress did not seem to be appreciable, since the formation of necking was not observed before the maximum load was recorded.

The variation of the ultimate stress as a function of temperature (from $+60^{o}C$ to $-120^{o}C$) has been plotted and is shown in Figures 9.4 and 9.5 for types U B and U C of all the grades of HIPS tested, respectively. It can be seen that the experimental results generate a set of smooth curves associated with the rubber content of the materials examined. These figures clearly confirm that the temperature has a strong influence on the yielding characteristics of HIPS. As the temperature is lowered, the ultimate stress increases from relatively low values ($17\ MN/m^2$ at $+60^{o}C$ for material U B with 5.55% rubber content) to sensibly higher values ($75\ MN/m^2$ at $-120^{o}C$ for the same material). At about $-20^{o}C$ to $-40^{o}C$, the experimental curves for all materials show a point of inflection which coincides with the β-transition of the crystal polystyrene. The β-transition which was shown to be unrelated to the variations of the loss factor and low strain properties of HIPS with temperature is ostensibly associated with the fracture behaviour of these materials.

The reason for the strong temperature dependence of the fracture properties is believed to be the molecular reorientation and structural change which gives rise to a relative rigidity of the polymer. This aspect of the fracture mechanism will be further expounded when analysing the results of the fracture toughness experiments.

The effect of rubber content on the ultimate strength of various types of HIPS is demonstrated in Figures 9.6 and 9.7, where the stress is plotted versus the volume fraction of the rubber at various temperatures.

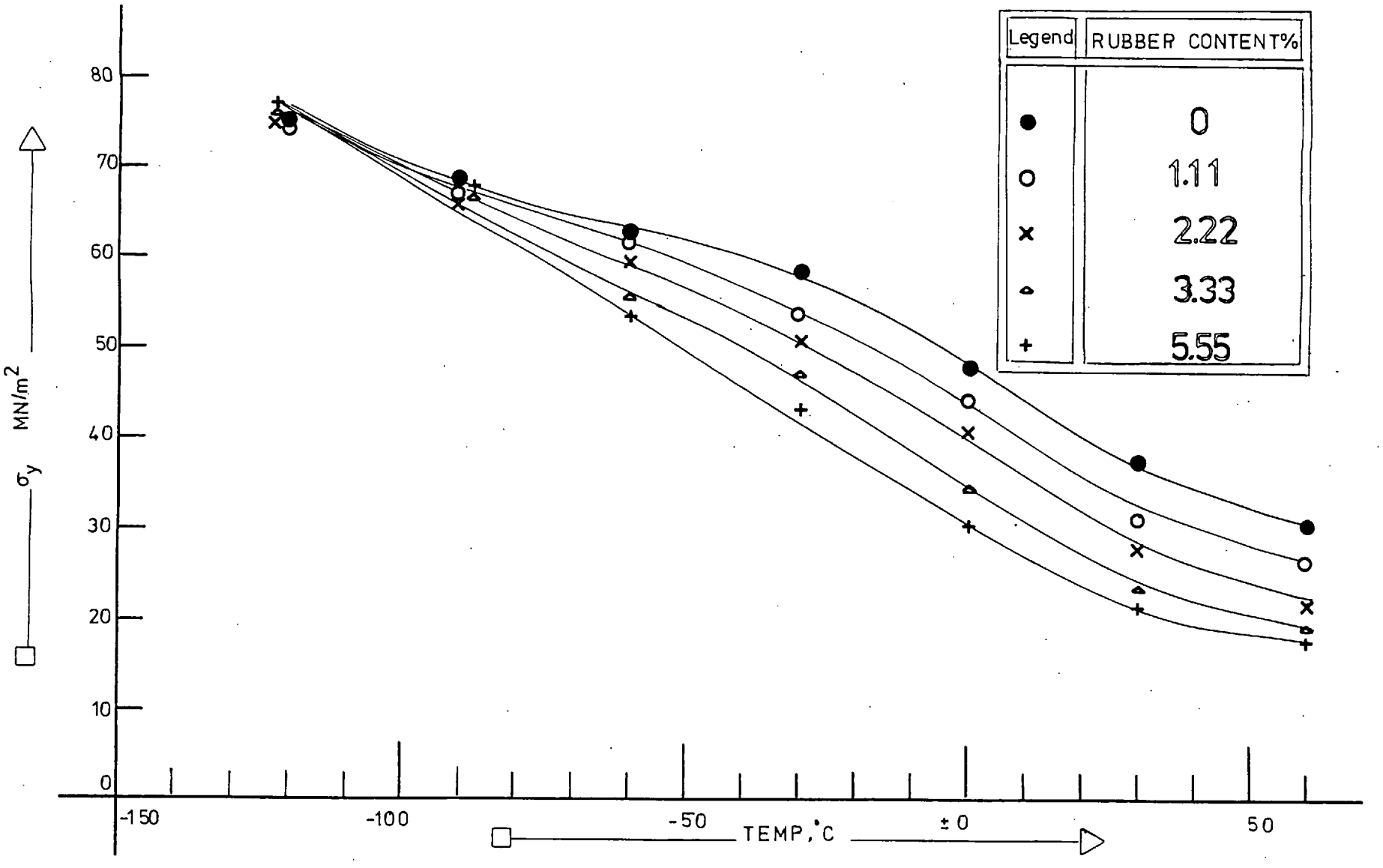


Figure 9.4: Ultimate fracture stress versus temperature for various grades of HIPS (type U B)

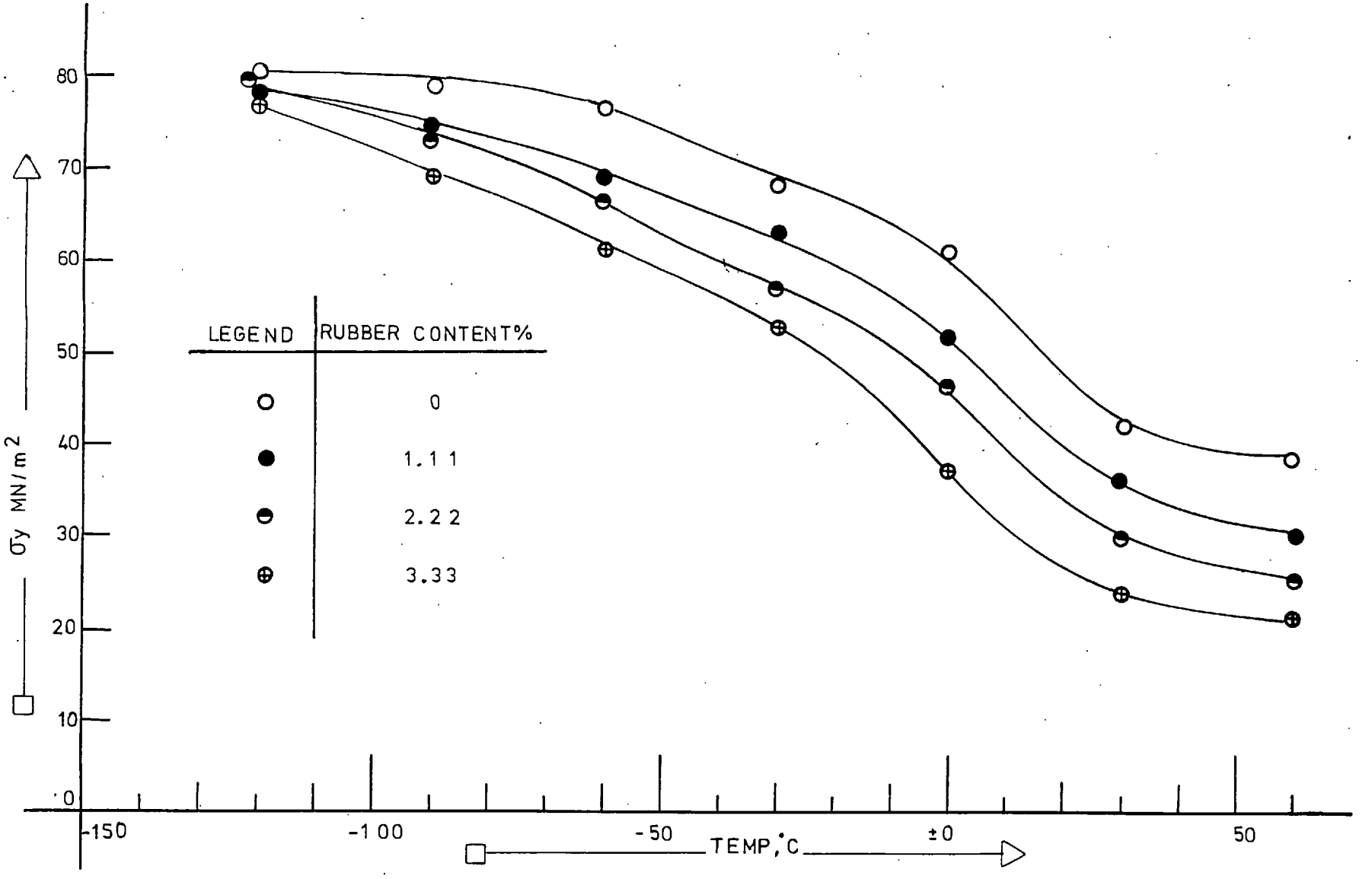


Figure 9.5: Ultimate fracture stress versus temperature for various grades of HIPS (type U C)

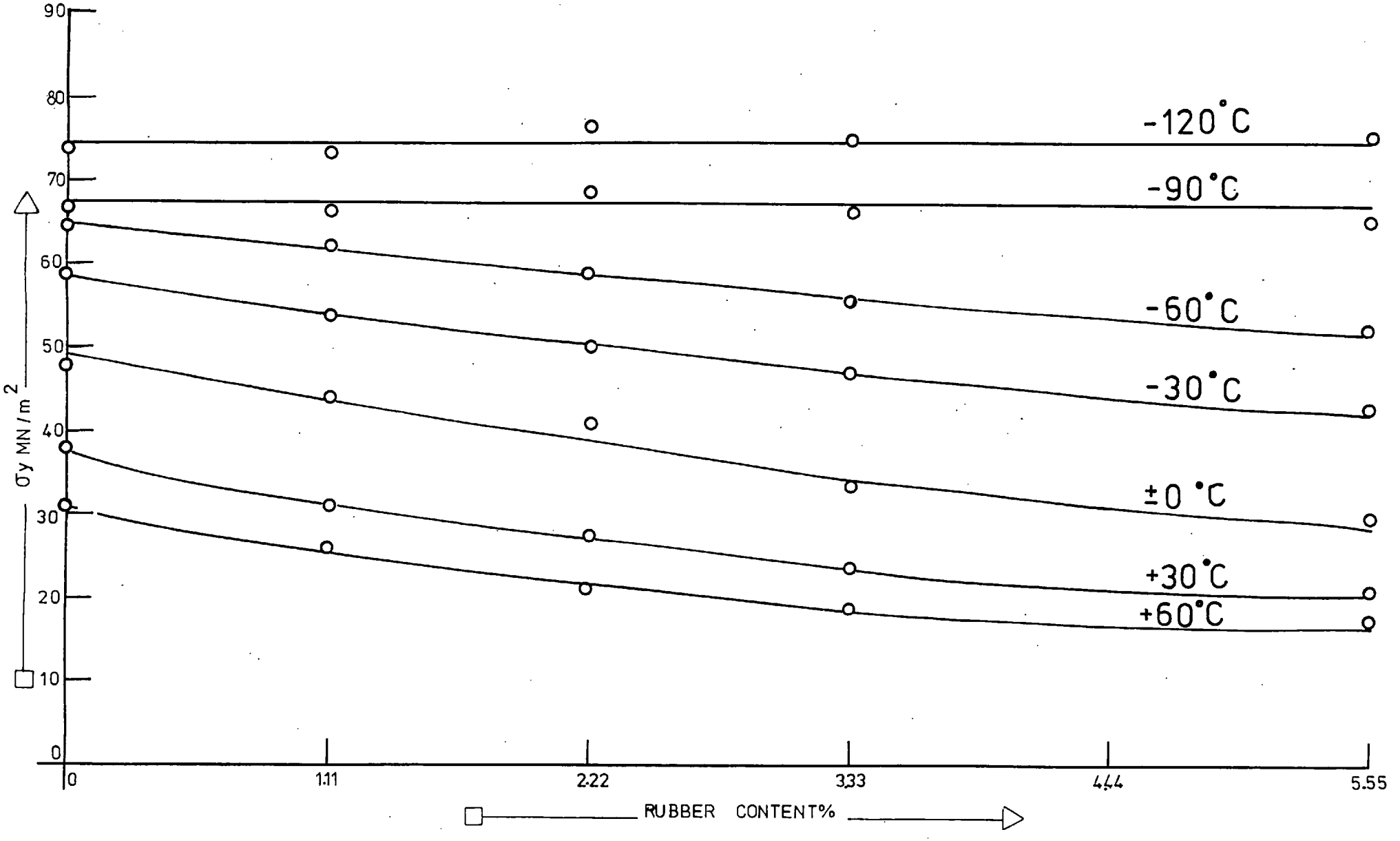


Figure 9.6: The effect of rubber on the ultimate fracture stress of HIPS (type U B) at various temperature levels

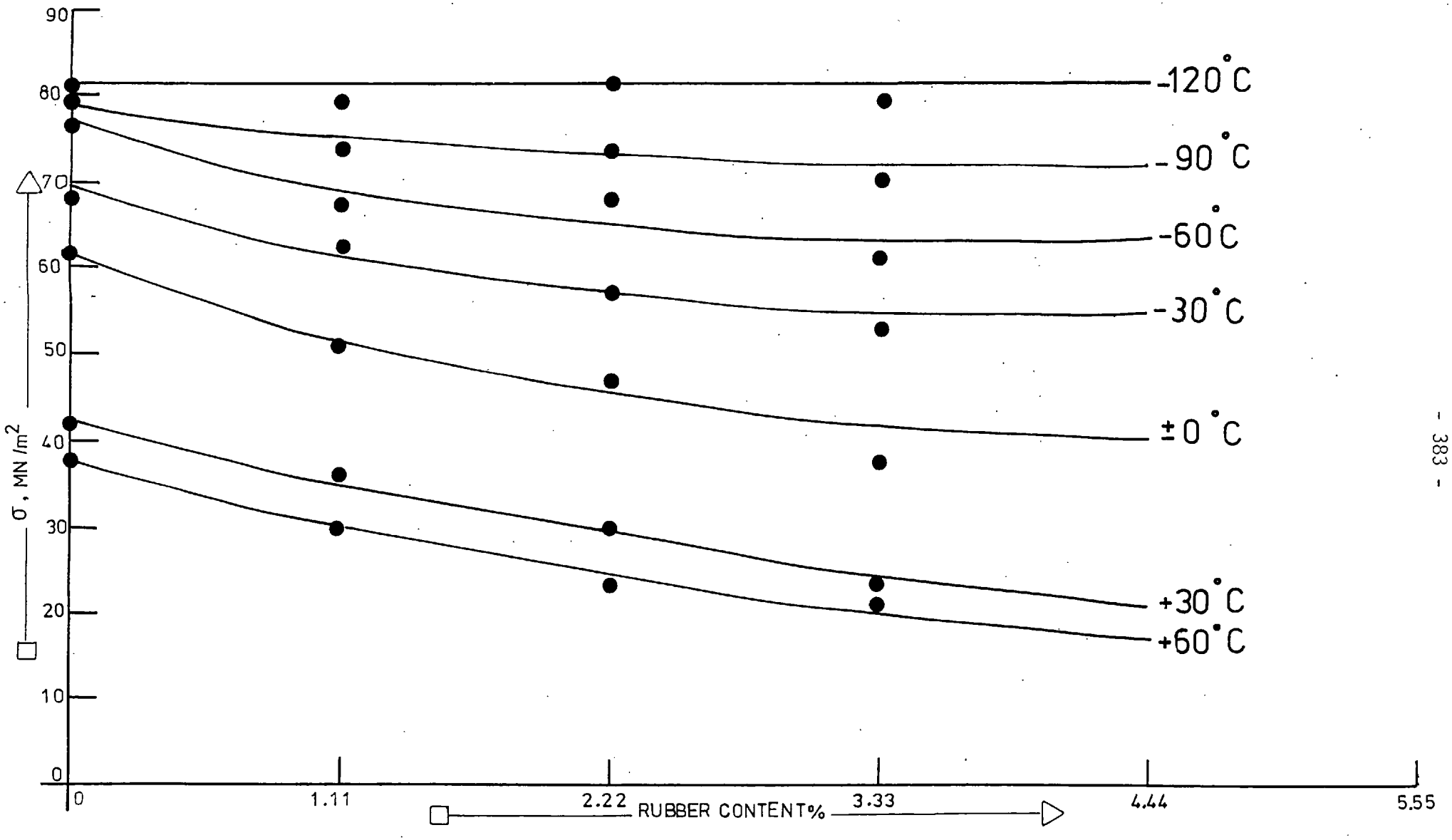


Figure 9.7: The effect of rubber on the ultimate fracture stress of HIPS (type U C) at various temperature levels

Figure 9.8 shows the photographs of typical fractures for various types of HIPS. Generally, both full yielding and craze formation (depending on the temperature and the amount of rubber used in the material) can usually be detected on the specimens. Full yielding and extensive craze formation in medium to high impact PS produces an opaque area in the strained region. Typical partial crazing in crystal PS at all temperatures and various types of HIPS at very low temperatures (i.e. $T < 120^{o}C$) is manifested by the formation of a large sequence of narrow craze bands which appear as internal cracks. As a general rule, the formation of crazes and plastic zones in HIPS materials becomes less conspicuous and is confined to thinner layers of highly strained zones as the temperature decreases.

9.3.2 Effect of Temperature on the Fracture Toughness of CPS

Values of fracture toughness were obtained as a function of temperature for two types of unmodified crystal polystyrene (grades U BO and U CO), using single-edge notched specimens. The temperature range considered was from $+60^{o}C$ to below $-140^{o}C$. At every temperature interval (varying from $20^{o}C$ to $40^{o}C$), a number of specimens (normally between five to eight) which contained initial cracks of different lengths, were tested and thereby consistent fracture toughness values were obtained for both types of CPS. All specimens exhibited brittle fracture independent of the test temperature. Consequently, only a very small craze growth (< 0.05 mm) was detected which did not cause any subsequent stable crack growth, even at the highest test temperature.

The fracture toughness experimental results are shown in Figures 9.9 and 9.10 for the two types of CPS, U-BO and U-CO, respectively. The behaviour illustrated by these curves shows that the toughness increases with decreasing temperature within the temperature range $+60^{o}C$ *

continued on page 383

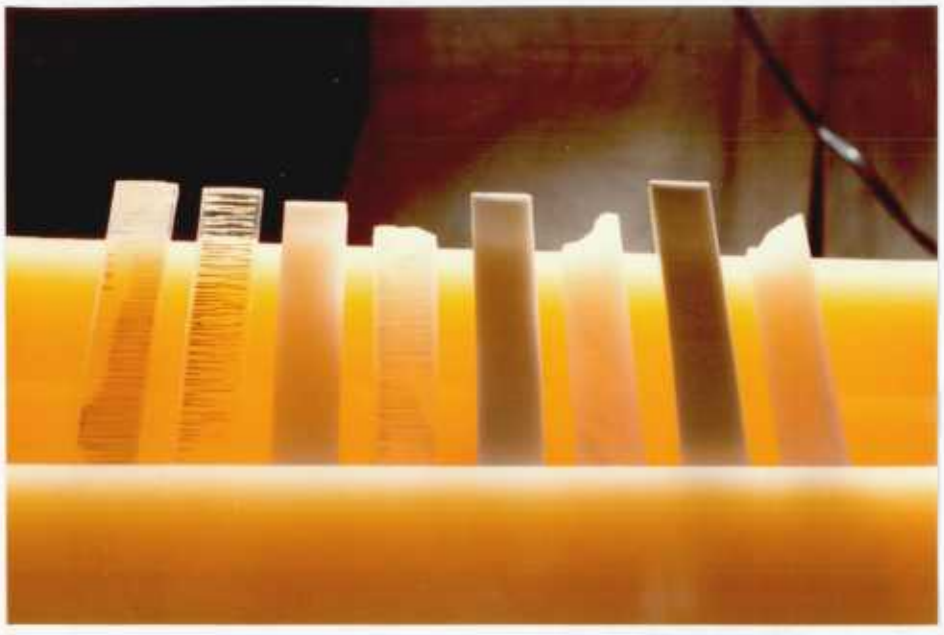


Figure 9.8: Types of fracture under uniform tensile loads. From the left:

1 & 2 : CPS (0% rubber content) tested at +60°C and -120°C. respectively. Note the typical partial craze formation in a brittle fracture

3 & 4 : $HIPS_0$ (1.11% rubber content) tested at +60°C and -120°C, respectively. Note the extensive craze formation at the higher temperature and the partial crazing typical of a brittle material at the lower temperature

5 & 6 : $HIPS_0$ (2.22% rubber content) tested at +60°C and -120°C, respectively

7 & 8 : $HIPS_0$ (3.33% rubber content) tested at +60°C and -120°C, respectively

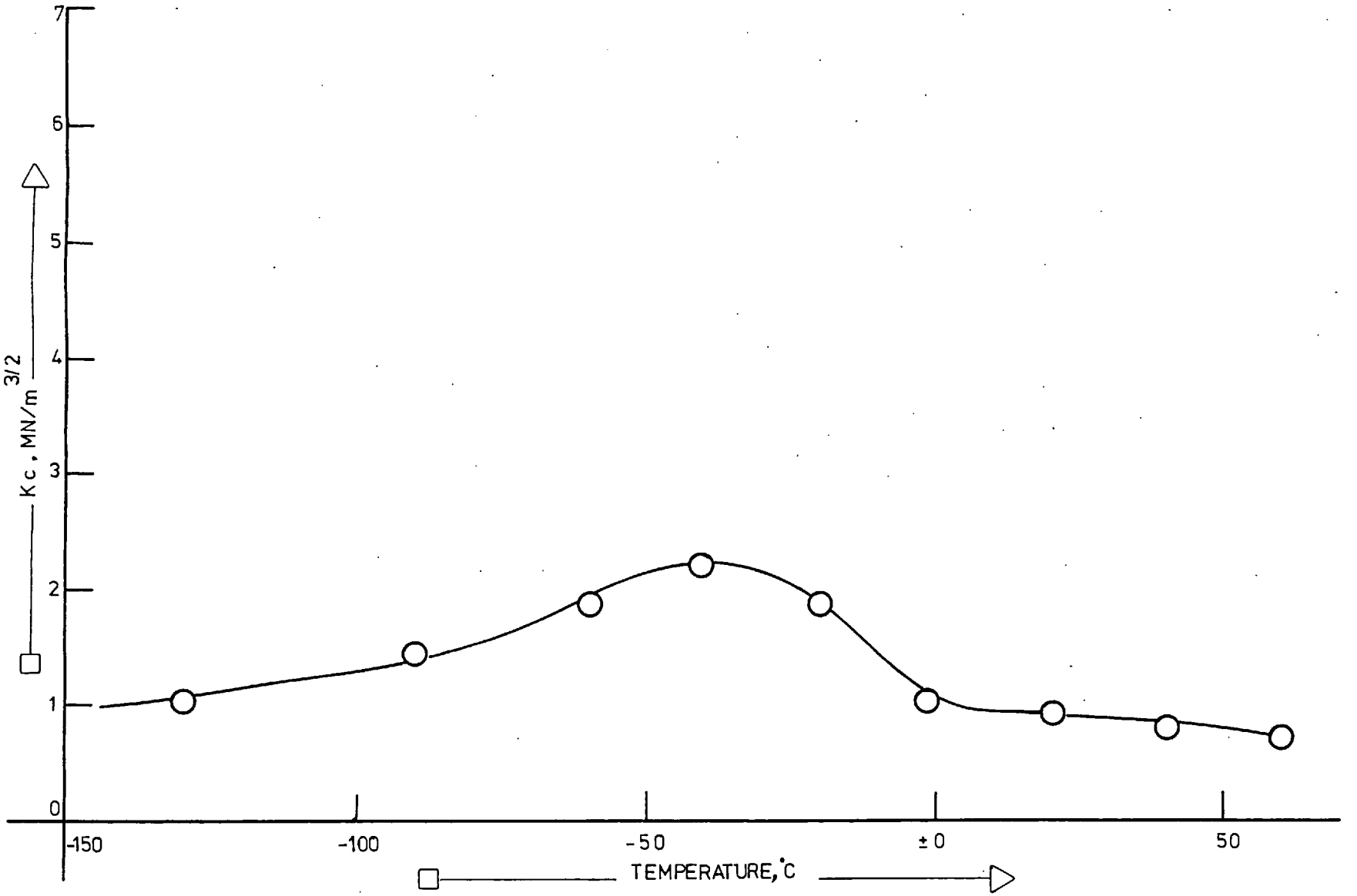


Figure 9.9: The effect of temperature on the fracture toughness of CPS (grade U 80) at 0.01 cm/min cross-head speed. Each point represents the average K_c evaluated for 5 to 8 specimens having different initial crack lengths

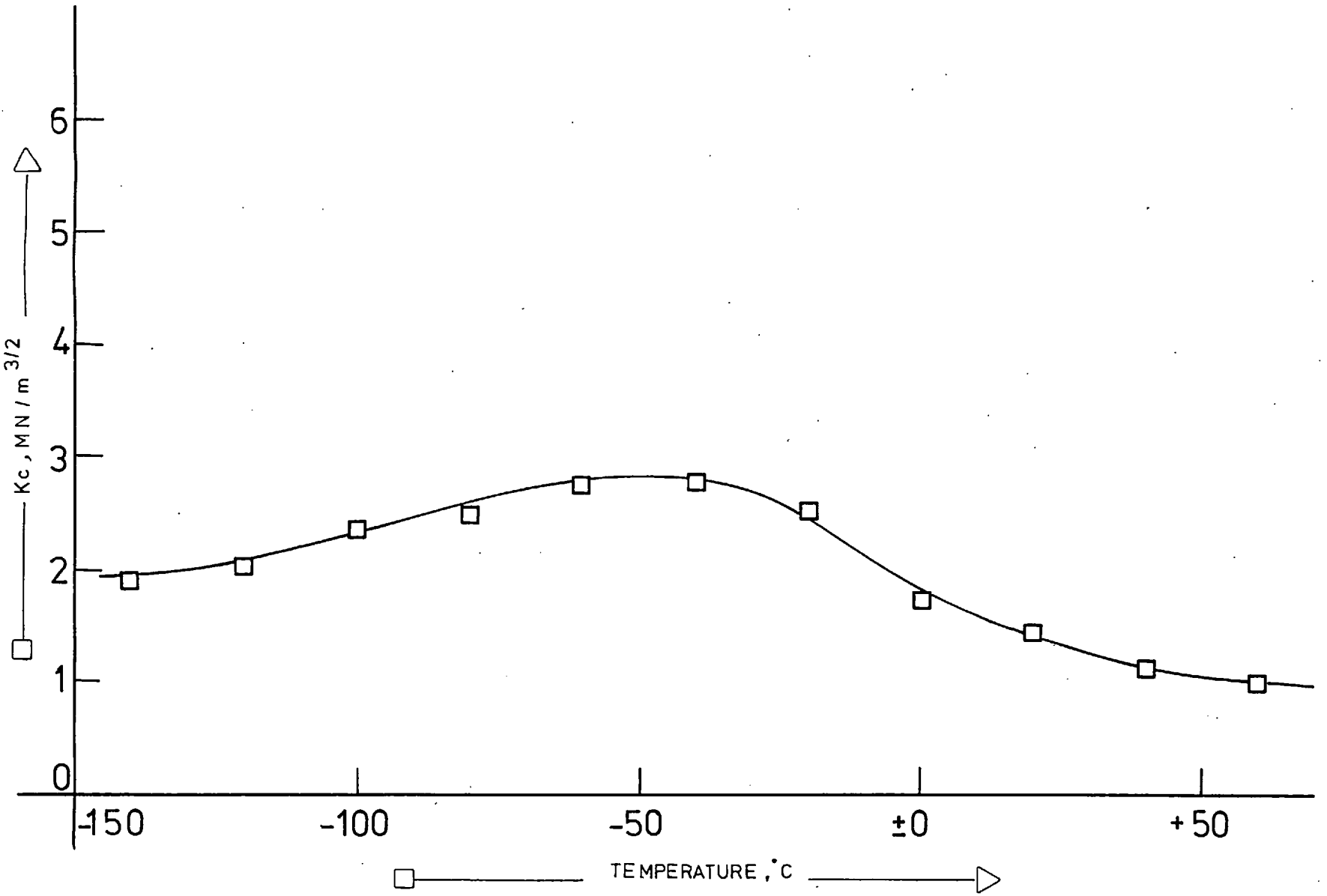


Figure 9.10: The effect of temperature on the fracture toughness for CPS (grade U C0) at 0.01 cm/min cross-head speed. Each point represents the average K_c evaluated for 5 to 8 specimens having different initial crack lengths

The fact that the experimental curves tend to become independent of the rubber content at lower temperatures indicates that the effect of the rubber (and hence its capacity for craze initiation) reduces and becomes almost negligible beyond the rubber glass transition temperature (-75°C to -80°C). In fact, an increase from zero rubber content in CPS (type U C) to 3.33% rubber content in HIPS (type U C) causes a decrease of about 45% in the ultimate stress at +60°C, but only about 5% at -90°C.

The experimental results have shown that some differences existed between the performances of type U B and U C of HIPS. Material U B had generally a 10% to 20% lower ultimate stress than type U C. It was also more influenced by the rubber glass transition temperature in the sense that near and below this temperature, the ultimate stress of all grades of U B tended more rapidly towards a constant value independent of their rubber content, whereas the U C materials showed perceivable differences, even at -120°C. The relatively high fracture strength in the case of the U C materials is believed to be mainly due to a higher molecular weight of the PS matrix employed.

The elongation of specimens tended to be small for CPS and appreciably larger for HIPS, especially at high temperatures. Typical results for the two types of failure are as follows:

1. Material U B0 (zero rubber content) at -120°C has an elongation to break of about 2.5 mm corresponding to 3.3% strain.

2. Material U B3.33 (3.33% rubber content) at +30°C has an elongation to break of about 45 mm corresponding to 60% strain.

* The continuation from page 384

to -40°C and thereafter decreases smoothly with decrease in temperature. The transitional temperature at which the maximum fracture toughness is obtained coincides for both types of CPS. The result reported by Parvin (1975) for a commercial grade of these materials also shows a peak at about -20°C for the computed fracture toughness values. It is interesting to note that the experimental curves obtained for the ultimate fracture stress of these materials have shown a point of inflection at about the same transitional temperature (see the previous section). On the other hand, the low strain properties (such as modulus of elasticity and the loss factor) show no significant variation at or near this transitional temperature. The increase in the toughness and fracture stress at this temperature can be caused by either one or a combination of the following phenomena:

1. The presence of 1.35% mineral oil: The mineral oil which is usually added for processing purposes acts as a plasticising agent and thence enhances the fracture toughness of the material. Boldt's (1973) experimental results on some CPS and HIPS are in support of this idea in which a large improvement was indicated for the elongation to break (a parameter approximately equivalent to the fracture toughness) at room temperature (see section 5.3 of Chapter 5). At the glass transition of the mineral oil (assumed to be around -40°C), the optimum oil-toughening process will occur, giving rise to a significant increase in the fracture toughness of CPS at this temperature.

2. Molecular structural changes: The fracture toughness peak at -40°C can be correlated to the β-transition of CPS. Martin et al (1956) found evidence of a similar peak at -30°C for thermal expansion. Chang & Bestul (1968) reported a change in the slope of the specific heat temperature plot at -23°C. Illers (1961) showed a secondary dynamic loss peak for crystal and modified PS in the region of 25°C to 60°C at frequencies varying from 0.05 to 40 Hz. This is in agreement with the experimental results previously noted for CPS (section 8.4 of Chapter 8)*. As discussed by Boyer (1968), the β-transition temperature is a strong function of the testing speed and could drop as low as -30°C while the α-transition still remains a a constant temperature. He suggested that the β-transition is caused by a molecular crankshaft motion (i.e. a specific motion about the chain axis) in CPS material.

9.3.3 Effect of Temperature on the Fracture Toughness of HIPS

120 mm wide single-edge notched specimens made from compression moulded sheets of various grades of specially prepared HIPS were tested at 0.01 cm/min Instron cross-head speed within the temperature range -140°C to +60°C. Fracture toughness values at crack initiation and at maximum applied load were computed for specimens containing cracks of various lengths (normally in the range of 10 mm < a < 40 mm) at temperature intervals of about 20°C. The initiation values obtained for all materials

---

* Although the β-transition recorded for U CO occurred at a temperature somewhat below the one quoted by Illers.

and at all testing temperatures were notable for being independent of the initial crack lengths and therefore were quite accurately described by the K_c criterion. This was mainly because of the use of comparatively wide specimens (that is, the craze length << specimen width) which caused a predominantly semi-brittle* fracture in these materials. The instability values (computed at maximum applied load but using the initial crack lengths) were, however, less consistent at higher temperatures ($T > 20^{o}C$) and a deviation from the linear fracture theory of about 5% to 10% was obtained†. The average instability values computed at temperatures above $20^{o}C$ should therefore be regarded as apparent fracture toughnesses.

The variations of fracture toughness computed at crack initiation and at maximum applied load as a function of temperature are shown in Figures 9.11 to 9.17 for various grades of HIPS materials tested. The experimental curves for both sets of initiation and instability data show that the K_c values increase with increasing temperature in the region $T < -80^{o}C$ to $-75^{o}C$, reaching a maximum at around this temperature, and then smoothly decreasing with increasing temperature. The glass transition temperature of PBD rubber employed in these polymers is about $-80^{o}C$ which approximately coincides with the peak obtained for the previously mentioned results. The peak observed for CPS at about $-40^{o}C$ due to the β-transition did not appear to influence the fracture toughness of their rubber-modified

---

* See Chapter 6 (section 6.8) for the definitions of fracture behaviour in HIPS. In the case of semi-brittle fracture, the instability point (the instant of unstable crack growth) normally coincides with the point of maximum load application.

† The derivation from the fracture mechanics theory is defined by equation (6.17) of Chapter 6.

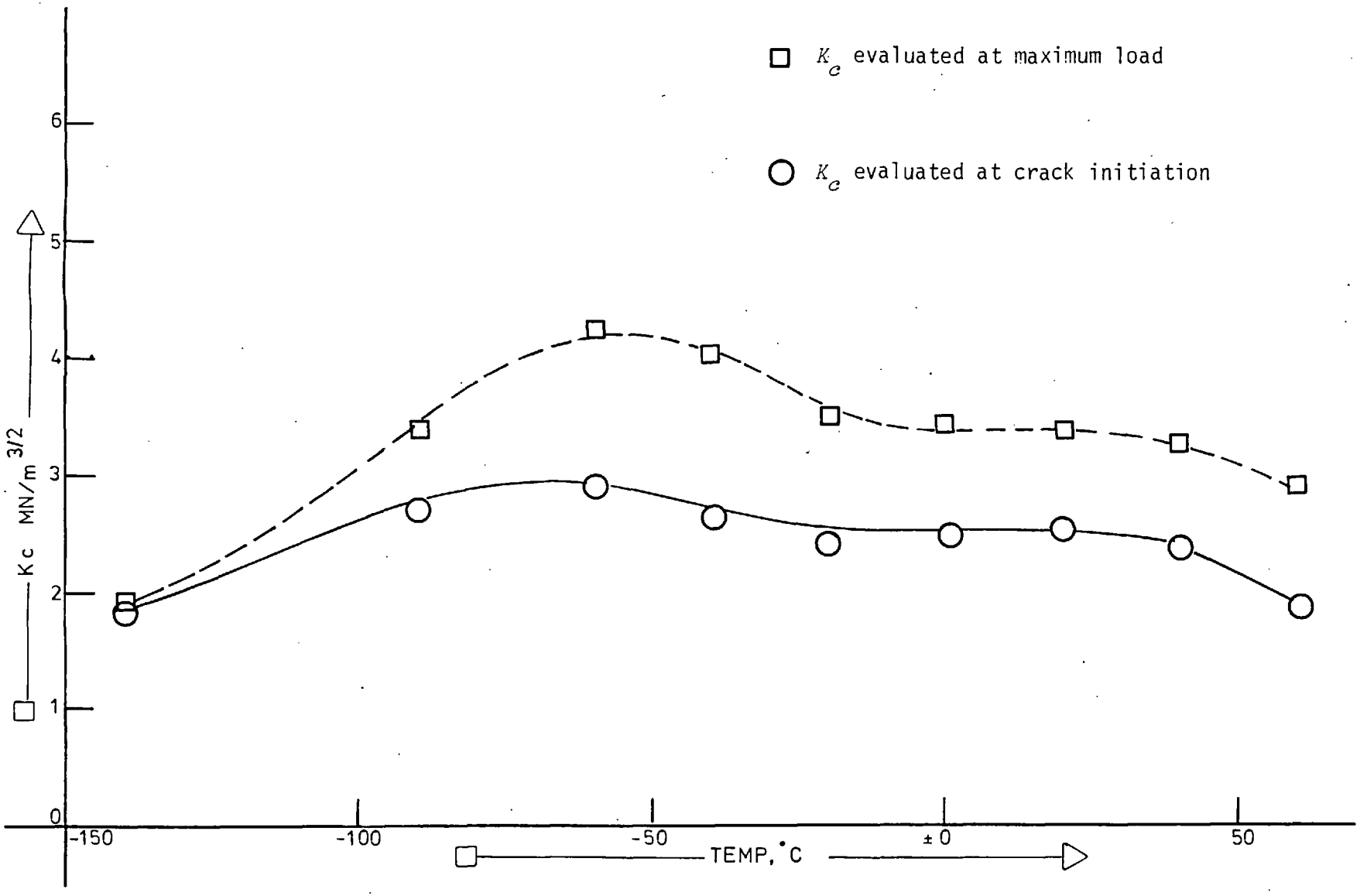


Figure 9.11: The effect of temperature on the fracture toughness of HIPS (grade U B1.11) at 0.01 cm/min cross-head speed. Each point represents the average K_c value obtained for 5 to 8 specimens having different initial crack lengths

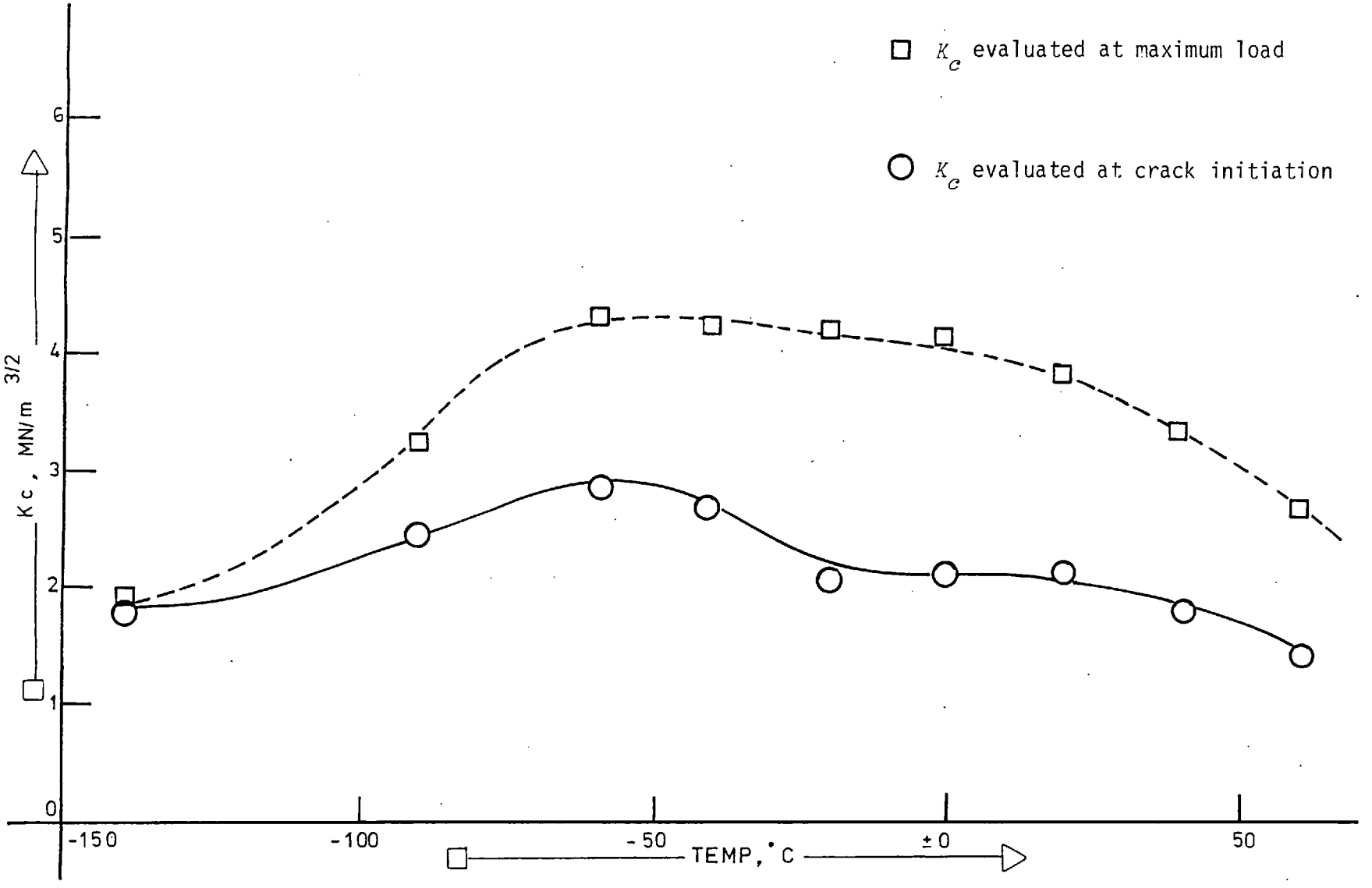


Figure 9.12: The effect of temperature on the fracture toughness of HIPS (grade II B2.22) at 0.01 cm/min cross-head speed. Each point represents the average K_c value obtained for 5 to 8 specimens having different initial crack lengths

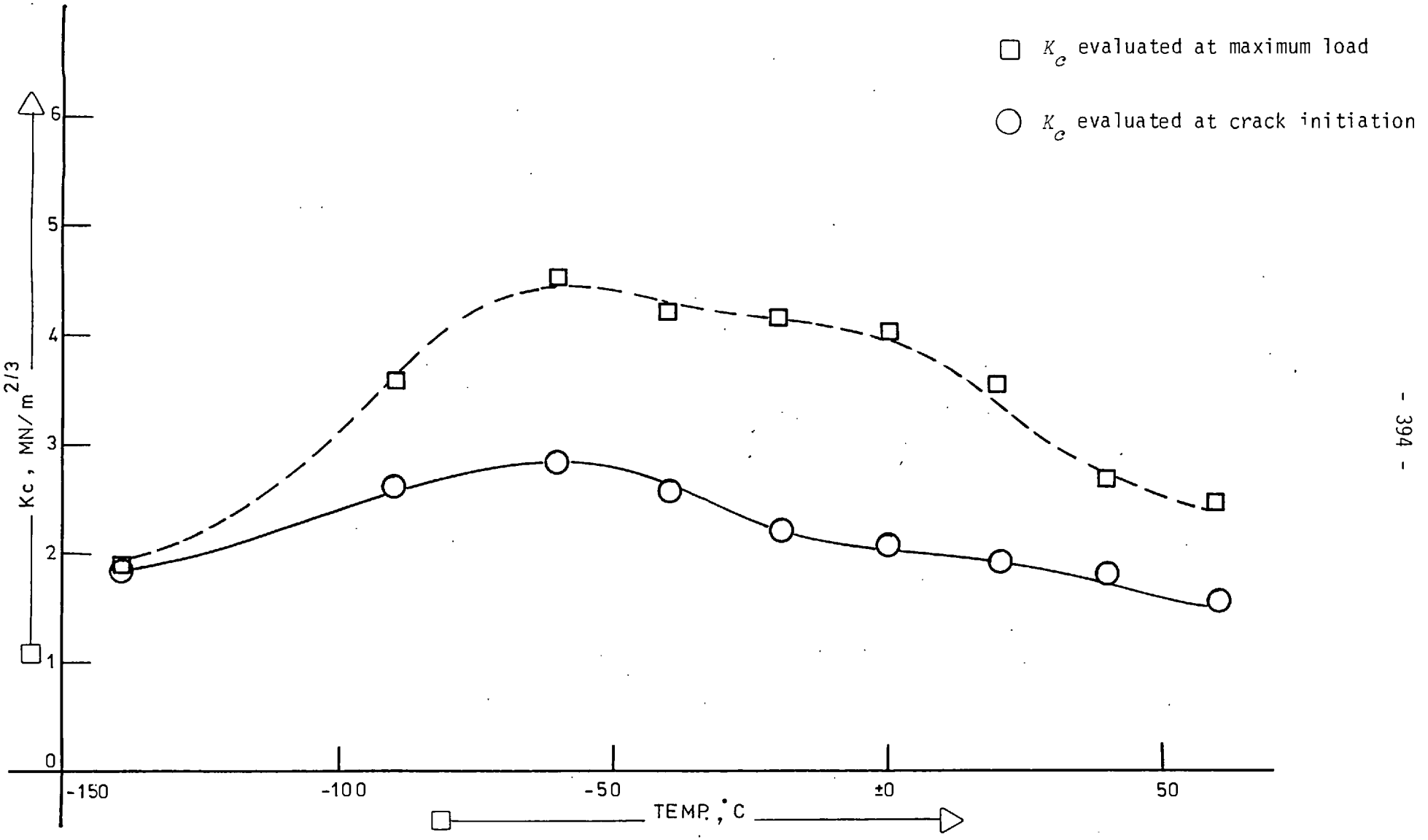


Figure 9.13: The effect of temperature on the fracture toughness of HIPS (grade U B3.33) at 0.01 cm/min cross-head speed. Each point represents the average K_c valued obtained for 5 to 8 specimens having different initial crack lengths

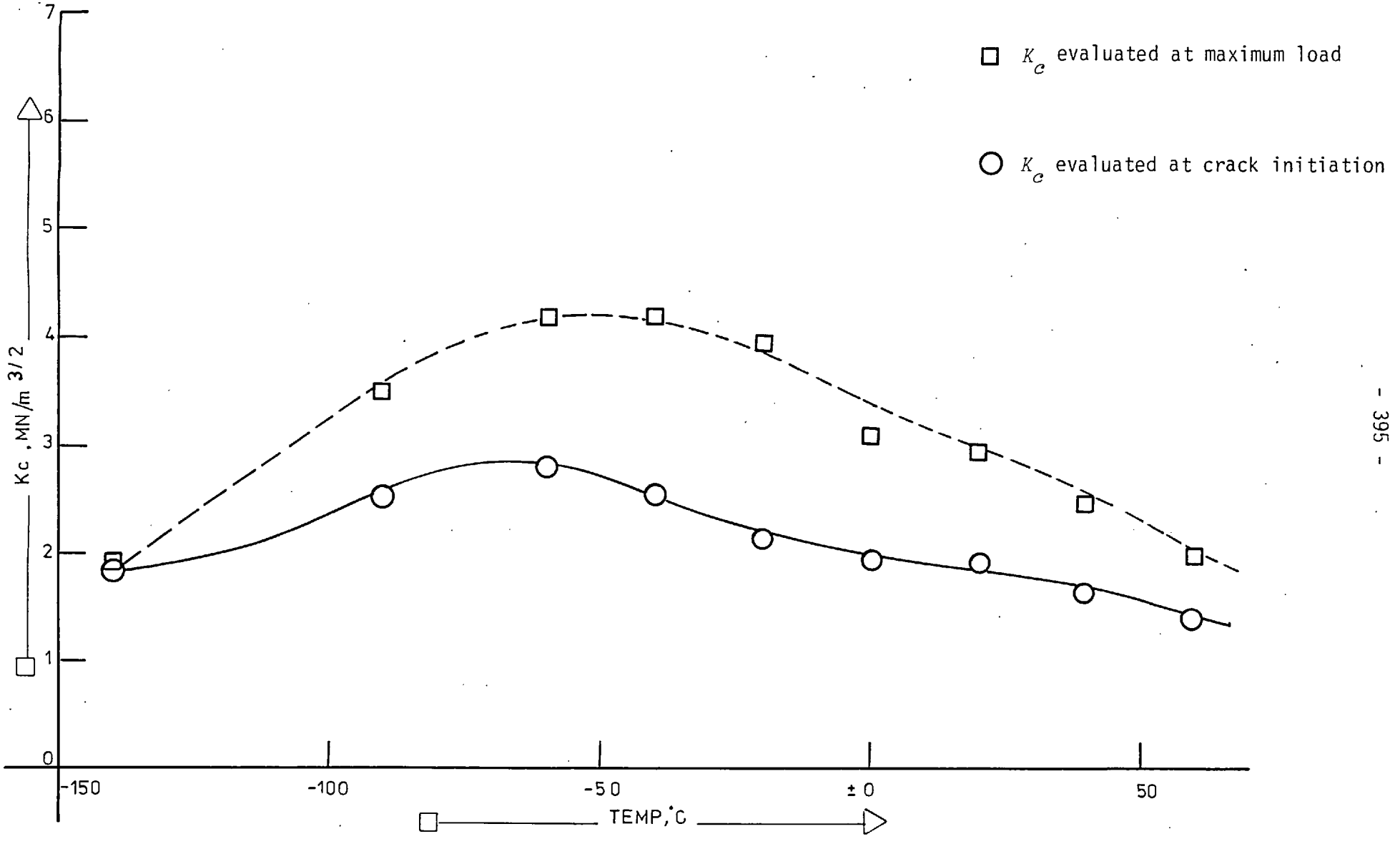


Figure 9.14: The effect of temperature on the fracture toughness of HIPS (grade U B5.55) at 0.01 cm/min cross-head speed. Each point represents the average K_c value obtained for 5 to 8 specimens having different initial crack lengths

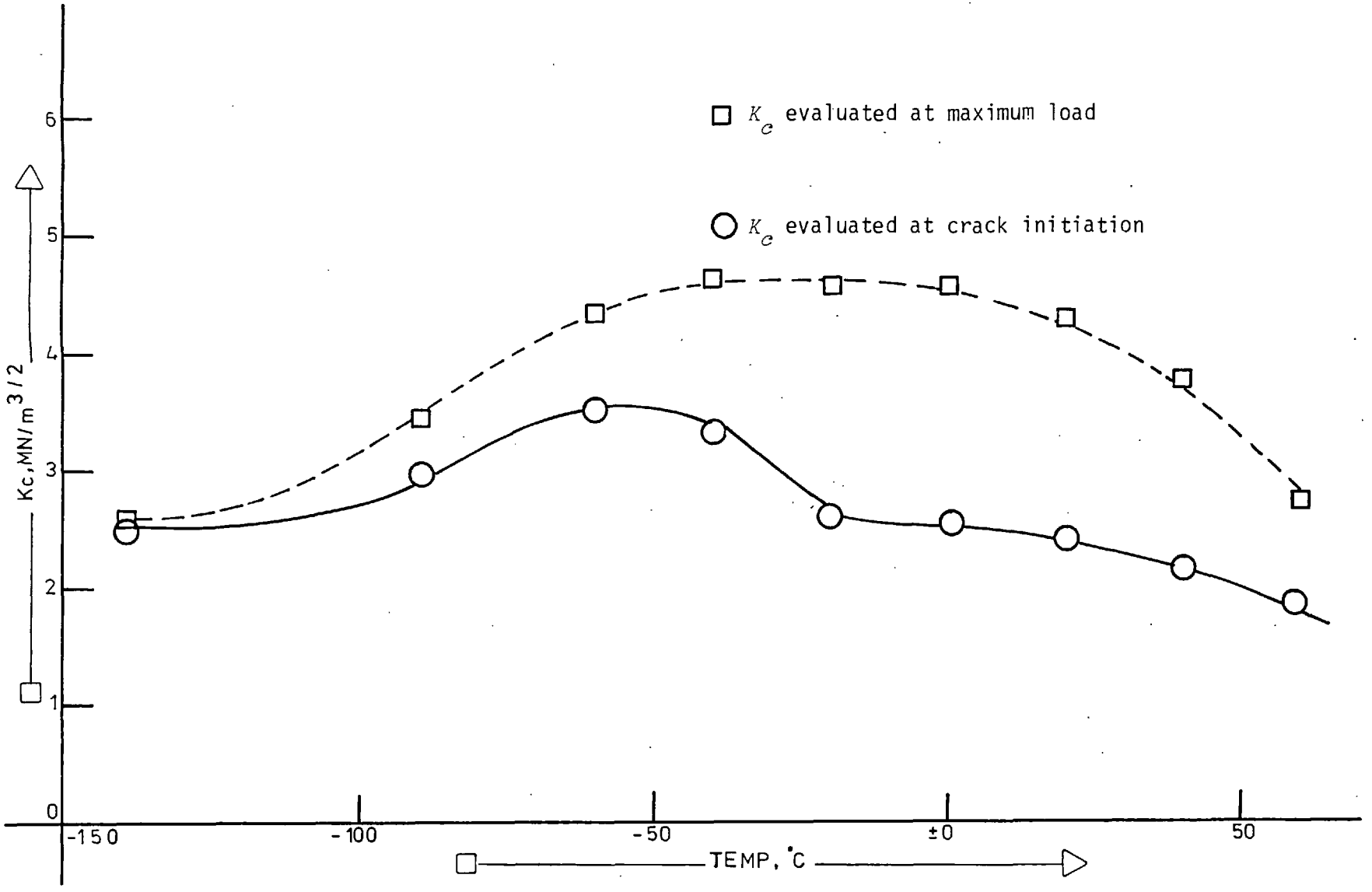


Figure 9.15: The effect of temperature on the fracture toughness of HIPS (grade II C1.11) at 0.01 cm/min cross-head speed. Each point represents the average K_c value obtained for 5 to 8 specimens having different initial crack lengths

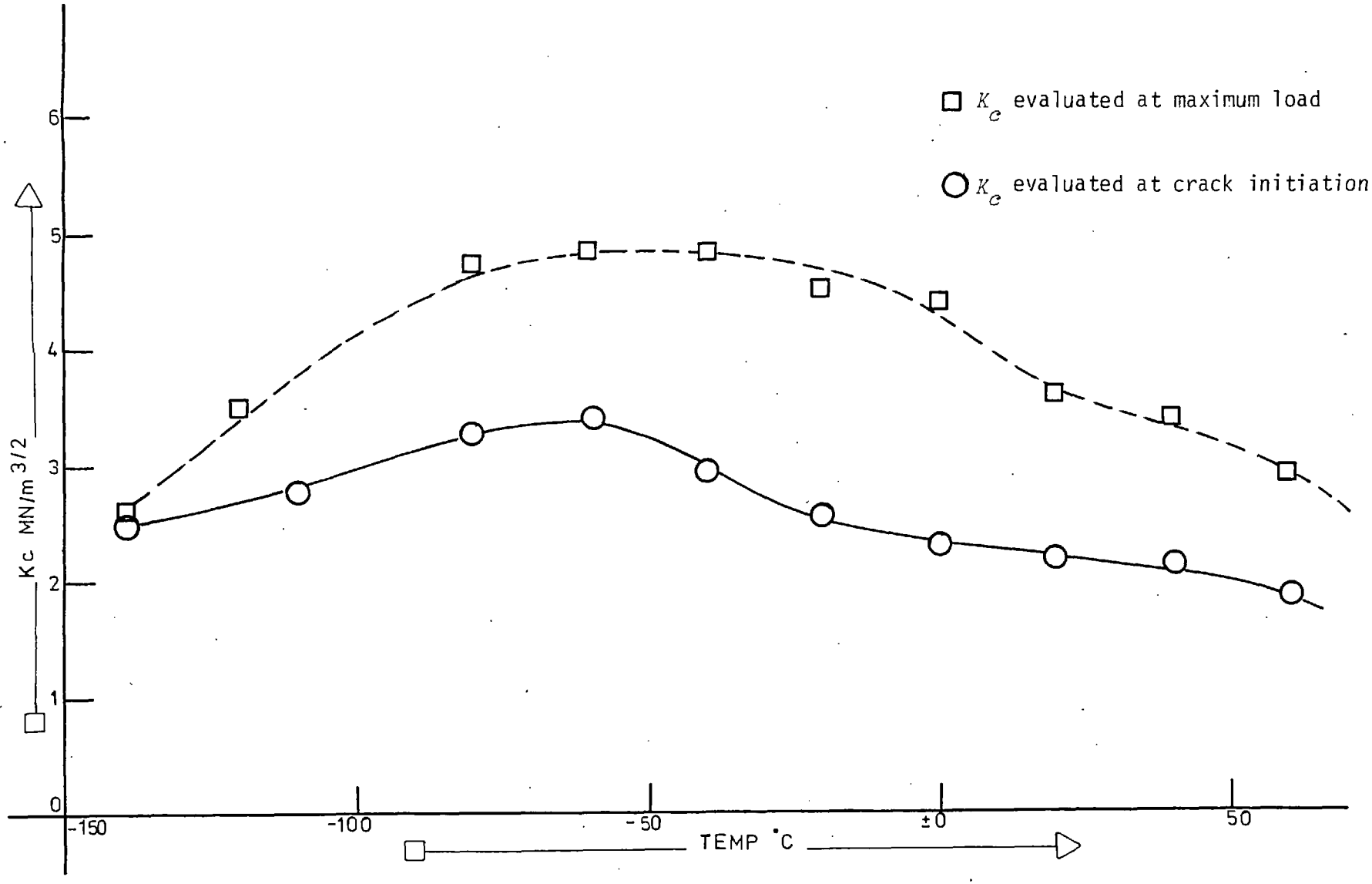


Figure 9.16: The effect of temperature on the fracture toughness of HIPS (grade II C?.22) at 0.01 cm/min cross-head speed. Each point represents the average K_c value obtained for 5 to 8 specimens having different initial crack lengths

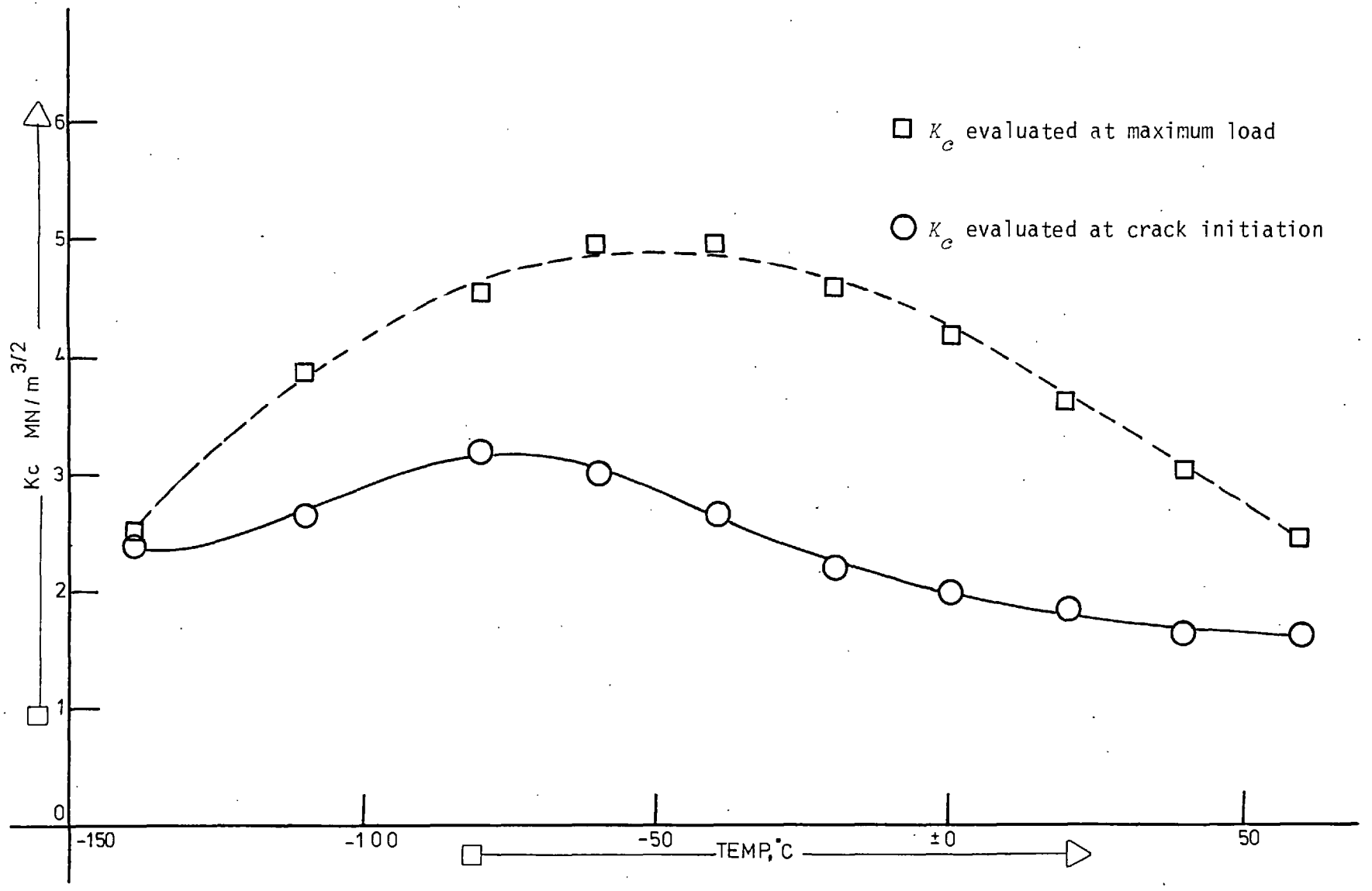


Figure 9.17: The effect of temperature on the fracture toughness of HIPS (grade U C3.33) at 0.01 cm/min cross-head speed. Each point represents the average K_c value obtained for 5 to 8 specimens having different initial crack lengths

derivatives. Below the rubber glass transition temperature, specimens made from various types of HIPS all broke in a semi-brittle manner manifesting limited craze growth and stable cracking. The extent of this slow crack growth is demonstrated by the differences obtained between the initiation and instability K_c values (Figures 9.11 to 9.17). It can be seen that these differences maximise at around -50°C to -30°C (depending on the material used), indicating comparatively long slow cracking at about these temperatures. At temperatures below -120°C to -140°C, the fracture occurred in a purely brittle manner and no crazing and slow crack growth was observed for any grades of HIPS tested. The initiation and instability curves, therefore, coincide at these very low temperatures. Figure 9.18 shows light micrographs of fractured surfaces at different temperatures for typical grades of HIPS. Generally, the amount of crazing manifested by opacity of the materials increases with increasing temperature showing a maximum craze formation at the highest temperature examined (i.e. at +60°C). It is worth noting that the amount of whitening shown in these photographs does not correspond to the craze length at initiation but rather describes the total crazing and the extent of slow crack growth at final fracture.

Theoretically, the craze length at crack initiation for specimens containing comparatively long initial cracks is approximately defined by:

$$r_c = \frac{\pi}{8} \frac{K_c^2}{\sigma_y^2} \qquad (9.1)$$

where σ_y and K_c denote the ultimate fracture stress and fracture toughness values, respectively. Although the fracture toughness increases with decreasing temperature in the region of T > -90°C, the craze zone length, r_c, will decrease, since the fracture stress, σ_y, increases more rapidly

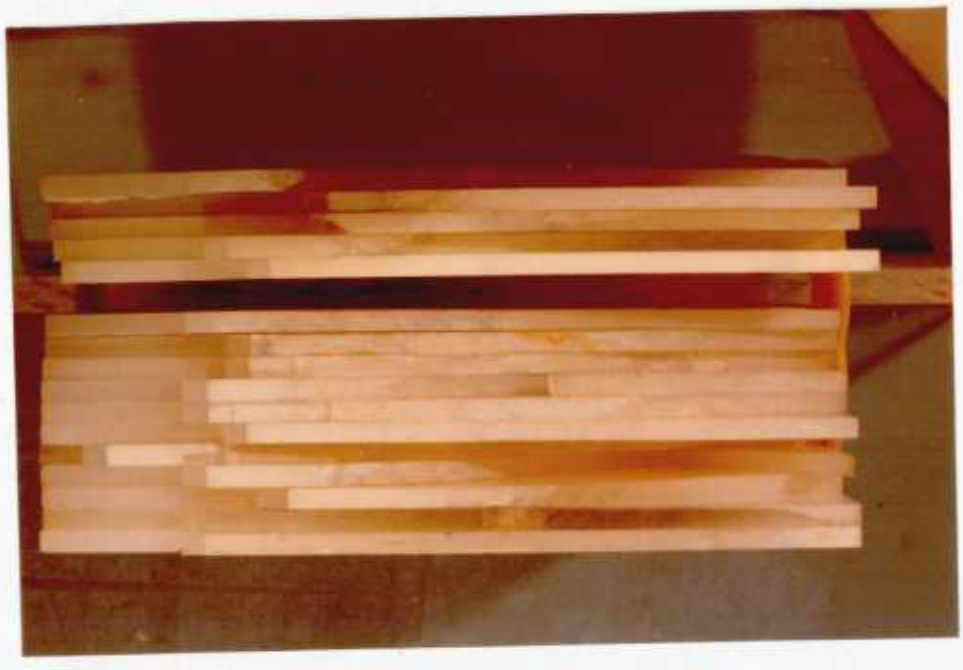


Figure 9.18: Fracture surfaces of some specially prepared samples of HIPS at various temperatures

as the temperature decreases. The typical computed craze zone lengths at crack initiation are:

Material U C3.33 (containing 3.33% rubber) { at $+60^{o}C$, r_c = 0.23 cm; at $-60^{o}C$, r_c = 0.09 cm

Material U C1.11 (containing 1.11% rubber) { at $+60^{o}C$, r_c = 0.15 cm; at $-60^{o}C$, r_c = 0.10 cm

The results described above are in close agreement with the experimental data obtained for HIPS materials.

The work by Parvin (1976) on the temperature-dependence of the fracture toughness in a commercial grade of HIPS similarly indicates substantial increases in fracture toughness with decreasing temperature in the range of $-80^{o}C < T < +20^{o}C$; although, as pointed out here, an analysis of the fracture surfaces showed a much greater craze formation at higher temperatures. Similar work was performed by Plati (1975) on the impact strength of an identical polymer. Plati's data for the impact resistance, conversely, demonstrates a sharp decrease with decreasing temperature within the above temperature range*. The Plati analysis is not, however, conclusive since it does not distinguish the initiation and propagation resistances. It is the author's belief that for HIPS, generally, the initiation impact resistance either increases or remains fairly constant as the temperature decreases, while the propagation impact resistance drops markedly at lower temperatures. The proof of this can be given as follows:

The fracture toughness, K_c, and the initiation impact strength, G_i, are correlated by:

---

* The impact strengths reported by Plati (1975) are G = 16 kJ/m^2 (at $+20^{o}C$) and G = 4 kJ/m^2 (at $-80^{o}C$).

$$G_i = \frac{K_c^2}{(1 - \nu^2)\, E} \tag{9.2}$$

where E and ν are the modulus and Poisson ratio of the material, respectively (see section 3.3 of Chapter 3). It has been shown that the modulus of elasticity remains fairly constant within a wide temperature range ($-60^{o}C < T < +60^{o}C$)*. If the fracture toughness increases substantially with decreasing temperature (as shown in this work), the right hand side ratio in equation (9.2) increases with the second power of K_c, assuming a constant modulus. Consequently, it is more likely that the initiation impact strength similarly increases with decreasing temperature, at least within the temperature range quoted by Plati.

The propagation impact resistance, being an aggregate composite property, generally depends on the rubber content of the polymer composite which, in turn, gives rise to a proportional increase in craze formation†. Since the volume of the crazed regions in HIPS reduces with decreasing temperature, the propagation impact resistance should similarly decrease

---

* See Chapter 8, section 8.4. Similarly, the experimental results obtained for some typical grades of HIPS by Cigna (1970) exhibit only a 10% to 15% reduction in modulus as the temperature increased from $-50^{o}C$ to $+50^{o}C$. The increase in the fracture strength within the temperature range $-50^{o}C < T < +20^{o}C$ was reported to be about 350% (Parvin (1975)) for the same material. There is a relatively sharp decrease in the modulus of HIPS near the glass transition temperature of CPS ($T_g \simeq 120^{o}C$) and PBD ($T_g \simeq -80^{o}C$). However, these variations do not occur within the temperature range quoted above.

† See Chapter 5, section 5.8, and also Chapter 7, section 7.8.

with a lowering of temperature*.

From the experimental analysis and the subsequent discussion presented here, it can be concluded that the variation of the initiation impact strength and the fracture toughness with temperature do not only depend on the crazing mechanism, but are also strongly affected by the amount of viscoelastic energy dissipation at the crack tip. The energy dissipation is itself influenced by the activation energy of the material which varies with temperature due to some change occurring in the molecular structure of the polymer.

---

* Direct experimental analysis of impact resistances of various types of HIPS at different temperatures has not been attempted here. For future research, it would therefore be of interest to find out to what extent the initiation and propagation resistances vary with temperature and thereby to assess the influence of the rubber and polystyrene glass transitions on these parameters.

9.4 THE RÔLE OF RUBBER IN HIPS WITH REFERENCE TO TEMPERATURE VARIATION

More light can be thrown on the effect of rubber content on the fracture toughness of HIPS by comparing the results obtained for materials with different rubber contents with those described for CPS. Plots of K_c versus nominal rubber fractional volume at different temperature intervals are shown in Figures 9.19 (type U B) and 9.20 (type U C). The striking feature described by these graphs is that the K_c maximises at around 1% rubber content for type U B and at around 1% to 2% rubber content for type U C, and then remains fairly constant (or decreases slightly, depending on the temperature or material used). The optimum rubber toughening is achieved at temperatures above $10^{o}C$ to $20^{o}C$ and is also in the range $-80^{o}C < T < -50^{o}C$. The rubber toughening effect is negligible at around $-30^{o}C$ which is near to the β-transition temperature of CPS ($T_\beta = -40^{o}C$). The reason for this behaviour is due to the fact that the β-transition, which is influenced by the presence of rubber, shifts to a lower temperature and interlocks with the rubber glass transition at about $-80^{o}C$. Since the increase in the fracture toughness of CPS due to the β-transition is almost identical to that obtained for HIPS materials due to the presence of rubber at $-40^{o}C$, there will be no relative improvement in the fracture strength of these polymers around this temperature.

It is interesting to note that the apparent fracture behaviour quantified by the amount of craze growth and slow cracking increases significantly with increasing rubber level. As previously shown, the craze length generated at the crack tip is approximately a square function of the ratio of the fracture toughness to the fracture stress. Since the ultimate fracture stress of HIPS materials decreases uniformly with an increase in rubber content, the craze length will increase, as the square of the rubber content, while the fracture toughness values may remain

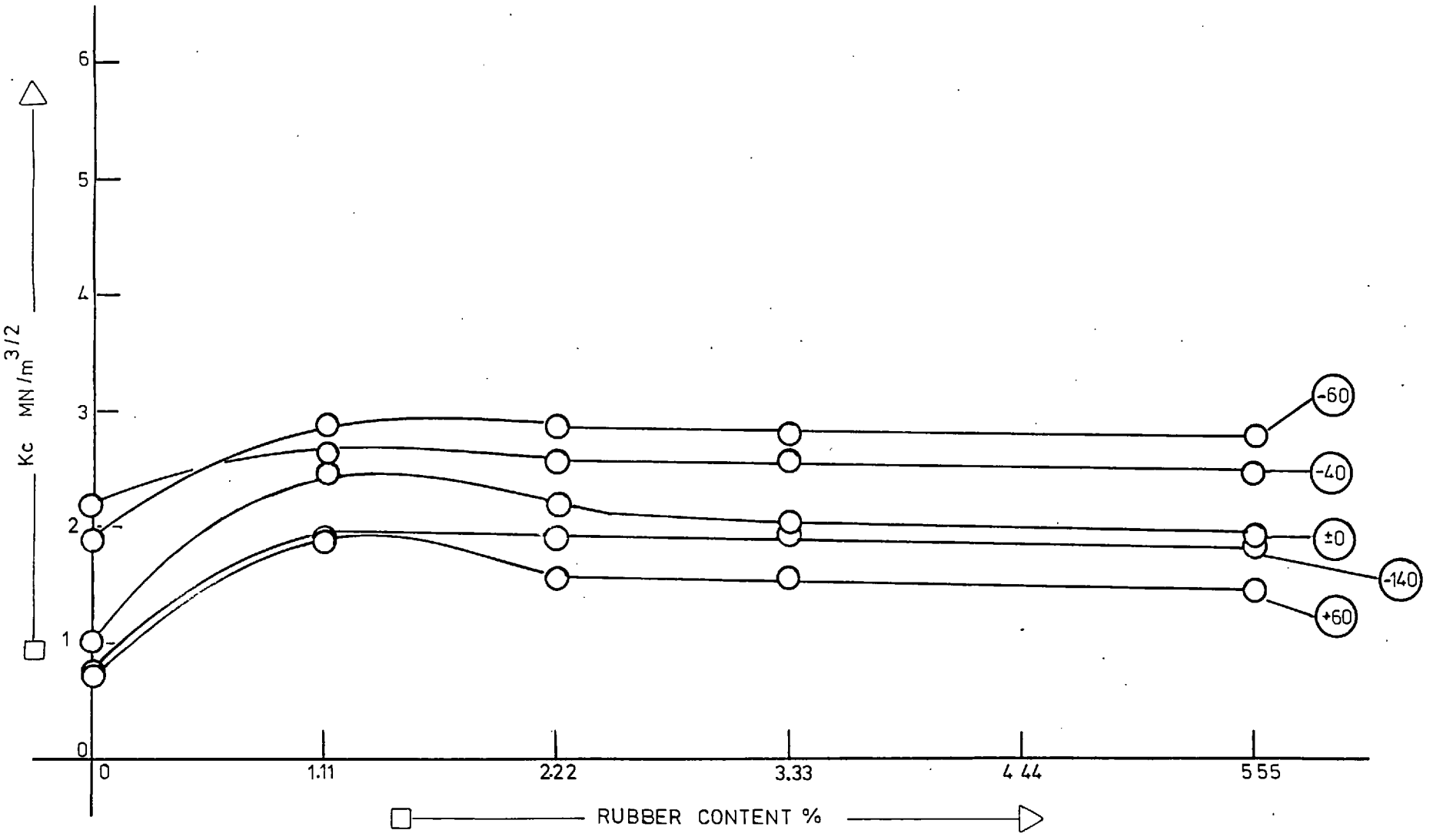


Figure 9.19: The effect of rubber on the fracture toughness of HIPS (type II B) at various temperatures

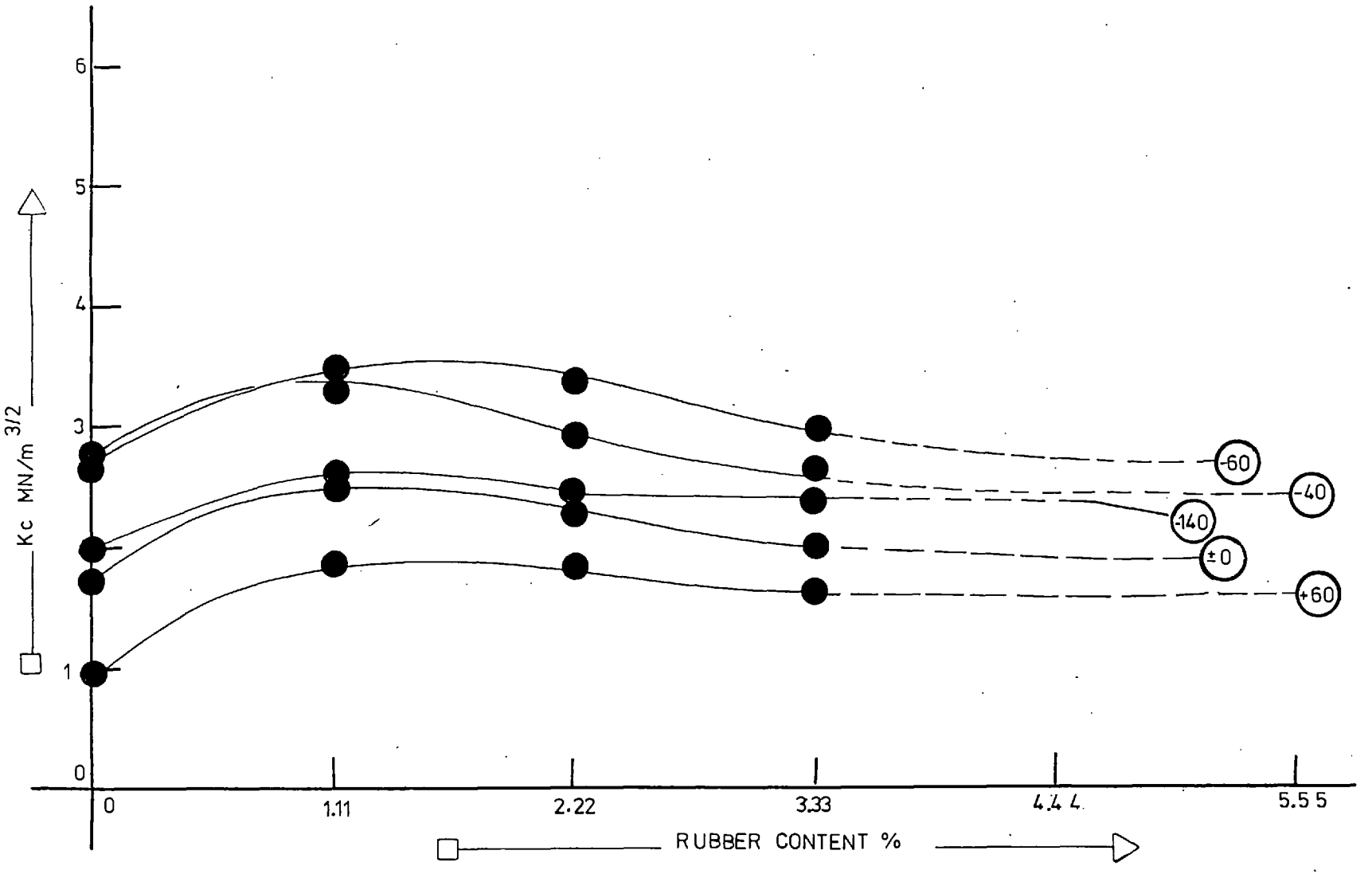


Figure 9.20: The effect of rubber on the fracture toughness of HIPS (type U C) at various temperatures

fairly constant. This is an important conclusion that can be drawn from the present experiments, clarifying the fact that a mere analysis of the fracture surfaces does not necessarily provide a correct basis for assessing the real toughness of rubber-modified polymers.

Finally, it is worth analysing the effect of material thickness on the apparent fracture toughness computed using Parvin's bimodal fracture model. This model was previously studied in Chapter 3, where it was shown that the plane strain fracture toughness, K_{1c}, and the plane stress fracture toughness, K_{2c}, are related to the apparent measured fracture toughness, K_c, by the following equation:

$$K_c = K_{1c} + \frac{K_{2c}^2}{\pi B \sigma_y^2} (K_{2c} - K_{1c}) \qquad (9.3)$$

The plane strain fracture toughness is theoretically obtained if the through-thickness strain is prevented. Under this circumstance, crazing cannot occur since its appearance induces a considerable through-thickness displacement. If the craze formation is not allowed, the fracture toughness of a modified PS material should tend to that of the crystal PS. This means that K_{1c} can be equated to the fracture toughness of the parent CPS, assuming no improvement in plane strain values of a rubber-modified PS. Having established this hypothesis, the plane stress fracture toughnesses can be deduced from equation (9.3), replacing K_{1c} and K_c with the fracture toughness values computed for CPS and its rubber-modified derivatives, respectively. The typical plane stress and plane strain fracture toughnesses for the U C2.22 containing 2.22% rubber are:

at $+50^{o}C$, K_{1c} = 1.05 $MN/m^{3/2}$, K_{2c} = 2.2 $MN/m^{3/2}$

at $0^{o}C$, K_{1c} = 1.7 $MN/m^{3/2}$, K_{2c} = 3.1 $MN/m^{3/2}$

at $-40^{o}C$, K_{1c} = 2.75 $MN/m^{3/2}$, K_{2c} = 3.3 $MN/m^{3/2}$

at $-80^{o}C$, K_{1c} = 2.55 $MN/m^{3/2}$, K_{2c} = 4.4 $MN/m^{3/2}$

at $-120^{o}C$, K_{1c} = 1.9 $MN/m^{3/2}$, K_{2c} = 4.5 $MN/m^{3/2}$

In general, the plane stress fracture toughness is smaller than the apparent fracture toughness obtained and therefore its computation will be of no practical interest. On the other hand, the most severe fracture occurs when a perfect constraint is exerted at the crack tip so that no crazing is allowed. However, this hypothetical constraint does not apply in practice. In fact, the experimental work on specimens which contained glue-covered surfaces* have proved that a further application of constraining materials does not cause a weaker fracture toughness. In designing a polymeric component, the calculations should therefore be based on the valid fracture toughness values under specified environmental conditions and within a given ambient temperature. Here, a valid fracture toughness means that the computed K_c must remain independent of the crack and specimen configurations.

---

* This experimental work has already been described in section 6.5.

CHAPTER 10

CONCLUSION

The primary aim of the work presented in this thesis was to develop a quantitative understanding of the mechanical and fracture behaviour of various types of high impact polystyrene with specific reference to their rubber contents and the consequent toughening processes involved. The theoretical and experimental findings of this survey are not, however, confined to these polymers alone, but may provide information which will be of considerable importance in future research work on a broader field of polymers, e.g. rubber combinations ranging from ABS, MBS (methylmeth-acrylate acrylonitrile butadiene styrene) and PVC/nitrile rubber blends to modified epoxide resins. From a general point of view, three aspects of the behaviour of these polymers have been considered to be of most interest to plastic manufacturers and designers. These are:

1. The elastic and yield properties;

2. The low strain rate fracture toughness; and

3. The high strain rate resistance (impact strength).

Discussions and conclusions relating to these specific factors have already been given in detail in the preceding chapters of this thesis, and here a summary of the discussions is presented together with an outline of possible future research in this field.

10.1 CONTRIBUTIONS

An introduction to the subject of elastic criteria of particulate-filled composites, crazing phenomenon, fracture mechanics and impact theories was given in Part I. In spite of the considerable number of valuable results already available, the work is still in an evolutionary stage. The preliminary literature survey given highlights the limitations of conventional elastic and fracture mechanics concepts and discusses the difficulties encountered when applying these theories for rubber particulate-filled composites. The subsequent chapters of this thesis have been directed to aiding the development of composite criteria upon which the elastic and fracture behaviour of these polymers can be analysed.

In Chapter 5, the low strain properties and yield stress of some specially prepared HIPS, having different nominal rubber fractional volumes, have been measured experimentally. It was shown that the yield and modulus values of these polymers decrease significantly with increasing rubber content. On average, a monotonical decrease of about 6% to 8% in the modulus of elasticity and yield stress was recorded for every 1% increase in the rubber fraction. On the other hand, the elongation to break (an implicit parameter exhibiting the extent of ductility of a material) was shown to increase several fold by the addition of a small fractional volume of rubber in the parent brittle PS matrix.

Electron microscopic analyses of the morphology of some experimental and commercial grades of HIPS have revealed a random dispersion of quasi-spherical (or spheroidal) rubber particles of a radius of about 3.5 to 6 μm, depending on the grade examined. These particles consisted of occluded PS sub-particles (80%) separated by thin layers (about 0.07 μm thick) of PBD rubber (20%). The micrographs of HIPS specimens subjected to tensile stresses have shown the production of multiple crazes emanating

from each particle on a plane perpendicular to the direction of the applied load. The crazing phenomenon has been confirmed to be the principal contributor to the toughening mechanism which was always accompanied by a substantial reduction in the stiffness and yield stress of the material.

An analytical craze formation model based on the previously mentioned experimental observations has been developed which excellently described the comparatively large deformation at rupture suffered by rubber-modified polymers.

The low strain properties, such as modulus of elasticity and bulk modulus of particulate-filled composites, can be evaluated if an appropriate model is chosen. In particular, when studying the elastic behaviour of HIPS, one must allow for the phase inversion occurring in the composite aggregate and PBD/PS particles. The analytical method proposed in Chapter 5 for computing the shear modulus of HIPS has principally been based on the Lewis & Neilsen theory for the suspension of relatively hard particles in a soft medium and the Hill theory for suspension of relatively soft elastic particles in a solid matrix. The computed moduli for various types of HIPS containing different rubber contents employing the two-stage calculation method proposed, have been shown to be satisfactory, as they were clearly correlated to the experimental data obtained. Subsequently, the influence of anisotropic dispersions of particles on the overall elastic properties of these materials have been analysed, using a simple theoretical model. When employing this model on certain specially prepared HIPS materials, the results indicated an almost perfect isotropic dispersion of particles in these polymers.

The experiments which have been described in Chapter 6 demonstrated that the linear theory of fracture mechanics can be successfully applied to characterise the brittle fracture of CPS and HIPS materials at room

temperature. In a systematic experimental analysis of the fracture behaviour of certain commercial types of HIPS, it has been shown that the prerequisite conditions of brittle fracture can generally be sustained if appropriate specimen geometry, crack configuration and notching technique are employed. Consequently, consistent and accurate fracture toughness values were obtained at the craze initiation, crack initiation and maximum applied load, using 100 mm wide single-edge notched specimens. Additionally, thin layers of Araldite were applied to the crack surfaces of some single-edge notched specimens to induce plane strain conditions and the fracture performance was studied. The experimental results obtained for these tests have indicated that the fracture toughness values were identical for both the glued and exposed specimens, although the cracking speed was significantly increased when Araldite covered the specimens. In discussing the fracture behaviour of these polymers, it was stated that the apparent brittle fracture should be associated with predominantly plane strain conditions which may be enhanced by the introduction of a constraining material covering the surfaces of the specimen. On the other hand, the rapid rupture of wide single-edge notched specimens with glued surfaces was partially attributed to the impact caused by the sudden fracture of these fragile constraints.

The picture which has emerged from the analysis of certain specially prepared grades of HIPS having various rubber contents was that the fracture toughness increased quite significantly with a small addition of rubber; however, there was no further improvement after 2% nominal rubber fractional volume. The limited toughening process involved is attributed to opposing effects of the rubber particles which both initiate and control the craze growth.

In Chapter 7, the impact behaviour of various types of commercial and

experimental HIPS material have been analysed. The conventional theories derived for homogeneous brittle and ductile materials were found to be inaccurate when fracture of rubber-modified polymers are studied. On the other hand, the modification of basic linear fracture theory for a situation where limited plastic flow, crazing and stable crack growth take place, have been shown to render an approximate solution but only for a narrow range of low impact grades of HIPS. Faced with these difficulties, a universal impact theory has been developed which provides a unique method of analysis, whereby the impact data obtained for a wide spectrum of brittle to ductile composite polymers can accurately be assessed. According to this theory, the energy loss in an impact test constitutes the energy consumed in the initiation of a crack, the energy dissipated while the crack propagates and the energy losses due to extraneous factors (such as the kinetic energy of the broken pieces and vibrational energy losses of the testing machine). It was shown experimentally (which is in accordance with the composite theory proposed) that the initiation resistance of a composite polymer merely depends on the composite matrix properties and does not vary effectively with the level of rubber grafting. However, the propagation resistance was seen to increase linearly as the rubber phase volume fraction became greater. The propagation impact resistance was found, therefore, to be useful for rating the various grades of HIPS in an order of merit.

The analysis of the dynamic mechanical results, described in Chapter 8, has provided an informative understanding of the molecular motions and possible transitional temperatures which occur as a result of the presence of the constitutive components of HIPS composites. Plots of the input-output phase angle versus temperature have generally shown two major transitional temperatures corresponding to the polystyrene and polybutadiene

glass transitions. The rubber peak, occurring at about -75°C to -80°C, was found to increase monotonically with additional rubber content. Although it can be concluded that the presence of a low temperature dampening peak in a glassy polymer is, in effect, an indication of a two-phase system, the size of this peak does not appear to be directly correlated to the actual degree of toughness. On the other hand, for a family of similarly prepared HIPS, the curves of bulk properties (such as modulus of elasticity and yield stress) versus temperature have shown almost identical transitional regions corresponding to the dynamic peaks observed in a *tan* Ω-temperature plot.

In Chapter 9, the effect of temperature on the yield strength and fracture toughness of various types of specially prepared HIPS has been studied. The initial interpretation of the results inferred that the apparent fracture behaviour of these materials, as quantified by the amount of crazing and slow crack growth, increased with increasing temperature. In contrast, the experimental results reported in this work have indicated a significant drop in the yield stress at higher temperatures.

The fracture toughness-temperature curves for various types of crystal polystyrene have exhibited a secondary peak at -40°C which can be correlated to the β-transition temperature of these materials. For HIPS, however, this peak was interlocked with the rubber glass transition at -75°C to -80°C. As a result of this study, the toughening effect of rubber at various temperatures has been analysed, whereby it was shown to be most efficient at higher temperatures (T > 20°C) but was almost insignificant in the vicinity of the PS β-transitional temperature (T = -40°C) and beyond the rubber glass transitional temperature (T < -80°C).

10.2 RECOMMENDATIONS FOR FUTURE RESEARCH

The analytical procedures developed in this thesis provide information which will be of considerable use in future research on rubber-modified polymers. Firstly, the methods developed in Chapters 5 to 9 are immediately applicable to design procedures of HIPS materials. Secondly, the theoretical models suggested for the evaluation of moduli, relative elongation to break and the impact resistance can be adopted as a basis for the analysis of newly processed particulate-filled polymers, as well as the other commercial rubber-modified polymers, such as ABS, MBS, and PVC/nitrile rubber blends.

Furthermore, it is interesting to analyse the effect of temperature on the initiation and propagation impact resistances of similarly prepared HIPS containing various rubber contents. The results of such a study will be of considerable interest to those who are concerned with the fracture of ductile and semi-ductile materials.

In Chapter 6, SEN and SN specimens have been employed to study the fracture behaviour of various types of HIPS materials. The question which may arise here is whether specimens with different crack configurations and subjected to different forms of loading should yield identical results, as reported by this work. In particular, the use of three-point bend single-edge notched specimens is recommended inasmuch as the results can be directly compared with those obtained from the Charpy impact specimens.

APPENDIX A

THE ISOLATED SPHERICAL INCLUSION

Goodier (1933) analysed the stress-strain behaviour of an infinite elastic body containing a single spherical particle, which was in a state of uniform uniaxial tension, σ, at points remote from the particle. Figure 2.4 of Chapter 2 illustrates the Goodier's model in a spherical system of coordinates. The Goodier theory is a rigorous basis for the analysis of particulate-filled composites containing spherical (or quasi-spherical) particles perfectly bounded to the matrix.

Let u_r, u_θ and u_ψ be the displacements along the radius, r, and at right angles to it in the meridian and orbital planes of the sphere, respectively. The specimen is under a tensile stress, σ, along the X_3-axis. The u_ψ component would naturally vanish since the problem is symmetrical. Hence, the displacement of any arbitrary point, like $A(r,\psi,\theta)$, outside the inclusion will always lie on the meridian planes of the spherical inclusion, and the other components, u_r and u_θ, do not involve the ψ-coordinate. The following equations, given by Goodier, define the displacement of a specimen in a region outside the inclusion:

$$u_r = \left[\left(\frac{H_1 O^3}{r^2} - \frac{H_2 O^5}{r^4} \right) + \left(\frac{H_3 O^3}{r^2} - \frac{H_4 O^5}{r^4} \right) \cos 2\theta \right] \frac{\sigma}{\mu} + u_r^* \qquad (A.1)$$

$$u_\theta = - \left[\frac{H_5 O^3}{r^2} + \frac{H_6 O^5}{r^4} \sin 2\theta \right] \frac{\sigma}{\mu} + u_\theta^* \qquad (A.2)$$

where O is the radius of the inclusion, and H_1, H_2, H_3, H_4, H_5 and H_6 are constants in terms of ν and ν' (Poisson ratios of the media and the inclusion, respectively), and the ratio of the modulus of rigidity of the media, μ, and the inclusion, μ'. u_r^* and u_θ^* are uniform displacements of

a complete elastic solid subjected to a uniform tensile stress, that is:

$$u_r^* = \frac{\sigma\, O}{4\mu}\left[\frac{1-\nu}{1+\nu} + \cos 2\theta\right]$$

$$u_\theta^* = -\frac{\sigma\, O}{4\mu}\sin 2\theta \qquad \text{(A.3)}$$

The constants H_1, H_2, H_3, H_4, H_5 and H_6 of equations (A.1) and (A.2) are given by:

$$H_1 = \frac{n_o - 1}{8}\,\frac{2\,(1-2\nu')(6-5\nu)\,n_o + 3 + 19\,\nu' - 20\,\nu\,\nu'}{\left[(7-5\nu)\,n_o + (8-10\nu)\right]\left[2\,(1-2\nu')\,n_o + (1+\nu')\right]}$$

$$+\frac{1}{4}\,\frac{n_o\,(1-2\nu')(1+\nu) - 1 + 2\,\nu\,\nu' + \nu}{(1+\nu)\left[2\,(1-2\nu')\,n_o + (1+\nu')\right]}$$

$$H_2 = \frac{3\,(n_o - 1)}{8}\,\frac{1}{(7-5\nu)\,n_o + (8-10\nu)}$$

$$H_3 = \frac{5}{3}\,(5-4\nu)\,H_2$$

$$H_5 = \frac{2\,(1-2\nu)\,H_3}{(5-4\nu)}$$

$$H_4 = 3H_2 \quad ; \quad H_6 = 2H_2 \quad ; \quad n_o = \frac{\mu}{\mu'}$$

The displacement variance due to the presence of a single spherical inclusion along the x_j-axis is given by:

$$\Delta X_3^p = (u_r - u_r^*)\cos\theta - (u_\theta - u_\theta^*)\sin\theta$$

$$\Delta X_1^p = (u_r - u_r^*)\sin\theta\cos\psi + (u_\theta - u_\theta^*)\cos\theta\cos\psi \qquad \text{(A.4)}$$

$$\Delta X_2^p = (u_r - u_r^*)\sin\theta\sin\psi - (u_\theta - u_\theta^*)\cos\theta\sin\psi$$

The stresses imposed by the presence of the particles for a region outside the particle boundary are defined by:

$$\sigma_r = 2\sigma \left[\frac{H'_1 O^3}{r^3} + \frac{H'_2 O^5}{r^5} + \left(\frac{H'_3 O^3}{r^3} + \frac{H'_4 O^5}{r^5} \right) \cos 2\theta \right] \tag{A.5}$$

$$\sigma_\theta = 2\sigma \left[\frac{H'_5 O^3}{r^3} + \frac{H'_6 O^5}{r^5} + \left(\frac{H'_7 O^3}{r^3} + \frac{H'_8 O^5}{r^5} \right) \cos 2\theta \right] \tag{A.6}$$

$$\sigma_\psi = 2\sigma \left[\frac{H'_9 O^3}{r^3} + \frac{H'_{10} O^5}{r^5} + \left(\frac{H'_{11} O^3}{r^3} + \frac{H'_{12} O^5}{r^5} \right) \cos 2\theta \right]$$

$$\sigma_{r\theta} = + 2\sigma \left[\frac{H'_{13} O^3}{r^3} + \frac{H'_{14} O^5}{r^5} \right] \sin 2\theta \tag{A.7}$$

$$\sigma_{r\psi} = \sigma_{\theta\psi} = 0 \tag{A.8}$$

where coefficients H'_i (i = 1, 2, ..., 14) are functions of ν, ν' and n_o.

Goodier's equations show that the maximum stress occur at the equator of the spherical inclusion. The stress concentration caused by the particle falls very rapidly with distance from its surface, therefore indicating the localised nature of the stress field. In special cases, a uniform tensile stress at a distance from a spherical cavity produces a tensile loop stress, σ_o, around the equator of the cavity in the direction of applied stress, and of a concentration magnitude of about 2.05 (assuming $\nu \simeq 0.33$). On the other hand, a rigid spherical inclusion ($\mu' \simeq \infty$), representing the worst possible case of an inclusion more rigid than the matrix, induces tensile stress concentrations at the planes of the sphere of a magnitude of about 1.95 σ.

APPENDIX B

THE CHARPY SPECIMEN

The stress intensity factor of a three-point bend beam containing a single-edge crack (Charpy specimen) is given by (see Figure 4.1 of Chapter 4):

$$K = \sigma \sqrt{a} \left[\eta_o + \eta_1 \left(\frac{a}{D}\right) + \eta_2 \left(\frac{a}{D}\right)^2 + \eta_3 \left(\frac{a}{D}\right)^3 + \eta_4 \left(\frac{a}{D}\right)^4 \right] = \sigma Y \sqrt{a} \qquad (B.1)$$

where a = crack length

σ = gross applied stress

D = specimen width along the crack

Y = geometrical factor introduced to account for finite width effect

The coefficients of the above polynomial depend on the span to depth ratio (S_p/D) of the specimen and have been computed by Gross & Srawley (1966) for various specimen configurations. Table B.1 collates the numerical values of the coefficients of this fourth degree polynomical against S_p/D.

The elastic strain energy stored in a Charpy specimen is given by (Timoshenko (1951)):

$$U = \tfrac{1}{2} \left(\frac{B D^2 \sigma}{6 S_p}\right)^2 C \qquad (B.2)$$

where C = specimen compliance

B = specimen thickness

Equation (4.19) derived in section 4.4 of Chapter 4 describes the compliance in terms of the intensity factor. Substituting equations (4.19) and (B.1) in equation (B.2) gives:

TABLE B.1

The coefficients of the Y polynomial*

Coefficients	S_p/D								
	4	5	6	7	8	9	10	11	12
n_0	1.93	1.937	1.945	1.952	1.96	1.967	1.975	1.982	1.990
n_1	- 3.07	- 2.99	- 2.91	- 2.83	- 2.75	- 2.67	- 2.59	- 2.51	- 2.43
n_2	14.53	14.312	14.095	13.877	13.66	13.442	13.225	13.007	12.790
n_3	-25.11	-24.827	-24.545	-24.262	-23.98	-23.697	-23.415	-23.132	-22.850
n_4	25.80	25.655	25.51	25.365	25.220	25.075	24.930	24.785	24.640

* Brown & Srawley (1966)

$$U = B\,D\,\frac{K^2}{E_{red}}\,\Phi\,(S_p/D, a/D) \tag{B.3}$$

where E_{red} is the reduced modulus of elasticity, and the function Φ is defined by:

$$\Phi = \left[\frac{1}{(a/D)}\int Y^2(a/D)\,d(a/D) + \frac{(S_p/D)}{9(a/D)}\right]/Y^2 \tag{B.4}$$

The geometry function, Φ, can either by computed analytically using equations (B.4) and (B.1), or determined experimentally by measuring the specimen compliance subjected to a static load, as detailed in Chapter 7. The experimental measurement has been carried out by Plati & Williams (1975) and the results are collated in Table B.2. For computing purposes, these results are also expressed in a polynomial form in a log-log plane as follows:

$$Y = \psi_1 X + \psi_2 X^2 + \psi_3 X^3 + \psi_4 X^4 + \psi_5 X^5 + \psi_6 X^6 \pm 2 \times 10^{-8}$$

where $Y = log\ \Phi$, and $X = -\ log\ (a/D)$.

The coefficients of this polynomial are given for different span width ratios in Table B.3.

TABLE B.2

CHARPY CALIBRATION FUNCTION

A / D	Φ				
	S_p/D= 4	S_p/D= 6	S_p/D= 8	S_p/D=10	S_p/D=12
0.04	1.681	2.456	3.197	3.904	4.580
0.06	1.183	1.715	2.220	2.700	3.155
0.08	0.933	1.340	1.725	2.089	2.432
0.10	0.781	1.112	1.423	1.716	1.990
0.12	0.680	0.957	1.217	1.461	1.688
0.14	0.605	0.844	1.067	1.274	1.467
0.16	0.550	0.757	0.950	1.130	1.297
0.18	0.505	0.688	0.858	1.015	1.161
0.20	0.468	0.631	0.781	0.921	1.050
0.22	0.438	0.584	0.718	0.842	0.956
0.24	0.413	0.543	0.664	0.775	0.877
0.26	0.391	0.508	0.616	0.716	0.808
0.28	0.371	0.477	0.575	0.665	0.748
0.30	0.354	0.450	0.538	0.619	0.694
0.32	0.339	0.425	0.505	0.578	0.647
0.34	0.324	0.403	0.475	0.542	0.603
0.36	0.311	0.382	0.447	0.508	0.564
0.38	0.299	0.363	0.422	0.477	0.527
0.40	0.287	0.345	0.398	0.448	0.494
0.42	0.276	0.328	0.376	0.421	0.462
0.44	0.265	0.311	0.355	0.395	0.433
0.46	0.254	0.296	0.335	0.371	0.405
0.48	0.244	0.287	0.316	0.349	0.379
0.50	0.233	0.267	0.298	0.327	0.355
0.52	0.224	0.253	0.281	0.307	0.332
0.54	0.214	0.240	0.265	0.288	0.310
0.56	0.205	0.228	0.249	0.270	0.290
0.58	0.196	0.216	0.235	0.253	0.271
0.60	0.187	0.205	0.222	0.238	0.253
1.00	0.000	0.000	0.000	0.000	0.000

* After Plati & Williams (1975)

TABLE B.3

The coefficients of the Φ polynomial

S_p/D	4	6	8	10	12
ψ_1	0.472745	0.459418	0.448416	0.438677	0.437392
ψ_2	-0.822365	-0.571559	-0.332259	-0.100584	0.068089
ψ_3	1.018265	0.690945	0.317650	-0.093797	-0.382703
ψ_4	-0.566424	-0.321486	0.013065	0.417717	0.688010
ψ_5	0.166343	0.075176	-0.091181	-0.299732	-0.433270
ψ_6	-0.017705	0.003082	0.028742	0.071685	0.098247

APPENDIX C

PROGRAM FOR CALCULATING FRACTURE TOUGHNESS

This program is written in FORTRAN IV and was run on a CDC 6400 at the Imperial College Computer Centre. In the version listed here, the program evaluates the fracture toughness of single-edge notched specimens but it can easily be modified to perform calculations for specimens containing surface notched and other types of crack configuration*. The program also provides some comments on the fracture behaviour and limitations of the linear fracture mechanics theory applied. Furthermore, the statistical analysis of the data obtained are described in terms of the maximum, minimum and mean values, variance, standard deviation, standard error, skewness and Kurtosis of the results. The deviation from linear fracture mechanics theory, as defined by equation (6.17) of Chapter 6, is also evaluated and indicated by the program.

The program also enables the production of graphs of the results for each batch of specimens. These graphs comprise the plots of stress versus crack depth, stress*Y-factor versus inversed square root of the crack length, intensity factor versus the crack length, and intensity factor versus the percentage of specimens having a value equal to or greater than a specified fracture toughness. The program listing is given as follows†.

---

* A simplified version of the program for surface notched specimens is also quoted here, which can simply be co-operated with the main program mentioned above.

† The program calls the library subroutines ELLICE and E02ACF, the listings of which are not given here. These are, however, available at the Computer Centre of Imperial College and may be directly called from the CERNUP and NAG4F softwares.

Program 1 (SEN Specimens)

```
      PROGRAM KANYAR(INPUT,OUTPUT,TAPE5=INPUT,TAPE6=OUTPUT,TAPE62)
C                                TEST 19
      REAL MEAN,M9X,MIN,K ,MATER
      DIMENSION AB(4),MATER(10),GLUE(12),LOAD(12),K(50),O(50),D(50),EPY(
     +50),FIP(32),A(2),X1(50),X2(50)
     +,N2(50),N3(50),N4(50)
      COMMON/C1/SIGMAY
      COMMON/C2/SIGMA
      COMMON/C3/DMAX,D1,MAX
      COMMON/C4/W,T,MEAN
      COMMON/C6/GLUE,LOAD,MATER
      COMMON/C7/J,D,O,K
      COMMON/C8/SIGMAR
      DATA(AB(I)=10H MACHINED ,10HSINGLE EDG,10HE--NOTCHED ,10HSPECIMENS
     +)
      DATA BB,SB,SD,DD/100.,0.,0.,0./
      DATA(MATER(II),II=1,6)/10HMATERIAL -,10HHIGH IMPAC,10HT POLYSTYR,
     +10HENE, GRADE,10HBPS,       ,10H           /
C
C     PRELIMINARY TERMS
      M2=1
      M3=1
      M4=1
      N2(M2)=0
      N3(M3)=0
      N4(M4)=0
      MIN=1000000.00000
      MAX=0.0
      SUM=0.0
      VARIANC=0.0
      GAMMA=0.0
      BETA=0.0
C     INPUT THE INITIAL DATA OF THE TEST
  155 READ(5,2) T,W,SIGMAY,CS,CH,SIGMAR,GLUE,LOAD
    2 FORMAT(N,2F5.3,F5.0,F5.2,F5.2,F5.0,4(/6A10))
      IF(T.LE..0) STOP
      READ(5,3) J ,RM,GLUEFF
    3 FORMAT(I2,2F5.2)
C     WRITE TITLE
      WRITE(6,1) AB
    1 FORMAT(1H1,///,50(*.*),*STRESS INTENSITY FACTOR EVALUATION*,50(*.*
     +),//44(*.*),43X,4A10,4X,44(*.*),//)
C     INPUT CRACK DIMENSIONS
      READ(5,30) (D(I),I=1,J)
   30 FORMAT(F5.3)
C     OUTPUT THE INITIAL DATA
      WRITE(6,19)T,W,RM,SIGMAY,CS,CH,MATER,GLUE,LOAD
   19 FORMAT(5X,*SPECIMEN NOMINAL THICKNESS, T=*,F5.3,*CM.,  SPECIMEN WI
     +DTH, W=*,F5.3,*CM.,  NOTCH CUTTING RADIUS, RM=*,F6.3,*CM.*,/5X,
     +     *YIELD STRESS, SIGMAY=*,F5.0,*KG./SQ.CM.,  CROSS HEAD SPEED, C
     +S=*,F5.2,*CM./MIN.  ,CHART SPEED, CH=*,F5.2,*CM./MIN.,*/5X,10A10/,
     +5X,10A10,/,5X,10A10)
      WRITE(6,94)
   94 FORMAT('1',//135('*'),/,  * NO  SPEC. THICK.  CRACK LENGTH  CRACKE
     +D ARCH  APPL. LOAD  CROSS STRESS  NET SIGMA  INTENS. FACTOR  PLAS
     +TICITY RADIUS  FRACTURE TOUGHNESS,/,'*',4H(CM),10X,4H(CM),7X,*(PER CEN
     +T)*,5X,*(KG./SQ.CM)*,4X,*(KG./SQ.CM)*,3X,*(KG./SQ.CM)*,2X,14H(M.N./M.**
     +1.5),8X,*(CM.)*,/,135('*'),/)
C     CALCULATIONS
```

```
      DO 6N=1,J
C       CHECK NOTCH DIMENSIONS REGARDING TO THE THEORETICAL LIMITS
C     READ THE ACCURATE THICKNESS OF THE FRACTURED SP. AROUND THE CRACK
      READ(5,107) TT
  107 FORMAT(F4.3)
      T=TT
      YYY=D(N)/W
      IF(YYY.LE..4)GO TO 10
      N2(M2)=N
      M2=M2+1
C     INPUT LOAD AND FRACTURE MANNER
   10 READ(5,11) F,FRAC1,FRAC2
   11 FORMAT(X,F3.0,2A6)
C     GLUE EFFECT ON TOTAL LOAD SHAREING
      F=F/GLUEFF
C     CHECK LOADING
      SIGMA=F/W/T
      P=(SIGMAY-SIGMA)/SIGMAY
      IF(ABS(P).GE.0.25) GO TO 12
      N3(M3)=N
      M3=M3+1
C     CALCUTION OF KC
   12 E=D(N)/W
      Y=1.99-0.41*E+18.7*E**2-38.48*E**3+53.85*E**4
      K(N)=Y*SQRT(D(N))*SIGMA*0.009807
      RRY(N)=K(N)**2/SIGMAP**2/2./3.14159/(.009807)**2
C     CHECK THE VALIDITY OF THE PLANE-STRAIN CONDITION
      PS=(K(N)/0.009807/SIGMAY)**2
      PV=T-PS*2.5
      IF(PV.GE.0.) GO TO 112
      N4(M4)=N
      M4=M4+1
  112 CONTINUE
C     CRACK AREA, NET STRESS
      AREA=T*D(N)
      PERCENT=100.*AREA/(T*W)
      SIGMAN=F/(W*T-AREA)
C     OUTPUT INITIAL DIMENSION,LOAD,KC,AND FRACTURE MANNER
      WRITE(6,14) N,T,D(N),PERCENT,F,SIGMA,SIGMAN,K(N),RRY(N),FRAC1,FRAC
     +2
   14 FORMAT(X,I2,6X,F4.3,9X,F5.3,10X,F4.1,9X,F4.0,9X,F4.0,9X,F4.0,10X,F
     +4.2,13X,F5.3,10X,2A6,/)
C     EXTRA TERMS
      D(N)=SIGMA
C     STATISTICAL TERMS
C     EVALUATION OF MEAN,MIN,MAX(OF KC AND D)
      SUM=SUM+K(N)
      IF(K(N).GT.MAX) MAX=K(N)
      IF(K(N).LE.MIN) MIN=K(N)
    6 CONTINUE
      MEAN=SUM/FLOAT(J)
      DMAX=D(J)
      D1=D(1)
C     VARIANCE,STANDARD ERROR,AND STANDARD DEVIATION
      DO 9 N=1,J
      VARIANC=VARIANC+((K(N)-MEAN)**2)/(FLOAT(J)-1.)
    9 CONTINUE
      STADEV=SQRT(VARIANC)
      STAERR=STADEV/(SQRT(FLOAT(J)))
C     SKEWNESS AND KURTOSIS
      DO 17 N=1,J
   17 GAMMA=GAMMA+((K(N)-MEAN)**3)/FLOAT(J)
      DO 19 N=1,J
   18 BETA=BETA+((K(N)-MEAN)**4)/FLOAT(J)
      GAMMA=GAMMA/STADEV**3
      BETA=BETA/STADEV**4
C          CALCULATE DEVIATION FROM THE LINEAR FRACTURE MECHANICS.
      DO 15 N=1,J
      X1(N)=D(N)/W
   15 X2(N)=K(N)-MEAN
      CALL SORM(X1,X2,J,A,B,PERROR)
```

```
      DELEMT=A(2)
C     OUTPUT PERCENTAGE OF BRITTLE OR DUCTILE FAILURE
      WRITE(6,100)
  100 FORMAT(%,/135('-'))
      WRITE(6,28) J,BB,SB,SD,DD
   28 FORMAT(10%,'AMONG',I2,'SPECIMENS',F5.1,'PER CENT HAVE FAILED IN BR
     +ITTLE MANNER',F5.1,'PER CENT IN SEMI-BRITTLE MANNER,',F5.1,'PER CE
     +NT',/,10%,'IN SEMI-DUCTILE MANNER , AND',F5.1,'PERCENT IN PURELY D
     +UCTILE MANNER.')
C     OUTPUT CAUTIONS AND COMMENTS
  131 IF(M2.LT.2) GO TO 130
      M2=M2-1
      WRITE(6,16)(N2(M),M=1,M2)
   16 FORMAT(10%,'NOTCH GEOMETRY OUTSTRIPS THE THEORETICAL LIMITS FOR SP
     +ECIMENS NO.',(20(I2,',')))
  130 IF(M3.LE.2) GO TO 132
      M3=M3-1
      WRITE(6,13) (N3(M),M=1,M3)
   13 FORMAT(10%,'LOAD EXCEEDS 3/4 OF THE RELEVANT YIELD STRESS FOR SPEC
     +MENS NO. =',/10%,I2,',',I2,33(',',I2))
  132 IF(M4.LT.2) GO TO 139
      M4=M4-1
  139 WRITE(6,74)(N4(M),M=1,M4)
   74 FORMAT(10%,'PLANE-STRAIN CONDITION COULD NOT BE MAINTAINED FOR SPEC
     +IMENS NO.=',/10%,I2,',',I2,33(',',I2))
C     OUTPUT STATISTICS
      WRITE(6,20) MAX,MIN,MEAN,VARIANC,STADEV,STAERR,GAMMA,BETA,DELEMT
   20 FORMAT(%,//135(%'='),//,
     +10%,'MAXIMUM STRESS INTENSITY FACTOR =',F4.2,/
     +10%,'MINIMUM STRESS INTENSITY FACTOR =',F4.2,/
     +10%,'MEAN STRESS INTENSITY FACTOR =',F4.2,/
     +10%,'VARIANCE OF THE STRESS INTENSITY FACTOR RESULTS =',F5.3,/
     +10%,'STANDARD DEVIATION OF THE RESULTS =',F5.3,/
     +10%,'STANDARD ERROR OF THE RESULTS =',F5.3,/
     +10%,'SKEWNESS OF THE RESULTS =',F5.3,/
     +10%,'KURTOSIS OF THE RESULTS =',F6.3/
     +10%,'DEVIATION FROM THE LINEAR FRACTURE MECHANICS THEORY=',F6.3)
C     PLOTTING SUBROUTINES
      CALL DRAW0
      CALL DRAW
      CALL DRAW1
      CALL ENPLOT
      GO TO 155
      END
      SUBROUTINE DRAW0
      COMMON/C1/SIGMAY
      REAL MAX,MEAN
      COMMON/C3/DMAX,D1,MAX
      COMMON/C4/W,T,MEAN
      COMMON/C5/U,V,WW,VV,UU,VU
C     CRACK DEPTH,UNIT ON THE X-AXIS
      U=AINT(DMAX*1000.0/9.+1.)/100.
C     STRESS,UNIT ON THE Y-AXIS
      V=AINT((SIGMAY+70.)/4.5/9.81+1.)
C     PERCENTAGE OF THE NOTCHED AREA,UNIT ON THE X-AXIS
      CAREAM=DMAX*T
      PERCM=100.*CAREAM/T/W
      WW=PERCM/9.
C     INTENSITY FACTOR,UNIT ON THE Y-AXIS
      VV=AINT(MAX/.45 +2.0)/10.
C     INV. SQ. PT. OF THE CRACK DEPTH, UNIT ON THE X-AXIS
      SICDM=1./SQRT(D1*10.)
      UU=AINT((SICDM/9.*100.+1.))/100.
C     STRESS*(Y-FACTOR) ,UNIT ON THE Y-AXIS
      SIGFA=MEAN *(1.+D1/100.)
      VU=AINT(SIGFA/5.0+1.)
      RETURN
      END
      SUBROUTINE DRAW
      INTEGER SLOT
      DIMENSION LOAD(12),GLUE(12),MATED(10),P(10),KT(10)
```

```
      COMMON/C6/GLUE,LOAD,MATER
      COMMON/C5/U,V,WW,VV,UU,VU
C     DRAWING OF BORDERS AROUND EACH FRAME
      CALL START(2)
      CALL FACTOR(.82)
      CALL PLOT(0.0,0.0,-3)
      CALL PLOT(0.0,13.0,2)
      CALL PLOT(21.,13.0,2)
      CALL PLOT(21.0,0.0,2)
      CALL PLOT(0.0,0.0,2)
      CALL PLOT(0.0,6.5,3)
      CALL PLOT(21.0,6.5,2)
      CALL PLOT(10.5,0.0,3)
      CALL PLOT(10.5,13.0,2)
C     DRAWING OF THE AXES IN EACH FRAME
      CALL PEN(4)
C  A- FRAME NO.1
      CALL PLOT(1.0,7.5,-3)
      CALL AXIS(0.0,0.0,17HCRACK DEPTH  (MM),-17,9.0,0.0,0.0,U)
      CALL AXIS(0.0,0.0,25HAPPLIED STRESS  (MN/M**2),25,4.5,90.,0.,V)
      CALL AXIS(0.0,4.5,30HPERCENTAGE OF THE NOTCHED AREA,30,9.,0.,.0,WW
     +)
C  B- FRAME NO.2
      CALL PLOT(10.5,0.,-3)
      CALL AXIS(0.,0.,17HCRACK DEPTH  (MM),-17,9.0,.0,.0,U)
      CALL AXIS(.0,.0,29HINTENSITY FACTOR  (MN/M**3/2),29,4.5,90.,0.,VV)
C  C- FRAME NO.3
      CALL AXIS(0.0,4.5,30HPERCENTAGE OF THE NOTCHED AREA,30,9.,0.,.0,WW
     +)
      CALL PLOT(-10.5,-6.5,-3)
      CALL AXIS(.0,.0,51HINVERSED SQUARE ROOT OF THE CRACK DEPTH  MM**(-
     +1/2),-51,9.,0.,0.0,UU)
      CALL AXIS(.0,.0,28HSTRESS * Y-FACTOR  (MN/M**2),28,5.0,90.0,0.0000
     +,VU)
C  D- FRAME NO.4
      CALL PLOT(10.5,0.0,-3)
      CALL PLOT(9.0,0.0,+2)
      R(1)=1.0
      R(2)=2.0
      R(3)=3.0
      R(4)=4.0
      R(5)=5.0
      R(6)=6.0
      R(7)=8.0
      R(8)=10.
      R(9)=15.
      R(10)=20.0
      R(11)=25.0
      R(12)=30.0
      R(13)=40.0
      R(14)=50.0
      R(15)=60.0
      R(16)=80.0
      R(17)=100.0
      DO 1 I=1,17
      X=ALOG10(R(I))*4.5
    1 CALL SYMBOL(X,-0.035,0.070,13,0.0,-1)
      DO 2 I=1,7
      X=ALOG10(R(I))*4.5 -0.04
    2 CALL NUMBER(X,-.20,0.11,R(I),0.0,-1)
      DO 3 I=8,17
      X=ALOG10(R(I))*4.5-.11
    3 CALL NUMBER(X,-.20,0.11,R(I),0.0,-1)
      CALL SYMBOL(0.50,-0.55,0.14,57HPERCENTAGE OF SP. HAVING A VALUE EQ
     +UAL OR GREATER THAN R(C,0,5)
      CALL AXIS(0.0,0.0,29HINTENSITY FACTOR  (MN/M**3/2),29,5.000,90.000
     +,.0,VV)
C     TITLE
      CALL PEN(1)
      CALL PLOT(-11.5,-1.0,-3)
```

```
      READ(5,99999)KT
99999 FORMAT(7A10)
      CALL SYMBOL(1.0,15.0,.16,97HFRACTURE TOUGHNESS IN MACHINED SINGLE
     +EDGE-NOTCHED SPECIMENS(PRODUCED BY A FLY CUTTER, R=60.0 MM),.0,97)
      CALL SYMBOL(1.0,14.4,.107,MATER,0.,100)
      CALL SYMBOL(1.0,14.0,.107,KT,0.,70)
      CALL SYMBOL(1.0,13.6,.107,GLUE,0.,120)
      CALL SYMBOL(1.0,13.2,.107,LOAD,0.,120)
C     FRAME NO.1
      CALL PLOT(7.5,12.0,-3)
      CALL SYMBOL(.0,-.60,.10,25HMEAN KC-VALUES (THEORY)  ,.0,25)
      CALL SYMBOL(.0,-.2,.10,25HGROSS STRESS (EMPIRICAL) ,.0,25)
      CALL SYMBOL(0.0,-.40,.10,25HYIELDING LINE (THEORY)   ,0.,25)
      CALL SYMBOL(2.5,-.15,.1,11,0.0,-1)
      CALL PEN(4)
      CALL PLOT(2.5,-.35,3)
      CALL PLOT(2.8,-.35,2)
      CALL PLOT(2.5,-.35,2)
      CALL PEN(3)
      CALL PLOT(2.5,-.55,3)
      CALL PLOT(2.8,-.55,2)
      CALL PLOT(2.5,-.55,2)
      CALL PEN(1)
C     FRAME NO.2
      CALL PLOT(10.5,-4.1,-3)
      CALL SYMBOL(0.0,0.0,.1,23HEXPERIMENTAL RESULS    ,.0,23)
      CALL SYMBOL(0.0,-.2,.1,23HAVERAGE KC-VALUE(EXP.) ,.0,23)
      CALL SYMBOL(2.3,.05,.10,2,0.0,-1)
      CALL PEN(4)
      CALL PLOT(2.3,-.2,3)
      CALL PLOT(2.6,-.2,2)
      CALL PEN(1)
      CALL PLOT(0.,0.4,-3)
C     FRAME NO.4
      CALL PLOT(-4.0,-5.3,-3)
      CALL SYMBOL(+0.0,-1.0,0.14,26HSTATISTICAL INVESTIGATIONS,.0,26)
      CALL PLOT(-14.0,-3.0,-3)
      CALL PEN(2)
      CALL PLOT(-1.0,-1.0,3)
      CALL PLOT(20.,-1.0,2)
      CALL PEN(1)
      RETURN
      END
      SUBROUTINE DRAW1
      REAL MEAN,K
      DIMENSION D(50),O(50),K(50)
      COMMON/C1/SIGMAY
      COMMON/C7/J,D,O,K
      COMMON/C5/U,V,WW,VV,UU,VU
      COMMON/C4/W,T,MEAN
      COMMON/C8/SIGMAP
C     DRAW STRESS VERSUS CRACK DEPTH
      DO1N=1,J
      X1=D(N)/U*10.
      Y=O(N)/9.81/V
    1 CALL SYMBOL(X1+1.0,Y+7.5,0.070,11,0.0,-1)
C     DRAW YIELD AND RUPTURE STRESS LINES & FRACTURE TOUGHNESS FOR KC=KC-MEAN
      II=3
      CALL PEN(4)
      R=(D(J)-D(1))/30.
      DO 2 N=1,31
      DX=D(1)+FLOAT(N-1)*R
      X=DX*10./U
      CAREA=DX*T
      PER=CAREA/T/W
      Y=SIGMAP*(1.-PER)/9.81/V
      CALL PLOT(X+1.,Y+7.5,II)
    2 II=2
      II=II+1
```

```
      CALL PEN(3)
      DO 5 N=1,31
      DX=D(1)+FLOAT(N-1)*A
      X=DX*10./U
      E=DX/W
      B=1.99-0.41*E+18.7*E**2-38.48*E**3+53.85*E**4
      A6=B*SQRT(DX)
      SIGMA=MEAN/A6*10.
      Y=SIGMA/V
      CALLPLOT(X+1.,Y+7.5,II)
    5 II=2
C     DRAW  KC-VALUES  VERSUS THE CRACK DEPTH
      CALL PEN(1)
      DO 3 N=1,J
      X=D(N)/U*10.
      Y=K(N)/VV
    3 CALL SYMBOL(X+11.5,Y+7.5,0.07,2,0.,-1)
      X=0.
      Y=MEAN/VV
      CALL PLOT(X+11.5,Y+7.5,+3)
      CALL PEN(4)
      CALL PLOT(X+20.5,Y+7.5,2)
      CALL PEN(1)
C     DRAW  1/(SQRT OF THE CRACK DEPTH)*Y-FACTOR AGAINST THE CRACK DEPTH
      DO 4 N=1,J
      X=1./(SQRT(D(N)*10.))/UU
      XX=1./SQRT(D(N)/100.)
      Y=K(N)*XX/VU
    4 CALL SYMBOL(X+1.,Y+1.,0.07,14,0.,-1)
C     DRAW STATISTICS
C     SORT KC
   15 IK=0
      DO 21 I=1,J-1
      IF(K(I).LE.K(I+1))GOTO 21
      BA=K(I)
      K(I)=K(I+1)
      K(I+1)=BA
      IK=IK+1
   21 CONTINUE
      IF(IK.NE.0)GO TO 15
      DO 6 I=1,J
      N=I
      XX=100.*FLOAT(I)/FLOAT(J)
      X=ALOG10(XX)*4.5
      JJ=J-N+1
      Y=K(JJ)/VV
    6 CALL SYMBOL(X+11.5,Y+1.0,0.0700,5,0.0,-1)
      RETURN
      END
```

Program 2 (SF Specimens)

```
00100 PROGRAM KKK(INPUT,OUTPUT,TAPE5=INPUT,TAPE6=OUTPUT)
00101 EXTERNAL FI
00110 11 READ(5,3)A,C,D,P
00120 3 FORMAT(F5.2,2F4.2,F3.0)
00130 IF(A.LE.0) STOP
00150 B=48.50/1000.
00151 C=C/1000.
00160 A=A/1000.
00170 D=D/1000.
00180 P=P*9.81
00181 R=(C**2+A**2/4.)/(2.*C)
00182 TANALF=A/(2.*(R-C))
00183 ALFA=2.*ATAN(TANALF)
00184 S1=ALFA*R**2/2.
00185 S2=(R-C)*A/2.
00186 AREA=S1-S2
00190 SG=P/(B*D)/1.E+6
00200 SN=P/(D*B-AREA)/1.E+6
00201 XK1=1.+.12*(1.-C/A)
00202 H=3.14159*C/2./D
00203 XK2=SIN(H)/COS(H)
00204 XK3=SQRT(XK2/H)
00205 XK4=SG*SQRT(3.14159*C)
00206 XK=XK1*XK3*XK4/FI(A,C)
00240 WRITE(6,1)A,C,D,B,SN,SG,XK
00250 1 FORMAT(8F10.3)
00251 GO TO 11
11115 END
20001 FUNCTION FI(X,Y)
20002 Z1=(X**2-Y**2)/X**2
20004 Z=SQRT(Z1)
20005 FI=ELLICE(Z)
20006 RETURN
20007 END
```

APPENDIX D

COMPUTER PROGRAM FOR IMPACT ANALYSIS

This program is written in FORTRAN IV and was run on the CDC 6400. The program, firstly, analyses the impact results on the basis of linear and yielding fracture mechanics assumptions, as described in Chapter 7. As a result, a line fit and a second degree fit on the energy-$BD\phi$ and energy-ligament area plots are produced, displaying the validity of the brittle and ductile impact theories applied. The pertinent ductile and brittle impact resistances of the material tested are then given in terms of the initial slopes of these plots and the corresponding errors involved are mentioned.

Subsequently, the program attempts to modify the impact data by adding incremental crack lengths pertaining to the slow crack growth and plastic zone length to the initial crack until the best straight line is achieved.

Finally, the impact data are studied on the basis of the composite theory expounded in Chapter 7, so that the initiation and propagation resistances of the material tested are computed.

The program also produces graphs of the results for each test, corresponding to the brittle, ductile and composite impact theories.

The program listed here* is followed by a sample of input and output print out.

---

* The program calls the standard library subroutine NAG4F, the listing of which is not given here (see the footnote of Appendix C).

```
      PROGRAM IMPACT(INPUT,OUTPUT,TAPE5=INPUT,TAPE6=OUTPUT,TAPE62)
      EXTERNAL E01,E02,E03,E04,E05,EXTRAP
      DIMENSION  S(60),B(60),D(60),A(60),X(64),U(64),W(66),R(3),SIG(3),
     +LIG(66),SSIG(3),RR(3),NUM(1),LTIT(3),UX(66)
     +,V(66,2),VV(66,1),Z(2,1),WORK(700),D2(66),DZZ(66),CONSTA(66),F(66)
     +,E(66)
      LOGICAL LLL,LLLL,EPR
      REAL LIG
      LLL=LLLL=.TRUE.
      CALL START(2)
      CALL FACTOR(0.7)
      CALL INTENSE(3)
      CALL NEWPAGE
      CALL BORDOFF
      READ(5,5)  (LTIT(I),I=1,3),G
    5 FORMAT(3A10,F4.1)
      READ(5,4432) N,SW,C,A0
 4432 FORMAT(I2,F2.0,2F5.3)
      C=C*10.
      DO 44332 I=1,N
44332 S(I)=SW
      READ(5,1)  (B(I),D(I),A(I),U(I),I=1,N)
    1 FORMAT((3F4.2,F5.1))
      WRITE(6,9)  (LTIT(I),I=1,3)
    9 FORMAT(1H ,16X,3A10,///,6X,*A= ORIGINAL DATA*,/,6X,16(*=*),//,
     +5X,*SPAN*,6X,1HD,8X,1HB,8X,1HA,6X,5HB*D*0,3X,7HB*(D-A),3X,*ENERGY*,
     +/,X,4(5X,*(MM)*),3X,7H(MM**2),2X,7H(MM**2),4X,*(MJ)*,/,6X,65(*-*))
      CALL SYMBOL(0.05,14.46,0.63,LTIT,0.0,30)
      W(N+1)=1000.
      M=2
      IP=1
      IM=66
      IN=2
      DO 2 I=1,N
      A(I)=A(I)*0.886
      CALL FI(S(I),B(I),D(I),A(I),X(I))
      W(I)=1.
      LIG(I)=D(I)*(B(I)-A(I))
      WRITE(6,3)  S(I),B(I),D(I),A(I),X(I),LIG(I),U(I)
    3 FORMAT(X,F9.1,3F9.2,2F9.2,F9.0)
      A(I)=A(I)+A0-C
      V(I,1)=LIG(I)
      V(I,2)=X(I)
      VV(I,1)=U(I)-G
    2 CONTINUE
      WRITE(6,80)
   80 FORMAT(X,/,6X,65(*-*),//,6X,*1- ADD-PLOT*,*:*)
      DO30I0=1,N
      E(I0)=(U(I0)-G)/X(I0)
   30 F(I0)=LIG(I0)/X(I0)
      N=N+1
      V(N,1)=0.
      V(N,2)=0
      VV(N,1)=1.E-50
      CALL LOOP(V,Z,VV,N,M,IP,IM,IN,EPP,WORK)
      EPROP=0
      DO 49 I=1,N
      ZZ=Z(1,1)*V(I,1)+Z(2,1)*V(I,2)
      D2(I)=VV(I,1)-ZZ
      EPROP=D2(I)**2+EPROP
      DZZ(I)=V(I,2)*V(I,1)*Z(1,1)/Z(2,1)
   49 CONTINUE
      EPROP=SQRT(EPROP/(FLOAT(N-1)))
      N=N-1
      U(N+1)=G
```

```
      NUM(1)=N+2
      X(N+1)=0.
      LIG(N+1)=0.
      DZZ(N+1)=0.
      X(N+2)=0.0
      LIG(N+2)=0.0
      U(N+2)=0.0.
      DZZ(N+2)=0.0
      CALL  GRAF(X,U,NUM,1,-1,13HB*D*D(A/D) MM,13,10HENERGY MJ ,10,9.6,6
     +.)
      CALL GRAF(LIG,U,NUM,1,-1,10HB*(D-A) MM,10,10HENERGY MJ ,10,9.6,6.)
      CALL GRAF(DZZ,U,NUM,1,-1,12H(BR+K*DU) MM,12,10HENERGY MJ ,10,9.6,
     +6.)
      N=N+1
      CALL E02ADF(N,X,U,W,3,NO,SIG,R,LLL)
      SE10=SIG(3)/SQRT(FLOAT(N-2))
      IF(R(1).GE.G) R(1)=6
      SLOPE1=R(2)-2.*SQRT(ABS(R(3)*(6-R(1))))
      WRITE(6,7) LLL,NO,(R(I),I=1,3),SE10,SLOPE1
      CALL E02ADF(N,LIG,U,W,3,NNO,SSIG,RR,LLLL)
      SE20=SSIG(3)/SQRT(FLOAT(N-2))
      IF(RR(3).LE.0.) GO TO 13.
      IF(RR(1).LE.6) RR(1)=6
      SLOPE2=RR(2)+2.*SQRT(RR(3)*(RR(1)-6))
      GO TO 14
   13 IF(RR(1).GE.6) RR(1)=6
      SLOPE2=RR(2)-2.*SQRT(RR(3)*(RR(1)-6))
23451 FORMAT(6X,*LIGAMENT AREA PLOT:*)
   14 WRITE(6,23451)
      WRITE(6,7)LLLL,NNO,(RR(I),I=1,3),SE20,SLOPE2
      CALL E02ADF(N,X,U,W,2,NO,SIG,R,LLL)
      SE30=SIG(2)/SQRT(FLOAT(N-2))
      WRITE(6,432)
  432 FORMAT(X,/,6X,*1- BDO-PLOT:*)
      WRITE(6,10) LLL,NO,(R(I),I=1,2),SE30
      CALL E02ADF(N,LIG,U,W,2,NNO,SSIG,RR,LLLL)
      SE40=SSIG(2)/SQRT(FLOAT(N-2))
      WRITE(6,2794)
 2794 FORMAT(/,6X,*LIGAMENT AREA PLOT*,*:*)
      WRITE(6,10)LLLL,NNO,(RR(I),I=1,2),SE40
      WRITE(6,43569)
43569 FORMAT(6X,65(*-*),//,6X,*MODIFICATATION PROCEDURE*,/,6X,24(*=*),
     +//)
      N=N-1
      SDP=SIG(2)
C
      CALL E02ADF(N,X,U,W,3,NO,SIG,R,LLL)
      IF(R(3).GE.0.) GO TO 44889
88110 DO 4 J=1,150
      STEP=C*FLOAT(J-1)
      STEPP=STEP+A0
      IF(STEPP.GT.4.) GO TO 44889
      DO 6 I=1,N
      A(I)=A(I)+C
      CALL FI(S(I),B(I),D(I),A(I),X(I))
    6 CONTINUE
      CALL E02ADF(N,X,U,W,3,NO,SIG,R,LLL)
      SE50=SIG(3)/SQRT(FLOAT(N-1))
      WRITE(6,12)STEPP,SE50,LLL,NO,(R(I),I=1,3)
   12 FORMAT(6X,*TABLE CRACK GROWTH=*,F6.4,* (MM),  STANDARD ERROR=*,
     +F7.4,* *,4H(MJ),/,6X,L1,I1,*:SECOND DEGREE CURVE FIT=*,3F10.4)
C
    7 FORMAT(6*,L1,I1,*:SECOND DEGREE CURVE FIT=*,F5.1,*+*,
     +F5.3,3H(X+,F5.3,11H*(X+C  (MJ),/,6X,*STANDARD ERROR=*,
     +F6.3,X,4H(MJ),*  INITIAL SLOPE =*,F6.3,10H (KJ/M**2),/)
   10 FORMAT(6X,L1,I1,*:LINE FIT=*,E10.4,*+*,E10.4,3H*X ,
     +4H(MJ),  ',6X,*STANDARD ERROR=*,F6.3,5H (MJ))
C
      IF(R(3).GT.0.) GO TO 8
      SDP=SIG(2)
    4 CONTINUE
    8 IF(ABS(R(2)).LT.0.5E-3) GO TO 88888
```

```
      A0=STEPP-C
      DO 818 I=1,N
  818 A(I)=A(I)-C-C/10.
      C=C/10.
      GO TO 88118
88888 WRITE(6,603)
  603 FORMAT(//,6X,*B=CORRECTED DATA*,/6X,16(*=*))
      WRITE(6,72)
   72 FORMAT(X,//,6X,*SPAN*,6X,1HD,8X,1HP,8X,1HA,6X,5HB*D*D,3X,
     +7HB*(D-A),3X,*ENERGY*,/,X,4(5X,*(MM)*),3X,7H(MM**2),
     +2X,7H(MM**2),4X,*(MJ)*,/,4X,65(*-*))
      DO 13246 I=1,N
      LIG(I)=D(I)*(B(I)-A(I))
C
      WRITE(6,3)S(I),B(I),D(I),A(I),X(I),LIG(I),U(I)
13246 CONTINUE
      CALL GRAF(X,U,NUM,1,-1,13HB*D*D(A+C) MM,13,10HENERGY MJ ,10,9.6,6.
     +)
      GO TO 44879
44889 WRITE(6,20)
   20 FORMAT(1H,//,10X,*PLASTIC CORRECTION DOES NOT CONVERGE*)
44879 DO 12457 I=1,N+1
12457 CONSTA(I)=6
      WRITE(6,189) (V(I,1),V(I,2),CONSTA(I),VV(I,1),DZ(I),I=1,N+1)
  189 FORMAT(//,6X,*C= COMPOSITE THEORY*,/,6X,19(*=*),//,6X,7HB*(D-A),
     +4X,5HB*D*U,4X,*KINETIC*,4X,*ENERGY*,4X,*DIFFER*,/,
     +6X,7H(MN**2),3X,7H(MM**2),4X,*(M J)*,5X,*(M J)*,6X,*(MJ)*,
     +/,(2X,5F10.2))
      WRITE(6,188) ERR,Z
  188 FORMAT(6X,65(*-*),/,6X,*************L2,*************,/,6X,/,
     +6X,*PROPAG. RESIS.=*,F6.4,10H (KJ/M**2),
     +*  INITIAT. RESIS.=*,F6.3,10H (KJ/M**2))
      WRITE(6,187) ERROR
  187 FORMAT(//,6X,*STANDARD ERROR=*,F5.3,5H (MJ),/)
      CALL NEWPAGE
      CALL BORDOFF
      CALL SYMBOL(0.05,14.46,0.63,LTIT,0.0,30)
      N=N+1
      E(N)=0
      F(N)=0
       CALL GRAF(F,E,N,1,-1,15H(1-A/D)/D(A/D)),15,23H(U-K)/(B*D*D(A/D)
     +KJ/M,23,9.6,6.0)
      CALL ENPLOT
      STOP
      END
      SUBROUTINE FI(SS,BB,DD,AA,XAXIS)
      EXTERNAL E01,E02,E03,E04,E05,EXTRAP
      S=SS/BB
      A=AA/BB
      IF(S.GE.4..AND.S.LE.12.) GO TO 1
      CALL EXTRAP(S,A,ANS)
      GO TO 2
    1 IF(S.GT.6.) GO TO 3
      ANS=E01(A)+(E02(A)-E01(A))*(S-4.)/2.
      GO TO 2
    3 IF(S.GT.8.) GO TO 4
      ANS=E02(A)+(E03(A)-E02(A))*(S-6.)/2.
      GO TO 2
    4 IF(S.GT.10.) GO TO 5
      ANS=E03(A)+(E04(A)-E03(A))*(S-8.)/2.
      GO TO 2
    5 ANS=E04(A)+(E05(A)-E04(A))*(S-10.)/2.
    2 XAXIS=ANS*BB*DD
      RETURN
      END
      SUBROUTINE EXTRAP(P,AAAAA,ANS)
      EXTERNAL E01,E02,E03,E04,E05
      LOGICAL LLLL
      DIMENSION Y(5),EIG(5),W(5),S(5),P(4)
      DATA S(1),S(2),S(3),S(4),S(5),W(1),W(2),W(3),W(4),W(5)
     +          /4.,6.,8.,10.,12.,1.,1.,1.,1.,1./
      A=AAAAA
```

```
      Y(1)=E01(A)
      Y(2)=E02(A)
      Y(3)=E03(A)
      Y(4)=E04(A)
      Y(5)=E05(A)
      CALL E02ABF(5,3,Y,M,4,ND,STG,P,LLLL)
      ANS=P(1)+P(2)*P+P(3)*P**2+P(4)*P**3
      RETURN
      END
      FUNCTION E01(X)
      DATA A,B,C,D,E,F
     +          /0.47274538063E-5,-0.822365026414,1.01826500429,-0.566424147
     +056,               0.166342888932,-0.017705624124?/
      T=-ALOG10(X)
      Y=A+T+B*T**2+C*T**3+D*T**4+E*T**5+F*T**6
      E01=10.**(Y)-1.
      RETURN
      END
      FUNCTION E02(X)
      DATA A,B,C,D,E,F
     +          /0.459417835619,-0.571558563308,0.690945209795,-0.32148611
     +9865,              0.070517585925D,-0.0030823537966?/
      T=-ALOG10(X)
      Y=A+T+B*T**2+C*T**3+D*T**4+E*T**5+F*T**6
      E02=10.**(Y)-1.
      RETURN
      END
      FUNCTION E03(X)
      DATA A,B,C,D,E,F
     +          /0.448416351284,-0.332259109332,0.317650071357,0.013065251
     +2460,              -0.091181235202S,0.028742458876?/
      T=-ALOG10(X)
      Y=A+T+B*T**2+C*T**3+D*T**4+E*T**5+F*T**6
      E03=10.**(Y)-1.
      RETURN
      END
      FUNCTION E04(X)
      DATA A,B,C,D,E,F
     +          /0.438677134948,-0.100558389194,-0.093797277010,0.41771669
     +3692,              -0.299732360822,0.071685574285?/
      T=-ALOG10(X)
      Y=A+T+B*T**2+C*T**3+D*T**4+E*T**5+F*T**6
      E04=10.**(Y)-1.
      RETURN
      END
      FUNCTION E05(X)
      DATA A,B,C,D,E,F
     +          /0.437392903379,0.068089556424S,-0.382703647464,0.68801068
     +2884,              -0.433269743848,0.098247019100?/
      T=-ALOG10(X)
      Y=A+T+B*T**2+C*T**3+D*T**4+E*T**5+F*T**6
      E05=10.**(Y)-1.
      RETURN
      END
      NOTRACE
      SUBROUTINE LS00S' (A,X,B,M,N,IP,IM,IN,EPP,WORK)
      DIMENSION A(IM,N),X(IN,IP),B(IM,IP),WORK(1)
      LOGICAL EPP
      DATA ETRE/1.0E-14/
      IMP1=M*N+6*N+M+1
      IMP2=6*N+M+1
      IMP3=5*N+1
      IMP4=4*N+1
      JO=IMP3-1
      JO1=2*N
      CALL PSOC'1,A,WORK,IMP2),M,N,IN)
      CALL DECOMP(M,N,WORK,IMP2),WORK(1),WORK(IMP1),EPP,WORK(5*N+1),
     +            WORK(3*N+1))
      IF(.NOT. EPP) RETURN
      ETA=ETRE**2
      DO 55  I=1,IP
      DO 10  I=1,M
```

```
      JU=JO+I
   10 WORK(JU)=B(I,K)
      CALL SLV  (M,N,WORK(IMP2),WORK(1),WORK(IMP1),WORK(IMP3),
     +           WORK(2*N+1),WORK(IMP4))
      DO 15  I=1,M
      JU=JO+I
   15 WORK(JU)=-PROD2(A,WORK(2*N+1),IM,1,N,I,-B(I,K))
      CALL SLV  (M,N,WORK(IMP2),WORK(1),WORK(IMP1),WORK(IMP3),
     +           WORK(N+1),WORK(IMP4))
      YNORM0=0
      ENORM1=0
      DO 20  I=1,N
      JU=JO1+I
      YNORM0=YNORM0+WORK(JU)**2
      JU=N+I
   20 ENORM1=ENORM1+WORK(JU)**2
      IF(ENORM1.LE. 0.0625*YNORM0) GO TO 25
      ERR=.FALSE.
      RETURN
   25 DO 30  I=1,N
      JU=JO1+I
      JU1=N+I
   30 WORK(JU)=WORK(JU)+WORK(JU1)
      IF(ENORM1 .LT. ETA*YNORM0) GO TO 45
      DO 35  I=1,M
      JU=JO+I
   35 WORK(JU)=-PROD2(A,WORK(2*N+1),IM,1,N,I,-B(I,K))
      CALL SLV  (M,N,WORK(IMP2),WORK(1),WORK(IMP1),WORK(IMP3),
     +           WORK(N+1),WORK(IMP4))
      ENORM0=ENORM1
      ENORM1=0
      DO 40  I=1,N
      JU=N+I
   40 ENORM1=ENORM1+WORK(JU)**2
      IF(ENORM1 .LE. 0.0625*ENORM0) GO TO 25
   45 DO 50  I=1,N
      JU=JO1+I
   50 X(I,K)=WORK(JU)
   55 CONTINUE
      RETURN
      END
      SUBROUTINE DECOMP(M,N,QR,ALPHA,IPIVOT,ERR,YA,SUM)
      DIMENSION QR(M,N),ALPHA(N),IPIVOT(N),YA(N),SUM(N)
      LOGICAL ERR
      DO 5  J=1,N
C
C       ***  J TH. COLUMN SUM  ***
      SUM(J)=PROD1(QR(1,J),QR(1,J),1,M)
    5 IPIVOT(J)=J
C
      DO 40  K=1,N
C     ***  K TH. HOUSEHOLDER TRANSFORMATION  ***
      SIGMA=SUM(K)
      JBAR=K
      L=K+1
      IF(L.GT.N) GO TO 11
      DO 10  J=L,N
      IF(SIGMA .GE. SUM(J)) GO TO 10
      SIGMA=SUM(J)
      JBAR=J
   10 CONTINUE
   11 CONTINUE
      IF(JBAR .EQ. K) GO TO 20
C     ***  COLUMN INTERCHANGE  ***
      I=IPIVOT(K)
      IPIVOT(K)=IPIVOT(JBAR)
      IPIVOT(JBAR)=I
      SUM(JBAR)=SUM(K)
      SUM(K)=SIGMA
      DO 15  I=1,M
```

```
      SIGMA=QR(I,I)
      QR(I,K)=QR(I,JBAR)
   15 QR(I,JBAR)=SIGMA
   20 CONTINUE
      SIGMA=PROD1(QR(1,K),QR(1,K),K,M)
      IF (SIGMA .NE. 0.0) GO TO 22
      ERR=.FALSE.
      RETURN
   22 QRKK=QR(K,K)
      ALPHA(K)=SQRT(SIGMA)
      IF(QRKK .GE. 0.0)  ALPHA(K)=-ALPHA(K)
      ALPHAK=ALPHA(K)
      BETA=1.0/(SIGMA-QRKK*ALPHAK)
      QR(K,K)=QRKK-ALPHAK
      IF (L.GT.N) GO TO 40
      DO 25  J=L,N
   25 YA(J)=BETA*PROD1(QR(1,K),QR(1,J),K,M)
      DO 35  J=L,N
      DO 30  I=K,M
   30 QR(I,J)=QR(I,J)-QR(I,K)*YA(J)
   35 SUM(J)=SUM(J)-QR(K,J)**2
   40 CONTINUE
      RETURN
      END
      SUBROUTINE SLV  (N,N,QR,ALPHA,IPIVOT,R,Y,Z)
      DIMENSION  QR(M,N),ALPHA(N),R(M),Y(N),IPIVOT(N),Z(N)
      DO 10  J=1,N
      GAMMA=PROD1(QR(1,J),R,J,M)/(ALPHA(J)*QR(J,J))
      DO 5  I=J,M
    5 R(I)=R(I)+GAMMA*QR(I,J)
   10 CONTINUE
      Z(N)=R(N)/ALPHA(N)
      NIT=N-1
      DO 15  I=1,NIT
      L=N-I
      LA=L+1
   15 Z(L)=-PROD2(QR,Z,M,LA,N,L,-R(L))/ALPHA(L)
      DO 20  I=1,N
      JU=IPIVOT(I)
   20 Y(JU)=Z(I)
      RETURN
      END
      FUNCTION PROD1(A,B,M,N)
      DIMENSION A(1),B(1)
      DOUBLE PRECISION SUM
C
      SUM=0.
      DO 5  I=M,N
    5 SUM=SUM+DBLE(A(I))*DBLE(B(I))
      PROD1=SUM
      RETURN
      END
      FUNCTION PROD2(A,B,MD,M,N,I,VAL)
      DIMENSION A(MD,1),B(1)
      DOUBLE PRECISION SUM
      SUM=VAL
      DO 5  J=M,N
    5 SUM=SUM+DBLE(A(I,J))*DBLE(B(J))
      PROD2=SUM
      RETURN
      END
      SUBROUTINE PROC1(A,QR,M,N,IM)
      DIMENSION A(IM,N),QR(M,N)
C
      DO 5 I=1,M
      DO 5 J=1,N
    5 QR(I,J)=A(I,J)
      RETURN
      END
```

Title — Uk

IMPACT STRENGTH (HIPS,USSE) 11.0

86	41	0.01	0.51

6.383.150.47108.4
6.363.140.57105.1
6.333.270.64105.1
6.273.150.74 97.4
6.393.180.86 95.2
6.333.191.16 95.2
6.373.161.21 89.7
6.373.151.36 87.5
6.353.151.38 88.6
6.363.171.50 86.4
6.353.271.59 83.1
6.243.161.70 80.8
6.373.191.87 77.5
6.413.162.12 74.2
6.353.202.16 75.3
6.373.162.18 73.1
6.303.152.36 68.6
6.323.242.44 68.6
6.323.182.51 65.3
6.353.172.77 60.8
6.393.162.83 63.1
6.363.162.84 61.9
6.363.142.92 58.6
6.363.142.96 58.6
6.333.143.05 53.0
6.39 3.17 3.19 59.7

D	B	a	I

1. No.
2. Span
3. Initial Correction
4. Incremental Step

IMPACT STRENGTH (HIPS,USSE)

A= ORIGINAL DATA
==========

SPAN (MM)	D (MM)	B (MM)	A (MM)	B*D*D (MM**2)	B*(D-A) (MM**2)	ENERGY (MJ)
41.0	6.38	3.15	.42	34.04	18.79	108.
41.0	6.36	3.14	.51	28.67	18.38	105.
41.0	6.33	3.27	.57	26.94	18.84	105.
41.0	6.27	3.15	.66	22.76	17.69	97.
41.0	6.39	3.18	.76	20.65	17.90	95.
41.0	6.33	3.19	1.03	16.01	16.91	95.
41.0	6.37	3.16	1.07	15.42	16.74	90.
41.0	6.37	3.15	1.20	13.95	16.27	88.
41.0	6.35	3.15	1.22	13.74	16.15	89.
41.0	6.36	3.17	1.33	12.92	15.95	86.
41.0	6.35	3.27	1.41	12.67	16.16	83.
41.0	6.24	3.16	1.51	11.34	14.96	81.
41.0	6.37	3.19	1.66	10.81	15.04	78.
41.0	6.41	3.16	1.88	9.67	14.32	74.
41.0	6.35	3.20	1.91	9.52	14.20	75.
41.0	6.37	3.16	1.93	9.36	14.03	73.
41.0	6.30	3.15	2.09	8.54	13.26	69.
41.0	6.32	3.24	2.16	8.55	13.47	69.
41.0	6.32	3.18	2.22	8.17	13.03	65.
41.0	6.35	3.17	2.45	7.44	12.35	61.
41.0	6.39	3.16	2.51	7.32	12.27	63.
41.0	6.36	3.16	2.52	7.24	12.15	62.
41.0	6.36	3.14	2.59	6.99	11.85	59.
41.0	6.36	3.14	2.62	6.89	11.74	59.
41.0	6.33	3.14	2.70	6.61	11.39	53.
41.0	6.38	3.17	2.83	6.43	11.27	60.

1- BDO-PLOT:
T2:SECOND DEGREE CURVE FIT= 11.0+7.683*X -.151*X**2 (MJ)
STANDARD ERROR= 4.131 (MJ) INITIAL SLOPE = 7.683 (KJ/M**2)

LIGAMENT AREA PLOT:
T2:SECOND DEGREE CURVE FIT= 11.0+2.412*X+ .141*X**2 (MJ)
STANDARD ERROR= .859 (MJ) INITIAL SLOPE = 2.412 (KJ/M**2)

1- BDO-PLOT:
T1:LINE FIT= .1125E+02+ .4363E+01*X (MJ)
STANDARD ERROR=91.583 (MJ)

LIGAMENT AREA PLOT:
T1:LINE FIT= .1098E+02+ .4611E+01*X (MJ)
STANDARD ERROR= 5.953 (MJ)

MODIFICATATION PROCEDURE
==========

```
STABLE CRACK GROWTH=2.7000 (MM),  STANDARD ERROR=   .7589 (MJ)
T2:SECOND DEGREE CURVE FIT=    39.9823   12.4408    -.1093
STABLE CRACK GROWTH=2.8000 (MM),  STANDARD ERROR=   .7616 (MJ)
T2:SECOND DEGREE CURVE FIT=    41.8198   12.4545    -.0866
STABLE CRACK GROWTH=2.9000 (MM),  STANDARD ERROR=   .7644 (MJ)
T2:SECOND DEGREE CURVE FIT=    43.6518   12.4817    -.0646
STABLE CRACK GROWTH=3.0000 (MM),  STANDARD ERROR=   .7673 (MJ)
T2:SECOND DEGREE CURVE FIT=    45.4813   12.5221    -.0432
STABLE CRACK GROWTH=3.1000 (MM),  STANDARD ERROR=   .7702 (MJ)
T2:SECOND DEGREE CURVE FIT=    47.3111   12.5755    -.0227
STABLE CRACK GROWTH=3.2000 (MM),  STANDARD ERROR=   .7733 (MJ)
T2:SECOND DEGREE CURVE FIT=    49.1442   12.6412    -.0029
STABLE CRACK GROWTH=3.3000 (MM),  STANDARD ERROR=   .7765 (MJ)
T2:SECOND DEGREE CURVE FIT=    50.9835   12.7186     .0159
STABLE CRACK GROWTH=3.2000 (MM),  STANDARD ERROR=   .7733 (MJ)
T2:SECOND DEGREE CURVE FIT=    49.1442   12.6412    -.0029
STABLE CRACK GROWTH=3.2100 (MM),  STANDARD ERROR=   .7736 (MJ)
T2:SECOND DEGREE CURVE FIT=    49.3278   12.6484    -.0010
STABLE CRACK GROWTH=3.2200 (MM),  STANDARD ERROR=   .7739 (MJ)
T2:SECOND DEGREE CURVE FIT=    49.5115   12.6557     .0009
STABLE CRACK GROWTH=3.2100 (MM),  STANDARD ERROR=   .7736 (MJ)
T2:SECOND DEGREE CURVE FIT=    49.3278   12.6484    -.0010
STABLE CRACK GROWTH=3.2110 (MM),  STANDARD ERROR=   .7737 (MJ)
T2:SECOND DEGREE CURVE FIT=    49.3462   12.6491    -.0008
STABLE CRACK GROWTH=3.2120 (MM),  STANDARD ERROR=   .7737 (MJ)
T2:SECOND DEGREE CURVE FIT=    49.3645   12.6498    -.0006
STABLE CRACK GROWTH=3.2130 (MM),  STANDARD ERROR=   .7737 (MJ)
T2:SECOND DEGREE CURVE FIT=    49.3829   12.6506    -.0004
STABLE CRACK GROWTH=3.2140 (MM),  STANDARD ERROR=   .7738 (MJ)
T2:SECOND DEGREE CURVE FIT=    49.4013   12.6513    -.0003
STABLE CRACK GROWTH=3.2150 (MM),  STANDARD ERROR=   .7738 (MJ)
T2:SECOND DEGREE CURVE FIT=    49.4196   12.6520    -.0001
STABLE CRACK GROWTH=3.2160 (MM),  STANDARD ERROR=   .7738 (MJ)
T2:SECOND DEGREE CURVE FIT=    49.4380   12.6528     .0001
```

B=CORRECTED DATA
==========

SPAN (MM)	D (MM)	B (MM)	A (MM)	B*D*D (MM**2)	B*(D-A) (MM**2)	ENERGY (MJ)
41.0	6.38	3.15	3.63	4.56	8.65	108.
41.0	6.36	3.14	3.72	4.33	8.29	105.
41.0	6.33	3.27	3.78	4.33	8.33	105.
41.0	6.27	3.15	3.87	3.90	7.55	97.
41.0	6.39	3.18	3.98	3.94	7.67	95.
41.0	6.33	3.19	4.24	3.35	6.66	95.
41.0	6.37	3.16	4.29	3.31	6.58	90.
41.0	6.37	3.15	4.42	3.06	6.14	88.
41.0	6.35	3.15	4.44	3.00	6.02	89.
41.0	6.36	3.17	4.54	2.85	5.75	86.
41.0	6.35	3.27	4.62	2.78	5.64	83.
41.0	6.24	3.16	4.72	2.35	4.80	81.
41.0	6.37	3.19	4.87	2.33	4.78	78.
41.0	6.41	3.16	5.09	2.00	4.16	74.
41.0	6.35	3.20	5.13	1.88	3.90	75.
41.0	6.37	3.16	5.15	1.86	3.86	73.
41.0	6.30	3.15	5.31	1.49	3.13	69.
41.0	6.32	3.24	5.38	1.45	3.05	69.
41.0	6.32	3.18	5.44	1.33	2.80	65.
41.0	6.35	3.17	5.67	1.01	2.15	61.
41.0	6.39	3.16	5.72	.99	2.11	63.
41.0	6.36	3.16	5.73	.93	1.98	62.
41.0	6.36	3.14	5.80	.82	1.75	59.
41.0	6.36	3.14	5.84	.76	1.64	59.
41.0	6.33	3.14	5.92	.60	1.29	53.
41.0	6.38	3.17	6.04	.50	1.07	60.

C= COMPOSITE THEORY
==========

B*(D-A) (MM**2)	B*D*D (MM**2)	KINETIC (M J)	ENERGY (M J)	DIFFER (MJ)
18.79	34.04	11.00	97.40	-2.89
18.38	28.67	11.00	94.10	-.19
18.84	26.94	11.00	94.10	-.51
17.69	22.76	11.00	86.40	-.27
17.90	20.65	11.00	84.20	-1.53
16.91	16.01	11.00	84.20	6.10
16.74	15.42	11.00	78.70	1.76
16.27	13.95	11.00	76.50	2.58
16.15	13.74	11.00	77.60	4.32
15.95	12.92	11.00	75.40	3.58
16.16	12.67	11.00	72.10	-.32
14.96	11.34	11.00	69.80	3.08
15.04	10.81	11.00	66.50	-.07
14.32	9.67	11.00	63.20	.32
14.20	9.52	11.00	64.30	2.02
14.03	9.36	11.00	62.10	.61
13.26	8.54	11.00	57.60	-.28
13.47	8.55	11.00	57.60	-1.10
13.03	8.17	11.00	54.30	-2.37
12.35	7.44	11.00	49.80	-3.67
12.27	7.32	11.00	52.10	-.97
12.15	7.24	11.00	50.90	-1.63
11.85	6.99	11.00	47.60	-3.58
11.74	6.89	11.00	47.60	-3.07
11.39	6.61	11.00	42.00	-7.12
11.27	6.43	11.00	48.70	.22
0	0	11.00	.00	.00

++++++++++ T++++++++++

PROPAG. RESIS.=3.8279 (KJ/M**2) INITIAT. RESIS.= .834 (KJ/M**2)

STANDARD ERROR= .545 (MJ)

REFERENCES

(a) Books of Standards and Manuals

ASTM BOOKS OF STANDARDS (1972a)

"Impact Resistance of Rigid Plastic Sheeting or Parts by Means of a Tup (Falling Weight)",

Part 27, Designation: D3029-72, pp. 787,793.

ASTM BOOKS OF STANDARDS (1972b)

"Impact Resistance of Plastics and Electrical Insulating Materials",

Part 27, Designation: D256-72a, pp. 71-88.

ASTM BOOKS OF STANDARD (1972c)

"Tensile Properties of Plastics",

Part 27, Designation: D638-71a, pp. 185,194.

ASTM BOOKS OF STANDARD (1972d)

"Dynamic Mechanical Properties of Plastics by Means of a Torsional Pendulum",

Part 27, Designation: D2236-70, pp. 645,649.

ASTM BOOKS OF STANDARDS (1973)

"Plane Strain Fracture Toughness of Metallic Materials",

Part 31, Designation: E399-72, pp. 960-979.

BRITISH STANDARDS INSTITUTION (1965)

"Impact Strength",

Part 3, Designation: BS 2782, pp. 149-169.

RHEOVIBRON (1973)

"Direct Reading Dynamic Viscoelastometer",

Instruction Manual, No. 62, Toyo Baldwin Company Limited.

US STEEL CORPORATION - CHEMICAL SECTION (1976)
"Data Log",
Private communications.

(b) Bibliography

ADAMS, C.H., JACKSON, G.B., and McCARTHY, R.A. (1956)
"The utility of impact testing as a criterion of toughness",
Soc. Plastic Eng. J., 12 (13) pp. 121-128.

AGARWAL, B.D., and BROUTMAN, L.J. (1974)
"Three-dimensional finite element analysis of spherical particle composites",
Fibre Sci. Technol., 7 (1) pp. 63-77.

ANDERSON, W.E. (1969)
Battelle Northwest, Report SA-2290.

ANDREWS, E.H. (1964)
"Crystalline morphology in thin films of natural rubber; crystallisation under strain",
Proc. Roy. Soc. 227 (Series A) pp. 562-570.

ANDREWS, E.H. (1968)
Fracture in Polymers,
Oliver & Boyd Limited, Edinburgh/London.

ANDREWS, E.H. (1974)
"Generalised theory of fracture mechanics",
J. Mat. Sci., 9 (6) pp. 887-894.

BALL, G.L. (1971)
"Dynamic mechanical properties; the torsion pendulum and ASTM",
Soc. Plastic Eng., Tech. Paper, 9 (77) pp. 71-77.

BAUMANN, R. (1912)

"Experiment on the effect of width of speciment on the notched bar impact strength",

Z. Ver. Dtsch. Ing., 56, pp. 1311-1314.

BAUER, O., GOELER, F., and SACHS, G. (1928)

"Research on copper and brass",

Z. für Metallkunde, 20, p. 202.

BEGLEY, J.A., and LANDES, J.D. (1972)

"The *J*-integral as a fracture criterion",

Fracture Toughness, *Proc. 1971 National Symp. on Fracture Mechanics*, Part II, ASTM STP514, pp. 1-20.

BILBY, B.A., COTTRELL, A.H., and SWINDON, K.H. (1963)

"The speed of plastic yield from a notch",

Proc. Roy. Soc., 272 (Series A) pp. 304-314.

BIRCH, M.W., and WILLIAMS, J.G. (1977)

"The effect of rate on the impact fracture toughness of polymers",

Int. J. Fracture, to be published.

BLUHM, J.I. (1961)

"A model for the effect of thickness on fracture toughness",

Proc. ASTM, 61, pp. 1324-1331.

BLUHM, J.I. (1962)

"Geometry effect on shear lip and fracture toughness transition temperature for bimodal fracture",

Proc. ASTM, 62, pp. 914-923.

BOBALEK, E.G., and EVANS, R.M. (1961)

Soc. Plastic Eng. Trans., 1, p. 93.

BOLDT, F.A. (1973)

"Impact/crystal polyblends",

Private communication (US Steel Corporation).

BOOGART, V.D.A., and TURNER, C.E. (1963)

"Fracture mechanics - A review of the principles with special reference to applications for glassy plastics in sheet form",

Trans. J. Plast. Inst., 31 (94) pp. 109-117.

BOWIE, O.L. (1964)

"Rectangular tensile sheet with symmetric edge cracks",

J. Appl. Mech., 31 (2) pp. 208-212.

BOYER, R.F. (1968)

"Dependence of mechanical properties on molecular motion in polymers",

Polym. Eng. & Sci., 8 (3) pp. 161-185.

BOYER, R.F., KESKKULA, H., and PLATT, A.E. (1970)

"Styrene polymers",

in Encyclopaedia of Polymer Science and Technology, 13, pp. 128-447, John Wiley & Sons Incorporated.

BRANDRUP, J., and IMMERGUT, E.H. (1974)

Polymer Handbook,

Wiley-Interscience, New York.

BROUTMAN, L.J., and PANIZZA, G. (1971)

Int. J. Polym. Mat., 1, p. 95.

BROWN, H.R. (1973)

"A critical examination of the impact test for glassy polymers",

J. Mat. Sci., 8, pp. 941-948.

BROWN, W.F., and SRAWLEY, J.E. (1966)

"Plane strain crack toughness of high strength metallic materials",

ASTM, STP 410.

BRUGGEMAN, D.A. (1937)

"Die Elastischen Konstanten der Quasiisotropen Mischkörper aus Isotropen Substanzen",

Ann. Phys., 29 p. 160.

BUCKNALL, C.B. (1967)

"The relationship between the structure and mechanical properties of rubber-modified thermoplastics",

Br. Plast., 41 (11 & 12), pp. 118-122 & 84-86.

BUCKNALL, C.B. (1969)

"Current research on the structure and mechanical properties of rubber-modified thermoplastics",

J. Mat. Sci., 4 (1) pp. 214-230.

BUCKNALL, C.B. (1977)

Toughened Plastics,

Materials Science Series, Applied Science Publishers, London.

BUCKNALL, C.B., and CLAYTON, D. (1972)

"Rubber toughening of plastics",

J. Mat. Sci., 7, pp. 202-210.

BUCKNALL, C.B., CLAYTON, D., and KEAST, W.E. (1972)

"Rubber toughening of plastics",

J. Mat. Sci., 7, pp. 1443-1453.

BUCKNALL, C.B., and SMITH, R.R. (1965)

"Stress whitening in HIPS",

Polymer, 6, pp. 437-446.

BUCKNALL, C.B., and STREET, D.G. (1967)

"The fracture behaviour of polyblends over a range of temperatures",

Soc. Chem. Ind. Monograph, 26, pp. 272-280.

BUDIANSKY, B. (1965)

"On the elastic moduli of some heterogeneous materials",

J. Mech. Phys. Solids, 13, pp. 223-227.

BUDIANSKY, B. (1970)

"Thermal and thermoelastic properties of isotropic composites",

J. Comp. Mat., 4, pp. 286-295.

BURDEKIN, F.E., and STONE, D.E.W. (1966)

"The crack opening displacement approach to fracture mechanics in yielding materials",

J. Strain Anal., 1, pp. 145-153.

BURNS, R., and WERRING, W.W. (1938)

"The impact testing of plastics",

Symp. on Impact Testing, Proc. ASTM, 38, pp. 39-52.

CALLENDAR, L.H. (1942)

"New methods for mechanical testing of plastics",

Br. Plast., 13 (155 & 156) pp. 445 & 506.

CHANG, S.S., and BESTUL, A.B. (1968)

"Heat capacities for atactic polystyrene of narrow molecular weight distribution to 360^{o}K",

J. Polym. Sci., Part A2, 6 (5) pp. 849-860.

CHARLTON, M.G., and FARMER, S.N. (1947)

"The impact strength of plastics materials",

Br. Plast., 19 (216) p. 208.

CHARPY, G. (1901)

"Memo on the testing of metals by means of notched bars bent under the application of shocks",

Intern. Assoc. Testing Materials.

CHARPY, G. (1912)

"Report on impact tests and work of the Committee",

Intern. Assoc. Testing Materials (6th Congress), New York, Paper 4.

CHELL, C.G. (1975)

"The stress intensity factors for centre and edge cracked sheets subjected to an arbitrary loading",

Eng. Fract. Mech., 7 (1) pp. 137-152.

CHURCH, H.F., and DAYNES, H. (1937)

"The falling weight impact test for ebonite",

Inst. Rubber Ind. Trans., 13 (2) p. 96.

CIGNA, G. (1970)

"Dynamic mechanical properties, structure and composition of impact polystyrene",

J. Appl. Polym. Sci., 14, pp. 1781-1793.

COTTRELL, A.H. (1961)

"Theoretical aspects of radiation damage and brittle fracture in steel pressure vessels",

Iron & Steel Inst., Special Report No. 69, p. 281.

DAVIES, E.A. (1971)

"The elastic constants of a two-phase composite material",

J. Phys. (Appl. Phys.), D4, pp. 1176-1181.

DEWEY, J.M. (1947)

"The elastic constants of materials loaded with non-rigid fillers",

J. Appl. Phys., 18, pp. 578-581.

DICKIE, R.A. (1973)

"Heterogeneous polymer-polymer composites - Theory of viscoelastic properties and equivalent mechanical models",

J. Appl. Polym. Sci., 17, pp. 45-63.

DUFFY, A.R., McCLURE, G.M., EIBER, R.J., and MAXEY, W.A. (1969)

Fracture,

(ed. Liebowitz, H.), Volume 5, Academic Press.

DUGDALE, D.S. (1960)

"Yielding of steel sheets containing slits",

J. Mech. Phys. Solids, 8, pp. 100-104.

DUNN, B.W. (1897)

"A photographic impact testing machine",

J. Franklin Inst., 144, pp. 321-348.

DUNN, B.W. (1898)

"A photographic impact testing machine",

J. Franklin Inst., 145, pp. 36-47.

EINSTEIN, A. (1906)

Investigations on the Theory of Brownian Motion,

Dover Publishers Incorporated, New York (Translated 1965), pp. 36-62.

ERDOGAN, F.E. (1962)

"On the stress distribution in plates with colinear cuts under arbitrary load",

Proc. 4th US Nat. Congress Applied Mech., University of California at Berkeley.

ESHELBY, J.D. (1957)

"Determination of the elastic field of an ellipsoidal inclusion and related problems",

Proc. Roy. Soc., 241 (Series A) pp. 376-396.

FENNER, D.N. (1973)

"Stress singularity analysis using the eigenfunction-expansion methods",

Ph.D. Thesis, University of London.

FERGUSON, R.J. (1973)

"The fracture of rubber-modified polystyrene",

Ph.D. Thesis, University of London.

FERGUSON, R.J., MARSHALL, G.P., and WILLIAMS, J.G. (1973)

"The fracture of rubber-modified polystyrene",

Polymer, 14, pp. 451-459.

FERGUSON, R.J., and WILLIAMS, J.G. (1973)

"Some observations on the fracture of poly(ethyleneterephthalate) film",

Polymer, 14, pp. 103-106.

FETTWEISS, F.W. (1929)

"Critical resumé on the notch impact test",

Archiv. für das Eisenhüttenwesen, 2, pp. 625-660.

FILLUNGER, P. (1924)

"On notched bar impact values",

Testing, 1 (1) pp. 23,32.

FRASER, R.A.W., and WARD, I.M. (1974)

"The fracture behaviour of notched specimens of polymethylmethacrylate",

J. Mat. Sci., 9 (10) pp. 1624-1630.

GOODIER, J.N. (1933)

"Concentration of stress around spherical and cylindrical inclusions and flaws",

J. Appl. Mech., 55 (7) pp. 39-44.

GOODIER, J.N., and FIELD, F.A. (1962)

"Plastic energy dissipation in crack propagation",

Proc. Int. Conf. on Fracture of Solids, Maple Valley, Washington.

GRIFFITH, A.A. (1921)

"The phenomena of rupture and flaw in solids",

Phil. Trans. Roy. Soc. London, 221 (Series A) pp. 163-198.

GRIFFITH, A.A. (1924)

"The theory of rupture",

Proc. 1st Int. Congress on Applied Mech., Delft, pp. 55-63.

GROSS, B., and SRAWLEY, J.E. (1965)

"Stress intensity factors for three-point bend specimens by boundary collocation",

NASA Technical Note, NASA TN D-3092.

HAIGH, B.H. (1930)

"Brittle fractures in metals",

Engineering, 130, pp. 685,717 & 715.

HALPIN, J.C. (1964)

"Fracture of amorphous polymer solids; time to break",

J. Appl. Phys., 35 (11) pp. 3133-3141.

HALPIN, J.C. (1969)

"Stiffness and expansion estimates for oriented short fibre composites",

J. Comp. Mat., 3, p. 732.

HASHIN, Z (1959)

"The moduli of an elastic solid containing spherical particles of another elastic material",

Proc. IUTAM Symp. on Non-Homogeneity in Elasticity and Plasticity, Warsaw Poland, Pergamon Press, New York, pp. 463-478.

HASHIN, Z. (1962)

"The elastic moduli of heterogeneous materials",

J. Appl. Mech., 29 (Series E) pp. 143-150.

HASHIN, Z. (1964)

"Theory of mechanical behaviour of heterogeneous media",

Appl. Mech. Review, 17 (1) pp. 1-9.

HASHIN, Z. (1970)

"Complex moduli of viscoelastic composites",

Int. J. Solid Structures, 6 (5 & 6) pp. 539-552 & 797-807.

HASHIN, Z., and SHTRIKMAN, S. (1961)

"Note on a variational approach to the theory of elastic composite materials",

J. Franklin Inst., 271, pp. 336-341.

HASHIN, Z., and SHTRIKMAN, S. (1962)

"On some variational principles in anisotropic and non-homogeneous elasticity",

J. Mech. Phys. Solids, 10, p. 335.

HASHIN, Z., and SHTRIKMAN, S. (1963)

"A variational approach to the theory of elastic behaviour of multi-phase materials",

J. Mech. Phys. Solids, 11, p. 127.

HAYES, D.J. (1970)

"Some applications of elastic-plastic stress analysis to fracture mechanics",

Ph.D. Thesis, University of London.

HAYES, D.J., and WILLIAMS, J.G. (1972)

"A practical method for determining Dugdale model solution for cracked bodies of arbitrary shape",

Int. J. Fract. Mech., 8 (3) pp. 239-256.

HAZEN, T. (1943)

"Toughness of moulding materials",

Modern Plastics, 21 (2) p. 103.

HERSHEY, A.V. (1954)

"The elasticity of an isotropic aggregate of anisotropic cubic crystals",

J. Appl. Mech., 21, p. 236.

HILL, R. (1965)

"A self-consistent mechanics of composite materials",

J. Mech. Phys. Solids, 13, pp. 213-222.

HODGKINSON, J.M. (1977)

Private communications, Imperial College.

HOFFMAN, R.D., and RICHMOND, O. (1976)

"Application of the Dugdale model to crazing and fracture in rubber-modified PS",

Annual Meeting of the Division of High Polymer Physics, American Physical Society, Atlanta, Georgia, 29 March - 1 April.

HOUNSFIELD , L.H. (1946)

"Commercial testing",

Plastics, Part 2, Tensometer Limited, Pub. No. 121.

HOUNSFIELD, L.H. (1948)

See Lethersich (1948).

HOWARD, I.G., and OTTER, N.R. (1975)

"On the elastic deformation of a sheet containing an edge crack",

J. Mech. Phys. Solids, 22 (2) pp. 139-149.

HULSE, G., and TAYLOR, W. (1957)

"Impact testing of toughened polystyrene",

Br. Plast., 30 (2) pp. 66-70 & 80.

ILLERS, K.H. (1961)

Zeit Elektrochemie, 56, p. 679.

INGLIS, C.E. (1913)

"Stress in a plate due to the presence of cracks and sharp corners",

Trans. Inst. Naval Arch., 60, pp. 219-225.

IRWIN, G.R. (1948)

"Fracture dynamics - Fracturing of metals",

ASTM, Cleveland, pp. 147-166.

IRWIN, G.R. (1956)

"Onset of fast crack propagation in high strength steel and aluminium alloys",

Proc. 1955 Sagamore Conf. on Strength Limitations of Metals, Syracuse University, New York, pp. 289-305.

IRWIN, G.R. (1960a)

"Fracture mechanics in structural mechanics",

Proc. 1st Naval Symp. on Structural Mechanics, Pergamon Press, New York, pp. 557-594.

IRWIN, G.R. (1960b)

"Fracture testing of high strength sheet materials under conditions appropriate for stress analysis",

US Nav. Res. Memo, Report 5486.

IRWIN, G.R. (1960c)

"Plastic zone near a crack and fracture toughness",

Proc. 7th Sagamore Ordnance Materials Res. Conf., Racquette Lake, New York, Syracuse University Press, METE 661-611/F.

IRWIN, G.R. (1962)

"Crack extension force for a part-through crack in a plate",

J. Appl. Mech., 29, p. 651.

IRWIN, G.R. (1964)

"Structural aspects of brittle fracture",

Appl. Mat. Res., 3 (2) p. 65.

IRWIN, G.R., and KIES, J.A. (1952)

"Fracturing and fracture dynamics",

Weld. J., 31 (Research Suppl.) pp. 95S-100S

IRWIN, G.R., and KIES, J.A. (1954)

"Critical energy rate analysis of fracture strength of large welded structures",

Weld. J., 33 (Research Suppl.) pp. 193S-198S.

IRWIN, G.R. (1957)

"Analysis of stresses and strains near the end of a crack traversing a plate",

J. Appl. Mech., 24, pp. 361-364.

ISHERWOOD, D.P., and WILLIAMS, J.G. (1970)

"The effect of stress-strain properties on notched tensile failure in plane stress",

Eng. Fract. Mech., 2, pp. 19-35.

IZOD, E.G. (1903)

"Testing brittleness of steel - Pendulum apparatus for testing steel as regards brittleness",

Engineering, 76, pp. 431 & 418.

KATO, K. (1967a)

"Osmium tetroxide procedures for light and electron microscopy of ABS plastics",

Polym. Eng. & Sci., 7 (1) pp. 38-39.

KATO, K. (1967b)

"Elektronenmicroskopichen Darstellung van ABS Kunststoffen",

Kolloid-Zeitschrift und Zeitschrift für Polymere, KZZPA, 220, p. 24.

KELLY, A.A. (1973)

Strong Solids,

2nd edition, Clarendon Press, Oxford.

KERNER, E.H. (1956a)

"The electrical conductivity of composite media",

Proc. Phys. Soc., 698, pp. 802-807.

KERNER, E.H. (1956b)

"The elastic and thermoelastic properties of composite media",

Proc. Phys. Soc., 69B, pp. 808-813.

KESKKULA, H., TURLEY, S.G., and BOYER, R.F. (1971)

"The significance of the rubber damping peak in rubber-modified polymers",

J. Appl. Polym. Sci., 15, pp. 351-367.

KNOTT, J.F. (1973)

Fundamentals of Fracture Mechanics,

Butterworth, London.

KOO, G.P. (1974)

"Dynamic mechanical testing of polymers",

Plastics Eng., 30 (5) pp. 33-38.

KUNTZE, W. (1932)

"Kohäsionfestigkeit (cohesion strength)",

Mitt der Deutschen Materialprüf, 20, pp. 1-60.

LAVENGOOD, R.E., NICOLAIS, L., and NARKIS, M. (1973)

"A deformational mechanism in particulate-filled glassy polymers",

J. Appl. Polym. Sci., 17, pp. 1173-1185.

LAVERY, J.H., and SOUTHWELL, R.V. (1934)

"New methods of testing by impact",

Inst. Civ. Engrs., Selected Paper No. 142.

LAWS, N. (1973)

"On the thermostatics of composite materials",

J. Mech. Phys. Solids, 21, pp. 9-17.

LAWS, N. (1974)

"The overall thermoelastic moduli of transversely isotropic composites according to the self-consistent method",

Int. J. Eng. Sci., 12, pp. 79-87.

LEIDNER, J., and WOODHAMS, R.T. (1974)

"The strength of polymeric composites containing spherical fillers",

J. Appl. Polym. Sci., 18, pp. 1639-1654.

LETHERSICH, W. (1946)

"Determination of the plastic and brittle states of pool bitumens",

J. Soc. Chem. Ind., 65 (7) p. 190 (ERA Report Ref. A/T95).

LETHERSICH, W. (1948)

"Impact testing - Critical resume",

The British Allied Industries Research Association, Technical Report Ref. L/T186.

LEVER, A.E., and RHYS, J. (1957)

The Properties and Testing of Plastic Materials,

Temple Press, London.

LEWIS, T.B., and NIELSEN, L.E. (1970)

"Dynamic mechanical properties of particulate-filled composites",

J. Appl. Polym. Sci., 14, pp. 1449-1471.

LIEBOWITZ, H. (1968)

"Fracture - An advanced treatise",

in Mathematical Fundamentals, Volume II, Academic Press, New York.

LIU, H.W. (1965)

"Fracture toughness testing and its applications",

ASTM, STP 381, p. 23.

LUBIN, G., and WINANS, R.R. (1944)

"Preliminary studied on a drop ball impact machine",

ASTM Bull., No. 128, p. 13.

LUDWIK, P. (1923)

"What is there in the notch impact test?",

Stahl U. Eisen, 43, p. 1427.

MACKENZIE, J.K. (1950)

"The elastic constants of solid containing spherical holes",

Proc. Phys. Soc., 63 (Series B) pp. 2-11.

MANN, H.C. (1937)

"A fundamental study of the design of impact test specimens",

Proc. ASTM, 37, p. 102.

MARSHALL, G.P., COUTTS, L.H., and WILLIAMS, J.G. (1974)

"Temperature effects in the fracture of PMMA",

J. Mat. Sci., 9, pp. 1409-1419.

MARSHALL, G.P., CULVER, L.E., and WILLIAMS, J.G. (1973)

"Fracture phenomena in polystyrene",

Int. J. Fracture, 9 (3) pp. 259-309.

MARSHALL, G.P., WILLIAMS, J.G., and TURNER, C.E. (1973)

"Fracture toughness and absorbed energy measurements in impact tests on brittle materials",

J. Mat. Sci., 8, p. 949.

MARTIN, G.M., ROGERS, S.S., and MANDELKERN, L. (1956)

"Temperature relations of amorphous polymers over an extended temperature range",

J. Polym. Sci., 20 (Letters to Editor) pp. 579-581.

MATSUO, M. (1969)

"Fine structures and fracture processes in plastic/rubber two-phase polymer system",

Polym. Eng. & Sci., 9 (3)pp. 206-212.

MATSUO, M., NOZAKI, C., and JYO, Y. (1969)

"Fine structures and fracture processes in plastic/rubber two-phase polymer system",

Polym. Eng. & Sci., 9 (3) pp. 197-205.

MOORE, J.D. (1971)

"An electron microscope study of the microstructure of some rubber-reinforced polystyrene",

Polymer, 12 (8) pp. 478-486.

MORRIS, A.C. (1968)

"Impact strength of thermoplastics",

Plastics & Polymers, 36 (125) pp. 433-443.

MOSER, M. (1925)

"A new method of interpreting notched bar impact test results",

Trans. ASTM, 7, p. 297.

MOSER, M. (1937)

"The development and present position of Continental research on the notched bar impact test",

Manchester Symp., Manchester Assoc. of Engrs., p. 97.

McCLINTOCK, F.A., and IRWIN, G.R. (1965)

"Plasticity aspects of fracture mechanics",

Fracture Toughness Testing and its Applications, ASTM, STP 381, pp. 84-113.

McCRUM, N.G., READ, B.E., and WILLIAMS, G. (1967)

Anelastic and Dielectric Effects in Polymeric Solids,

John Wiley & Sons, London/New York/Sydney.

McGEARY, R.K. (1961)

"Mechanical packing of spherical particles",

J. Am. Ceram. Soc., 44 (10) pp. 513-522.

NADI, A., and MANJOINE, M.J. (1941)

"High speed tension tests at elevated temperatures",

Trans. Am. Soc. Mech. Engrs., 63 (2) p. A77.

NICOLAIS, L., and NARKIS, M. (1973)

"Stress-strain behaviour of styrene-acrylonitrile/glass bead composites in the glassy region",

Polym. Eng. & Sci., 11 (3) pp. 194-199.

NIELSEN, L.E. (1966)

"Simple theory of stress-strain properties of filled polymers",

J. Appl. Polym. Sci., 10, pp. 97-103.

NIELSEN, L.E. (1973)

"Thermal conductivity of particulate-filled polymers",

J. Appl. Polym. Sci., 17, pp. 3819-3820.

NIELSEN, L.E. (1974)

Mechanical Properties of Polymers and Composites,

Marcel Dekker Incorporated, New York.

OLDROYD, J.G. (1956)

"The effect of small viscous inclusions on the mechanical properties of an elastic solid",

in Deformation and Flow of Solids (ed. Grammel), Springer Verlag, Berlin, pp. 304-313.

OROWAN, E. (1945)

"Notch brittleness and the strength of metals",

Trans. Inst. Engrs. Shipbldrs. in Scot., 89, Paper 1063, p. 165.

OROWAN, E. (1949)

"Fracture and strength of solids",

Rep. Prog. Phys., 12, pp. 185-232.

PARIS, P.C., and SIH, G.C. (1965)

"Stress analysis of cracks",

Fracture Toughness Testing and its Applications, ASTM, STP 381, pp. 30-81.

PARIS, P.C., SIH, G.C., and ERDOGAN, F. (1962)

"Crack tip stress intensity factors for plane extension and plate bearing problems",

J. Appl. Mech., 29, p. 306.

PARVIN, M. (1975)

"Thickness, temperature and environmental effects in the fracture of polymers",

Ph.D. Thesis, University of London.

PARVIN, M., and WILLIAMS, J.G. (1975)

"Ductile-brittle fracture transitions in PC",

Int. J. Fracture, 11 (6) pp. 963-972.

PARVIN, M., and WILLIAMS, J.G. (1976)

"The effect of temperature on the fracture of rubber-modified polystyrene",

J. Mat. Sci., 11, pp. 2045-2050.

PETRENKO, S.N. (1925)

"Comparative slow bend and impact notched bar tests on some metals",

US Bureau of Standards, Technical Paper 289, p. 315.

PLATI, E. (1975)

"Application of fracture mechanics to the impact behaviour of polymers",

Ph.D. Thesis, University of London.

PLATI, E., and WILLIAMS, J.G. (1975a)

"The determination of the fracture parameters for polymers in impact",

Polym. Eng. & Sci., 15 (16) pp. 470-477.

PLATI, E., and WILLIAMS, J.G. (1975b)

"Effect of temperature on the impact fracture toughness of polymers",

Polymer, 16, pp. 915-920.

RICE, J.R. (1967)

"Stress due to a sharp notch in a work-hardening elastic material loaded by longitudinal shear",

J. Appl. Mech., 34, p. 287.

RICE, J.R. (1968)

"A path-independent integral and approximation analysis of strain concentration by notches and cracks",

J. Appl. Mech., 35, pp. 379-386.

RICE, J.R. (1973)

"Elastic-plastic fracture mechanics",

Eng. Fract Mech. (Compendium), 5, pp. 1019-1022.

RICE, J.R., PARIS, P.C., and MERKLE, J.G. (1973)

"Some further results of J-integral analysis and estimates",

Progress in Flow Growth and Fracture Toughness Testing, ASTM, STP 536, pp. 231-245.

RICE, J.R., and ROSENGREN, G.F. (1968)

"Plane strain deformation near a crack tip in a power law hardening material",

J. Mech. Phys. Solids, 16, pp. 1-12.

ROELIG, H. (1945)

"The dependence of damping and dynamic modulus on temperature as a means of evaluating the elastic behaviour of raw and vulcanised rubber",

Rubber Chem. Technol., 18, pp. 62-70 (translated from *Kautschuk*, 19, (1943), pp. 47-49).

RUSSELL, S.8. (1898)

"Experiments with a new machine for testing materials by impacts",

Trans. Am. Soc. Civ. Engrs., 39, pp. 237-272.

SATO, Y., and FURUKAWA, J. (1962)

"A molecular theory of filler reinforcement based upon the conception of internal deformation - A rough approximation of the internal deformation",

Rubber Chem. Technol., 35, p. 857 & 36, pp. 1081-1106.

SAUERWALD, F., and WIELAND, H. (1926)

"The notched impact test of Schüler-Moser and the notch toughness of brass, copper and aluminium at different temperatures",

Stahl U. Eisen, 46, p. 546.

SCOTT, G.D. (1960)

"Packing of spheres",

Nature, 188 (4754) pp. 908-909.

SIH, G.C. (1962)

"On the singular character of thermal stresses near a crack tip",

J. Appl. Mech., 29, p. 587.

SIH, G.C. (1973)

Method of Analysis and Solution to Crack Problems,

Noordhof International Publishing, Leyden.

SMITH, T.L. (1963)

"Ultimate tensile properties of elastomers. 1. Characterisation by a time and temperature independent failure envelope",

J. Polym. Sci., Part A, 1 (12) pp. 3597-3615.

SMITH, T.L. (1964)

"Relations between ultimate tensile properties of elastomers and their structure",

Proc. Roy. Soc., 282 (Series A) pp. 102-113.

SMITH, F.W. (1966)

The Boeing Company, SDRM No. 17, August 1966.

SNEDDON, I.N. (1946)

"The distribution of stress in the neighbourhood of a crack in an elastic solid",

Proc. Roy. Soc. London, 187 (Series A) pp. 229-260.

SRAWLEY, J.E., and BROWN, W.F. (1965)

"Fracture toughness testing methods",

Fracture Toughness Testing and its Applications, ASTM, STP 381, pp. 133-198.

STEPHENSON, C.E. (1957)

"An appraisal of the Izod impact test for plastics",

Br. Plast., 3, pp. 99-104.

STOCK, C.R. (1944)

"A ball impact tester for plastics",

ASTM Bull., No. 130, p. 21.

SWEDENBORG, . (1734)

"Traité de Fer".

TAKAYANAGI, M. (1963)

"Viscoelastic properties of crystalline polymers",

Memoirs of the Faculty of Engineering (Kyushu University), 23 (1) pp. 41-96.

TAKAYANAGI, M., HARIMA, H., and IWATA, Y. (1963)

"Viscoelastic behaviour of polymer blends and its comparison with model experiments",

Memoirs of the Faculty of Engineering (Kyushu University), 23 (1) pp. 1-13.

TELFAIR, D., and NASON, H.K. (1943)

"Impact testing of plastics - Energy consideration",

Modern Plastics, 20 (11) p. 85 (also, *Proc. ASTM*, 43, p. 1211).

THEOCARIS, P.S. (1974)

"Determination of crack opening displacement by the method of caustics",

J. Strain Anal., 9 (3) pp. 197-205.

TIMOSHENKO, S.P., and GOODIER, J.N. (1970)

Theory of Elasticity,

McGraw-Hill Book Company, New York/London/Tokyo.

TREDGOLD, D.T. (1924)

Strength of Cast Iron,

J. Taylor, London, pp. 245-268.

THURSTON, R.H. (1874,1875,1876)

"On the mechanical properties of materials of construction",

Trans. Am. Soc. Civ. Engrs., 3, pp. 1-30, 4, pp. 265-276, 6, p. 102.

TURLEY, S.G. (1963)

"A dynamic mechanical study of rubber-modified polystyrenes",

J. Polym. Sci., Part C, 1, pp. 101-116.

TURLEY, S.G. (1967)

ACS Preprints, Chicago, p. 1524.

TURNER, C.E. (1972)

"Fracture mechanics and strength of non-metallic materials",

Phys. Bull., 23, pp. 669-672.

VINCENT, P.I. (1971)

"Impact tests and service performance of thermoplastics",

Plastic Inst. Monograph.

VITMAN, F., and STEPANOV, W. (1939)

"On the influence of the deformation rate on the brittleness of steel",

J. Tech. Phys. (USSR), 9, p. 1070.

WEISS, V., and SESSLER, J.G. (1962)

"Analysis of the effect of test temperature on the notch strength of high strength sheet alloys",

ASTM, STP 302, pp. 3-20.

WEISS, V., and YUKAWA, S. (1965)

"Critical appraisal of fracture mechanics",

Fracture Toughness Testing and its Applications, ASTM, STP 381, pp. 1-26.

WELLS, A.A. (1965)

"The application of fracture mechanics to yielding materials",

Proc. Roy. Soc., 285 (Series A) p. 34.

WESTERGAARD, H.M. (1939)

"Bearing pressures and cracks",

J. Appl. Mech., 61 (Series A) pp. 49-53.

WETTON, R.E., MOORE, J.D., and INGRAM, P. (1973)

"Transition magnitudes and impact improvement in rubber-modified plastics",

Polymer, 14, pp. 161-166.

WIGGLESWORTH, L.A. (1957)

"Stress distribution in a notched plate",

Mathematika, 4 (7) pp. 76-96.

WILKINSON, C.S., and GEHMAN, S.D. (1950)

"Hysteresis determinations with the Goodyear-Roelig machine",

Anal. Chem., 22 (2) pp. 283-289.

WILLIAMS, J.G. (1972)

"Viscoelastic and thermal effects on crack growth in PMMA",

Int. J. Fract. Mech., 8 (4) pp. 393-401.

WILLIAMS, J.G. (1973)

Stress Analysis of Polymers,

Longman, London.

WILLIAMS, J.G., and BIRCH, M.W. (1977)

"The impact testing of polymers - A reassessment",

Proc. 4th Int. Conf. on Fracture (ICF4), 1, Part IV, pp. 501-528,

University of Waterloo, Ontario, Canada.

WILLIAMS, M.L. (1957)

"Stress distribution at the base of a stationary crack",

J. Appl. Mech., 24, p. 104.

WOLSTENHOLME, W.E., PREGUM, S.E., and STARK, C.E. (1964)

"Factors influencing Izod impact properties of thermoplastics measured with autographic impact test",

J. Appl. Polym. Sci., 18, p. 119.

YOSHINO, M., and TAKAYANAGI, M. (1959)

Japan Soc. Test. Mat., 8, p. 330.

ZENER, C., and HOLLOMAN, J.H. (1944)

"Plastic flow and rupture of metals",

Trans. Am. Soc. Metals, 33, pp. 163-235.

ZINZOW, W.A. (1938)

"Discussion on the impact testing of plastics",

Proc. ASTM, 38, p. 52.

AN IMPACT STRENGTH ANALYSIS OF SOME RUBBER MODIFIED POLYSTYRENES

by

K. Nikpur and J.G. Williams

Department of Mechanical Engineering
Imperial College of Science and Technology
London SW7 2BX

ABSTRACT

The classification of impact failures is discussed and four types are defined; namely, brittle, semi-brittle, semi-ductile and ductile. The failures observed in rubber modified polystyrenes are shown to be semi-ductile in which the absorbed energy is essentially linear with ligament area because of extensive crazing but with a deviation caused by the subsequent brittle fracture of the matrix. It is shown that it is possible to deduce an equivalent ductile energy per unit area, G_d, and a true matrix toughness, G_c. G_d is shown to be proportional to rubber content in two sets of blended resins while G_c remains constant. The method was also successful on several commercial grades.

INTRODUCTION

There has been a good deal of success in using linear elastic fracture mechanics to describe crack growth in polymers (e.g. 1,2,3) and, in particular, brittle failures in impact (4,5). In common with other materials, however, interest inevitably turns to describing materials which show sufficient toughness not to be fully brittle and, indeed, materials which are quite ductile. Fully ductile behaviour may neither need, nor yield to, description in fracture mechanics terms but there is much interest in materials which show substantial ductility along with brittle failures. Such materials are the rubber modified polystyrenes, which are investigated here. The addition of rubber particles to the polystyrene matrix induces craze formation which provides a ductile process but the inherently brittle matrix is unchanged.

This paper discusses the classification of impact failures and then describes a series of experiments on various types of rubber modified polystyrene. The analysis of the results in fracture mechanics terms is then considered.

FRACTURE CLASSIFICATION AND ANALYSIS

It is normal practice to classify the impact failures of polymers in either the Izod or Charpy tests according to the degree of deformation encountered (e.g. 6). One extreme is the brittle fracture in which there is a flat, smooth surface with little or no distortion. This is illustrated in Figure 1(a), together with the triangular load deflection diagram which is associated with this type of fracture. The other extreme is that of ductile failure in which there is gross plastic deformation in the ligament of the specimen which results in large energy absorption and a load-deflection diagram, as shown in Figure 1(d). In conventional testing, the impact strength is described in terms of the energy absorbed, U_1, per unit of ligament area, A. i.e.

$$Impact\ strength = U_1/A$$

For ductile failures, this parameter is often reasonably constant with specimen geometry, although it really describes the energy to deform the ligament prior to, and perhaps during, fracture while the energy per unit area to actually cause rupture is a very small part of the total.

For the brittle failure, the energy per unit area is not constant since the fracture is initiated as a classical Griffith type when:

$$\frac{dU_1}{da} = G_c$$

This analysis has now been very thoroughly investigated for the impact test (e.g. 5) and a true measure of G_c is given by:

$$G_c = \frac{U_1}{B\ D\ \phi} \qquad \text{——— (1)}$$

where B = specimen breadth;

D = specimen depth; and

ϕ = a geometrical factor which can be deduced for any geometry (4).

If impact tests are performed with specimens with various crack lengths, the energy should be linear with ϕ for brittle fracture (and not ligament area), while for ductile failure it will be linear with ligament area (and not ϕ).

Between these two extremes, it is useful to identify intermediate cases and these are also illustrated in Figure 1. The first (Figure 1(b)) may be termed semi-brittle and describes those cases which are essentially brittle but with some curvature in the loading line. This may be caused either by the growth of a plastic zone prior to crack initiation or by slow stable crack growth prior to crack instability. Providing the zone size or crack growth are small, a satisfactory solution for G_c may be obtained by correcting ϕ by using a crack length to which a length correction is added. The U_1 versus uncorrected ϕ in this case is almost linear but with a slight downward curvature, as illustrated in Figure 2. The length correction is chosen to achieve a straight line with minimum deviation. Also shown in Figure 2 is a positive intercept on the energy axis, U_k, which is the kinetic energy which may be determined separately. The addition of either a plastic zone or crack growth term generally produces substantial G_c values with little scatter and the method has been shown to work well on polyethylene and PTFE (7).

It should be noted in passing here that in the often very low G_c values of purely brittle failures, there is a major problem with kinetic energy scatter which is best corrected by taking a lower bound on the U_1 versus $BD\phi$ graph (8).

The second intermediate case, and that to be studied here, is shown in Figure 1(c) and is termed semi-ductile. Here, a fully plastic ligament is formed but there is subsequently an unstable brittle fracture. U_1 is now

predominantly governed by ligament area, as in the ductile case, but there is now some upward curvature on this graph, particularly at the smaller crack lengths (high areas), as shown in Figure 3. The intercepts are often unreliable on ductile plots since the linearity is caused by a uniform zone width in the ligament which does not occur for small areas. For the semi-ductile values, however, there is generally a positive intercept on the energy axis of U_k.

It is suggested here that this type of fracture may be usefully described by attributing an apparent surface energy, G_d, to give the plastic deformation and a subsequent true crack propagation value, G_c. The energy equation now becomes:

$$U_1 = G_c B D \phi + G_d A \qquad \text{——} \quad (2)$$

and this will now be investigated when applied to rubber modified polystyrene polymers. Such behaviour is probably unique to rubber modified polymers since the rubber modification results in craze initiation from the rubber particles. This is the energy absorption process which renders the process ductile but it occurs essentially with no distortion of the crack tip, and consequent blunting, since there is a substantial volume increase during crazing. Thus, large amounts of energy may be absorbed in these systems without the geometry changes induced in the ductile deformation of most homogeneous materials.

EXPERIMENTAL PROGRAMME

Three groups of materials were tested. In one series, a 5.55% rubber modified grade was back-blended with the unmodified matrix polystyrene to give rubber contents of 0, 1.11, 2.22, 3.33 and 5.55% rubber. In a second series, a 3.33% composite was used, giving only four values. Care was taken in the blending operation to minimise any molecular weight changes in the polystyrene and only small changes were observed. This was found to be the most satisfactory way of producing materials in which only one variable, in this case rubber content, was varied. In addition, a group of commercial resins termed Super, Standard and Medium impact polystyrenes were also tested and analysed.

Charpy impact specimens with a test span of 41 mm, B = 3.1 mm and D = 6.3 mm were machined from extruded sheets and sharp notches of various lengths were cut with a single point fly cutter. For each test, a set of specimens with various crack lengths was broken in an accurate pendulum impact machine (9) at 20°C and the energies recorded.

RESULTS

Only one material, S1 (the polystyrene used in the first series), showed brittle failure and Figure 4 shows U_1 plotted versus $BD\phi$. The considerable scatter due to kinetic energy is apparent but there is a well-defined lower bound (8) which gives G_c = 0.41 kJ/m^2.

All the other materials gave pronounced non-linearity when plotted on the basis of $BD\phi$ but, on a ligament area basis, gave linearity over some of the data, as shown in Figure 5 for material S3. This form is that for semi-ductile behaviour (see Figure 3). For small ligament areas, i.e. long crack lengths, we have that (5):

$$B\ D\ \phi \rightarrow A/2$$

so that equation (2) becomes:

$$U_1 = (G_d + G_c/2)\ A$$

Thus, a line drawn, as shown in Figure 5, will give an average G_d value given by:

$$G_{d_{av}} = G_d + G_c/2$$

The two separate values may be obtained by using equation (2) for all the points and this was done using two methods. In the first, equation (2) was written as:

$$U_1 = G_c\ (B\ D\ \phi + k\ A)$$

and k was adjusted using a computer program to give a minimum deviation from a straight line. G_c is given by the slope of this line and $G_d = k\ G_c$. Figure 6 shows the data plotted as U_1 versus $BD\phi + kA$ after this analysis has been

performed indicating good linearity. The alternative is to rearrange the equation as:

$$\frac{U_1 - U_k}{B\ D\ \phi} = G_c + G_d \frac{A}{B\ D\ \phi}$$

and then replot the data, as shown in Figure 7, where G_d is the slope and G_c is the intercept. Similar plots for the commercial grades are shown in Figure 8, again showing good linearity. The two methods gave identical results and Table I shows the collected data for all the materials tested.

DISCUSSION

Table I indicates quite close agreement between $G_{d_{av}}$ and $G_d + G_c/2$, in accordance with the theoretical expectations. G_c is always the smaller of the two values and, for the higher energies, is difficult to determine with precision. However, it is clear that, for the two sets of blended materials, G_c remains essentially constant at the resin value for the various rubber contents. This supports the concept that the energy described in G_d is dissipated prior to fracture and a crack then propagates through the matrix material which is initiated at G_c.

G_d is strongly dependent on rubber content as expected and Figure 9 shows a linear dependence for both materials. The matrix resin of the SS series behaved as if it contained some modifier since it exhibited crazing and gave semi-ductile data. A comparison of the two lines in Figure 9 would indicate an equivalent rubber content of 0.67% and it is suggested that this may be due to the presence of mineral oil which can behave in a similar way to rubber.

The linear dependence of G_d on rubber content is sensible since the particle sizes are the same for all the materials, so that each rubber content reflects the number of particles. It is these particles which generate the crazes which absorb the energy so that G_d would be proportional to the number of them and hence to the rubber content. It is of interest to note that, although G_c is slightly higher for the SS materials, the G_d dependence of rubber content is the same, indicating that it is not governed by G_c.

The rubber content of the commercial grades is not known but they may be estimated from the G_d values and Figure 9. The Super grades (C1,2) appear to have up to 6.5% rubber, the Standard (C3-8) 5.2%, and the Medium (C9,10) 3.5%. It is notable, however, that the matrix toughness, G_c, is substantially greater (× 3.5) in the Super grades and the Standard (× 2) than the Medium grades, indicating the necessity of not only higher rubber contents, but also tougher matrices to achieve high toughness.

ACKNOWLEDGEMENT

The authors wish to express their appreciation to US Steel Chemicals, who provided the materials used here and also financial support.

REFERENCES

1. Marshall, G.P., Coutts, L.H., and Williams, J.G.
J. Mater. Sci., 9, 1974, 1409.

2. Parvin, M., and Williams, J.G.
J. Mater. Sci., 11, 1976, 2045.

3. Williams, J.G.
Polym. Engng & Sci., 17, 1977, 144.

4. Plati, E., and Williams, J.G.
Polym. Engng & Sci., 15, 1975, 470.

5. Williams, J.G., and Birch, M.W.
Proc. 4th Int. Conf. on Fracture (ICF4), 1, Part IV, 1977, 501,
University of Waterloo, Canada, 19-24 June.

6. Vincent, P.I.
"Impact Tests and Service Performance of Thermoplastics",
Plastics Inst. Monograph, 1971.

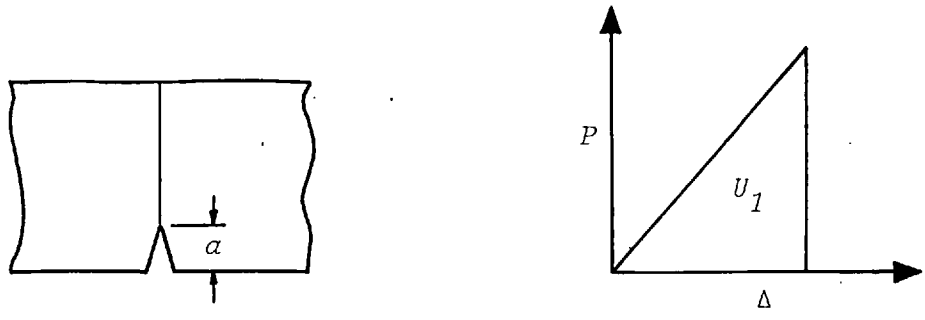
7. Birch, M.W., and Williams, J.G.
Int. J. Fracture, to be published.

8. Newmann, L.V., and Williams, J.G.
"The Impact Behaviour of ABS Over a Range of Temperatures", in preparation.

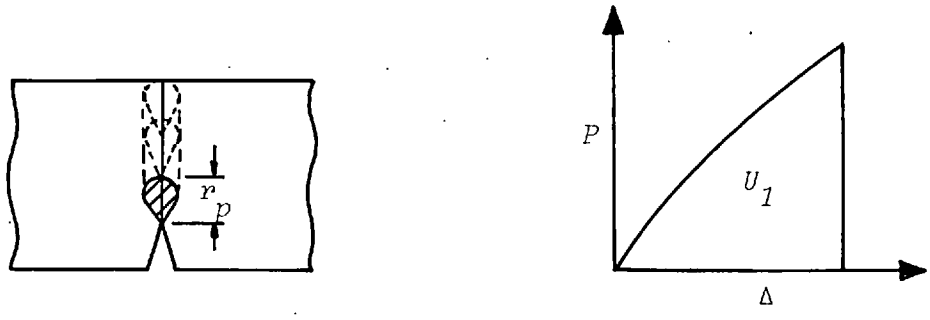
9. Plati, E., and Williams, J.G.
Polymer, 16, 1975, 915.

TABLE I

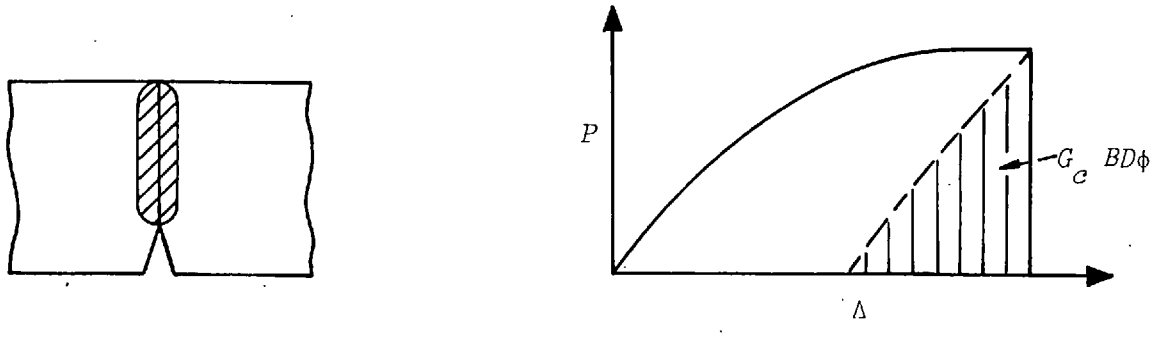
Grade	Rubber Content (% vol.)	$G_{d_{av}}$ (kJ/m^2)	G_d (kJ/m^2)	G_c (kJ/m^2)	$G_d + G_c/2$ (kJ/m^2)
S1	0	-	-	0.4	-
S2	1.11	1.2	1.0	0.4	1.2
S3	2.22	2.7	2.5	0.3	2.65
S4	3.33	4.1	3.9	0.3	4.05
S5	5.55	6.1	5.6	0.4	5.8
SS1	0	1.1	0.8	0.5	1.05
SS2	1.11	1.5	1.6	0.5	1.85
SS3	2.22	3.6	3.6	0.2	3.7
SS4	3.33	4.8	4.4	0.4	4.6
C1 } "Super"	-	6.7	6.3	1.1	6.85
C2 } "Super"	-	4.7	4.8	0.9	5.25
C3	-	4.3	4.0	0.8	4.4
C4	-	4.4	4.0	0.8	4.4
C5 } "Standard"	-	4.4	3.9	0.7	4.25
C6 } "Standard"	-	4.0	3.8	0.8	4.2
C7	-	4.0	3.6	0.8	4.0
C8	-	3.5	3.2	0.7	3.55
C9 } "Medium"	-	3.1	2.9	0.4	3.1
C10 } "Medium"	-	2.5	2.4	0.3	2.55



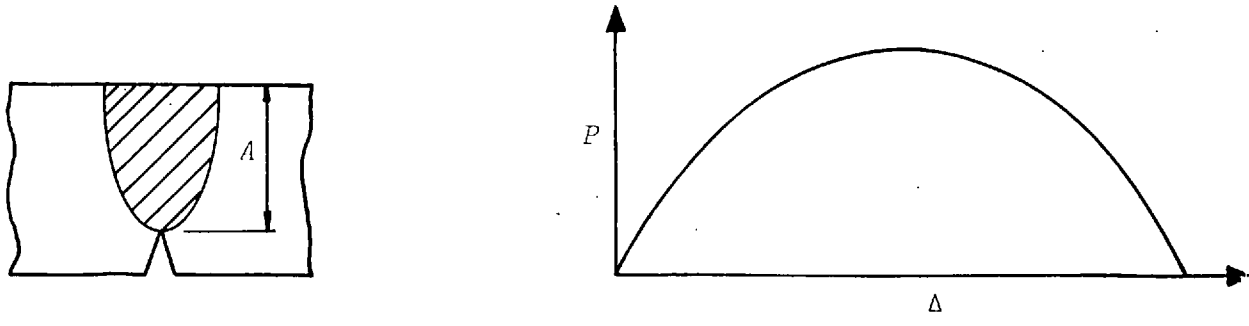
(a) Brittle



(b) Semi-brittle



(c) Semi-ductile



(d) Ductile

Figure 1: Modes of failure

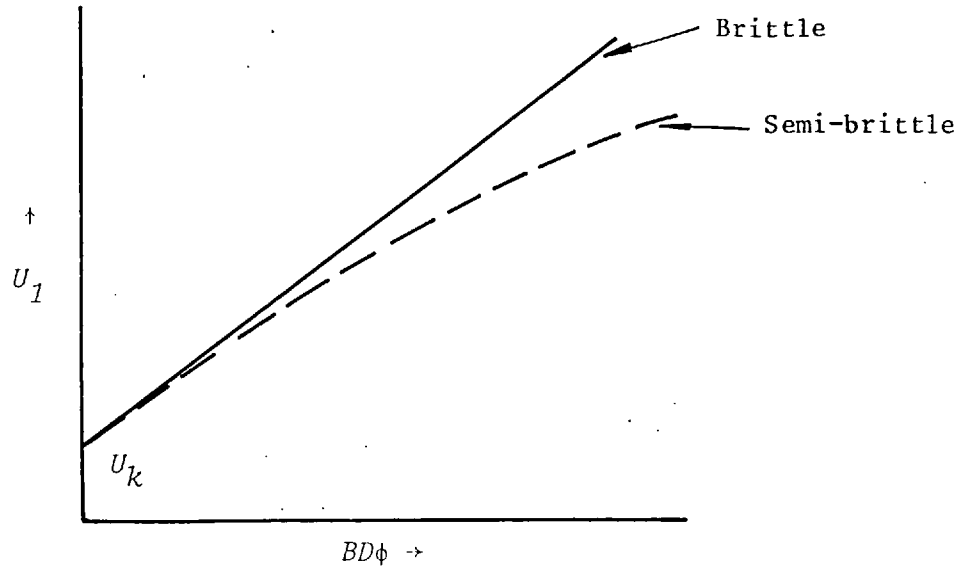


Figure 2: Brittle and semi-brittle behaviour

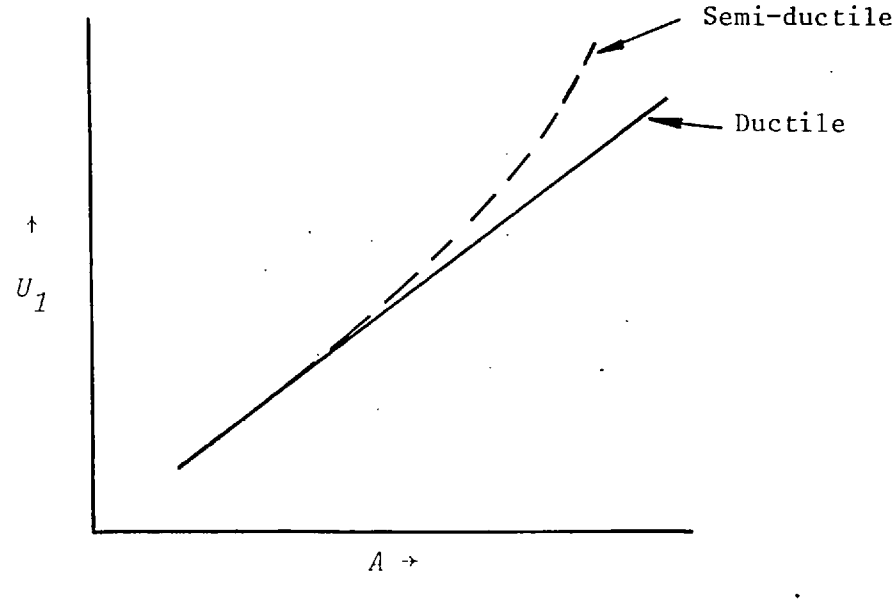


Figure 3: Ductile and semi-ductile behaviour

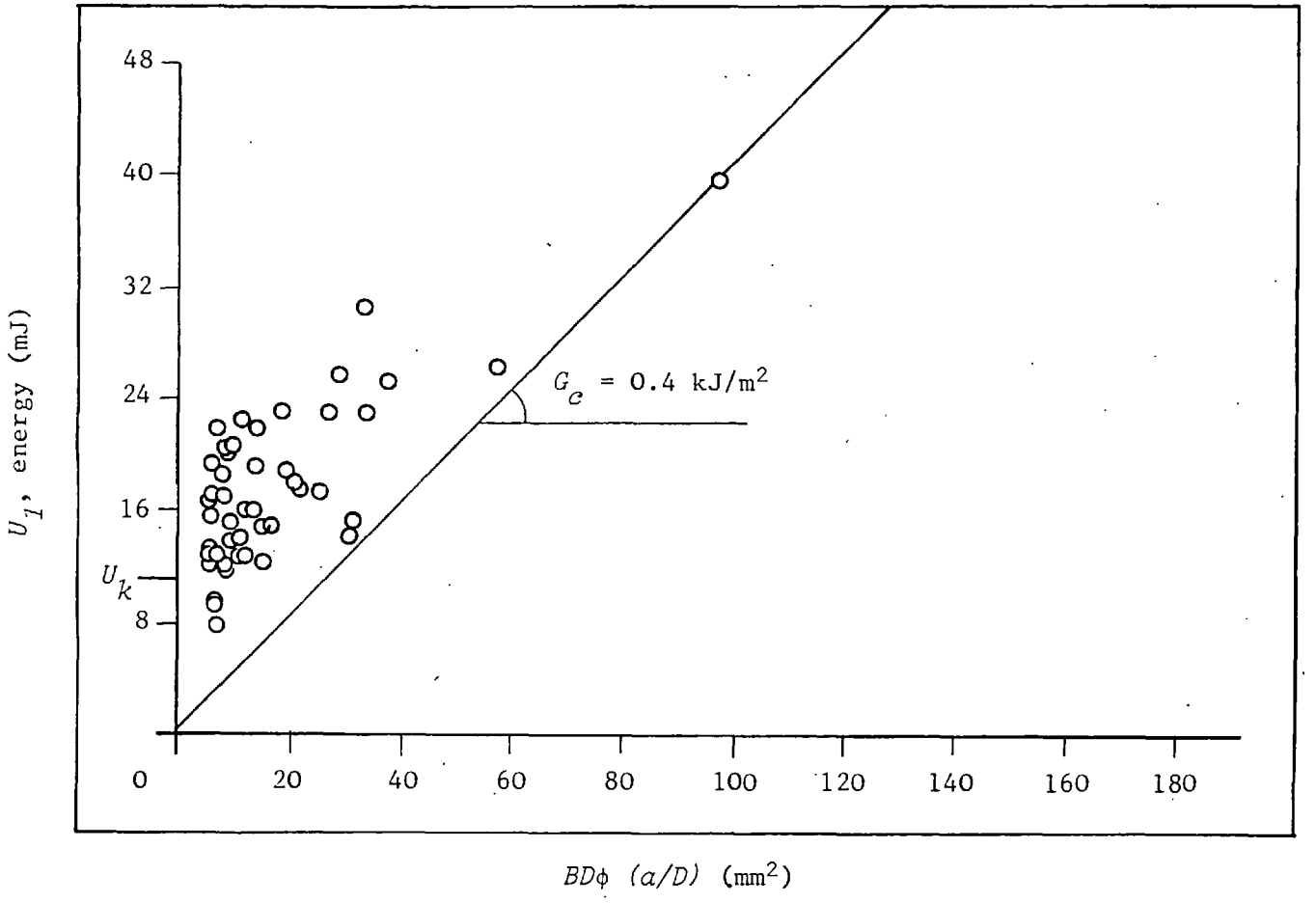


Figure 4: Grade S1 (0% rubber content) - Plotted on the basis of brittle theory

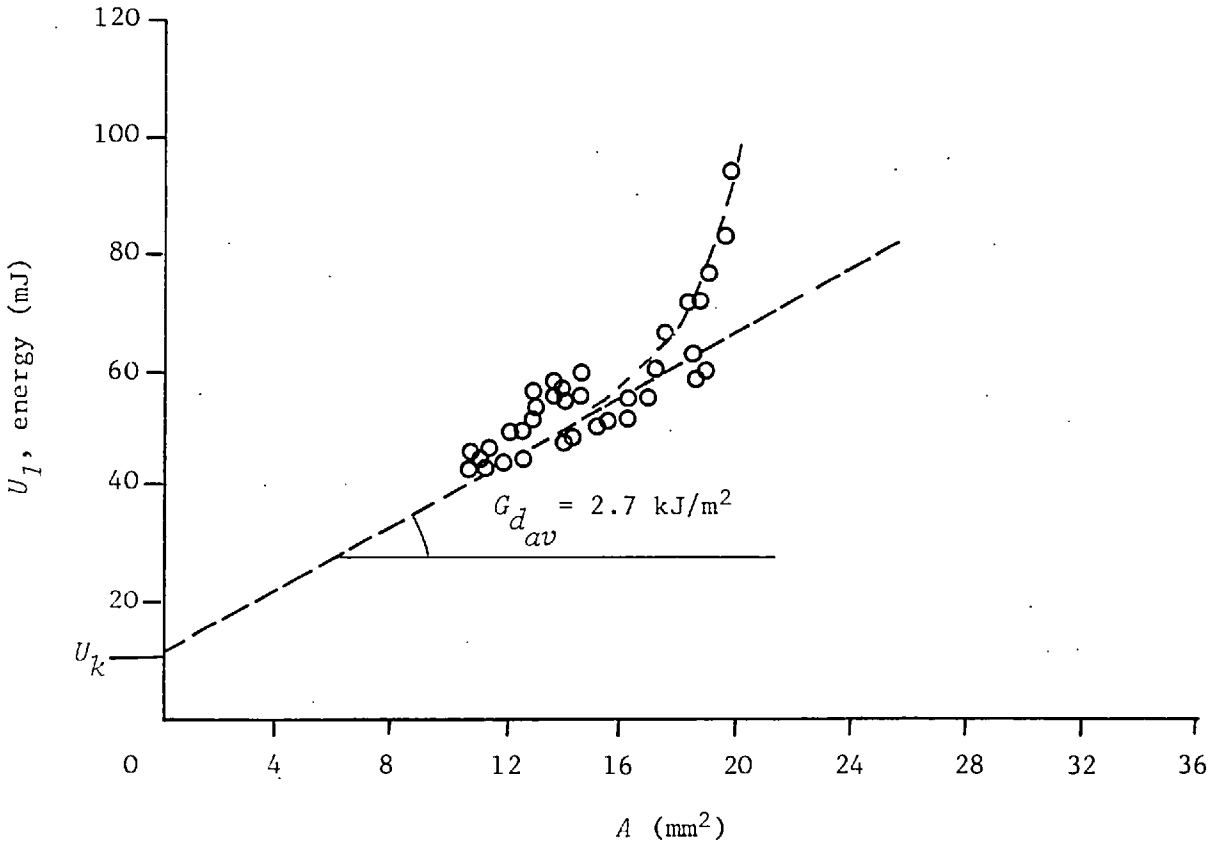


Figure 5: Grade S3 (2.22% rubber content) - Energy versus ligament area

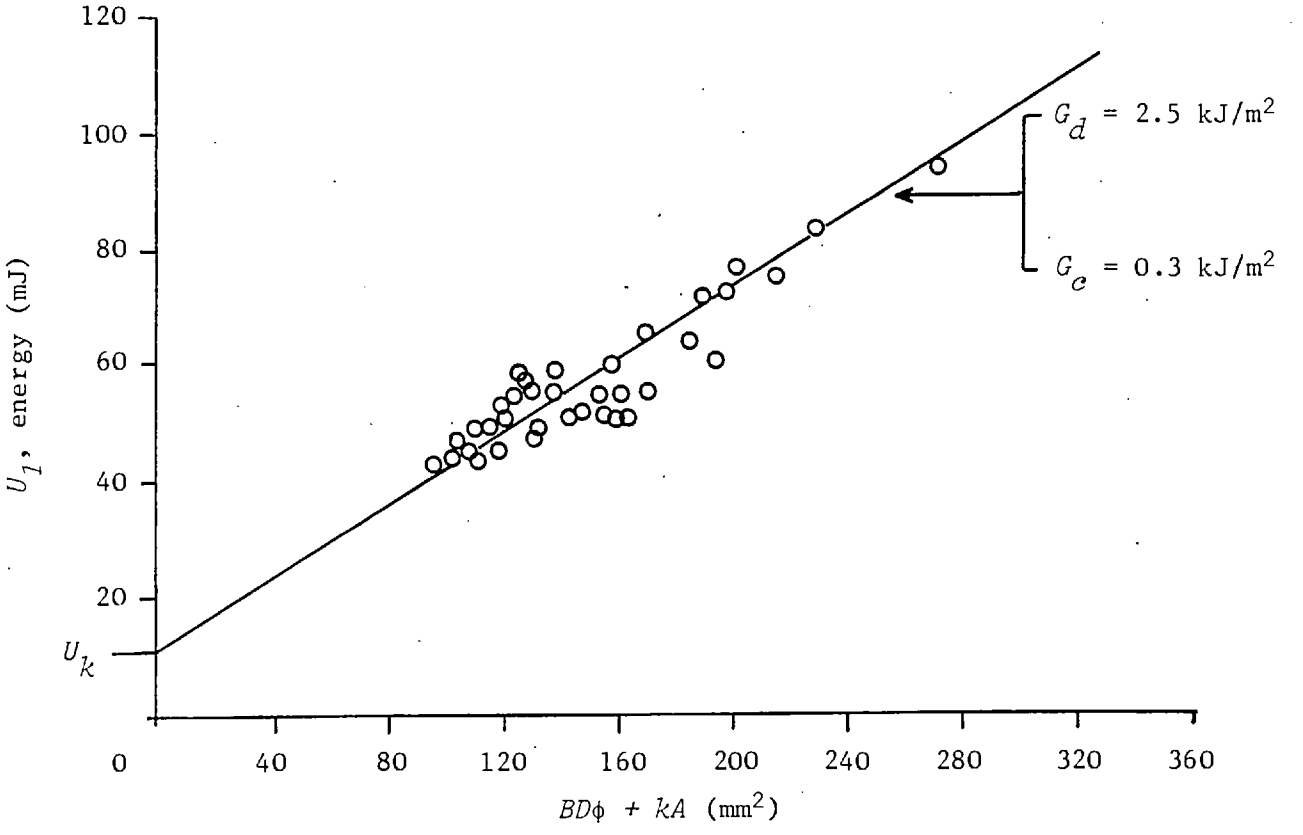


Figure 6: Grade S3 (2.22% rubber content) - Numerical analysis of data (k = 8.33)

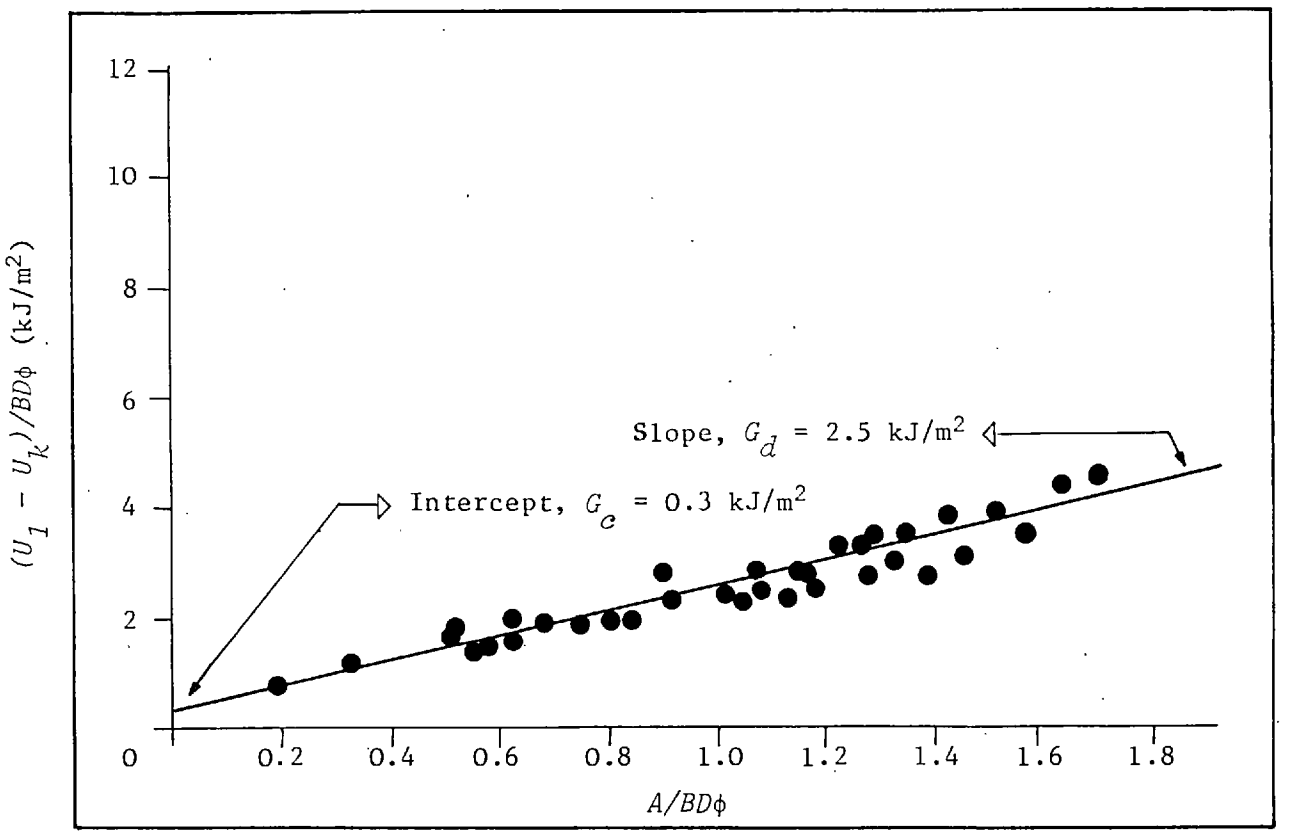


Figure 7: Grade S3 (2.22% rubber content) - Graphical analysis data

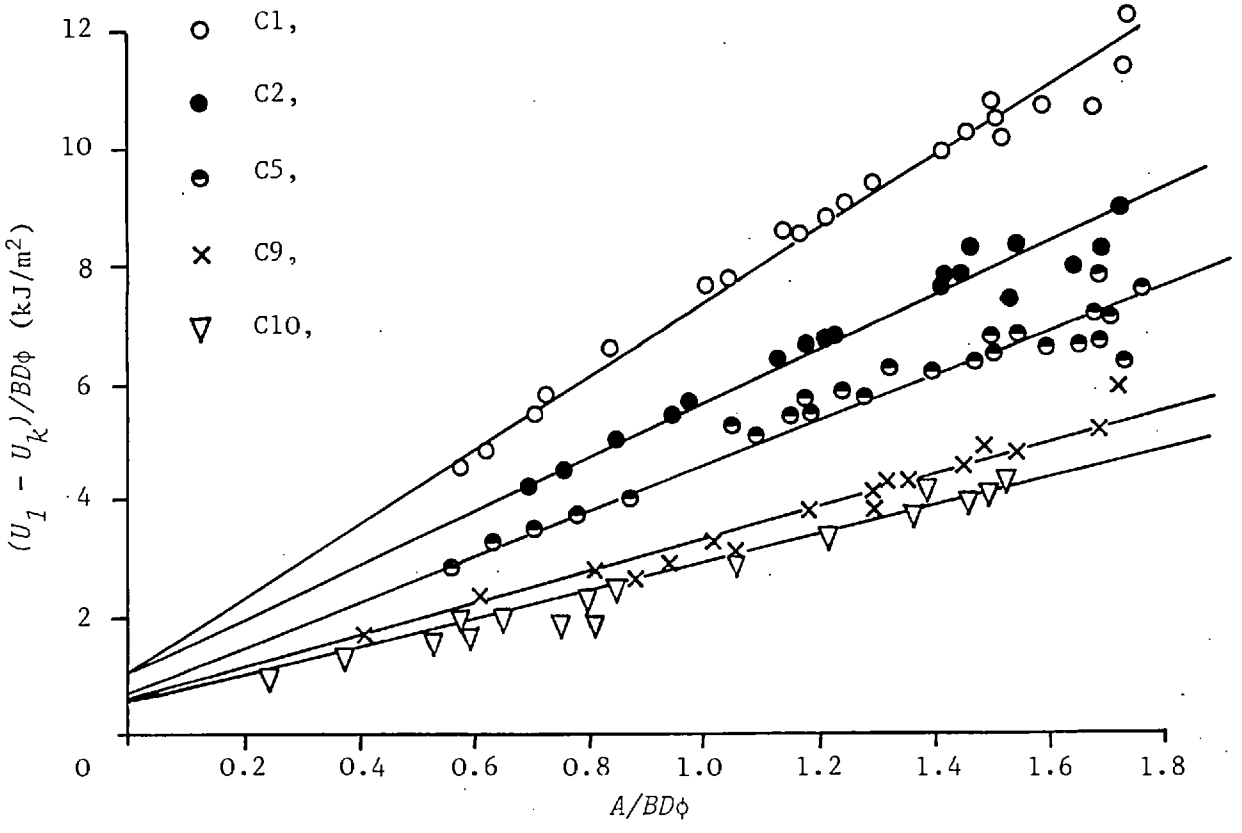


Figure 8: Commercial materials, Super, Standard and Medium grades

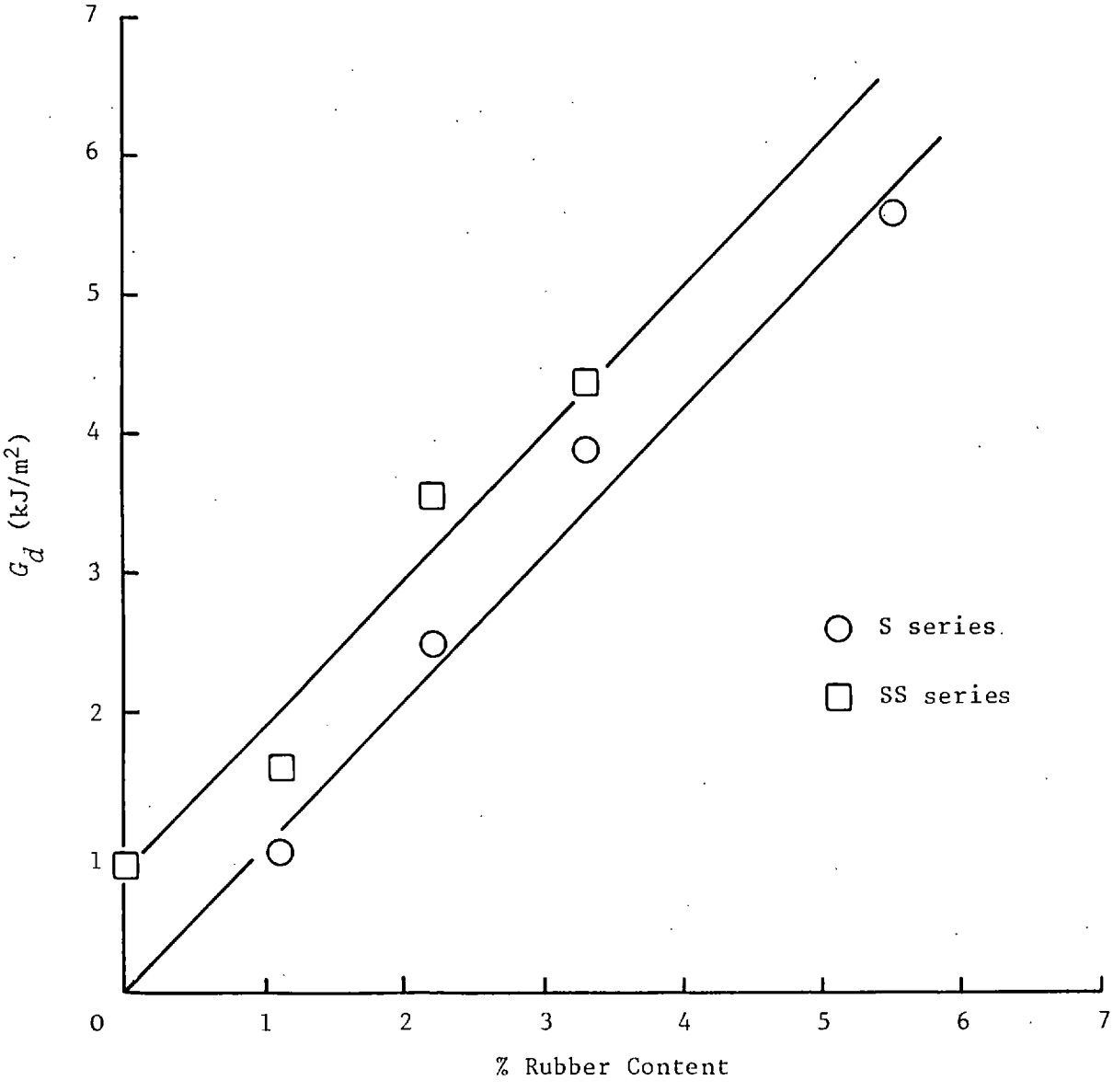


Figure 9: G_d as a function of rubber content